



MONASH University

Analysis of the interaction between α_2 -antiplasmin and plasmin(ogen)

Bernadine G.C. Lu

Bachelor of Biomedical Science (Honours)

Submitted in total fulfilment of the requirement of the degree of
Doctor of Philosophy
May 2013



A C B D

Australian Centre for Blood Diseases

Australian Centre for Blood Diseases
6th Floor Burnet Building,
89 Commercial Road, Melbourne 3004, Victoria, Australia

ERRATA

- p 14 Section 1.4.1, line 3-4: "whereas Type II" for "whereas Type I"
- p 107 Para 1, line 4: "Figure 3.12A" for "Figure 3.10A" and "Figure 3.12B" for "Figure 3.10B"
Para 1, line 5-6: "Figure 3.12C" for "Figure 3.10C"
Para 1, line 7: "Figure 3.12D" for "Figure 3.10D"
Para 1, line 9: "Figure 3.12E" for "Figure 3.10E"
Para 2, line 1: "Figure 3.10A" for "Figure 3.11A" and "Figure 3.10B" for "Figure 3.11B"
Para 2, line 4: "Figure 3.10C" for "Figure 3.11C" and "Figure 3.10D" for "Figure 3.11D"
Para 2, line 7: "Figure 3.11A" for "Figure 3.12A" and "Figure 3.11B" for "Figure 3.12B"
Para 2, line 9-10: "Figure 3.11C" for "Figure 3.12C" and "Figure 3.11D" for "Figure 3.12D"
- p 152 Figure 4.5, line 7 in legend: "Michaelis constant" for "Michaelis Menton"
- p 154 Figure 4.6, line 7 in legend: "Michaelis constant" for "Michaelis Menton"

ADDENDUM

- p 14 Section 1.4, line 11: Delete "Lys⁷⁷-Lys⁷⁸" and add "Lys⁶², Arg⁶⁸ and Lys⁷⁷"
- p 26 Line 4: Comment: Upon cleavage of Lys¹⁵⁸-Ile¹⁵⁹ bond, uPA is converted to a two chain form and is held together by a single disulphide bond at Cys¹⁴⁸-Cys²⁷⁹.
- p 30 Table 1.1: Add to table legend "Clade classification, known function and dysfunction (high or low levels) of human serpins."
- p 58 Section 1.11, Para 2, line 3-4: Delete "three single point mutation at Thr103Asn, Lys296Ala and Ala117Gln" and read "three mutation sites which are Thr103Asn, Ala117Gln and tetra-alanine substitution at residues 296-299."
- p 89 Table 3.2: Add to the end of table legend "MW is in Daltons (Da) and extinction coefficient is in M⁻¹cm⁻¹"
- p 123 Figure 3.13: Comment: As stated in the figure legend on page 122, all proteins analysed (including WT) in this figure are recombinant α_2 -antiplasmin proteins.
- p 166 Para 1, line 12: Delete sentence starting with "No residual activity was observed..." and replace with "Fluorescence emission was not detected with active site-blocked plasmin which indicated that activity of plasmin was blocked (results not shown)."
- p 166 Para 2, Comment: In Figure 4.11 (p 169), higher active site-blocked plasmin (20-120nM) was only used for C Δ α_2 -antiplasmin which had the lowest affinity. WT, N Δ and N Δ C Δ have comparable affinity and 2-8nM of active site-blocked plasmin was used in the analyses of these α_2 -antiplasmin proteins.
- p 184 Para 2, line 4: Delete sentence beginning with "Unlike the CM5 chip..." and replace with "In contrast, orientation of ligand binding on a CM5 chip surface is random and as a consequence, the interaction of target analyte will be inconsistent."
- p 191 Para 2, line 7-8: Comment: Another method of expression of microplasmin in eukaryotic cells has been described using *Pichia pastoris* cells (Nagai et al, 2003 – Journal of Thrombosis and Haemostasis, Vol 1(2), p 307-313).
- p 222 Para 2: Comment: uPA was purchased and concentration supplied on the product was based on its assayed activity (Units) rather than molar concentration.
- p 231 Para 2: Comment: Approximately 1.5mg of His- μ PIg S741A was obtained from 200mg of inclusion bodies. 0.5mg of this protein was stored at -80°C and the remaining ~1mg was subjected to uPA activation and further purification process. Typical yield of His- μ PIg S741A is 0.4mg from 200mg of inclusion bodies. This amount is comparable to other microplasmin recombinant proteins produced (His- μ PIg and μ PIg WT) in Chapter 5.

p 243 Comment: His- μ Plm S741A used for non-covalent complex detection by size exclusion chromatography does not contain non-activatable μ Plg. As indicated in Figure 5.11 (p 235), His- μ Plm S741A was purified by Benzamidine affinity chromatography to remove His- μ Plg S741A that could not be activated.

p 245 Comment: Figure 5.14A shows a Western blot probed with anti-plasminogen antibody, therefore Δ α_2 -antiplasmin should not react with this antibody and therefore is not visible on the blot.

p 256 Para 1: Comment: 100nM binding affinity was seen between active site-blocked microplasmin and WT α_2 -antiplasmin in Chapter 7 but active site mutated microplasmin and Δ α_2 -antiplasmin (Chapter 5) could not be co-eluted by size exclusion chromatography. It was stated at the end of paragraph 1 that one possible explanation for this was that migration of Δ and His- μ Plm S741A through the gel filtration medium could have caused the two molecules to separate. Add at the end of paragraph 1:

"For a direct comparison, future work on the co-elution of WT α_2 -antiplasmin and active site-blocked microplasmin could be studied. Furthermore, the binding affinity of Δ α_2 -antiplasmin with μ Plm-S741A could be analysed to observe if the affinity remains at 100nM."

p 275 Figure 6.4: Comment: Panel A shows a figure of an SDS-PAGE whereas panel B is a Native-PAGE which visualises the protein in its native conformation. The protein bands shown in panel B does not reflect the molecular weight of the proteins but indicates that the folding and charge of H229A and E232A are slightly different.

p 285 Figure 6.7: Comment: Higher concentration of H229A and E232A could be used in kinetic assays to achieve progress curves that are similar to those in Figure 4.5A.

p 324 Section 7.3.2: Comment: Prior to evaluating the binding affinity of plasminogen variants via SPR, plasminogen preparations were verified that they were devoid of plasmin activity. Therefore, the slow dissociation phase observed in sensorgrams with plasminogen is not due to the presence of plasmin contaminants. Add at the end of paragraph 1:

"Residual plasmin activity of GluPlg, GluPlg Type I, GluPlg Type II and LysPlg were analysed with AMC fluorogenic substrate and compared with active plasmin. Fluorescence emission was not detected with all plasminogen preparations which indicated that there was no residual plasmin present in those purified samples (results not shown)."

p 353 Para 1: Comment: The study published by Lijnen et al (1981) demonstrated that the binding affinity of plasminogen to α_2 -antiplasmin is in the order of μ M whereas this study showed lower affinity at nM range. Lijnen and colleagues used purified α_2 -antiplasmin from plasma and as mentioned in this paragraph, plasma α_2 -antiplasmin has four potential glycosylation sites. Add to the end of paragraph 1:

"Furthermore, recombinant α_2 -antiplasmin proteins produced in this thesis does not contain any glycosylation. Future experiments should include plasma purified α_2 -antiplasmin to explore the potential role of glycosylation sites in the binding of plasminogen. Perhaps the discrepancy seen with affinity between the study by Lijnen et al (1981) and this thesis could be resolved."

p 354 Add to the end of paragraph 1:

"In humans, plasminogen and α_2 -antiplasmin circulates at a concentration of $\sim 2.4\mu$ M and $\sim 1\mu$ M respectively. Based on this knowledge, results obtained from this chapter would suggest that α_2 -antiplasmin circulates in complex with plasminogen in plasma. In order to confirm this observation, co-purification of α_2 -antiplasmin and plasminogen from plasma should be attempted."

p 365 Add at the end of the paragraph:

"This knowledge will enable us to discover new therapeutics such as antibodies or small peptides which blocks the interaction sites of α_2 -antiplasmin to plasmin, thus up-regulating the activity of plasmin, the natural clot-busting molecule, in pathological thrombotic events."

Notice 1

Under the Copyright Act 1968, this thesis must be used only under the normal conditions of scholarly fair dealing. In particular no results or conclusions should be extracted from it, nor should it be copied or closely paraphrased in whole or in part without the written consent of the author. Proper written acknowledgement should be made for any assistance obtained from this thesis.

Notice 2

I certify that I have made all reasonable efforts to secure copyright permissions for third-party content included in this thesis and have not knowingly added copyright content to my work without the owner's permission.

Principal supervisor: **Assoc. Prof. Paul Coughlin^{1,2}**

Co-supervisor: **Dr Anita Horvath¹**

From the ¹Australian Centre for Blood Diseases, Monash University, Melbourne, Victoria 3004, and the ²Department of Medicine and Haematology, Box Hill Hospital, Box Hill, Victoria 3128, Australia

Statement of Originality

I hereby declare that this thesis contains no material which has been accepted for the award of any other degree or diploma in any other university or institution. To the best of my knowledge and belief, this thesis contains no material previously published or written by another person, except where due reference has been made in the text of the thesis.

The results presented in Chapter 4 of this thesis were published in a peer-reviewed journal: Lu B.G.C., Sofian T., Law R.H.P., Coughlin P.B., Horvath A.J. (2011). Contribution of conserved lysine residues in the α_2 -antiplasmin C terminus to plasmin binding and inhibition. *The Journal of Biological Chemistry* 286, 24544-24552.

Bernadine G.C. Lu

May 2013

This page has been intentionally left blank.

Acknowledgements

Firstly, I would like to thank my supervisors Associate Professor Paul Coughlin and Dr Anita Horvath for supporting me in the last four years. Thank you for giving me the opportunity to travel overseas to present my work at ISTH, Kyoto, Japan. It was a great experience and cemented my enthusiasm and appreciation for scientific research. Thank you for teaching me to be independent and laying the foundation of my research career!

A big thank you to our collaborators from the Department of Biochemistry and Molecular Biology (Monash University), in particular Dr Ruby Law and Adam Quek, for providing purified plasminogen used in surface plasmon resonance experiments. Thank you for assisting me with the α_2 -antiplasmin/microplasmin crystallisation trials and allowing me to undertake this work in your laboratory.

I would like to express my appreciation to Dr Elizabeth Gardiner (Vascular Biology Laboratory, ACBD) and Dr Ping Fu (Molecular Endocrinology Laboratory, AMREP) for their advice and guidance during the development of the surface plasmon resonance experiments. I would also like to thank Dr Trifina Sofian, a former member of our laboratory, for sharing her knowledge and techniques which formed the basis of my PhD work. Thank you for always encouraging and checking in on my progress once in awhile.

I would like to thank everyone at the Australian Centre for Blood Diseases. In particular to all the members of the Fibrinolysis and Gene Regulation Laboratory, especially Associate Professor Robert Medcalf, thank you for always including me in all your lab events and encouraging me throughout this PhD journey. Special thanks to Amanda Au for always listening to my complaints and participating in my random conversations. Thank you for always supporting and advising me whenever I encounter any problems. I am glad that we were able to share this PhD 'adventure' and become really great friends! To Dr Rachael Borg, Elisa Cops, Maria Daglas, Roxann Freeman, Be'eri Neigo, Dr André Samson and Dr Maithili Sashindranath, thank you for making the lab a friendly and fun environment. I will always cherish the friendship we have formed and I will always remember all the good times we had in (and out of) the lab.

Last but not least, I would like to thank my family for all the support they have given me. Ma and Pa, thank you for giving me this opportunity to study in Australia. I would not be where I am today without your help and encouragement. I would like to thank all my siblings and their family. In particular, to my brothers, Joseph and Gabriel, and sister-in-law, Elaine, for always supporting me (financially and emotionally) and ensuring that I was always fed.

This page has been intentionally left blank.

Table of Contents

Statement of Originality	iii
Acknowledgements	v
Table of Contents	vii
Table of Figures	xiii
Manuscripts and conference abstracts arising from this thesis	xvii
Abbreviations	xviii
Abstract	xx
Chapter 1: Literature Review	1
1.1 Introduction to the Fibrinolytic System	3
1.2 Fibrin(ogen)	6
1.3 Serine Proteases	10
1.3.1 Structure of Serine Proteases	10
1.3.2 Serine Protease Mechanism of Function	11
1.4 Plasmin(ogen)	14
1.4.1 Plasminogen Glycoforms	14
1.4.2 Crystal Structure of Plasminogen.....	15
1.4.3 Kringle Domains of Plasminogen	16
1.4.4 Protease Domain	16
1.4.5 Microplasmin(ogen) and Miniplasmin(ogen).....	17
1.4.6 Other Roles of Plasmin(ogen) Outside of Fibrinolysis	17
1.4.7 Plasminogen Deficiency	17
1.5 Plasminogen Activators	24
1.5.1 Tissue-type Plasminogen Activator.....	24
1.5.2 Urokinase-type Plasminogen Activator	25
1.6 Inhibitors of the Fibrinolytic System	26
1.7 Serine Protease Inhibitors (Serpins)	27
1.7.1 Biological Roles of Human Serpins	27
1.7.2 Structure of Serpins	33
1.7.3 Serpin Inhibitory Mechanism.....	37
1.7.4 Conformational States of Serpins	40
1.7.5 Regulation of Serpin Activity	42

1.8	Inhibition of the Fibrinolytic System at the Level of Plasminogen Activators: PAI-I and PAI-II	46
1.8.1	Plasminogen Activator Inhibitor I (PAI-I)	46
1.8.2	Plasminogen Activator Inhibitor II (PAI-II)	47
1.9	Inhibition of Plasmin by α_2 -Antiplasmin	48
1.9.1	Reactive Centre Loop of α_2 -antiplasmin	48
1.9.2	The N-terminus of α_2 -antiplasmin	48
1.9.3	The C-terminus of α_2 -antiplasmin	49
1.9.4	X-ray Crystal Structure of Murine α_2 -antiplasmin	52
1.9.5	α_2 -antiplasmin Deficiency	52
1.10	Other Regulators of the Fibrinolytic System.....	56
1.10.1	Thrombin Activatable Fibrinolysis Inhibitor (TAFI)	56
1.10.2	α_2 -Macroglobulin	57
1.10.3	Neuroserpin.....	57
1.11	Current Thrombolytic Therapy	58
1.12	Development of New Thrombolytics	59
1.12.1	Plasmin as a Direct Therapeutic Agent.....	59
1.12.2	Potential Therapeutic Role of α_2 -Antiplasmin.....	60
1.13	Aims and Hypotheses	61

Chapter 2: General Materials and Methods 63

2.1	General Reagents	64
2.2	Apparatus and Equipment	64
2.3	Bacterial Cells	66
2.3.1	<i>Escherichia coli</i> BL21(DE3)pLysS	66
2.3.2	<i>Escherichia coli</i> XL-10 Gold	66
2.4	Plasmids and Vectors.....	67
2.4.1	pET(3a)His.....	67
2.4.2	pGEMT-easy	67
2.5	Molecular Biology	68
2.5.1	Polymerase Chain Reaction (PCR)	68
2.5.2	DNA Electrophoresis	68
2.5.3	DNA Purification.....	68
2.5.4	Preparation of Chemically Competent <i>Escherichia coli</i> Cells.....	69
2.5.5	Transformation of Chemically Competent <i>Escherichia coli</i> Cells	69
2.5.6	Ligations.....	69

2.5.7	Colony PCR.....	70
2.5.8	pGEMT-easy Cloning	70
2.5.9	DNA Sequencing	71
2.5.10	Site-Directed Mutagenesis.....	71
2.6	Protein Biochemistry.....	74
2.6.1	Sodium Dodecyl Sulfate-Polyacrylamide Gel Electrophoresis (SDS-PAGE)	74
2.6.2	Non-Denaturing Polyacrylamide Gel Electrophoresis (Native-PAGE)	75
2.6.3	Transverse Urea Gradient Polyacrylamide Gel Electrophoresis (TUG-PAGE)	76
2.6.4	Western Blotting	77
2.6.5	Coomassie Brilliant Blue.....	77
2.6.6	Protein Concentration Determination	78

Chapter 3: Expression and Purification of Recombinant α_2 -antiplasmin Proteins ...
..... **79**

3.1	Introduction.....	81
3.2	Methods.....	82
3.2.1	Generation of Human α_2 -antiplasmin Bacterial Expression Construct.....	82
3.2.2	Sequence Alignment, Molecular Weight, Extinction Co-efficient and Isoelectric Point (pI).....	83
3.2.3	Large Scale Expression of Recombinant Human α_2 -antiplasmin.....	83
3.2.4	Purification on Nickel Chelate Affinity Chromatography	84
3.2.5	Purification on Anion Exchange Affinity Chromatography	86
3.2.6	Western Blot Analysis of Recombinant Human α_2 -antiplasmin	86
3.2.7	Circular Dichroism Analysis of Recombinant Human α_2 -antiplasmin.....	87
3.3	Results	88
3.3.1	Generation of N- and/or C-terminally Truncated Human α_2 -antiplasmin Constructs	88
3.3.2	Mutagenesis of the Human α_2 -antiplasmin C-terminus	94
3.3.3	Recombinant Human α_2 -antiplasmin Wild-type Expression and Purification	95
3.3.4	Recombinant Human α_2 -antiplasmin Variants Expression and Purification	101
3.3.5	Circular Dichroism Analysis of Recombinant α_2 -antiplasmin	121
3.4	Discussion	124
3.5	Conclusion.....	126

Chapter 4: Contribution of Conserved Lysine Residues in the α_2-antiplasmin C-terminus to Plasmin Inhibition and Binding	127
4.1 Introduction	129
4.2 Methods	134
4.2.1 Enzyme-Inhibitor Kinetics	134
4.2.2 Stoichiometry of Inhibition (<i>S</i>).....	134
4.2.3 Rates of Inhibition (<i>k_a</i>)	134
4.2.4 Binding Affinity (<i>K_D</i>)	136
4.3 Results	138
4.3.1 Stoichiometry of Inhibition between Recombinant Human α_2 -Antiplasmin and Plasmin	138
4.3.2 Rate of Plasmin Inhibition of Recombinant Human α_2 -Antiplasmin Variants – Continuous Method	149
4.3.3 Rate of Plasmin Inhibition of Recombinant Human α_2 -Antiplasmin Variants – Discontinuous Method.....	162
4.3.4 Binding Affinity of Recombinant Human α_2 -Antiplasmin Variants for Active Site-blocked Plasmin.....	166
4.4 Discussion.....	180
4.5 Conclusion	188

Chapter 5: Expression, Purification and Non-covalent Complex Studies of Microplasmin(ogen)	189
5.1 Introduction	191
5.2 Methods	192
5.2.1 Generation of Microplasminogen Expression Constructs.....	192
5.2.2 Trial Expression of Microplasminogen	194
5.2.3 Large Scale Expression of Microplasminogen	194
5.2.4 Inclusion Bodies (IB) Purification	195
5.2.5 Denaturation of IB	195
5.2.6 Refolding of Microplasminogen from IB	196
5.2.7 Purification of Microplasminogen on Nickel Chelate Affinity Chromatography ..	197
5.2.8 Activation of Microplasminogen to Microplasmin	198
5.2.9 Preparation of Microplasmin.....	198
5.2.10 Purification of Microplasmin(ogen) on Cation Exchange Affinity Chromatography ..	199
5.2.11 Purification of Microplasmin on Benzamidine Affinity Chromatography.....	200
5.2.12 Purification of Microplasmin on Size Exclusion Chromatography.....	200
5.2.13 Western Blot Analysis Microplasmin(ogen)	201

5.2.14	Microplasmin/ α_2 -antiplasmin Co-complex Studies.....	201
5.2.15	Crystallisation Trials of Microplasmin/ α_2 -antiplasmin Co-complex.....	202
5.3	Results	203
5.3.1	Generation of Microplasminogen in pET(3a)His and pET(3a) Expression Vector	203
5.3.2	Trial Expression of Microplasminogen	209
5.3.3	Large Scale Expression, Inclusion Bodies Purification, Denaturation and Refolding	213
5.3.4	Large Scale Purification of Active Site Mutated Microplasminogen.....	219
5.3.5	Microplasminogen to Microplasmin: Activation Studies.....	222
5.3.6	Large Scale Purification of Active Site Mutated Microplasmin.....	231
5.3.7	Large Scale Purification of Wild-type Recombinant Microplasmin(ogen).....	236
5.3.8	Non-Covalent Complex Studies of Active Site Mutated Microplasmin with N-Terminally Truncated α_2 -Antiplasmin.....	242
5.3.9	Preliminary Crystallisation Trials of Non-Covalent Complex.....	253
5.4	Discussion	254
5.5	Conclusion.....	257

Chapter 6: Contribution of β -sheet C of α_2 -antiplasmin to Plasmin Inhibition and Binding 259

6.1	Introduction.....	261
6.2	Methods.....	263
6.2.1	Site-directed Mutagenesis of the β -sheet C of Human α_2 -antiplasmin.....	263
6.2.2	Expression and Purification of β -sheet C Mutant α_2 -antiplasmin	263
6.2.3	Western Blot Analysis of Recombinant β -sheet C Mutant Human α_2 -antiplasmin	263
6.2.4	Circular Dichroism Analysis of Recombinant β -sheet C Human α_2 -antiplasmin..	263
6.2.5	Native-PAGE Analysis of Recombinant β -sheet C Human α_2 -antiplasmin	264
6.2.6	Stoichiometry of Inhibition of β -sheet C Human α_2 -antiplasmin with Plasmin	264
6.2.7	Rate of Inhibition of β -sheet C Human α_2 -antiplasmin with Plasmin	264
6.2.8	Surface Plasmon Resonance to measure Binding Affinity	264
6.3	Results	265
6.3.1	Mutagenesis of β -sheet C α_2 -antiplasmin.....	265
6.3.2	Expression and Purification of β -sheet C α_2 -antiplasmin	269
6.3.3	Stoichiometry of Inhibition of β -sheet C mutant α_2 -antiplasmin	277
6.3.4	Plasmin Inhibition Rate of β -Sheet C α_2 -antiplasmin Mutants	283
6.3.5	Binding Affinity of β -sheet C α_2 -antiplasmin Mutants with Active Site-blocked Plasmin.....	289

6.3.6	Binding Affinity of β -sheet C α_2 -antiplasmin with Active Site-blocked Microplasmin .	293
6.4	Discussion.....	299
6.5	Conclusion	304
Chapter 7: Insights into the Binding of Different Conformational Forms of Plasmin(ogen) to α_2-antiplasmin		305
7.1	Introduction	307
7.2	Methods	310
7.2.1	Kinetic Studies	310
7.2.2	Binding Studies	311
7.3	Results	315
7.3.1	Kinetic Analysis of Recombinant Microplasmin.....	315
7.3.2	Plasminogen Binding to α_2 -antiplasmin	324
7.3.3	Plasmin Binding to α_2 -antiplasmin	337
7.3.4	Microplasmin(ogen) Binding to α_2 -antiplasmin.....	342
7.4	Discussion.....	352
7.5	Conclusion	356
Chapter 8: General Discussion.....		357
Chapter 9: Bibliography		369
Chapter 10: Appendices		393
Appendix 10.1	General Buffers.....	394
Appendix 10.2	Lu et al., 2011, published paper related to this thesis as described in Chapter 4	397
Appendix 10.3	Horvath et al., 2011, published paper related to the methods used in measuring the rate of plasmin inhibition by α_2 -antiplasmin as described in Chapters 4 and 6.....	406

Table of Figures

Figure		Page
Chapter 1		
1.1	Regulation of the fibrinolytic system	5
1.2	Structure of fibrinogen	9
1.3	Serine protease structure and inhibitory mechanism	13
1.4	Schematic of plasminogen	19
1.5	X-ray crystal structure of human plasminogen	21
1.6	Schematic representation of the conformational change that occurs from Glu-plasminogen (closed) to Lys-plasminogen (open)	23
1.7	Biological functions of serpins	29
1.8	General structure of serpins	34
1.9	Serpin inhibitory mechanism	39
1.10	Different conformational states of serpins	45
1.11	Sequence alignment of human and mouse α_2 -antiplasmin	51
1.12	X-ray crystal structure of murine α_2 -antiplasmin	55
Chapter 2		
2.1	Schematic diagram of site-directed mutagenesis using the Stratagene Quikchange kit	73
Chapter 3		
3.1	Cloning strategy for truncated α_2 -antiplasmin variants into the pET(3a)His expression vector	91
3.2	Sequence alignment of wild-type and truncated human α_2 -antiplasmin	93
3.3	Schematic representation of the C-terminus of human α_2 -antiplasmin and positions at which mutations were introduced	97
3.4	Purification of wild-type human α_2 -antiplasmin	99
3.5	Nickel affinity chromatography of N- or/and C-terminally truncated human α_2 -antiplasmin	103
3.6	Anion exchange chromatography of N- or/and C-terminally truncated human α_2 -antiplasmin	105
3.7	Nickel affinity and anion exchange chromatography of K464R	109
3.8	Nickel affinity chromatography of multiple C-terminal Lys to Ala mutations of human α_2 -antiplasmin	111
3.9	Anion exchange chromatography of multiple C-terminal Lys to Ala mutations of human α_2 -antiplasmin	113
3.10	Nickel affinity chromatography of 15 amino acid deletion of the C-terminus of human α_2 -antiplasmin	115
3.11	Anion exchange chromatography of 15 amino acid deletion of the C-terminus of α_2 -antiplasmin	117
3.12	Purification of human α_2 -antiplasmin containing five Lys to Ala mutation in the C-terminus	119
3.13	Circular dichroism analysis of α_2 -antiplasmin	123
Chapter 4		
4.1	Comparison of plasmin inhibition rate (k_a) between wild-type and single Lys to Ala mutation in the C-terminus of α_2 -antiplasmin	133
4.2	Stoichiometry of inhibition (SI) of WT, N- and/or C-terminally truncated human α_2 -antiplasmin	143

4.3	Stoichiometry of inhibition (<i>S</i>) of progressive Lys to Ala mutants of human α_2 -antiplasmin with plasmin	145
4.4	Stoichiometry of inhibition (<i>S</i>) of 15 amino acids truncation of human α_2 -antiplasmin with plasmin	147
4.5	Plasmin inhibition rate (k_a) by WT, N- and/or C-terminally truncated human α_2 -antiplasmin	153
4.6	Plasmin inhibition rate (k_a) by single Lys to Arg mutation in the C-terminus of human α_2 -antiplasmin	155
4.7	Plasmin inhibition rate (k_a) by multiple Lys to Ala mutations in the C-terminus of human α_2 -antiplasmin	157
4.8	Plasmin inhibition rate (k_a) by human α_2 -antiplasmin truncated by 15 amino acids	159
4.9	Comparison of plasmin inhibition rate (k_a) between wild-type and mutant α_2 -antiplasmin	161
4.10	Plasmin inhibition rate (k_a) of recombinant human α_2 -antiplasmin determined by discontinuous method	165
4.11	Sensorgrams of the binding of WT, N- and/or C-terminally truncated α_2 -antiplasmin to active site-blocked plasmin as measured by SPR	169
4.12	Sensorgrams of the binding of single Lys mutant α_2 -antiplasmin to active site-blocked plasmin as measured by SPR	171
4.13	Sensorgrams of the binding of progressive Lys to Ala mutant α_2 -antiplasmin to active site-blocked plasmin as measured by SPR	173
4.14	Sensorgrams of the binding of α_2 -antiplasmin truncated by 15 amino acids to active site-blocked plasmin as measured by SPR	175
4.15	Comparison of the binding affinity (K_D) between wild-type and mutant α_2 -antiplasmin for active site-blocked plasmin	179
4.16	Mechanism of serpin inhibition	183
Chapter 5		
5.1	Cloning strategy for microplasminogen variants into the pET(3a)His and pET(3a) expression vector	205
5.2	Sequence alignment of His- μ PIg S741A, His- μ PIg WT and μ PIg WT	207
5.3	Trial expression of microplasminogen as detected by Western blot of insoluble and soluble lysates	211
5.4	Inclusion bodies preparation of His- μ PIg S741A	215
5.5	Denaturation and refolding of His- μ PIg S741A	217
5.6	Nickel affinity purification of His- μ PIg S741A	221
5.7	Activation studies with varying concentration of uPA	225
5.8	Activation studies with varying incubation period of uPA with His- μ PIg S741A	227
5.9	Activation studies with tPA	229
5.10	Cation exchange chromatography of His- μ PIm S741A	233
5.11	Benzamidine affinity purification of His- μ PIm S741A	235
5.12	Purification of His- μ PIg WT and His- μ PIm WT	239
5.13	Purification of μ PIg WT and μ PIm WT	241
5.14	Detection of non-covalent complex of N Δ α_2 -antiplasmin with His- μ PIm S741A by Native-PAGE	245
5.15	Detection of non-covalent complex of N Δ α_2 -antiplasmin with His- μ PIm S741A by non-reduced SDS-PAGE	247
5.16	Purification of N Δ α_2 -antiplasmin and His- μ PIm S741A by size exclusion chromatography	249
5.17	Detection of non-covalent complex of N Δ α_2 -antiplasmin with His- μ PIm S741A by size exclusion chromatography	251

Chapter 6		
6.1	Sequence alignment of β -sheet C human α_2 -antiplasmin	267
6.2	Nickel affinity chromatography of β -sheet C α_2 -antiplasmin	271
6.3	Anion exchange chromatography of β -sheet C human α_2 -antiplasmin	273
6.4	Analysis of recombinant β -sheet C α_2 -antiplasmin on Western and Native-PAGE	275
6.5	Stoichiometry of inhibition (<i>S</i>) of β -sheet C α_2 -antiplasmin with plasmin	279
6.6	Circular dichroism analysis of β -sheet C α_2 -antiplasmin	281
6.7	Plasmin inhibition (k_a) by β -sheet C α_2 -antiplasmin	285
6.8	Comparison of plasmin inhibition rate (k_a) between wild-type and β -sheet C α_2 -antiplasmin	287
6.9	Sensorgrams of the binding of recombinant β -sheet C α_2 -antiplasmin to PlmCMK as measured by SPR	291
6.10	Sensorgrams of the binding of recombinant β -sheet C α_2 -antiplasmin to μ PlmCMK as measured by SPR	295
6.11	Comparison of the binding affinity (K_D) between β -sheet C α_2 -antiplasmin with PlmCMK or μ PlmCMK	297
6.12	Structure of murine α_2 -antiplasmin highlighting His ²²⁹ , Glu ²³² and Arg ²³³ in the β -sheet C region	303
Chapter 7		
7.1	Schematic of the different conformations of plasmin(ogen)	309
7.2	Determination of the K_M for μ Plm and AMC	313
7.3	Stoichiometry of Inhibition of human α_2 -antiplasmin with microplasmin	317
7.4	Microplasmin inhibition rate by wild-type and C-terminally truncated human α_2 -antiplasmin	319
7.5	Microplasmin inhibition rate of recombinant human α_2 -antiplasmin determined by discontinuous method	321
7.6	Comparison of the microplasmin inhibition rate between wild-type and C-terminally truncated α_2 -antiplasmin	323
7.7	Sensorgrams of the binding of recombinant α_2 -antiplasmin to GluPIg as measured by SPR	327
7.8	Sensorgrams of the binding of recombinant α_2 -antiplasmin to GluPIg Type I as measured by SPR	329
7.9	Sensorgrams of the binding of recombinant α_2 -antiplasmin to GluPIg Type II as measured by SPR	331
7.10	Sensorgrams of the binding of recombinant α_2 -antiplasmin to LysPIg as measured by SPR	333
7.11	Comparison of the K_D between WT and C Δ α_2 -antiplasmin for PIg variants	335
7.12	Sensorgrams of the binding of WT and C Δ α_2 -antiplasmin to Plm as measured by SPR	339
7.13	Comparison of the K_D between WT and C Δ α_2 -antiplasmin for plasmin variants	341
7.14	Sensorgrams of the binding of WT and C Δ α_2 -antiplasmin to μ PIg as measured by SPR	345
7.15	Sensorgrams of the binding of WT and C Δ α_2 -antiplasmin to μ PlmCMK as measured by SPR	347
7.16	Sensorgrams of the binding of WT and C Δ α_2 -antiplasmin to μ Plm as measured by SPR	349
7.17	Comparison of the K_D between WT and C Δ α_2 -antiplasmin for microplasmin(ogen) variants	351
Chapter 8		
8.1	Summary of main findings	367

Table		Page
Chapter 1		
1.1	Clade classification, known function and dysfunction of human serpins	30
Chapter 3		
3.1	Primer sequences for human α_2 -antiplasmin	85
3.2	Molecular weight (MW), extinction coefficient and isoelectric point (pI) of human α_2 -antiplasmin variants	89
Chapter 4		
4.1	Stoichiometry of inhibition (<i>S</i>) and plasmin inhibition rate (k_a) of single Lys to Ala mutation in the C-terminus of α_2 -antiplasmin versus WT α_2 -antiplasmin	131
4.2	Mean stoichiometry of inhibition (<i>S</i>) of plasmin by recombinant human α_2 -antiplasmin	141
4.3	Mean plasmin inhibition rate (k_a) of WT and mutant recombinant human α_2 -antiplasmin as measured by continuous assay	151
4.4	Mean plasmin inhibition rate (k_a) of plasmin for mutant recombinant human α_2 -antiplasmin as measured using the discontinuous assay	163
4.5	Mean binding affinity, association and dissociation constant of WT and mutant α_2 -antiplasmin mutants for active site-blocked plasmin as measured by surface plasmon resonance	177
Chapter 5		
5.1	Primer sequences for human μ PIg	193
5.2	Molecular weight (MW), extinction coefficient and isoelectric point (pI) of human μ PIg variants	208
Chapter 6		
6.1	Primer sequence for human β -sheet C α_2 -antiplasmin	262
6.2	Molecular weight (MW), extinction coefficient and isoelectric point (pI) of human β -sheet C α_2 -antiplasmin	268
6.3	Stoichiometry of inhibition (<i>S</i>) and plasmin inhibition rate (k_a) of β -sheet C α_2 -antiplasmin versus WT α_2 -antiplasmin	276
6.4	Mean binding affinity, association and dissociation constants of WT and β -sheet C α_2 -antiplasmin mutants for active site-blocked plasmin as measured by surface plasmon resonance	288
6.5	Mean binding affinity, association and dissociation constants of WT and β -sheet C α_2 -antiplasmin mutants for active site-blocked microplasmin as measured by surface plasmon resonance	292
Chapter 7		
7.1	Stoichiometry of inhibition (<i>S</i>) and microplasmin inhibition rate (k_a) measured by continuous and discontinuous assays with WT and C Δ α_2 -antiplasmin	314
7.2	Mean binding affinity, association and dissociation constants of plasmin(ogen) variants with WT or C Δ α_2 -antiplasmin as measured by SPR	336

Manuscripts and conference abstracts arising from this thesis

Published manuscripts:

Lu, B.G.C., Sofian, T., Law, R.H.P., Coughlin, P.B., Horvath, A.J. (2011). Contribution of conserved lysine residues in the α_2 -antiplasmin C terminus to plasmin binding and inhibition. *The Journal of Biological Chemistry* 286, 24544-24552. (Appendix 10.2)

Horvath, A.J., **Lu, B.G.C.**, Pike, R.N., and Bottemley, S.P. (2011). Chapter Eleven – Methods to measure the kinetic of protease inhibition by serpins. *Methods Enzymol* 501, 223-235. (Appendix 10.3)

Conference Abstracts:

Lu, B.G.C., Sofian, T., Law, R.H., Coughlin, P.B., Horvath, A.J. “Antiplasmin-plasmin interaction: Comprehensive study of the antiplasmin C-terminus region using surface plasmon resonance” *Oral presentation* at the 23rd Congress of the International Society on Thrombosis and Haemostasis, Kyoto, Japan, July 2011.

Lu, B.G.C., Law, R.H., Coughlin, P.B., Horvath, A.J. “Insights into the different conformational forms of plasmin(ogen)” *Poster presentation* at the 23rd Congress of the International Society on Thrombosis and Haemostasis, Kyoto, Japan, July 2011.

Lu, B.G.C., Sofian, T., Coughlin, P.B., Horvath, A.J. “Lysine residues in the antiplasmin C-terminus mediate only a part of the interaction with plasmin” *Oral presentation* by Assoc Prof Coughlin at the 22nd Congress of the International Society on Thrombosis and Haemostasis, Boston, USA, July 2009.

Sofian, T., **Lu, B.G.C.**, Hitchen, C., Horvath, A.J., Coughlin, P.B. “The extreme C-terminus of antiplasmin is most important in accelerating the plasmin-antiplasmin interaction” *Poster presentation* by Assoc Prof Coughlin at the 22nd Congress of the International Society on Thrombosis and Haemostasis, Boston, USA, July 2009.

Abbreviations

°C	Degree Celsius
[S]	Substrate concentration
μPIg	Microplasminogen
μPIm	Microplasmin
μPImCMK	Active site-blocked microplasmin
μX (eg. μM, μL)	Micro (10 ⁻⁶)
Abs	Absorbance
Ala, A	Alanine
AMC	H-Ala-Phe-Lys7-amino-4-methylcoumarin
ANOVA	Analysis of variance
Arg, R	Arginine
Asn, N	Asparagine
CD	Circular Dichroism
cDNA	Complementary DNA
CM5	Carboxymethylated dextran
CMK	D-Val-Phe-Lys chloromethyl ketone
DNA	Deoxyribonucleic acid
<i>E.coli</i>	<i>Escherichia coli</i>
EDTA	Ethylenediaminetetraacetic acid
et al.	And others
FT	Flowthrough
g	gram
Glu, E	Glutamic acid
GluPIg	Glu-plasminogen
hAP	human α ₂ -antiplasmin
His, H	Histidine
HPLC	High performance liquid chromatography
hr	Hr
IB	Inclusion bodies
Insol	Insoluble
IPTG	Isopropyl β-D-1-thiogalactopyranoside
<i>k'</i>	Apparent second-order association rate constant
K1-5	Kringle 1-5
<i>k_a</i>	Inhibition rate
<i>k_{a1}</i>	Association rate constant
<i>k_{a2}</i>	Forward rate constant
<i>K_D</i>	Binding affinity
<i>k_{d1}</i>	Dissociation rate constant
<i>k_{d2}</i>	Reverse rate constant
kDa	Kilodalton
KM	Michaelis-Menton constant
kobs	First-order association rate constant
LBS	Lysine binding site
Leu, L	Leucine
Lys, K	Lysine
LysPIg	Lys-plasminogen
M	Molar
m	Meter

mAU	Milliabsorbance units
MCR	Multiple cloning region
Min	Minutes
MW	Molecular weight
mX (eg. mg, mL)	Milli (10^{-3})
Ni ²⁺	Nickel ions
NS	Non-significant
NTA	Nitrilotriacetic acid
nX (eg. nM, ng)	Nano (10^{-9})
PAI-I/II	Plasminogen activator inhibitor I/II
PAP	Pan-apple domain
PAGE	Polyacrylamide gel electrophoresis
PBS	Phosphate buffered saline
pI	Isoelectric point
Plg	Plasminogen
Plm	Plasmin
PlmCMK	Active site-blocked plasmin
PMSF	Phenylmethylsulfonyl fluoride
Pro, P	Proline
PVDF	Polyvinylidene difluoride
RCL	Reactive centre loop
RPM	Revolutions per minute
RT	Room temperature
RU	Response unites
SDS	Sodium dodecyl sulphate
SDS-PAGE	Sodium dodecyl sulphate polyacrylamide gel electrophoresis
SE	Standard error of the mean
Ser, S	Serine
Serpin	Serine protease inhibitor
SM	Starting material
SP	Serine protease
Sol	Soluble
SPR	Surface plasmon resonance
SI	Stoichiometry of inhibition
TEMED	Tetramethylethylenediamine
tPA	Tissue-type plasminogen activator
uPA	Urokinase-type plasminogen activator
V _{max}	Maximum velocity
WT	Wild-type

Abstract

Plasminogen is a multi-domain molecule which consists of a pan-apple domain, five kringles and a serine protease domain. Activation of plasminogen to plasmin converts the zymogen to a potent enzyme which dissolves blood clots. α_2 -antiplasmin is the physiological inhibitor of plasmin. In addition to the conserved serpin core, α_2 -antiplasmin also possesses two unique N- and C-terminal extensions. The conserved lysine residues (Lys⁴²⁷, Lys⁴³⁴, Lys⁴⁴¹, Lys⁴⁴⁸ and Lys⁴⁶⁴) in the C-terminus are essential in mediating binding with plasmin kringle domains. Disrupting the interaction of the C-terminus to plasmin has been shown to decrease plasmin inhibition resulting in increased fibrinolysis. To better understand the interaction that occurs between α_2 -antiplasmin and plasmin, this study explored the basic biochemical and binding properties of these multi-domain molecules.

How the lysine residues within the C-terminus of α_2 -antiplasmin accelerate the binding to plasmin kringles remains poorly understood. To elucidate this, systematic and sequential mutation of the C-terminal lysines were generated. The effects of these recombinant α_2 -antiplasmin proteins on plasmin inhibition rate using kinetic assays and binding affinity via surface plasmon resonance were studied. WT α_2 -antiplasmin was a fast inhibitor of plasmin at a rate of $3.7 \times 10^7 \text{ M}^{-1}\text{s}^{-1}$. It was determined that the C-terminal lysine (Lys⁴⁶⁴) was individually the most important lysine residue for initiating binding to plasmin. The conserved internal lysine residues within the C-terminus of α_2 -antiplasmin individually contributed less, but together significantly enhanced plasmin inhibition and binding. When the C-terminus of α_2 -antiplasmin was removed, the binding affinity with active site-blocked plasmin remained high ($K_D = 49\text{nM}$), suggesting that an additional exosite interaction exists.

It was hypothesised that the exosite interaction may lie between the α_2 -antiplasmin serpin core and plasmin protease domain. Therefore, non-covalent complex studies with N-terminally truncated α_2 -antiplasmin and active site mutated microplasmin were performed. Recombinant microplasmin, a truncated form of plasmin, was generated. Biochemical studies to directly demonstrate complex formation between α_2 -antiplasmin and active site mutated microplasmin were inconclusive. Non-denaturing PAGE suggested an interaction but this was not confirmed on size exclusion chromatography. Structural studies were attempted but unsuccessful at present, however crystallisation trials are currently ongoing.

Two residues (His²²⁹ and Glu²³²) within the β -sheet C of α_2 -antiplasmin were identified as potential interaction points with plasmin(ogen). Recombinant α_2 -antiplasmin mutants with alanine substitutions at these two positions were generated. The effects of these mutants on plasmin inhibition rate, plasmin binding and microplasmin binding were investigated. Results showed that plasmin inhibition and microplasmin binding affinity remained unchanged. However,

plasmin binding affinity was affected by the single alanine substitution suggesting that His²²⁹ and Glu²³² of β -sheet C are involved in plasmin interaction, presumably towards the kringles and not the protease domain.

The mechanism by which α_2 -antiplasmin interacts with plasmin(ogen) remains unclear. Therefore, the binding of α_2 -antiplasmin with different plasmin(ogen) variants were studied via surface plasmon resonance to elucidate which region(s) may be exposed and participate in binding. It was determined that the interaction between Glu-plasminogen (Type I and Type II) and α_2 -antiplasmin was not lysine mediated. In contrast, binding of Lys-plasminogen and α_2 -antiplasmin was primarily driven by the exposure of lysine binding sites in the kringles. Conversion of microplasminogen to microplasmin greatly improved the binding affinity to α_2 -antiplasmin from ~1400nM to ~100nM. This indicated that the activation of the serine protease domain resulted in dramatic conformational change and increase in additional interaction points for α_2 -antiplasmin.

The results of these studies, taken together suggest that an additional exosite interaction occurs between one of the plasmin kringle domains and the α_2 -antiplasmin serpin core. Future studies exploring other residues within the β -sheet C or other regions within the serpin core of α_2 -antiplasmin are required to confirm the exosite interaction and the identities of the region(s) involved in α_2 -antiplasmin and plasmin(ogen).

This page has been intentionally left blank.

Chapter 1:

Literature review

This page has been intentionally left blank.

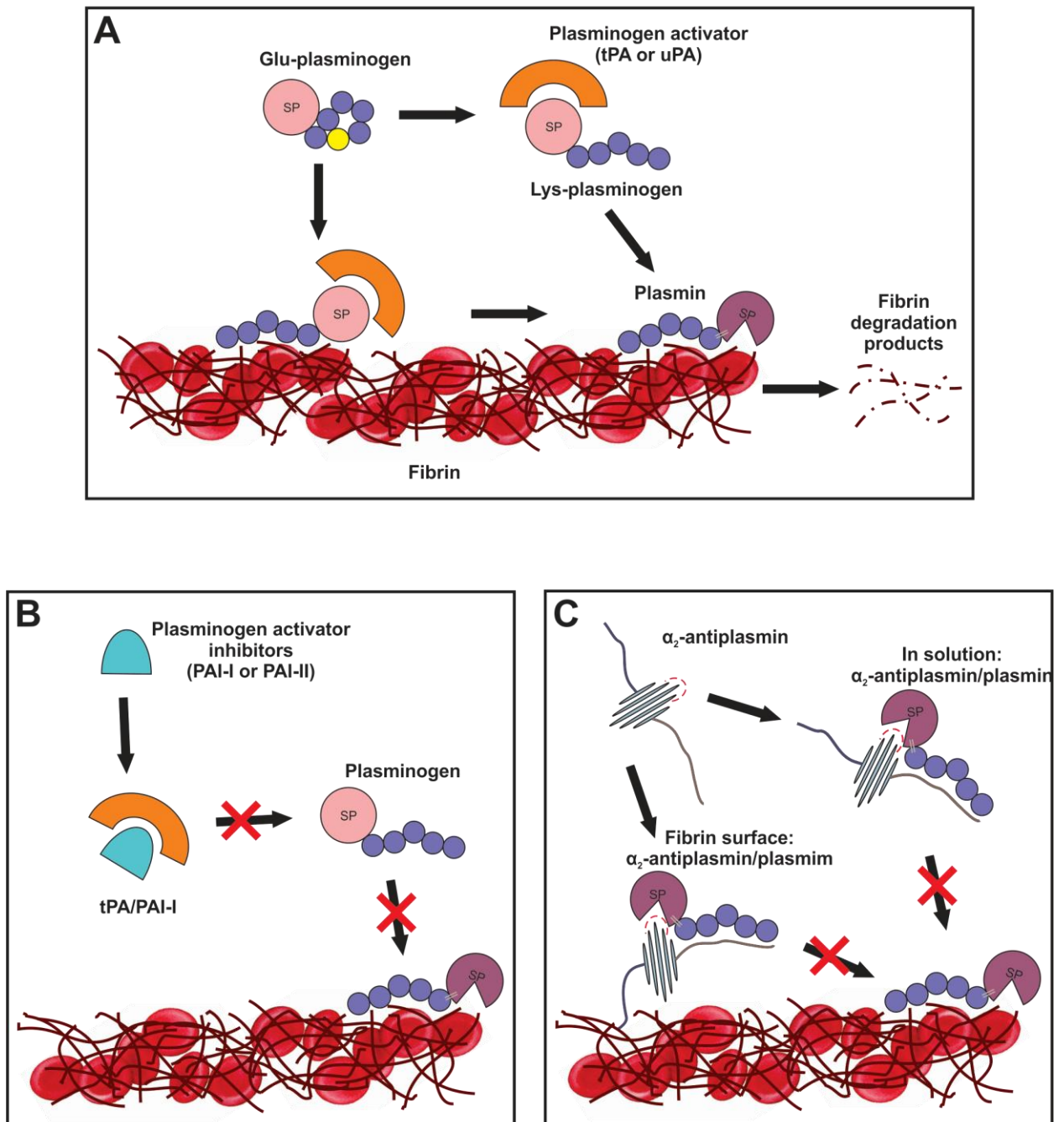
1.1 Introduction to the Fibrinolytic System

The fibrinolytic system is involved in regulating the dissolution of blood clots. Blood clots are formed in response to vascular injury and are composed of fibrin, platelets and red blood cells. Fibrin is required to hold the haemostatic clot together at the site of injury. Tight regulation between the fibrinolytic system and coagulation pathway is very important to ensure that homeostasis is maintained in the body. A variety of physiological processes such as thrombolysis, reproduction, embryogenesis and angiogenesis are involved in the fibrinolytic/coagulation system. Furthermore, dysfunction of the haemostatic system can lead to abnormal formation or dissolution of blood clots which has been implicated in cardiovascular, inflammatory and bleeding disorders. Stroke, myocardial infarction, deep vein thrombosis and pulmonary embolism are some examples of thrombotic disease. Pro-fibrinolytics such as plasminogen activating agents (eg. Alteplase) are used in disease states to prevent further pathological clot formation. One of the major drawbacks is the side effect of excessive bleeding which limits the use of these agents and hence there is a need for the development of new therapeutics.

Activation of the fibrinolytic system involves the conversion of an inactive zymogen, plasminogen, to the active counterpart, plasmin, which is the main protease required for the degradation of fibrin. This process is initiated by two major plasminogen activators which are tissue-type plasminogen activator (tPA) and urokinase-type plasminogen activator (uPA). Members of the serine protease inhibitor (serpin) family regulate the activity of plasmin, tPA and uPA. Plasmin activator inhibitors (PAI-I and PAI-II) stop the activity of tPA and uPA whereas the activity of plasmin is inhibited by α_2 -antiplasmin. The reaction between α_2 -antiplasmin and plasmin is very rapid and results in an inactive complex of these molecules. Dysregulation of any component in this system may cause excessive degradation of plasma proteins, such as extracellular matrices, by plasmin leading to haemorrhagic complications. On the other hand, inefficient plasmin conversion could cause decreased clot degradation. Figure 1.1 shows a schematic diagram of the fibrinolytic system.

Figure 1.1. Schematic of the fibrinolytic system. A) Plasminogen exists in two conformation known as Glu- (closed) and Lys-plasminogen (open). Plasminogen is activated to plasmin by plasminogen activators (tPA/uPA). Activation can occur on the fibrin clot or in solution. Plasmin is the main protease involved in regulating the breakdown of fibrin to fibrin degradation products. **B)** The fibrinolytic system can be inhibited at the level of plasminogen activators by plasminogen activator inhibitors (PAI-I/PAI-II). Once tPA or uPA is blocked, plasminogen cannot be converted to plasmin. **C)** α_2 -antiplasmin, the physiological inhibitor of plasmin, directly acts on the protease by forming an irreversible covalent complex either in solution or on the fibrin surface hindering clot breakdown.

Figure 1.1.
Regulation of the fibrinolytic system



1.2 Fibrin(ogen)

Fibrin(ogen) is the main component of blood clot forming the scaffold required to trap platelets and red blood cells. It is primarily synthesised as a 350 kDa protein by hepatocytes consisting of two identical subunits with each subunit comprised of three non-identical polypeptide chains termed $\text{A}\alpha$ chain, $\text{B}\beta$ chain and γ chain (Medved et al., 2009; Mosesson, 2005; Tsurupa et al., 2010; Undas and Ariëns, 2011). These chains form a triple helical coiled-coil linked by five symmetrical disulfide bridges at the NH_2 -terminal portion. The section where all six chains from both subunits converge, is known as region E (Blomback et al., 1976; Hoeprich and Doolittle, 1983; Madrazo et al., 2001; Mosesson, 2005). The C-terminal region (one in each subunit) of $\text{B}\beta$ and γ and a portion of $\text{A}\alpha$ is termed region D (Mosesson, 2005; Tsurupa et al., 2010). The remaining COOH-terminal region of residues 221-610 of the $\text{A}\alpha$ chain forms the flexible αC connector (residues 221-391) and the compact αC domain (residues 392-610) (Tsurupa et al., 2002). Residues 1-53 in the NH_2 -terminal region of the $\text{B}\beta$ chain is termed $\text{B}\beta\text{N}$. αC and $\text{B}\beta\text{N}$ region are named as such due to the fact that both regions are removed during the early stages of proteolysis and are therefore separate from the D and E regions (Medved et al., 2009). The structure of fibrinogen can be described as containing a central E region, two terminal D regions (D-E-D), two αC regions (each consisting of a αC connector and αC domain) and two $\text{B}\beta\text{N}$ regions (Medved et al., 2009; Tsurupa et al., 2010). The crystal structure of human fibrinogen has been solved and is shown in Figure 1.2A (Kollman et al., 2009). The key domains were previously elucidated from work using fibrinogen from other species (Kollman et al., 2009; Madrazo et al., 2001; Yee et al., 1997).

Fibrinogen is rather inert in circulation. Blood clot formation is triggered by conversion of fibrinogen to fibrin mediated by thrombin cleavage thereby triggering fibrin polymerisation. Thrombin cleaves two pairs of fibrinopeptide at residues 1-16 on the NH_2 -terminal portion of $\text{A}\alpha$ chain (FpA) and residues 1-14 of $\text{B}\beta$ chain (FpB) (Medved et al., 2009). This exposes polymerisation sites termed 'knobs' 'A' and 'B' which can interact with complementary sites termed 'holes' 'a' and 'b' located on the D regions (Figure 1.2B) (Medved and Nieuwenhuizen, 2003; Medved et al., 2009; Mosesson, 2005). This interaction is known as 'DD-E'. FpA is removed first which results in formation of the two-stranded protofibrils through the interaction of 'knob A' to 'hole a' (Blomback et al., 1978; Fowler et al., 1981; Medved and Nieuwenhuizen, 2003). The secondary binding is triggered when FpB is removed, promoting lateral assembly of protofibrils into a thicker fibre via 'knob B' interacting with 'hole b'. This process is necessary for the formation of a three dimensional network of fibrin mesh (Medved and Nieuwenhuizen, 2003; Mosesson et al., 1993). The two αC domains form intramolecular interaction, however upon fibrin polymerisation, this interaction dissociates and reassociates forming intermolecular contacts (αC -polymers) hence supporting further lateral growth of the fibrin mesh (Gorkun et al.,

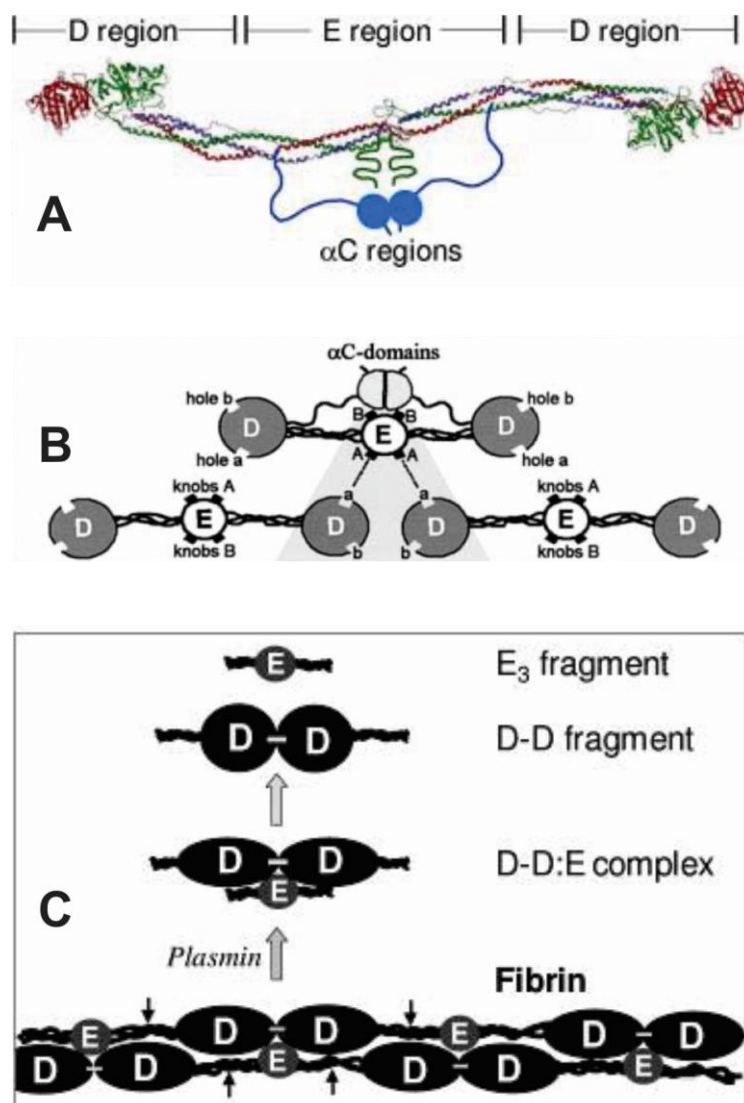
1994). In addition to thrombin activating fibrinogen, thrombin also plays a role in the conversion of Factor XIII to Factor XIIIa. Factor XIIIa further reinforces the fibrin structure by creating covalent cross-links. This occurs rapidly between the COOH-terminal region of γ chain with adjacent fibrin D regions (γ - γ cross-linking). Cross-linking has been reported to occur between α C-polymers but at a slower rate (Mosesson et al., 2001). Factor XIIIa is also responsible for incorporating the N-terminal region of α_2 -antiplasmin to a single Lys residue (Lys³⁰³) in the α C connector (refer to Section 1.9 for α_2 -antiplasmin) (Kimura and Aoki, 1986).

Fibrin degradation is mediated by the generation of plasmin in the vicinity or directly on the blood clot. Binding sites for tPA and plasminogen are cryptic in fibrinogen, however upon conversion to fibrin, conformational changes occur to the structure thus exposing these regions. A few binding sites have been identified in the fibrin structure, two in the D region and one in the α C domain (Medved and Nieuwenhuizen, 2003). In the D region, along the A α chain from residues 148-160 was determined to bind both tPA and plasminogen in a Lys-dependent manner (mediated by kringle domains) (Schielen et al., 1991). Under experimental conditions, it appears that this region has equal affinity for tPA and plasminogen, however it is believed that this site is saturated with plasminogen in circulation as the concentration is higher compared to tPA in physiological conditions (Bosma et al., 1988; Yakovlev et al., 2000). The second binding site in the D region is located on the γ chain at residues 315-323 (Yonekawa et al., 1992). This region only binds tPA in a Lys-independent manner most likely through its finger-like domain (refer to Section 1.5 for tPA) (Grailhe et al., 1994). Crystallisation studies of the D region in fibrinogen also revealed that A α 148-160 and γ 312-324 are located close to each other which suggests that the proximity may facilitate tPA activation of plasminogen (Spraggon et al., 1997; Weisel et al., 1994). The third region identified is in the α C domain residues 392-610 (Tsurupa and Medved, 2001). A specific region has yet to be mapped, however it was determined that both tPA and plasminogen were able to bind at two separate sites in a Lys-dependent manner (Tsurupa et al., 2011).

Congenital fibrinogen deficiency is a rare disorder and classified as either quantitative (afibrinogenemia or hypofibrinogenemia) or qualitative (dysfibrinogenemia) defects (Acharya and Dimichele, 2008). Afibrinogenemia (most severe form) usually manifest during the neonatal period, where 85% of cases presents with umbilical cord bleeding (Mannucci et al., 2004). Bleeding into skin, muscles and central nervous system also occurs. Hypofibrinogenemia and dysfibrinogenemia patients experience less frequent and severe bleeding events when compared to afibrinogenemia (Acharya and Dimichele, 2008). Fibrinogen replacement therapy is an effective treatment for patients with congenital fibrinogen deficiency (Bornikova et al., 2011).

Figure 1.2. Structure of fibrin(ogen). **A)** Ribbon diagram of fibrinogen with $A\alpha$ chain in blue, $B\beta$ chain in green and γ chain in red. The αC regions have not been crystallised and is represented by two blue spheres and connector. The D and E regions are labelled above the structure. **B)** DD-E interaction. Polymerisation sites termed 'knobs A' and 'B' interacting with complementary sites termed 'holes' 'a' and 'b'. **C)** Schematic representation of fibrin and fibrin degradation products by plasmin (adapted from Tsurupa et al., 2011).

Figure 1.2.
Structure of fibrin(ogen)



1.3 Serine Proteases

Proteases are divided into several classes which are cysteine, serine, metallo, aspartic acid, glutamic, asparagine and threonine (Rawlings et al., 2012). Serine proteases comprise nearly a third of known proteases and are named based on the presence of a serine residue at the core of the catalytic site (Di Cera, 2009; Hedstrom, 2002). They have been found to be involved in many physiological processes in humans such as fibrinolysis, coagulation and immune response. Furthermore, dysfunction of these serine proteases are linked with diseases such as cardiovascular and cancer (Hedstrom, 2002). Based on the MEROPS database, a collection of known proteases classified based on similarities in sequence and structure, serine proteases are grouped into 15 clans and 53 families (Rawlings et al., 2012).

The four main and common clans were first distinguished based on the presence of “Asp-His-Ser” residues referred to as the catalytic triad or charge relay system. Based on the MEROPS classification, these four clans were termed PA, SB, SC and SK with the representative serine protease in each group being chymotrypsin, subtilin, carboxypeptidase Y and Clp protease respectively (Hedstrom, 2002). Since then, novel catalytic triads and dyads have been discovered such as “His-Ser-His” and “Ser-Lys” (Di Cera, 2009; Ekici et al., 2008).

1.3.1 Structure of Serine Proteases

The general structure of the serine protease domain is typically characterised by two six-stranded beta barrels. The His-Asp-Ser catalytic triad is located between the two barrels (Hedstrom, 2002). Most serine proteases exist as zymogens, therefore proteolysis of the activation domain is required for conversion to active protease. The activation domain is usually located in the N-terminal portion of the protease domain (Di Cera, 2009). Using chymotrypsinogen as an example, conversion to the active form, chymotrypsin, requires cleavage between residues 15 and 16 (Neurath and Dixon, 1957). Upon cleavage, Ile¹⁶ forms a salt bridge with Asp¹⁹⁴ which triggers structural rearrangement and reorganises the catalytic domain to its active conformation (Hedstrom, 2002).

Besides the core protease domain, some serine proteases are composed of additional regulatory domains such as kringles, N-terminal peptide, epidermal growth factor-like and fibronectin domains (Hedstrom, 2002; Schaller and Gerber, 2011). Examples of serine proteases containing such regions are plasminogen, tPA and uPA which are reviewed in later sections.

1.3.2 Serine Protease Mechanism of Function

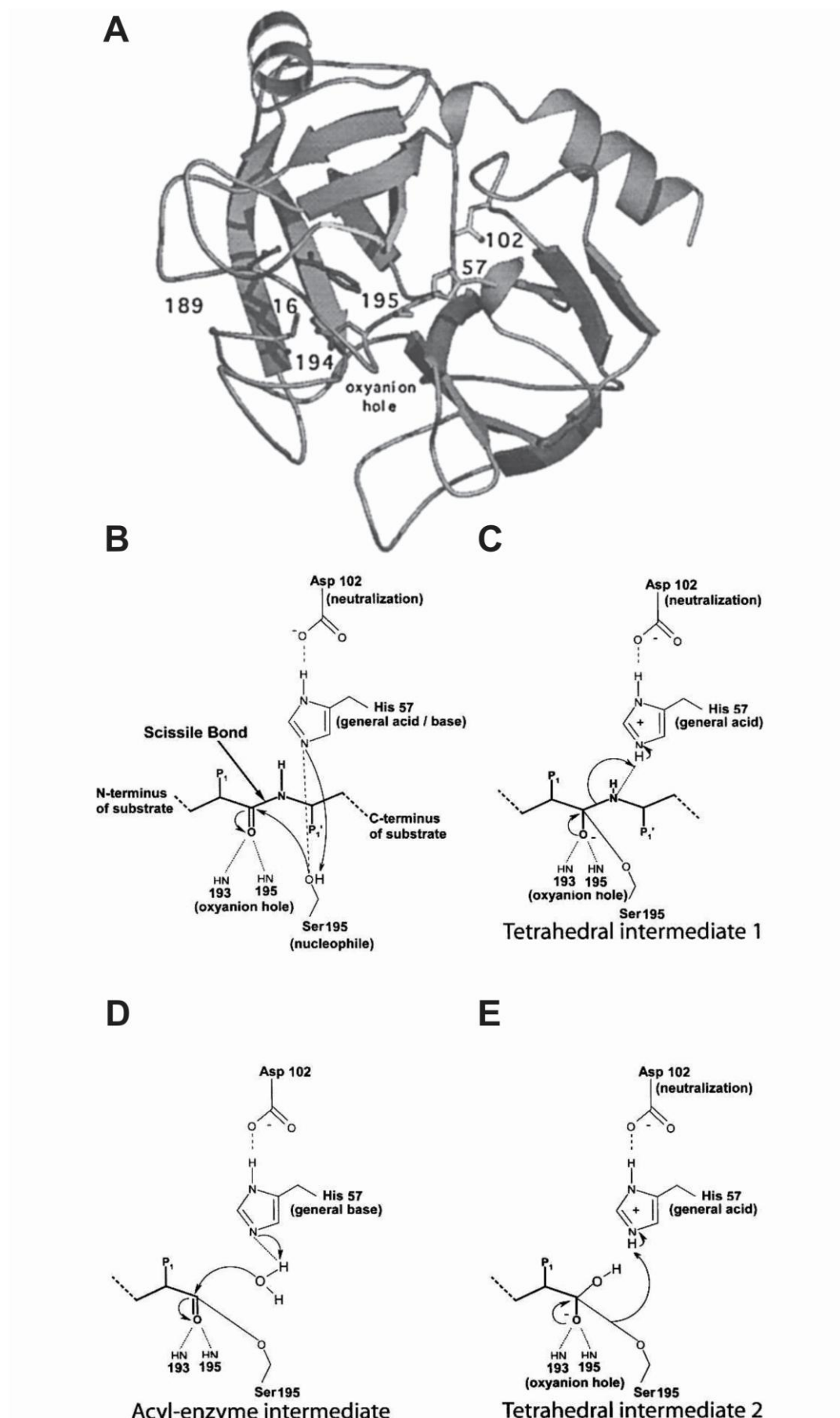
The following general steps are required for serine proteases to hydrolyse a peptide bond: 1) Activation of the amide bond via interaction of carbonyl oxygen with a general acid, 2) Activation of water through a general base and 3) Protonation of amine prior to expulsion (Hedstrom, 2002).

To better understand this complicated mechanism, chymotrypsin will be used as an example to demonstrate the reaction that occurs at the catalytic triad (Figure 1.3A). Chymotrypsin, with the catalytic triad residues of His⁵⁷, Asp¹⁰² and Ser¹⁹⁵, is a member of the PA clan and S1 family. The S1 family is the largest family of serine proteases. The first three dimensional structure was determined in 1967 by Matthews and colleagues and has been refined since then (Freer et al., 1970; Matthews et al., 1967). The catalytic neutrophile is Ser¹⁹⁵ which attacks the carbonyl of peptide substrate with the assistance of His⁵⁷ as a general base forming a tetrahedral intermediate (Figure 1.3B and C). The tetrahedral intermediate is stabilised by hydrogen bond between His⁵⁷-H⁺ and Asp¹⁰² and interaction with atoms Gly¹⁹³ and Ser¹⁹⁵ which forms a positively charged pocket known as the oxyanion hole. The tetrahedral then collapses with the release of the C-terminus of the peptide yielding the acyl-enzyme intermediate (Figure 1.3D). This acyl-enzyme intermediate is then attacked by water molecule, again mediated by His⁵⁷ as a general base, to form a second tetrahedral intermediate (Figure 1.3E). The final collapse releases the N-terminal peptide of the substrate and expulsion of residue Ser¹⁹⁵ (Ekici et al., 2008; Hedstrom, 2002).

The catalytic triad of serine proteases can be disrupted by natural inhibitors in the human circulatory system. These inhibitors, known as serpins, form an irreversible complex with the protease which causes a permanent distortion of the catalytic site rendering it inactive (Hedstrom, 2002). The serpin mechanism will be reviewed in Section 1.7.

Figure 1.3. Serine protease structure and inhibitory mechanism. A) Structure of chymotrypsin with the catalytic triad located at His⁵⁷, Asp¹⁰² and Ser¹⁹⁵ (adapted from Hedstrom, 2002). The proteolytic mechanism of serine proteases is demonstrated as follows **B)** Michaelis complex, **C)** Tetrahedral intermediate 1, **D)** Acyl-enzyme intermediate, **E)** Tetrahedral intermediate 2 (adapted from Ekici et al., 2008).

Figure 1.3.
Serine protease structure and inhibitory mechanism



1.4 Plasmin(ogen)

The principle enzyme in the fibrinolytic system mediating fibrin cleavage is plasmin. The zymogen plasminogen, is the precursor ~90 kDa molecule which is converted to its active form by plasminogen activators tPA and uPA. Plasmin(ogen) is a member of the S1 serine protease family and contains the classical “His-Asp-Ser” catalytic cleft. The gene is located on chromosome 6q26-6q27, contains 19 exons and 18 introns, and spans for 52.5kb (Castellino and Ploplis, 2005; Petersen et al., 1990). Plasminogen is secreted from the liver as an 810 amino acid molecule (Raum et al., 1980). The mature form, Glu-plasminogen, is generated by the removal of the 19 residue signal peptide resulting in a 791 amino acid protein (Forsgren et al., 1987). Lys-plasminogen, another form of N-terminally modified plasminogen, has been identified where the N-terminal peptide (NTP) or Pan-apple domain (PAP) is cleaved by plasmin at Lys⁶², Arg⁶⁸ and Lys⁷⁷ (Summaria et al., 1976). Figure 1.4 shows a schematic of the plasminogen molecule. Lys-plasminogen binds more avidly to fibrin surfaces and is more readily activated by tPA and uPA in comparison to Glu-plasminogen (Fredenburgh and Nesheim, 1992; Hoylaerts et al., 1982; Nesheim et al., 1990). Glu-plasminogen exists in a closed conformation whereas Lys-plasminogen has a more open conformation which makes the activation and binding sites more accessible in Lys-plasminogen (Lähtenmäki et al., 2005; Markus et al., 1978).

1.4.1 Plasminogen Glycoforms

Furthermore, plasminogen exists in two forms termed Type I and Type II which can be separated based on their affinity to lysine sepharose. The known differences between these two forms are the additional glycosylation site present in Type I (Asn²⁸⁹ and Thr³⁴⁶) whereas Type II only contains a single glycosylation at Thr³⁴⁶ (Hayes and Castellino, 1979a, b; Hayes and Castellino, 1979c). Type I exists at approximately 40% in circulation and Type II makes up the rest. Type II was determined to have approximately 10 times increased binding on cell surface when compared to Type I (Gonzalez-Gronow et al., 1989). However further characterisation revealed that the oligosaccharide side chains present on plasminogen may mediate binding to independent cell surface receptors (Gonzalez-Gronow et al., 2002; Gonzalez-Gronow et al., 2001). Type II was also shown to have an increased affinity for fibrin and α_2 -antiplasmin (Lijnen et al., 1981).

1.4.2 Crystal Structure of Plasminogen

The mature form of plasminogen is composed of the Pan-apple domain (PAP), five kringle domains (K1-5) and the protease domain. The PAP was characterised based on sequence similarities with the 'apple domains' of members from the prekallikrein family (Tordai et al., 1999). It was also suggested that the interactions made by PAP were mostly intramolecular-based thus maintaining Glu-plasminogen in a tight conformation (Banyai and Patthy, 1984; Ponting et al., 1992).

Recently, the crystal structure of Glu-plasminogen has been determined where all the domains were successfully visualised (Law et al., 2012; Xue et al., 2012). Law and colleagues crystallised Glu-plasminogen Type I and Type II to a resolution of 5.2Å and 2.45Å respectively (Law et al., 2012). Based on the crystal structure of Type II (Figure 1.5), it was revealed that PAP makes extensive contacts with the lysine binding sites (LBS) of K4 and K5. In addition to maintaining the molecule in the closed conformation, the PAP blocks the LBS of K4 and K5 which holds plasminogen in a relatively non-reactive form (Law et al., 2012). Furthermore, the cleavage site of plasmin at Lys⁷⁷-Lys⁷⁸ is buried suggesting that a certain degree of conformational change is required to expose this region for conversion to Lys-plasminogen (Law et al., 2012). The K3/K4 linker domain is closely associated with the SP domain and the activation loop protecting the zymogen from unwanted activation. Six out of the seven domains remained the same in Type I when compared with Type II Glu-plasminogen. K3 was the only region which could not be visualised in Type I crystal structure possibly due to the low resolution of the structure or the presence of the additional glycosylation site at Asn²⁸⁹ induced greater mobility in this region and thereby preventing its crystallisation (Law et al., 2012). It was observed that a hydrogen bond exists between Asn²⁸⁹ of K3 and SP domain in Type II which may contribute to the overall stability of the molecule in comparison to Type I. K1 remains unprotected in closed conformation and was suggested to be the initial mediator of fibrin and cell surface binding (Law et al., 2012). Similarly, Xue and colleagues solved the structure of Glu-plasminogen, in the presence of both glycoforms, to a resolution of 3.5Å (Xue et al., 2012).

The conversion from Glu-plasminogen to plasmin is a multistep process which includes conformational change and activation. Each domain within the plasminogen molecule has a role in protecting the zymogen from unwanted activation or recruitment on surfaces triggering a cascade of events. The structure of Lys-plasminogen has yet to be determined. However from observations seen in the Glu-plasminogen structure, it is suggested that Lys-plasminogen exists in a more open conformation due to the absence of PAP. Figure 1.6 is a schematic representation of the conformational change that occurs when Glu-plasminogen is converted to Lys-plasminogen.

1.4.3 Kringle Domains of Plasminogen

Plasmin(ogen) has five kringle domains, each domain is approximately 80 amino acids and consists of a triple-looped structure connected by three disulfide bridges: K1, Cys⁸⁴-Cys¹⁶²; K2, Cys¹⁶⁶-Cys²⁴³; K3, Cys²⁵⁶-Cys³³³; K4, Cys³⁵⁸-Cys⁴³⁵; K5, Cys⁴⁶²-Cys⁵⁴¹ (Castellino and Ploplis, 2005; Schaller and Gerber, 2011). K3 is the only domain which does not contain a functional LBS, however a single amino acid substitution at Lys³¹¹ to Asp alters the kringle to become a low affinity LBS (Burgin and Schaller, 1999). The kringle domains mediate binding of plasmin(ogen) to fibrin(ogen) (Suenson and Thorsen, 1981) and to the C-terminus of α_2 -antiplasmin (Gerber et al., 2010; Wiman et al., 1979). The affinity of the various kringles for 6-aminohexanoic acid from highest to lowest is as follows: K1>K4>K5>K2 (Schaller and Gerber, 2011). The same affinity model has been proposed for the binding α_2 -antiplasmin C-terminus (refer to Section 1.9 for α_2 -antiplasmin review) to kringle domains (Lu et al., 2011). The crystal structure of Glu-plasminogen identified that K1 is the only accessible kringle in the closed conformation and is likely to mediate initial recruitment on fibrin and cell surface (Law et al., 2012; Xue et al., 2012).

1.4.4 Protease Domain

As expected, the serine protease domain is a trypsin-like structure composed of two structurally similar sub-domains characterised by an antiparallel β -barrel where the catalytic domain is located in the centre of the two sub-domains (Law et al., 2012; Peisach et al., 1999). The catalytic triad have been identified to residues His⁶⁰³, Asp⁶⁴⁶ and Ser⁷⁴¹ (Castellino and Ploplis, 2005). The activation site is contained within this domain at Arg⁵⁶¹-Val⁵⁶². Activation by tPA and uPA (refer to Section 1.5 for review of plasminogen activators) converts the single chain plasminogen to a double chain molecule held by two disulfide bridge at Cys⁵⁴⁸-Cys⁶⁶⁶ and Cys⁵⁵⁸-Cys⁵⁶⁶ (Robbins et al., 1967). Once plasmin is generated, it is able to breakdown blood clots into fibrin degradation products. As summarised in Section 1.2, the main constituent of a blood clot is the complex molecule, fibrin. Interaction of plasmin(ogen) to fibrin is mediated by its kringle domains as previously described. A cascade of proteolytic events is triggered by plasmin on the A α chain to produce fragment X (260 kDa). Fragment X is then further degraded to fragment Y (160 kDa) and fragment D (100 kDa). Fragment Y undergoes a final cleavage to produce a second fragment D and fragment E (60 kDa) (Gaffney, 2001; Schaller and Gerber, 2011; Walker and Nesheim, 1999).

1.4.5 Microplasmin(ogen) and Miniplasmin(ogen)

Microplasminogen and miniplasminogen are plasminogen molecules lacking kringle domains. Both are produced through laboratory manipulations of full-length plasminogen as they are not found in human circulation (Medynski et al., 2007). Microplasminogen only contains the SP domain whereas miniplasminogen contains a single kringle domain (K5) and the SP domain (Ney and Pizzo, 1982; Wu et al., 1987). Microplasmin and miniplasmin can be produced by plasminogen activators (tPA and uPA) through the activation loop (Arg⁵⁶¹-Val⁵⁶²) in the intact SP domain (Medynski et al., 2007).

1.4.6 Other Roles of Plasmin(ogen) Outside of Fibrinolysis

In addition to its role in fibrinolysis, plasmin mediates many other physiological processes such as proteolysis of extracellular matrix to promote cell migration (Wong et al., 1992), wound healing and tissue remodelling (Creemers et al., 2000) and also tumour invasion and metastasis (Ranson et al., 1998).

1.4.7 Plasminogen Deficiency

Plasminogen deficiency is a rare autosomal recessive disorder which presents as having reduced levels of plasminogen leading to the development of pseudomembranes. The most prominent pseudomembranes are seen in the eyes and have been termed ligneous conjunctivitis (Mehta and Shapiro, 2008b; Schuster and Seregard, 2003). Other typically affected areas are the oropharynx, respiratory and genitourinary tract. Due to the lack of proteolytic capacity, wound healing is markedly inefficient and formations of lesions rich in fibrin are observed (Mehta and Shapiro, 2008b; Mingers et al., 1997).

Figure 1.4. Schematic of plasminogen. The plasminogen molecule is composed of the N-terminal peptide (NTP) also known as Pan-apple domain, five kringle domains (K1-K5) and the protease domain. The catalytic triad represented by red coloured circles and is located at His⁶⁰³, Asp⁶⁴⁶ and Ser⁷⁴¹. Lys⁷⁷-Lys⁷⁸ peptide bond is cleaved by plasmin in the conversion of Glu-plasminogen to Lys-plasminogen. Activation of plasminogen to plasmin occurs proteolytic cleavage of Arg⁵⁶¹-Val⁵⁶² bond indicated by the orange arrow (adapted from Schaller and Gerber, 2011).

Figure 1.4.
Schematic of plasminogen

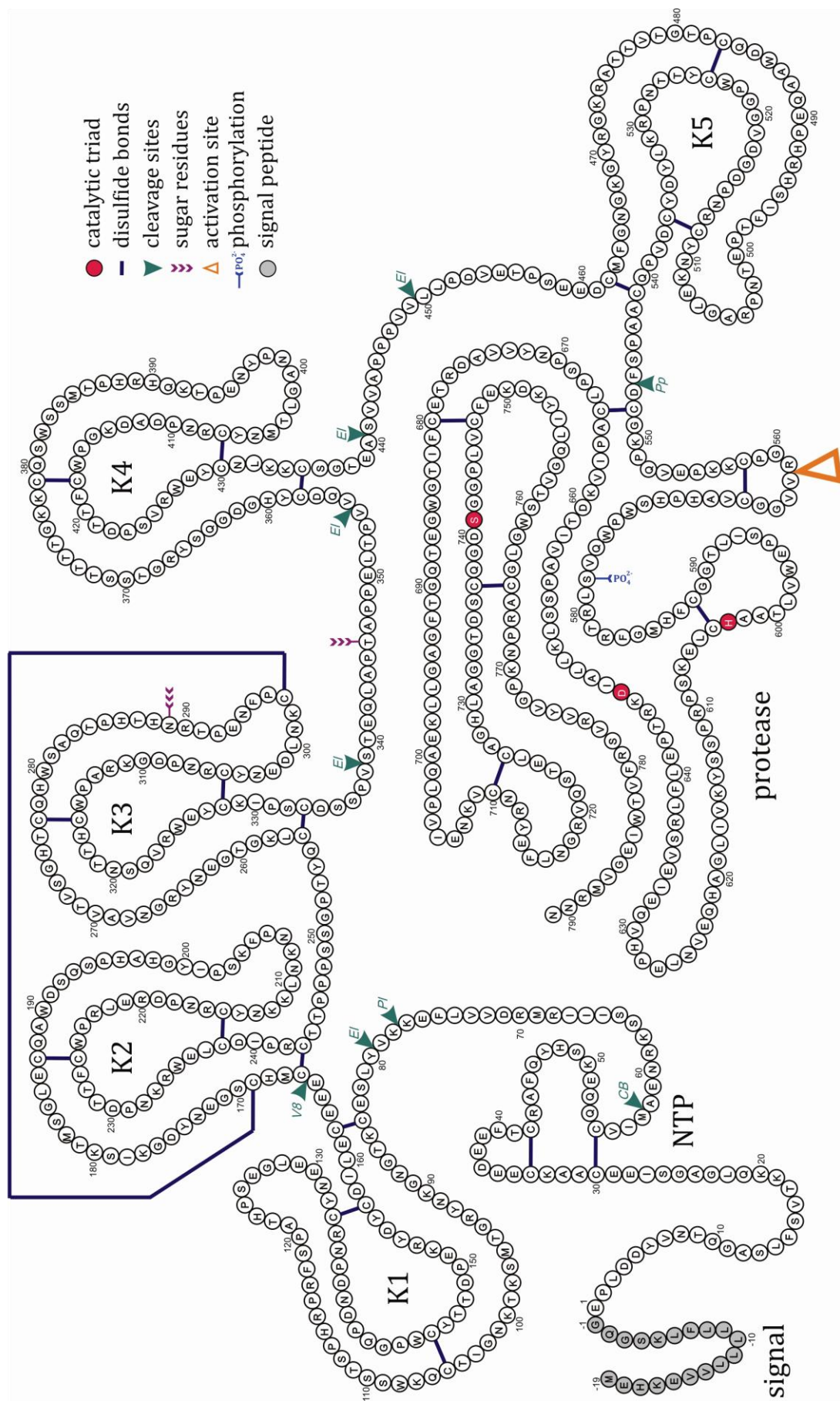


Figure 1.5. X-ray crystal structure of human plasminogen. The Pan-apple domain (PAp) is labelled in blue. The five kringle domains are coloured as follows: K1, pink; K2, yellow; K3, orange; K4, green; K5, purple. The protease domain is cyan. The lysine binding site (LBS) on K1 is indicated by the asterisk (*). (Adapted from Law et al., 2012)

Figure 1.5.
X-ray crystal structure of human plasminogen

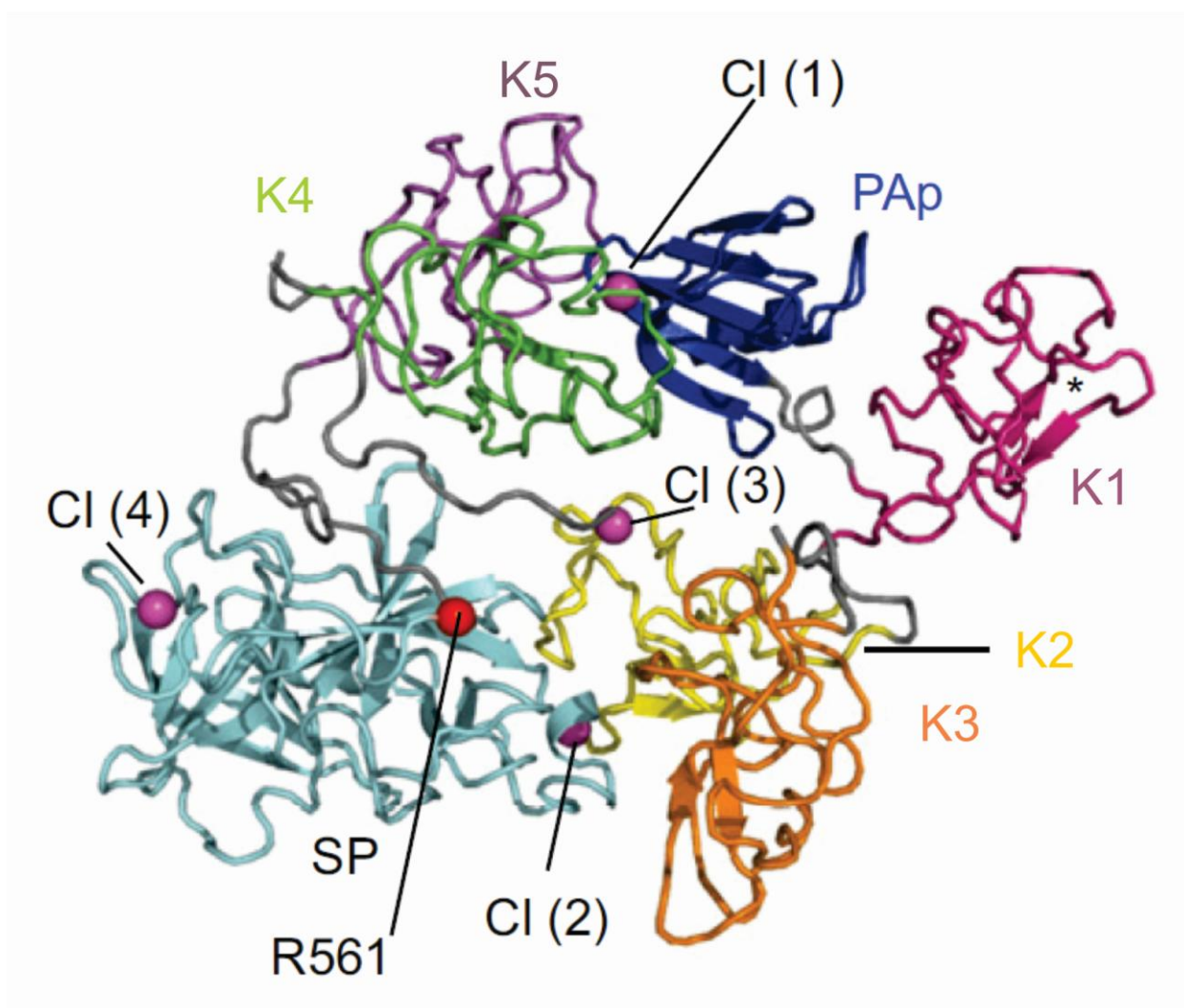
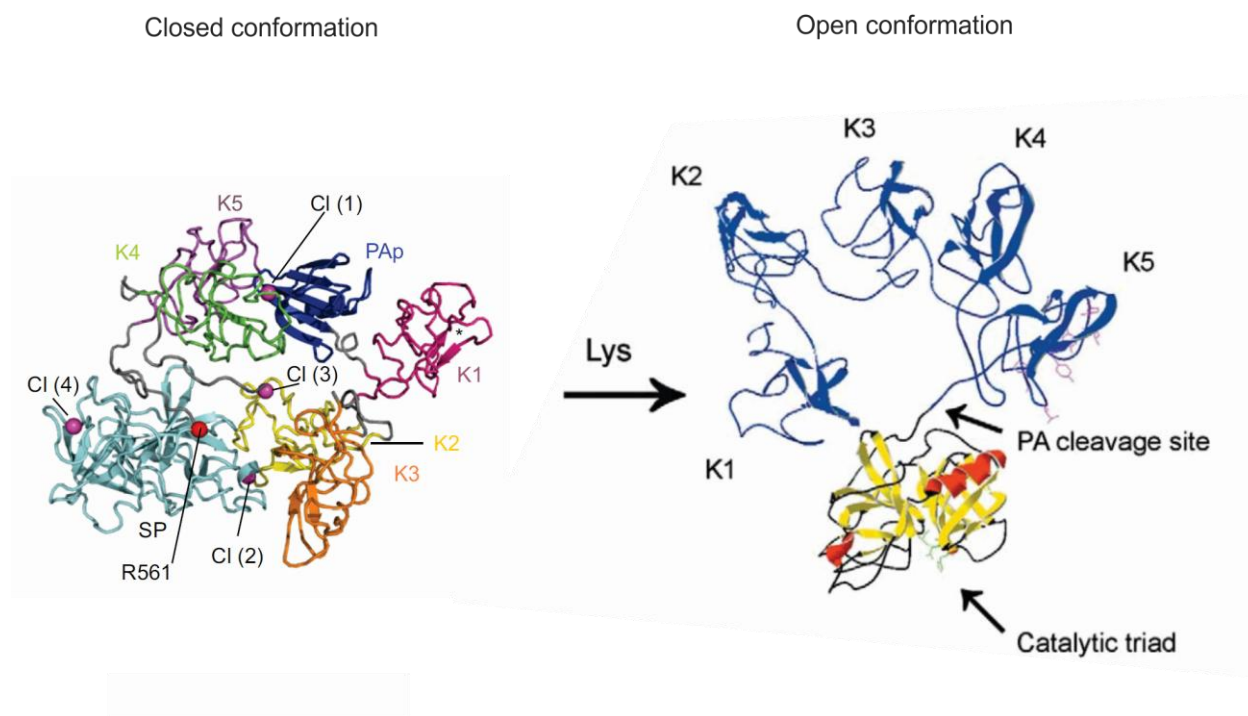


Figure 1.6. Schematic representation of the conformational change that occurs from Glu-plasminogen (closed) to Lys-plasminogen (open). Removal of the PAp induces conformational change from closed to open in plasminogen. This exposes plasminogen activation site and the catalytic domain in the serine protease domain and the lysine binding sites in the kringles (Adapted from Law et al., 2012 and Lähteenmäki et al., 2005)

Figure 1.6.
Schematic representation of the conformational change that occurs from Glu-plasminogen (closed) to Lys-plasminogen (open)



1.5 Plasminogen Activators

In circulation, plasminogen can be activated by two proteases, tPA and uPA. Both tPA and uPA catalyse the same Arg⁵⁶¹-Val⁵⁶² bond in plasminogen during the conversion to plasmin however they have different biological function. tPA is targeted to activate plasminogen on a fibrin clot, whereas uPA is mainly involved in conversion of plasminogen involved in extracellular matrix remodelling and regulating cell migration. Similar to plasmin, tPA and uPA are serine proteases and the principal inhibitors are PAI-I and PAI-II (these inhibitors will be further reviewed in Section 1.8).

1.5.1 Tissue-type Plasminogen Activator

Tissue-type plasminogen activator (tPA), the main activator of plasminogen, is synthesised as a 70 kDa (527 residues) single chain polypeptide by various cell types (endothelial cells and keratinocytes) (Rijken et al., 1981). The tPA gene is located on chromosome 8p12 spanning 32.4 kb and 14 exons (Ny et al., 1984). The tPA molecule is composed of five structural domains which are a finger-like domain (FN, residues 4-50), an epidermal growth factor-like region (EGF, residues 51-87), two kringle domains (K1, residues 87-175; K2, residues 176-262) which are homologous to those in plasminogen and the serine protease domain (SP, residues 276-527) (Pennica et al., 1983; Rijken and Lijnen, 2009). The catalytic triad is located at His³²², Asp³⁷¹ and Ser⁴⁷⁸ (Pennica et al., 1983). Experimental studies of the two kringle domains have revealed that only K2 contains an active LBS. Binding of plasminogen to tPA are mediated by K2 and FN domain (Ichinose et al., 1986; van Zonneveld et al., 1986). As described in Section 1.2, tPA binding sites on fibrin(ogen) has been localised to D region and α C domains (Medved and Nieuwenhuizen, 2003). The crystal structure of full-length tPA has yet to be determined, however X-ray crystal structure of individual domains (with the exception of K1) are available. Recently, a group has published a three dimensional structure of tPA as measured by small-angle X-ray scattering (SAXS) method and modelling known domains to available structures (Rathore et al., 2012).

Unlike other single chain serine proteases, the proenzyme form of tPA is active. His³²² and Ser⁴⁷⁸ of the catalytic domain are covalently bound. In the single chain form, Lys⁴²⁹ forms a salt bridge with Asp⁴⁷⁷ contributing to the additional active conformation (Renatus et al., 1997). The double chain form is produced by cleavage of the Arg²⁷⁵-Ile²⁷⁶ peptide bond by plasmin. Kallikrein or Factor Xa has also been reported to convert tPA to the two chain form. The two chain form is held together by a single disulfide bond at Cys²⁶³-Cys³⁹⁵ (Loscalzo, 1988). The single chain tPA is only 5-10-fold less active than the double chain tPA. Nevertheless, activity of

both single and double chain tPA when bound to fibrin appears to be comparable (Loscalzo, 1988; Tate et al., 1987). Plasminogen activation is increased by ~60-fold, from $0.01\mu\text{M}^{-1}\text{s}^{-1}$ to $0.63\mu\text{M}^{-1}\text{s}^{-1}$, in the presence of fibrin indicating that efficient activation of plasminogen by tPA requires fibrin (Hoylaerts et al., 1982). The mechanism by which plasminogen conversion by tPA is accelerated in the presence of fibrin remains unknown. It has been proposed that binding to fibrin induces conformational change in tPA which increases localisation of plasminogen on the tPA/fibrin surface, thus improving plasminogen activation (Longstaff et al., 2011).

In addition to its role in fibrinolysis, tPA is highly expressed in the central nervous system (CNS) specifically in the hippocampus, amygdala, cerebellum and hypothalamus. tPA has been implicated in many important roles such as memory, learning and endocrine functions. Plasminogen and PAI-I are also expressed in the CNS which indicates that plasminogen conversion can occur in the neuronal environment (Melchor and Strickland, 2005). Recent evidence have shown that tPA mediated plasmin generation is recruited to the site of neuronal injury as a clearance mechanism (Samson et al., 2009; Samson et al., 2012). Decreased levels of tPA/plasmin generation in the brain have been shown to contribute to accumulation of β -amyloid deposition in Alzheimer's disease (Melchor et al., 2003). Therefore tPA and plasmin have a significant role in maintaining homeostasis of the CNS. In contrast, it has been shown that excessive tPA present during pathological processes such as chronic brain injury leads to excitotoxicity (Hazell, 2007).

tPA deficiency in humans has not been reported (Brandt, 2002). Knockout mice (tPA^{-/-}) have been described to have normal thrombolytic capacity. However, they have an increased risk of developing thrombosis upon endotoxin induction (Carmeliet et al., 1994; de Giorgio-Miller et al., 2005).

1.5.2 Urokinase-type Plasminogen Activator

Urokinase-type plasminogen activator (uPA), is the other major endogenous activator of plasminogen. It is secreted in the lung, kidney and endothelial cell as a single chain polypeptide of 55 kDa (411 amino acids) (Bernik and Kwaan, 1969; Wun et al., 1982). The uPA gene is located on chromosome 10q24 spanning 6.4kb and 11 exons (Ricchio et al., 1985). Similar to tPA, uPA is a multidomain serine protease with three structural domains which are the epidermal growth factor-like region (EGF, residues 5-49), one kringle domain (K1, residues 50-131) and the serine protease domain containing the catalytic triad at His²⁰⁴, Asp²⁵⁵ and Ser³⁵⁶ (Kasai et al., 1985). The kringle domain of uPA does not contain a LBS and therefore the activity of uPA is not fibrin dependent. Recently, the crystal structure of uPA complexed with its inhibitor, PAI-I have been determined (Lin et al., 2011). Prior to this work, only individual crystal

structures of each uPA domain were available (Hansen et al., 1994; Li et al., 1994; Spraggon et al., 1997).

The proenzyme uPA is converted to its active two chain form by plasmin, kallikrein and Factor XIIa which results in a cleavage of Lys¹⁵⁸-Ile¹⁵⁹ and the formation of a single disulfide bond at Cys¹⁴⁸-Cys²⁷⁹ (Rijken and Lijnen, 2009; Schaller and Gerber, 2011). Furthermore an additional low molecular weight form (33 kDa) of two chain uPA has been described. This form is generated by plasmin or uPA cleaving itself at the peptide bond between Lys¹³⁵-Lys¹³⁶ and the molecule only contains the SP domain and lacks EGF and K1 (Gunzler et al., 1982; Steffens et al., 1982). Both forms are able to bind to plasminogen, however only the high molecular weight form can interact with the uPA receptor (uPAR) (Cesarman-Maus and Hajjar, 2005). uPAR is a cellular receptor which is proposed to bind uPA via the EGF domain (Appella et al., 1987). Binding of uPA/uPAR localises plasminogen activation on cell surfaces which have been shown to play an important physiological role in the clearance of fibrin induced inflammation (Connolly et al., 2010). uPA not only acts as a proteolytic enzyme in the fibrinolytic system, but is also involved in cell migration and adhesion, tissue remodelling and immune response (Lin et al., 2011).

Similar to tPA, uPA deficiency has not been described in humans. Mice with uPA deficiency have been reported to have normal thrombolytic capacity, however were shown to have increased fibrin deposits around organs (de Giorgio-Miller et al., 2005). Mice deficient with both tPA and uPA have a more severe phenotype with extensive fibrin deposition and delayed wound healing (Carmeliet et al., 1994).

1.6 Inhibitors of the Fibrinolytic System

Fibrinolysis can be inhibited at two levels. Firstly, by inhibition of plasminogen activation through the action of plasminogen activator inhibitors (PAIs) and secondly, direct plasmin inhibition by α_2 -antiplasmin. Both PAIs and α_2 -antiplasmin are serpins which act by forming an irreversible complex at the active site of the protease with the consequent proteolytic cleavage of the target molecule. Once this occurs, both protease and serpin lose their functionality. The following section explains the structure and mechanism of action of member of the serine protease inhibitor (serpin) family (Section 1.7). A brief review of PAIs (Section 1.8) and α_2 -antiplasmin (Section 1.9) will follow on.

1.7 Serine Protease Inhibitors (Serpins)

The term serpin is an acronym for **Serine Protease Inhibitor**. The initial identification of this superfamily was based on the observed similarity between the primary structure of three proteins, human antithrombin, human α_1 -proteinase inhibitor and egg white ovalbumin (Hunt and Dayhoff, 1980). Serpins constitutes the largest class of serine/cysteine peptidase inhibitors with over 3000 members identified across different species (mammals, plants, viruses etc.). 36 human serpins have been identified of which 9 are involved in processes regulating blood circulation (Law et al., 2006; Silverman et al., 2001; Silverman et al., 2010).

Initially serpins were named based on their ability to inhibit serine proteases. However as more members were identified, some lacked inhibitory properties (angiotensinogen and ovalbumin). The serpin superfamily was then divided into clades based on their phylogenic relationship. There are 16 clades (A to P) with 3-77 members in each clade (Irving et al., 2000). Each serpin is named according to clade group (X) and the number within the clade (y) (SERPINXy) (Irving et al., 2000; Law et al., 2006). Human serpins are members of the first nine clades (A-I), animal serpins occupy three clades, viral serpins in two and the remaining two clades are specifically taken up by plant and insect serpins (Gettins, 2002; Irving et al., 2000).

1.7.1 Biological Roles of Human Serpins

Of the 36 human serpins identified, 27 are inhibitory while the remaining 9 are non-inhibitory serpins. They are involved in a range of physiological processes such as fibrinolysis, blood coagulation and inflammation (Rau et al., 2007; Silverman et al., 2001). Figure 1.7 illustrates the diverse role that serpins play in the human system. Dysfunction of these serpins has been reported to be present in pathologies (Kaiserman et al., 2006). For example, angiotensinogen, a non-inhibitory serpin, is the precursor molecule of the blood pressure regulator angiotensin I and reduced production of this serpin is reported to cause hypertension (Jeunemaitre et al., 1999). Antichymotrypsin is responsible for inhibiting cathepsin G and its deficiency results in emphysema (Gooptu et al., 2000). Centerin is expressed in normal and malignant germinal centre of B cells and has been linked as a marker in B cell lymphomas (Paterson et al., 2008). Deficiency in α_2 -antiplasmin, the main inhibitor of plasmin has been reported to result in abnormal bleeding (Miles et al., 1982). An extensive list of all known human serpins with its function and dysfunction are shown on Table 1.1.

Figure 1.7. Biological functions of serpins. Human serpins are involved in a variety of physiological processes. Serpins in red have been implicated in protease inhibition whereas others appear to have non-inhibitory roles (green) (adapted from Silverman et al., 2001).

Figure 1.7.
Biological functions of serpins

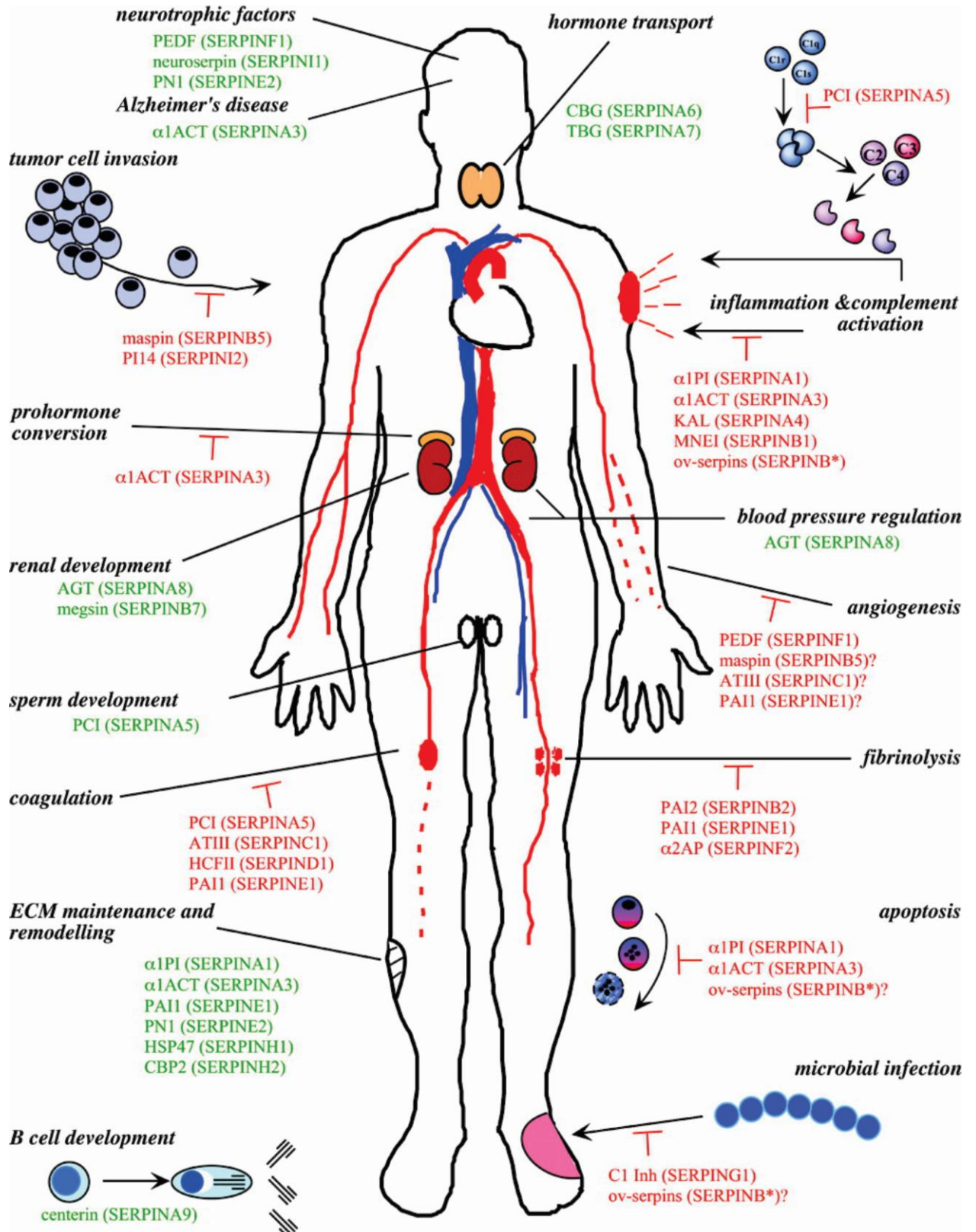


Table 1.1. Clade classification, known function and dysfunction (high or low levels) of human serpins (Adapted and expanded from Gettins, 2002)

Serpin name	Alternative name	Function	Dysfunction	References
Serpin A1	Antitrypsin	Inhibits human neutrophil elastase	Emphysema, cirrhosis	(Lomas et al., 1992; Lomas et al., 1993)
Serpin A2	Antitrypsin-related protein	Pseudogene, uncharacterised	-	(Seixas et al., 2007)
Serpin A3	Antichymotrypsin	Inhibition of Cathepsin G	Emphysema	(Gooptu et al., 2000)
Serpin A4	Kallistatin	Inhibition of kallikrein, regulation of vascular function	Renal and cardiovascular	(Chao et al., 1996; Liu et al., 2012)
Serpin A5	Protein C inhibitor	Inhibition of active protein C	Angioedema, chronic active plaques in multiple sclerosis	(Geiger, 2007; Han et al., 2008)
Serpin A6	Corticosteroid-binding globulin	Cortisol binding	Chronic fatigue	(Klieber et al., 2007; Torpy et al., 2004)
Serpin A7	Thyroxine-binding globulin	Thyroxine binding	Hypothyroidism	(Bartalena et al., 1992; Zhou et al., 2006)
Serpin A8	Angiotensinogen	Release of angiotensin I by rennin cleavage	Hypertension	(Jeunemaitre et al., 1999)
Serpin A9	Centerin	Inhibition of trypsin and trypsin-like proteases	Highly expressed in B cell lymphomas	(Paterson et al., 2008)
Serpin A10	Protein Z-dependent proteinase inhibitor	Binds to protein Z and inhibits Factor Xia	Venous thromboembolic disease	(Corral et al., 2006; Han et al., 2000)
Serpin A11	-	Not characterised	-	-
Serpin A12	Vaspin	Insulin-sensitising adipocytokine	Increased vaspin correlates with insulin resistance in Type II diabetes	(Hida et al., 2005; Teshigawara et al., 2012)
Serpin B1	Monocyte neutrophil I elastase inhibitor	Inhibition of neutrophil elastase	Mouse knockouts are presented with neutrophil survival defects and immune deficiency	(Benarafa et al., 2007; Remold-O'Donnell et al., 1992)
Serpin B2	Plasminogen activator inhibitor (PAI-II)	Inhibition of uPA	Mouse knockouts are presented with no obvious change in phenotype	(Dougherty et al., 1999)
Serpin B3	Squamous cell carcinoma antigen-I	Inhibitor of papain-like cysteine proteases	Mouse knockouts are presented with increased production of mucus in asthma	(Schick et al., 1998; Sivaprasad et al., 2011)
Serpin B4	Squamous cell carcinoma antigen-II	Inhibitor of cathepsin G and chymase	Same as Serpin B3	(Schick et al., 1997)

Serpin B5	Maspin	Tumour suppressor	Increased maspin correlates with improved prognosis in tumour growth	(Goulet et al., 2012; Goulet et al., 2011)
Serpin B6	Proteinase inhibitor-6	Inhibitor of cathepsin G	Moderate to severe hearing loss	(Sirmaci et al., 2010)
Serpin B7	Megsin	Megakaryocyte maturation	Overexpression correlates with kidney disease	(Miyata et al., 2002; Miyata et al., 2007)
Serpin B8	Cytoplasmic antiproteinase 8	Inhibitor of furin	Linked with development of psoriasis	(Dahlen et al., 1998; Sun et al., 2010)
Serpin B9	Cytoplasmic antiproteinase 9	Inhibitor of granzyme B	Mouse knockout presents with immune dysfunction	(Rizzitelli et al., 2012)
Serpin B10	Bomapin	Thrombin and trypsin inhibitor	-	(Riewald et al., 1998)
Serpin B11	Epipin	Non-inhibitory	-	(Askew et al., 2007)
Serpin B12	Yukopin	Inhibits trypsin-like proteases	-	(Askew et al., 2001)
Serpin B13	Headpin	Inhibition of cathepsin K and L	Decreased headpin correlates with poor clinical outcome in squamous cell carcinomas	(de Koning et al., 2009; Jayakumar et al., 2003)
Serpin C1	Antithrombin	Inhibitor of thrombin and Factor Xa	Thrombosis and clotting disorder	(Perry and Carrell, 1996)
Serpin D1	Heparin cofactor II	Inhibitor of thrombin	Mouse knockouts are lethal	(Aihara et al., 2007)
Serpin E1	Plasminogen activator inhibitor I (PAI-I)	Inhibitor of thrombin, uPA and tPA	Cardiovascular disease	(Gils and Declerck, 2004)
Serpin E2	Protease nexin I	Inhibitor of uPA and rPA	Male infertility	(Murer et al., 2001)
Serpin E3	Nexin-related serine protease inhibitor	Not characterised	-	-
Serpin F1	Pigment epithelium derived factor	Non-inhibitory, potent anti-angiogenic molecule	Osteogenesis imperfect type VI	(Doll et al., 2003; Homan et al., 2011)
Serpin F2	α_2 -antiplasmin	Inhibitor of plasmin	Abnormal bleeding	(Miles et al., 1982; Moroi and Aoki, 1976)
Serpin G1	C1 inhibitor	Inhibitor of C1 esterase	Angioedema, age-related macular degeneration	(Aulak et al., 1993; Ennis et al., 2008)
Serpin H1	47 kDa heat shock protein	Non-inhibitory, molecular chaperone for collagens	Osteogenesis imperfect	(Christiansen et al., 2010; Hirayoshi et al., 1991)
Serpin I1	Neuroserpin	Inhibitor of uPA, tPA and plasmin	Dementia	(Davis et al., 2002; Osterwalder et al., 1998)
Serpin I2	Pancpin	Inhibitor of cancer metastasis	Downregulated in pancreatic cancer cells, myopia	(Hysi et al., 2012; Ozaki et al., 1998)

This page has been intentionally left blank.

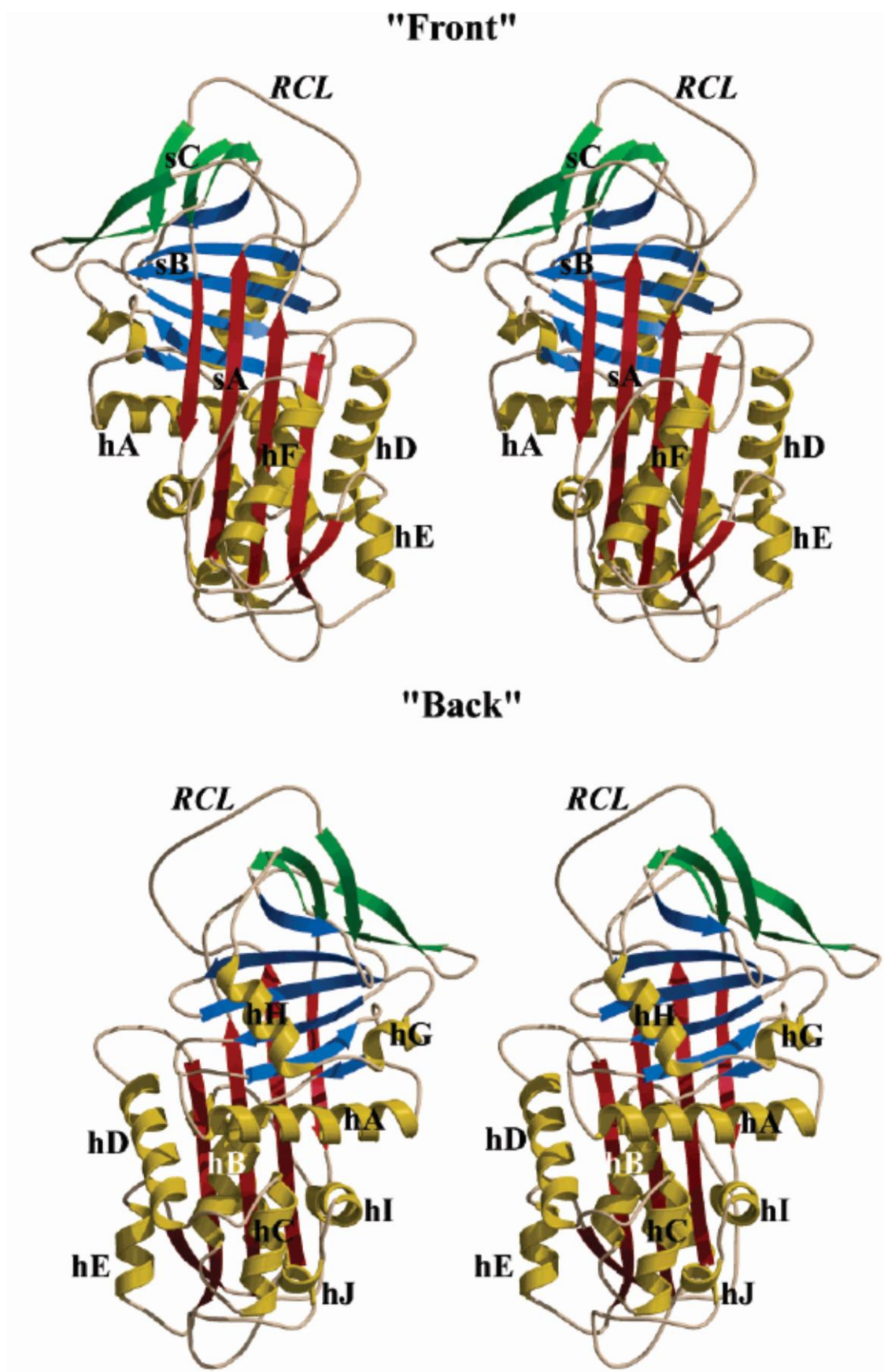
1.7.2 Structure of Serpins

Both inhibitory and non-inhibitory serpins contain the same general structure of three β -sheets (sA-sC) and 8-9 α -helices (hA-hI) (Figure 1.8). Near the COOH-region, an exposed loop exists between the β -sheet A and C (sA and sC) which is the reactive centre loop (RCL) (Irving et al., 2000). It is linked to strand 1 of β -sheet C (s1C) and strand 5 of β -sheet A (s5A) (Elliott et al., 1996). β -sheet A (sA) is the largest and contains five strands in which the first strand is only 5-6 residues and the rest are 12-15 residues. The breach and shutter regions are located at the top and bottom of sA respectively. All α -helices are located on the back of the molecule except for α -helix F (hF) which is found on the front of sA (Gettins, 2002).

The reactive centre loop (RCL), typically 20 amino acids in length, is the most variable region between serpins which determines the inhibitory and biological function of the molecule (Rau et al., 2007). α_1 -antitrypsin was the first serpin crystallised and showed the cleaved RCL inserted between the strands of β -sheet A (sA) (Baumann et al., 1991). Together with the uncleaved structure, the structural rearrangement experienced by a serpin molecule during inhibition was demonstrated. This indicates that the RCL is a flexible region and its function is mediated by highly conserved motifs in proximal and distal portion. Insertion of the RCL into β -sheet A (sA) involves opening of the breach and shutter region together with the movement of α -helix F (hF) (Baumann et al., 1991; Wei et al., 1994). Residues proximal (NH_2 -region) to the RCL are termed P residues (i.e. P4, P3, P2 etc.) and residues distal (COOH-region) to the RCL are P' residues (i.e. P2', P3', P4' etc.). Proteolytic cleavage of the RCL occurs at the P1-P1' peptide bond. The P1 residue is the major determinant of serpin specificity. Some serpins utilise an alternative residue within the RCL as P1 which enables it to inhibit multiple proteases (Schechter and Berger, 1967; Schechter and Berger 1968).

Figure 1.8. General structure of serpins. The structure of a typical serpin containing the reactive centre loop, three β -sheets (sA-sC) and nine α -helices (hA-hI) (adapted from Gettins, 2002).

Figure 1.8.
General structure of serpins



This page has been intentionally left blank.

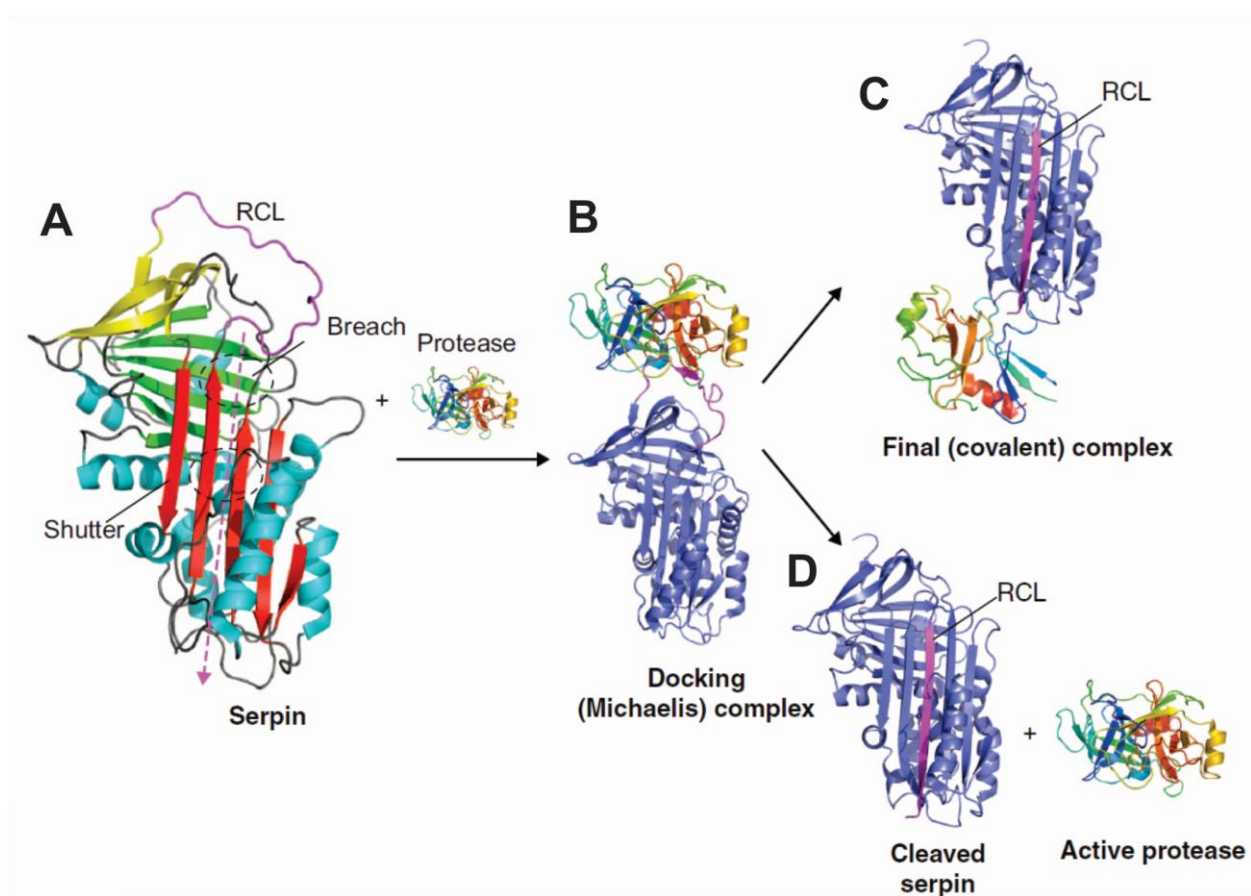
1.7.3 Serpin Inhibitory Mechanism

Unlike the Kunitz-Kazal type protease inhibitors that exhibit the 'lock and key' mechanism, serpins have a unique inhibition mechanism which involves the conformational change of the serpin molecule termed the 'stressed to relaxed' (S→R) transition (Law et al., 2006). The serpin molecule is in a metastable native conformation. Once the RCL is incorporated into β -sheet A, its stability is significantly increased (Rau et al., 2007). The metastability of serpins is important for its function as a protease inhibitor (Gettins, 2002). In this state, the serpin is placed under strain, however this is necessary for RCL translocation and deformation of the active site of proteinase in the inhibitory complex (Kaiserman et al., 2006).

Serpins inhibit serine proteases by forming an irreversible covalent complex, which results in the loss of both serpin and protease activity once the inhibitory complex is formed (Silverman et al., 2001). The initial step is the formation of a non-covalent Michaelis-Menton complex. This occurs when the exposed RCL of the serpin interacts with the protease. At this point, the complex is still reversible and therefore the fully functional protease may be released back into circulation or peptide bond cleavage may occur (Gettins, 2002). As the target enzyme recognition of serpin RCL, there is rapid conversion to an irreversible serpin-protease complex. Formation of this complex results in the cleavage of the P1 serpin bond at the RCL, releasing the P1' residues and moving the RCL 70Å across the molecule (Huntington et al., 2000). Serpins are called irreversible suicide inhibitors because once the RCL is cleaved it is no longer active. An ester bond is formed between the protease active site and the serpin P1 residues resulting in the insertion of the RCL into β -sheet A and forming an additional strand in β -sheet A. Once this occurs, the protease is dragged to the opposite pole of the serpin body, trapping the serpin-protease complex as an acyl-enzyme intermediate (Law et al., 2006). This process is termed acyl trapping. As the protease is dragged over the body of the serpin, it undergoes a loss of secondary structure and rearrangement of its active site. The catalytic serine residue moves 6Å away from the histidine residue rendering the protease inactive. Interaction of serpins with a non-target enzyme will result in the formation of RCL cleaved serpin and the release of the active protease, this reaction is known as substrate reaction (Huntington et al., 2000; Law et al., 2006). Figure 1.9 shows the serpin inhibitory mechanism.

Figure 1.9. Serpin inhibitory mechanism. **A)** Structure of native serpin with the RCL exposed at the top of the molecule. **B)** Michaelis or encounter complex formed when the protease is docked on the RCL of the serpin. Complex can either proceed down the inhibitory or substrate pathway. **C)** Inhibition pathway occurs when both serpin and protease are rendered inactive. The RCL is inserted into β -sheet A which drags the protease across the serpin molecule distorting the active site of the protease. **D)** Substrate pathway: Serpin undergoes substrate-like behaviour which results in an inactive serpin molecule and the release of active protease (adapted from Law et al., 2006).

Figure 1.9.
Serpin inhibitory mechanism



1.7.4 Conformational States of Serpins

Serpins exist in five conformational states which are the native, RCL cleaved, latent, delta (δ) and polymeric. The native (Figure 1.10A) and cleaved (Figure 1.10B) forms were previously described. Briefly, the native state is the active form where the RCL is exposed and able to interact with its target protease (Whisstock et al., 1998). It is also known as the metastable conformation due to the strain present within the molecule. Based on the α_1 -antitrypsin structure, the strain throughout the serpin molecule is due to the presence of hydrophobic pockets, overpacking of side chains and burial of polar groups in the hydrophobic core (Im et al., 1999; Lee et al., 1996; Ryu et al., 1996). The structure of ovalbumin was the first serpin solved in its native form (Stein et al., 1990). The secondary and tertiary structures within the core domain of serpins are similar with the exception of antithrombin and heparin cofactor II which will be further explained in Section 1.7.5. The RCL is the only region that is variable in each serpin (Gettins, 2002).

The RCL cleaved form (Figure 1.10B) is the final and most stable serpin form. The first published X-ray crystal structure was the RCL cleaved form α_1 -antitrypsin (Baumann et al., 1991). The RCL is cleaved at the P1-P1' peptide bond and separated by insertion of the RCL into the shutter and breach regions between the β -sheet A. The end product of this form is an inactive serpin.

The metastable state renders serpins to be more susceptible to spontaneous conformational rearrangement therefore serpin molecules can adopt structures which are more energetically stable but can result in a loss of inhibitory function. The latent form occurs when the uncleaved RCL inserts itself into the β -sheet A increasing its thermal stability of the serpin molecule (Figure 1.10C). The RCL is still intact and tethered on β -sheet C. However, the RCL becomes inaccessible to the protease resulting in an inactive form of serpin (Whisstock and Bottomley, 2006). This phenomena was first seen in the crystal structure of PAI-I (Mottonen et al., 1992). However, in the case of PAI-I, this is more likely a regulatory mechanism. PAI-I spontaneously converts to the latent form which allows circulation of the serpin in an inactive form and its activity is recovered through the interaction with tissue glycoprotein vitronectin (Lawrence et al., 1994; Lawrence et al., 1997). It has been reported that binding of PAI-I to vitronectin increases the half-life of active PAI-I from 1-2 hour to 4-6 hour (Lindahl et al., 1989). Active PAI-I has a 200-fold increased affinity for its target protease in comparison to latent PAI-I (Lawrence et al., 1997). Other latent serpins have been described in disease states. Some examples include; 1) latent α_1 -antichymotrypsin, which is one of the causes of chronic obstructive pulmonary disease, 2) latent neuroserpin causes accumulation of inclusion bodies in the brain of patients with dementia and 3) latent antithrombin increases the onset of thrombosis (Chang and Lomas, 1998; Onda et al., 2005; Zhou et al., 1999).

The δ form (Figure 1.10D) has a similar conformation to the latent form however the RCL is partially inserted into β -sheet A together with another sequence to mimic full insertion (Whisstock and Bottomley, 2006). This form is observed in a naturally occurring variant of α_1 -antichymotrypsin (Leu55Pro). The crystal structure revealed that the additional sequence which is inserted in β -sheet A is filled by an unfolded loop of helix F. δ form has high structural and thermal stability. In addition to that, δ form has an increased tendency to form polymers (Gooptu et al., 2000).

Serpins have an increased propensity to polymerise to achieve a more stable conformation. The existence of naturally occurring mutation increases the tendency of polymer formation resulting in pathologic diseases termed 'serpinopathies' (Whisstock and Bottomley, 2006). The most common and best characterised mechanism of polymer formation is where the RCL of one molecule interacts with β -sheet A of a second serpin molecule generating a continuous chain of inactivated serpin (Chang et al., 1997). The dysfunction has been associated with s4A (β -sheet A strand 4) linkage (Gooptu and Lomas, 2009). Polymer formation seen in Z α_1 -antitrypsin (Glu342Lys) is the best defined pathology seen as accumulation of polymeric α_1 -antitrypsin in hepatocytes which is implicated in cirrhosis and hepatocellular carcinoma (Lomas et al., 1992). Accumulation of protein in the liver results in lack of circulating α_1 -antitrypsin hence there is lack of clearance of neutrophil elastase in the lungs which may predispose to early onset panlobular emphysema (Eriksson et al., 1986; Sveger, 1976). S (Glu264Val) and I (Arg39Cys) α_1 -antitrypsin causes milder forms of disease because there is less disruption to β -sheet A, thus slower rates of polymer formation (Dafforn et al., 1999).

Familial encephalopathy with neuroserpin inclusion bodies (FENIB) is another well characterised serpinopathy. This is an autosomal dominant disease characterised with the formation of neuroserpin polymers within the deeper layers of the cerebral cortex and substantia nigra. Multiple mutations in the gene have been reported which are Ser49Pro, Ser52Arg, His338Arg, Gly392AGly and Gly392Arg (arranged from mild to severe symptoms) (Belorgey et al., 2002; Belorgey et al., 2004; Coutelier et al., 2008; Davis et al., 2002). The more severe forms have mutations within the shutter region which suggest that the incorporation of the RCL into β -sheet A is unstable and increases its tendency to polymerise. Neuroserpin polymers are inactive, however the accumulation of the aggregated protein itself is sufficient to cause the clinical phenotype seen in FENIB (Davis et al., 2002). A more detailed description of neuroserpin is reviewed in Section 1.10.3.

Other forms of polymerisation outside of s4A linkage have been characterised. The β -sheet C strand 1 (sC1) linkage forming a C-sheet dimer has been observed in crystallography studies of antithrombin and tengpin (Carrell et al., 1994; Zhang et al., 2008). The mechanism for sC1 linkage has been suggested to be mediated by β -sheet C displacement when the RCL

inserts into β -sheet A (Gooptu and Lomas, 2009). Another polymerisation identified is called s7A seen in the crystal structure of PAI-I. The structure revealed that the RCL of one molecule anneals as strand 7A of β -sheet A (Sharp et al., 1999).

1.7.5 Regulation of Serpin Activity

As previously described, PAI-I spontaneously converts to the latent form and is reactivated in the presence of vitronectin. This is one example of serpin regulation. This section will describe the regulation by glycosaminoglycan (GAG) through the binding mechanism or allosteric mechanism (Gettins, 2002). To explain the two regulation mechanisms of GAG's, the serpins antithrombin and heparin cofactor II will be used as examples.

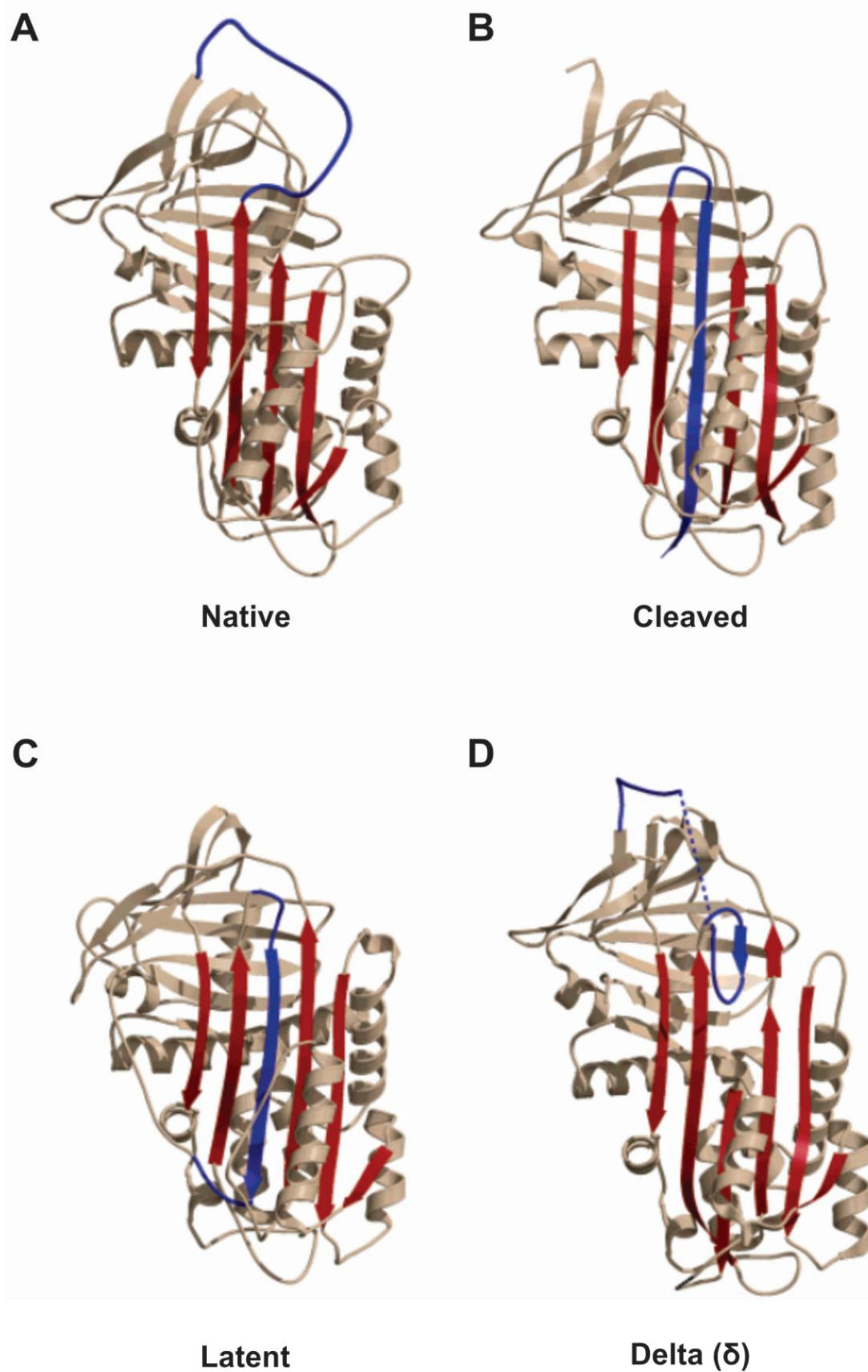
The protease targets for antithrombin are Factor Xa and thrombin with an inhibition rate of 2000 and 7000 $M^{-1}s^{-1}$ respectively (Bjork and Olson, 1997; Izaguirre et al., 2003). The binding of heparin to antithrombin accelerated thrombin inhibition by ~ 10000 -fold (Rezaie and Olson, 2000; Turk et al., 1997). In the absence of heparin, the RCL of antithrombin is partially inserted rendering it inaccessible to the proteinase. Binding of heparin induces expulsion of the RCL and reorientation of the P1 residue to a more accessible position. It has been reported that heparin binding mediates a conformational change in helix D, triggering repositioning of the RCL (Belzar et al., 2002; Meagher et al., 2000). Binding of heparin to antithrombin has been identified to a five-saccharide region known as pentasaccharide (Casu et al., 1981; Lindahl et al., 1981). Studies using this pentasaccharide sequence of heparin have revealed that antithrombin possesses two separate mechanism of action for Factor Xa and thrombin. The pentasaccharide accelerates Factor Xa inhibition by ~ 300 -fold whereas only a slight (~ 2 -fold) increase in inhibition was seen for thrombin. Therefore, it was suggested that Factor Xa inhibition is based on a conformational change or allosteric mechanism. Longer heparin chains were required for the acceleration of thrombin inhibition through a bridging mechanism where GAG binding sites were required on both serpin and protease. The bridging mechanism involves a ternary structure of serpin (antithrombin), protease (thrombin) and GAG (heparin) (Olson et al., 1992). Further experiments have revealed that Factor Xa inhibition is accelerated in the presence of long chain heparin which demonstrates that regulation of Factor Xa is mediated by both bridging and allosteric mechanism (Rezaie, 1998).

Heparin cofactor II is an inhibitor of thrombin however it is not a substitute for antithrombin in deficiency (Griffith et al., 1983). Alone, heparin cofactor II is a more potent inhibitor of chymotrypsin and cathepsin G (Griffith et al., 1985). It has been proposed that the binding of heparin cofactor II to GAG (dermatan sulphate or heparin) induces expulsion of the RCL and displacement of the highly acidic 80-residue N-terminal extension. The N-terminal

extension then binds to thrombin exosite I which in turn orientates the protease catalytic site to the RCL of the serpin (Van Deerlin and Tollefsen, 1991). Once this occurs, thrombin inhibition is increased by 10,000-fold. The bridging mechanism observed in heparin cofactor II/thrombin/GAG is analogous to antithrombin/thrombin/GAG (Tollefsen et al., 1983).

Figure 1.10. Different conformational states of serpin. **A)** In its native state, the RCL (blue) is exposed and able to interact with its target protease. **B)** Cleaved serpin is the final and most stable form which results in the inactivation of the serpin molecule. **C)** Latent form occurs when the uncleaved RCL inserts into β -sheet A rendering the molecule inactive. **D)** Delta (δ) form have a partially inserted RCL in β -sheet A together with an additional sequence which mimics full insertion (adapted from Gettins, 2002).

Figure 1.10.
Different conformational states of serpins



1.8 Inhibition of the Fibrinolytic System at the Level of Plasminogen Activators: PAI-I and PAI-II

The previous section describes serpin function and regulation in general. As mentioned in the introduction, a number of molecules within the fibrinolytic system, in particular PAI-I, PAI-II and α_2 -antiplasmin, are serpins and they are all important in regulating and maintaining a haemostatic environment in the human circulation. The start of this literature review looked at the activation of the fibrinolytic system and its role in fibrin clot degradation. This leads us to the following section which is how fibrinolysis is regulated. Referring to Figure 1.1, fibrinolysis can firstly be inhibited at the level of plasminogen activators, PAI-I and PAI-II.

1.8.1 Plasminogen Activator Inhibitor I (PAI-I)

The main physiological inhibitor of tPA, PAI-I, is a single chain glycoprotein with a molecular weight of 50 kDa and is composed of 379 amino acids (Pannekoek et al., 1986). It is secreted by a range of cells types including endothelial cells and hepatocytes. The PAI-I gene is located on chromosome 7q21.3-q22 spanning 12.2 kb and 9 exons (Loskutoff et al., 1987). The P1-P1' bond is located at Arg³⁴⁶-Met³⁴⁷ and is able to inhibit both single and two chain tPA and only two chain uPA (Pannekoek et al., 1986). The rate of inhibition has been reported as $2.5\text{-}4 \times 10^7 \text{ M}^{-1}\text{s}^{-1}$ and $1 \times 10^7 \text{ M}^{-1}\text{s}^{-1}$ for two chain tPA and uPA respectively (Alessi et al., 1988). PAI-I also inhibits thrombin ($1.1 \times 10^3 \text{ M}^{-1}\text{s}^{-1}$) and plasmin ($6.6 \times 10^5 \text{ M}^{-1}\text{s}^{-1}$), but at a slower second order rate constant (Schaller and Gerber, 2011).

The crystal structures of the active and latent conformations of PAI-I have been determined (Sharp et al., 1999; Stout et al., 2000). Recently, the complex structure of PAI-I/uPA has been solved to a resolution of 2.3Å by Lin and colleagues (2011). The crystallisation of this complex revealed new insights on how uPA interacts with PAI-I. Extensive interaction of P4-P3' residues within the RCL to the catalytic site of uPA were seen. In addition to that, exosite interactions beyond the RCL were identified. The uPA 37-loop and 147-loop interacts with PAI-I β -sheet B and C respectively (Lin et al., 2011). The crystal structure further confirms structural specificity of PAI-I with its target protease uPA and tPA.

PAI-I deficiency in humans rarely exhibit spontaneous bleeding events and usually present with mild to moderate bleeding symptoms (Fay et al., 1997; Fay et al., 1992; Mehta and Shapiro, 2008a).

1.8.2 Plasminogen Activator Inhibitor II (PAI-II)

PAI-II, another member of the serpin superfamily, was first isolated in human placenta. Levels of PAI-II in human plasma are only significantly present during pregnancy and perhaps play a role in placenta maintenance or embryonic development (Lecander and Astedt, 1986). PAI-II gene is located on chromosome 18q21.2-q22 spanning 16.4 kb and 8 exons (Ye et al., 1989). It was determined that PAI-II does not contain a complete signal sequence, therefore is not secreted and remains in the intracellular compartment as a non-glycosylated 47 kDa protein (393 amino acids) (Genton et al., 1987). A study by Mikus and colleagues (1996) suggested that due to the lack of signal peptide, intracellular PAI-II readily polymerises which adds to reduced secretion (Mikus and Ny, 1996). A small portion of single chain PAI-II is secreted via a facultative translocation pathway as a 60 kDa (415 amino acids) protein. PAI-II inhibits both single and two chain tPA with an inhibition rate of $1.0 \times 10^4 \text{ M}^{-1}\text{s}^{-1}$ and $2.6 \times 10^5 \text{ M}^{-1}\text{s}^{-1}$ respectively. It is also able to inhibit two chain uPA at a rate of $2.4\text{-}2.7 \times 10^6 \text{ M}^{-1}\text{s}^{-1}$ (Mikus et al., 1993).

1.9 Inhibition of Plasmin by α_2 -antiplasmin

The serpin α_2 -antiplasmin, previously known as α_2 -plasmin inhibitor, is the main inhibitor of plasmin. α_2 -antiplasmin is present in plasma at a concentration of $\sim 1\mu\text{M}$ and is unique among the serpin family due to the presence of N- and C-terminal extensions beyond its inhibitory core. (Coughlin, 2005; Moroi and Aoki, 1976). The N- and C-terminal extensions are unusual as they are the most extensive when compared to the other members of the serpin superfamily. The molecular weight of α_2 -antiplasmin 67 kDa (464 amino acids) and is primarily secreted in the liver (Saito et al., 1982). The gene is located on chromosome 17p13.3 spanning 16 kb and 10 exons (Hirosawa et al., 1988).

1.9.1 Reactive Centre Loop of α_2 -antiplasmin

The P1-P1' peptide bond is located at Arg³⁷⁶-Met³⁷⁷ within the 17 amino acid RCL (Holmes et al., 1987b). The length of RCL is important because the naturally occurring mutation found in α_2 -antiplasmin Enschede results in an addition of alanine into the RCL. The RCL of 18 amino acids, is rendered inactive (Holmes et al., 1987a). α_2 -antiplasmin forms an inactive stoichiometric complex of 1:1 with plasmin in two steps. The first step is the formation of a fast reversible second order complex followed by a formation of a slower first order (Lijnen, 2001; Wiman et al., 1979). The inhibition rate of the second order is very fast at $2 \times 10^7 \text{ M}^{-1}\text{s}^{-1}$ and the rate is dependent on the availability of the lysine binding site and the active site of the plasmin molecule (Wiman et al., 1978; Wiman et al., 1979). α_2 -antiplasmin is known to inhibit both trypsin and chymotrypsin at a rate of $2.5 \times 10^5 \text{ M}^{-1}\text{s}^{-1}$ and $1.7 \times 10^5 \text{ M}^{-1}\text{s}^{-1}$ respectively (Nobar et al., 2004; Potempa et al., 1988).

1.9.2 The N-terminus of α_2 -antiplasmin

The N-terminus of α_2 -antiplasmin extends for 43 amino acids from Met¹-Cys⁴³. α_2 -antiplasmin is found to exist in two N-terminally different forms in human circulation. 30% of circulating α_2 -antiplasmin exists as the full 464 amino acid form with methionine as its N-terminus (Met- α_2 -antiplasmin) (Bangert et al., 1993; Sumi et al., 1989). The remaining 70% of circulating α_2 -antiplasmin is proteolytically cleaved at the first 12 amino acid sequence yielding a shorted form of α_2 -antiplasmin with asparagine as its N-terminus (Asn- α_2 -antiplasmin) (Bangert et al., 1993). The N-terminus cross-links to fibrin via Factor XIIIa during clot formation. The important residue glutamine (Gln¹⁴) is believed to play a key role in cross-linking to fibrin (Kimura and Aoki, 1986; Lee et al., 2001; Tsurupa et al., 2010). Cross-linking of α_2 -antiplasmin

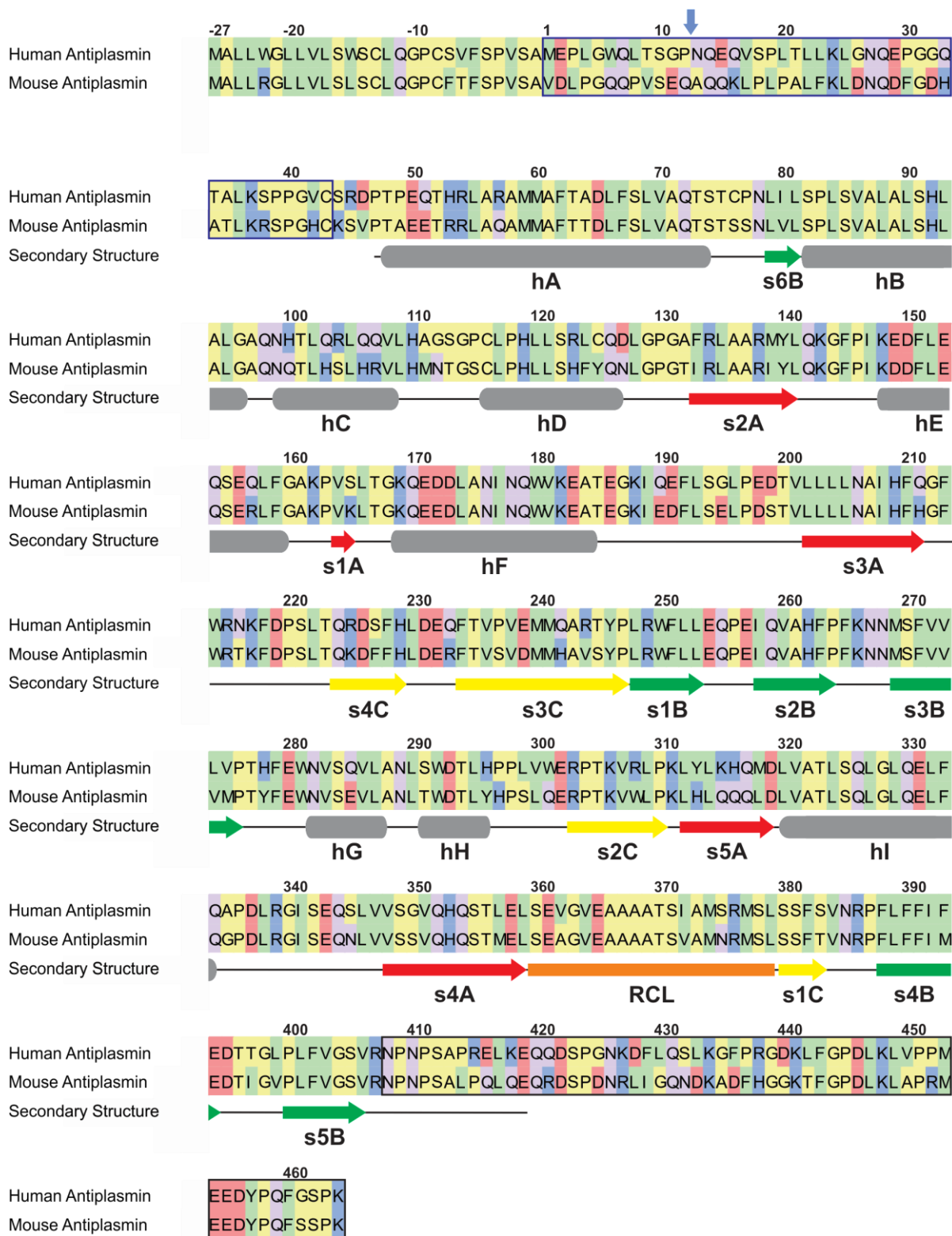
to fibrin increases the resistance of fibrin to the fibrinolytic process thereby preventing clot dissolution. This indicates that the N-terminus is required to localise α_2 -antiplasmin to the clot surface (Bangert et al., 1993; Kimura et al., 1985). The protease responsible for cleaving the peptide bond at Pro¹²-Asn¹³ has been identified as α_2 -antiplasmin cleaving enzyme (APCE), which is a protein homologous to fibroblast activation protein (Lee et al., 2006). This proteolytic mechanism may be an important process as the 452 amino acid form of α_2 -antiplasmin is ~13-fold faster at cross-linking to fibrin when compared to Met- α_2 -antiplasmin (Lee et al., 2004).

1.9.3 The C-terminus of α_2 -antiplasmin

The C-terminus of α_2 -antiplasmin is significantly important because of its ability to interact with the lysine binding sites (LBS) of plasmin. The LBS is located within the kringle domains of plasmin (Frank et al., 2003; Wiman et al., 1979). The C-terminal extension is located after the conserved proline and extends for 55 amino acids from Asn⁴¹⁰-Lys⁴⁶⁴. The C-terminus of α_2 -antiplasmin contains six lysines, five of which are conserved between species (Lys⁴²⁷, Lys⁴³⁴, Lys⁴⁴¹, Lys⁴⁴⁸ and Lys⁴⁶⁴), and it is known to mediate binding to kringle domains of plasmin(ogen) (Gerber et al., 2010). Figure 1.11 shows the sequence of human α_2 -antiplasmin compared to mouse α_2 -antiplasmin. There is a 61% sequence homology of the C-terminus of human and mouse α_2 -antiplasmin, indicating that this region is well conserved. A study with low molecular weight plasmin which lacks the LBS showed a 30-60-fold decrease in the rate of interaction when compared to full-length plasmin and α_2 -antiplasmin (Wiman et al., 1978). This informs that the LBS are required for the fast association of plasmin to α_2 -antiplasmin. Mutation of Lys⁴⁶⁴ (Lys464Ala) decreased the interaction between plasmin and α_2 -antiplasmin, suggesting that the most C-terminal lysine is important in the initial docking to the kringle domain of plasmin while the other residues complete the association via a zipper-like mechanism (Frank et al., 2003). However a study conducted by Wang and colleagues (2003) determined that Lys⁴⁴⁸ is the main lysine residue involved in the interaction with the LBS of plasmin. This observation completely contradicted the finding of Frank and colleagues (2003) (Frank et al., 2003; Wang et al., 2006; Wang et al., 2003). Further to this, Gerber and colleagues (2010) studied the binding of kringle domains to C-terminal peptide and showed that Lys⁴⁶⁴ was the most important which corresponds with observations seen by Frank and colleagues (Frank et al., 2003; Gerber et al., 2010). Due to the inconclusive results, a systematic and sequential study on the mutagenesis of full-length α_2 -antiplasmin C-terminus with intact plasmin was performed in our laboratory and it was determined that indeed Lys⁴⁶⁴, the most C-terminal lysine, was the most important. This results will be further reviewed in Chapter 4 and the published article is as attached at the end of this thesis (Appendix 10.3) (Lu et al., 2011).

Figure 1.11. Sequence alignment of human and murine α_2 -antiplasmin. N- and C-terminal extensions are boxed in blue and black respectively. Blue arrow indicates cleavage site for the generation of human Asn- α_2 -antiplasmin. Secondary structures are shown below the alignment. The numbering of human α_2 -antiplasmin is shown above and based on the full-length secreted form of 464 residues. Figure was produced with PFAAT (Caffrey et al., 2007).

Figure 1.11.
Sequence alignment of human and mouse α_2 -antiplasmin



1.9.4 X-ray Crystal Structure of Murine α_2 -antiplasmin

The crystal structure of human α_2 -antiplasmin is yet to be determined, however the X-ray crystal structure of an N-terminally truncated murine α_2 -antiplasmin was solved to a resolution of 2.65Å (Figure 1.12) (Law et al., 2008). As expected, the serpin core of murine α_2 -antiplasmin is composed of three β -sheets and nine α -helices. The start of the C-terminus is closely associated with the body of the serpin, however the complete tail was not successfully solved. This suggests that the C-terminus is a highly flexible region and could potentially act as a 'hook' when binding to kringle domains of plasmin which in turn orientates the active site to RCL of antiplasmin (Law et al., 2008).

1.9.5 α_2 -antiplasmin Deficiency

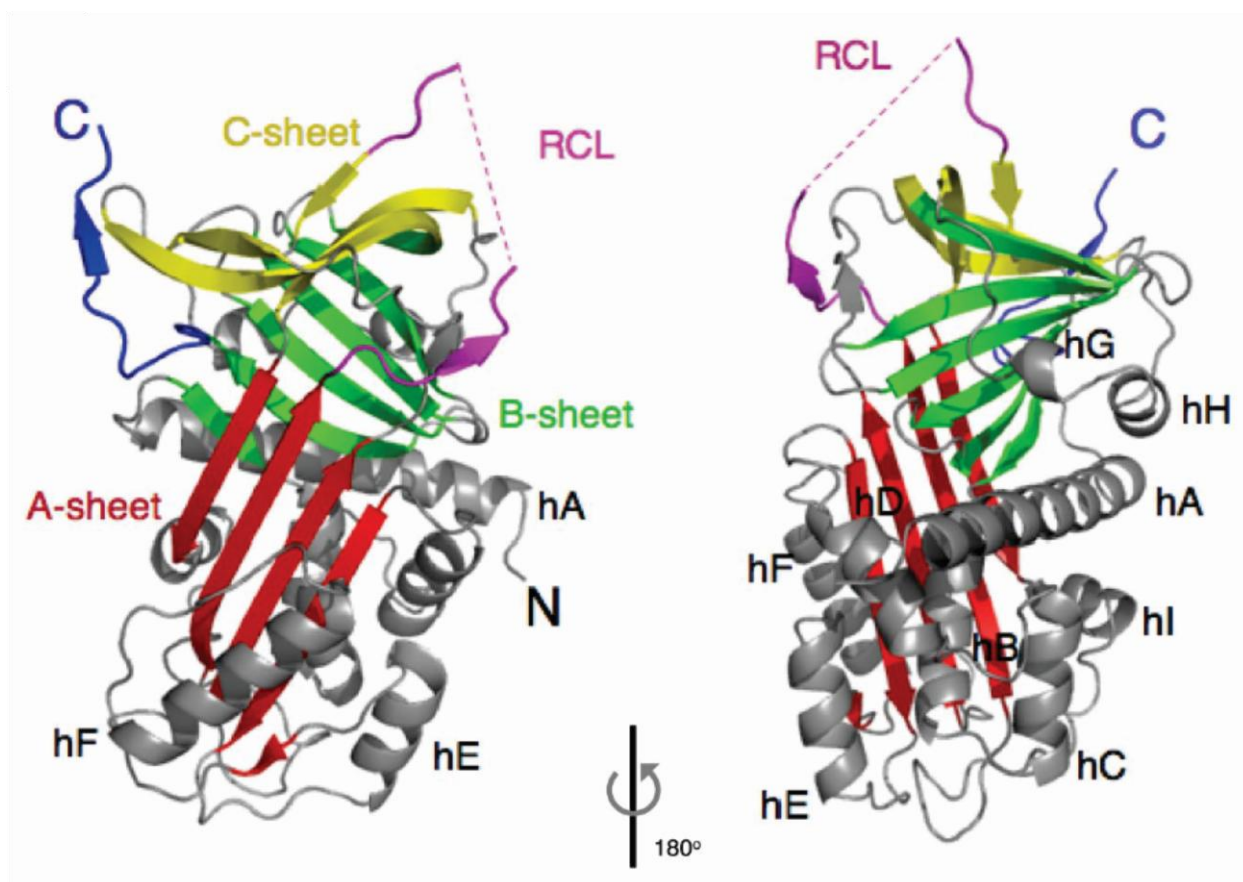
Congenital α_2 -antiplasmin deficiency is a rare autosomal recessive disorder (Aoki et al., 1979). Homozygotes have a severe bleeding disorder whereas heterozygotes present with a milder bleeding tendency and have been shown to manifest to a severe disorder later in life (Ikematsu et al., 1996; Koie et al., 1978). To date, five α_2 -antiplasmin deficiencies have been classified in humans. The first was identified in 1987 and was named α_2 -antiplasmin Enschede. As previously described, an additional alanine in the RCL causes a qualitative change in the molecule which reduces its ability to inhibit plasmin (Holmes et al., 1987a; Kluft et al., 1987). α_2 -antiplasmin Okinawa presents with a deletion of amino acid Glu¹⁴⁹ resulting in structural alteration and loss of plasmin inhibitory function. Secretion of this mutated protein into the circulation is decreased (Miura et al., 1989). The third mutation discovered was an elongation of the α_2 -antiplasmin protein as a consequence of a frameshift mutation in the gene. Similar to α_2 -antiplasmin Okinawa, intracellular transport from endoplasmic reticulum to golgi complex is reduced hence effecting secretion from cells (Miura and Aoki, 1990). A missense mutation at the P8' residue within the RCL (Val384Met) alters the inhibitory potential of α_2 -antiplasmin and patients present with an increased bleeding tendency (Lind and Thorsen, 1999). A single thymine deletion at position 332 results in a frameshift mutation. The mutant protein consists of the first 83 amino acids plus an additional 11 new amino acids and lacks the RCL. Therefore the inactive protein is only 94 amino acids in contrast to the full-length active protein of 464 amino acids (Yoshinaga et al., 2002).

The first α_2 -antiplasmin deficient mice were genetically engineered by Lijnen and colleagues in 1999. Surprisingly, the time required for these mice to recover from tail bleeds was not significantly different from its wild-type counterparts (Lijnen et al., 1999). Perhaps other plasmin inhibitors in the mouse circulatory system are important unlike what was observed from humans with congenital α_2 -antiplasmin deficiency. Further experiments with α_2 -antiplasmin

deficient mice were performed by Matsuno and colleagues (2002) where they measured clot occlusion time in arterial and venous thrombosis. No difference in occlusion time was observed in an arterial thrombosis model when they compared α_2 -antiplasmin deficient with wild-type mice. Spontaneous reperfusion of arteries was observed for all α_2 -antiplasmin deficient mice within 90 minutes of occlusion however only 50% of WT mice were able to maintain vascular integrity. On the other hand, venous thrombosis formation time was significantly increased in the α_2 -antiplasmin deficient mice. Spontaneous reperfusion of veins in α_2 -antiplasmin deficient mice was achieved within 60 minutes. These observations suggest that α_2 -antiplasmin plays an important role in the regulation of thrombus in the venous but not the arterial system (Matsuno et al., 2002).

Figure 1.12. X-ray crystal structure of murine α_2 -antiplasmin. Overall structure of mouse α_2 -antiplasmin with the β -sheet A in red, β -sheet B in green and β -sheet C in yellow. The nine α -helices are labelled hA to hI. The RCL is in magenta and missing residues are represented as dashed lines. N- and C-terminal regions are as indicated (adapted from Law et al., 2008).

Figure 1.12.
X-ray crystal structure of murine α_2 -antiplasmin



1.10 Other Regulators of the Fibrinolytic System

Described previously are the major inhibitors of the fibrinolytic system. In this section, three additional proteins which are TAFI, α_2 -macroglobulin and neuroserpin will be reviewed. These proteins have diverse function however all are involved in the regulation of the fibrinolytic system.

1.10.1 Thrombin Activatable Fibrinolysis Inhibitor (TAFI)

Studies have shown a regulatory link between the blood coagulation pathway and fibrinolysis through a protein called thrombin activatable fibrinolysis inhibitor (TAFI), a plasma zymogen. The TAFI gene is mapped to chromosome 13q14.1 spanning 48 kb and 11 exons (Tsai and Drayna, 1992). It is a member of the metallo-carboxypeptidase family which are responsible for hydrolysing C-terminal peptide bonds (Bouma et al., 2001). The zymogen is synthesised in the liver as a polypeptide of 423 amino acids (60 kDa). Once secreted, the signal peptide is removed and the protein circulates in the 403 amino acid (56 kDa) form. TAFI is activated by thrombin or plasmin which results in cleavage of the Arg⁹²-Ala⁹³ peptide bond releasing the active protease, TAFIa, of 308 amino acids (36 kDa) and the activation peptide (92 amino acids, 20 kDa) (Declerck, 2011). Plasmin is a more potent activator of TAFI in comparison with thrombin. TAFI activation is increased by ~1000-fold in the presence of both thrombin and thrombomodulin (Bajzar et al., 1996). TAFIa conversion is enhanced in the presence of plasmin and heparin but not as significant as thrombin/thrombomodulin (Mao et al., 1999).

When plasmin cleaves fibrin, it exposes carboxy-terminal lysines which increases recruitment of free plasmin(ogen) in the circulation on the blood clot. Localisation of plasmin(ogen) on the fibrin surface enhances plasmin generation and fibrin degradation. TAFIa has high affinity for carboxy-terminal lysines and is drawn towards the partially degraded clot. TAFIa removes these lysines therefore decreasing plasmin generation and preventing further clot breakdown which leads to inhibition of fibrinolysis (Boffa et al., 1998; Cesarman-Maus and Hajjar, 2005; Declerck, 2011). The physiological inhibitor of TAFIa has not been identified however it has been shown that TAFIa spontaneously inactivates after ~8 min at 37°C (Boffa et al., 1998). The x-ray crystal structure of TAFIa revealed a 'dynamic flap' region within the catalytic domain and as the name suggests, it is a mobile site. It was suggested that the activation peptide, which is removed upon thrombin or plasmin activation, stabilises the dynamic flap region. Instability of this region causes increased mobility of the catalytic domain which eventually leads to irreversible conformational change rendering the enzyme inactive (Marx et

al., 2008). A study by Sanglas and colleagues support this theory and demonstrated that unstable TAFIa is prone to polymer formation (Sanglas et al., 2010). These observations explain the spontaneous inactivation of TAFIa.

Increased TAFI levels in plasma is correlated with having a slightly increase risk of venous thrombosis. TAFI-deficient mice did not exhibit any change in phenotype when compared to wild-type mice. TAFI in thrombotic or inflammatory states demonstrated varied results in studies and the exact role still remains elusive (Libourel et al., 2002; van Tilburg et al., 2000).

1.10.2 α_2 -macroglobulin

α_2 -macroglobulin is one of the major protease inhibitors present in plasma and is known to inhibit a diverse range of proteases (Armstrong and Quigley, 1999; Rehman et al., 2012). The gene is located on chromosome 12p13.3-p12.3 spanning 48 kb and 36 exons (Matthijs et al., 1992). It is synthesised in the liver as a large single chain glycoprotein of 1451 amino acids (180 kDa). α_2 -macroglobulin exists in a tetrameric form, with a total molecular weight of 720 kDa, connected by two interchain disulfide bridges (Cys²⁵⁵-Cys⁴⁰⁸ and Cys⁴⁰⁸-Cys²⁵⁵). Each of the subunits are arranged in an anti parallel orientation (Jensen and Sottrup-Jensen, 1986). Five functional sites have been characterised on this tetrameric protein: 1) Bait region, 2) Internal thiol ester, 3) Receptor binding site, 4) Transglutaminase reactive site, and 5) Zinc binding (metalloprotein). Limited proteolysis of the bait region by proteases induces a conformational change which results in the trapping of the protease in the central cavity of the large tetrameric molecule (Borth, 1992). Only one bait region is accessible to plasmin, therefore one tetramer can inhibit one mol of plasmin. The plasmin inhibition rate by α_2 -macroglobulin has been determined to be $1.34 \times 10^5 \text{ M}^{-1}\text{s}^{-1}$ (Steiner et al., 1987).

1.10.3 Neuroserpin

Neuroserpin is predominantly found in the brain and has recently been found to be expressed in other human organs such as skin and liver (Cheret et al., 2012; Hastings et al., 1997). It is expressed as a single glycoprotein of 394 amino acids (55 kDa). The gene is located on chromosome 3q26.1 spanning 89.8 kb and 9 exons (Schrimpf et al., 1997). It is a member of the serpin superfamily and the P1-P1' peptide bond is located at Arg³⁴⁶-Met³⁴⁷ (Hastings et al., 1997). In the brain, neuroserpin functions in maintaining the neuronal environment which includes axon and dendritic growth via non-inhibitory pathway. It has been reported that

neuroserpin regulates tPA, uPA and plasmin in the brain (Lee et al., 2012). Single and two chain tPA is inhibited at a rate of $6.2 \times 10^5 \text{ M}^{-1}\text{s}^{-1}$ and $8.0 \times 10^4 \text{ M}^{-1}\text{s}^{-1}$ respectively. Plasmin inhibition by neuroserpin occurs at a much slower second order rate constant of $3.6 \times 10^2 \text{ M}^{-1}\text{s}^{-1}$ (Hastings et al., 1997). As described in section 1.7.4, misfolding of neuroserpin has been described in the disease progression of FENIB. As expected, the crystal structure of native neuroserpin revealed that the core domain is composed of three β -sheets, nine α -helices and the RCL (Ricagno et al., 2009).

1.11 Current Thrombolytic Therapy

Thrombolytic agents available today are derivatives of plasminogen activators. These drugs are introduced to increase plasminogen conversion to plasmin promoting fibrin degradation during thrombotic events. Intravenous recombinant tPA (Alteplase) is the current gold standard in the treatment of cardiovascular events such as stroke, myocardial infarction and pulmonary embolism. However, treatment using tPA is limited to a narrow time window of 4.5 hour. Administration after 4.5 hour is associated with an increase bleeding tendency where the risks outweigh the benefits therefore use after the therapeutic window is not recommended (Donnan et al., 2011; Lees et al., 2010; Tausky et al., 2011). Compilation of trials conducted has found that treatment of tPA at 90 min is twice as beneficial as treatment at 3 hour. Due to the nature of cardiovascular events, only a small percentage of patients would receive intravenous tPA because time from the onset of symptom to initiation of thrombolytic therapy may be more than 4.5 hour. Other unwarranted effects of tPA use include angioedema and systemic embolism (Lees et al., 2010).

Due to the side effects and narrow therapeutic window of using Alteplase, other thrombolytics are being developed and trialled. Two examples are tenecteplase and desmoteplase. Tenecteplase is recombinant tPA containing three mutation sites at Thr103Asn, Lys296Ala and tetra-alanine substitution at residues 296-299. These mutations prolongs the tPA half-life and increases inactivation by PAI-I (Melandri et al., 2009). Recent Phase IIb trials in Australia have shown positive outcomes where patients receiving tenecteplase had better reperfusion and clinical outcomes calling for Phase III trials to be conducted (Parsons et al., 2012).

Desmoteplase was first derived from bat saliva (plasminogen activator α 1) and in contrast to tPA, it does not contain the kringle 2 domain and have been shown to lack neurotoxicity. It is highly fibrin specific, therefore reduces risk of systemic bleeding (von Kummer et al., 2012). Phase III clinical trials, Desmoteplase in Acute Ischemic Stroke-3 and -4 (DIAS-3 and DIAS-4) are ongoing. Previous trials (DIAS-2) have shown improved reperfusion and

clinical outcomes (Hacke et al., 2005). In addition to that, the therapeutic window for desmoteplase administration is up to 9 hour (von Kummer et al., 2012).

1.12 Development of New Thrombolytics

1.12.1 Plasmin as a Direct Therapeutic Agent

Plasmin is a preferred thrombolytic agent as it acts directly on the fibrin clot and does not require activation by plasminogen activators. Previous work of intravenous administration of plasmin for the dissolution of thrombus was unsuccessful (Boyles et al., 1960). Recent work has shown that intravenous administration of plasmin is ineffective due to the presence of the natural plasmin inhibitor, α_2 -antiplasmin, which acts by quickly neutralising injected plasmin. In light of this knowledge, Marder and colleagues have demonstrated that plasmin administered directly at the site of the thrombus via regional catheter-delivery method was able to demonstrate effective thrombolysis (Marder et al., 2001). By introducing plasmin in the vicinity of the thrombus, plasmin is able to quickly localise on the fibrin surface thus protected from α_2 -inactivation. Studies have shown that unlike recombinant tPA, the administration of intravenous plasmin is not associated with increased bleeding. Once clot dissolution is completed, plasmin is neutralised by circulating α_2 -antiplasmin (Marder, 2008). Using this mode of administration, plasmin therapy is shown to be effective in removing thrombus in a model of rabbit middle cerebral artery (Marder et al., 2010a). Plasmin treatment is not only limited to stroke models, but it is also shown to be promising therapy in deep vein thrombosis (Marder, 2009).

Other derivatives of plasmin, such as microplasmin, have shown thrombolytic potential. Microplasmin only contains the protease core and lacks the five kringle domains. It has been shown to be safe and does not increase risk of bleeding in rabbit stroke models (Lapchak et al., 2002). More recently, a trial on human patients with ischemic stroke further demonstrate its haemostatic safety. However, effectiveness of microplasmin as a thrombolytic was not seen which could be explained by the small sample number of patients (Thijs et al., 2009).

Using recombinant technology, plasmin molecule containing kringle 1 and protease domain (Δ K2-K5) has been generated. The kringle 1 is attached to the protease domain and was chosen in this case because it was shown to have the highest affinity to fibrin. Δ K2-K5 was shown to retain fibrin binding ability and its enzymatic properties were unchanged when compared to full-length plasmin (Marder et al., 2010b). Recent studies with rat transient stroke model demonstrated that Δ K2-K5 does not increase risk of bleeding and was effective at removing thrombus (Crumrine et al., 2012).

1.12.2 Potential Therapeutic Role of α_2 -antiplasmin

Plasmin degradation of fibrin clot can be optimised by inhibiting the natural inhibitor, α_2 -antiplasmin, from inactivating plasmin in circulation. As described previously, α_2 -antiplasmin is unique due to the presence of the N- and C-terminal extensions. The N-terminus localises the inhibitor on the fibrin surface which makes it an effective inhibitor of plasmin in the vicinity of the clot. Sheffield and colleagues made a fusion protein where residues 13-42 of α_2 -antiplasmin were attached to albumin. The study demonstrated that the albumin fusion protein was able to cross-link to the fibrin clot and therefore act as a competitor to circulating α_2 -antiplasmin. Furthermore, the inactivation of plasmin near the fibrin clot was slowed down (Sheffield et al., 2009).

Another group generated monoclonal antibodies against α_2 -antiplasmin and identified two regions to which the antibodies interacted with. The first epitope region was located in the N-terminal region of α_2 -antiplasmin. The antibody decreased cross-linking properties of α_2 -antiplasmin which in turn increased clot lysis. The exact location of the second epitope was not known, but was suggested to be in a region where conformational change is mediated. Binding of antibodies to this region significantly increased the stoichiometry of inhibition of α_2 -antiplasmin to binding making the inhibitor a substrate (Sazonova et al., 2007).

Targeting the C-terminal extension of α_2 -antiplasmin could potentially be another target for the development of therapeutics. It is known that in the absence of the C-terminus, inhibition of plasmin is decreased by 30-60-fold (Lu et al., 2011). Therefore, blocking of this region may increase the half-life of circulating plasmin which may result in increased thrombolysis.

Studying the interaction of plasmin/ α_2 -antiplasmin may prove to be beneficial in gaining a greater understanding of these multi-domain molecules and its complex interaction. Increased knowledge of the fundamentals involved in plasmin/ α_2 -antiplasmin association may lead to the development of new therapeutic agents aimed in blocking the interaction site(s) of α_2 -antiplasmin, thus up-regulating plasmin clot dissolution activity during thrombotic events.

1.13 Aims and Hypotheses

The C-terminus of α_2 -antiplasmin has been shown to initiate binding to plasmin via the kringle domains, which in turn orientates the reactive centre loop of α_2 -antiplasmin to the active site of plasmin. The hypotheses of this project are that the lysine residues within the C-terminus are critical for rapid interaction between plasmin and α_2 -antiplasmin. As the number of lysine to alanine mutations are introduced on the C-terminus, the slower the rate of plasmin inhibition and weaker the binding affinity. Previous results have shown that α_2 -antiplasmin lacking the complete C-terminus still have a notable plasmin inhibition rate. Therefore, it was further hypothesised that an additional exosite region exists beyond the C-terminus and reactive centre loop.

In order to explore these hypotheses, several aims were established.

1. To generate progressive Lys to Ala mutations in five conserved lysine residues within the C-terminus of α_2 -antiplasmin by site directed mutagenesis. N-terminally, C-terminally and double (N- and C-terminally) truncated α_2 -antiplasmin mutant were produced to demonstrate importance of each tail region. Furthermore, 15 amino acids were removed from the C-terminus. These recombinant proteins were then generated and purified. Plasmin inhibition and binding of mutant α_2 -antiplasmin were determined and characterised against wild-type α_2 -antiplasmin. A binding assay to measure the affinity of plasmin/ α_2 -antiplasmin interaction was established and optimised.
2. To identify the additional interaction site which may exist between α_2 -antiplasmin and plasmin. To achieve these aims, this section was divided into three sub-aims.
 - a. The x-ray crystal structure of the α_2 -antiplasmin/microplasmin encounter complex was attempted to directly visualise the potential exosite region. In order to achieve this, a bacterial expression system was set up for the production of recombinant microplasmin(ogen).
 - b. The second section explored the interaction of β -sheet C region of α_2 -antiplasmin in binding to the protease domain of plasmin.
 - c. Finally, binding studies of α_2 -antiplasmin with various forms of plasmin(ogen) were studied in an attempt to further understand the interaction of these multi-domain molecules.

This page has been intentionally left blank.

Chapter 2:

General materials and methods

2.1 General Reagents

All chemicals and reagents used were of analytical grade. Chemicals and reagents bought were obtained from local companies or sourced from local importers from overseas manufacturers. All primers were purchased from Sigma Aldrich (NSW, Australia). Commonly used buffers are listed in Appendix 10.1.

2.2 Apparatus and Equipment

Centrifuges

Beckman J-6M/E centrifuge, Sorvall RC-5B refrigerated superspeed centrifuge and Sorvall RC 5B plus were used with SS-34 and SLA-1500 rotors and Beckman coulter Allegra X-12R centrifuge were used for large volumes. Biofuge pico Haraeus and Eppendorf centrifuge 5415R were used for eppendorf tubes.

DNA Electrophoresis

The Wide Mini-Sub-cell GT from BioRad was used for DNA gel electrophoresis.

DNA Visualisation

DNA gels were visualised using the Chemigenius Bioimaging System from Syngene and Red Imaging System by Alpha Innotech.

Electrophoresis Power Supply

BioRad Power Pac 300.

High Performance Liquid Chromatography (HPLC)

AKTA-UPC 900 HPLC system from GE Healthcare was used for the purification of recombinant proteins.

Kinetic Assays

Flourogenic assays were performed using a Fluostar Optima plate reader from BMG Labtech.

pH Meter

pH of solutions were adjusted using the pH meter from Oakton.

Polymerase Chain Reaction (PCR)

PCR was performed using a Perkin Elmer GeneAmp PCR System 9700.

Protein Electrophoresis Visualisation

Coomassie stained SDS-PAGE were visualised using the EPSON Perfection V700.

Scales

Powdered chemicals and reagents were weighed using the Mettler Toledo PB3002-S and AG204.

SDS-PAGE apparatus

SDS-PAGE was performed using the Mini-Protean III electrophoresis system from BioRad.

Shakers and Incubators

Orbital mixer, orbital mixer incubators, vortex mixer, suspension mixer, dry block heater and waterbath are all from Ratek. Incubator used was from Thermoline.

Spectrophotometer

The Nanodrop ND-1000 Spectrophotometer from Biolab was used.

Surface Plasmon Resonance (SPR)

BIACore T100 and T200 from GE Healthcare were used to measure surface plasmon resonance in binding assays.

Western Blotting

The Mini-Protean II Trans blot module for Western blotting from BioRad was used.

2.3 Bacterial Cells

2.3.1 *Escherichia coli* BL21(DE3)pLysS

The *E.coli* strain of BL21(DE3)pLysS were used for protein expression. This strain contains the following genotype: *E.coli* B F⁻ *dcm ompT hsdS*(r₈m₈) *gal* λ(DE3) [pLysS Cam^r]. High-efficiency protein expression is achieved from T7 promoter-driven expression vectors such as the pET vector. BL21(DE3)pLysS contains the lysogenic phage λ(DE3) which encodes the T7 RNA polymerase gene under the control of the *lac* UV5 promoter. The pLysS plasmid carried by this strain encodes for the T7 lysosyme which reduces the expression of protein controlled by the T7 promoter but does not interfere with expression levels during isopropyl-1-thio-β-D-galactopyranoside (IPTG) induction. Additionally, *ompT* results in mutation of the outer membrane protein protease which reduces proteolysis of expressed proteins.

2.3.2 *Escherichia coli* XL-10 Gold

The *E.coli* strain of XL-10 Gold Ultracompetent cells, were used for the propagation and cloning of plasmids due to its high transformation efficiency. This strain contains the following genotype: Tet^r D(*mcrA*)183 Δ(*mcrCB-hsdSMR-mrr*) 173 *endA1 supE44 thi-1 recA1 gyrA96 relA1 lac* Hte [F' *proAB lac*^qΔ*M15* Tn10 (Tet^r) Amy Cam^r]. These cells are deficient in all known restriction system and endonucleases which improves the quality of miniprep DNA. The Hte phenotype increases transformation efficiency of ligated and large DNA molecules. The *lac*^qΔ*M15* gene present on the F' episome allows blue-white colour screening for recombinant plasmids.

2.4 Plasmids and Vectors

2.4.1 pET(3a)His

The pET(3a) vector developed by Novagen was modified by Associate Professor Paul Coughlin to include a 6xHistidine-tag. The pET(3a)His expression system was used to generate N-terminally His-tagged recombinant proteins in *E.coli*. The expression of the target gene in the pET system is driven by the T7 promoter. In the *E.coli* genome, the *lac* promoter is located upstream of the T7 gene. Addition of IPTG results in the derepression of the *lac* promoter which in turns allow transcription and translation of the T7 gene, resulting in the generation of the T7 RNA polymerase. T7 RNA polymerase produced will bind to the T7 promoter on the pET vector and results in expression of the target gene.

2.4.2 pGEMT-easy

The pGEMT-easy vector was used for cloning PCR products. The vector uses T-overhangs at the insertion site to improve efficiency of PCR product ligations and prevents recircularisation. It contains numerous restriction sites within the multiple cloning region. The multiple cloning region is flanked by restriction enzyme EcoRI, BstZI and NotI, which provides three single-enzyme digestions for the release of the insert. The pGEMT-easy vector contains T7 and SP6 polymerase promoters which flank a multiple cloning region within the α -peptide coding region of the enzyme β -galactosidase. Insertional inactivation of the α -peptide allows recombinant clones to be identified by blue/white screening on indicator plates.

2.5 Molecular Biology

2.5.1 Polymerase Chain Reaction (PCR)

Genes of interest were amplified using the Gene Amp PCR system 9700 (Perkin Elmer, Rowville, Australia). A basic PCR reaction usually consisted of the following reagents: 10x PCR buffer, 10mM dNTP mix, 50mM MgSO₄, 10μM of each forward and reverse primer, DNA polymerase (0.05units/μL) and ~10ng DNA template. Specific PCR conditions and primer pairs are described in subsequent chapters.

2.5.2 DNA Electrophoresis

Agarose gel electrophoresis was used to separate DNA. Gels were made by dissolving agarose in 1x TAE buffer to the final concentration of 1% in a microwave oven. When the agarose is cooled to ~60°C ethidium bromide was added to the final concentration of 0.5μg/mL. The gel was poured into a Biorad Mini-Sub-cell GT gel apparatus system and left to set at room temperature. DNA samples were mixed with DNA loading bugger and loaded into the wells. Samples along with DNA markers were electrophoresed at 80V in 1x TAE buffer for 45 minutes. DNA bands were visualised under ultraviolet (UV) illumination in either a Chemigenius Bioimaging System or Red Imaging System.

2.5.3 DNA Purification

2.5.3.1 Mini Preparation

Mini Prep DNA was obtained from 1.5-5mL overnight culture of *E.coli* in LB media containing ampicillin (100μg/mL). DNA was purified using the Qiagen Miniprep kit (Doncaster, Australia) following manufacturer's instructions.

2.5.3.2 Gel Extraction and Purification of DNA

DNA bands separated via electrophoresis were excised from the agarose gel using a sterile scalpel under UV light. Excised bands were purified using the Qiagen Gel Extraction kit (Doncaster, Australia) following manufacturer's instructions.

2.5.4 Preparation of Chemically Competent *Escherichia coli* Cells

BL21(DE3)pLysS and XL-10 Gold competent *E.coli* cells were prepared chemically using a rubidium chloride method. Frozen cells from glycerol stocks were streaked onto a LB agar plate in the absence of any antibiotics, and left to grow overnight at 37°C. A single colony was inoculated into 5mL of LB media and grown overnight in a shaking incubator at 37°C. The culture was diluted 1:100 into 100mL of LB media and grown in a shaking incubator at 37°C until an OD_{550nm} of 0.5-0.6 was reached. The bacterial cells were then placed on ice for 15 minutes before centrifugation at 3000 x g for 15 minutes. The supernatant was discarded and the cell pellet was resuspended in 40mL of Transformation buffer I (30mM potassium acetate, 100mM rubidium chloride, 10mM calcium chloride, 50mM magnesium chloride, 15% (v/v) glycerol) and placed on ice for 15 minutes. The cells were centrifuged at 3000 x g for 15 minutes. The supernatant was discarded and the cell pellet was resuspended in 4mL of Transformation buffer II (10mM MOPS, 75mM calcium chloride, 10mM rubidium chloride, 15% (v/v) glycerol) and placed on ice for 15 minutes. Cells were used immediately or snap frozen in liquid nitrogen in 100µL aliquots and stored at -80°C until required.

2.5.5 Transformation of Chemically Competent *Escherichia coli* Cells

1µL of DNA (or 3-5µL for ligation reactions) was added to 50µL of chemically competent *E.coli* cells and incubated on ice for 20 minutes. The reaction was then heat shocked for 60 seconds at 42°C and then placed on ice for an additional 2 minutes. 950µL of LB media was added to the cells and incubated at 37°C for an additional 20 minutes. 100µL of the reaction was then spread on an LB agar plate containing ampicillin (100µg/mL) with a glass spreader. The plates were incubated overnight at 37°C to allow growth of colonies. Colony plates were then stored at 4°C until required for up to 1 month.

2.5.6 Ligations

50ng of vector was incubated with a 3-fold excess of cDNA insert, T4 DNA ligase and 2x ligation buffer in a reaction of 10µL. The reaction was mixed and incubated at room temperature for 30 minutes. 3-5µL of the reaction was then transformed into chemically competent *E.coli* cells or stored at -20°C until further use.

2.5.7 Colony PCR

Colony PCR was used to determine whether a transformed colony contained the cDNA insert of interest in the correct orientation in respect to the T7 promoter. 20µL PCR reactions were set up containing either two gene specific primer, or plasmid specific primer and a gene specific primer, in a standard reaction as previously described (section 2.5.1). Using a sterile toothpick and under aseptic techniques, each colony was inoculated firstly into the PCR reaction and then into 5mL LB media containing ampicillin (100µg/mL). Specific PCR conditions and primer pairs are outlined in the relevant chapters. Agarose electrophoresis was used to separate the PCR products which were visualised using ethidium bromide under a UV illuminator. Colonies confirmed having the insert of interest and in the correct orientation were cultured overnight in a shaking incubator at 37°C. DNA was extracted by mini preparation as previously described in section 2.5.3.1.

2.5.8 pGEMT-easy Cloning

pGEMT-easy vector (Promega, NSW, Australia) was used as the first step of cloning in PCR products before being cloned into the subsequent expression vector. An adenosine tail, “A-tailing”, was added to the 3’ ends of blunted DNA before ligation to the pGEMT-easy vector. The reaction contained the following: 5 units of Taq polymerase, 0.2mM dATP, 1.5mM MgCl₂ and 10x Taq reaction buffer. The A-tailing reaction was incubated at 70°C for 30 minutes. The reaction was loaded on a 1% agarose gel (section 2.5.2) and subsequently gel purified using the Qiagen gel extraction kit (section 2.5.3.2). 3.5µL of purified product was ligated to 25ng of pGEMT-easy vector containing 1 unit of T4 DNA ligase and 2x ligation buffer. The ligation reaction was incubated at 4°C overnight before transformation into XL-Gold *E.coli* (section 2.5.5). The transformed cells were then plated onto an LB agar plate containing 50µg/mL ampicillin, 0.5mM IPTG and 20µg/mL Xgal. The lacZ gene which encodes for the enzyme galactosidase is positioned within the cloning site in the pGEMT-easy vector. Ligation of the insert into this region will disrupt the lacZ gene, therefore rendering them unable to produce the enzyme. Cells containing the vector that did not take up the cDNA of interest will still have the intact lacZ gene, therefore able to cleave the Xgal present in the plate forming blue colonies. Cells with the cDNA insert will form white colonies. Colony PCR (section 2.5.7) was performed on the positive colonies (white colonies) to verify that the correct insert is present at the appropriate orientation. Selected colonies were then prepared for mini preparation (section 2.3.5.1) and plasmids were sent for DNA sequencing to confirm authenticity.

2.5.9 DNA Sequencing

DNA sequencing was performed by Micromon (Monash University, Clayton, Australia). 5µL of DNA sample at 200ng/µL concentration per sequencing reaction were sent to the centre. Plasmid specific primers (i.e. T7 primers) were supplied by the institute. 5µM of gene specific primers were sent together with DNA sample if required.

2.5.10 Site-Directed Mutagenesis

To produce single amino acid mutations in the plasmid of interest, the QuikChange Site Directed Mutagenesis kit (Stratagene, USA) was used. The mutation was introduced through the design of two complementary synthetic oligonucleotide primers. Specifics of each primer pairs are described in subsequent chapters. To extend the mutagenic primers during the temperature cycling, a DNA polymerase with proof reading capabilities, Pfu, was employed. Sample reactions of a total volume of 50µL were set up as follows: 10x QuikChange reaction buffer, 100ng/µL DNA template, 125ng sense mutagenic primer, 125ng antisense mutagenic primer, 0.2mM dNTPs, Pfu Turbo DNA polymerase.

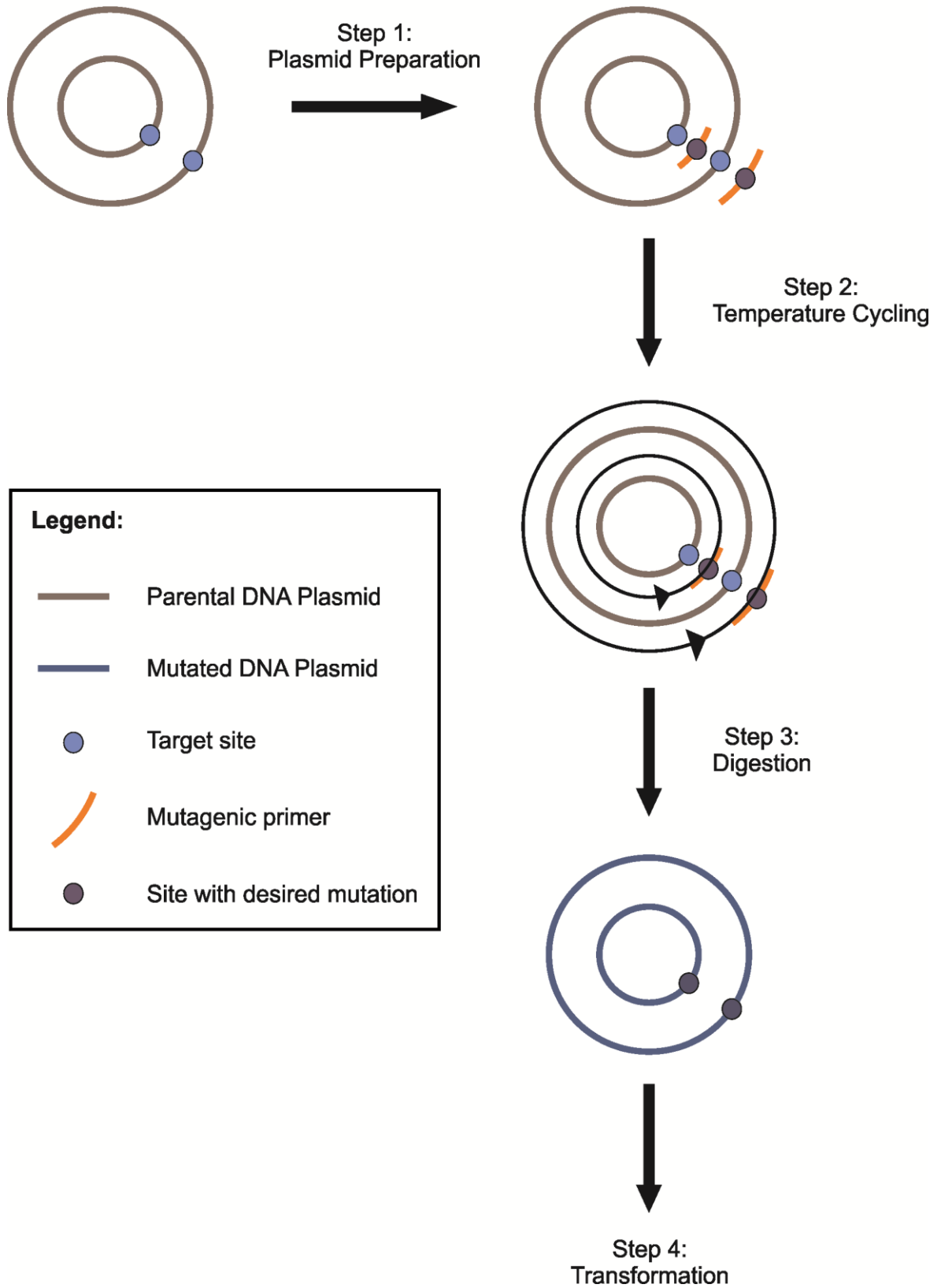
The basic PCR cycling parameters were as follows:

1 cycle	95°C for 30 seconds
18 cycles	95°C for 30 seconds
	55°C for 1 minute
	68°C for 1min/kb of plasmid length

DpnI, a restriction enzyme which cuts at methylated GATC sequence that is present in non-mutated parental DNA, was then added to the PCR reaction. The reaction was incubated at 37°C for 2 hours to ensure complete digestion. These reactions were then used to transform XL-10 Gold *E.coli* (section 2.5.5). A few of the resultant colonies were selected and grown up in LB media for mini preparation (section 2.5.3.1). Plasmids were sent for sequencing to confirm the desired mutation.

Figure 2.1. Schematic diagram of site-directed mutagenesis using the Stratagene Quikchange kit. Step 1: Gene in plasmid with target site for mutation. Step 2: Plasmid is denatured and annealing of mutagenic primers containing the desired mutation. Step 3: DpnI digests methylated non-mutated parental DNA plasmid leaving behind mutated plasmid. Step 4: Transformation of mutated DNA plasmid into XL-10 Gold competent cells (diagram adapted from Quikchange site-directed mutagenesis kit instruction manual).

Figure 2.1.
Schematic diagram of site-directed mutagenesis
using the Stratagene Quikchange kit



2.6 Protein Biochemistry

2.6.1 Sodium Dodecyl Sulfate Polyacrylamide Gel Electrophoresis (SDS-PAGE)

SDS-PAGE is used to separate proteins based on their molecular weight. SDS is an anionic detergent which denatures the protein molecule making it linear and it coats the protein with a negative charge that is proportional to its molecular weight. The distance of migration is assumed to be directly related to the size of the protein. A Tris-glycine buffering system was used in this method based on the Laemmli method.

The gels are prepared by casting two different layers of acrylamide between glass plates. The first poured is the resolving gel which is responsible for separating proteins. The stacking gel, poured second, has a lower pH and percentage of acrylamide which allow the protein to stack into thin layers so that they migrate at the same distance once they reach the resolving gel.

The composition of resolving and stacking gels are as follows:

	<u>12.5% Resolving Gel</u>	<u>4% Stacking Gel</u>
1.5M Tris-HCl pH8.8	2.5mL	-
0.5M Tris-HCl pH6.8	-	2.5mL
40% acrylamide (37.5:1)	3.1mL	1mL
dH ₂ O	4.3mL	6.4mL
10% SDS	100μL	100μL
10% APS	50μL	50μL
TEMED	5μL	10μL

Ammonium persulfate (APS) and N, N, N', N'- Tetramethylethylenediamine (TEMED) were added to the acrylamide to the mixture last to allow crosslinking and gel hardening. Protein samples were prepared by boiling for five minutes in the presence of 5x SDS-PAGE loading dye. SDS and heat denatures the protein in the sample. The loading dye contains bromophenol blue which help track the migration of the protein, and β-mercaptoethanol (BME) reduces any disulphide bond present. The Mini-Protean III electrophoresis system (Biorad, Australia) was used to separate the proteins. Fermentas pre-stained page rulers were ran alongside the samples. Electrophoresis was ran at 200V for 50minutes, or until the dye-front has reached the end of the gels in 1x SDS-PAGE buffer. To detect protein bands, the gel was stained with Coomassie brilliant blue buffer (section 2.6.5). Gels also can be transferred onto Immobilon-P PVDF membrane for Western blotting (section 2.6.4).

2.6.2 Non-Denaturing Polyacrylamide Gel Electrophoresis (Native-PAGE)

Native-PAGE separates proteins according to their intrinsic properties as they migrate through a polyacrylamide gel matrix. The proteins are analysed under non-denaturing or native condition due to the absence of SDS.

The composition of the resolving and stacking gels are as below:

	<u>Resolving Gel (8%)</u>	<u>Stacking Gel (4%)</u>
40% acrylamide (29:1)	2mL	1mL
1.5M Tris-HCl pH8.8	2.5mL	-
0.5M Tris-HCl pH6.8	-	2.5mL
dH ₂ O	5.5mL	6.5mL
10% APS	50µL	50µL
TEMED	5µL	10µL

The gels were poured in a similar manner as previously described for SDS-PAGE (section 2.6.1). The samples were prepared by mixing with 5x Native-PAGE loading dye and electrophoresis was ran in 1x Native-PAGE buffer at a constant current of 15mA per gel until the dye front has ran through the stacker, and 30mA per gel until the gel front has reached the end of the resolving gel. Gels were then stained with Coomassie brilliant blue buffer (section 2.6.5) or transferred onto Immobilon-P PVDF membrane for Western blotting (section 2.6.4).

2.6.3 Transverse Urea Gradient Polyacrylamide Gel Electrophoresis (TUG-PAGE)

TUG-PAGE was prepared using a Biorad Mini Protean II SDS-PAGE system. A U-shaped template was sandwich between two glass plates with bull-dog clips to secure the edges. 3mL of 0M urea solution and 3mL of 8M urea solution was loaded into a gradient maker.

The composition of the urea solutions are as follows:

	<u>0M Urea</u>	<u>8M Urea</u>
40% acrylamide (37.5:1)	2mL	2mL
1.5M Tris-HCl pH8.8	2.5mL	2.5mL
Urea	-	4.8g
dH ₂ O	5.5mL	Make up to 10mL
10% APS	12μL	12μL
TEMED	3μL	3μL

APS and TEMED were added to each gradient solution. The solution was then pumped into the glass plate with the 8M urea solution filling the glass plates first then followed by the 0M urea solution. The U-shaped template was removed once the gel was set and the glass plate was rotated 90° and 1mL Native gel stacker was poured. 100μg of recombinant protein was prepared by mixing with 5x Native-PAGE loading dye and loaded evenly across the stacking gel. The tank was filled with 1x Native-PAGE buffer and the protein was electrophoresed as previously described for Native-PAGE (section 2.6.2). Gels were stained with Coomassie (section 2.6.5.1) to detect protein band.

2.6.4 Western Blotting

Proteins on an SDS-PAGE can be transferred onto Immobilon-P PVDF membrane for detection via immunodetection. A 'sandwich' was prepared, cathode side down, with the gel holder. A sponge was placed first, followed by Whatman paper, the gel, the pre-soaked Immobilon-P PVDF membrane in 100% methanol, followed by Whatman paper, sponge and the gel holder. The gel holder was placed in the Biorad Mini Protean II Western blot apparatus with the gel facing cathode. The 'sandwich' was transferred at 80V for 1 hour in 1x Western buffer. The membrane will be imprinted with the same protein bands which were present on the gel. The membrane was blocked with 5% (w/v) skim milk in PBS containing 0.1% Tween 20 (PBS-Tween) for 30 minutes to prevent any non-specific binding of antibodies to the surface of the membrane. The membrane was then incubated with primary antibody at specified dilutions in 0.5% skim milk/PBS-Tween or 5% skim milk for a minimum of 1 hour or overnight at 4°C. The membrane was then washed in PBS-Tween for five minutes, three times. The membrane was then incubated in a HRP-conjugated secondary antibody at specified dilutions in 0.5% skim milk/PBS-Tween or 5% skim milk for 45 minutes. The membrane was washed three times in PBS-Tween at 5 minute intervals. 1mL of Supersignal West Pico Chemiluminescent Substrate (Pierce; 0.5mL peroxide solution and 0.5mL enhancer solution) was added to the blots. The HRP that was conjugated to the secondary antibody oxidises the peroxide and the reaction releases light. This light was detected by exposing the membrane to medical x-ray films (AGFA). The membrane can be stained with Coomassie Blue for protein band detection (section 2.6.5.2).

2.6.5 Coomassie Brilliant Blue

2.6.5.1 Protein Detection on SDS-PAGE

To detect the protein, electrophoresed gels were stained with Coomassie Blue buffer for ~20 minutes and transferred to Coomassie destain buffer for ~1 hour or until the bands were visible and the gel becomes clear.

2.6.5.2 Protein Detection on Immobilon-P PVDF

Protein that has been transferred onto Immobilon-P PVDF can be stained with Coomassie Blue buffer for ~5 min and transferred to Coomassie destain buffer for ~10 min or until the bands were visible.

2.6.6 Protein Concentration Determination

Tryptophan and tyrosine residues absorb UV light at 280nm and remain fairly consistent in many proteins. Therefore the absorbance of protein solution at 280nm can be used to determine their concentration. The extinction coefficient and the molecular weight of each recombinant protein were determined using the full amino acid sequence and the Peptide Properties Calculator (<http://web.expasy.org/protparam/>). Protein concentration was determined by Equation 2.1.

Equation 2.1:

$$\begin{aligned} & \textit{Protein concentration (mg/mL)} \\ &= Abs_{280nm} (\textit{units. cm}^{-1}) \times \frac{\textit{Molecular weight (g/mol)}}{\textit{Extinction coefficient (U. mL. mg}^{-1}. \textit{cm}^{-1})} \end{aligned}$$

2 μ L of purified protein sample was pipetted onto the pedestal of the Nanodrop ND-1000 Spectrophotometer against an appropriate blank sample of the buffer. Details of the individual molecular weight and extinction coefficient of each protein are reported in subsequent chapters.

Chapter 3:

Expression and purification of recombinant α_2 -antiplasmin proteins

This page has been intentionally left blank.

3.1 Introduction

α_2 -antiplasmin is the main physiological inhibitor of plasmin. It is unique among the serpin family due to the presence of the N- and C-terminal regions (Coughlin, 2005). α_2 -antiplasmin is synthesised in the liver as a 464 amino acid form with methionine at its N-terminus (Met- α_2 -antiplasmin), however it undergoes proteolytic cleavage of 12 amino acids yielding the 452 amino acid form with asparagine at the N-terminus (Asn- α_2 -antiplasmin). The N-terminus is cross-linked to fibrin by factor XIIIa, thereby localising α_2 -antiplasmin to the clot. In addition, the Asn-form has been shown to cross-link to fibrin 13-times faster than the Met-form (Lee et al., 2004). The C-terminus extends 55 amino acids from Asn⁴¹⁰ to Lys⁴⁶⁴ and is important in the initial interaction with kringle domains of plasmin. The lysine residues (Lys⁴²⁷, Lys⁴³⁴, Lys⁴⁴¹, Lys⁴⁴⁸ and Lys⁴⁶⁴) in the C-terminus are key in mediating the binding event with plasmin kringle domains (Frank et al., 2003; Lu et al., 2011).

Our laboratory has previously published the X-ray crystal structure of murine α_2 -antiplasmin. In this, the structure revealed the typical serpin core-fold of nine α -helices, three β -sheets and a reactive centre loop (RCL), however the C-terminus could not be modelled suggesting that this region is highly flexible (Law et al., 2008; Sofian, 2009). Furthermore, detailed characterisation of murine α_2 -antiplasmin in the absence and/or presence of the N- and/or C-terminus have been completed. Results revealed that in the absence of the C-terminus, plasmin inhibition rates were reduced by ~40-fold (Sofian, 2009). Nevertheless, review of human α_2 -antiplasmin was lacking especially regarding the lysine residues (Lys⁴²⁷, Lys⁴³⁴, Lys⁴⁴¹, Lys⁴⁴⁸ and Lys⁴⁶⁴) within the C-terminus. Studies addressing the importance of these lysine residues have been published, however amino acid substitutions introduced at lysine residues were inconsistent in charge (Wang et al., 2006; Wang et al., 2003). Another group used peptides which consisted of the C-terminal region of the α_2 -antiplasmin and measured its interaction with kringle domain(s) of plasmin (Frank et al., 2003; Gerber et al., 2010).

Therefore, a systematic and sequential study on the mutagenesis of C-terminal lysines of full-length human α_2 -antiplasmin was presented. This chapter described the cloning and protein expression of recombinant wild-type human Asn- α_2 -antiplasmin along with truncated variants of the N- and/or C-terminal extension. Multiple Lys to Ala mutations were introduced in the C-terminus of α_2 -antiplasmin and the C-terminal region was shortened by 15 amino acids. All recombinant proteins were generated in a bacterial expression system and were purified to homogeneity. Each recombinant α_2 -antiplasmin mutant was assessed by CD spectrometry to confirm that the proteins produced retained their native fold. Further kinetic and binding characterisation of these proteins will be described in Chapter 4.

3.2 Methods

3.2.1 Generation of Human α_2 -antiplasmin Bacterial Expression Construct

Human WT α_2 -antiplasmin cDNA was isolated from a liver cDNA library using PCR with primers 5'-GGA TCC ACC CCA GGA GCA GGT GTC CC-3' and 5'-GGA TCC TCA CTT GGG GCT GCC AAA C-3'. The product was cloned into the pET(3a)His expression vector and sequenced for authenticity. This construct was then used as the template to clone the other mutant α_2 -antiplasmin recombinant expression vectors.

3.2.1.1 Generation of N- and/or C-terminally Truncated Human α_2 -antiplasmin Constructs

To generate the antiplasmin N- and/or C-terminally truncated construct (N Δ , C Δ , N Δ C Δ , L449 Δ), primers (Table 3.1) were designed to introduce the START 'Met' codon at Cys⁴³, a STOP codon at Pro⁴¹⁴ and a STOP codon at Leu⁴⁴⁹. Sample reactions were set up as indicated in section 2.5.1.

The PCR cycling parameters were as follows:

1 cycle	94°C for 2 seconds
30 cycles	94°C for 30 seconds
	55°C for 30 seconds
	68°C for 2 minutes

The PCR products were ran on an agarose gel and purified (section 2.5.3.2). An adenosine tail was then added to the 3' ends and the construct was ligated into the pGEMT-easy vector (section 2.5.8). Positive colonies and pET(3a)His vector were then digested with BamHI in a 37°C waterbath, overnight. Digestion reactions with a total volume of 50 μ L were set up as follows: pGEMT-easy α_2 -antiplasmin plasmid, 10x BamHI buffer, 10x BSA, 20units BamHI. 1 μ L of calf intestinal phosphatase (CIP) was added to the pET(3a)His reaction after BamHI reaction was completed. CIP was added to minimise recirculation of the pET(3a)His vector during ligation reaction. *BamHI* digestion reactions were ran on an agarose gel and purified (section 2.5.3.2). The α_2 -antiplasmin cDNA were then cloned into the BamHI site of pET(3a)His vector (section 2.5.6). Colony PCR (section 2.5.7) was performed to identify which bacterial colonies contain the insert in the correct orientation. Positive colonies were

cultured overnight at 37°C in LB media and plasmid DNA was extracted using the Qiagen miniprep kit (section 2.5.3.1). Plasmid DNA was sent for sequencing to confirm authenticity.

3.2.1.2 Site-directed Mutagenesis of the C-terminus of Human α_2 -antiplasmin

The QuikChange site-directed mutagenesis kit (Stratagene) (section 2.5.10) was used on the WT α_2 -antiplasmin template in which alanine was substituted for lysine residues along the C-terminus of antiplasmin. The mutagenic forward primer was designed to contain the GCA codon which would replace lysine at Lys⁴²⁷, Lys⁴³⁴, Lys⁴⁴¹, Lys⁴⁴⁸ and Lys⁴⁶⁴. Table 3.1 shows the list of primers designed to introduce the mutations. Several mutations within the C-terminus of α_2 -antiplasmin were made as follows: K464A, K448A/K464A, K441A/K448A/K464A, K434A/K441A/K448A/K464A, K427A/K434A/K441A/K448A/K464WT and K448A/L449 Δ . All constructs were nucleotide sequenced to confirm the mutations introduced.

3.2.2 Sequence Alignment, Molecular Weight, Extinction Co-efficient and Isoelectric Point (pI)

Nucleotide sequence obtained after DNA sequencing was translated to amino acid sequence using the Translate tool. The sequence was then aligned using the Multalin tool. The ProtParam tool was used to calculate the theoretical molecular weight, extinction co-efficient and isoelectric point (pI) using the amino acid sequence of recombinant human antiplasmin. All these can be accessed from ExPASy website (<http://expasy.org/tools/>).

3.2.3 Large Scale Expression of Recombinant Human α_2 -antiplasmin

The production of recombinant α_2 -antiplasmin in a bacterial expression system and its subsequent purification is well established in our laboratory. In this study, wild-type (WT) and mutant α_2 -antiplasmin proteins were produced in the same manner.

E.coli BL21(DE3)pLys cells transformed with either WT or mutant α_2 -antiplasmin plasmid (see section 2.5.5 for transformation protocol) were used to inoculate a culture of 2x tryptone-yeast medium (2x TY) supplemented with 100 μ g/mL ampicillin and grown overnight in a shaking incubator at 37°C, rotating at 220rpm. The cell cultures were then diluted 1:10 in fresh 2x TY

media supplemented with 100µg/mL ampicillin and grown for a further 2 hr at 37°C and 220rpm. The cells were induced with a final IPTG concentration of 0.01mM and grown for another 4-5 hr at 30°C and 220rpm. Cells were harvested by centrifugation at 3500rpm (Beckman JS-4.2 rotor) for 20 min at 4°C. The supernatant was discarded and the cell pellet was lysed to obtain soluble pellet or stored at -80°C until further use.

To obtain soluble recombinant α_2 -antiplasmin, the cell pellet was resuspended in Lysis buffer (50mM NaPO₄ pH8.0, 150mM NaCl, 20mM Imidazole) containing 1mg/mL lysozyme, 0.2mg/mL DNase, 1:1000 protease inhibitor cocktail (Sigma), and 0.01% PMSF per liter of cell culture. The cells were allowed to rest on ice for 20 min. The cell lysates were then frozen in liquid nitrogen and then completely thawed in a 37°C water bath. This freeze-thaw cycle was performed three times to completely lyse the cells. The lysate was centrifuged (Sorvall SS34 rotor) at 15,000rpm, 4°C for 20 min. The supernatant was transferred to a clean tube for the first stage of purification. A 5µL sample of the supernatant was collected and analysed on 12.5% SDS-PAGE.

3.2.4 Purification on Nickel Chelate Affinity Chromatography

WT and mutant recombinant α_2 -antiplasmin were expressed with a hexahistidine tag on the N-terminal region of the protein which allowed the first purification step by affinity chromatography. The hexahistidine residues on the recombinant protein bound tightly to the nickel ions in a column. Non-tagged proteins were removed under washing conditions. High concentration of imidazole in the elution buffer was used to competitively displace the histidine residues from the column which resulted in the elution of the tagged proteins.

A 1mL Nickel-HisTrap column was used on the AKTA-UPC 900 HPLC system. The column was equilibrated with 5 column volumes of HisTrap Buffer A (20mM NaPO₄ pH8.0, 150mM NaCl, 20mM Imidazole), followed by 5 column volume of HisTrap Buffer B (20mM NaPO₄ pH8.0, 150mM NaCl, 500mM Imidazole) and then re-equilibrated back to HisTrap Buffer A. Soluble supernatant was loaded onto the HisTrap column in 10mL batches. Unbound protein fractions were collected for analysis by SDS-PAGE. The bound protein was eluted with a linear gradient of Imidazole (20mM to 500mM) over 10 column volumes at 1mL/min and 1mL fractions were collected in 96-well deep plates. Peak protein fractions were run on a 12.5% SDS-PAGE and gels were subsequently analysed by Coomassie staining (section 2.6.5). Peak fractions were then pooled, placed in a dialysis tubing (Spectra/por 12-14kDa cut-off) and dialysed in MonoQ Buffer A (20mM Tris-HCl pH8.0, 0.1mM EDTA) for 2 hr at 4°C to prepare the sample for second stage purification.

Table 3.1 Primer sequences for human α_2 -antiplasmin.

Primer Name	Orientation	Nucleotide Sequence (5' → 3')	Purpose
#318	Sense	GGATCCAACCAGGAGCAGGTGTCC	α_2 -antiplasmin forward and reverse primers
#319	Antisense	GGATCCTCACTTGGGGCTGCCAAA	
#422	Sense	GTTTGGCAGCCCCGCATGAGGATCCGGC	Lys ⁴⁶⁴ → Ala ⁴⁶⁴
#423	Antisense	GCCGGATCCTCATGCGGGGCTGCCAAAC	
#424	Sense	GGCCCTGACTTAGCACTTGTGCCCCCC	Lys ⁴⁴⁸ → Ala ⁴⁴⁸
#425	Antisense	GGGGGGCACAAGTGCTAAGTCAGGGCC	
#426	Sense	CCCCCGCGGAGACGCACTTTTCGGCCCTG	Lys ⁴⁴¹ → Ala ⁴⁴¹
#427	Antisense	CAGGGCCGAAAAGTGCGTCTCCGCGGGGG	
#428	Antisense	GCGGGGGAAGCCTGCCAGGCTCTGGAGG	Lys ⁴³⁴ → Ala ⁴³⁴
#429	Sense	CCTCCAGAGCCTGGCAGGCTTCCCCCGC	
#430	Sense	GGATTCCCCGGGCAACGCAGACTTCCTCCAGAGCC	Lys ⁴²⁷ → Ala ⁴²⁷
#431	Antisense	GGCTCTGGAGGAAGTCTGCGTTGCCCGGGGAATCC	
#432	Antisense	GGATCCTCATGCACTGGGGTTGGG	Pro ⁴¹⁴ → Stop
#433	Antisense	GGATCCTCATTTTAAGTCAGGGCC	Leu ⁴⁴⁹ → Stop
#435	Antisense	GCCGGATCCTCACTTGGGGCTGCCAAAC	Lys ⁴⁶⁴ → Arg ⁴⁶⁴
#436	Sense	GTTTGGCAGCCCCAAGTGAGGATCCGGC	
#437	Sense	GGCCCTGACTTAGCATGATTATCCGGC	Lys ⁴⁴⁸ → Ala ⁴⁴⁸ (for K448A/L449 Δ)
#439	Antisense	GCCGGATCCTCATGCTAAGTCAGGGCC	
#444	Sense	AGGATCCATGAGCAGAGACCCACC	Cys ⁴³ → Met
T7for	Sense	AATACGACTCACTATAG	Vector specific (pET(3a)His)
T7rev	Antisense	GGCGACTCGTTATTGATCG	
M13for	Sense	GTAAAACGACGGCCAGT	Vector specific (pGEMT-easy)
M13rev	Antisense	CAGGAAACAGCTATGAC	

3.2.5 Purification on Anion Exchange Affinity Chromatography

This stage of purification involves the binding of negatively charged protein to the positively charged column. The high concentration of negatively charged chloride ions in the elution buffer competes for binding to the column which results in the elution of the protein of interest. This method of separation is very selective because different protein elute at different concentration of salt due to the differences in the external charge of the protein. α_2 -antiplasmin has a theoretical pI of ~6 and the buffers used in this method is pH8.0 for the protein to be negatively charged.

Tricorn MonoQ 5/50 GL column (GE Healthcare) was used for this protocol. The column was equilibrated by 5 column volume of MonoQ Buffer A (20mM Tris-HCl pH8.0, 0.1mM EDTA), followed by 5 column volume of MonoQ Buffer B (20mM Tris-HCl pH8.0, 0.1mM EDTA, 0.5M NaCl) then re-equilibrated back to MonoQ Buffer A. The protein sample was transferred out of the dialysis tubing and filtered through a 0.2 μ M membrane to remove any precipitated protein. The sample was then loaded onto the system using a 10mL sample loop. The protein was eluted with increasing linear concentration of NaCl (0 to 0.5M) over 30 column volumes at 1mL/min. 500 μ L fractions were collected in a 96-well deep plate. Peak fractions were analysed on 12.5% SDS-PAGE and subsequently stained with Coomassie to determine the purity of the protein of interest. Aliquots of recombinant protein were stored at -80°C and protein concentration were determined using direct measurement at 280nm (section 2.6.6).

3.2.6 Western Blot Analysis of Recombinant Human α_2 -antiplasmin

Recombinant α_2 -antiplasmin proteins were ran on a 12.5% SDS-PAGE (section 2.6.1) and were subsequently transferred onto Immobilon-P PVDF membrane as described in section 2.6.4. Membranes were incubated with 1:2000 dilution of primary antibody (anti 6xHisTag raised in mouse), followed by 1:5000 dilution of the secondary antibody (anti-mouse).

3.2.7 Circular Dichroism Analysis of Recombinant Human α_2 -antiplasmin

Circular dichroism (CD) analysis was performed on a Jasco J-815 spectropolarimeter (Jasco, Easton, MD, USA) using a 0.1cm path length cuvette with a protein concentration of 200 μ g/mL in 20mM Tris-HCl and 0.1mM EDTA. The CD spectrum of recombinant antiplasmin (WT and mutants) was performed in the far-ultraviolet range. Spectral measurements were recorded from 190-260nm at room temperature, with a one second response time.

3.3 Results

3.3.1 Generation of N- and/or C-terminally Truncated Human α_2 -antiplasmin Constructs

Wild-type (WT) human α_2 -antiplasmin was initially isolated from a liver cDNA library using PCR (see section 3.2.1) by Ms Corrine Hitchen. Subsequently, this was used as a template to clone all single/multiple Lys to Ala mutants and truncated variants of α_2 -antiplasmin.

The N-terminally truncated (N Δ) α_2 -antiplasmin mutant was generated by designing primers to delete 43 amino acids from the N-terminus of the full-length protein (#319 and #444 – see Table 3.1). The C-terminally truncated (C Δ) α_2 -antiplasmin mutant was generated by introducing a stop codon at Pro414 by using mutagenic primers (#318 and #432 – see Table 3.1) designed specifically for this deletion. A double truncation of both tails was also generated to produce the N- and C-terminally truncated (N Δ C Δ) α_2 -antiplasmin mutant (#432 and #444 – see Table 3.1). Figure 3.1 outlines the strategy for cloning truncated variants of α_2 -antiplasmin.

All variants were sequenced for authenticity. Sequence alignment is shown on Figure 3.2 of WT α_2 -antiplasmin and truncated variants. Table 3.2 is a summary of the extinction coefficient, molecular weight (MW) and isoelectric point (pI) of WT and α_2 -antiplasmin variants as calculated from the predicted amino acid sequence.

Table 3.2 Molecular weight (MW), extinction coefficient and isoelectric point (pI) of human α_2 -antiplasmin variants. MW is in Daltons (Da) and extinction coefficient is in $M^{-1}s^{-1}$. Parameters were calculated using the Protparam Tool available at the following website: <http://web.expasy.org/protparam/>

Recombinant α_2 -antiplasmin	MW	Extinction Coefficient	pI
WT	51549	39210	6.13
N Δ	48494	39085	6.13
C Δ	45764	37720	6.21
N Δ C Δ	42709	37595	6.21
K448A	51492	39210	6.05
K464A	51492	39210	6.05
K464R	51577	39210	6.13
K448A/K464A	51435	39210	5.97
K441A/K448A/K464A	51378	39210	5.90
K434A/K441A/K448A/K464A	51321	39210	5.82
K427A/K434A/K441A/K448A/K464A	51264	39210	5.75
K427A/K434A/K441A/K448A/K464WT	51321	39210	5.82
L449 Δ	49733	37720	6.31
K448A/L449 Δ	49676	37720	6.22

Figure 3.1. Cloning strategy for truncated human α_2 -antiplasmin variants into the pET(3a)His expression vector. The α_2 -antiplasmin gene was amplified with the corresponding primers to isolate WT and truncated variants. The PCR products were subcloned into the pGEMT-easy vector and excised with BamHI. The insert was then cloned in-frame with the 6xHistidine (His) tag via BamHI restriction site in the multiple cloning region (MCR).

Figure 3.1.
Cloning strategy for truncated human α_2 -antiplasmin variants into the pET(3a)His expression vector

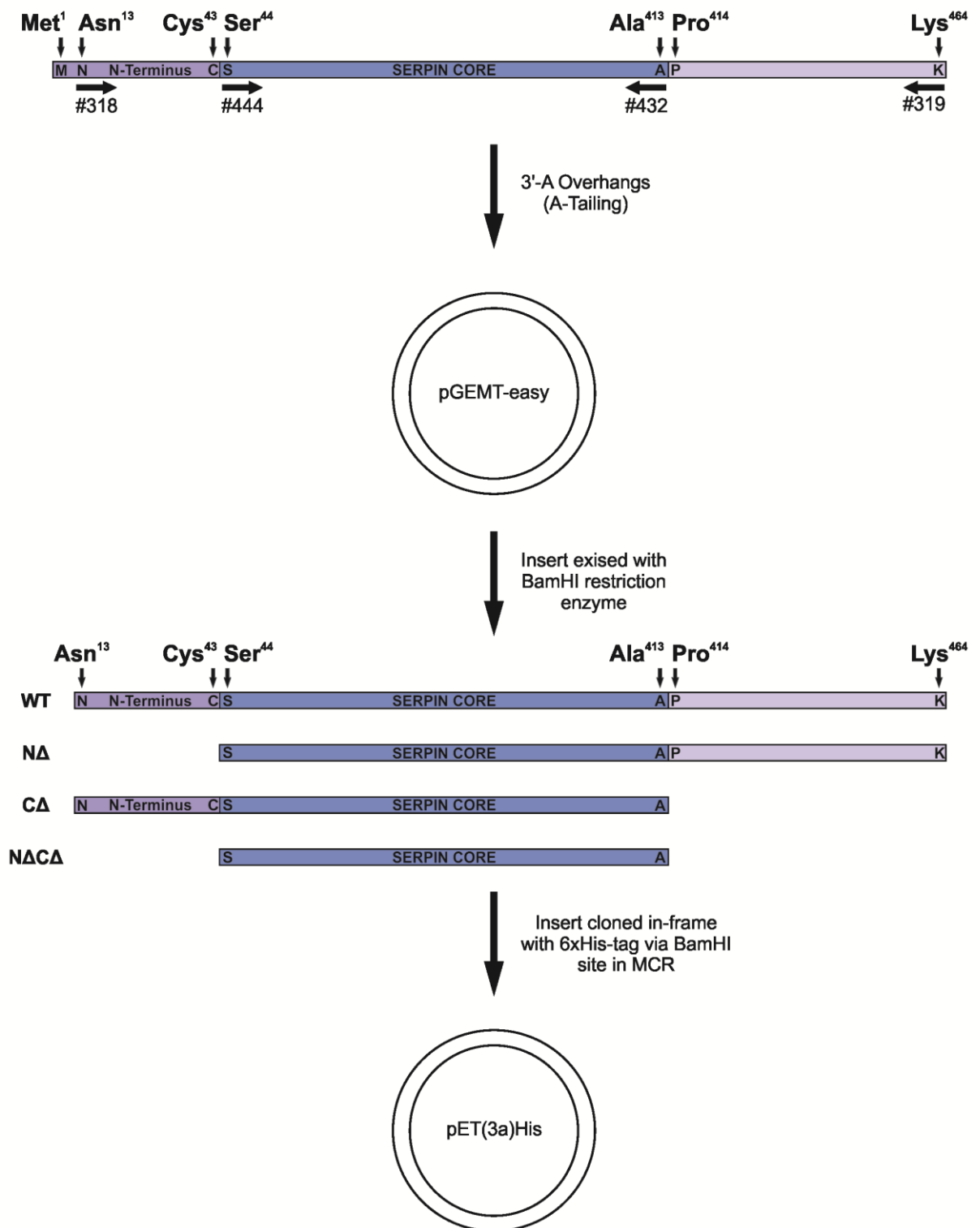


Figure 3.2. Sequence alignment of wild-type and truncated human α_2 -antiplasmin.

Wild-type (WT) human α_2 -antiplasmin and three truncated α_2 -antiplasmin mutants (N Δ , C Δ and N Δ C Δ) were generated, expressed and purified. The region highlighted in grey is the 6xHistidine tag. WT and C Δ α_2 -antiplasmin produced is the Asn form, where the first 13 amino acid is not present. The first 43 amino acids have been removed to produce the N Δ variants. In the C Δ α_2 -antiplasmin variants, 50 amino acids have been deleted in the C-terminal region. The numbering of recombinant α_2 -antiplasmin variants was based on the secreted 464 residue form.

Figure 3.2. Sequence alignment of wild-type and truncated human α_2 -antiplasmin

	13			50
WT	MHHHHHH	GSNQEQVSL	TLLKLGNOEP	GGQTALKSPPGVCSRDPTE
NA				MHHHHHH GSMSRDPTPE
CA	MHHHHHH	GSNQEQVSL	TLLKLGNOEP	GGQTALKSPPGVCSRDPTE
NA Δ				MHHHHHH GSMSRDPTPE
	51			100
WT	QTHRLARAMM	AFTADLFSLV	AQTSTCPNLI	LSPLSVALALSHLALGAQNH
NA	QTHRLARAMM	AFTADLFSLV	AQTSTCPNLI	LSPLSVALALSHLALGAQNH
CA	QTHRLARAMM	AFTADLFSLV	AQTSTCPNLI	LSPLSVALALSHLALGAQNH
NA Δ	QTHRLARAMM	AFTADLFSLV	AQTSTCPNLI	LSPLSVALALSHLALGAQNH
	101			150
WT	TLQRLQQVLH	AGSGPCLPHL	LSRLCQDLGP	GAFRLAARMYLQKGFPIKED
NA	TLQRLQQVLH	AGSGPCLPHL	LSRLCQDLGP	GAFRLAARMYLQKGFPIKED
CA	TLQRLQQVLH	AGSGPCLPHL	LSRLCQDLGP	GAFRLAARMYLQKGFPIKED
NA Δ	TLQRLQQVLH	AGSGPCLPHL	LSRLCQDLGP	GAFRLAARMYLQKGFPIKED
	151			200
WT	FLEQSEQLFG	AKPVSLTGKQ	EDDLANINQW	VKEATEGKIQEFLSGLPEDT
NA	FLEQSEQLFG	AKPVSLTGKQ	EDDLANINQW	VKEATEGKIQEFLSGLPEDT
CA	FLEQSEQLFG	AKPVSLTGKQ	EDDLANINQW	VKEATEGKIQEFLSGLPEDT
NA Δ	FLEQSEQLFG	AKPVSLTGKQ	EDDLANINQW	VKEATEGKIQEFLSGLPEDT
	201			250
WT	VLLLLNAIHF	QGFWRNKFD	SLTQRDSFHL	DEQFTVPVEMMQARTYPLRW
NA	VLLLLNAIHF	QGFWRNKFD	SLTQRDSFHL	DEQFTVPVEMMQARTYPLRW
CA	VLLLLNAIHF	QGFWRNKFD	SLTQRDSFHL	DEQFTVPVEMMQARTYPLRW
NA Δ	VLLLLNAIHF	QGFWRNKFD	SLTQRDSFHL	DEQFTVPVEMMQARTYPLRW
	251			300
WT	FLLEQPEIQV	AHFPPKNNMS	FVVLVPTHFE	WNVSQVLANLSWDTLHPPLV
NA	FLLEQPEIQV	AHFPPKNNMS	FVVLVPTHFE	WNVSQVLANLSWDTLHPPLV
CA	FLLEQPEIQV	AHFPPKNNMS	FVVLVPTHFE	WNVSQVLANLSWDTLHPPLV
NA Δ	FLLEQPEIQV	AHFPPKNNMS	FVVLVPTHFE	WNVSQVLANLSWDTLHPPLV
	301			350
WT	WERPTKVRLP	KLYLKHQMDL	VATLSQLGLQ	ELFQAPDLRGISEQSLVVS
NA	WERPTKVRLP	KLYLKHQMDL	VATLSQLGLQ	ELFQAPDLRGISEQSLVVS
CA	WERPTKVRLP	KLYLKHQMDL	VATLSQLGLQ	ELFQAPDLRGISEQSLVVS
NA Δ	WERPTKVRLP	KLYLKHQMDL	VATLSQLGLQ	ELFQAPDLRGISEQSLVVS
	351			400
WT	VQHQSTLELS	EVGVEAAAAT	SIAMSRMSLS	SFSVNRPFLFFIFEDTTGLP
NA	VQHQSTLELS	EVGVEAAAAT	SIAMSRMSLS	SFSVNRPFLFFIFEDTTGLP
CA	VQHQSTLELS	EVGVEAAAAT	SIAMSRMSLS	SFSVNRPFLFFIFEDTTGLP
NA Δ	VQHQSTLELS	EVGVEAAAAT	SIAMSRMSLS	SFSVNRPFLFFIFEDTTGLP
	401			450
WT	LFVGSVRNPN	P SAPRELKEQ	QDS PGNKDFL	QSLKGFPRGDKLFGPDLKLV
NA	LFVGSVRNPN	P SAPRELKEQ	QDS PGNKDFL	QSLKGFPRGDKLFGPDLKLV
CA	LFVGSVRNPN	PSA		
NA Δ	LFVGSVRNPN	PSA		
	451	464		
WT	PPMEEDYPQF	GSPK		
NA	PPMEEDYPQF	GSPK		
CA				
NA Δ				

3.3.2 Mutagenesis of the Human α_2 -antiplasmin C-terminus

Site-directed mutagenesis using a PCR protocol was performed on pET-His(3a) vector containing the α_2 -antiplasmin cDNA template (Figure 2.1). Lys to Ala mutations in the C-terminus of WT antiplasmin gene were introduced by designing mutagenic primers (Table 3.1) and the Quikchange mutagenesis kit was used. Several mutations (single or multiple Lys to Ala) within the C-terminus of α_2 -antiplasmin were made as follows: K448A, K464A, K464R, K448A/K464A, K441A/K448A/K464A, K434A/K441A/K448A/K464A and K427A/K434A/K441A/K448A/K464WT. A stop codon was introduced at position 437 to shorten the C-terminus: L449 Δ and K448A/L449 Δ . Figure 3.3 is a schematic representation of the C-terminal of α_2 -antiplasmin and the position at which the mutations were introduced. DNA sequencing confirmed authenticity of the clones generated.

3.3.3 Recombinant Human α_2 -antiplasmin Wild-type Expression and Purification

An established expression and purification protocol for recombinant α_2 -antiplasmin has been previously described in my honours thesis (Lu, 2008) and recently published (Lu et al., 2011). This section describes the large scale purification of WT α_2 -antiplasmin. A two-step chromatographic purification protocol was carried out to remove contaminating proteins and to purify the protein of interest to homogeneity. The first step was purification by nickel affinity chromatography which involves binding of soluble protein lysate to a HisTrap column. Bound proteins were eluted with a 0-500mM imidazole gradient. Figure 3.4A shows a typical elution profile for WT α_2 -antiplasmin. Peak fractions were analysed on a Coomassie stained 12.5% SDS-PAGE (Figure 3.4B). At the predicted molecular mass of α_2 -antiplasmin, two dominant bands were observed at approximately 55kDa. Western blot of peak fractions revealed that WT α_2 -antiplasmin protein runs below the 55kDa band marker indicating that the slightly higher band was a contaminant (Figure 3.4C). Significant amount of contaminating material at various molecular weights were also observed on the SDS-PAGE.

A second purification step was carried out to remove the contaminating materials. Peak fractions from the HisTrap column were pooled and dialysed in MonoQ Buffer A. The sample was then bound to an anion exchange column (MonoQ) and a 0-500mM NaCl gradient was generated for protein elution. A typical elution profile of WT α_2 -antiplasmin is shown on Figure 3.4D. WT α_2 -antiplasmin was eluted out as a single peak at approximately 30% concentration of MonoQ Buffer B. The fractions corresponding to this peak were analysed on a Coomassie stained 12.5% SDS-PAGE and is shown in Figure 3.4E. A dominant band was seen at ~55kDa which corresponds to the molecular weight of WT α_2 -antiplasmin. Fraction number 18 (Figure 3.4D) was collected and the final protein concentration was calculated from the absorbance at 280nm. The yield of protein obtained for WT α_2 -antiplasmin was ~0.35mg per litre of culture.

Figure 3.3. Schematic representation of the C-terminus of human α_2 -antiplasmin and positions at which mutations were introduced. WT α_2 -antiplasmin and various mutants (Lys to Ala mutations or truncations) of the C-terminus were generated, expressed and purified. *Dashes* represent the wild-type sequence, and the introduction of a stop codon is indicated (Δ).

Figure 3.3.
Schematic representation of the C-terminus of human α_2 -antiplasmin
and positions at which mutations were introduced

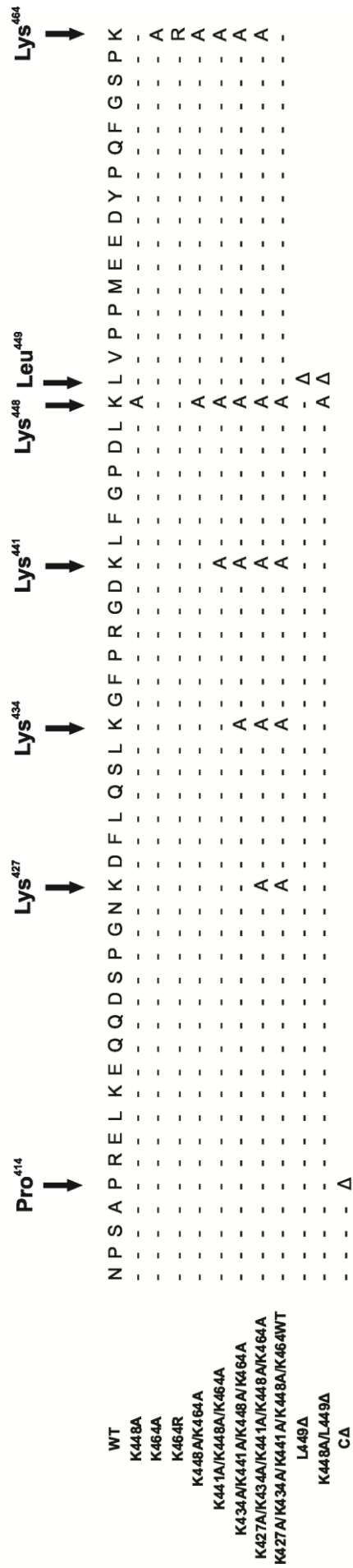
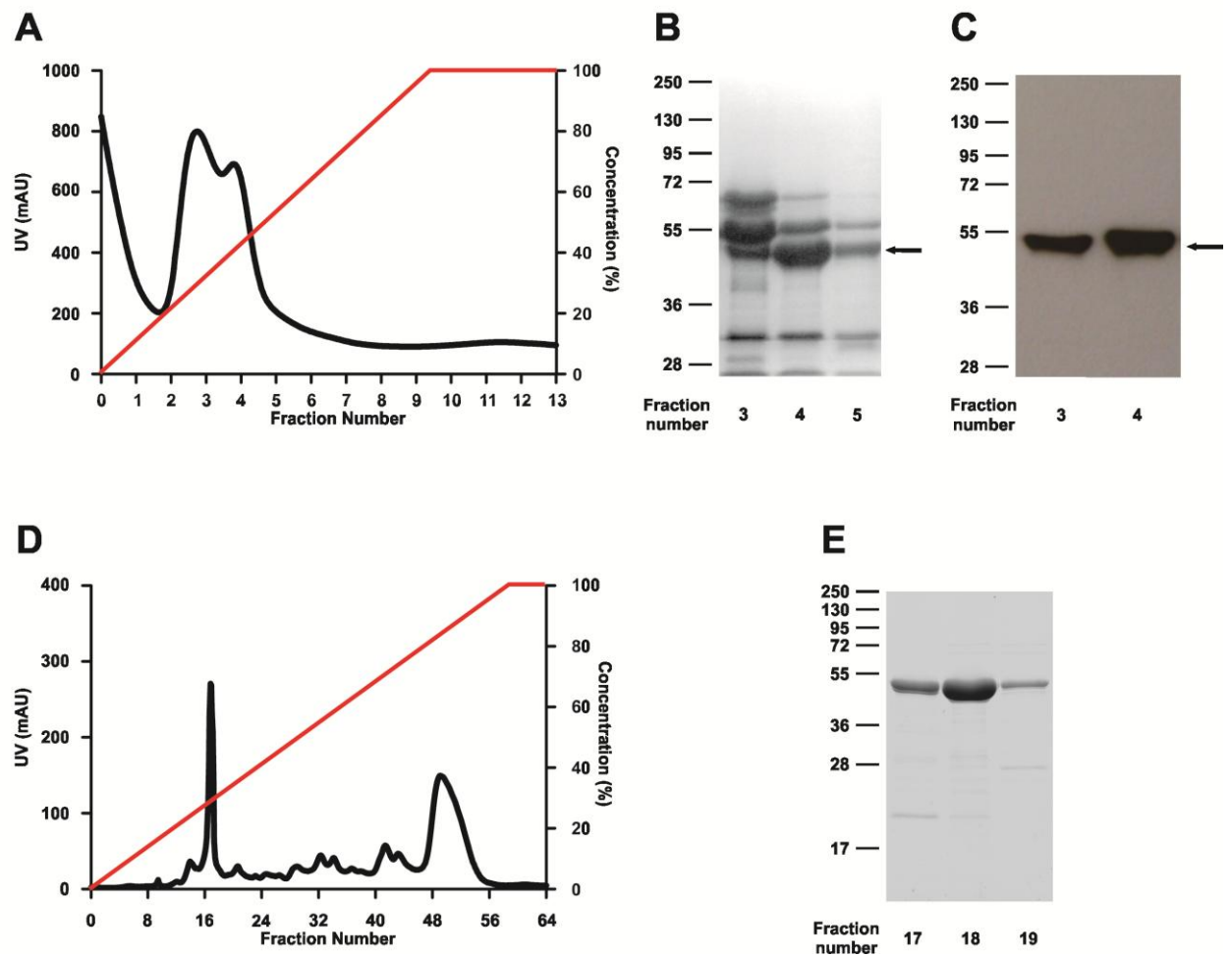


Figure 3.4. Purification of wild-type human α_2 -antiplasmin. **A)** Elution profile of WT α_2 -antiplasmin from HisTrap column. Protein absorbance is in mAU (black lines) and the percentage of HisTrap Buffer B (red). 1mL fractions were collected and numbered accordingly. **B)** The peak fractions from nickel affinity chromatography were analysed on a Coomassie stained 12.5% SDS-PAGE. Arrow indicates WT α_2 -antiplasmin. **C)** Fractions 3 and 4 from HisTrap purification analysed by Western blot using anti-His antibody. **D)** Elution profile of WT α_2 -antiplasmin from MonoQ column. Protein absorbance is shown in mAU (black) and the percentage of MonoQ Buffer B (red). 500 μ L fractions were collected and numbered accordingly. **E)** Peak fractions of anion affinity purification analysed on a Coomassie stained 12.5% SDS-PAGE. Molecular weight markers are in kDa.

Figure 3.4.
Purification of wild-type human α_2 -antiplasmin



This page has been intentionally left blank.

3.3.4 Recombinant Human α_2 -antiplasmin Variants Expression and Purification

This section describes the large scale purification of N- and/or C-terminally truncated (N Δ , C Δ and N Δ C Δ) proteins, single Lys to Arg mutant (K464R), progressive Lys to Ala mutations (K448A/K464A, K441A/K448A/K464A, K434A/K441A/K448A/K464A, K427A/K434A/K441A/K448A/K464A and K427A/K434A/K441A/K448A/K464WT) and shortening of the C-terminus by 15 amino acids (L449 Δ and K448A/L449 Δ). Purification of single Lys to Ala (K448A and K464A) and truncated (C Δ) α_2 -antiplasmin has been previously described (Lu, 2008; Lu et al., 2011). As described in section 3.3.3, purification of α_2 -antiplasmin is a two-step process which involves: i) Nickel affinity chromatography (HisTrap) and ii) Anion exchange chromatography (MonoQ).

N- and/or C-terminally truncated α_2 -antiplasmin

N Δ , C Δ and N Δ C Δ proteins were generated as soluble proteins in the *E.coli* expression system. A single peak was observed after nickel affinity purification of N Δ α_2 -antiplasmin (Figure 3.5A). Peak fractions were analysed on a Coomassie stained 12.5% SDS-PAGE which showed a dominant band at ~48kDa, corresponding to the predicted molecular weight mass of N Δ (Figure 3.5B). Double peaks were observed for the nickel affinity purification of both C Δ (Figure 3.5C) and N Δ C Δ (Figure 3.5E). Analysis of peak fractions on Coomassie stained SDS-PAGE showed that a protein band corresponding to the MW was observed at ~45kDa for C Δ (Figure 3.5D) and ~40kDa for N Δ C Δ (Figure 3.5F) as indicated by the black arrows.

Second stage purification was performed on the anion exchange column to purify N Δ (Figure 3.6A), C Δ (Figure 3.6C) and N Δ C Δ (Figure 3.6E) to homogeneity. Multiple peaks were observed on the MonoQ purification of N Δ C Δ (Figure 3.6E) when compared to the chromatograms of N Δ and C Δ . This suggests that protein expression for N Δ C Δ α_2 -antiplasmin were low and dominated by bacterial proteins. Nevertheless, peak fractions were analysed on a Coomassie stained SDS-PAGE and revealed that a dominant protein band corresponding to the predicted MW was observed at ~48kDa for N Δ (Figure 3.6B), ~45kDa for C Δ (Figure 3.6D) and ~40kDa for N Δ C Δ (Figure 3.6F). Protein yield for N Δ and C Δ were approximately 0.3mg per litre of culture, whereas the yield for N Δ C Δ was 0.1mg/L.

Figure 3.5. Nickel affinity chromatography of N- or/and C- terminally truncated human α_2 -antiplasmin. **A)** Elution profile of N Δ . **B)** Peak fractions from N Δ purification were analysed on Coomassie stained 12.5% SDS-PAGE. **C)** Elution profile of C Δ . **D)** Peak fractions from C Δ purification were analysed on Coomassie stained 12.5% SDS-PAGE. **E)** Elution profiles of N Δ C Δ . **F)** Peak fractions of N Δ C Δ were analysed on Coomassie stained 12.5% SDS-PAGE. Elution profiles show protein absorbance in mAU (black lines) and the percentage of HisTrap Buffer B (red). 1mL fractions were collected and numbered accordingly. Arrow indicates recombinant protein of interest. Molecular weight markers are in kDa.

Figure 3.5.
Nickel affinity chromatography of N- or/and C- terminally truncated human α_2 -antiplasmin

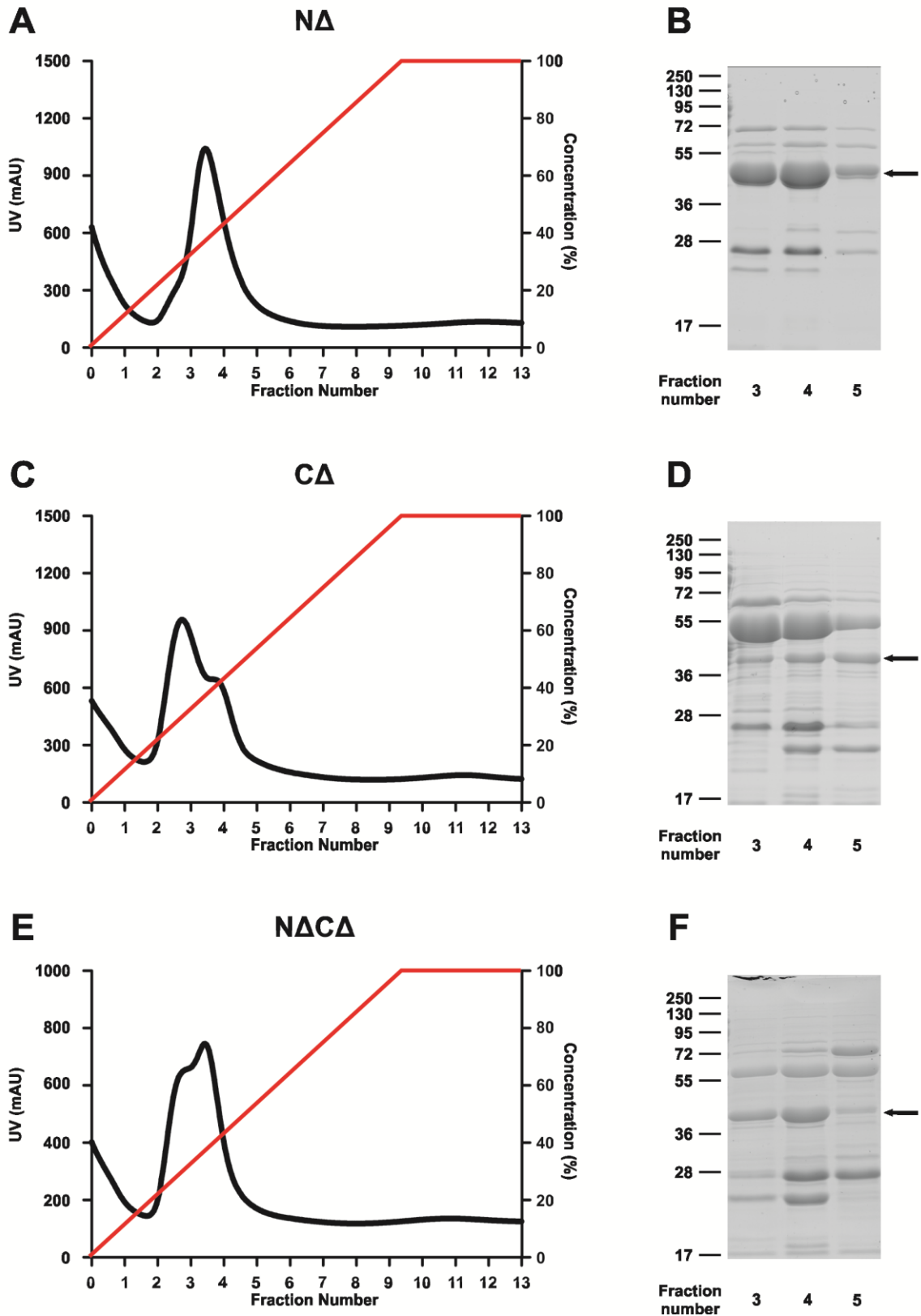
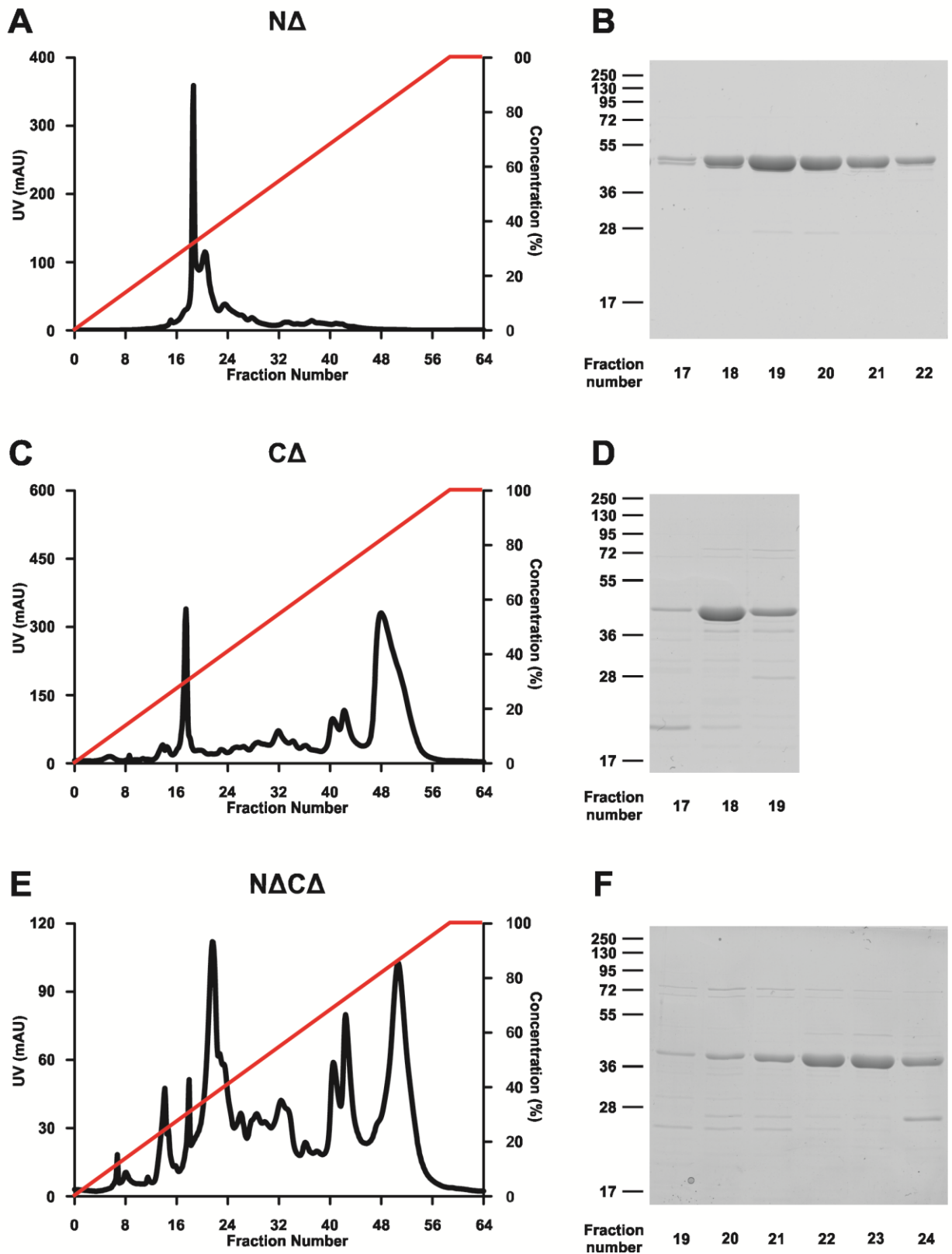


Figure 3.6. Anion exchange chromatography of N- or/and C- terminally truncated human α_2 -antiplasmin. **A)** Elution profile of N Δ . **B)** Peak fractions from N Δ purification were analysed on Coomassie stained 12.5% SDS-PAGE. **C)** Elution profile of C Δ . **D)** Peak fractions from C Δ purification were analysed on Coomassie stained 12.5% SDS-PAGE. **E)** Elution profiles of N Δ C Δ . **F)** Peak fractions of N Δ C Δ were analysed on Coomassie stained 12.5% SDS-PAGE. Elution profiles show protein absorbance in mAU (black lines) and the percentage of MonoQ Buffer B (red). 500 μ L fractions were collected and numbered accordingly. Molecular weight markers are in kDa.

Figure 3.6.
Anion exchange chromatography of N- or/and C- terminally truncated human α_2 -antiplasmin



Single Lys to Arg mutation at position 464 of α_2 -antiplasmin

Soluble protein obtained from K464R expression was first purified on a nickel affinity purification column. The chromatogram revealed that double peaks were obtained from the purification (Figure 3.7A). Analysis of the peak fractions revealed that the protein of interest was eluted in the second peak (fractions 5-7) when analysed on a Coomassie stained SDS-PAGE. A protein band was observed at ~55kDa which corresponds to the predicted MW of K464R (Figure 3.7B). A second purification on an anion exchange column was performed to separate the protein of interest to homogeneity. A single peak was observed on the chromatogram (Figure 3.7C) and analysis of the peak fractions on a Coomassie stained SDS-PAGE revealed a dominant protein band at the molecular weight marker (~55kDa) which corresponds to K464R (Figure 3.7D). Protein yield for K464R was 0.4mg per litre of culture.

Progressive Lys to Ala mutation within the C-terminus of α_2 -antiplasmin

Progressive Lys to Ala α_2 -antiplasmin mutants (K448A/K464A, K441A/K448A/K464A, K434A/K441A/K448A/K464A, and K427A/K434A/K441A/K448A/K464WT) were first purified on the nickel affinity column. Double peaks were obtained from purification of these mutants (K448A/K464A – Figure 3.8A; K441A/K448A/K464A – Figure 3.8C; K434A/K441A/K448A/K464A – Figure 3.8E); K427A/K434A/K441A/K448A/K464WT – Figure 3.8G). Analysis of peak fractions on a Coomassie stained SDS-PAGE revealed that protein of interest was eluted in the second peak (fractions 3-5). Multiple Lys to Ala mutants showed a band at ~50kDa which corresponds to the predicted MW of the protein (K448A/K464A – Figure 3.8B; K441A/K448A/K464A – Figure 3.8D; K434A/K441A/K448A/K464A – Figure 3.8F; K427A/K434A/K441A/K448A/K464WT – Figure 3.8H).

To further purify the protein of interest and to remove contaminating protein, peak fractions were pooled and prepared for second stage purification on an anion exchange column. Elution profile for K448A/K464A (Figure 3.9A), K441A/K448A/K464A (Figure 3.9C) and K434A/K441A/K448A/K464A (Figure 3.9E) produced a single dominant peak. Chromatogram of K427A/K434A/K441A/K448A/K464A showed a double peak (Figure 3.9G). Analysis of peak fractions on a Coomassie stained SDS-PAGE revealed a dominant band at ~50kDa which corresponds to the predicted MW of the protein (K448A/K464A – Figure 3.9B; K441A/K448A/K464A – Figure 3.9D; K434A/K441A/K448A/K464A – Figure 3.9F). A double band was observed at fraction 19 of K448A/K464A and was therefore excluded from the protein pool (Figure 3.9B). Analysis of fractions eluted from K427A/K434A/K441A/K448A/K464A purification revealed that the second peak contained the protein of interest (Figure 3.9H). Protein yields for multiple Lys to Ala mutants were between 0.2 and 0.4mg per litre of culture.

A mutant containing five Lys to Ala substitution (K427A/K434A/K441A/K448A/K464A) was also generated, expressed and purified as described above. Nickel affinity purification revealed that the protein was abundantly produced as seen on the chromatogram (Figure 3.12A) and its corresponding Coomassie stained SDS-PAGE (Figure 3.12B). A single peak was observed when the protein was further purified on the anion affinity column (Figure 3.12C), however when the peak fractions were analysed on a Coomassie stained 12.5% SDS-PAGE, two protein bands at similar molecular weight was seen (Figure 3.12D). Further analysis of this two bands were analysed on Western blot to detect the presence of a full-length C-terminus (Figure 3.12E). The membrane was probed with anti-sheepC peptide where this antibody binds to a specific region of the C-terminus with the sequence corresponding to 'LFGPDLKLVPPMEEDYPQFGSPK'. It is observed that only the protein with a slightly higher molecular weight reacted to this antibody. Absence of an immunoreactive band in the second band demonstrates that around 40% of the purified protein does not contain an intact C-terminus. From this evidence, K427A/K434A/K441A/K448A/K464A will be omitted from further kinetic and binding studies.

15 amino acid truncation of the C-terminus of α_2 -antiplasmin

L449 Δ (Figure 3.10A) and K448A/L449 Δ (Figure 3.10C) were purified on nickel affinity column and two peak fractions were observed on the chromatogram. Analysis on a Coomassie stained SDS-PAGE revealed that the second peak contained the protein of interest which appears as a band at ~50kDa (L449 Δ – Figure 3.10B; K448A/L449 Δ – Figure 3.10D). Second stage purification on an anion exchange column was performed to remove contaminating proteins and to purify L449 Δ and K448A/L449 Δ to homogeneity. A single dominant peak was observed on the chromatogram (L449 Δ – Figure 3.11A; K448A/L449 Δ – Figure 3.11C). Further analysis of peak fraction on a Coomassie stained SDS-PAGE revealed a single protein band at ~50kDa which corresponds with the predicted MW of the protein of interest (L449 Δ – Figure 3.11B; K448A/L449 Δ – Figure 3.11D). Protein yield for both L449 Δ and K448A/L449 Δ were ~0.3mg per litre of culture.

Soluble mutant recombinant α_2 -antiplasmin proteins, with the exception of K427A/K434A/K441A/K448A/K464A, were able to be expressed and purified under the same condition as WT α_2 -antiplasmin with minor variation in expression levels. The yield of protein obtained ranges from 0.1-0.4mg per litre of culture.

Figure 3.7. Nickel affinity and anion exchange chromatography of K464R. **A)** Elution profile of K464R from nickel affinity purification. **B)** Peak fractions from HisTrap purification of K464R analysed on Coomassie stained 12.5% SDS-PAGE. **C)** Elution profile of K464R from anion exchange chromatography. **D)** Peak fractions from MonoQ purification of K464R analysed on Coomassie stained 12.5% SDS-PAGE. Arrow indicates recombinant protein of interest. Molecular weight markers are in kDa.

Figure 3.7.
Nickel affinity and anion exchange chromatography of K464R

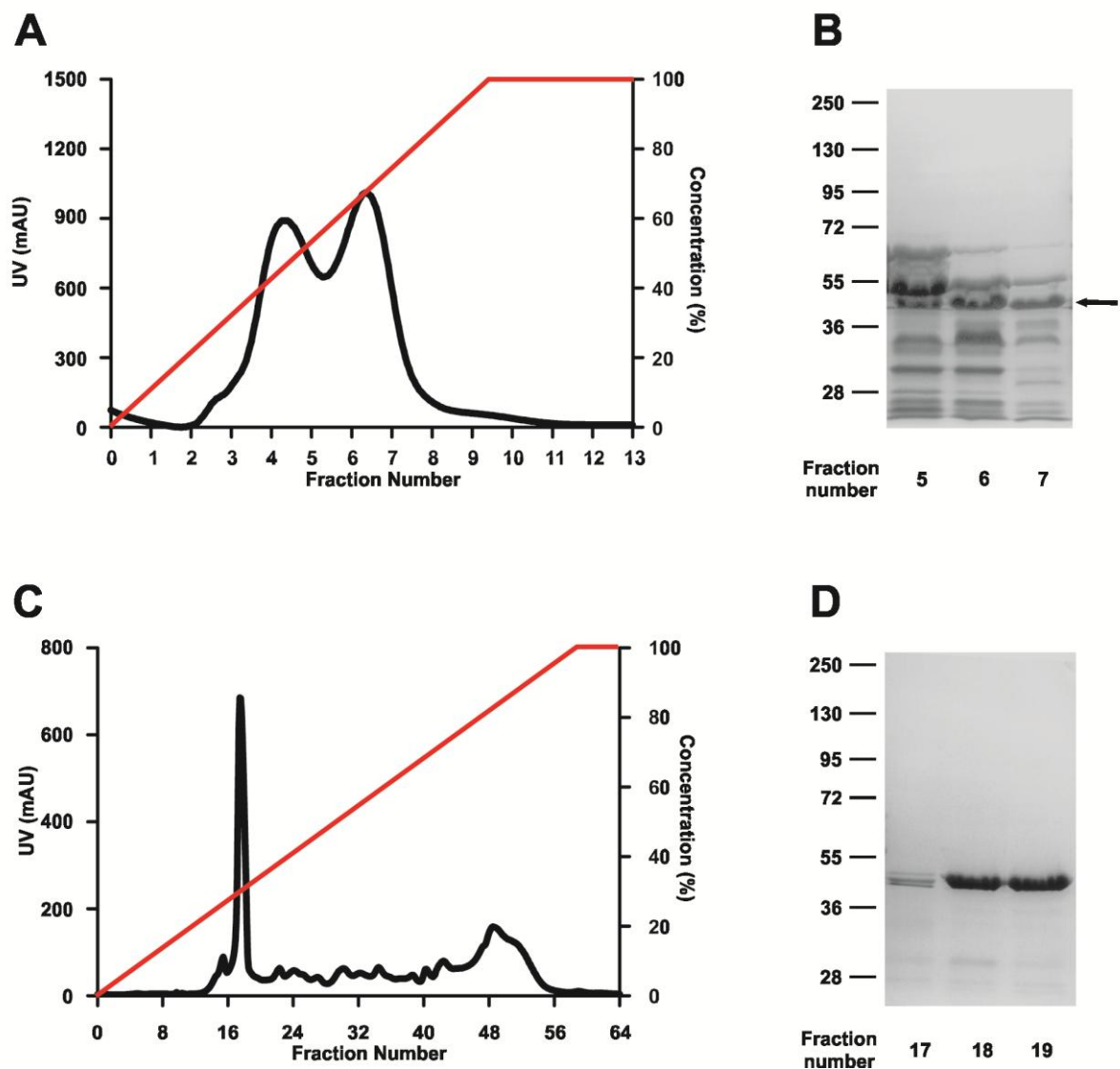


Figure 3.8. Nickel affinity chromatography of multiple C-terminal Lys to Ala mutations of human α_2 -antiplasmin. **A)** Elution profile of K448A/K464A. **B)** Peak fractions from K448A/K464A purification were analysed on Coomassie stained 12.5% SDS-PAGE. **C)** Elution profile of K441A/K448A/K464A. **D)** Peak fractions from K441A/K448A/K464A purification were analysed on Coomassie stained 12.5% SDS-PAGE. **E)** Elution profiles of K434A/K441A/K448A/K464A. **F)** Peak fractions of K434A/K441A/K448A/K464A were analysed on Coomassie stained 12.5% SDS-PAGE. **G)** Elution profile of K427A/K434A/K441A/K448A/K464WT. **H)** Peak fractions of K427A/K434A/K441A/K448A/K464WT were analysed on Coomassie stained 12.5% SDS-PAGE. Elution profiles show protein absorbance in mAU (black lines) and the percentage of HisTrap Buffer B (red). 1mL fractions were collected and numbered accordingly. Arrow indicates recombinant protein of interest. Molecular weight markers are in kDa.

Figure 3.8.
Nickel affinity chromatography of multiple C-terminal Lys to Ala
mutations of human α_2 -antiplasmin

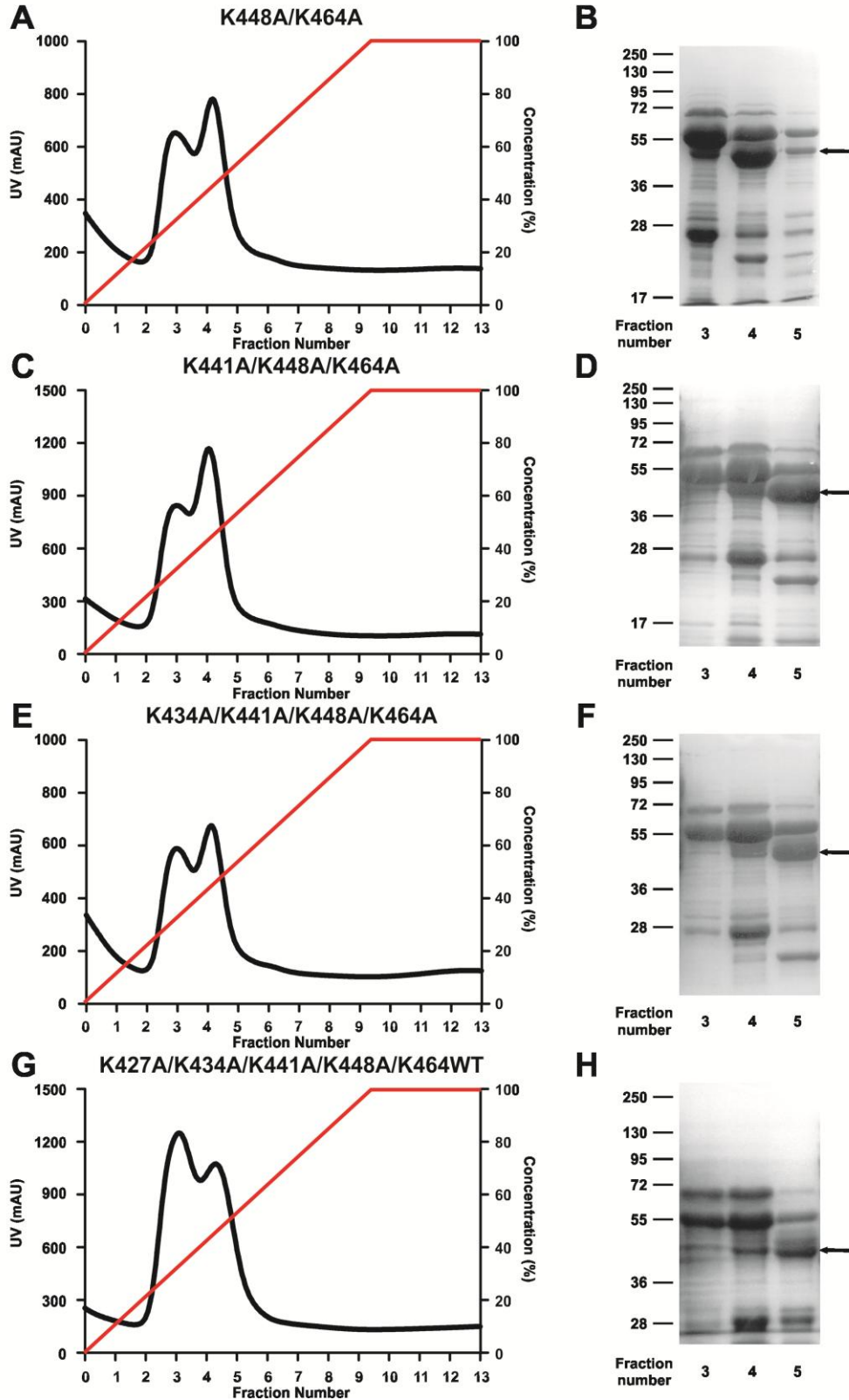


Figure 3.9. Anion exchange chromatography of multiple C-terminal Lys to Ala mutations of human α_2 -antiplasmin. **A)** Elution profile of K448A/K464A. **B)** Peak fractions from K448A/K464A purification were analysed on Coomassie stained 12.5% SDS-PAGE. **C)** Elution profile of K441A/K448A/K464A. **D)** Peak fractions from K441A/K448A/K464A purification were analysed on Coomassie stained 12.5% SDS-PAGE. **E)** Elution profiles of K434A/K441A/K448A/K464A. **F)** Peak fractions of K434A/K441A/K448A/K464A were analysed on Coomassie stained 12.5% SDS-PAGE. **G)** Elution profile of K427A/K434A/K441A/K448A/K464WT. **H)** Peak fractions of K427A/K434A/K441A/K448A/K464WT were analysed on Coomassie stained 12.5% SDS-PAGE. Elution profiles show protein absorbance in mAU (black lines) and the percentage of MonoQ Buffer B (red). 500 μ L fractions were collected and numbered accordingly. Molecular weight markers are in kDa.

Figure 3.9.
Anion exchange chromatography of multiple C-terminal Lys to Ala mutations of human α_2 -antiplasmin

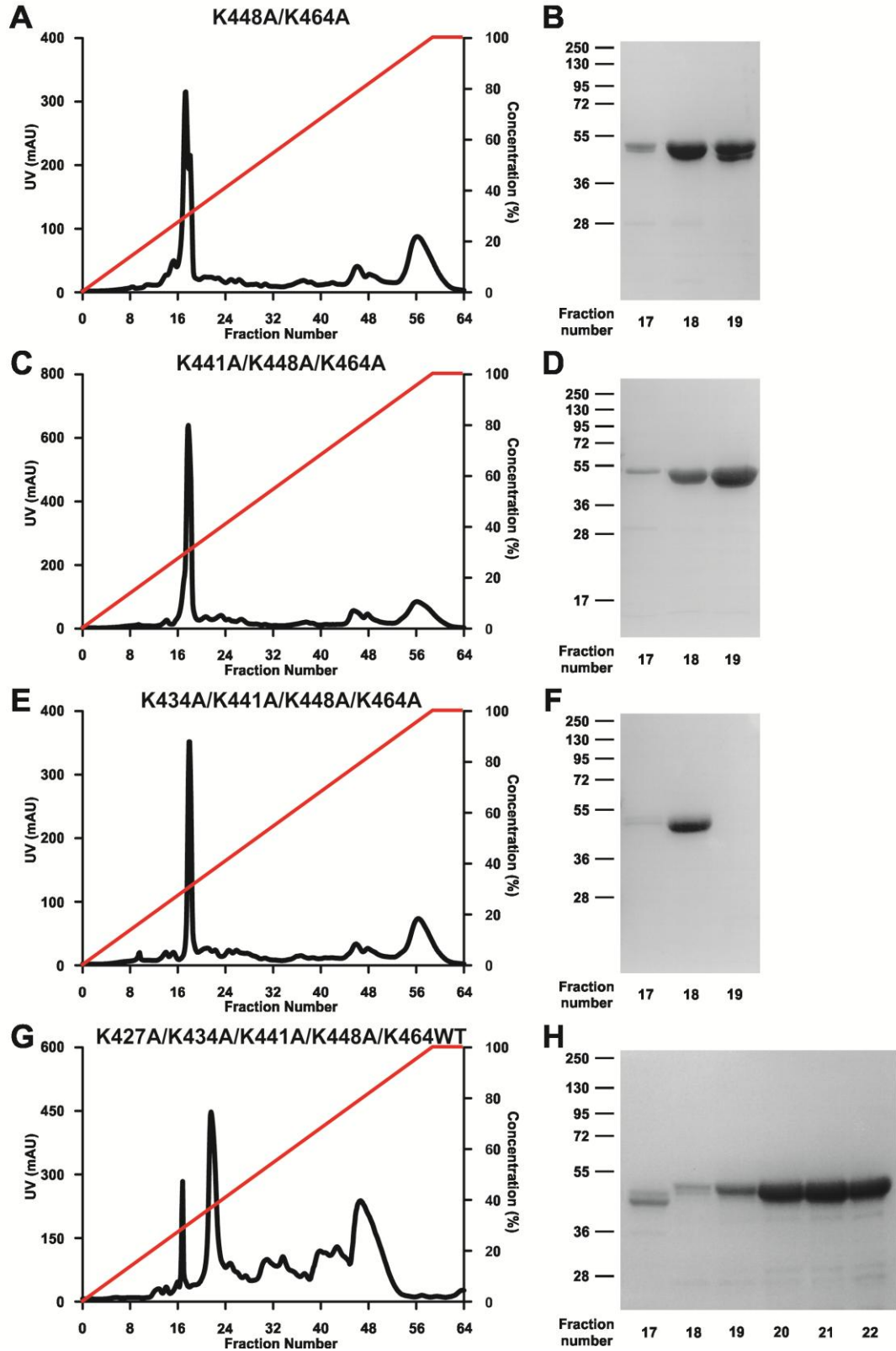


Figure 3.10. Nickel affinity chromatography of 15 amino acid deletion of the C-terminus of human α_2 -antiplasmin. A) Elution profile of L449 Δ . **B)** Peak fractions from L448 Δ purification were analysed on Coomassie stained 12.5% SDS-PAGE. **C)** Elution profiles of K448A/L449 Δ . **D)** Peak fractions of K448A/L449 Δ were analysed on Coomassie stained 12.5% SDS-PAGE. Elution profiles show protein absorbance in mAU (black lines) and the percentage of HisTrap Buffer B (red). 1mL fractions were collected and numbered accordingly. Arrow indicates recombinant protein of interest. Molecular weight markers are in kDa.

Figure 3.10.
Nickel affinity chromatography of 15 amino acid deletion of the C-terminus of human α_2 -antiplasmin

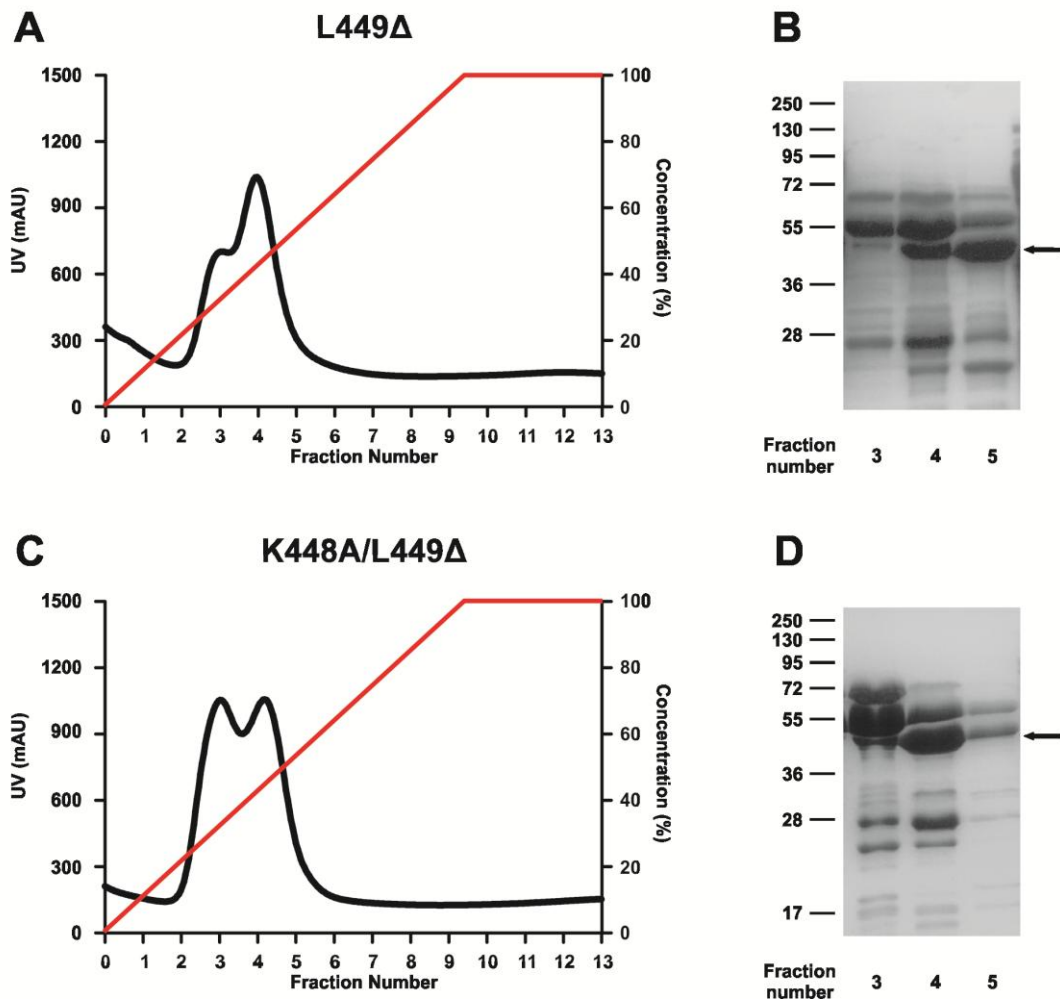


Figure 3.11. Anion exchange chromatography of 15 amino acid deletion of the C-terminus of human α_2 -antiplasmin. **A)** Elution profile of L449 Δ . **B)** Peak fractions from L448 Δ purification were analysed on Coomassie stained 12.5% SDS-PAGE. **C)** Elution profiles of K448A/L449 Δ . **D)** Peak fractions of K448A/L449 Δ were analysed on Coomassie stained 12.5% SDS-PAGE. Elution profiles show protein absorbance in mAU (black lines) and the percentage of MonoQ Buffer B (red). 500 μ L fractions were collected and numbered accordingly. Molecular weight markers are in kDa.

Figure 3.11.
Anion exchange chromatography of 15 amino acid deletion of the C-terminus of human α_2 -antiplasmin

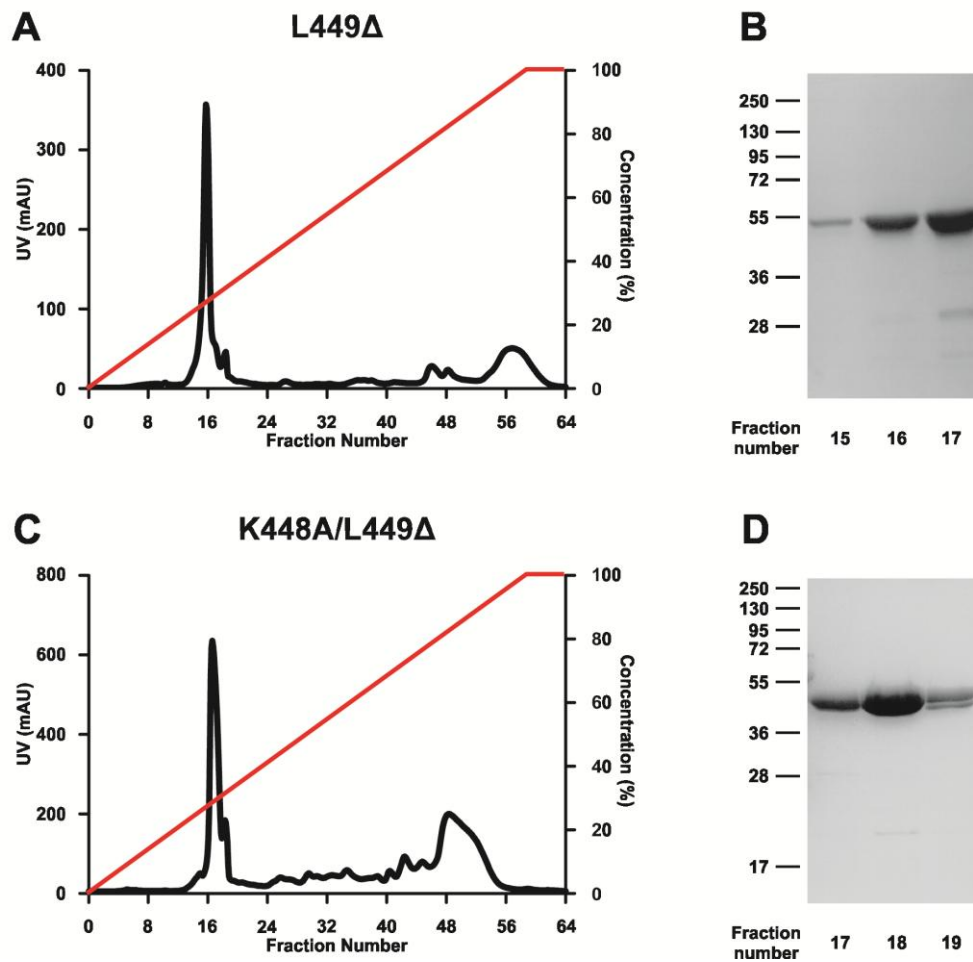
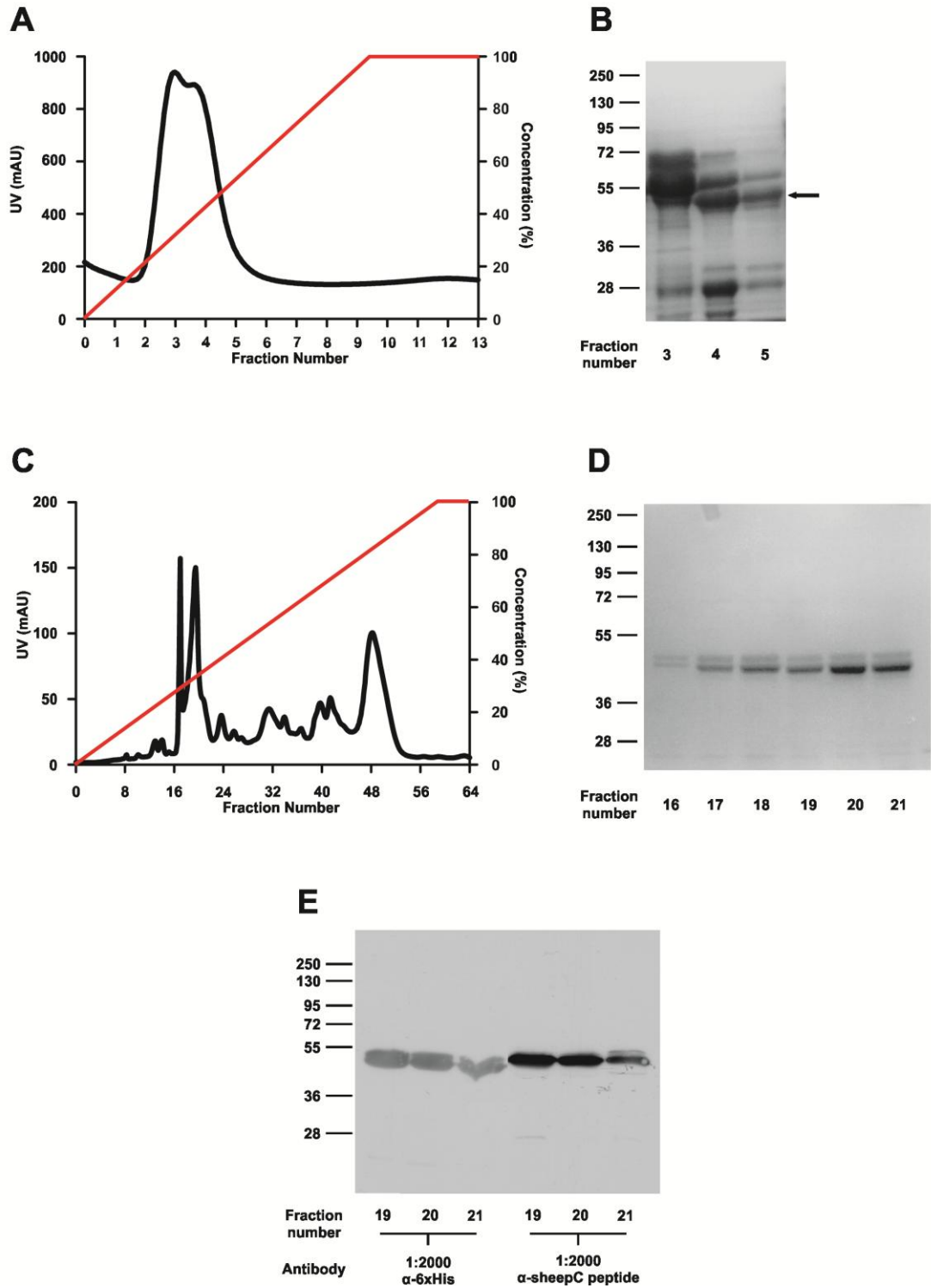


Figure 3.12. Purification of human α_2 -antiplasmin containing five Lys to Ala mutation in the C-terminus. **A)** Elution profile of K427A/K434A/K441A/K448A/K464A from HisTrap column. Protein absorbance is in mAU (black lines) and the percentage of HisTrap Buffer B (red). 1mL fractions were collected and numbered accordingly. **B)** Peak fractions of nickel purification analysed on a Coomassie stained 12.5% SDS-PAGE. Arrow indicates K427A/K434A/K441A/K448A/K464A. **C)** Elution profile of K427A/K434A/K441A/K448A/K464A α_2 -antiplasmin from MonoQ column. Protein absorbance is in mAU (black) and the percentage of MonoQ Buffer B (red). 500 μ L fractions were collected and numbered accordingly. **D)** Peak fractions of anion affinity purification analysed on a Coomassie stained 12.5% SDS-PAGE. **E)** Membrane probed with anti-6xHistidine (α -6xHis) and an antibody specific to the C-terminus of α_2 -antiplasmin (LFGPDLKLVPPMEEDYPQFGSPK) (α -sheepC peptide). Molecular weight markers are in kDa.

Figure 3.12.
Purification of human α_2 -antiplasmin containing five Lys to Ala mutation in the C-terminus



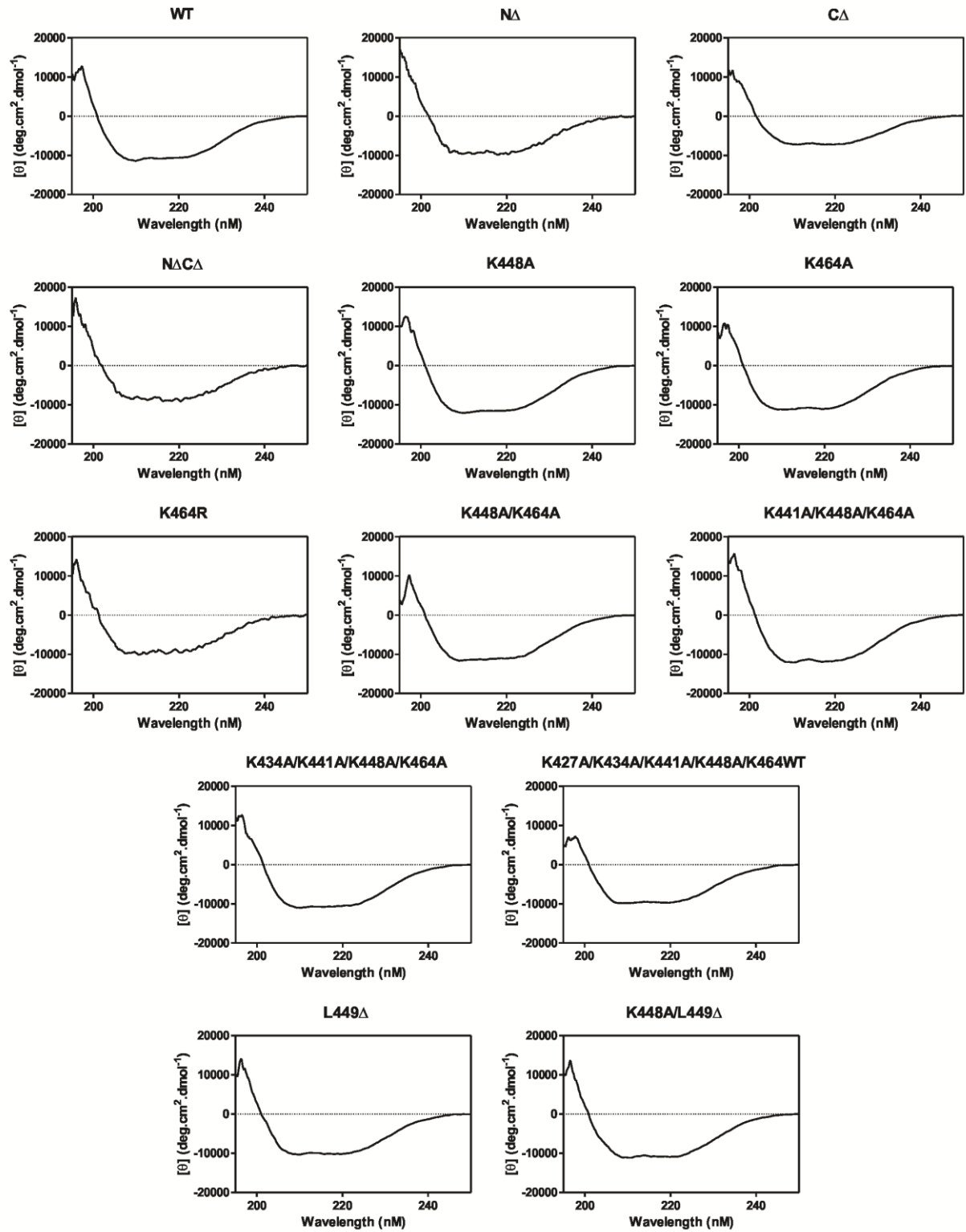
This page has been intentionally left blank.

3.3.5 Circular Dichroism Analysis of α_2 -antiplasmin

To ensure that recombinant WT and mutant α_2 -antiplasmin produced remained in their native conformation, all purified proteins were assessed by CD spectrometry. Mutant proteins produced CD spectra similar to WT α_2 -antiplasmin demonstrating that all recombinant proteins produced retained their native fold (Figure 3.13). Peak fractions for each of the recombinant protein were collected and used for further kinetic and binding studies which will be presented in Chapter 4.

Figure 3.13. Circular dichroism analysis of α_2 -antiplasmin. The CD spectrum of 200 μ g/mL recombinant α_2 -antiplasmin was determined from 195-250nm using a 0.1cm path length cuvette.

Figure 3.13.
Circular dichroism analysis of α_2 -antiplasmin



3.4 Discussion

α_2 -antiplasmin, the main inhibitor of plasmin, is present in the human circulation of 1 μ M (Wiman and Collen, 1977). The protein when compared to the other members of the serpin superfamily is unique due to the presence of the N- and C-terminal extensions. In circulation, the N- and C-terminus have been reported to undergo proteolytic modification resulting in different α_2 -antiplasmin isoforms (Lee et al., 2004). As such, purification of α_2 -antiplasmin from human plasma would result in isolation of multiple forms. A variety of expression protocols in different systems has been previously described (prokaryotic (Lee et al., 2000; Sumi et al., 1989), eukaryotic (Lee et al., 1999; Wang et al., 2003) and mammalian cell lines). In this chapter, a bacterial protein expression and purification system was chosen to produce recombinant α_2 -antiplasmin. Recombinant DNA technology allows the production of an array of mutant proteins which do not occur naturally in circulation which will add to our further understanding of the structure and function of the target protein.

Previous studies in our laboratory used murine α_2 -antiplasmin as human α_2 -antiplasmin expression and purification yielded low quantities of protein which were inadequate for crystallisation purposes (Sofian, 2009). During my honours year, the expression and purification for human α_2 -antiplasmin was optimised (Lu, 2008). In this study, WT and a range of mutant recombinant human α_2 -antiplasmin were designed, expressed, purified and characterised biochemically. The recombinant α_2 -antiplasmin protein produced was of the Asn-form, where 12 amino acids have been cleaved from the secreted form, with the addition of an N-terminal hexahistidine tag (His-tag) for purification purposes. Throughout this work, the numbering of α_2 -antiplasmin is based on the secreted Met-form of 464 amino acids. An N-terminally truncated (N Δ) α_2 -antiplasmin was produced where the start codon and His-tag were introduced at Cys⁴³. The C-terminally truncated (C Δ) α_2 -antiplasmin was generated whereby a STOP codon was introduced at Pro⁴¹⁴. A double truncation of N- and C-terminal extensions, where the serpin core remained intact, was also made (N Δ C Δ). The lysine residues (Lys⁴²⁷, Lys⁴³⁴, Lys⁴⁴¹, Lys⁴⁴⁸ and Lys⁴⁶⁴) within the C-terminus were mutated singularly (K464R) or progressively (K448A/K464A, K441A/K448A/K464A, K434A/K441A/K448A/K464A and K427A/K434A/K441A/K464WT). The C-terminus was shortened by 15 amino acids by the introduction of the stop codon at Leu⁴⁴⁹ (L449 Δ , K448A/L449 Δ).

All recombinant α_2 -antiplasmin were expressed in *Escherichia coli* as a soluble protein. Combinations of nickel affinity and anion exchange chromatography have successfully isolated the recombinant human α_2 -antiplasmin from contaminating bacterial proteins. Truncations of N- and C-terminal regions alone, and shortening of the C-terminus by 15 amino acids did not significantly alter protein expression levels. However, low protein expression was observed most prominently with the N Δ C Δ protein. As seen from the chromatogram from the anion

exchange chromatography step (Figure 3.9E), the peak fraction of interest only reached a maximum of 120mAU and was hard to identify as there were many other major peak fractions seen from the elution profile. The N Δ C Δ protein had undergone the most dramatic change considering both the N- and C-terminal extensions were removed when compared to full-length, N Δ , C Δ and the other α_2 -antiplasmin mutants (single and multiple Lys to Ala substitutions). The removal of both regions may have affected the stability of the protein and increased the insolubility of the protein in the bacterial expression system. Furthermore, Cys⁴³ have been removed in N-terminally truncated α_2 -antiplasmin proteins produced in this thesis. It has been shown that Cys⁴³ forms a disulphide bond with Cys¹¹⁶ and the removal of this may have altered α_2 -antiplasmin stability (Christensen et al., 1997). It is surprising that absence of the N- and C-terminus has an effect on the stability of the protein as the truncations made are consistent with other members of the serpin superfamily.

Abundant soluble proteins for all multiple Lys to Ala mutants except for the quintuple Lys to Ala mutant (K427A/K434A/K441A/K448A/K464WT) were obtained in this chapter. During second stage purification, it was observed that two species were present in the peak fraction. Further analysis by Western blot with an antibody specific to the final 23 amino acids of the C-terminal region revealed that ~60% of purified protein did not contain this region of the C-terminus (Figure 3.12E). Introduction of five Lys to Ala mutation may have increased the propensity of the protein being cleaved by bacterial proteases. Nevertheless, the majority of the desired recombinant α_2 -antiplasmin proteins were successfully produced with a final protein yield of between 0.1-0.4 mg per L of culture.

WT and mutant α_2 -antiplasmin were assessed by CD spectrometry. Mutant α_2 -antiplasmin proteins produced CD spectra similar to WT α_2 -antiplasmin, demonstrating that the mutant proteins retained their native fold. This result further corresponds with our kinetic analysis of the stoichiometry of inhibition between recombinant α_2 -antiplasmin and human plasmin described in Chapter 4.

3.5 Conclusion

This chapter describes a straightforward and practical method for obtaining abundant recombinant α_2 -antiplasmin in its native conformation. The method describes *Escherichia coli* as an effective expression system for the production of human α_2 -antiplasmin. Proteins are secreted in a soluble form therefore no solubilisation or refolding protocols were necessary. A variety of recombinant α_2 -antiplasmin proteins were successfully purified and will be further characterised by kinetic and affinity assays in the following chapter.

Chapter 4:

Contribution of conserved lysine residues in the α_2 -antiplasmin C-terminus to plasmin inhibition and binding

This page has been intentionally left blank.

4.1 Introduction

Prior to this work, it was poorly understood how the C-terminus accelerates binding to kringle domains of plasmin and which residues are involved. The C-terminus of human α_2 -antiplasmin contains six lysine residues, five of which are conserved between species (Lys⁴²⁷, Lys⁴³⁴, Lys⁴⁴¹, Lys⁴⁴⁸ and Lys⁴⁶⁴). These lysines are important in mediating the binding of the C-terminal region to kringle domains of plasmin(ogen) (Coughlin, 2005). A previous study showed that the antiplasmin/plasmin association was reduced when a synthetic peptide corresponding to the final 26 amino acids of the C-terminus blocked the association to plasmin, indicating that this region has high affinity for plasmin kringle domains (Hortin et al., 1988). Another study with microplasmin and full-length α_2 -antiplasmin showed a 30-60 reduction in association rate constant implicating the importance of C-terminal to kringle interaction in accelerating the inhibitory mechanism (Wiman et al., 1978). However, the relative importance assigned to the C-terminal lysine compared with other internal lysine residues differs in published studies. A group that studied the binding of kringle domains to C-terminal peptide containing Lys to Ala substitutions showed that the Lys⁴⁶⁴, the most C-terminal lysine, was the most important contributor to binding for plasmin kringle domains (Frank et al., 2003; Gerber et al., 2010). However, plasmin inhibition studies by Wang and colleagues indicated that Lys⁴⁴⁸ in full-length antiplasmin was most important in the interaction with plasmin (Wang et al., 2006; Wang et al., 2003).

In previous work in our laboratory, single Lys to Ala mutations were introduced at positions 427, 434, 441, 448 and 464 along the C-terminus of full-length human α_2 -antiplasmin (Lu, 2008). Plasmin inhibition rate (k_a) for each of the recombinant α_2 -antiplasmin was measured and it was noted that mutants containing single-site substitution at Lys⁴²⁷, Lys⁴³⁴ and Lys⁴⁴¹ had significant decrease in plasmin inhibition rate when compared with wild-type (WT) antiplasmin (Table 4.1 and Figure 4.1). Mutation at Lys⁴⁴⁸ and Lys⁴⁶⁴ showed the most significant decrease in plasmin inhibition rate of 2.7-fold and 4.9-fold respectively. From this observation, it was concluded that Lys⁴⁶⁴ is the most important lysine residue in the C-terminus. A C-terminally truncated mutant of antiplasmin was also generated, and showed the most impressive decrease in plasmin inhibition of ~40-folds when compare to all other recombinant antiplasmin (Table 4.1 and Figure 4.1). Even though our previous data indicate that Lys⁴⁶⁴ is the most important lysine, its affect when mutated (K464A, $k_a = 1.0 \times 10^7 \text{ M}^{-1}\text{s}^{-1}$) does not correspond to the plasmin inhibition rate when the whole C-terminus is absent (C Δ , $k_a = 9.2 \times 10^5 \text{ M}^{-1}\text{s}^{-1}$). Perhaps all the lysine residues are collectively important or there are other residues within the C-terminus which are mediating the interaction with plasmin.

Therefore, to fully understand the role of the C-terminal lysine residues in the interaction with kringle domains of plasmin, this chapter describes the systematic and sequential study on

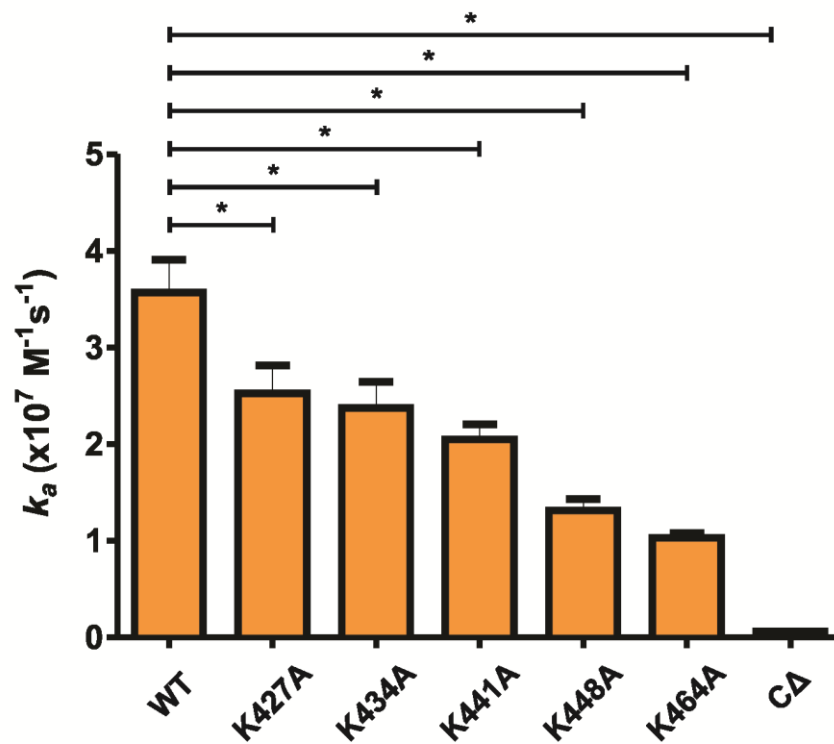
the mutagenesis of multiple Lys to Ala in the C-terminus of human α_2 -antiplasmin (Lys⁴²⁷, Lys⁴³⁴, Lys⁴⁴¹, Lys⁴⁴⁸ and Lys⁴⁶⁴). Plasmin inhibition rate (k_a) for full-length human α_2 -antiplasmin and intact plasmin were investigated. Truncations of N- and/or C-terminal regions of α_2 -antiplasmin were also generated. The N-terminal region of α_2 -antiplasmin has not been implicated in the interaction with the plasmin molecule. Therefore to confirm this, plasmin inhibition rates of these truncations were determined and compared with wild-type α_2 -antiplasmin. The primary hypothesis being tested in this chapter is that lysine residues at the extreme as well as internally along the C-terminal extension of α_2 -antiplasmin accelerate the inhibition of plasmin. The importance of the C-terminus was further evaluated by shortening the α_2 -antiplasmin molecule by 15 amino acids and comparing its plasmin inhibition rate with wild-type α_2 -antiplasmin. Furthermore, the binding affinity (K_D) of wild-type α_2 -antiplasmin and various mutants for active site-blocked plasmin were also carried out. A sensitive binding assay using surface plasmon resonance (SPR) was established to measure the binding affinity between the two molecules. The results presented in this chapter, with some minor exclusions, was recently published in a peer reviewed journal article and is attached at the end of this thesis (Appendix 10.2) (Lu et al., 2011).

Table 4.1. Stoichiometry of inhibition (S) and plasmin inhibition rate (k_a) of single Lys to Ala mutation in the C-terminus of α_2 -antiplasmin versus WT α_2 -antiplasmin.

Recombinant α_2 -antiplasmin	$S \pm SE$ (n=3)	$k_a \pm SE$ ($M^{-1}s^{-1}$) (n=3)
WT	1.03 ± 0.02	$3.68 \pm 0.34 \times 10^7$
K427A	0.94 ± 0.02	$2.38 \pm 0.29 \times 10^7$
K434A	0.99 ± 0.01	$2.35 \pm 0.28 \times 10^7$
K441A	1.03 ± 0.02	$2.11 \pm 0.16 \times 10^7$
K448A	0.99 ± 0.003	$1.31 \pm 0.12 \times 10^7$
K464A	0.98 ± 0.003	$1.01 \pm 0.05 \times 10^7$
C Δ	1.49 ± 0.02	$9.22 \pm 0.24 \times 10^5$

Figure 4.1. Comparison of plasmin inhibition rate (k_a) between wild-type and single Lys to Ala mutation in C-terminus of α_2 -antiplasmin. The k_a for plasmin and α_2 -antiplasmin variants were measured as described in Section 4.2.3.1. Statistics were assessed by one-way ANOVA with Newman-Keuls post-hoc correction. “*” refers to statistically significant data of $p < 0.05$. Each of the protein is represented by the mean ($n=3$) with error bars representing \pm SE (Lu et al., 2011).

Figure 4.1.
Comparison of plasmin inhibition rate (k_a) between WT and single Lys to Ala mutation in the C-terminus of α_2 -antiplasmin



4.2 Methods

4.2.1 Enzyme-Inhibitor Kinetics

All kinetic assay reactions were made up in Kinetic buffer (20mM Tris-HCl pH8.0, 150mM NaCl and 0.01% Tween-20) in a 1% bovine serum albumin (BSA) coated PerkinElmer Optiplate. Fluorogenic substrate, H-Ala-Phe-Lys-7-amino-4-methylcoumarin (AMC) (Bachem, Bubendorf, Switzerland), was used to measure plasmin activity. Fluorescence was measured at 355/460nm at 25°C using a FLUOstar Optima plate reader (BMG Labtech, Victoria, Australia). All kinetic reactions were performed in triplicates (Appendix 10.3) (Horvath et al., 2011).

4.2.2 Stoichiometry of Inhibition (*SI*)

The stoichiometry of inhibition (*SI*) of all recombinant human α_2 -antiplasmin was determined by titration with human plasmin (Hematologic Technologies, Essex Junction, VT). 8nM of human plasmin was incubated with wild-type (WT) and mutant α_2 -antiplasmin at various concentration (2-16nM) for 1 hr at 37°C. After incubation, the reaction was diluted 1/8 (final plasmin concentration of 1nM) and residual plasmin activity was assayed in the presence of 200 μ M (final concentration) fluorogenic substrate, AMC. Each experiment was performed in duplicates and the *SI* for each recombinant α_2 -antiplasmin was determined by averaging three separate experiments. Fluorescence signal was detected over 20 min at 355/460nm, and the resulting plots were analysed using linear regression analysis on GraphPad Prism 5 software. The rate of fluorescence increase is proportional to residual plasmin activity. This value was then plotted against the serpin:protease ratio. The points were analysed using linear regression and the line was extrapolated to the x-intercept which represents the serpin:protease ratio which results in zero protease activity.

4.2.3 Rates of Inhibition (k_a)

4.2.3.1 Continuous Method

The rate of plasmin inhibition by recombinant α_2 -antiplasmin was determined using the continuous or progress curve method. Human plasmin (0.5nM) was reacted with various concentrations of recombinant WT or mutant α_2 -antiplasmin (1-40nM), in the presence of 1mM (final concentration) of fluorogenic AMC substrate. The increase in fluorescence resulting from substrate hydrolysis was continuously measured for 1 hr. The raw data was fitted using non-linear regression in GraphPad Prism 5 software (Equation 4.1) where *P* is the concentration

of product at time t , V_0 is the initial velocity, and k_{obs} is the apparent first-order rate constant (Schechter and Plotnick, 2004).

Equation 4.1:

$$P = \frac{V_0}{k_{obs}} \times [1 - e^{(-k_{obs}t)}]$$

The k_{obs} value for each antiplasmin concentration was calculated by Equation 4.1. Each k_{obs} value was plotted against the respective antiplasmin concentration. Linear regression analysis was performed to obtain the uncorrected rate of inhibition, k' . Equation 4.2 was used to account for fluorogenic substrate competition, where the rate of inhibition was adjusted with the SI , substrate concentration ($[S]$), and Michaelis constant ($K_m = 150\mu\text{M}$) of the substrate to give the second-order rate constant, k_a .

Equation 4.2:

$$k_a = k' \times \left(1 + \frac{[S]}{K_M}\right) \times SI$$

4.2.3.2 Discontinuous Method

5-20nM of recombinant α_2 -antiplasmin (K434A/K441A/K448A/K464A, C Δ and N Δ C Δ) and 0.5nM human plasmin were incubated at different time points (0-5 mins) in a 96 well PerkinElmer Optiplate. At the end of the incubation period, residual protease activity was determined by adding the fluorogenic AMC substrate at a final concentration of 200 μM . Fluorescence emission was monitored for 20 min.

The observed pseudo first-order rate constant (k_{obs}) were determined from the slope of the linear plot of the natural log of residual protease activity versus time (seconds). The calculated k_{obs} were then plotted against serpin concentration. This slope represents the second-order rate constant (k') which was then corrected by multiplying the value with the SI to obtain the rate of inhibition (k_a).

4.2.4 Binding Affinity (K_D)

4.2.4.1 Preparation of Active Site-Blocked Plasmin

Active site-blocked plasmin (PlmCMK) was produced by incubating human plasmin with a 1000-fold molar excess of D-Val-Phe-Lys chloromethyl ketone (Calbiochem) at 37°C for 1 hr. Active site-blocked plasmin was then dialysed overnight at 4°C in Running buffer (0.01M HEPES pH7.4, 0.15M NaCl, 50µM EDTA and 0.05% surfactant P20 (GE Healthcare)). To confirm that the active site was completely blocked, the activity of active site-blocked plasmin was checked against active plasmin in the presence of 200µM fluorogenic AMC substrate.

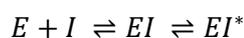
4.2.4.2 Surface Plasmon Resonance (SPR) to measure Binding Affinity (K_D)

The interactions between active site-blocked plasmin and various recombinant α_2 -antiplasmin (WT, K448A, K464A, K464R, K448A/K464A, K441A/K448A/K464A, K434A/K441A/K448A/K464A, K427A/K434A/K441A/K448A/K464WT, L449 Δ , K448A/L449 Δ , CA, NA) were determined via surface plasmon resonance (SPR) using the BIAcore T100 system (GE Healthcare).

To measure the binding affinity and rate of plasmin association of α_2 -antiplasmin to active site-blocked plasmin, hexahistidine-tagged WT or mutant α_2 -antiplasmin were immobilised on the nitrilotriacetic acid (NTA) surface of a NTA chip (GE Healthcare) according to manufacturer's instructions. All experiments were carried out in running buffer at a flow rate of 10µL/min and performed in triplicates. The NTA surface was activated by injecting 500µM NiCl₂ for 1 min. 20nM of WT or mutant α_2 -antiplasmin was immobilised (ligand) onto the surface on one flow cell for 1 min. A flow cell containing no immobilised α_2 -antiplasmin was used to account for nonspecific binding to the NTA surface. Six different concentrations of active site-blocked plasmin (analyte) were injected for 1 min of association time, followed by 10 min of dissociation time. The concentration range of active site-blocked plasmin (2-120nM) was adjusted for each α_2 -antiplasmin variant. After each concentration cycle, the NTA surface was completely stripped with Regeneration buffer (0.01M HEPES pH7.4, 0.15M NaCl, 0.35M EDTA and 0.05% surfactant P20) at a flow rate of 30µL/min for 2 min. NTA surface activation and α_2 -antiplasmin immobilisation were performed at each active site-blocked plasmin concentration. The injection needle was cleaned with an extra wash of Running buffer after each subsequent step.

Real-time binding curves were monitored on a sensorgram as resonance units (RU) over time. All experiments were conducted with a blank flow cell (with no immobilised ligand) running in parallel and subjected under the same running conditions. The final sensorgram produced was corrected with the blank flow cell to account for any non-specific binding. For kinetic and binding affinity analysis of recombinant α_2 -antiplasmin with active site-blocked plasmin, the two-state reaction model provided in the BIAcoreT100 evaluation software (Version 1.1.1) was used (Equation 4.3). This model describes a 1:1 binding of analyte to ligand, followed by a secondary interaction that stabilises the two molecules. Chi²-analysis (χ^2) supported this model. The overall binding affinity (K_D) was calculated using Equation 4.4 (Karlsson and Fält, 1997).

Equation 4.3:



Equation 4.4:

$$K_D = \frac{k_{d1}}{k_{a1}} \times \frac{k_{d2}}{k_{d2} + k_{a2}}$$

4.3 Results

4.3.1 Stoichiometry of Inhibition between Recombinant Human α_2 -Antiplasmin and Plasmin

For each of the recombinant proteins generated in Chapter 3, the *SI* was determined to establish that the proteins were correctly folded and functional. Increasing concentrations of recombinant α_2 -antiplasmin (2-16nM) were incubated with a constant concentration (8nM) of plasmin at 37°C for 1 hr. Residual protease activity was assayed and plotted against the serpin:protease ratio. Figures 4.2-4.4 show that as serpin ratio increases, there is a linear decrease in protease activity. The *SI* of each recombinant protein was determined by extrapolating to the serpin:protease ratio which resulted in complete loss of protease activity (the x-intercept). For each protein, this was carried out and the *SI* values are summarised in Table 4.2. The results are as described below.

SI of Wild-type, N- and/or C-terminally truncated α_2 -antiplasmin

Mutations within the C-terminal and N-terminal region of α_2 -antiplasmin would not be expected to have an effect on the inhibitory mechanism because this property resides in the serpin core domain.

The *SI* of WT α_2 -antiplasmin was found to be 1.0 (Figure 4.2A and Table 4.2) which corresponds with published values (Shieh and Travis, 1987) and mouse α_2 -antiplasmin with plasmin (Law et al., 2008). N-terminally truncated α_2 -antiplasmin (N Δ) showed a *SI* of 1.0 which corresponds with its WT counterpart (Figure 4.2B). When the C-terminus (C Δ) was removed, there was a slight increase in the *SI* when measured against plasmin as seen in Figure 4.2C (C Δ , *SI* = 1.5). Furthermore when both the N- and C-terminal extensions were removed (N Δ C Δ), the *SI* with plasmin increased to 1.8 (Figure 4.2D).

Both WT and N Δ α_2 -antiplasmin were shown to have an *SI* of approximately 1.0 which indicates that the proteins were correctly folded and functional. The *SI* of C Δ and N Δ C Δ protein were observed to be 1.5 and 1.8 respectively which is higher than WT. This result suggests that the C- and N-terminus may play a role in the structural stability of human α_2 -antiplasmin.

SI of Progressive Lys to Ala mutations within the C-terminus of α_2 -antiplasmin

To examine the role of lysine residues in the α_2 -antiplasmin C-terminus, a series of mutant recombinant proteins with multiple lysine to alanine mutations were produced. The *SI* of K448A/K464A, K441A/K448A/K464A, K434A/K441A/K448A/K464A and K427A/K434A/K441A/K448A/K464WT are shown in Figure 4.3A to D respectively. These progressive lysine mutants gave an *SI* of approximately 1.0 (Table 4.2) which corresponds with WT α_2 -antiplasmin indicating that the efficiency of these proteins as a plasmin inhibitor had not been changed by the introduction of multiple lysine substitution in the C-terminus.

In addition, the most C-terminal lysine was substituted with arginine (K464R) to further investigate the importance of the positive charge of Lys⁴⁶⁴. The *SI* showed a slight increase to 1.15 (Figure 4.3E). This change is minor and consequently indicates that recombinant K464R is functional.

SI of α_2 -antiplasmin with 15 amino acids truncated

It was previously shown that Lys⁴⁶⁴ is the most important lysine residue followed by Lys⁴⁴⁸ (Lu et al., 2011). Therefore, to further demonstrate the importance of these two residues, 15 amino acids were truncated from the C-terminus of α_2 -antiplasmin. L449 Δ (Figure 4.4A) and K448A/L449 Δ (Figure 4.4B) gave an *SI* of 1.0-1.1 (Table 4.2) and corresponds with WT α_2 -antiplasmin. Results indicate that removal of the last 15 amino acid within the C-terminus of α_2 -antiplasmin does not alter the functional properties of the serpin.

This page has been intentionally left blank.

Table 4.2. Mean stoichiometry of Inhibition (SI) of plasmin by recombinant human α_2 -antiplasmin. Plasmin (1 nM) was incubated with WT or mutant α_2 -antiplasmin (0.2-2 nM) for 1 hr at 37°C. Residual protease activity was measured in the presence fluorogenic substrate ([AMC] = 0.2 mM). Results with “#” were previously presented in my honours thesis (2008).

Recombinant α_2-antiplasmin	SI \pm SE (n=3)
WT[#]	1.03 \pm 0.02
NΔ	1.03 \pm 0.02
CΔ[#]	1.49 \pm 0.02
NΔCΔ	1.78 \pm 0.01
K464A[#]	0.98 \pm 0.003
K464R	1.15 \pm 0.005
K448A/K464A	0.96 \pm 0.01
K441A/K448A/K464A	0.97 \pm 0.02
K434A/K441A/K448A/K464A	1.02 \pm 0.03
K427A/K434A/K441A/K448A/K464WT	1.01 \pm 0.01
L449Δ	1.02 \pm 0.04
K448A/L449Δ	1.08 \pm 0.02

Figure 4.2. Stoichiometry of inhibition (*SI*) of WT, N- and/or C-terminally truncated human α_2 -antiplasmin with plasmin. A constant plasmin concentration was incubated with varying amount of recombinant α_2 -antiplasmin at the indicated serpin:protease ratio. Once the reaction was completed, residual protease activity was assayed. The *SI* was obtained by extrapolating to where protease activity equals zero. **A)** *SI* of WT α_2 -antiplasmin. **B)** *SI* of N Δ α_2 -antiplasmin. **C)** *SI* of C Δ α_2 -antiplasmin. **D)** *SI* of N Δ C Δ α_2 -antiplasmin.

Figure 4.2.
Stoichiometry of inhibition (*S*) of WT, N- and/or C-terminally truncated human α_2 -antiplasmin with plasmin

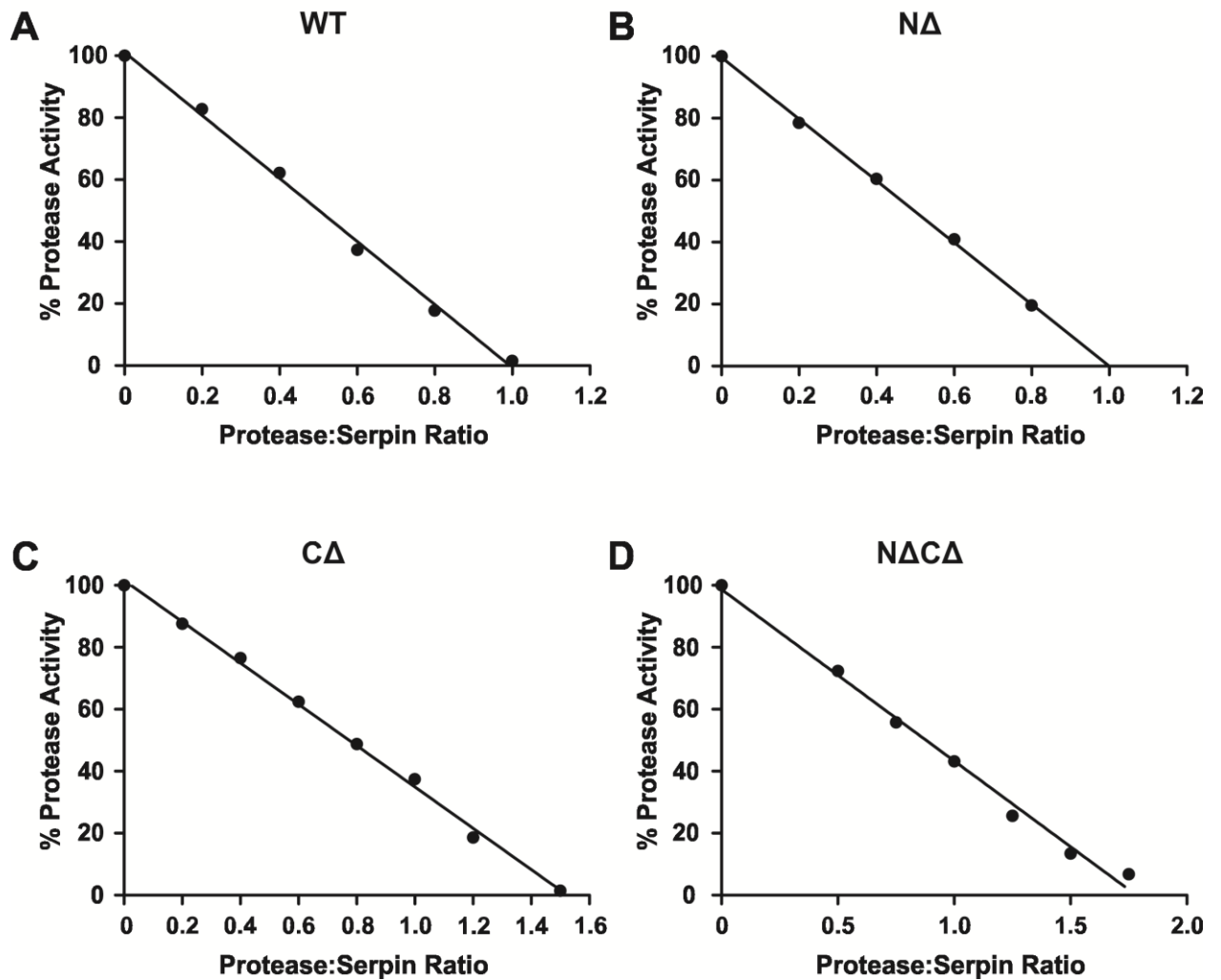


Figure 4.3. Stoichiometry of inhibition (SI) of progressive Lys to Ala mutants of human α_2 -antiplasmin with plasmin. A constant plasmin concentration was incubated with varying amount of recombinant α_2 -antiplasmin at the indicated serpin:protease ratio. Once the reaction was completed, residual protease activity was assayed. The SI was obtained by extrapolating to where protease activity equals zero. **A)** SI of K448A/K464A α_2 -antiplasmin. **B)** SI of K441A/K448A/K464A α_2 -antiplasmin. **C)** SI of K434A/K441A/K448A/K464A α_2 -antiplasmin. **D)** SI of K427A/K434A/K441A/K448A/K464WT α_2 -antiplasmin. **E)** SI of K464R α_2 -antiplasmin.

Figure 4.3.
Stoichiometry of inhibition (S) of progressive Lys to Ala mutants of human α_2 -antiplasmin with plasmin

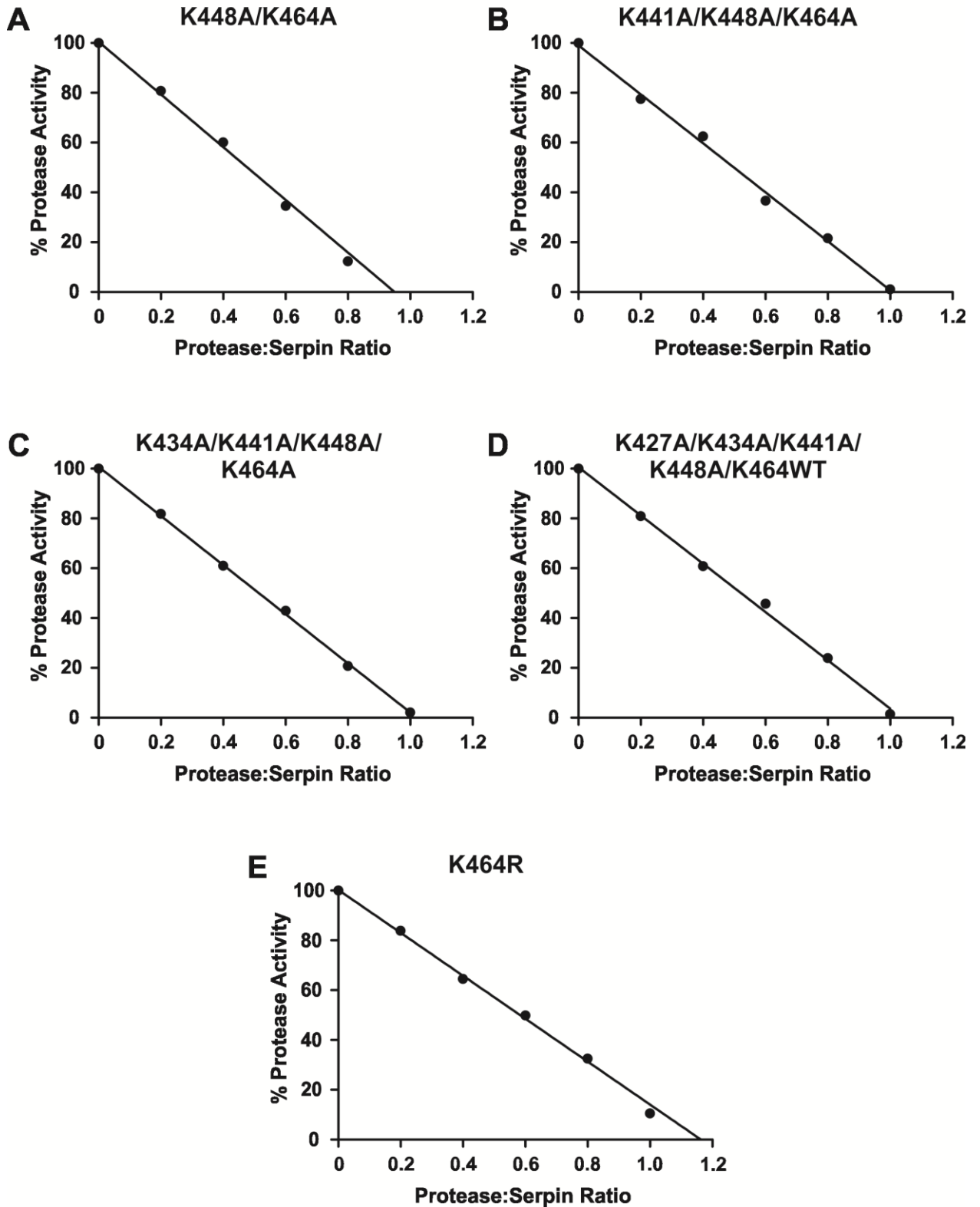
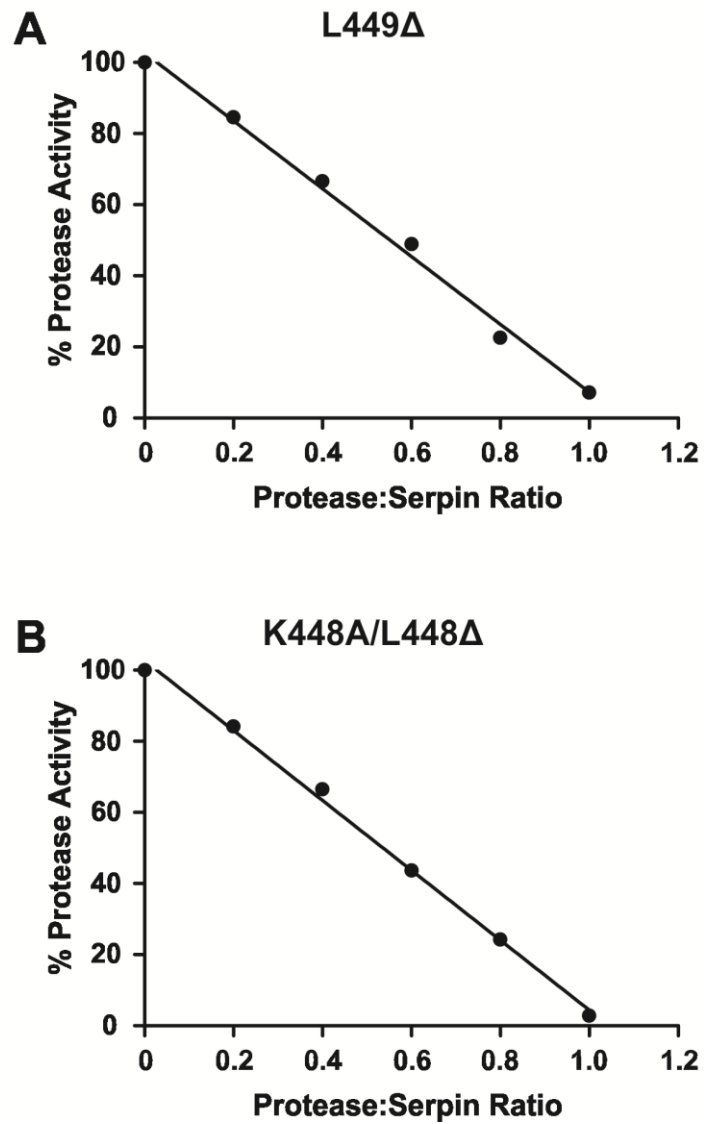


Figure 4.4. Stoichiometry of inhibition (*SI*) of 15 amino acids truncation of human α_2 -antiplasmin with plasmin. A constant plasmin concentration was incubated with varying amount of recombinant α_2 -antiplasmin at the indicated serpin:protease ratio. Once the reaction was completed, residual protease activity was assayed. The *SI* was obtained by extrapolating to where protease activity equals zero. **A)** *SI* of L449 Δ α_2 -antiplasmin. **B)** *SI* of K448A/L449 Δ α_2 -antiplasmin.

Figure 4.4.
Stoichiometry of inhibition (SI) of 15 amino acids
truncation of human α_2 -antiplasmin with plasmin



This page has been intentionally left blank.

4.3.2 Rate of Plasmin Inhibition of Recombinant Human α_2 -Antiplasmin Variants – Continuous Method

Kinetic studies using a protease inhibition assay (continuous method) were performed to measure the rate of plasmin inhibition by WT and mutant α_2 -antiplasmin. The continuous assay was established in the laboratory using a sensitive fluorogenic substrate (AMC) and enables the measurement of low amounts of plasmin activity. Plasmin inhibition rates are presented in Table 4.3 and the corresponding progress curves are presented in Figures 4.5-4.8.

k_a of wild-type, N- and/or C-terminally truncated α_2 -antiplasmin

Figure 4.5A shows the progress curve obtained from WT α_2 -antiplasmin using the continuous assay where residual protease activity was measured in fluorescence units. The observed association rates (k_{obs}) for each serpin concentration was determined (Equation 4.1; Section 4.2.3.1). Each k_{obs} value was plotted against serpin concentration and linear regression analysis performed to calculate the gradient of the slope giving the uncorrected plasmin inhibition rate, k' (Figure 4.5B). The true plasmin inhibition rate (k_a) was obtained by taking into account the SI of the serpin, $[S]$ and K_M (Equation 4.2; Section 4.2.3.1). As expected, recombinant WT α_2 -antiplasmin was a fast inhibitor of human plasmin with a k_a of $3.7 \times 10^7 \text{ M}^{-1}\text{s}^{-1}$ and corresponds to published results (Christensen et al., 1996).

In the absence of the N-terminus (N Δ) (Figure 4.5C & D), the plasmin inhibition rate remains unchanged (N Δ , $k_a = 4.3 \times 10^7 \text{ M}^{-1}\text{s}^{-1}$) when compared with WT α_2 -antiplasmin (WT, $k_a = 3.7 \times 10^7 \text{ M}^{-1}\text{s}^{-1}$). Observations confirm that the N-terminal region of α_2 -antiplasmin is not involved in accelerating the inhibitory mechanism this serpin.

As expected, when the C-terminus was removed (C Δ) (Figure 4.5E & F), there was a 40-fold reduction in plasmin inhibition rate ($k_a = 9.2 \times 10^5 \text{ M}^{-1}\text{s}^{-1}$) (Lu, 2008; Lu et al., 2011). This result corresponds with the reaction between full-length α_2 -antiplasmin with microplasmin in a previously published study (Wiman et al., 1978).

The double truncation of the N- and C-terminal region (N Δ C Δ) (Figure 4.5G & H) resulted in a 65-fold decrease in plasmin inhibition ($k_a = 5.7 \times 10^5 \text{ M}^{-1}\text{s}^{-1}$). There was no significant difference between the plasmin inhibition rate obtained for C Δ and N Δ C Δ (Figure 4.9). Further confirming that the N-terminus does not contribute to the inhibitory mechanism of α_2 -antiplasmin, and demonstrating that the C-terminus is responsible for accelerating plasmin inhibition.

k_a of progressive Lys to Ala mutations within the C-terminus of α_2 -antiplasmin

The primary hypothesis being tested in this chapter is that lysine residues at the extreme C-terminus of α_2 -antiplasmin as well as internally along the C-terminal extension accelerate the inhibition of plasmin. The K464A mutant produced the greatest reduction of 3.6-fold in the plasmin inhibition rate when compared to all other individual Lys to Ala mutations (K427A, K434A, K441A and K448A) (Figure 4.1 and Table 4.1). To further investigate the importance of the positive charge of Lys⁴⁶⁴, a single Lys to Arg mutation was introduced at position 464 (K464R) (Figure 4.6A & B). There was a ~2-fold reduction in plasmin inhibition rate by K464R when compared to K464A ($k_a = 5.3 \times 10^6 \text{ M}^{-1}\text{s}^{-1}$). Results indicate that even though Arg and Lys are both positively charged amino acids, Lys cannot be substituted by Arg.

The plasmin inhibition rate observed with individual Lys to Ala mutants (Table 4.1) were small when compared with the complete removal of the C-terminus, the effect of progressive mutations of the Lys residues in this region was examined. The k_a for K448A/K464A (Figure 4.7A & B), K441A/K448A/K464A (Figure 4.7C & D) and K434A/K441A/K448A/K464A (Figure 4.7E & F) were 4.9×10^6 , 2.2×10^6 and $8.2 \times 10^5 \text{ M}^{-1}\text{s}^{-1}$ respectively. Compared to K464A α_2 -antiplasmin, each added Lys to Ala mutation resulted in an additional ~2-fold reduction in plasmin inhibition rate (Table 4.3). The overall reduction in the rate of plasmin inhibition observed with the four-residue substitution (K434A/K441A/K448A/K464A) was 45-fold, which is comparable with the effect of removing the entire C-terminus (C Δ , $k_a = 9.2 \times 10^5 \text{ M}^{-1}\text{s}^{-1}$).

The relative importance of the Lys⁴⁶⁴, the most C-terminal lysine, compared with the internal lysine residues was further addressed by measuring the rate of plasmin inhibition of a mutant in which Lys⁴⁶⁴ was preserved while the internal lysines were mutated to alanine (K427A/K434A/K441A/K448A/K464WT) (Figure 4.7G & H). This mutant demonstrated a 5.2-fold decrease in plasmin inhibition rate ($k_a = 7.1 \times 10^6 \text{ M}^{-1}\text{s}^{-1}$) when compared to WT α_2 -antiplasmin.

k_a of α_2 -antiplasmin with 15 amino acids truncated

The importance of the C-terminal lysine was further evaluated by producing a mutant in which a stop codon was introduced after Lys448 (L449 Δ) (Figure 4.8A & B). Despite this mutant possessing a C-terminal lysine, it showed a rate reduction in plasmin inhibition ($k_a = 1.1 \times 10^7 \text{ M}^{-1}\text{s}^{-1}$) of 3.4-fold when compared to WT α_2 -antiplasmin. Additionally, when the L449 Δ mutant was modified by substituting Lys⁴⁴⁸ with alanine (K448A/L449 Δ) (Figure 4.8C & D), there was a further decrease in plasmin inhibition rate ($k_a = 2.8 \times 10^6 \text{ M}^{-1}\text{s}^{-1}$).

Table 4.3. Mean plasmin inhibition rate (k_a) for WT and mutant recombinant human α_2 -antiplasmin as measured by continuous assay. “#” indicates results obtained from my honours thesis (2008).

Recombinant α_2 -antiplasmin	$k_a \pm SE (M^{-1}s^{-1}) (n=3)$
WT#	$3.68 \pm 0.34 \times 10^7$
N Δ	$4.27 \pm 0.61 \times 10^7$
C Δ #	$9.22 \pm 0.24 \times 10^5$
N Δ C Δ	$5.72 \pm 0.14 \times 10^5$
K464A#	$1.01 \pm 0.05 \times 10^7$
K464R	$5.33 \pm 0.06 \times 10^6$
K448A/K464A	$4.91 \pm 0.52 \times 10^6$
K441A/K448A/K464A	$2.19 \pm 0.05 \times 10^6$
K434A/K441A/K448A/K464A	$8.22 \pm 0.52 \times 10^5$
K427A/K434A/K441A/K448A/K464WT	$7.09 \pm 0.15 \times 10^6$
L449 Δ	$1.08 \pm 0.02 \times 10^7$
K448A/L449 Δ	$2.75 \pm 0.07 \times 10^6$

Figure 4.5. Plasmin inhibition rate (k_a) by wild-type, N- and/or C-terminally truncated human α_2 -antiplasmin. Progress curves of the interaction between plasmin and α_2 -antiplasmin measured in fluorescence units. Black lines represent raw curves. Red line represents control protease only. Each curve was analysed and fitted (orange lines) using non-linear regression using Equation 4.1 to determine the k_{obs} at each serpin concentration. k_{obs} were plotted against α_2 -antiplasmin concentration and linear regression analysis was used to determine the k' . The plasmin inhibition rate (k_a) was determined by factoring in the Michaelis constant (K_M), substrate concentration [S] and the S_I as described using Equation 4.2. **A&B)** Progress curves and k_a of WT α_2 -antiplasmin. **C&D)** Progress curves and k_a of N Δ α_2 -antiplasmin. **E&F)** Progress curves and k_a of C Δ α_2 -antiplasmin. **G&H)** Progress curves and k_a of N Δ C Δ α_2 -antiplasmin.

Figure 4.5.
Plasmin inhibition rate (k_a) by WT, N- and/or C-terminally truncated human α_2 -antiplasmin

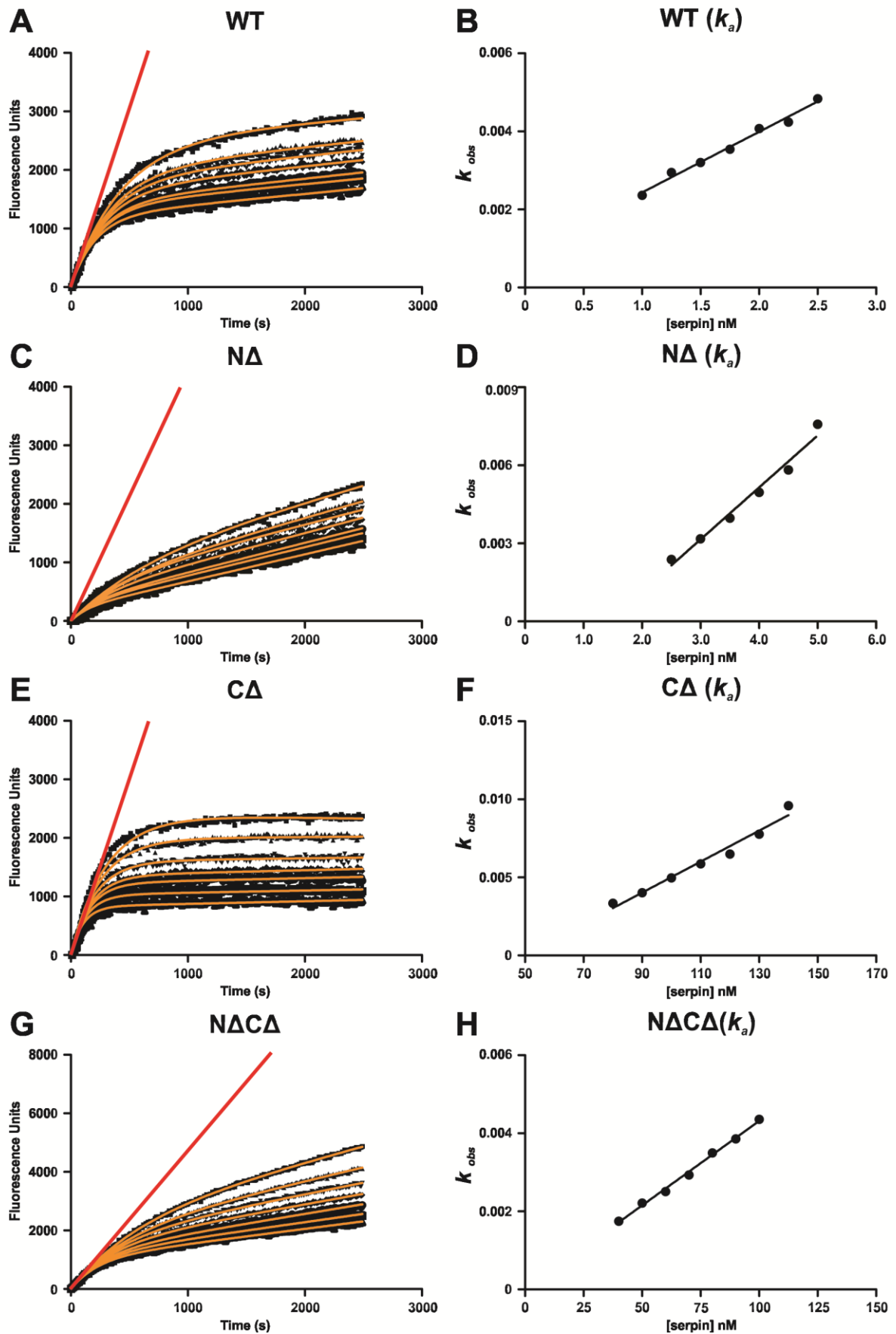


Figure 4.6. Plasmin inhibition rate (k_a) by single Lys to Arg mutation in the C-terminus of human α_2 -antiplasmin. Progress curves of the interaction between plasmin and α_2 -antiplasmin measured in fluorescence units. Black lines represent raw curves. Red line represents control protease only. Each curve was analysed and fitted (orange lines) using non-linear regression using Equation 4.1 to determine the k_{obs} at each serpin concentration. k_{obs} were plotted against α_2 -antiplasmin concentration and linear regression analysis was used to determine the k' . The plasmin inhibition rate (k_a) was determined by factoring in the Michaelis constant (K_M), substrate concentration [S] and the SI as described using Equation 4.2. **A&B)** Progress curves and k_a of K464R α_2 -antiplasmin.

Figure 4.6.
Plasmin inhibition rate (k_a) by single Lys to Arg mutation in the C-terminus of human α_2 -antiplasmin

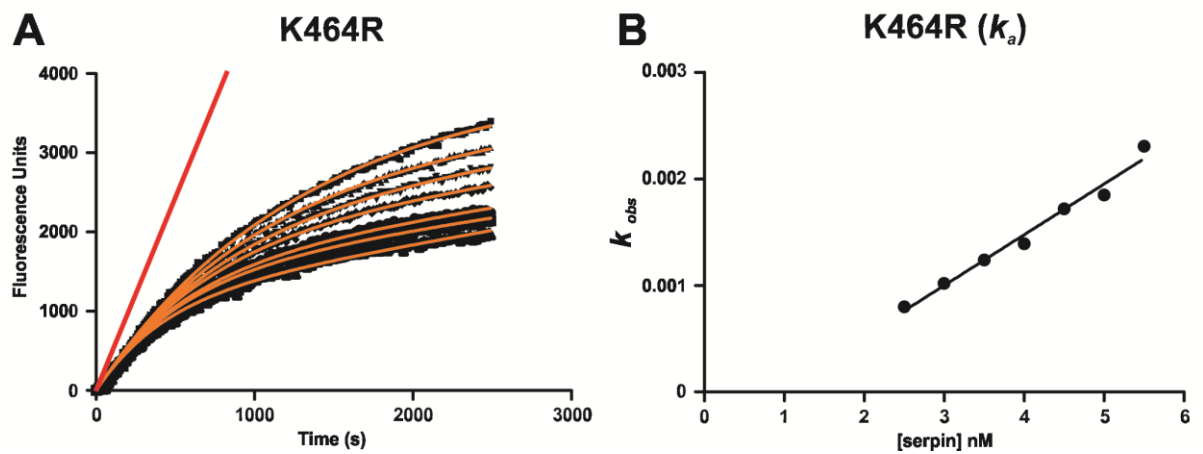


Figure 4.7. Plasmin inhibition rate (k_a) by multiple Lys to Ala mutations in the C-terminus of human α_2 -antiplasmin. Progress curves of the interaction between plasmin and α_2 -antiplasmin measured in fluorescence units. Black lines represent raw curves. Red line represents control protease only. Each curve was analysed and fitted (orange lines) using non-linear regression using Equation 4.1 to determine the k_{obs} at each serpin concentration. k_{obs} were plotted against α_2 -antiplasmin concentration and linear regression analysis was used to determine the k' . The plasmin inhibition rate (k_a) was determined by factoring in the Michaelis Menton (K_M), substrate concentration [S] and the S/I as described using Equation 4.2. **A&B)** Progress curves and k_a of K448A/K464A α_2 -antiplasmin. **C&D)** Progress curves and k_a of K441A/K448A/K464A α_2 -antiplasmin. **E&F)** Progress curves and k_a of K434A/K441A/K448A/K464A α_2 -antiplasmin. **G&H)** Progress curves and k_a of K427A/K434A/K441A/K448A/K464WT α_2 -antiplasmin.

Figure 4.7.
Plasmin inhibition rate (k_a) by multiple Lys to Ala mutations in the C-terminus of human α_2 -antiplasmin

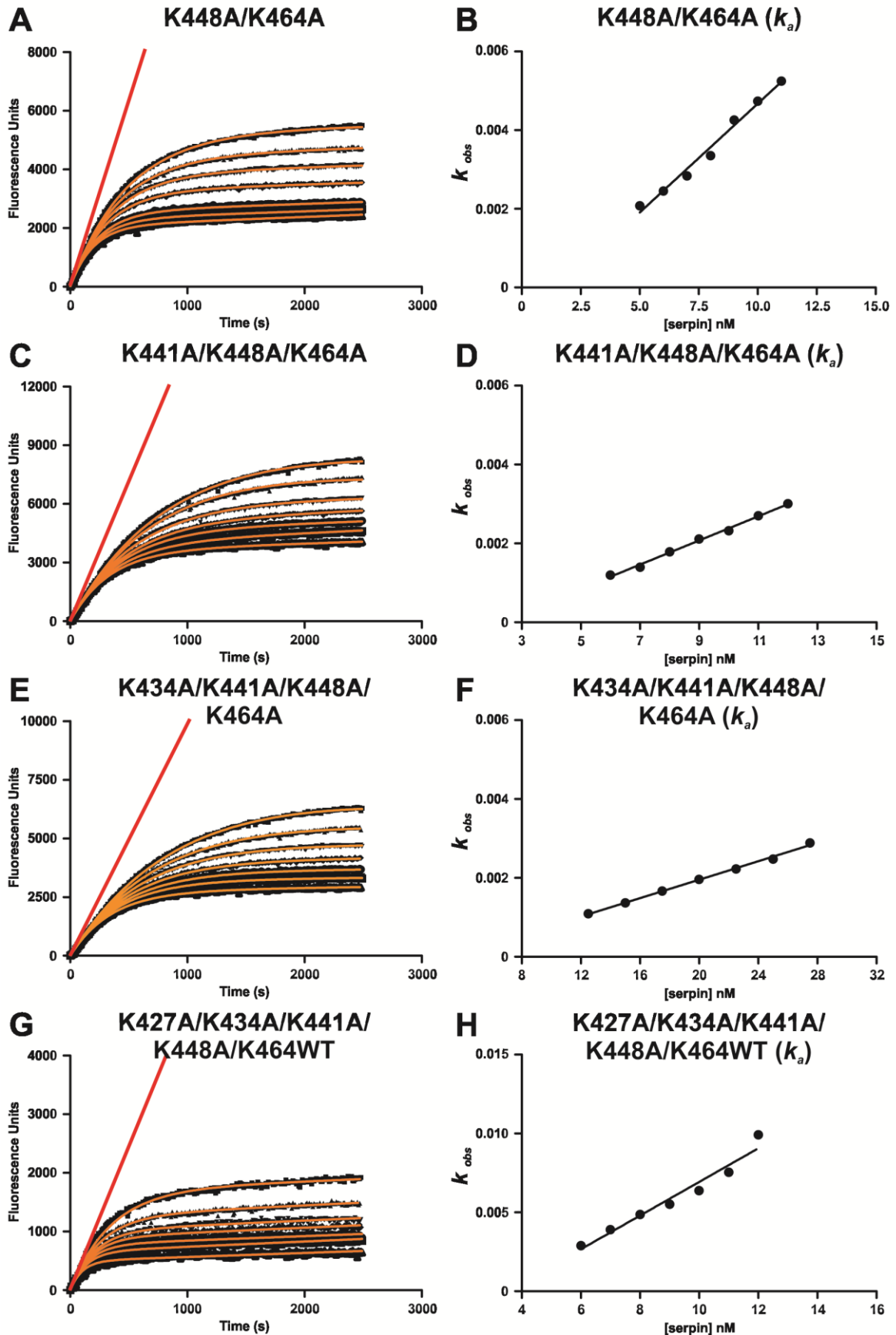


Figure 4.8. Plasmin inhibition rate (k_a) by human α_2 -antiplasmin truncated by 15 amino acids. Progress curves of the interaction between plasmin and α_2 -antiplasmin measured in fluorescence units. Black lines represent raw curves. Red line represents control protease only. Each curve was analysed and fitted (orange lines) using non-linear regression using Equation 4.1 to determine the k_{obs} at each serpin concentration. k_{obs} were plotted against α_2 -antiplasmin concentration and linear regression analysis was used to determine the k' . The plasmin inhibition rate (k_a) was determined by factoring in the Michaelis Menton (K_M), substrate concentration [S] and the S/I as described using Equation 4.2. **A&B)** Progress curves and k_a of L449 Δ α_2 -antiplasmin. **C&D)** Progress curves and k_a of K448A/L449 Δ α_2 -antiplasmin.

Figure 4.8.
Plasmin inhibition rate (k_a) by human α_2 -antiplasmin truncated by 15 amino acids

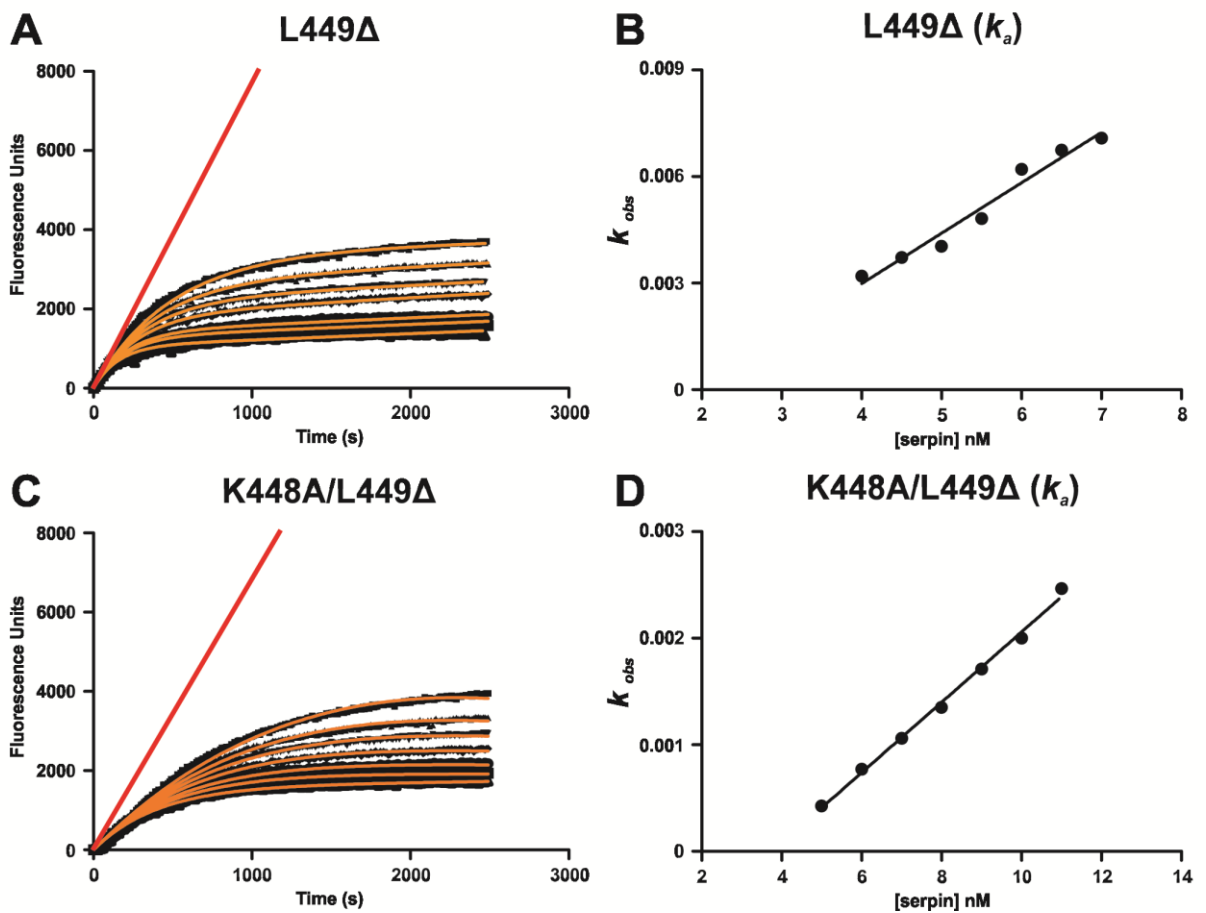


Figure 4.9. Comparison of plasmin inhibition rate (k_a) between wild-type and mutant α_2 -antiplasmin. The k_a for plasmin and α_2 -antiplasmin variants were measured as described in Section 4.2.3.1. Statistics were assessed by one-way ANOVA with Newman-Keuls post-hoc correction. “*” refers to statistically significant data with a p-value of $p < 0.05$. “ns” refers to non-statistically significant data ($p > 0.05$). Each of the data point represents the mean ($n=3$) with error bars representing \pm SE of each protein.

Figure 4.9.
Comparison of plasmin inhibition rate (k_a) between wild-type and mutant α_2 -antiplasmin

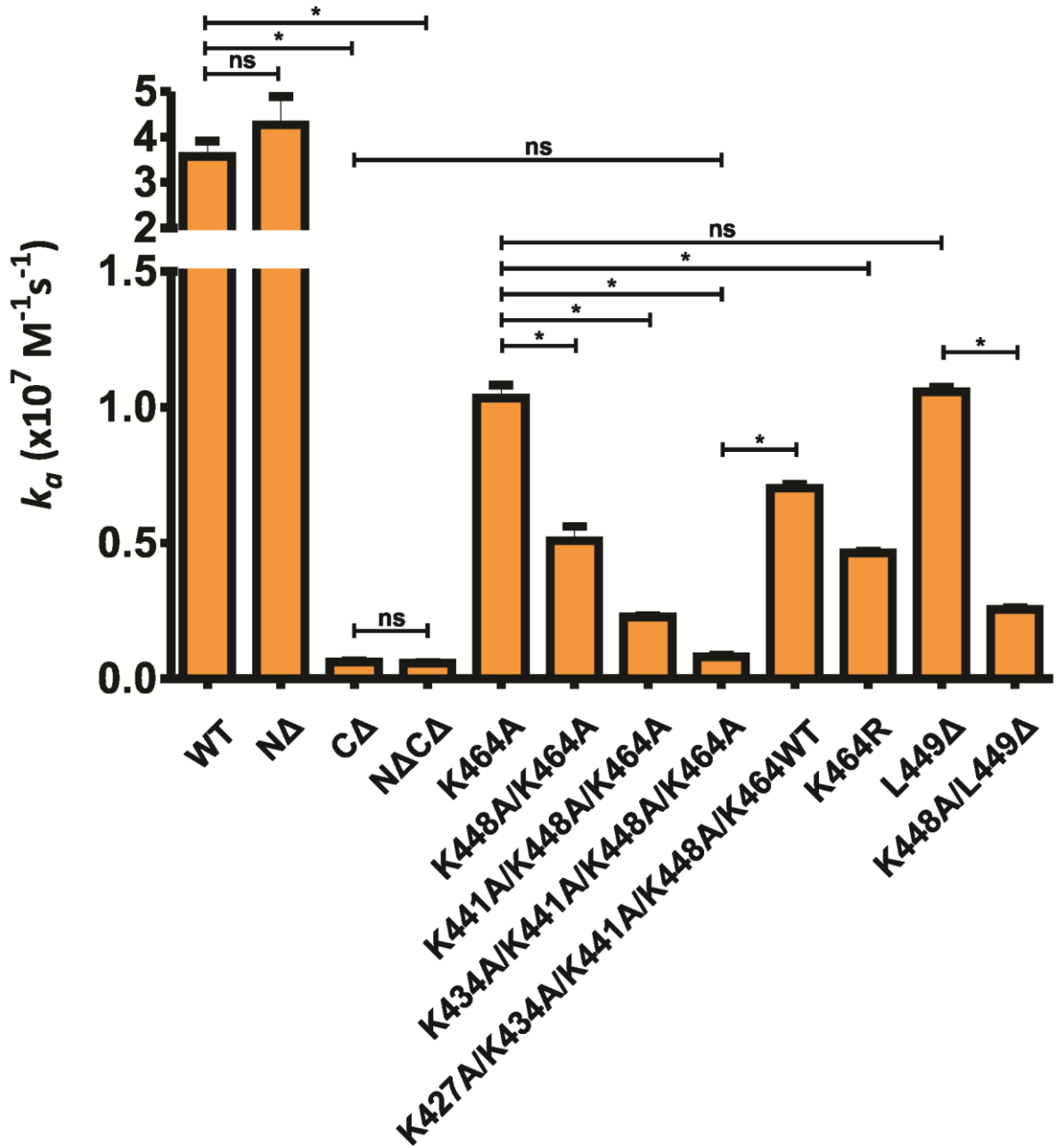


Table 4.4. Mean plasmin inhibition rate (k_a) of plasmin for mutant recombinant human α_2 -antiplasmin as determined using the discontinuous assay. Results with “#” have been presented in my honours thesis (2008).

Recombinant α_2-antiplasmin	$k_a \pm SE$ ($M^{-1}s^{-1}$) (n=3)
CΔ[#]	$3.80 \pm 0.08 \times 10^5$
NΔCΔ	$1.86 \pm 0.15 \times 10^5$
K434A/K441A/K448A/K464A	$4.63 \pm 0.51 \times 10^5$

4.3.3 Rate of Plasmin Inhibition of Recombinant Human α_2 -Antiplasmin Variants – Discontinuous Method

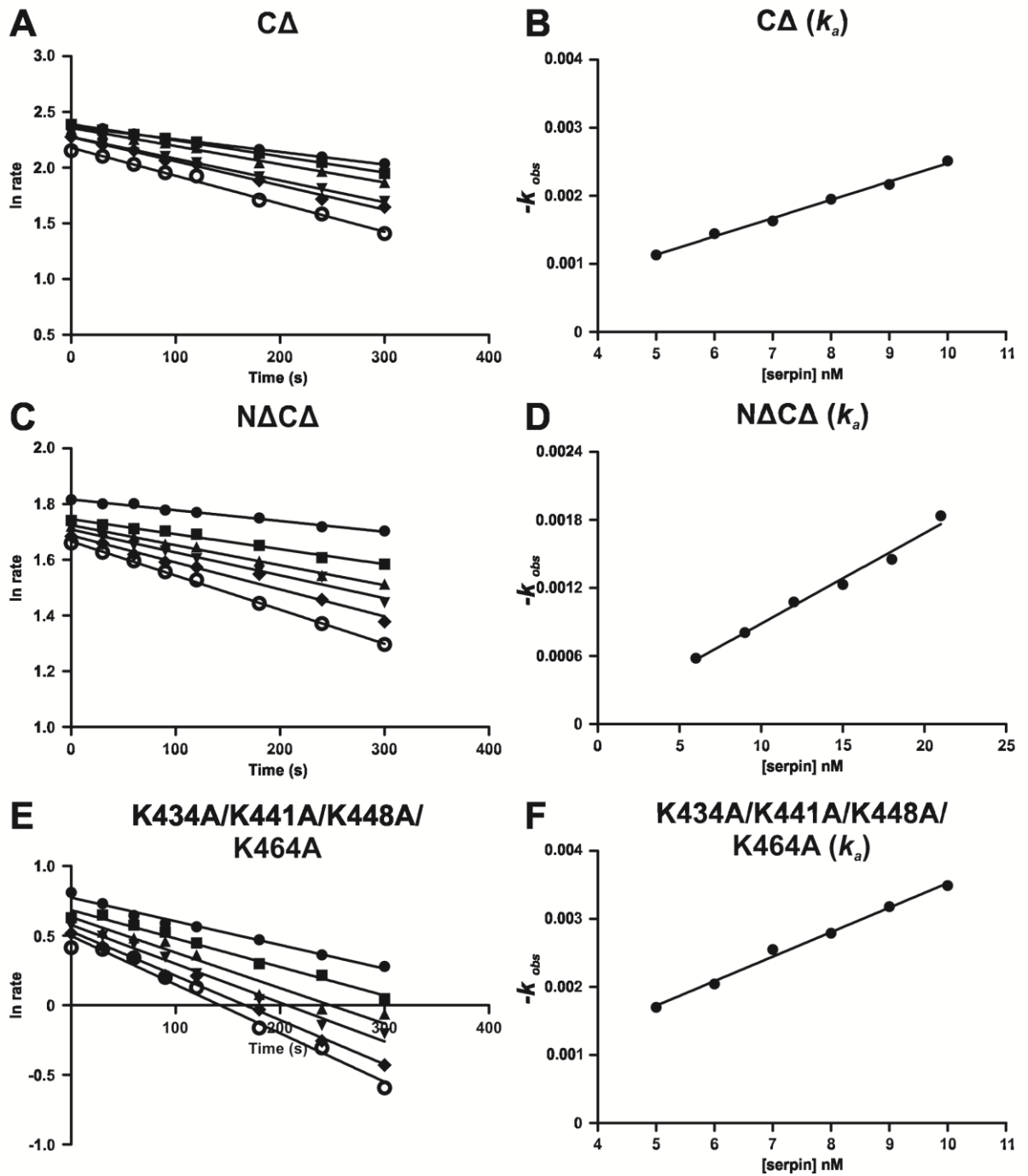
The plasmin inhibition rates obtained from C Δ , N Δ C Δ , and K434A/K441A/K448A/K464A α_2 -antiplasmin were found to be significantly slower compared to WT α_2 -antiplasmin when the continuous assay was used. Furthermore, large amounts of recombinant protein were used to reach the maximum velocity (V_{max}). Therefore, the discontinuous assay was employed to analyse the association rate of C Δ , N Δ C Δ , and K434A/K441A/K448A/K464A α_2 -antiplasmin as this protocol is suitable for measuring inhibition rates of less than $10^6 \text{ M}^{-1}\text{s}^{-1}$ and does not rely on V_{max} being reached (Olson et al., 1993). This assay requires the use of a smaller quantity of protein and measures the residual protease activity as an end-point measurement.

Different concentrations of recombinant α_2 -antiplasmin (5-20 nM) were incubated with a fixed amount of plasmin (0.5nM) at various time points (0-5 min) after which fluorogenic substrate (200 μM) was added and residual protease activity measured. A linear relationship was observed when the log of protease activity was plotted against time (C Δ – Figure 4.10A; N Δ C Δ – Figure 4.10C; K434A/K441A/K448A/K464A – Figure 4.10E). The observed association rate (k_{obs}) of each concentration was then obtained by performing a linear regression analysis on each data set. Each k_{obs} value were then plotted against serpin concentration and the slope of the line gave the uncorrected plasmin inhibition rate, k' (C Δ – Figure 4.10B; N Δ C Δ – Figure 4.10D; K434A/K441A/K448A/K464A – Figure 4.10F). The true plasmin inhibition rate, k_a , was obtained by correcting with the $S/$ of the serpin.

The plasmin inhibition rate of C Δ , N Δ C Δ , and K434A/K441A/K448A/K464A α_2 -antiplasmin obtained from this method are 3.8×10^5 , 1.9×10^5 and $4.6 \times 10^5 \text{ M}^{-1}\text{s}^{-1}$ respectively (Table 4.4). The discontinuous assay resulted in a ~2-fold discrepancy in plasmin inhibition rates when compared to the continuous assay.

Figure 4.10. Plasmin inhibition rate (k_a) of recombinant human α_2 -antiplasmin determined by discontinuous method. Semilog plots in panels A, C and E are of residual plasmin activity versus time for reactions at varying concentration of recombinant α_2 -antiplasmin. Section 4.2.3.2 describes how the k_a for plasmin and α_2 -antiplasmin variants were measured. **A&B)** Semilog plots and k_a of C Δ α_2 -antiplasmin. **C&D)** Semilog plots and k_a of N Δ C Δ α_2 -antiplasmin. **E&F)** Semilog plots and k_a of K434A/K441A/K448A/K464A α_2 -antiplasmin.

Figure 4.10.
Plasmin inhibition rate (k_a) of recombinant human α_2 -antiplasmin determined by discontinuous method



4.3.4 Binding Affinity of Recombinant Human α_2 -Antiplasmin Variants for Active Site-blocked Plasmin

The plasmin inhibition constants derived from the enzyme-inhibitor kinetics were derived from measuring the inhibition of plasmin amidolytic activity. To corroborate these results and to partition the α_2 -antiplasmin/plasmin interaction between the serpin core versus the C-terminal extension, surface plasmon resonance (SPR) was used to directly measure the binding affinity of recombinant human α_2 -antiplasmin for human plasmin. Binding of WT and mutants α_2 -antiplasmin to active site-blocked plasmin was observed in real time. The association and dissociation constants were calculated to obtain the binding affinity (K_D) (Table 4.5). In this study, active site-blocked plasmin was used to prevent the formation of the covalent α_2 -antiplasmin/plasmin complex. Plasmin was irreversibly blocked with a plasmin inhibitor (CMK) as described in Section 4.2.4.1. To ensure that plasmin activity was completely blocked, residual activity was assayed with the fluorogenic substrate (AMC) and compared with active plasmin. Fluorescence emission was not detected with active site-blocked plasmin which indicated that the activity of plasmin was blocked (results not shown). Sensorgrams for the interaction between active site-blocked (PlmCMK) and α_2 -antiplasmin are shown in Figures 4.11-4.14 and collated data are presented in Table 4.5. To achieve similar response units (RU) as WT α_2 -antiplasmin (Figure 4.11A), a higher concentration of active site-blocked plasmin was used with α_2 -antiplasmin mutants, which accounts for the difference in shape of the binding curves observed in the sensorgrams. All experiments were conducted in parallel with a blank flow cell to monitor non-specific binding and subtracted with test flow cells.

K_D of wild-type, N- and/or C-terminally truncated α_2 -antiplasmin

Figure 4.11A shows the sensorgram of WT α_2 -antiplasmin binding to PlmCMK. The initial upward slope from 0-60 seconds (s) is the association phase which is followed by the dissociation phase from 60-360s. As the concentration of the analyte, PlmCMK, increases, there is an increase in the response units (RU) observed on the sensorgram. The K_D of WT α_2 -antiplasmin for PlmCMK was determined to be 1.6nM, indicating a high affinity interaction. The affinity for PlmCMK remains unchanged when the N-terminus of α_2 -antiplasmin (N Δ - Figure 4.11B) was removed ($K_D = 1.0$ nM). In the absence of the C-terminal region (C Δ - Figure 4.11C), there was a 31-fold reduction in binding affinity ($K_D = 50$ nM). Even though there was a significant decrease in the binding between WT and C Δ to PlmCMK (Figure 4.15), affinity of C Δ α_2 -antiplasmin remains high. When both the N- and C-terminus (N Δ C Δ - Figure 4.11D) were removed, the binding affinity ($K_D = 1.3$ nM) remained unchanged and is non-statically different when compared to WT α_2 -antiplasmin (Figure 4.15). Change in binding affinity is consistent with trends seen in plasmin inhibition rates (k_a) except for N Δ C Δ .

The discrepancy seen with $N\Delta C\Delta$ in plasmin inhibition and binding will be further explored in the discussion section.

In order to obtain the binding affinity of α_2 -antiplasmin to PlmCMK, plasmin association (k_{a1}), dissociation (k_{d1}), forward (k_{a2}) and reverse (k_{d2}) rate constant were also generated. For all recombinant α_2 -antiplasmin tested in this chapter, the rate of plasmin association (k_{a1}) obtained using SPR was very similar to the rate of plasmin inhibition (k_a) previously obtained using kinetic analysis. The dissociation rate constant (k_{d1}) and the forward and reverse rate constants (k_{a2} and k_{d2}) remained relatively unchanged for all recombinant α_2 -antiplasmin (WT and mutants) with active site-blocked plasmin (Table 4.5).

K_D of single Lys mutations within the C-terminus of α_2 -antiplasmin

Single Lys to Ala mutants at position 448 (K448A – Figure 4.12A; $K_D = 2.0\text{nM}$) and 464 (K464A – Figure 4.12B; $K_D = 5.2\text{nM}$) showed decreases in binding affinity of 1.3- and 3.3-fold respectively when compared to WT α_2 -antiplasmin. To further investigate the importance of Lys⁴⁶⁴, a single Lys to Arg mutation was introduced at position 464 (K464R – Figure 4.12C; $K_D = 21\text{nM}$). There was a ~4-fold reduction in binding affinity by K464R when compared to K464A. Overall measurements of binding affinity were consistent with trends observed with plasmin inhibition as determined by kinetic analysis.

K_D of progressive Lys to Ala mutations within the C-terminus of α_2 -antiplasmin

Sequential mutation of the lysine residues within the C-terminus resulted in a progressive decrease in the binding affinity, which corresponds to the observations made with the plasmin inhibition rate (Section 4.2). K448A/K464A (Figure 4.13A; $K_D = 10\text{nM}$) showed a 2-fold reduction in binding affinity when compared to K464A. K441A/K448A/K464A (Figure 4.13B; $K_D = 29\text{nM}$) produced a 2.8-fold reduction in affinity when compared to K448/K464A. The binding for K434A/K441A/K448A/K464A (Figure 4.13C; $K_D = 42\text{nM}$) was similar to that obtained when the C-terminus was removed (C Δ). The binding for K427A/K434A/K441A/K448A/K464WT (Figure 4.13D) was 13nM which corresponds to an 8.4-fold decrease when compared to WT α_2 -antiplasmin.

K_D of α_2 -antiplasmin with 15 amino acids truncated

The importance of the last 15 amino acid sequence of the C-terminus of α_2 -antiplasmin was further evaluated by introducing a stop codon at Leu⁴⁴⁹. The binding affinity of L449 Δ (Figure 4.14A; $K_D = 6.4\text{nM}$) was similar to that obtained for K464A ($K_D = 5.2\text{nM}$). This confirms and supports the results observed with plasmin inhibition rate (k_a) using protease assays. Subsequently when the L449 Δ mutant was modified by substituting Lys⁴⁴⁸ with alanine (K448A/L449 Δ ; Figure 4.14B), this resulted in a 17-fold reduction in binding affinity (27nM) compared with WT α_2 -antiplasmin.

Figure 4.11. Sensorgrams of the binding of WT, N- and/or C-terminally truncated α_2 -antiplasmin to active site-blocked plasmin as measured by SPR. Recombinant α_2 -antiplasmin (20nM) was immobilised on a NTA chip. The binding of various concentrations of active site-blocked plasmin to α_2 -antiplasmin was monitored in real time. Blue lines are raw curves and fitted curves are in black. **A)** Binding of active site-blocked plasmin (2-8nM) to WT ($\chi^2 = 0.21$). **B)** Binding of active site-blocked plasmin (2-8nM) to N Δ ($\chi^2 = 0.13$). **C)** Binding of active site-blocked plasmin (20-120nM) to C Δ ($\chi^2 = 0.60$). **D)** Binding of active site-blocked plasmin (2-8nM) to N Δ C Δ ($\chi^2 = 0.61$).

Figure 4.11.
Sensorgrams of the binding of WT, N- and/or C-terminally truncated α_2 -antiplasmin to active site-blocked plasmin as measured by SPR

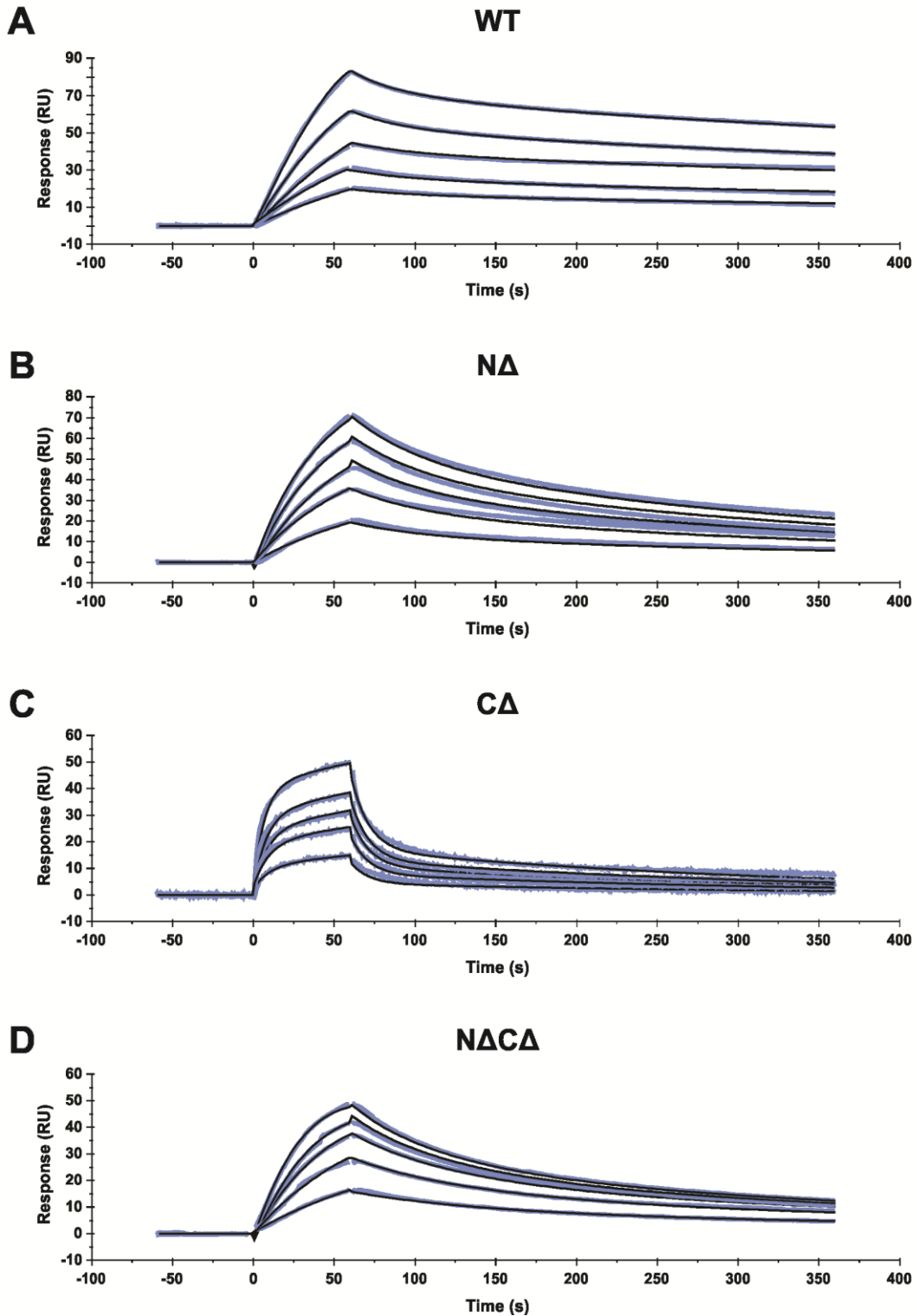


Figure 4.12. Sensorgrams of the binding of single Lys mutant α_2 -antiplasmin to active site-blocked plasmin as measured by SPR. Recombinant α_2 -antiplasmin (20nM) was immobilised on a NTA chip. The binding of various concentrations of active site-blocked plasmin to α_2 -antiplasmin was monitored in real time. Blue lines are raw curves and fitted curves are in black. **A)** Binding of active site-blocked plasmin (2.5-12.5nM) to K448A ($\chi^2 = 0.88$). **B)** Binding of active site-blocked plasmin (4-20nM) to K464A ($\chi^2 = 0.30$). **C)** Binding of active site-blocked plasmin (6-30nM) to K464R ($\chi^2 = 0.41$).

Figure 4.12.
Sensorgrams of the binding of single Lys mutant α_2 -antiplasmin to active site-blocked plasmin as measured by SPR

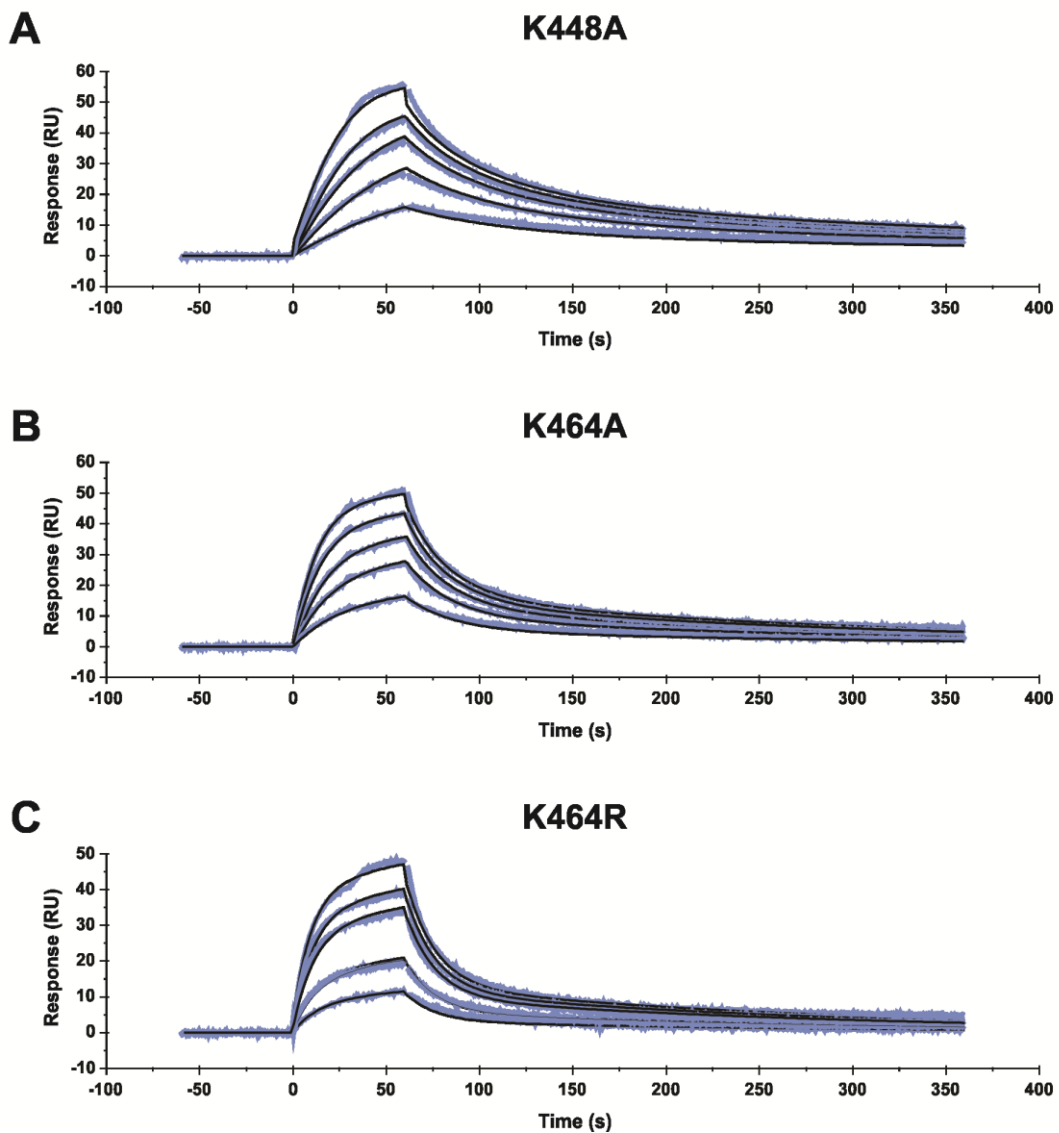


Figure 4.13. Sensorgrams of the binding of progressive Lys to Ala mutant α_2 -antiplasmin to active site-blocked plasmin as measured by SPR. Recombinant α_2 -antiplasmin (20nM) was immobilised on a NTA chip. The binding of various concentrations of active site-blocked plasmin to α_2 -antiplasmin was monitored in real time. Blue lines are raw curves and fitted curves are in black. **A)** Binding of active site-blocked plasmin (6-36nM) to K448A/K464A ($\chi^2 = 0.34$). **B)** Binding of active site-blocked plasmin (10-80nM) to K441A/K448A/K464A ($\chi^2 = 0.31$). **C)** Binding of active site-blocked plasmin (20-100nM) to K434A.K441A/K448A/K464A ($\chi^2 = 0.54$). **D)** Binding of active site-blocked plasmin (8-40nM) to K427A/K434A/K441A/K448A/K464WT ($\chi^2 = 0.54$).

Figure 4.13.
Sensorgrams of the binding of progressive Lys to Ala mutant α_2 -antiplasmin to active site-blocked plasmin as measured by SPR

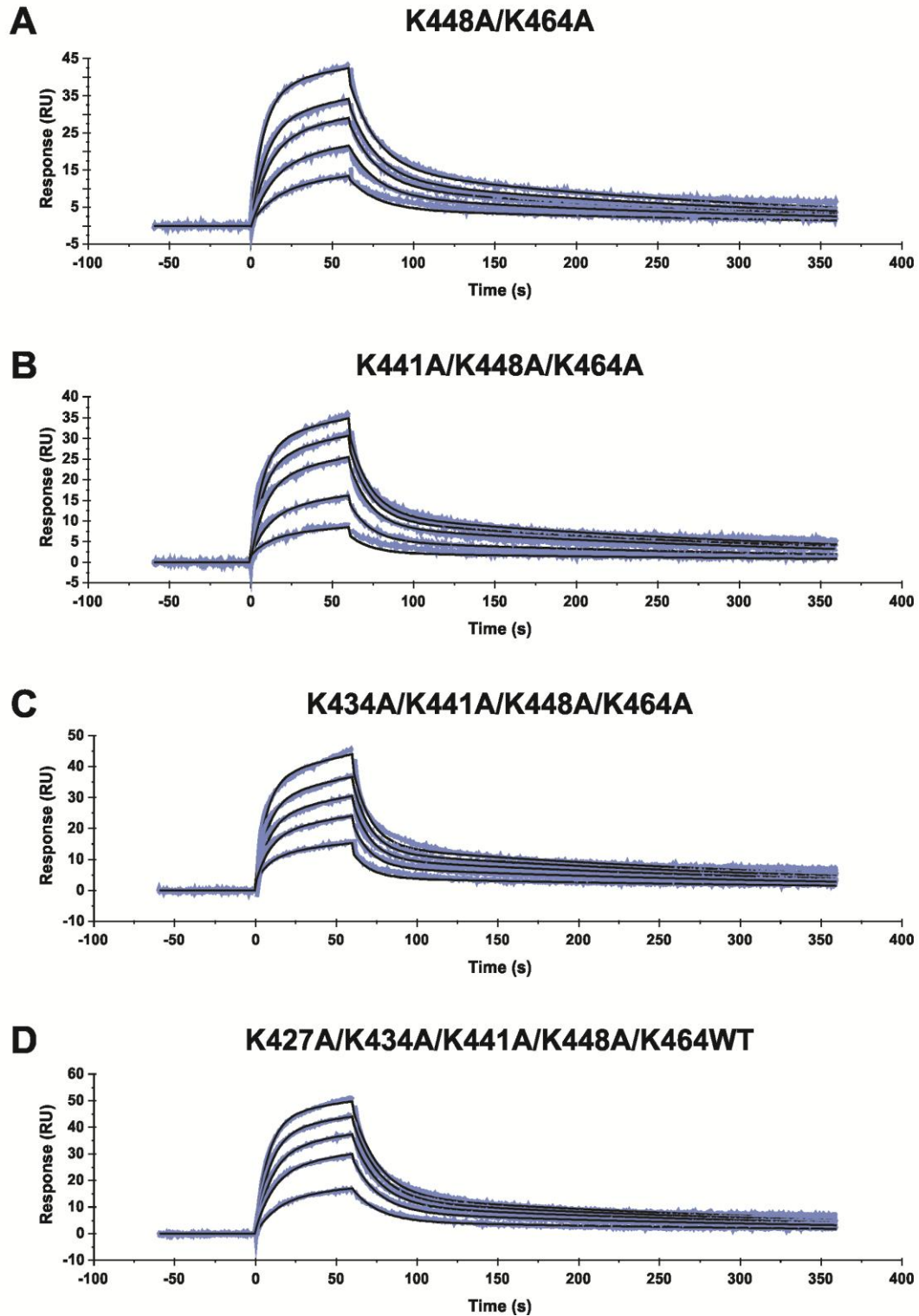
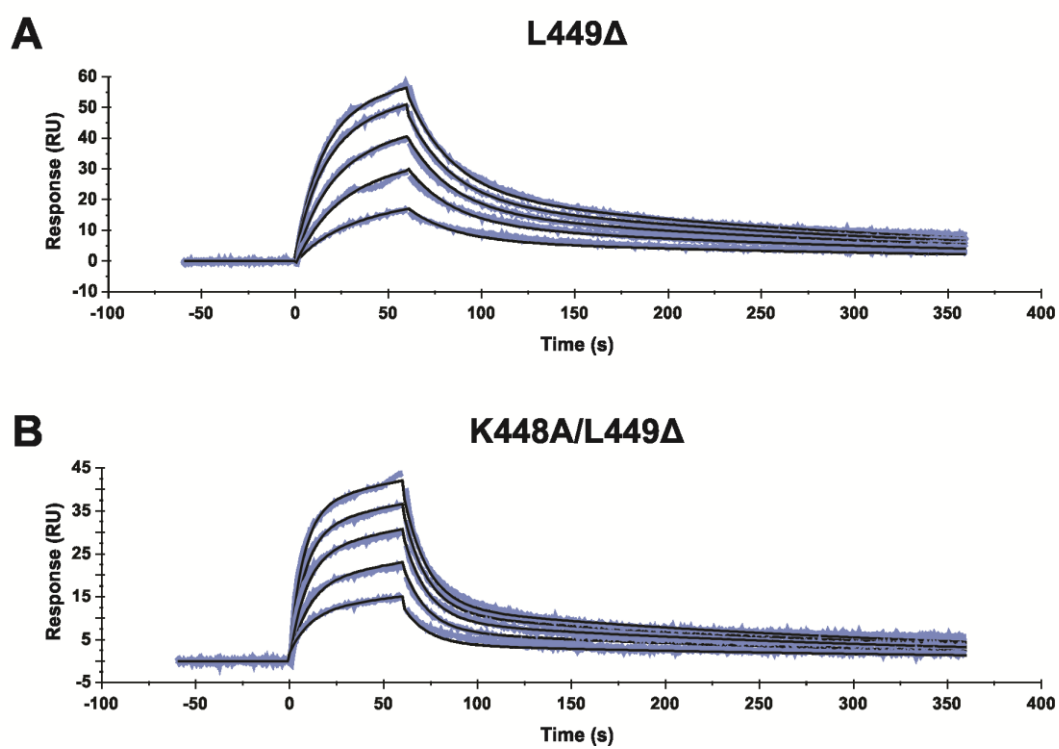


Figure 4.14. Sensorgrams of the binding of α_2 -antiplasmin truncated by 15 amino acids to active site-blocked plasmin as measured by SPR. Recombinant α_2 -antiplasmin (20nM) was immobilised on a NTA chip. The binding of various concentrations of active site-blocked plasmin to α_2 -antiplasmin was monitored in real time. Blue lines are raw curves and fitted curves are in black. **A)** Binding of active site-blocked plasmin (4-20nM) to L449 Δ ($\chi^2 = 0.59$). **B)** Binding of active site-blocked plasmin (10-50nM) to K448A/L449 Δ ($\chi^2 = 0.49$).

Figure 4.14.
Sensorgrams of the binding of α_2 -antiplasmin truncated by 15 amino acids to active site-blocked plasmin as measured by SPR



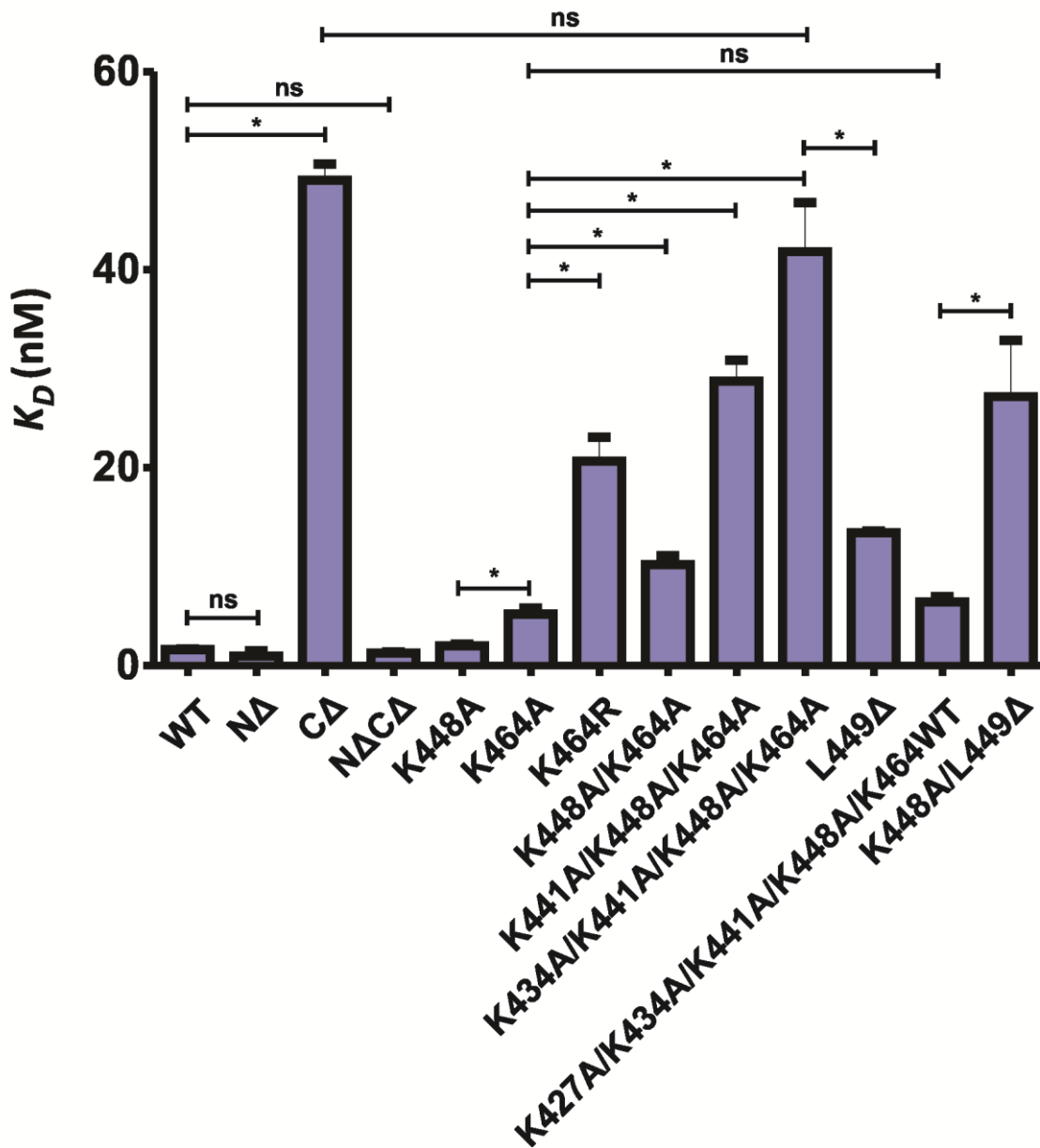
This page has been intentionally left blank.

Table 4.5. Mean binding affinity, association and dissociation constants of WT and mutant α_2 -antiplasmin mutants for active site-blocked plasmin as measured by surface plasmon resonance (n=3-6).

Recombinant α_2 -antiplasmin	$K_D \pm SE$ (nM)	k_{a1} ($M^{-1}s^{-1}$)	k_{d1} (1/s)	k_{a2} (1/s)	k_{d2} (1/s)
WT	1.6 \pm 0.1	2.1 $\times 10^7$	0.09	0.007	0.005
N Δ	1.0 0.7	1.1 $\times 10^7$	0.02	0.009	0.003
C Δ	49 \pm 1.7	5.1 $\times 10^5$	0.08	0.008	0.004
N Δ C Δ	1.3 \pm 0.1	9.5 $\times 10^6$	0.02	0.003	0.003
K448A	2.0 \pm 0.1	1.1 $\times 10^7$	0.05	0.004	0.003
K464A	5.2 \pm 0.6	3.9 $\times 10^6$	0.05	0.006	0.004
K464R	21 \pm 2.4	1.4 $\times 10^6$	0.06	0.006	0.004
K448A/K464A	10 \pm 1.0	2.0 $\times 10^6$	0.05	0.007	0.005
K441A/K448A/K464A	29 \pm 2.1	7.8 $\times 10^5$	0.07	0.008	0.004
K434A/K441A/K448A/K464A	42 \pm 5.0	5.9 $\times 10^5$	0.08	0.008	0.003
K427A/K434A/K441A/K448A/K464WT	13 \pm 0.2	1.6 $\times 10^6$	0.06	0.006	0.003
L449 Δ	6.4 \pm 0.6	2.9 $\times 10^6$	0.05	0.006	0.004
K448A/L449 Δ	27 \pm 5.7	1.2 $\times 10^6$	0.08	0.006	0.004

Figure 4.15. Comparison of binding affinity (K_D) between wild-type and mutant α_2 -antiplasmin for active site-blocked plasmin. The K_D for plasmin and α_2 -antiplasmin variants were measured as described in Section 4.2.4. Statistics were assessed by one-way ANOVA with Newman-Keuls post-hoc correction. “*” refers to statistically significant data with a p-value of $p < 0.05$. “ns” refers to non-statistically significant data ($p > 0.05$). Each data point represents the mean ($n=3-6$) with error bars representing \pm SE of each protein.

Figure 4.15.
Comparison of binding affinity (K_D) between wild-type and mutant α_2 -antiplasmin for active site-blocked plasmin



4.4 Discussion

This is the first comprehensive measurement of the kinetics of α_2 -antiplasmin/plasmin interaction employing two different methods. By incorporating a fluorogenic substrate with high affinity for plasmin, the continuous assay was used to accurately measure the rate of plasmin inhibition for WT α_2 -antiplasmin and mutants. In addition, α_2 -antiplasmin/plasmin interaction via surface plasmon resonance (SPR) was independently observed. In both methods, a comprehensive set of recombinant α_2 -antiplasmin variants and their inhibition/binding rate with plasmin were analysed. It is important to recognise that the two methods measure different kinetic rate constants. Using Figure 4.16 as a reference schematic, SPR measures the initial rate of interaction (k_1) between α_2 -antiplasmin and plasmin. The protease inhibition assay measures the overall rate at which the irreversible covalent α_2 -antiplasmin/plasmin complex is formed, resulting in complete inhibition; therefore, this takes into account k_1 , k_2 and k_4 (Figure 4.15). We were able to obtain comparable rates of plasmin inhibition (k_a) and association rate (k_{a1}) despite the fact that both methods measure different values. This indicates that the rapid interaction is predominantly due to the formation of the initial reversible encounter α_2 -antiplasmin/plasmin complex, thus suggesting that the rate-limiting step occurs when the covalent α_2 -antiplasmin/plasmin complex is formed.

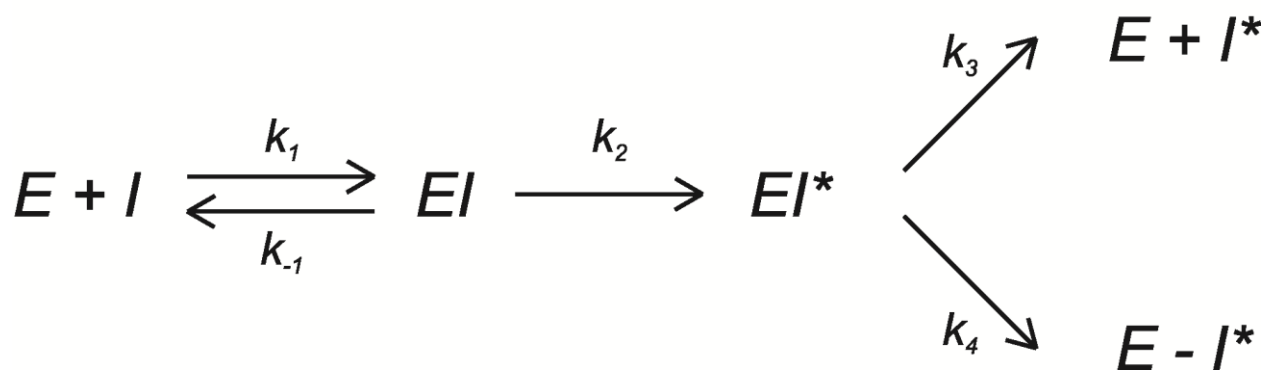
One of the potential consequences of introducing a mutation into a protein is that the mutation changes the structure of the protein, thereby altering the inhibitory activity of the serpin. Therefore, the determination of the stoichiometry of inhibition (SI) was important in evaluating the efficiency of each recombinant protein as a protease inhibitor. In the kinetic assay, a fraction of the reaction may have gone down the substrate pathway (Figure 4.15). Thus the SI value is important in obtaining a true value when calculating the plasmin inhibition rate as it accounts for the balance between the substrate and inhibition reactions (Schechter and Plotnick, 2004). It was shown in Chapter 3 that all recombinant α_2 -antiplasmin generated retained their native fold (Figure 3.13). The SI for WT α_2 -antiplasmin was determined to be ~ 1.0 which corresponds with published values (Law et al., 2008; Shieh and Travis, 1987). All other α_2 -antiplasmin mutants were determined to have an SI of between 1.0 and 1.2 except for $N\Delta C\Delta$ which was calculated to have an SI of 1.8. The SI values obtained suggest that multiple Lys to Ala mutations within the C-terminus of α_2 -antiplasmin did not compromise the folding of the serpin structure and that singularly, the N- or C-terminal extensions are not essential for the folding of α_2 -antiplasmin to the metastable active conformation. However, when both N- and C-terminal extensions are absent, the efficiency of α_2 -antiplasmin as a plasmin inhibitor was reduced. It was evident from the generation of recombinant $N\Delta C\Delta$ that the expression levels were low (see Chapter 3). The removal of N- and C-terminal regions may have affected the stability of the protein and may have increased the propensity of the protein to be converted to latent or polymer form.

Compared to most other serpins, α_2 -antiplasmin is unique because of the presence of both an extensive N-terminus spanning 43 amino acids and C-terminus of 55 amino acids. Previous studies with N- and/or C- terminal truncations of mouse α_2 -antiplasmin found that no significant increase in *SI* was observed (Sofian, 2009). This is true for the murine system, nevertheless the human system may be different. C1-inhibitor and heparin cofactor II (HCII) are two examples of serpins which possess an N-terminal region which is longer than α_2 -antiplasmin. It has been shown that truncation of the 75 amino acid N-terminus of HCII resulted in decreased specificity for heparin but its activity towards α -thrombin and chymotrypsin remained unchanged (Baglin et al., 2002; Van Deerlin and Tollefsen, 1991). Truncations of the N-terminus of C1-inhibitor also revealed that the inhibitory mechanism of the serpin is not affected in the absence of the N-terminal region (Beinrohr et al., 2007; Coutinho et al., 1994; Rossi et al., 2010). A known serpin which contains N- and C-terminal extensions is pigment epithelium-derived factor (PEDF) however this molecule is a non-inhibitory member of the serpin family therefore the role of the extensions in inhibitory mechanism cannot be explored (Simonovic et al., 2001; Tombran-Tink et al., 2005). A serpin which possess a C-terminus, thermoplin, from the thermophilic bacteria *Thermobifida fusca*, has been implicated in enhancing stability of the protein structure at elevated temperatures (Fulton et al., 2005; Irving et al., 2003). Therefore, it is possible that the N- and C-terminal region in the human α_2 -antiplasmin may play a role in stability during protein folding and the removal of these regions might affect the inhibitory efficiency.

Prior to the work presented in this thesis, studies investigating the binding affinity of α_2 -antiplasmin/plasmin have been limited. The only other study that used SPR to measure the interaction between α_2 -antiplasmin and plasmin were Wang and colleagues (Wang et al., 2006). In this study, a carboxymethyl dextrane surface chip (CM5) was used to immobilise plasminogen or kringle 1-3 on the surface. This study determined that Lys⁴⁴⁸ was more important than Lys⁴⁶⁴ which is in contradiction to results from this current study and Schaller and colleagues (Frank et al., 2003; Gerber et al., 2010). The limitation of binding studies performed by Wang and colleagues were that the mutations chosen to replace the lysine residues within the C-terminus were inconsistent in charge. They also studied the interaction with plasminogen or kringle 1-3 (K1-3), but not the complete plasmin molecule. This prompted the current study to measure the binding affinity of plasmin with α_2 -antiplasmin recombinant proteins produced.

Figure 4.16. Mechanism of serpin inhibition. I represents the serpin and E represents the protease. The forward rate constant of serpin with protease is represented as k_1 . The association rate constant (k_{a1}) measured in surface plasmon resonance studies is equal to k_1 . The reverse rate constant is k_{-1} . The rate at which conformational change (EI^*) occurs is denoted as k_2 . k_3 occurs during substrate reaction which results in cleaved serpin and release of active protease ($E+I^*$). Formation of serpin/protease covalent complex ($E-I^*$) results in complete inhibition and the rate constant is represented as k_4 .

Figure 4.16.
Mechanism of serpin inhibition



One of the challenging aims in this study was to establish a binding assay using surface plasmon resonance (SPR) between human α_2 -antiplasmin and plasmin. One of the advantages of using SPR is that binding of α_2 -antiplasmin/plasmin is monitored in real time. The technology is very sensitive, therefore extremely low concentrations of ligand and analyte are required to generate a detectable response. In this study, α_2 -antiplasmin was assigned as the ligand (protein immobilised on the chip surface). It is well known that the end product of α_2 -antiplasmin/plasmin is an irreversible covalent complex. In order to obtain accurate binding data, clear association and dissociation curves are required. If a covalent complex is formed, the dissociation phase will not be seen. Due to this fact, plasmin was irreversibly blocked with a commercially available plasmin inhibitor, CMK (D-Val-Phe-Lys Chloromethyl Ketone) to prevent the covalent complex formation. Therefore, active site-blocked plasmin (PI_mCMK) was chosen as the analyte in this work. In order to account for non-specific binding of PI_mCMK to the chip surface, a blank cell which does not contain immobilised ligand was used. All experiments conducted showed that baseline RU levels were maintained in the blank flow cell indicating that PI_mCMK does not bind non-specifically to the chip surface (results not shown). Nevertheless, each sensorgram produced in this thesis was subtracted with the blank flow cell to account for non-specific binding.

All recombinant human α_2 -antiplasmin generated is N-terminally His-tagged, therefore the nitrilotriacetic acid (NTA) chip was chosen to immobilise the His-tagged proteins in this present study. The benefits of using this chip are that the immobilised ligand, in this case α_2 -antiplasmin, will bind to the surface in a consistent orientation via the His-tag. In contrast, orientation of ligand binding on a CM5 chip is random and as a consequence, the interaction of target analyte will be inconsistent. Another benefit of using the NTA chip is the regeneration capability of the surface. Nickel ions (Ni^{2+}) chelating of the NTA surface are required for the capture of His-tagged proteins. Once the His-tagged proteins are bound, regeneration of the surface is a simple injection of buffer containing high concentration of EDTA which will remove both Ni^{2+} and His-tagged proteins. The surface is then ready for another immobilisation cycle. With this feature, the NTA chip can be used numerous times with different ligand being immobilised if desired. This aspect is unique to the NTA chip in comparison to the CM5 chip. Once the ligand is coupled onto a CM5 chip, the protein is permanently fixed to the surface. After multiple cycles and regeneration, the protein surface may degrade and binding of analyte to the ligand may be affected. By using the NTA chip, this problem will not occur as a fresh ligand layer is immobilised at each binding cycle.

The disadvantage of using the NTA chip was that leaching of His-tagged α_2 -antiplasmin from the surface layer was quite evident (results not shown). It was observed that if high amounts of His-tagged α_2 -antiplasmin were immobilised on the surface, the baseline level (>500 RU) of captured His-tagged protein will fall rapidly over time (process is known as

leaching), especially in the first 5 min. To minimise this problem, low levels of His-tagged α_2 -antiplasmin (50-100 RU) were captured on the NTA/Ni²⁺ surface and each concentration run was kept under 30 min. In this study, this issue was lessened by setting the analyte association time to 1 min and dissociation time to 5min, therefore each concentration cycle was less than 10 min and all variants tested were subjected to the same conditions.

The two-state reaction model describes a 1:1 binding of analyte to immobilised ligand, followed by a secondary interaction that stabilizes the two molecules. It is known that the interaction of α_2 -antiplasmin to plasmin induces a conformational change, therefore the two-state reaction model was used for data analysis. k_{a1} and k_{d1} are association and dissociation rate constants whereas k_{a2} and k_{d2} are forward and reverse conformation change constants based on Equation 4.3. This method of analysis is commonly used in many other different studies which describe conformational change in their molecules of interests (Lund-Katz et al., 2010; Sota et al., 1998).

The effects of the N- and/or C-terminal deletions on the rate of plasmin inhibition were investigated. Full-length human α_2 -antiplasmin was observed to have a inhibition rate of $3.7 \times 10^7 \text{ M}^{-1}\text{s}^{-1}$ which corresponds with published values (Christensen et al., 1996). As expected, the binding affinity of α_2 -antiplasmin to plasmin was high ($K_D = 1.6\text{nM}$). It was demonstrated that the N-terminus does not affect the binding affinity or rate of plasmin inhibition as the results produced are similar to that of full-length α_2 -antiplasmin. The absence of the C-terminus (C Δ) reduced both the rate of plasmin inhibition and binding affinity by ~40-fold when compared to full-length α_2 -antiplasmin. The most unexpected result was obtained when the mutant lacking both the N- and C-terminus (N Δ C Δ) was analysed. N Δ C Δ showed the expected decrease in plasmin inhibition rate as C Δ , however binding affinity was similar to wild-type α_2 -antiplasmin. The reason for this is unclear. The SI of N Δ C Δ was reported to be 1.8 and may be evidence of formation of latent and polymeric forms. Perhaps this may cause the recombinant N Δ C Δ to bind non-specifically to active site-blocked plasmin hence producing a high binding affinity. It is important to note that N Δ C Δ protein generated is lacking a cysteine amino acid at position 43 (Figure 1.10). Cysteines are known for their importance in intra-molecular disulfide bonding and the removal of Cys⁴³ in the α_2 -antiplasmin molecule may have altered structural stability thus increasing its propensity to become misfolded. It has been published that Cys⁴³ forms a disulphide bond with Cys¹¹⁶ and is highly conserved between species (Christensen et al., 1997). Therefore, to further explore this possibility, incorporation of Cys⁴³ and incremental additions of amino acids at the N-terminal region of α_2 -antiplasmin will be considered.

As previously determined, Lys⁴⁶⁴ is the most important lysine residue within the C-terminal region of α_2 -antiplasmin (Lu, 2008; Lu et al., 2011). To further confirm that the lysine

at 464 cannot be replaced with any other residue, a mutant where the lysine was mutated to arginine was generated. Arginine has the same positive charge in its side chains as lysine. From the inhibition and binding affinity data, we were able to show that Lys⁴⁶⁴ cannot be replaced with another residue, even of the same charge. Several studies have shown that arginine residues can improve stability in protein structures because arginine has the ability to form more electrostatic interactions as it contains three asymmetrical nitrogen atoms, whereas lysine only has one (Borders et al., 1994; Sokalingam et al., 2012). The ability for arginine to form multiple bonds may have affected the structure of the C-terminus and in turn altered the accessibility of the other lysine residues to the plasmin kringle domains, therefore decreasing binding affinity and rate of plasmin inhibition.

Using protease inhibition and binding affinity data, we were able to demonstrate a progressive decrease in rate of plasmin association, inhibition and binding affinity with consecutive Lys to Ala mutations within the C-terminus of α_2 -antiplasmin. We showed that all conserved lysine residues (Lys⁴²⁷, Lys⁴³⁴, Lys⁴⁴¹, Lys⁴⁴⁸ and Lys⁴⁶⁴) play a role in the interaction with kringle domains of plasmin, with the most C-terminal lysine (Lys⁴⁶⁴) being the main mediator, followed by Lys⁴⁴⁸, which corresponds with previously published data (Frank et al., 2003; Gerber et al., 2010). Individually, the internal lysine residues appear to have a minor function in the interaction with plasmin. However, as demonstrated by several of our α_2 -antiplasmin mutants, primarily K434A/K441A/K448A/K464A and C Δ , we were able to show that when five of the lysines were mutated, the rate of plasmin inhibition and binding was reduced when compared to the C-terminally truncated α_2 -antiplasmin protein. This indicates that the lysine residues within the C-terminus of α_2 -antiplasmin are the primary mediators in the binding to the kringle domains and that removal of these residues will result in the loss of C-terminal binding. Furthermore, K427A/K434A/K441A/K448A/K464WT demonstrated that even with the presence of the most C-terminal lysine with all the internal lysines mutated, the plasmin inhibition rate obtained was not comparable with WT α_2 -antiplasmin. Therefore, each conserved lysine residue in the C-terminus of α_2 -antiplasmin participates in the binding and inhibition of plasmin.

Previous studies by Frank and colleagues used individual recombinant plasmin kringle domains (K1, K3, K3mut, K4 and K5) to examine the affinity of the isolated α_2 -antiplasmin C-terminus. K1 had the highest affinity, followed by K4, K5 and K2 (Frank et al., 2003). In further experiments, Gerber *et al.* examined the affinity of the recombinant plasmin kringle domains (K1, K1-3, K4 and K4-5) (Gerber et al., 2010). They demonstrated that progressive mutations of lysine residues within the C-terminus of α_2 -antiplasmin decrease the affinity for K1-3, although the greatest contribution to binding was attributable to Lys⁴⁶⁴ and Lys⁴⁴⁸. The apparent lack of effect on the affinity of mutations of Lys⁴¹⁸, Lys⁴²⁷, Lys⁴³⁴ and Lys⁴⁴¹ may be explained by the fact that only two lysine binding kringle domains were present in the K1-3

protein as it is known that K3 does not bind to lysines (Marti et al., 1994). The discrepancy between our results and those of Gerber and colleagues can be accounted for by difference in experimental approaches. They measured the association constants of isolated kringle domains with the C-terminal portion of α_2 -antiplasmin. By contrast, this study describes the rate of plasmin inhibition and binding affinity of full-length α_2 -antiplasmin with intact plasmin.

C Δ , N Δ C Δ and K434A/K441A/K448A/K464A were analysed using the discontinuous method as this protocol is suitable in measuring rates of less than $10^6 \text{ M}^{-1}\text{s}^{-1}$ (Horvath et al., 2011; Olson et al., 1993). The discontinuous method produced results which were ~2-fold slower when compared to the continuous method. Employment of stopped-flow kinetics, as described by Christensen and colleagues (1996), could be considered in future work to compare slower inhibitory rates ($k_a < 10^6 \text{ M}^{-1}\text{s}^{-1}$).

One striking observation made in this study is that the rate of plasmin inhibition and binding affinity of plasmin with C-terminally truncated (C Δ) were relatively high ($k_a = 3.8\text{-}9.2 \times 10^5 \text{ M}^{-1}\text{s}^{-1}$; $K_D = 49\text{nM}$). It is important to note that SPR studies were performed with active site-blocked plasmin, suggesting that the rapid association and high affinity observed in the absence of the C-terminal extensions may be mediated by exosite interactions between the serpin body and the protease. The interactions between the α_2 -antiplasmin core domain, outside the immediate vicinity of P1-P1', and the active site cleft of plasmin are also likely to contribute specificity to the serpin/protease interaction. Having additional exosite interactions is not uncommon in the serpin inhibition mechanism, as it may aid in the recognition of its target protein (Lin et al., 2011; Whisstock et al., 2010).

4.5 Conclusion

In summary, detailed kinetic and binding studies of the interaction between α_2 -antiplasmin and plasmin has been described in this chapter. Within the α_2 -antiplasmin C-terminus, the contribution of the conserved lysine residues to the interaction with the plasmin kringle domains has been measured. This study demonstrates that the C-terminal lysine, Lys⁴⁶⁴, is the single most important amino acid. The remaining conserved lysine residues within the C-terminus individually contribute less, but together significantly enhance the rate of serpin/protease association. These data support the zipper model of interaction whereby Lys⁴⁶⁴ binds initially to plasmin (most likely at K1), followed by progressive binding of the other conserved lysines (Lys⁴⁴⁸, Lys⁴⁴¹ and Lys⁴³⁴) to the remaining lysine binding kringle domains. Results seen with Δ α_2 -antiplasmin and plasmin highlighted the importance of exosite interactions between the α_2 -antiplasmin core serpin domain and protease, which provides additional mechanism of specificity in the serpin/protease interaction. Exosite interaction between α_2 -antiplasmin and plasmin will be further investigated in Chapters 5 and 6.

Chapter 5:

Expression, purification and non-covalent complex studies of microplasmin(ogen)

This page has been intentionally left blank.

5.1 Introduction

Plasmin (Plm) is a serine protease which circulates in the body in its inactive precursor form, plasminogen (Plg). Plg exists in two forms, Glu-plasminogen (Glu-Plg) and Lys-plasminogen (Lys-Plg). Glu-Plg, the predominant circulating molecule, contains the N-terminal peptide (Glu¹-Lys⁷⁷), protease domain and five kringle domains (K1-5) (Parry et al., 1998) and is 791 amino acids in length. Lys-Plg is generated by plasmin hydrolysis where the N-terminal peptide is cleaved at Lys⁷⁷-Lys⁷⁸, yielding a zymogen which is more readily activated by plasminogen activators and has a higher affinity for fibrin compared to Glu-Plg. Plasmin(ogen) is a multi-domain molecule and it is known that a high degree of structural mobility occurs during the transition between plasminogen to plasmin. Due to this fact, crystallisation of full-length plasminogen was challenging and the structure was only recently determined (Law et al., 2012). Therefore, a shortened form of plasminogen which lacks all kringle domains to minimise structural mobility is a more favourable molecule for further crystallisation studies with α_2 -antiplasmin.

Microplasminogen (μ Plg), a truncated form of Plg which only contains the protease domain (Pro⁵⁴²-Asn⁷⁹¹), does not naturally occur in human circulation but can be produced by either proteolytic cleavage of Plg or recombinant protein technology. There are a number of methods which describe the expression and purification of μ Plg. Briefly, μ Plg has been produced in prokaryotic expression system (*Escherichia coli* (Ma et al., 2007; Medynski et al., 2007; Parry et al., 1998)), in eukaryotic cells (High Five cells (Peisach et al., 1999) and Sf9 cells (Wang et al., 1995)). Another method of obtaining μ Plg is through proteolytic cleavage of full-length plasminogen by active plasmin (Shi and Wu, 1988; Wu et al., 1987). The activation site (Arg⁵⁶¹-Val⁵⁶²) is present, therefore μ Plg can be converted to microplasmin (μ Plm) by plasminogen activators. The crystal structure of mutant μ Plg (Peisach et al., 1999) and ternary structure of μ Plm-staphylokinase- μ Plm (Parry et al., 1998) have also been previously described.

One of the important observations seen from Chapter 4 was the high binding affinity seen with active site-blocked plasmin and C-terminally truncated α_2 -antiplasmin ($K_D = 50$ nM). This led to the hypothesis that an additional exosite interaction may exist outside of the conventional RCL to protease active site and the α_2 -antiplasmin C-terminal to kringle domains. This interaction may lie between the serpin core and protease domain and to explore this theory, crystallisation of α_2 -antiplasmin and μ Plm complex may provide a direct visualisation of this exosite interaction. Therefore, the aims of this chapter were first, to establish an expression, purification and activation protocol for μ Plg/ μ Plm (active and active site mutated). Further to this, active site mutated μ Plm and N-terminally truncated antiplasmin complex were produced and biochemical studies (Native-PAGE and non-reduced SDS-PAGE) were performed to determine if the non-covalent complex could be generated and purified (gel filtration) for crystallisation.

5.2 Methods

5.2.1 Generation of Microplasminogen Expression Constructs

Human WT plasminogen (Plg) was isolated from a liver cDNA library and using PCR and the active site of Plg was mutated (Plg S741A) by Ms Corrine Hitchen (previous research assistant in our laboratory). Subsequently, microplasminogen (μ Plg) was isolated from Plg S741A with primers 5'- AGGATCCATGGCGGCCCTTCATTTG-3' (#4434) and 5'- GGATCCTTAATTATTTCTCATC-3' (#445). The product was cloned into either the pET(3a)His or pET(3a) expression vector and sequenced for authenticity. Site-directed mutagenesis was performed with primers #453 and #454 to return the active site to WT (Table 5.1). The following clones were generated: His- μ Plg S741A, His- μ Plg WT and μ Plg WT.

As previously described in section 3.2.2, sequence alignment, molecular weight, extinction co-efficient and isoelectric point (pI) were determined using the Translate, Multalin and ProtParam tool which are accessible from the ExPASy website (<http://expasy.org/tools/>).

Table 5.1. Primer sequences for human μ PIg.

Primer Name	Orientation	Nucleotide Sequence (5' → 3')
#443	Sense	AGGATCCATGGCGGCCCTTCATTTG
#445	Antisense	GGATCCTTAATTATTTCTCATC
#453	Sense	GCCAGGGTGACAGTGGAGGTCCTCTGG
#454	Antisense	CCAGAGGACCTCCACTGTCACCCTGGC

5.2.2 Trial Expression of Microplasminogen

As the production of recombinant μ PIg in a bacterial expression system has yet to be established in our laboratory, trial induction and expression of μ PIg was carried out to determine the optimal conditions for producing this protein. Based on available protocols by other scientific groups (Medynski et al., 2007; Parry et al., 1998), relevant changes to their protocol were made to suit the protein production conditions for our laboratory.

Escherichia coli BL21(DE3)pLys cells were transformed with either pETHis- μ PIg or pET- μ PIg as described in section 2.5.5. The transformed cells were used to inoculate a 5mL culture of 2x tryptone-yeast medium (2x TY) supplemented with 100 μ g/mL ampicillin and grown overnight (o/n) in a shaking incubator at 37°C, rotating at 220rpm. The cell culture were then diluted 1:10 in fresh 2x TY media supplemented with 100 μ g/mL ampicillin and grown for a further 2 hr at 37°C with rotation at 220rpm. The cells were induced with three different concentration of IPTG (0.5mM, 1mM and 2mM final concentration) and grown for another 3 hr at 37°C and 220rpm. Cells were harvested by centrifugation at 3000rpm (Beckman coulter Allegra X-12R) for 10 min at room temperature (RT). The supernatant was discarded and the cell pellet was resuspended in 50 μ L of IB Lysis buffer (50mM Tris-HCl pH8.0, 100mM NaCl, 1% Triton X-100, 5mM MgCl₂, 1mg/mL lysozyme, 0.1mg/mL DNase, 0.01% PMSF and 1:1000 protease inhibitor cocktail). The cells were incubated on ice for 20 min before it was completely frozen down in liquid nitrogen, and then completely thawed in a 37°C water bath. This freeze-thaw cycle was repeated three times. The lysates was centrifuged (Biofuge pico Haraeus) at 13,000rpm at RT for 10 min. Soluble and insoluble samples were prepared for analysis on a 12.5% SDS-PAGE (section 2.6.1) and subsequently analysed by Western blot (section 2.6.4) (Refer to section 5.2.13 for details on primary and secondary antibodies used).

5.2.3 Large Scale Expression of Microplasminogen

E.coli BL21 transformed with either pETHis- μ PIg or pET- μ PIg were inoculated into a culture of 2x TY containing 100 μ g/mL ampicillin and grown overnight in a shaking incubator at 37°C, rotating at 220rpm. The cell culture was diluted into fresh 2x TY supplemented with 100 μ g/mL ampicillin and grown for a further 2 hr under the same conditions. The cells were then induced with a final IPTG concentration of 1mM and grown for another 3 hr at 37°C and 220rpm. Cells were harvested by centrifugation at 3500rpm (Beckman JS-4.2 rotor) for 20 min at 4°C. The supernatant was discarded and the cell pellet was lysed or stored at -80°C until further use.

5.2.4 Inclusion Bodies (IB) Purification

Recombinant μ PIg were produced as insoluble protein in the bacteria, therefore μ PIg will be found in the inclusion bodies (IB) of the bacteria. IB were obtained from lysing the cell pellet with μ PIg Lysis buffer and the lysis method is as described in section 5.2.3. The supernatant of the lysis process was discarded and the insoluble pellet, where the IB is present, was kept.

The IB pellet was washed with Wash buffer 1 (50mM Tris-HCl pH8.0, 0.5% Triton X-100, 100mM NaCl and 1mM EDTA) using a homogeniser (Wheaton Dounce Tissue Homogeniser 15 mL). For every 1mg of IB pellet, 15 mL of Wash buffer 1 was used. The homogenised pellet was transferred to a centrifugal tube and spun down (Sorval SS34 rotor) at 13,000rpm for 20 min at 4°C. The supernatant was discarded and the IB pellet was again homogenised with Wash buffer 1. The homogenising and centrifugation step was repeated three times. A small sample of the supernatant at each wash step was collected before it was discarded for Western blot analysis.

After the third wash with Wash buffer 1, the IB pellet was further washed into Wash buffer 2 (50mM Tris-HCl pH8.0 and 1mM EDTA) using a homogeniser. Again, for every 1mg of IB pellet, 15 mL of Wash buffer 2 was used. The homogenised pellet was centrifuged at 13,000rpm for 20 min at 4°C. The supernatant was discarded and the IB pellet was homogenised with Wash buffer 2 and centrifuged for a total of three times. Again, a small sample of supernatant was collected at each wash step for Western blot analysis. At the final centrifugation step, the IB pellet was divided into 100-200mg aliquots and stored at -80°C until further use. A small sample of IB was collected for analysis by Western blot.

5.2.5 Denaturation of IB

The IB pellet was denatured in Denaturing buffer (8M Urea, 50mM Tris-HCl pH8.0, 1mM EDTA and 10mM BME). For every 100mg of IB pellet, 10mL of Denaturing buffer was used. The IB pellet was allowed to denature at RT on a suspension mixer for 6-8 hr. The reaction was then centrifuged at 13,000rpm for 20 min at 4°C. The pellet was discarded and the soluble supernatant was used for refolding of μ PIg. A small sample of soluble and insoluble material was collected for analysis by Western blot.

5.2.6 Refolding of Microplasminogen from IB

Soluble denatured IB pellet was applied into a syringe and allowed to slowly drip through a needle (Terumo, 26g x 1/2") into Refolding buffer (50mM Tris-HCl pH8.0, 50mM NaCl, 1.25mM reduced glutathione and 0.125mM oxidised glutathione). For every 10mL of denatured IB, 150mL of Refolding buffer was used. This process was done o/n at 4°C and refolding was performed at slow mixing with a magnetic stirrer.

Refolded material was centrifuged at 13,000rpm for 20 min at 4°C and immediately placed into a dialysis tubing (Spectra/por 12-14 kDa cut-off) and dialysed into 5L μ PIg HisTrap A buffer (50mM Tris-HCl pH8.0 and 100mM NaCl) for 3 hr at 4°C followed by two additional 5L buffer changes. The second dialysis was again performed for 3 hr at 4°C, and at the final buffer change, the refolded material was allowed to dialysed o/n at 4°C. The dialysed material was filtered through a 0.2 μ M filter disc and kept cold before first stage purification. See section 5.2.7 for first stage purification of pETHis- μ PIg. pET- μ PIg was activated to μ PIm (section 5.2.9) straight after dialysis or purification of pET- μ PIg begins at section 5.2.10.

5.2.7 Purification of Microplasminogen on Nickel Chelate Affinity Chromatography

pET(3a)His- μ PIg (His- μ PIg WT and His- μ PIg S741A) were expressed with a hexahistidine tag on the N-terminal region of the protein. Whereas pET(3a)- μ PIg does not contain a hexahistidine tag therefore the first stage purification for this expression vector was on a cation exchange affinity column (section 5.2.10).

A 1mL Nickel-HisTrap column was used on the AKTA-UPC 900 HPLC system. The column was equilibrated with 5 column volumes of μ PIg HisTrap Buffer A (50mM Tris-HCl pH8.0, 100mM NaCl and 20mM Imidazole), followed by 5 column volume of μ PIg HisTrap Buffer B (50mM Tris-HCl pH8.0, 100mM NaCl and 500mM Imidazole) and then re-equilibrated back to μ PIg HisTrap buffer A. Due to the amount of refolded material present (>150mL), the soluble refolded μ PIg was loaded onto the HisTrap column using a peristaltic pump in a cold room at approximately 1mL/min. Once the sample has been loaded, the HisTrap column was transferred back to the HPLC system and the bound protein was eluted with a linear gradient of Imidazole (20mM to 500mM) over 10 column volumes at 1mL/min and 1mL fractions were collected in 96-well deep plates. Peak protein fractions were ran on a 12.5% SDS-PAGE and subsequently transferred onto Immobilon-P PVDF membrane for Western blot analysis. Peak fractions were then pooled, placed in a dialysis tubing (Spectra/por 12-14kDa cut-off) and dialysed in MonoS buffer A (20mM MES pH6.5 and 10% Sucrose) for 2 hr at 4°C to prepare for urokinase activation (section 5.2.9) or for the next purification step (section 5.2.10).

5.2.8 Activation of Microplasminogen to Microplasmin

5.2.8.1 Activation Studies with Urokinase Plasminogen Activator

Varying concentration (40 to 120units/mL/ μ M) of urokinase plasminogen activator (uPA) was incubated with a fixed amount of μ PIg (4 μ M) for 2 hr at 37°C. Once the reactions were completed, the samples were prepared for analysis on a 12.5% SDS-PAGE (section 2.6.1) and Coomassie blue staining (section 2.6.5.1). Activation of full-length plasminogen was also set up as a control.

A fixed amount of uPA (40units/mL/ μ M) was incubated with a fixed amount of μ PIg (4 μ M) for varying time lengths (15, 30, 45, 60, 90 and 120min) at 37°C. Once the reactions were completed, the samples were prepared for SDS-PAGE and subsequently transferred for Western analysis. The membrane was then probed with an antibody against plasminogen and analysed by Coomassie stain.

5.2.8.2 Activation Studies with Tissue-type Plasminogen Activator

Varying concentration of tissue-type plasminogen activator (tPA) was incubated with a fixed amount of μ PIg at a ratio of 50:1, 10:1 and 2:1 (μ PIg:tPA) for different time lengths (2-22 hr) at 37°C. Once the reactions were completed, the samples were prepared for analysis on a 12.5% SDS-PAGE and subsequently transferred for Western blot analysis. The membrane was probed with an antibody against plasminogen and analysed by Coomassie stain.

5.2.9 Preparation of Microplasmin

Protein concentration of dialysed pooled HisTrap fractions (from section 5.2.7) were determined using direct measurement at 280nm (section 2.6.6). 40Units/mL/ μ M of uPA was added to the reaction and incubated at 37°C on slow rotation. The sample was then filtered through a 0.2 μ M membrane and placed on ice until purification on a cation exchange affinity column (section 5.2.10).

5.2.10 Purification of Microplasmin(ogen) on Cation Exchange Affinity Chromatography

This stage of purification involves the binding of positively charged protein to the negatively charged column. μ PIg and μ PIm has a theoretical pI of ~8 and therefore the buffers used for this method is at pH6.5 for the protein to be positively charged.

Tricorn MonoS 5/50 GL column (GE Healthcare) was used for this protocol. The column was equilibrated by 5 column volume of MonoS buffer A (20mM MES pH6.5 and 10% Sucrose), followed by 5 column volume of MonoS buffer B (20mM MES pH6.5, 10% Sucrose and 1M NaCl) then re-equilibrated back to MonoS buffer A. The protein sample was transferred out of the dialysis tubing and filtered through a 0.2 μ M filter membrane to remove any precipitated protein. The sample was then loaded onto the system using a 10mL sample loop. The protein was eluted with increasing linear concentration of NaCl (0 to 1M) over 20 column volumes at 1mL/min. 500 μ L fractions were collected in a 96-well deep plate. Peak fractions were ran on a 12.5% SDS-PAGE and subsequently transferred to Immobilon-P PVDF for Western blot analysis and Coomassie staining.

For recombinant μ PIg, peak fractions were pooled and aliquots of recombinant protein were stored at -80°C until further use. Protein concentration of recombinant μ PIg was determined by direct measurement at 280nm (section 2.6.6).

For recombinant μ PIm purification, peak fractions were then pooled and placed in a dialysis tubing (Spectra/por 12-14kDa cut-off) and dialysed in Benzamidine binding buffer (50mM Tris-HCl pH7.4 and 0.5M NaCl) for 2 hr at 4°C. The sample was then filtered through a 0.2 μ M membrane and placed on ice for further purification (section 5.2.11).

5.2.11 Purification of Microplasmin on Benzamidine Affinity Chromatography

This stage of purification involves the separation of trypsin and trypsin-like serine proteases. A 1 mL HiTrap Benzamidine FF column (GE Healthcare) was used for this protocol. The column was equilibrated with 5 column volume of MQH₂O followed by 5 column volume of Benzamidine binding buffer. The filtered protein sample was then applied onto the column using a 10mL sample loop at 1mL/min. Once the protein has bound to the column, it was then washed with 5 column volume of Benzamidine wash buffer (50mM Tris-HCl pH7.4, 1M NaCl and 20mM p-aminobenzamidine) before eluting with Benzamidine elution buffer (50mM Glycine pH3.0). The protein was then eluted with decreasing linear pH gradient (pH7.4 to pH3.0) over 10 column volume at 1mL/min. 1mL fractions were collected in a 96-well deep plate. μ Plm-WT fractions were kept at low pH, whereas μ Plm-S741A fractions were neutralised with 60 μ L of 1M Tris-HCl pH9.0. Peak fractions were analysed on 12.5% SDS-PAGE and subsequently transferred onto Immobilon-P PVDF for Western blot analysis and Coomassie staining to determine the purity of the purified protein of interest. Protein concentration of recombinant μ Plm was determined by direct measurement at 280nm (section 2.6.6). Purified protein were stored at -80°C or purified further by size exclusion chromatography (section 5.2.12) for crystallisation purposes.

5.2.12 Purification of Microplasmin on Size Exclusion Chromatography

To remove any polymeric species which may be observed with recombinant μ Plm or N Δ , size exclusion chromatography on the Superdex 75 column (GE Healthcare) was performed. The column was equilibrated with one column volume (25 mL) of MQH₂O followed by one column volume of Gel Filtration Buffer (25mM Tris-HCl pH8.0, 150mM NaCl, 5% Glycerol and 0.05% NaAz). 0.5mL or 1mL of the protein sample was loaded using a 500 μ L or 1mL sample loop. 200 μ L fractions were collected on a 96-well plate and peak fractions were ran on a 12.5% SDS-PAGE and subsequently transferred onto Immobilon-P PVDF for Western blot. In addition, gel filtration standards (Biorad) were loaded onto the column.

5.2.13 Western Blot Analysis Microplasmin(ogen)

Recombinant μ PIg and μ PIm proteins were ran on a 12.5% SDS-PAGE (section 2.6.1) and were subsequently transferred onto Immobilon-P PVDF membrane as described in section 2.6.4. Membranes were incubated with 1:3000 dilution of primary antibody (anti-plasminogen raised in sheep), followed by 1:5000 dilution of the secondary antibody (anti-sheep/goat).

5.2.14 Microplasmin/ α_2 -antiplasmin Co-complex Studies

5.2.14.1 Detection of Microplasmin/ α_2 -antiplasmin Co-complex on Native-PAGE

μ PIm was incubated with hAP at a 1:1 and 2:1 molar ratio at 37°C for 30min. A minimum of 10 μ g of total protein in the reaction was then analysed on a native or acid native-PAGE as previously described in section 2.6.2. The protein on the gel were then transferred onto Immobilon-P PVDF membrane for Western blotting (section 5.2.13) and subsequently stained with Coomassie (section 2.6.5.2).

5.2.14.2 Detection of Microplasmin/ α_2 -antiplasmin Co-complex on Non-reduced SDS-PAGE

μ PIm was incubated with hAP at a 1:1 and 1:2 molar ratio at 37°C for 30min. A minimum of 1 μ g of total protein in the reaction was then analysed on a non-reduced SDS-PAGE. The gel is composed of the same constituents as described in section 2.6.1 and ran in the same manner. The difference is the preparation of the sample which involves addition of 5x non-reduced SDS-PAGE loading dye which does not contain BME and the sample does not require any boiling. The gel was then stained with Coomassie to visualise the protein band (section 2.6.5.1).

5.2.14.3 Detection of Microplasmin/ α_2 -antiplasmin Co-complex by Co-purification on Size Exclusion Column

μ Plm was incubated with hAP at a 1:1 molar ratio at 37°C for 30min. The protein sample was then syringe filtered through a 0.2 μ m filter disc to remove any precipitated protein. The sample was then loaded onto the gel filtration column as previously described in section 5.2.12. Peak fractions were run on a 12.5% SDS-PAGE and subsequently transferred onto Immobilon-P PVDF membrane for Western analysis.

5.2.15 Crystallisation Trials of Microplasmin/ α_2 -antiplasmin Co-complex

5.2.15.1 Sample Preparation of Recombinant Δ hAP and Recombinant His- μ Plm-S741A

Recombinant hAP and His- μ Plm were expressed and purified as previously described (Chapter 3 and Chapter 5 respectively). To obtain an optimal concentration for crystallisation trials, hAP and His- μ Plm were concentrated separately on an Ultrafree-0.5 centrifugal filter device (Millipore) by centrifuging at 14,000 x g at 4°C until the protein was concentrated to approximately 5-12mg/mL as determined by direct protein concentration measurement at 280nm. The protein was then added together at a 1:1 molar ratio and incubated for 30-60 min at RT. The protein sample was then centrifuged at 13,000rpm at 4°C to remove any protein which may have precipitated before setting up the crystallisation trays.

5.2.15.2 Preliminary Crystallisation Screening Trials of Microplasmin/ α_2 -antiplasmin Non-covalent Co-complex

Crystallisation trial experiments were performed using the hanging drop method. A 10mL polypropylene syringe (without a needle) was used to apply a uniform layer of vacuum grease around the rims of a 24-well plate (Linbro) and leaving a 10mm gap. 1 μ L of 1:1 μ Plm/hAP protein mixture was first placed in the centre of a coverslip and was mixed with 1 μ L of reservoir buffer. The coverslip was flipped so that the protein drop is on the bottom, and this was placed over the appropriate well with reservoir buffer.

Precipitant conditions were performed using commercially available crystallisation kits (Sigma and Hampton 1). The conditions in these kits varied in buffer type, pH, precipitant type, concentration and additives.

5.3 Results

5.3.1 Generation of Microplasminogen in pET(3a)His and pET(3a) Expression Vector

Microplasminogen S741A (μ Plg S741A) was initially isolated from the full-length plasminogen template by PCR (section 5.2.1) using generated primers #443 and #445 (Table 5.1). Subsequently, this product was introduced into the pET(3a)His expression vector via the BamHI site in the multiple cloning region. This was to generate recombinant μ Plg with a poly-Histidine tag and resulted with His- μ Plg S741A expression construct. This variant contains an N-terminal hexahistidine-tag (His-tag) and is catalytically inactive due to the single amino acid change at position 741. The active site was returned to wild-type (WT) with mutagenic primers (#453 and #454 – see Table 5.1) to produce the second expression construct of His- μ Plg WT. A variant which did not possess the N-terminal His-tag was also generated by subcloning μ Plg WT into the BamHI region of the pET(3a) expression vector. Therefore, three expression constructs were generated: His- μ Plg S741A, His- μ Plg WT and μ Plg WT. Figure 5.1 outlines the strategy for cloning human μ Plg.

All variants were sequenced for authenticity. Sequence alignment of all variants produced is shown on Figure 5.2. Table 5.2 is a summary of the extinction coefficient, molecular weight (MW) and isoelectric point (pI) of μ Plg variants as calculated from the predicted amino acid sequence.

Figure 5.1. Cloning strategy for microplasminogen variants into the pET(3a)His and pET(3a) expression vector. The plasminogen (plg) gene containing active site mutation (S741A) was amplified with the corresponding primers to isolate μ Plg. The PCR product was cloned in-frame with the 6xHistidine (His) tag via BamHI restriction site in the multiple cloning region (MCR) producing **A)** His- μ Plg S741A. Site-directed mutagenesis was performed to mutate the Alanine at position 741 to Serine and cloned into **B)** pET(3a)His expression vector (His- μ Plg WT) and **C)** pET(3a) expression vector (μ Plg WT).

Figure 5.1.
Cloning strategy for microplasminogen variants into the pET(3a)His and pET(3a) expression vector

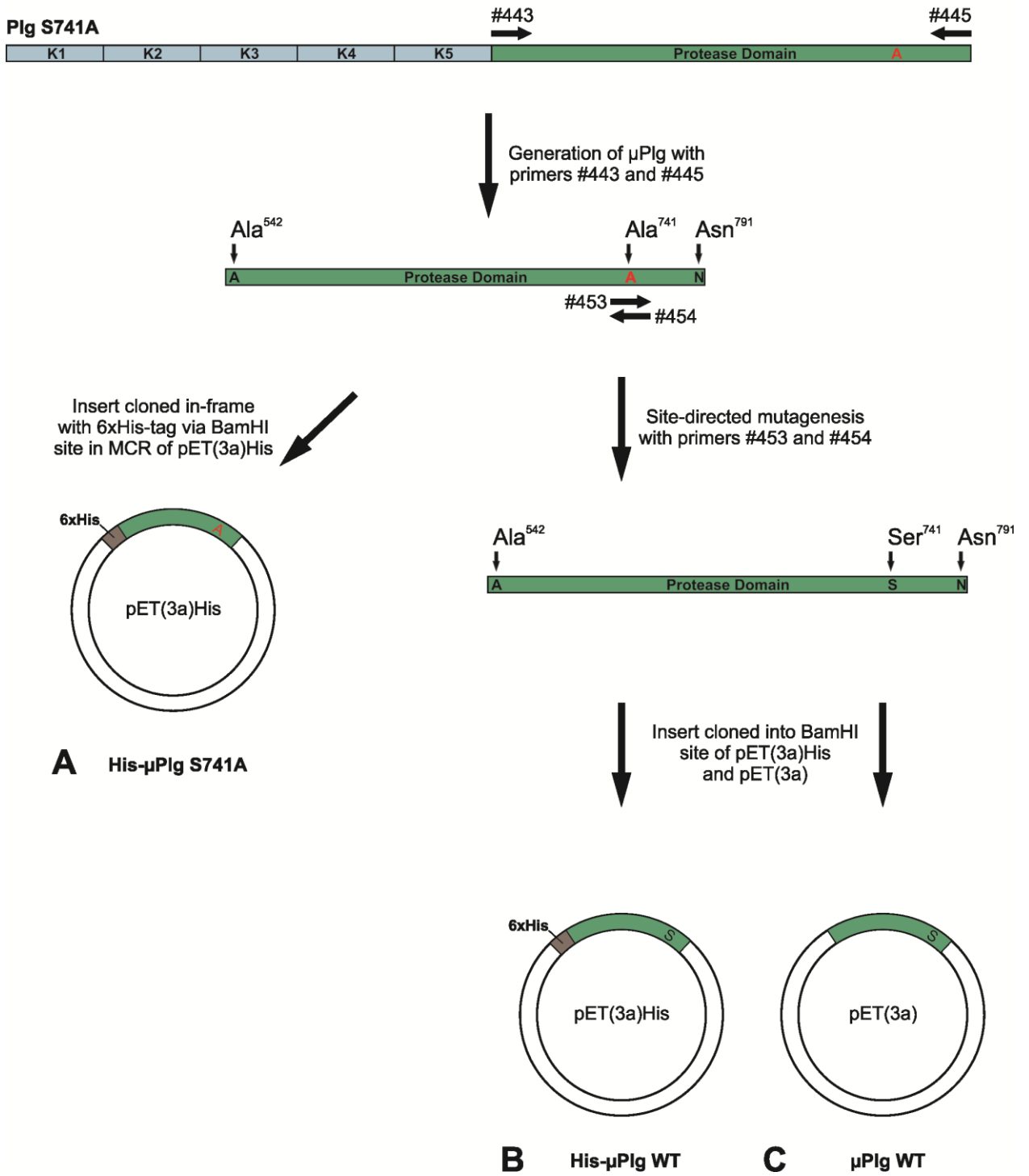


Figure 5.2. Sequence alignment His- μ PIg S741A, His- μ PIg WT and μ PIg WT. His-tagged wild-type (His- μ PIg WT) and active site mutated (His- μ PIg S741A) human microplasminogen were generated, expressed and purified. The region highlighted in grey is the 6xHistidine tag. μ PIg consists of the protease domain (Ala⁵⁴²-Asn⁷⁹¹) and lacks all five kringles. The active site of μ PIg is rendered inactive by a single amino acid change at position 741 where the Serine residue (highlighted in yellow) is replaced with Alanine (highlighted in green). Recombinant μ PIg was also produced without a His-tag (μ PIg WT) for binding studies. The numbering of recombinant μ PIg variants was based on the full-length plasminogen form of 791 amino acids.

Figure 5.2.
Sequence alignment of His- μ Plg S741A,
His- μ Plg WT and μ Plg WT

		542				580
His- μ Plg S741A	MMHHHHHGS	MAAPSFDCGK	PQVEPKKCPG	RVVGGCVAHP	HSWPWQVSLR	
His- μ Plg WT	MMHHHHHGS	MAAPSFDCGK	PQVEPKKCPG	RVVGGCVAHP	HSWPWQVSLR	
μ Plg WT		MAAPSFDCGK	PQVEPKKCPG	RVVGGCVAHP	HSWPWQVSLR	
		581				630
His- μ Plg S741A	TRFGMHFCGG	TLI SPEWVLT	AAHCLEKSPR	PSSYKVILGA	HQEVNLEPHV	
His- μ Plg WT	TRFGMHFCGG	TLI SPEWVLT	AAHCLEKSPR	PSSYKVILGA	HQEVNLEPHV	
μ Plg WT	TRFGMHFCGG	TLI SPEWVLT	AAHCLEKSPR	PSSYKVILGA	HQEVNLEPHV	
		631				680
His- μ Plg S741A	QEIEVSRLFL	EPTRKDIALL	KLSSPAVITD	KVIPACLPS P	NYVVADRTEC	
His- μ Plg WT	QEIEVSRLFL	EPTRKDIALL	KLSSPAVITD	KVIPACLPS P	NYVVADRTEC	
μ Plg WT	QEIEVSRLFL	EPTRKDIALL	KLSSPAVITD	KVIPACLPS P	NYVVADRTEC	
		681				730
His- μ Plg S741A	FITGWGETQG	TFGAGLLKEA	QLPVIENKVC	NRYEFLNGRV	QSTELCAGHL	
His- μ Plg WT	FITGWGETQG	TFGAGLLKEA	QLPVIENKVC	NRYEFLNGRV	QSTELCAGHL	
μ Plg WT	FITGWGETQG	TFGAGLLKEA	QLPVIENKVC	NRYEFLNGRV	QSTELCAGHL	
		731				780
His- μ Plg S741A	AGGTDSCQGD	GGPLVCFEK	DKYILQGVTS	WGLGCARPKN	PGVYVRVSRF	
His- μ Plg WT	AGGTDSCQGD	GGPLVCFEK	DKYILQGVTS	WGLGCARPKN	PGVYVRVSRF	
μ Plg WT	AGGTDSCQGD	GGPLVCFEK	DKYILQGVTS	WGLGCARPKN	PGVYVRVSRF	
		781	791			
His- μ Plg S741A	VTWIEGVMRN	N				
His- μ Plg WT	VTWIEGVMRN	N				
μ Plg WT	VTWIEGVMRN	N				

Table 5.2. Molecular weight (MW), extinction coefficient and isoelectric point (pI) of human μ PIg variants. Parameters were calculated using the ProtParam Tool available at the following website: <http://web.expasy.org/protparam/>

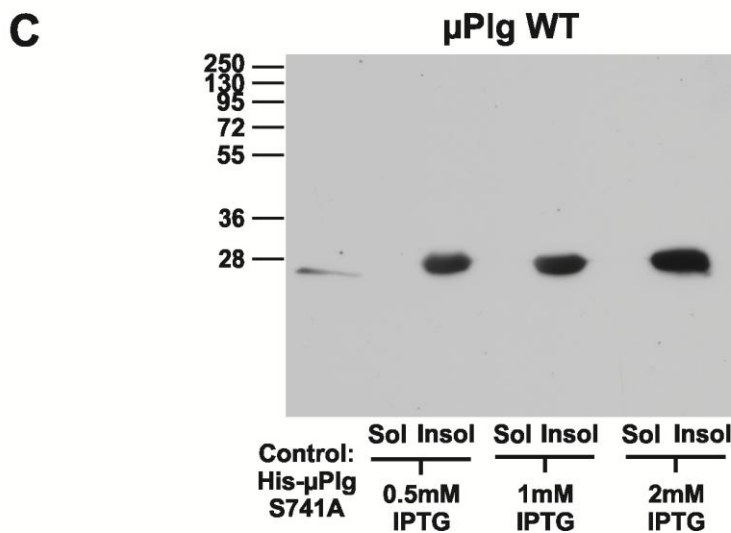
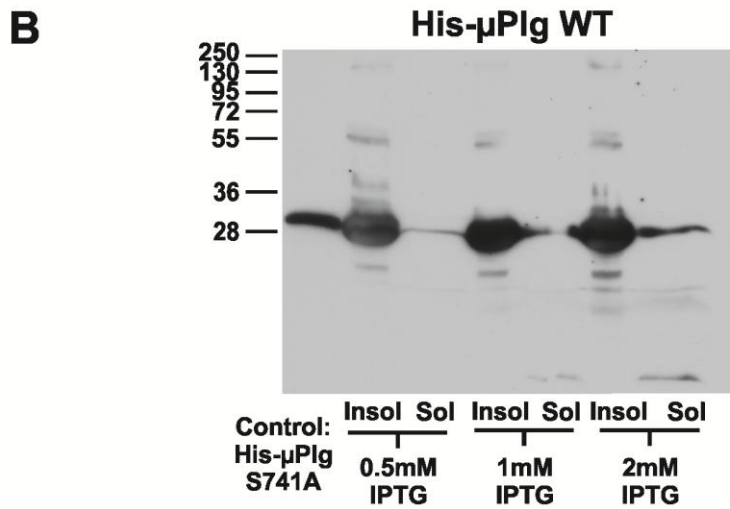
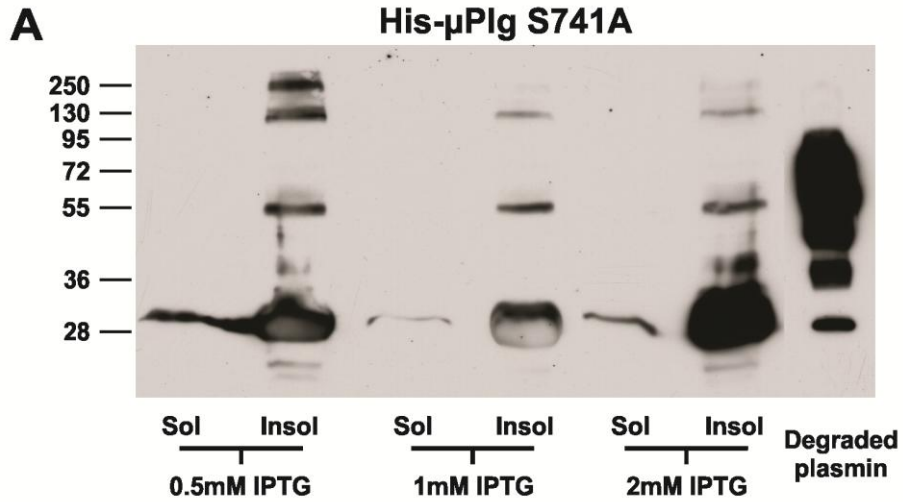
Recombinant μPIg	MW	Extinction Coefficient	pI
His-μPIg S741A	28516	41200	8.25
His-μPIg WT	28516	41200	8.25
μPIg WT	27434	41200	8.24

5.3.2 Trial Expression of Microplasminogen

Initial small scale trial expressions were set up to determine if μ Plg could be expressed in the *Escherichia coli* bacterial expression system. Protein expression cultures (5mL) were prepared and were induced at varying IPTG concentration (0.5mM, 1mM and 2mM) for 3 hrs at 37°C. Insoluble and soluble bacterial lysates were collected and samples were prepared for Western blot analysis. Figure 5.3 shows the Western blot analysis for His- μ Plg S741A (Figure 5.3A), His- μ Plg WT (Figure 5.3B) and μ Plg WT (Figure 5.3C) probed with an antibody against human Plg. In all the μ Plg expression trials, a predominant band is seen at approximately 28kDa, which corresponds to the predicted molecular weight of μ Plg, in the insoluble fraction of all IPTG induction concentration. From the Western blots, it was determined that μ Plg was produced in the insoluble pellet and required denaturing and refolding procedure before further purification. The expression level of all recombinant μ Plg appeared to be consistent at each IPTG concentration. 1mM final concentration of IPTG was selected for all large scale expression of μ Plg variants.

Figure 5.3. Trial expression of microplasminogen as detected by Western blot of insoluble and soluble lysates. 5mL cultures were prepared and protein production was produced by inducing with varying amounts of IPTG at 37°C for 3 hrs. Insoluble (Insol) and soluble (Sol) bacterial lysates were collected. Samples were ran on a reduced 12.5% SDS-PAGE and subsequently analysed on Western blots with an antibody against plasminogen. Relative molecular weight in kDa is as indicated on the left of each Western. Recombinant μ PIg was seen predominantly in the insoluble fraction at approximately 28kDa. **A)** Trial expression of His- μ PIg S741A. **B)** Trial expression of His- μ PIg WT. **C)** Trial expression of μ PIg WT.

Figure 5.3.
Trial expression of microplasminogen as detected by
Western blot of insoluble and soluble lysates



This page has been intentionally left blank.

5.3.3 Large Scale Expression, Inclusion Bodies Purification, Denaturation and Refolding

In this section, the large scale expression and inclusion bodies (IB) preparation of recombinant μ PIg was described. A 3 litre culture was prepared and insoluble cell lysates containing IB pellets were collected. To separate the IB pellet from cellular debris, the insoluble cell lysate was homogenised and washed with buffer containing Triton-X (Wash Buffer 1). Samples of soluble supernatant were collected after each wash step and analysed by Western blot. Figure 5.4 shows the IB purification of His- μ PIg S741A. His- μ PIg S741A was the dominant band at 28 kDa, which corresponds to the predicted weight of μ PIg. It can be seen by both Western blotting and the Coomassie staining that insoluble μ PIg was still present in the IB pellet and was not solubilised during the Wash steps. Similar results were obtained for His- μ PIg WT and μ PIg-WT (data not shown). Approximately 0.6g of IB pellet was obtained for each 1L of culture.

To solubilise recombinant μ PIg, 8M urea was applied to 200mg of IB. Urea is a known denaturant, and promotes unfolding hence improving the solubility of proteins (Bennion and Daggett, 2003). Soluble and insoluble samples of His- μ PIg S741A were collected and analysed on a Western blot as shown in Figure 5.5. A large majority (~80%) of His- μ PIg S741A was solubilised in 8M Urea. Similar results were obtained for His- μ PIg WT and μ PIg-WT (data not shown).

Solubilised and unfolded μ PIg was then slowly dripped into refolding buffer to commence reformation of disulphide bonds. This step reduced the concentration of urea to help in the refolding process. In addition, glutathione reduced and oxidised (ratio of 10:1) were added to the buffer to enhance disulphide bond formation (Clark, 2001). Soluble and insoluble samples of His- μ PIg S741A were collected and analysed on a Western blot as shown in Figure 5.5. Approximately 75% of the denatured sample of His- μ PIg S741A (Figure 5.5) was solubilised and refolded. Recombinant μ PIg was ~90% pure at the end of the refolding stage as seen in Figure 5.5B. Similar results were obtained for His- μ PIg WT and μ PIg-WT (data not shown). The soluble fractions were then further dialysed to remove excess urea as described in section 5.2.6 before first stage of purification.

Figure 5.4. Inclusion bodies preparation of His- μ PIg S741A. Recombinant μ PIg was produced as an insoluble protein contained within the inclusion bodies (IB). To separate the IB from the cellular debris, buffer containing Triton-X (Wash Buffer 1) was performed. The second wash buffer (Wash Buffer 2) removes Triton-X from the IB pellet. The final purified IB pellet will contain the insoluble form of μ PIg seen as the dominant band at approximately 28kDa as indicated by the black arrows. Relative molecular weight in kDa is as indicated on the left of each Western. Samples were collected at each subsequent step and analysed on a Western blot with an antibody against plasminogen. **A)** Western blot of IB wash of His- μ PIg S741A. **B)** Coomassie stained Western membrane of His- μ PIg S741A.

Figure 5.4.
Inclusion bodies preparation of His- μ PIg S741A

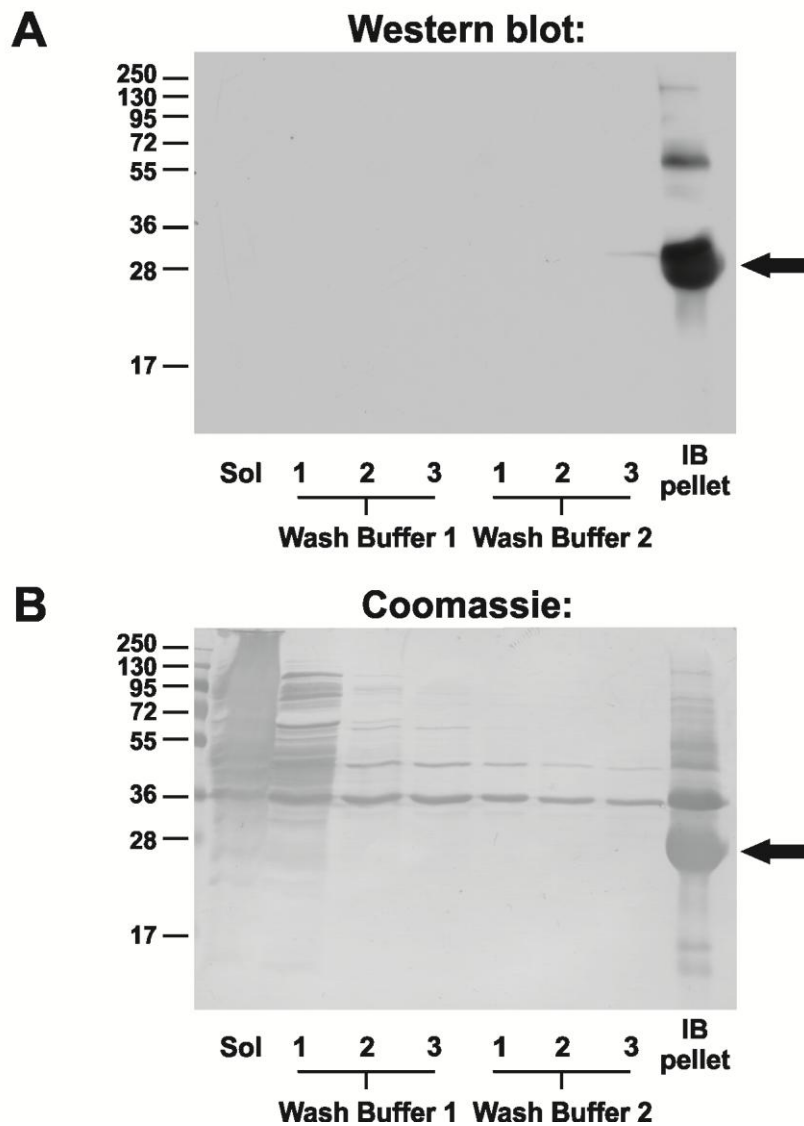
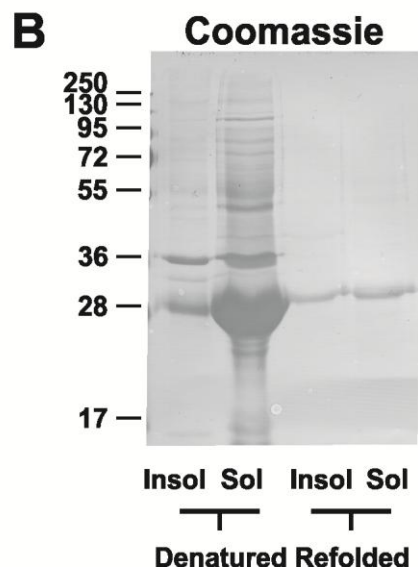
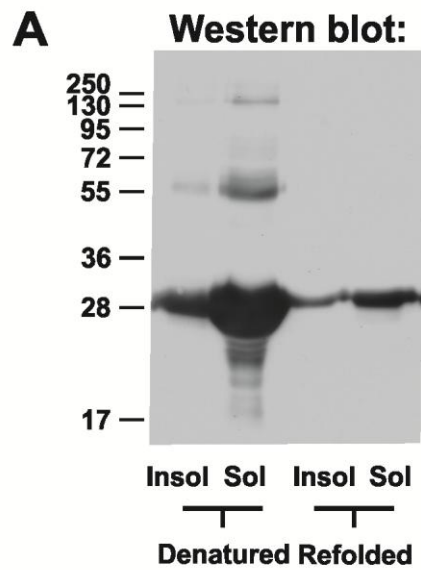


Figure 5.5. Denaturation and refolding of His- μ PIg S741A. Purified inclusion bodies (IB) were solubilised in buffer containing 8M Urea for 6-8 hrs at room temperature. The solution was then slowly dripped into refolding buffer to commence formation of μ PIg in its native conformation. Insoluble (Insol) and soluble (Sol) samples were collected at each step and analysed on a Western blot with an antibody against plasminogen. μ PIg seen as the dominant band at approximately 28kDa. Relative molecular weight in kDa is as indicated on the left of each Western. **A)** Western blot of denaturation and refolding of His- μ PIg S741A. **B)** Coomassie stained Western membrane of His- μ PIg S741A.

Figure 5.5.
Denaturation and refolding of His- μ PIg S741A



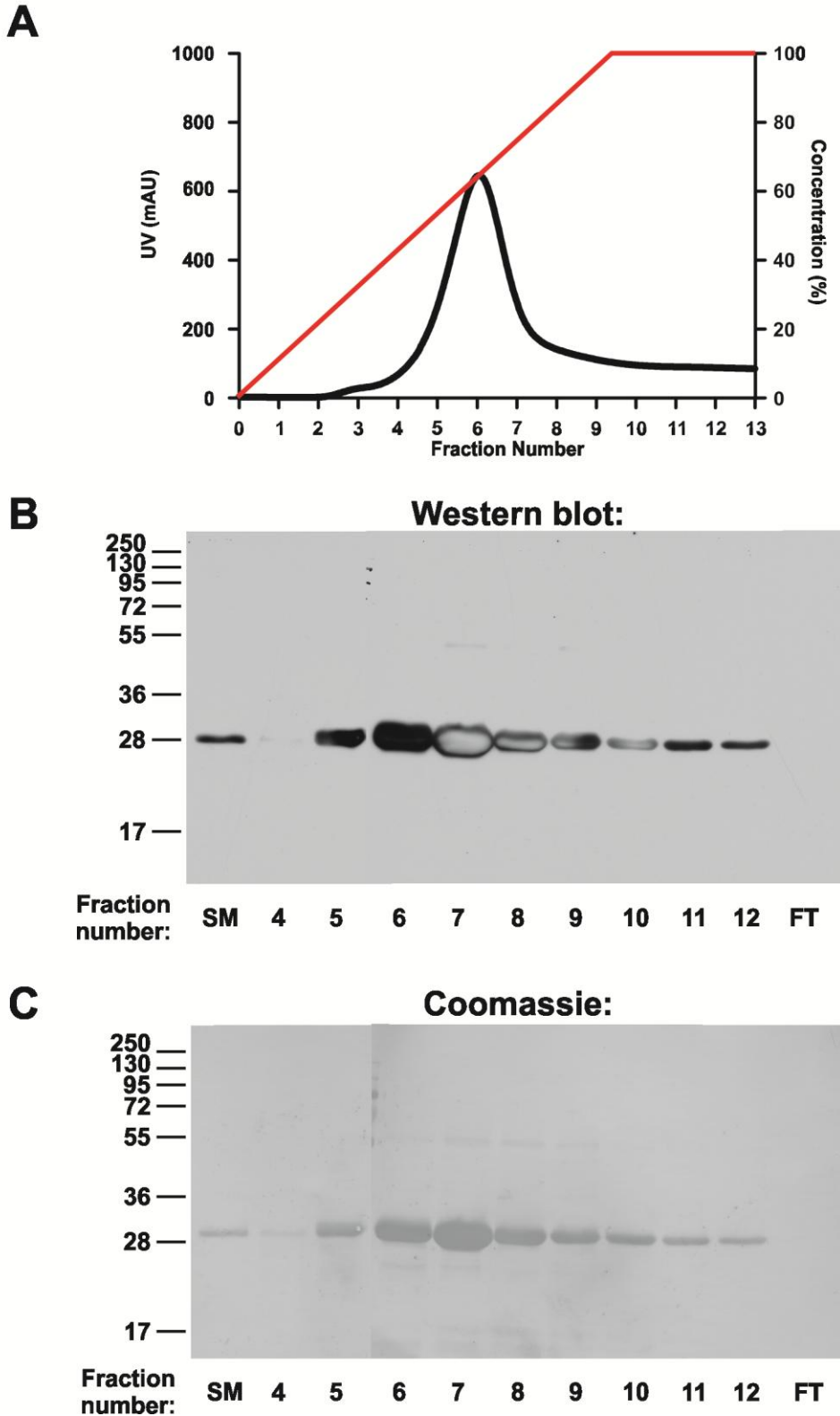
This page has been intentionally left blank.

5.3.4 Large Scale Purification of Active Site Mutated Microplasminogen

Active site mutated microplasminogen (His- μ PIg S741A) was further purified by nickel affinity chromatography. The soluble and refolded solution was bound to the column, where it was washed and then eluted with a 0-500mM imidazole gradient. Figure 5.6A shows a typical elution profile of His- μ PIg S741A. Peak fractions were analysed by Western blotting with an antibody against plasminogen (Figure 5.6B). A dominant band was observed at approximately 28kDa which corresponds to the predicted mass of μ PIg. The Western blot was subsequently stained with Coomassie (Figure 5.6C). Purified His- μ PIg S741A is ~98% homogenous as seen in Figure 5.6C.

Figure 5.6. Nickel affinity chromatography of His- μ PIg S741A. **A)** Elution profile of His- μ PIg S741A from the HisTrap column. Protein absorbance is in mAU (black lines) and the percentage of HisTrap Buffer B (red). 1mL fractions were collected and numbered accordingly. **B)** Fractions of nickel purification were ran on a 12.5% SDS-PAGE and subsequently analysed on Western blot with an antibody against plasminogen. **C)** The Western was then analysed by Coomassie staining. His- μ PIg S741A is seen as the dominant band at approximately 28kDa. Relative molecular weight in kDa is as indicated on the left of the Western.

Figure 5.6.
Nickel affinity chromatography of His- μ PIg S741A



5.3.5 Microplasminogen to Microplasmin: Activation Studies

As the activation site of μPlg (Arg⁵⁶¹-Val⁵⁶²) was left intact, μPlg can be activated by plasminogen activators to form microplasmin (μPlm). This section describes the activation studies performed with urokinase (uPA) and tissue-type plasminogen activator (tPA) to identify the optimal conditions for μPlm formation.

A fixed amount of His- μPlg S741A and Glu-plasminogen (Glu-Plg – control) was incubated with different concentrations of uPA (40-120 Units/mL/ μM) for 2 hr at 37°C. At the end of the incubation period, the reaction was prepared for analysis on a Coomassie stained 12.5% SDS-PAGE. Figure 5.7A shows that Glu-Plg migrates at approximately 95 kDa. Activation with uPA resulted in its conversion to plasmin (Plm) which appeared as a band at 72 kDa. Glu-Plg was fully activated at 40 Units/mL/ μM . Figure 5.7B shows a band migrating above 28 kDa and corresponds to His- μPlg S741A. Activation of His- μPlg S741A with uPA resulted in the cleavage of recombinant μPlg to His- μPlm S741A. An additional band is observed migrating below 28 kDa on SDS-PAGE corresponds to His- μPlm S741A. The conversion efficiency of μPlg to μPlm did not change with increasing amounts of uPA with approximately 60% of material converted to μPlm across all concentrations. Based on the results obtained from the control Glu-Plg reaction, uPA concentration of 40 Units/mL/ μM was chosen.

Using 40 Units/mL/ μM of uPA, studies with varying incubating period (15-120 min) was performed with a fixed amount of His- μPlg S741A at 37°C. At the end of each incubation period, the reaction was prepared for Western blot analysis with an antibody against plasminogen and the membrane was subsequently stained with Coomassie. As shown in Figure 5.8, activation levels to His- μPlm did not change when the reaction was incubated for 15-120 min. Based on the results obtained, the incubation period for uPA activation of 2 hrs was selected.

Activation studies with tPA is shown on Figure 5.9. A constant amount of His- μPlg S741A was incubated with varying concentration of tPA (ratio of 50:1, 10:1 and 2:1) and for different time lengths (2-22 hr) at 37°C. A control reaction with Glu-Plg was prepared with tPA at a ratio of 50:1. The reaction was then prepared for Western blot analysis with an antibody against plasminogen (Figure 5.9A) and stained with Coomassie (Figure 5.9B). His- μPlg S741A migrates above 28 kDa and activation with tPA resulted in the cleavage of His- μPlg to His- μPlm which is observed as a band below 28 kDa. Glu-Plg migrates at 95 kDa and activation with tPA results in the formation of plasmin (72 kDa) and other plasmin degradation products (bands below 72 kDa). At a range of temperature from 25-40°C and extended incubation period, plasmin is known to autolyse to smaller fragments (Jespersen et al., 1986). From Figure 5.9B, it was seen that the conversion of His- μPlg to His- μPlm with tPA was approximately 60%. Increased concentration of tPA and length of incubation did not improve tPA activation of His- μPlg .

The results obtained with tPA did not differ from uPA activation. ~60% of recombinant His- μ PIg S741A could be activated to His- μ PIm S741A which suggests that only a proportion of recombinant μ PIg was correctly folded. Based on these observations, it was determined that future activation of recombinant μ PIg would be carried out with 40 Units/mL/ μ M of uPA for 2 hrs at 37°C.

Figure 5.7. Activation studies with varying concentration of uPA. Increasing amount of urokinase plasminogen activator (uPA) from 40-120 Units/mL/ μ M was incubated with a fixed amount of GluPlg and His- μ Plg S741A for 2 hrs at 37°C. The reaction was then analysed on a Coomassie stained 12.5% SDS-PAGE. **A)** Coomassie stained SDS-PAGE of the activation of GluPlg (black arrow) to plasmin (Plm – Blue arrow). Red arrow points to uPA. **B)** Coomassie stained SDS-PAGE of the activation of His- μ Plg S741A (black arrow) to His- μ Plm S741A (blue arrow). Red arrow points to uPA. Relative molecular weight in kDa is as indicated on the left of the SDS-PAGE.

Figure 5.7.
Activation studies with varying concentration of uPA

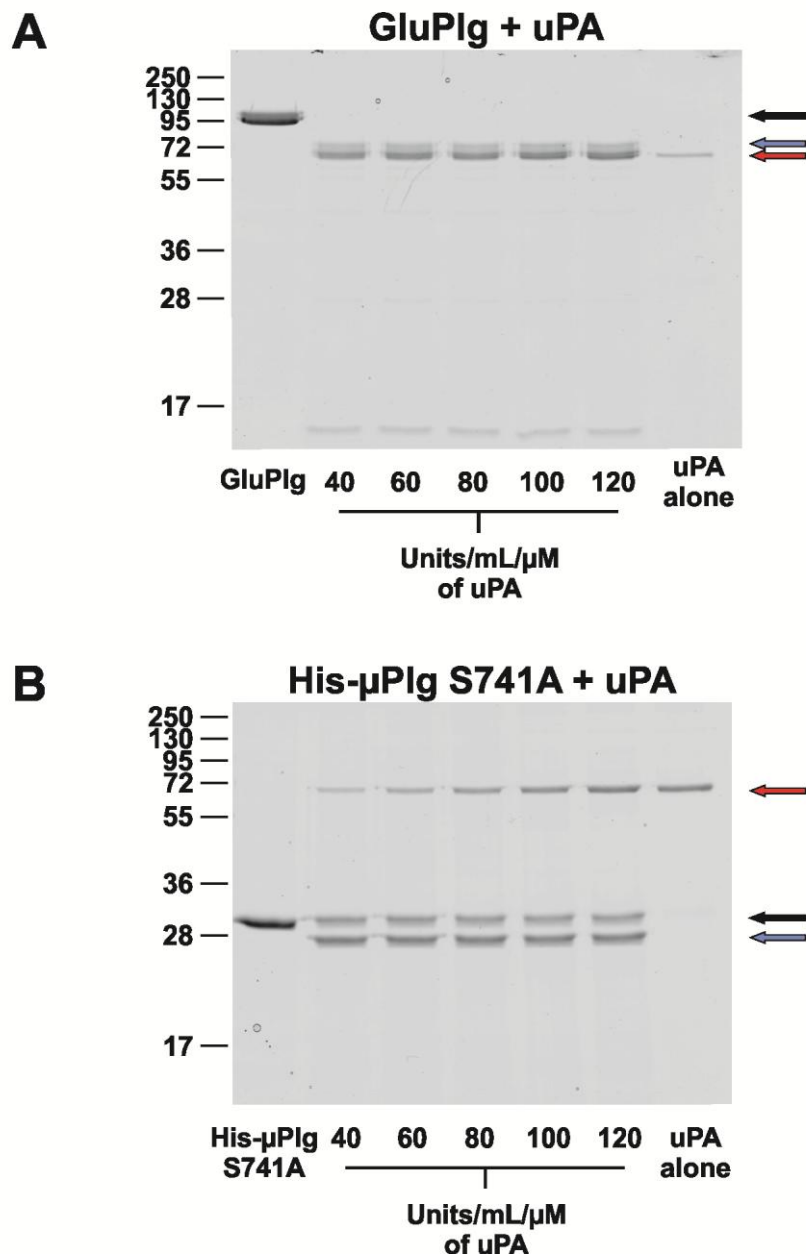


Figure 5.8. Activation studies with varying incubation period of uPA with His- μ PIg S741A. 40 Units/mL/ μ M of uPA was incubated with a fixed amount of His- μ PIg S741A for different length of time (15-120mins) at 37°C. Each reaction was ran on a 12.5% SDS-PAGE and subsequently transferred to a Western blot. **A)** Western blot of the activation of His- μ PIg S741A (black arrow) to His- μ PIg S741A (blue arrow) as detected with an antibody against plasminogen. **B)** Coomassie stained Western blot of the activation of His- μ PIg S741A (black arrow) to His- μ PIg S741A (blue arrow). Red arrow points to uPA. Bands seen at approximately 55kDa were bacterial contaminating protein. Relative molecular weight in kDa is as indicated on the left of the Western.

Figure 5.8.
Activation studies with varying incubation period of uPA
with His- μ PIg S741A

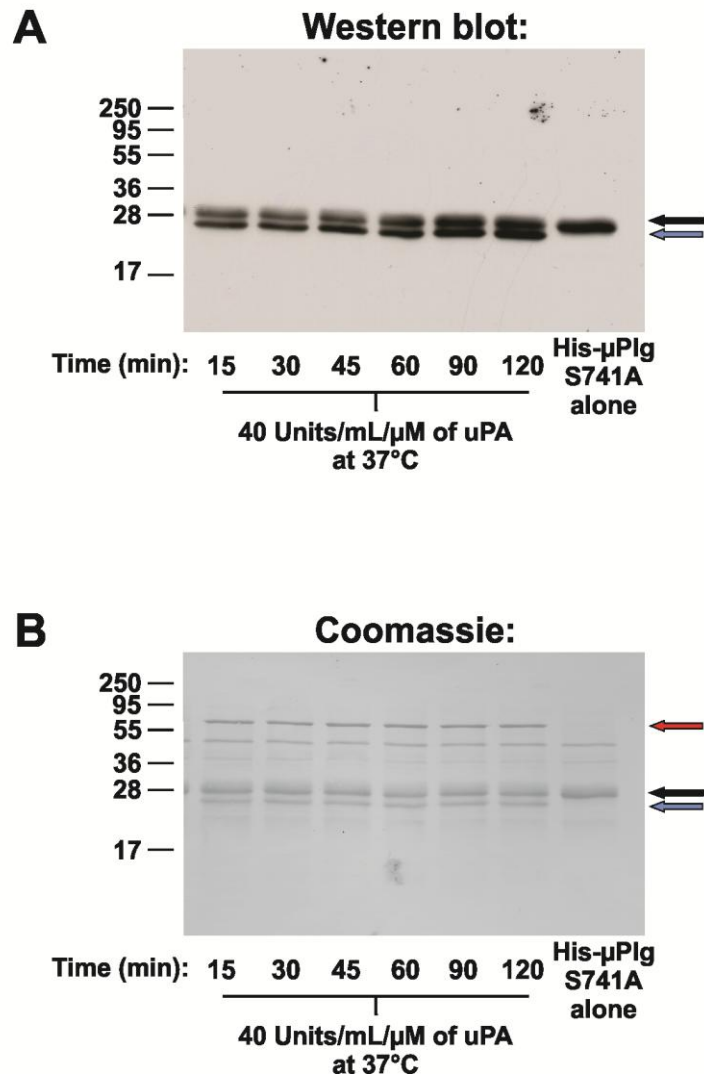


Figure 5.9. Activation studies with tPA. A constant amount of His- μ PIg S741A was incubated with varying tPA concentration (μ PIg:tPA ratios = 50:1; 10:1; 2:1) and with different time length (2-22 hrs) at 37°C. As a control, GluPIg was incubated with tPA at a ratio of 50:1 for 2-22 hrs. Each reaction was ran on a 12.5% SDS-PAGE and subsequently transferred to a Western blot. **A)** Western blot of the activation of His- μ PIg S741A (black arrow) to His- μ PIm S741A (blue arrow) as detected with an antibody against plasminogen. **B)** Coomassie stained Western blot of the activation of His- μ PIg S741A (black arrow) to His- μ PIm S741A (blue arrow). Red arrow points to uPA. Relative molecular weight in kDa is as indicated on the left of the Western.

This page has been intentionally left blank.

5.3.6 Large Scale Purification of Active Site Mutated Microplasmin

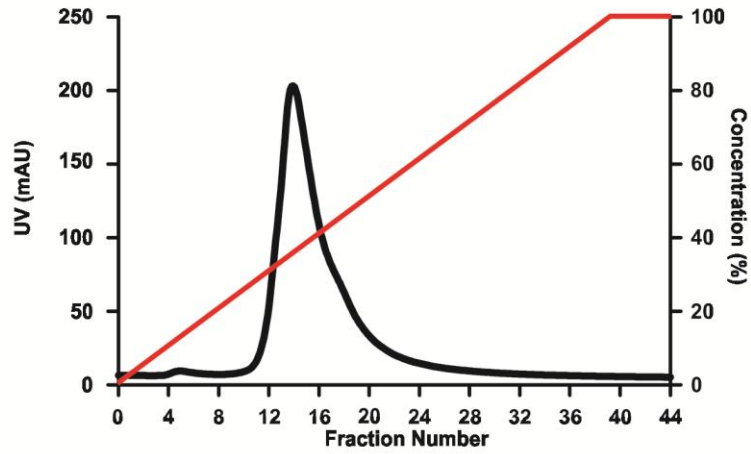
Large scale expression of His- μ PIg S741A was undertaken to generate large quantities of protein for crystallisation studies. Two chromatographic protocols were carried out to remove contaminating proteins and to purify the protein of interest to homogeneity. The first step was the removal of uPA from the μ PIm activation reaction (containing uPA, His- μ PIg S741A and His-PIm S741A) by purification on the cation affinity column (MonoS). uPA is negatively charged and therefore is not retained in the MonoS column. Figure 5.10A shows a typical elution profile for His- μ PIm S741A. Peak fractions were analysed on a Western blot and is shown in Figure 5.10B. Two bands were observed at ~28 kDa which corresponds to His- μ PIg S741A (top band) and His- μ PIm S741A (bottom band). This purification step successfully removed uPA from the fractions as seen in Figure 5.10C.

A second purification step was carried out to remove His- μ PIg S741A and to purify correctly folded His- μ PIm S741A. In order to achieve this, peak fractions from the MonoS column were pooled and bound to the Benzamidine affinity column. The Benzamidine column binds to trypsin-like serine proteases which include μ PIm. Removal of incorrectly folded His- μ PIg S741A was achieved by an initial column wash with a buffer containing 1M salt and p-aminobenzamidine. Subsequently, elution of activated His- μ PIm S741A was performed with a linear decrease in pH of 7.4 to 3. A typical elution profile is seen in Figure 5.11A. A single peak is eluted at approximately pH 4.5. Peak fractions were analysed by Western blot and is shown in Figure 5.11B. A dominant band is seen at ~28 kDa which corresponds with His- μ PIm S741A. Fraction number 8 (Figure 5.11B & C) appears to be ~98% pure and contains small amounts of non-activated form. This fraction was collected and the final protein concentration was calculated from the absorbance of 280nm. The yield of protein obtained for His- μ PIm S741A was ~0.4mg per 200mg of IB pellet.

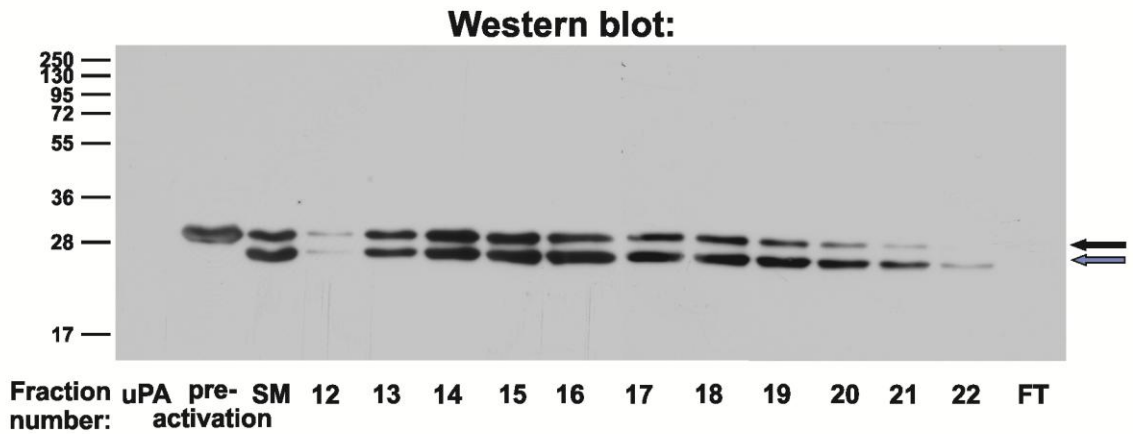
Figure 5.10. Cation exchange chromatography of His- μ PIg S741A. **A)** Elution profile of His- μ PIg S741A from the MonoS column. Protein absorbance is in mAU (black lines) and the percentage of MonoS Buffer B (red). 500 μ L fractions were collected and numbered accordingly. **B)** Fractions of MonoS purification were ran on a 12.5% SDS-PAGE and subsequently analysed on Western blot with an antibody against plasminogen. **C)** The Western was then analysed by Coomassie staining. His- μ PIg S741A is seen below the 28kDa (blue arrow). Approximately 40% of His- μ PIg S741A could not be activated and is shown by the black arrow. The red arrow points to tPA. Relative molecular weight in kDa is as indicated on the left of the Western.

Figure 5.10.
Cation exchange chromatography of His- μ Plm S741A

A



B



C

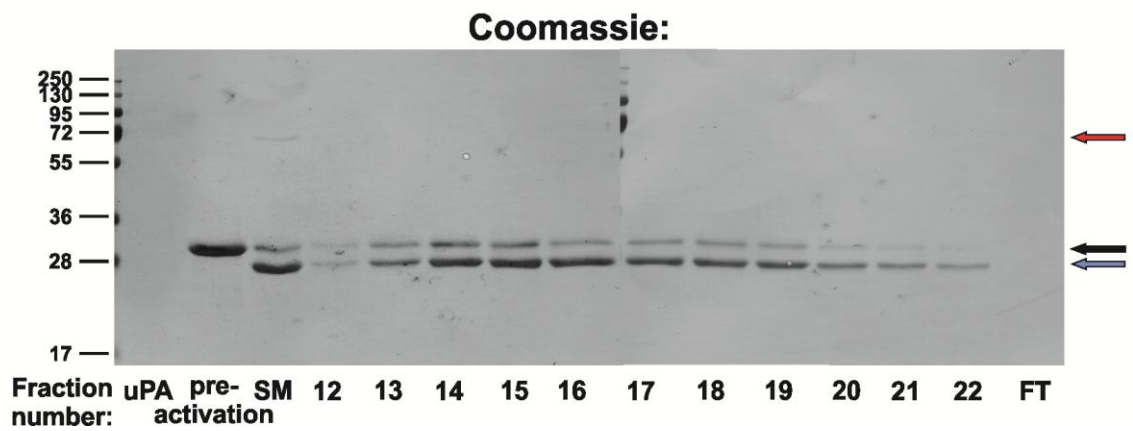
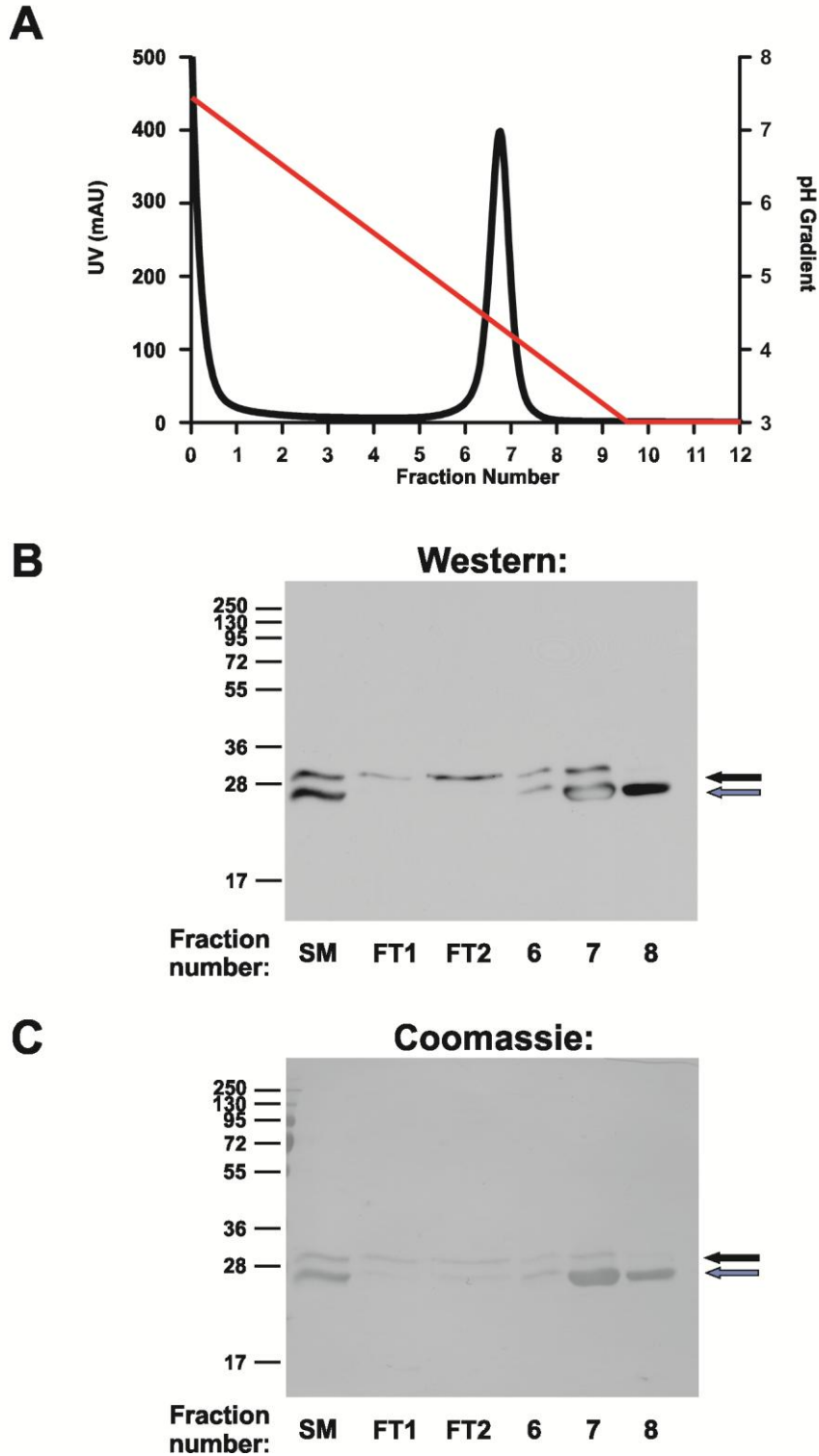


Figure 5.11. Benzamidine affinity chromatography of His- μ Plm S741A. **A)** Elution profile of His- μ Plm S741A from the Benzamidine column. Protein absorbance is in mAU (black lines) and the pH of Benzamidine Elution Buffer (red). 1mL fractions were collected and numbered accordingly. **B)** Fractions of Benzamidine purification were ran on a 12.5% SDS-PAGE and subsequently analysed on Western blot with an antibody against plasminogen. **C)** The Western was then analysed by Coomassie staining. His- μ Plm S741A is seen below the 28kDa (blue arrow). Majority of His- μ Plg S741A (black arrow) could be removed by benzamidine affinity purification. Relative molecular weight in kDa is as indicated on the left of the Western.

Figure 5.11.
Benzamidine affinity chromatography of
His- μ Plm S741A



5.3.7 Large Scale Purification of Wild-type Recombinant Microplasmin(ogen)

The expression, IB purification, denaturation and refolding of two proteins (His- μ PIg WT and μ PIg WT) are as described in section 5.2.3 to 5.2.6 of this chapter. To obtain homogenous protein, several purification stages were required and is as described in this section.

Purification of His-tagged wild-type microplasmin(ogen)

The refolded soluble His- μ PIg WT was first purified on a nickel affinity column. Figure 5.12A shows a typical elution profile of His- μ PIg WT. Recombinant His- μ PIg WT was eluted out at approximately 60% of HisTrap Buffer B. The major peak was analysed on a Western blot. The result shows a major protein band at 28kDa (Figure 5.12B). Purified His- μ PIg WT was then activated with uPA to His- μ PIm WT as described in section 5.2.9. To remove uPA, a second purification step was introduced on the cation affinity column. The sample was bound to the MonoS column and the elution profile is presented on Figure 5.12C. Peak fractions were eluted at ~30% of MonoS Buffer B and were analysed by Western blot (Figures 5.12D). Activation to His- μ PIm WT was ~80% efficient as observed on the Western blot. Finally, to remove non-activated His- μ PIm WT, peak fractions from MonoS were pooled and further purified on the benzamidine affinity column and the chromatogram is shown on Figure 5.12E. His- μ PIm WT was eluted at approximately pH5.0 (Figure 5.12E) and His- μ PIg WT was successfully removed after benzamidine purification as the major band was below 28 kDa and corresponds with His- μ PIm (Figure 5.12F). The final protein concentration was calculated from the absorbance at 280nm. Protein yield was ~0.4mg per 200mg of IB pellet.

Purification of wild-type microplasmin(ogen)

Soluble and refolded μ PIg WT were first purified on a MonoS column. As this protein does not contain the N-terminal his-tag, nickel affinity column cannot be used as the first stage of purification. The elution profile of μ PIg WT is shown on Figure 5.13A. Peak fractions were eluted at ~30% MonoS Buffer B. Peak fractions were analysed by Coomassie stained 12.5% SDS-PAGE (Figure 5.13B). Fraction 8 (~95% pure) was collected and protein concentration was determined by absorbance at 280nm. Protein yield was ~0.3mg per 200mg of IB pellet. μ PIg WT was collected for binding studies in Chapter 7.

To obtain μ PIm WT, directly after the refolding of μ PIg WT, the reaction was activated with 40 Units/mL/ μ M of uPA for 2 hr as described in section 5.2.9. The reaction was then applied on the cation affinity column (MonoS) to remove uPA. Figure 5.13C shows the elution profile of activated μ PIm WT. Peak fractions were eluted at ~30% concentration of MonoS Buffer B and were analysed on a Western blot (Figure 5.13D). Activation of μ PIm WT (below 28

kDa) was ~80% efficient with a band still observed above 28 kDa which corresponds with μ PIg. Peak fractions were then pooled and further purified on the benzamidine affinity column. A single peak was observed at ~pH5.0 (Figure 5.13E). The peak fractions were analysed on a Western blot and incorrectly folded μ PIg was successfully removed after Benzamidine purification as the band observed is below 28 kDa which corresponds with μ PIm (Figure 5.13F). The final protein concentration was calculated and protein yield was ~0.4mg per 200mg of IB pellet. Further binding characterisation was performed in Chapter 6 and 7.

Figure 5.12. Purification of His- μ PIg WT and His- μ PIIm WT. **A)** Chromatogram of His- μ PIg WT from the HisTrap column. Protein absorbance is in mAU (black lines) and the percentage of HisTrap Buffer B (red). 1mL fractions were collected and numbered accordingly. **B)** Fractions of HisTrap purification were run on a 12.5% SDS-PAGE and subsequently analysed on Western blot with an antibody against plasminogen. **C)** Chromatogram of His- μ PIIm WT from the MonoS column. Protein absorbance is in mAU (black lines) and the percentage of MonoS Buffer B (red). 500 μ L fractions were collected and numbered accordingly. **D)** Fractions of MonoS purification were run on a 12.5% SDS-PAGE and subsequently analysed on Western blot with an antibody against plasminogen. **E)** Elution profile of His- μ PIg WT from the Benzamidine column. Protein absorbance is in mAU (black lines) and the pH of Benzamidine Elution Buffer (red). 1mL fractions were collected and numbered accordingly. **F)** Fractions of Benzamidine purification were run on a 12.5% SDS-PAGE and subsequently analysed on Western blot with an antibody against plasminogen. His- μ PIIm WT is seen below the 28 kDa (blue arrow). Majority of His- μ PIg WT (black arrow) was removed by Benzamidine affinity chromatography. Relative molecular weight in kDa is as indicated on the left of the Western blots.

Figure 5.12.
Purification of His- μ PIg WT and His- μ PIm WT

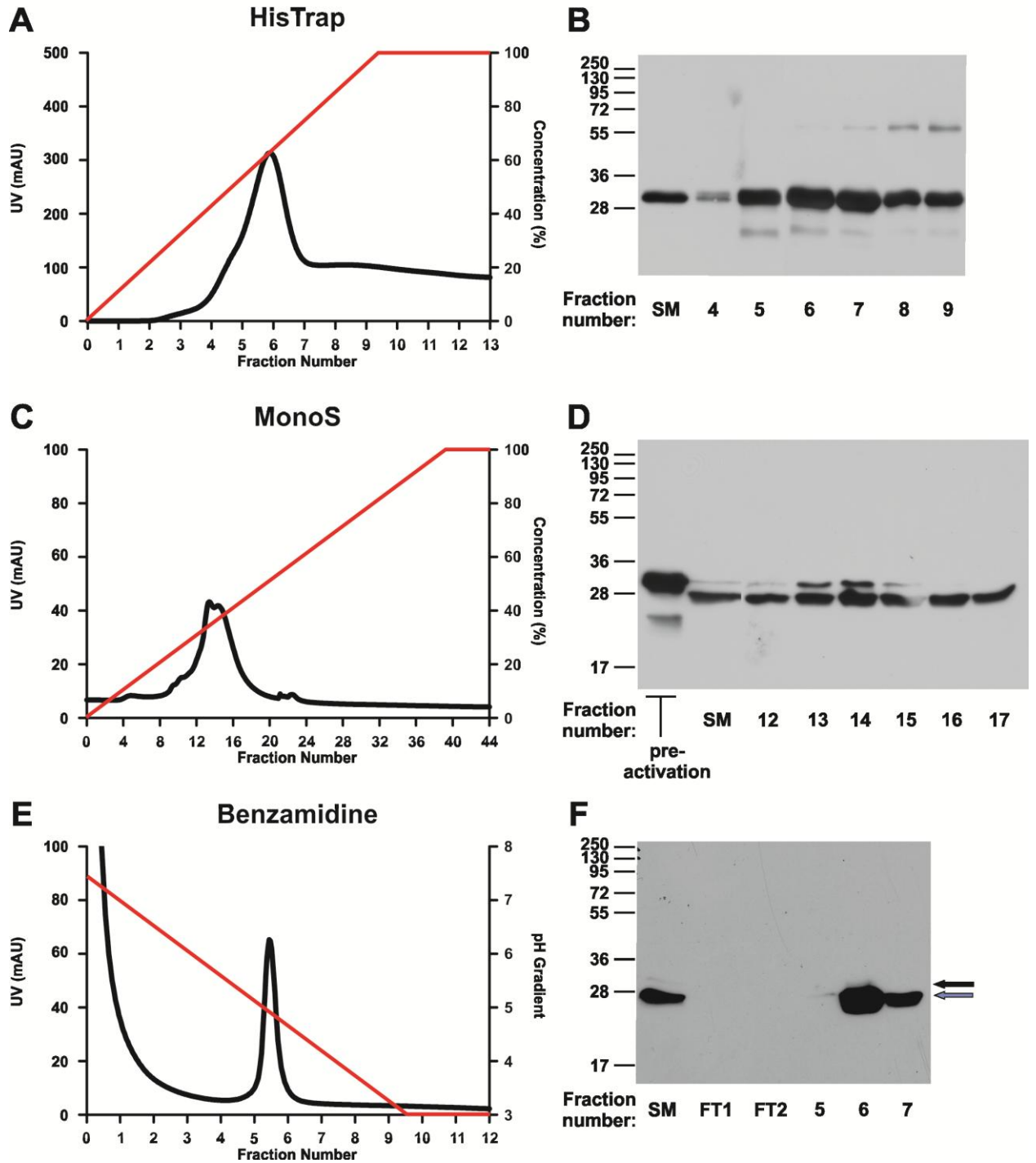
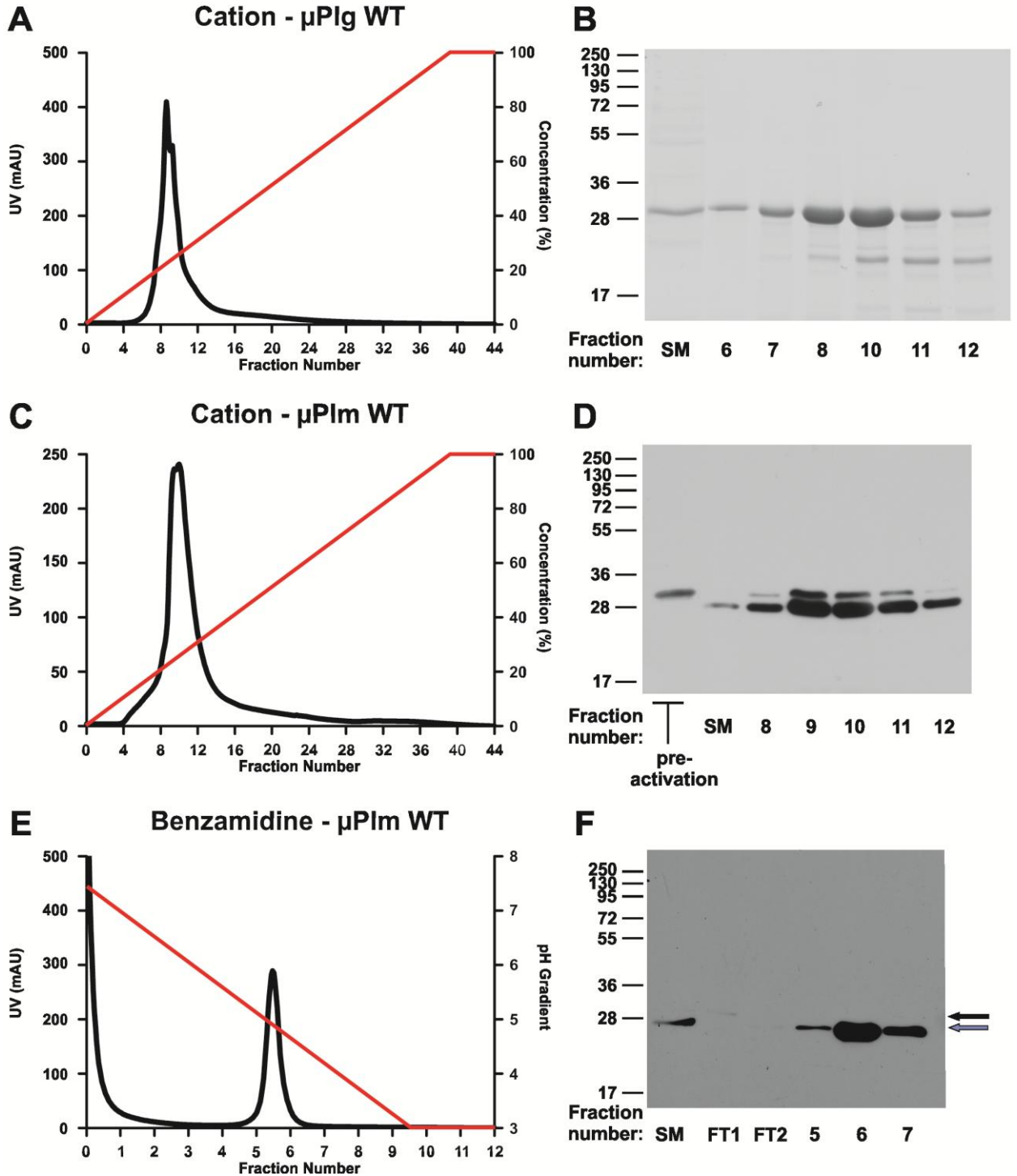


Figure 5.13. Purification of μ PIg WT and μ PIIm WT. **A)** Chromatogram of μ PIg WT from the cation affinity chromatography. Protein absorbance is in mAU (black lines) and the percentage of MonoS Buffer B (red). 500 μ L fractions were collected and numbered accordingly. **B)** Fractions of MonoS were ran on a 12.5% SDS-PAGE and subsequently analysed on Western blot with an antibody against plasminogen. **C)** Chromatogram of μ PIIm WT from the MonoS column. Protein absorbance is in mAU (black lines) and the percentage of MonoS Buffer B (red). 500 μ L fractions were collected and numbered accordingly. **D)** Fractions of MonoS purification were ran on a 12.5% SDS-PAGE and subsequently analysed on Western blot with an antibody against plasminogen. **E)** Elution profile of μ PIIm WT from the Benzamidine column. Protein absorbance is in mAU (black lines) and the pH of Benzamidine Elution Buffer (red). 1mL fractions were collected and numbered accordingly. **F)** Fractions of Benzamidine purification were ran on a 12.5% SDS-PAGE and subsequently analysed on Western blot with an antibody against plasminogen. μ PIIm WT is seen below the 28 kDa (blue arrow). Majority of μ PIg WT (black arrow) was removed by Benzamidine affinity chromatography. Relative molecular weight in kDa is as indicated on the left of the Western blots.

Figure 5.13.
Purification of μ PIg WT and μ PIm WT



5.3.8 Non-Covalent Complex Studies of Active Site Mutated Microplasmin with N-Terminally Truncated α_2 -Antiplasmin

One of the aims of this chapter was to crystallise the encounter complex of His- μ Plm S741A with N-terminally truncated α_2 -antiplasmin (N Δ) to visualise the interaction that occurs between the protease domain and serpin core. Before crystallisation trials were started, preliminary biochemical studies were carried to determine whether the non-covalent complex can be formed. Detection of non-covalent complex by Native-PAGE, non-reduced SDS-PAGE and size exclusion purification were carried out.

Non-covalent complex detection by Native-PAGE

The formation of the non-covalent complex was first examined on a Native-PAGE. N Δ was incubated with His- μ Plm WT or His- μ Plm S741A at a ratio of 1:1 or 1:2 (N Δ : μ Plm) for 30 min at 37°C. The reaction was then resolved on Native-PAGE and subsequently analysed by Western blotting with an antibody against plasminogen (Figure 5.14A). The membrane was then stained with Coomassie (Figure 5.15B). The control reaction with His- μ Plm WT which will form a covalent complex with N Δ clearly shows a shift down the Native-PAGE. This shift was weakly seen with the reaction with His- μ Plm S741A. A change in mobility compared to control as shown on the Native-PAGE with His- μ Plm S741A and N Δ suggests that non-covalent complex was formed.

Non-covalent complex detection by non-reduced SDS-PAGE

The non-covalent complex was also tested on non-reduced SDS-PAGE. N Δ or WT was incubated with Plm or His- μ Plm S741A at a ratio of 1:1 or 2:1 (N Δ : μ Plm) for 30 min at 37°C. The reaction was then prepared for analysis on a Coomassie stained non-reduced SDS-PAGE. Figure 5.15A shows the gel for the control reaction of WT or N Δ with Plm. There is a clear change in mobility when a covalent complex was formed with WT and Plm to a higher molecular weight band between 130 and 250kDa which corresponds with the predicted covalent complex mass of ~150kDa. However for the reaction with His- μ Plm S741A, a non-covalent complex could not be visualised on the non-reduced SDS-PAGE (Figure 5.15B). This result was expected as SDS contained in the gel causes protein to unfold and linearise.

Non-covalent complex detection by size exclusion chromatography

Size exclusion chromatography was carried out to examine whether non-covalent complex could be resolved into a single peak. Prior to complex incubation, His- μ Plm S741A and N Δ were purified by gel filtration column (Superdex 200) individually to remove polymeric species (Figure 5.16). His- μ Plm S741A was incubated with N Δ at a 1:1 ratio as previously described. The complex reaction was then loaded on the gel filtration column. Two distinct peaks were obtained on the chromatogram (Figure 5.17B). Analysis of the Coomassie stained SDS-PAGE showed that the first peak (fractions 68-71) was N Δ α_2 -antiplasmin as a band at around 50 kDa and the second peak (fractions 84-88) was His- μ Plm S741A which corresponds with the 28 kDa molecular weight marker (Figure 5.17C).

Figure 5.14. Detection of non-covalent complex of NΔ α_2 -antiplasmin with His- μ Plm S741A by Native-PAGE. NΔ hAP was incubated with either His- μ Plm WT or His- μ Plm S741A at a ratio of 1:1 or 1:2 for 30 min at 37°C. The reaction was then loaded on a Native-PAGE and transferred onto Immobilon-P PVDF membrane for Western blotting. **A)** Western blot with an antibody against plasminogen of non-covalent complex of NΔ with His- μ Plm S741A and control reaction of covalent NΔ and His- μ Plm WT complex. **B)** The Western blot was subsequently stained with Coomassie. The area indicated by the black arrow is indicative of covalent and non-covalent complex forming on the Native-PAGE.

Figure 5.14.
Detection of non-covalent complex of NΔ α₂-antiplasmin with His-μPlm S741A by Native-PAGE

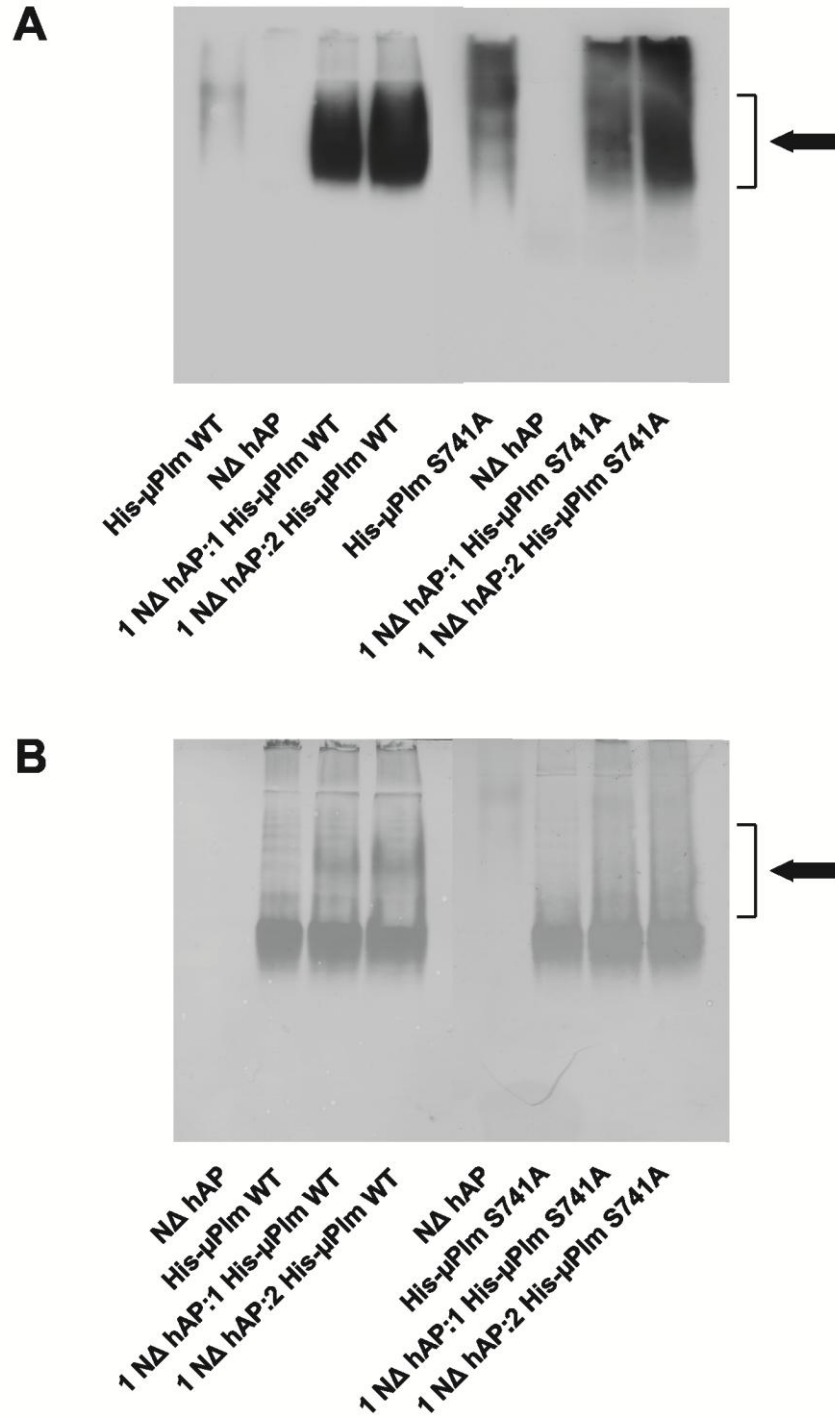


Figure 5.15. Detection of non-covalent complex of NΔ α_2 -antiplasmin with His- μ Plm S741A by non-reduced SDS-PAGE. A) As a control reaction, NΔ and WT hAP was incubated with Plasmin (Plm) at a ratio of 1:1 or 2:1 for 30 min at 37°C. The reaction was then loaded non-reduced on a 12.5% SDS-PAGE and analysed by Coomassie staining. Formation of covalent complex is seen as a higher molecular weight band at approximately 130 kDa as indicated by the black arrow. **B)** NΔ and WT hAP was incubated with His- μ Plm S741A at a ratio of 1:1 or 2:1 for 30 min at 37°C. The reaction was then loaded non-reduced on a 12.5% SDS-PAGE and analysed by Coomassie staining. Relative molecular weight in kDa is as shown on the left.

Figure 5.16. Purification of NΔ α_2 -antiplasmin and His- μ Plm S741A by size exclusion chromatography. To prepare NΔ hAP and His- μ Plm S741A for crystallisation trials, each recombinant protein was further purified on a size exclusion column (Superdex 200) to remove potential polymers. **A)** Chromatogram of NΔ hAP purification on the gel filtration column. **B)** Peak fractions were analysed on a Coomassie stained 12.5% SDS-PAGE. The dominant band at approximately 50kDa is NΔ hAP. **C)** Chromatogram of His- μ Plm S741A on the gel filtration column. **D)** Peak fractions were analysed on a Coomassie stained 12.5% SDS-PAGE. His- μ Plm S741A is seen at approximately 28kDa. Relative molecular weight in kDa is as shown on the left of each SDS-PAGE.

Figure 5.16.
Purification of NΔ α_2 -antiplasmin and His- μ PIII S741A
by size exclusion chromatography

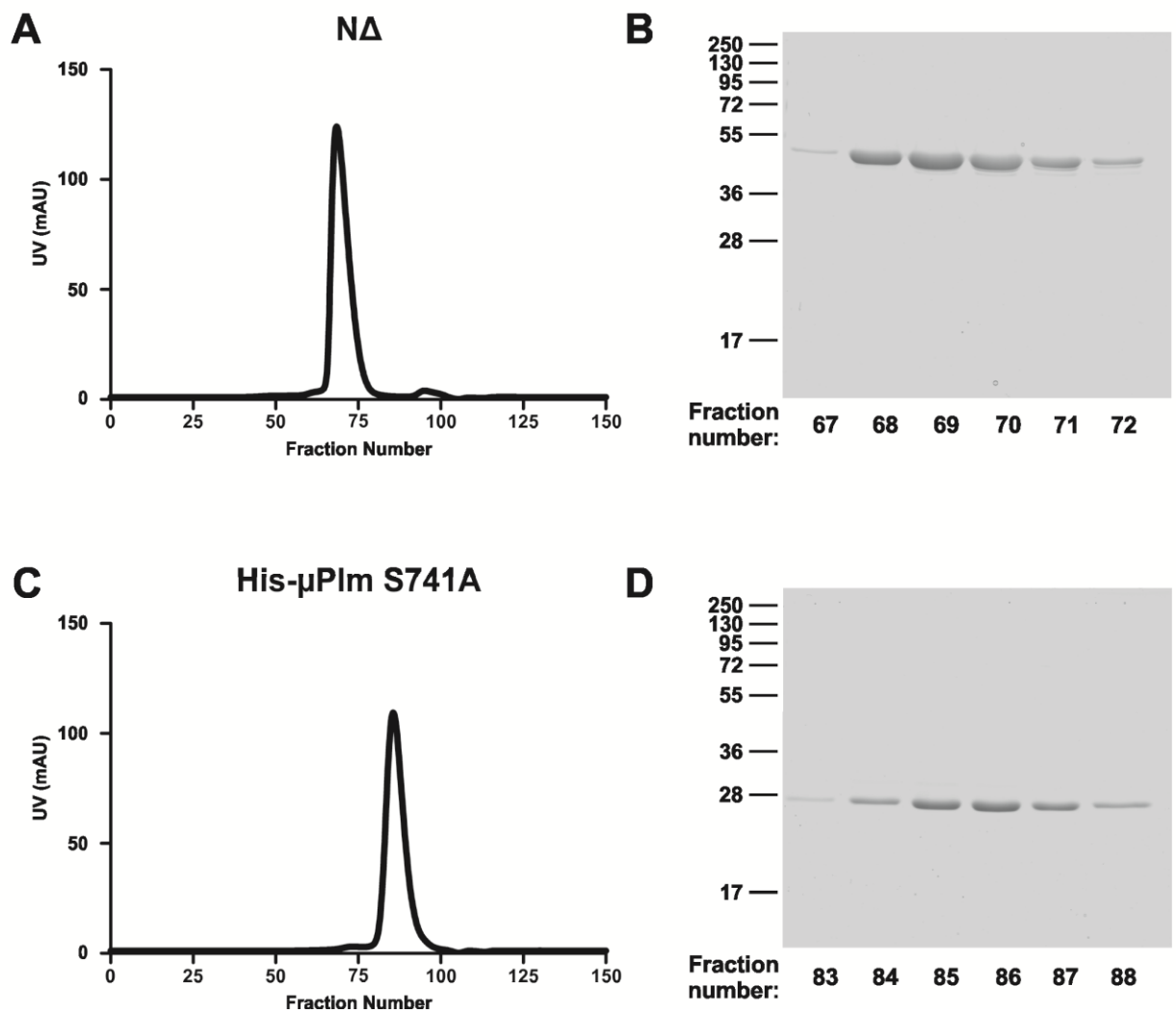
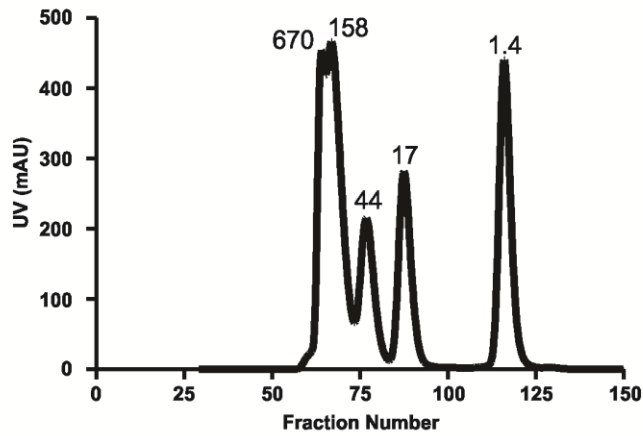


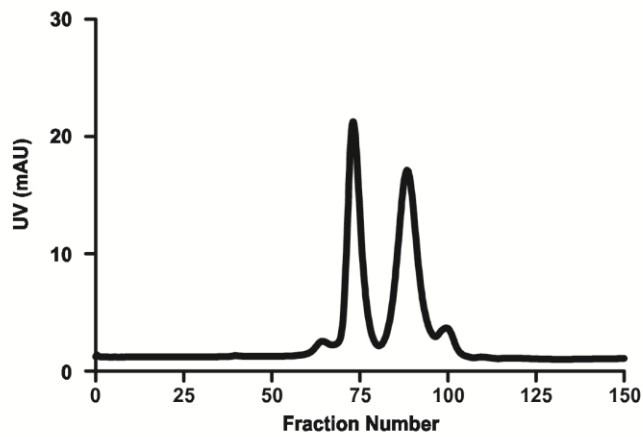
Figure 5.17. Detection of non-covalent complex of NΔ α_2 -antiplasmin with His- μ Plm S741A by size exclusion chromatography. NΔ hAP and His- μ Plm S741A was incubated at a 1:1 ratio for 1 hr at 37°C. The reaction was then loaded on a gel filtration column (Superdex 200). **A)** Gel filtration standards with their corresponding molecular weight in kDa. **B)** Chromatogram of non-covalent complex co-purification on the size exclusion column. **C)** Peak fractions were analysed on a Coomassie stained 12.5% SDS-PAGE. The first dominant peak is NΔ hAP which appears as a protein band at approximately 50kDa. The second peak is His- μ Plm S741 (28kDa). Non-covalent complex could not be separated by size exclusion chromatography. Relative molecular weight in kDa is as indicated on the left.

Figure 5.17.
Detection of non-covalent complex of $N\Delta \alpha_2$ -antiplasmin with His- μ Plm S741A by size exclusion chromatography

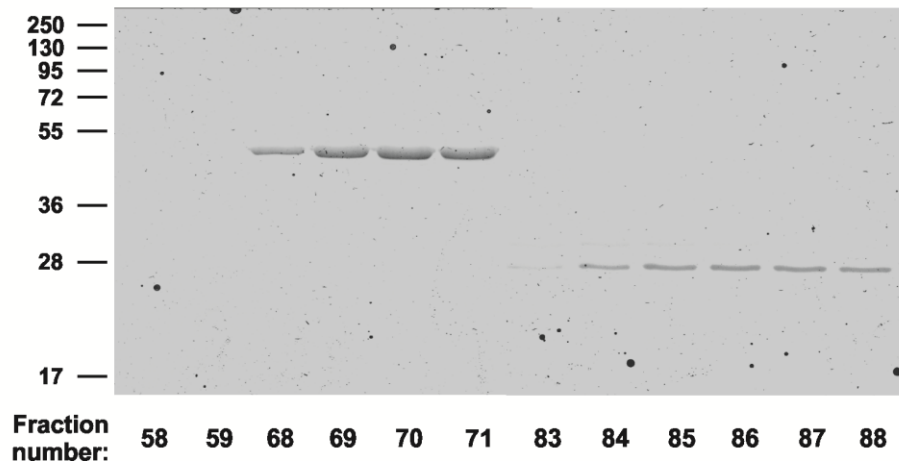
A



B



C



This page has been intentionally left blank.

5.3.9 Preliminary Crystallisation Trials of Non-Covalent Complex

Proteins used for crystallisation trials are required to be monomeric, therefore before commencement of trials, both NΔ and His-μPlm S741A were purified on the size exclusion column to remove potential polymeric forms. Figure 5.16A shows the chromatogram of NΔ α₂-antiplasmin purified from the Superdex 200 column. The peak fraction was analysed on a Coomassie stained SDS-PAGE and is seen on Figure 5.16B. A single band was observed at 50kDa which corresponds with its predicted mass. Figure 5.16C shows the chromatogram of His-μPlm S741A purified from gel filtration and the corresponding peak fraction was analysed on a Coomassie stained SDS-PAGE (Figure 5.16D) A single band was observed at 28kDa. Once the proteins were purified, the protein concentration was measured by absorbance at 280nm. Both proteins were incubated at a ratio of 1:1 and incubated as previously described in section 5.2.14. Preliminary crystallisation screenings were carried out with this 1:1 mixture using commercially available kits. Approximately 120 conditions were undertaken however no diffractable crystals were obtained as yet. The trays were set up in the Crystallisation Unit at the Department of Biochemistry and Molecular Biology, Monash University Clayton Campus. Crystallisation trials are still ongoing.

5.4 Discussion

One of the challenging aims in this study was to establish an expression and purification method for recombinant human μ PIg/ μ PIm. Several protocols on the isolation of μ PIg/ μ PIm from prokaryotic expression system (Medynski et al., 2007; Parry et al., 1998) and proteolytic cleavage of full-length PIg (Shi and Wu, 1988; Wu et al., 1987) have been previously reported. The production of μ PIg through recombinant protein production using a bacterial expression system was pursued. Due to prior success in the expression and purification of human α_2 -antiplasmin using the *E.coli* BL21 bacterial system, our protein expression protocols were optimised to suit μ PIm production (Lu et al., 2011).

The recombinant μ PIg generated was predicted to be 249 amino acids in length from Ala⁵⁴²-Asn⁷⁹¹ with a molecular weight of ~28kDa. Throughout this work, the numbering of μ PIg/ μ PIm was based on the full-length secreted form of 791 amino acids. In this study, the WT form of μ PIg was generated with and without an N-terminal hexahistidine tag (His- μ PIg WT and μ PIg WT). An active site mutated variant containing the N-terminal His-tag was also produced where Ser⁷⁴¹ was mutated to Ala (His- μ PIg S741A).

Trial expression revealed that all recombinant μ PIg variants (His- μ PIg S741A, His- μ PIg WT and μ PIg WT) were expressed as insoluble protein aggregates known as inclusion bodies (IB) in the cytoplasm of *E.coli*. The IB pellet was then extracted from the bacterial cells by freeze and thaw cycles. The insoluble cell lysates contains not only the IB, but also the bacterial cell wall and outer membrane proteins. These contaminants were removed with detergent (Triton X-100) with the help of a tissue homogeniser. On average, a 1L bacterial culture produced approximately 0.6mg of washed IB pellet for all μ PIg variants. The purified IB pellet was solubilised with a strong protein denaturant (8M Urea) which unfolds the protein. Native protein formation was then induced. This step is the most critical as μ PIg has to be correctly folded to its tertiary and quaternary structure to ensure that its functional and biological characteristics are retained. To aid with bond formation and refolding, glutathione oxidised and reduced were added at a ratio of 10:1. This ratio is similar to that found in the endoplasmic reticulum environment in vivo (Chakravarthi et al., 2006) to reproduce the optimum condition for correct protein folding. Once recombinant μ PIg was solubilised and refolded, activation and purification of the protein can commence.

The activation cleft Arg⁵⁶¹-Val⁵⁶² was left intact in all recombinant μ PIg variants generated. Therefore μ PIg conversion to μ PIm by plasminogen activators could occur. In this study, activation of μ PIg to μ PIm was achieved by uPA. Upon activation, two-chain μ PIm is formed where A-chain consists of residues 542-561 and B-chain consists of residues 562-791. Under reducing conditions of μ PIm, the disulphide linker dissociates from A-chain and B-chain

resulting in two protein bands at ~26kDa and ~2kDa when analysed on a SDS-PAGE. Non-activated form (μ PIg) is a single-chain, and therefore a single band at 28kDa is observed in reduced conditions on a SDS-PAGE. Due to this fact, conversion efficiency can be monitored by running activated sample on a reduced SDS-PAGE. A percentage of recombinant His- μ PIg S741A (~40%), His- μ PIg WT (~20%) and μ PIg WT (~20%) could not be activated and remained in the zymogen form (seen as the higher molecular weight form). This may be due to the fact that a proportion of recombinant μ PIg generated was misfolded. Therefore, the structure may be distorted and the activation cleft may not be accessible to plasminogen activators. uPA activation efficiency may in fact inform us of the effectiveness of the protein refolding step. This step may be a way to distinguish misfolded protein from protein in the correct conformation.

Combinations of nickel affinity, cation exchange and Benzamidine affinity chromatography have successfully isolated the recombinant μ PIg/ μ PIm. Nickel affinity purification was used to purify His-tagged μ PIg only (His- μ PIg S741A and His- μ PIg WT). This step assists in the removal of bacterial contaminant proteins which were also present in the IB pellet. Cation exchange chromatography was used to further purify μ PIg or activated μ PIm. This is particularly important in removing uPA from recombinant μ PIm generated. One important observation after MonoS purification was the fact that non-activated μ PIm co-eluted with activated μ PIm. A proportion of μ PIg produced was most likely misfolded and remained in its zymogen form even in the presence of plasminogen activators. Cation chromatography could not separate the non-activated form and therefore a final purification step with Benzamidine affinity column was performed. Before elution of the protein was commenced, the column was washed with a buffer containing *p*-aminobenzamidine (competitive elution) and a high concentration of NaCl. It was observed that activated μ PIm bound more avidly than non-activated μ PIm and therefore only the zymogen form was removed during the high salt wash. A low pH elution was introduced to displace μ PIm from the column. Previous studies have reported that μ PIm at neutral pH has the propensity to self degrade when stored for extended period of time (Medynski et al., 2007; Parry, 2001). Therefore, recombinant μ PIm was stored at a low pH to avoid this occurrence. Expression and purification levels remained constant in both pET(3a)His (His- μ PIm S741A and His- μ PIm WT) and pET(3a) expression vectors.

Our laboratory has solved the crystal structure of mouse α_2 -antiplasmin (Law et al., 2008) and recently full-length plasminogen (Law et al., 2012). However the structure of human α_2 -antiplasmin complexed with plasmin is yet to be determined. Both proteins are made up of multiple domains, which accounts for the difficulty in obtaining a crystal structure as yet. To simplify this complex interaction, in this chapter we attempted to crystallise the protease domain of plasmin and a truncated version of α_2 -antiplasmin.

The second challenging aim of this chapter was to obtain the crystal structure of the non-covalent complex between active site mutated μ Plm and N-terminally truncated antiplasmin. Observations from Chapter 4 led to the hypothesis that there may be an additional interaction between the protease domain and the serpin core which has yet to be identified. In order to address this, crystallisation of the encounter complex of these two molecules was attempted with the hope of visualising this interaction. Non-covalent complex formation of His- μ Plm S741A with N Δ was only demonstrated on Native-PAGE seen as a band-shift down the gel (Figure 5.14). Furthermore, in Chapter 7 it was shown that active site-blocked μ Plm interacted with α_2 -antiplasmin at a binding affinity of approximately 100nM (refer to section 7.3.4). From these observations, it was predicted that non-covalent complex formation could occur with α_2 -antiplasmin and His- μ Plm S741A. However, no evidence of non-covalent complex was seen the non-reduced SDS-PAGE (Figure 5.15) which is expected because SDS contained in the gel would have unfolded the protein and separated any non-covalent contacts during electrophoresis. Additionally, the complex could not be co-eluted from the gel filtration column (Figure 5.17). It is possible that interaction between His- μ Plm S741A and N Δ was not stable and migration through the gel filtration medium causes the two entities to separate due to the weak interaction. For a direct comparison, future work on the co-elution of WT α_2 -antiplasmin and active site-blocked microplasmin could be studied. Furthermore, the binding affinity of N Δ α_2 -antiplasmin with μ Plm-S741A could be analysed to observe if the affinity remains at 100nM.

Typically, crystallisation of a complex involves pre-incubation of the target proteins followed by co-purification before trays are set up (Huntington et al., 2000). However, attempts in purifying the His- μ Plm S741A and N Δ complex were not successful. Therefore we decided to mix the two proteins together in a 1:1 molar ratio and from this, crystallisation trays were set up. Several groups have attempted this method and crystals for uPA/PAI-I and antithrombin/FactorXa/Heparin were successfully generated (Johnson et al., 2006; Lin et al., 2011). To ensure high purity of the two proteins, a final gel filtration step was performed. This is to separate any potential polymeric form and to obtain homogeneous monomeric form of both proteins. It is important to note that a large amount of both His- μ Plm S741A and N Δ are required for crystallisation. As fresh proteins are preferred for optimum crystallisation conditions, both proteins have to be produced simultaneously. Obtaining the X-ray crystal structure of the non-covalent complex between His- μ Plm S741A and N Δ α_2 -antiplasmin is complicated and despite a number of trays being set-up, no diffractable crystals have formed. Expression and purification of both proteins are well established and crystallisation of the encounter complex is still ongoing. In addition to solving the crystal structure of the non-covalent μ Plm/ α_2 -antiplasmin complex, the covalent structure may add to the understanding of its final inactivated form.

5.5 Conclusion

This chapter describes the protocol in obtaining abundant recombinant μ PIg and μ PIm. *Escherichia coli* was determined to be a suitable expression system in the production of recombinant μ PIg/ μ PIm. Proteins were produced in the insoluble inclusion bodies. Solubilisation and refolding of these inclusion bodies were required to form native μ PIg/ μ PIm. μ PIg in the correct conformation was activated by plasminogen activators to μ PIm. Wild-type and active site mutated μ PIm has been successfully produced and will be further characterised by kinetic and affinity assays. Non-covalent complex formation between active site mutated μ PIm and N-terminally truncated α_2 -antiplasmin was demonstrated.

This page has been intentionally left blank.

Chapter 6:

Contribution of β -sheet C of α_2 -antiplasmin to plasmin inhibition and binding

This page has been intentionally left blank.

6.1 Introduction

Observations from Chapter 4 and a recent publication have revealed that binding affinity of human α_2 -antiplasmin lacking the C-terminal region to active site-blocked plasmin remains high ($K_D = 50\text{nM}$) (Lu et al., 2011). This interaction is unlikely to be reactive centre loop (RCL) mediated as the catalytic domain was blocked with a synthetic peptide (CMK). These data suggests that additional exosite region(s) may exist beyond the C-terminus/kringle domain interaction providing an additional mechanism of specificity in this complex interaction. It is common for serpins to possess additional points of interaction to increase its specificity towards its target protease. Some examples include tPA/PAI-I (Ibarra et al., 2004), uPA/PAI-I (Lin et al., 2011) and antithrombin/thrombin/heparin (Izaguirre and Olson, 2006; Izaguirre et al., 2003).

With our collaborators at the Department of Biochemistry and Molecular Biology (Monash University, Clayton), three residues were identified (His²²⁹, Glu²³² and Arg²³³) in the third and fourth strands of β -sheet C that could potentially interact with plasmin(ogen). These residues were identified based on molecular modelling of α_2 -antiplasmin/plasmin on the superposition of the X-ray crystal structure of PAI-I/uPA encounter complex (Lin et al., 2011). Previous reports have suggested that some serpins may form additional contacts via β -sheet C to promote added specificity in protease interaction. For example, 147-loop in uPA directly interacts with β -sheet C of PAI-I (Izaguirre and Olson, 2006; Lin et al., 2011).

To address the potential exosite interactions in the β -sheet C of human α_2 -antiplasmin with plasmin, this chapter describes the mutagenesis of His²²⁹ and Glu²³² to alanine. The murine α_2 -antiplasmin Arg²³³ is not conserved in human α_2 -antiplasmin and therefore was not mutated (Figure 1.10). The expression and subsequent purification of these recombinant β -sheet C mutants are described. The rate of plasmin inhibition (k_a) for the β -sheet C mutant α_2 -antiplasmin was investigated. To distinguish whether an interaction exist between the β -sheet C and the protease domain or β -sheet C and kringle domains, binding affinities (K_D) of mutant β -sheet C α_2 -antiplasmin for active site-blocked plasmin and microplasmin were carried out.

Table 6.1. Primer sequence for human β -Sheet C α_2 -antiplasmin.

Primer Name	Orientation	Nucleotide Sequence (5' → 3')
#449	Sense	CCAGAGAGACTCCTTCGCCCTGGACGAGCAGTTCACG
#450	Antisense	CGTGAACTGCTCGTCCAGGGCGAAGGAGTCTCTCTGG
#451	Sense	CCTTCCACCTGGACGCGCAGTTCACGGTGC
#454	Antisense	GCACCGTGAAGTGCAGGTCCAGGTGGAAGG

6.2 Methods

6.2.1 Site-directed Mutagenesis of the β -sheet C of Human α_2 -antiplasmin

Isolation of human WT α_2 -antiplasmin cDNA was as described in section 3.2.1. The QuikChange site-directed mutagenesis kit (Stratagene) (section 2.5.10) was used to introduce alanine at position 229 and 232 in the β -Sheet C of α_2 -antiplasmin. Table 6.1 shows the list of primers used to introduce the mutations. The following mutants were made: H229A and E232A. All constructs were nucleotide sequenced to confirm the authenticity of the mutations.

6.2.2 Expression and Purification of β -sheet C Mutant α_2 -antiplasmin

Expression and purification of human α_2 -antiplasmin is as described in Chapter 3. Briefly, sheet C mutant α_2 -antiplasmin plasmids were transformed into *E.coli* BL21 cells and were grown in 2x TY media. Cultures were induced with a final IPTG concentration of 0.01mM (section 3.2.3). Soluble supernatant of bacterial cell lysates were collected and purified on a HisTrap column. Protein of interest was eluted out with a buffer containing high concentration of imidazole (section 3.2.4). Peak fractions were collected and prepared for second stage purification on a MonoQ column. Recombinant β -sheet C α_2 -antiplasmin mutants were eluted with a buffer containing high concentration of NaCl (section 3.2.5). Recombinant proteins concentrations were determined and stored at -80°C until further use.

6.2.3 Western Blot Analysis of Recombinant β -sheet C Mutant Human α_2 -antiplasmin

Recombinant β -sheet C mutant proteins were ran on a 12.5% SDS-PAGE (section 2.6.1) and were subsequently transferred onto Immobilon-P PVDF membrane as described in section 2.6.4. Membranes were incubated with 1:2000 dilution of primary antibody (anti 6xHis-Tag raised in mouse) followed by 1:5000 dilution of the secondary antibody (anti-mouse).

6.2.4 Circular Dichroism Analysis of Recombinant β -sheet C Human α_2 -antiplasmin

CD analysis was performed on β -sheet C mutants as described in section 3.2.7.

6.2.5 Native-PAGE Analysis of Recombinant β -sheet C Human α_2 -antiplasmin

Native-PAGE gels were prepared and ran as described in section 2.6.4. 10 μ g of recombinant β -sheet C mutant proteins were electrophoresed and subsequently stained with Coomassie.

6.2.6 Stoichiometry of Inhibition of β -sheet C Human α_2 -antiplasmin with Plasmin

Determination of the stoichiometry of inhibition (*SI*) of recombinant β -sheet C mutants with plasmin is as described in section 4.2.2. Briefly, 8nM of human plasmin was incubated with 2-16nM of recombinant β -sheet C mutants for 1 hr at 37°C. The reaction was then diluted 1/8 and residual plasmin activity was assayed in the presence of 200 μ L fluorogenic substrate, AMC. Fluorescence signal was detected over 20 min at 355/460nm.

6.2.7 Rate of Inhibition of β -sheet C Human α_2 -antiplasmin with Plasmin

The rate of plasmin inhibition by mutant β -sheet C mutants was determined using the continuous method as described in section 4.2.3.1. Briefly, human plasmin (0.5nM) was reacted with 1-2.5nM of mutant α_2 -antiplasmin, in the presence of 1mM fluorogenic AMC substrate. The increase in fluorescence resulting from substrate hydrolysis was continuously measure for 1 hr at 355/460nm.

6.2.8 Surface Plasmon Resonance to measure Binding Affinity

The interaction between active site-blocked plasmin/microplasmin and mutant β -sheet C α_2 -antiplasmin were determined via surface plasmon resonance using the BIAcore T100 system as described in section 4.2.4.2. Active site-blocked plasmin (PI_mCMK) and active site-blocked microplasmin (μ PI_mCMK) was produced by incubating with a 1000-fold molar excess of D-Val-Phe-Lys chloromethyl ketone (CMK) at 37°C for 1 hr. Briefly, mutant α_2 -antiplasmin were immobilised on the NTA chip. Six different concentrations (0-8nM) of PI_mCMK or μ PI_mCMK were injected for 1 min of association time, followed by 10 min of dissociation time. The NTA surface was regenerated at each concentration cycle.

6.3 Results

6.3.1 Mutagenesis of β -sheet C α_2 -antiplasmin

Mutations in the β -sheet C of wild-type (WT) human α_2 -antiplasmin were introduced by using the Quikchange mutagenesis kit as previously described in Chapter 3. Mutagenic primers were designed (Table 6.1) to replace the amino acids at position His²²⁹ and Glu²³² with Ala. Nucleotide sequencing was performed to confirm all single-point substitutions and to ensure that no other mutations were introduced into the gene. Figure 6.1 shows the amino acid sequence of β -sheet C mutants aligned with WT α_2 -antiplasmin. Both mutants were verified to have the mutation of interest at the corresponding positions. The α_2 -antiplasmin mutants were named H229A and E232A. Table 6.2 is a summary of the extinction co-efficient, molecular weight (MW) and isoelectric point (pI) of the β -sheet C mutants as calculated from the predicted amino acid sequence.

Figure 6.1. Sequence alignment of β -sheet C human α_2 -antiplasmin. Wild-type (WT) human α_2 -antiplasmin and two β -sheet C α_2 -antiplasmin mutants (H229A and E232A) were generated, expressed and purified. Amino acid at position 229 and 232 were mutated to alanine as indicated by the red font and highlighted in green.

Figure 6.1. Sequence alignment of β-sheet C human α₂-antiplasmin

	13				50
WT	MHHHHHH	GSNQEQVSP	TLLKLGNOEP	GGQTALKSPP	GVCSRDPTE
H2 29A	MHHHHHH	GSNQEQVSP	TLLKLGNOEP	GGQTALKSPP	GVCSRDPTE
E2 32A	MHHHHHH	GSNQEQVSP	TLLKLGNOEP	GGQTALKSPP	GVCSRDPTE
	51				100
WT	QTHRLARAMM	AFTADLFSLV	AQTSTCPNLI	LSPLSVALAL	SHLALGAQNH
H2 29A	QTHRLARAMM	AFTADLFSLV	AQTSTCPNLI	LSPLSVALAL	SHLALGAQNH
E2 32A	QTHRLARAMM	AFTADLFSLV	AQTSTCPNLI	LSPLSVALAL	SHLALGAQNH
	101				150
WT	TLQRLQQVLH	AGSGPCLPHL	LSRLCQDLGP	GAFRLAARMY	LQKGFPIKED
H2 29A	TLQRLQQVLH	AGSGPCLPHL	LSRLCQDLGP	GAFRLAARMY	LQKGFPIKED
E2 32A	TLQRLQQVLH	AGSGPCLPHL	LSRLCQDLGP	GAFRLAARMY	LQKGFPIKED
	151				200
WT	FLEQSEQLFG	AKPVSLTGKQ	EDDLANINQW	VKEATEGKIQ	EFLSGLPEDT
H2 29A	FLEQSEQLFG	AKPVSLTGKQ	EDDLANINQW	VKEATEGKIQ	EFLSGLPEDT
E2 32A	FLEQSEQLFG	AKPVSLTGKQ	EDDLANINQW	VKEATEGKIQ	EFLSGLPEDT
	201				250
WT	VLLLLNAIHF	QGFWRNKFD	SLTQRDSFHL	DEQFTVPVEM	MQARTYPLRW
H2 29A	VLLLLNAIHF	QGFWRNKFD	SLTQRDSFHL	DEQFTVPVEM	MQARTYPLRW
E2 32A	VLLLLNAIHF	QGFWRNKFD	SLTQRDSFHL	DEQFTVPVEM	MQARTYPLRW
	251				300
WT	FLLEQPEIQV	AHFPPKNNMS	FVVLVPTHFE	WNVSQVLANL	SWDTLHPPLV
H2 29A	FLLEQPEIQV	AHFPPKNNMS	FVVLVPTHFE	WNVSQVLANL	SWDTLHPPLV
E2 32A	FLLEQPEIQV	AHFPPKNNMS	FVVLVPTHFE	WNVSQVLANL	SWDTLHPPLV
	301				350
WT	WERPTKVRLP	KLYLKHQMDL	VATLSQLGLQ	ELFQAPDLRG	ISEQSLVVS
H2 29A	WERPTKVRLP	KLYLKHQMDL	VATLSQLGLQ	ELFQAPDLRG	ISEQSLVVS
E2 32A	WERPTKVRLP	KLYLKHQMDL	VATLSQLGLQ	ELFQAPDLRG	ISEQSLVVS
	351				400
WT	VQHQSSTLELS	EVGVEAAAAT	SIAMSRMSLS	SFSVNRPFLF	FIFEDTTGLP
H2 29A	VQHQSSTLELS	EVGVEAAAAT	SIAMSRMSLS	SFSVNRPFLF	FIFEDTTGLP
E2 32A	VQHQSSTLELS	EVGVEAAAAT	SIAMSRMSLS	SFSVNRPFLF	FIFEDTTGLP
	401				450
WT	LFVGSVRNPN	PSAPRELKEQ	QDSPGNKDFL	QSLKGFPRGD	KLFGPDLKLV
H2 29A	LFVGSVRNPN	PSAPRELKEQ	QDSPGNKDFL	QSLKGFPRGD	KLFGPDLKLV
E2 32A	LFVGSVRNPN	PSAPRELKEQ	QDSPGNKDFL	QSLKGFPRGD	KLFGPDLKLV
	451	464			
WT	PPMEEDYPQF	GSPK			
H2 29A	PPMEEDYPQF	GSPK			
E2 32A	PPMEEDYPOF	GSPK			

Table 6.2. Molecular weight (MW), extinction coefficient and isoelectric point (pI) of human β -sheet C α_2 -antiplasmin. Parameters were calculated using the Protparam Tool available at the following website: <http://web.expasy.org/protparam/>

Recombinant α_2-antiplasmin	Molecular Weight (Daltons)	Extinction Coefficient ($M^{-1}cm^{-1}$)	Isoelectric Point
H229A	51483	39210	6.10
E232A	51491	39210	6.22

6.3.2 Expression and Purification of β -sheet C α_2 -antiplasmin

The expression and purification of β -sheet C mutant α_2 -antiplasmins was as described per the standard method in Chapter 3. A two-step purification method whereby HisTrap followed by MonoQ purification were carried out to purify β -sheet C mutant α_2 -antiplasmin to homogeneity.

The soluble lysate was bound to a nickel chelate affinity column (HisTrap) and protein of interest was eluted with a 0-500mM imidazole gradient. Figure 6.2A and C shows the corresponding chromatogram of H229A and E232A respectively. A single peak was observed for H229A whereas a double protein peak was obtained for E232A. When analysed on Coomassie stained 12.5% SDS-PAGE (Figure 6.2B and D), a major contaminating protein band appears at a slightly higher molecular weight and the second band directly below is most likely H229A and E232A recombinant α_2 -antiplasmin (as indicated by the arrow).

Fractions 2-4 of H229A and fractions 4-5 of E232A were pooled and applied onto the MonoQ column to further purify recombinant α_2 -antiplasmin. Figure 6.3A and C shows the corresponding chromatogram of H229A and E232A respectively. Protein of interest is eluted with a 0-500mM NaCl gradient in fraction number 18 and 19 when analysed on a Coomassie stained 12.5% SDS-PAGE (Figure 6.3B and D). A doublet was observed in fraction 17 in both H229A and E232A purification which is indicative of cleaved protein. Therefore fractions 18 and 19 were pooled to make up the final purified protein sample.

A Western blot of purified protein was performed with the anti-6xHis tag antibody to confirm that the band at the correct molecular weight for α_2 -antiplasmin was the protein of interest (Figure 6.4A). Analysis by Native-PAGE was also performed to ensure that the majority of proteins produced are in monomeric form (Figure 6.4B). Protein concentration was determined at absorbance at 280nm. Protein yields were approximately 0.1-0.4mg per litre of culture.

Figure 6.2. Nickel affinity chromatography of β -sheet C human α_2 -antiplasmin. **A)** Elution profile of H229A. **B)** Peak fractions from H229A purification were analysed on Coomassie stained 12.5% SDS-PAGE. **C)** Elution profile of E232A. **D)** Peak fractions from E232A purification were analysed on Coomassie stained 12.5% SDS-PAGE. Elution profiles show protein absorbance in mAU (black lines) and the percentage of HisTrap Buffer B (red). 1mL fractions were collected and numbered accordingly. Arrow indicates recombinant protein of interest. Relative molecular weight in kDa is as indicated on the left.

Figure 6.2.
Nickel affinity chromatography of β -sheet C human α_2 -antiplasmin

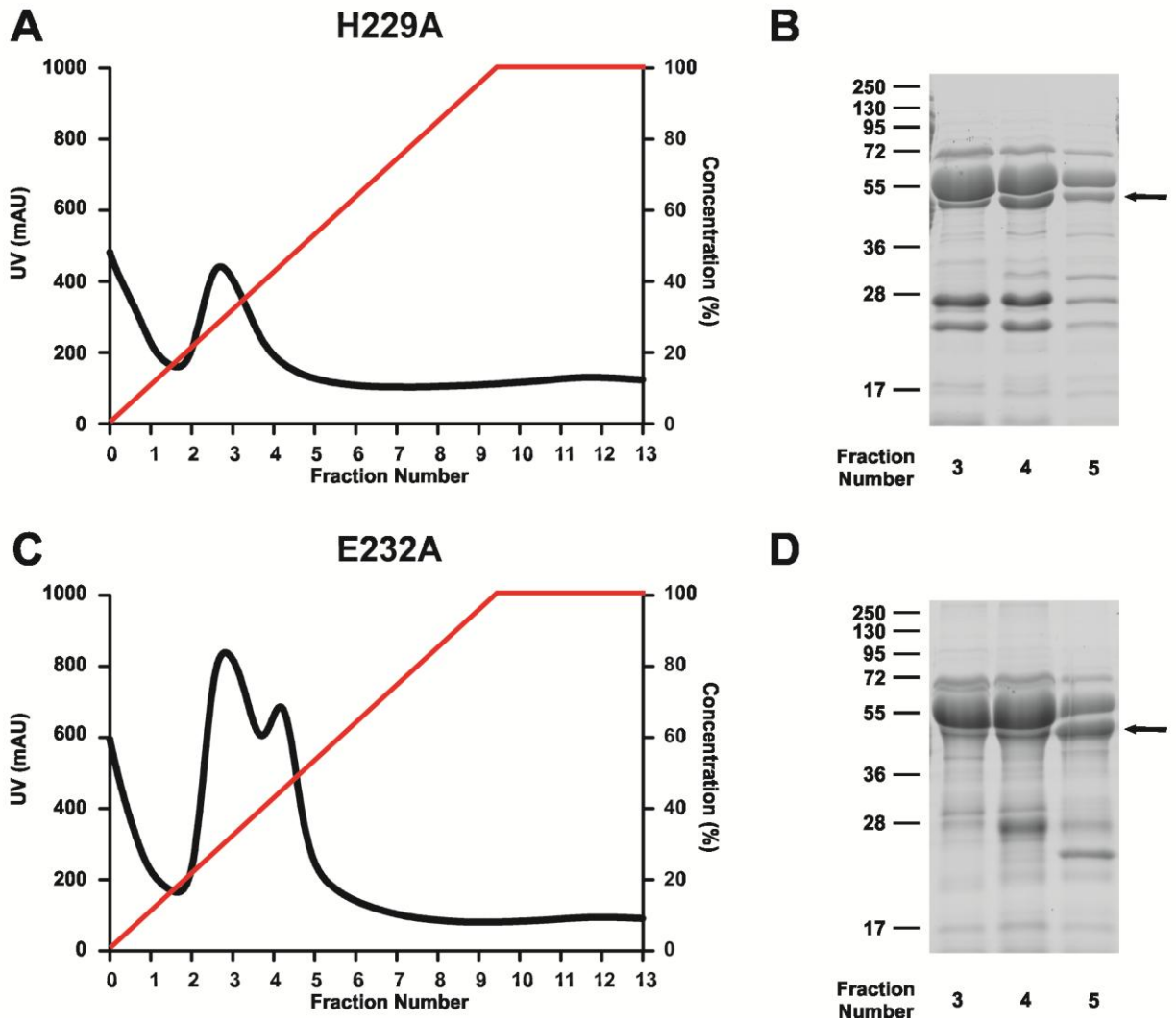


Figure 6.3. Anion exchange chromatography of β -sheet C human α_2 -antiplasmin. A) Elution profile of H229A. **B)** Peak fractions from H229A purification were analysed on Coomassie stained 12.5% SDS-PAGE. **C)** Elution profile of E232A. **D)** Peak fractions from E232A purification were analysed on Coomassie stained 12.5% SDS-PAGE. Elution profiles show protein absorbance in mAU (black lines) and the percentage of HisTrap Buffer B (red). 500 μ L fractions were collected and numbered accordingly. Relative molecular weight in kDa is as indicated on the left.

Figure 6.3.
Anion exchange chromatography of β -sheet C human α_2 -antiplasmin

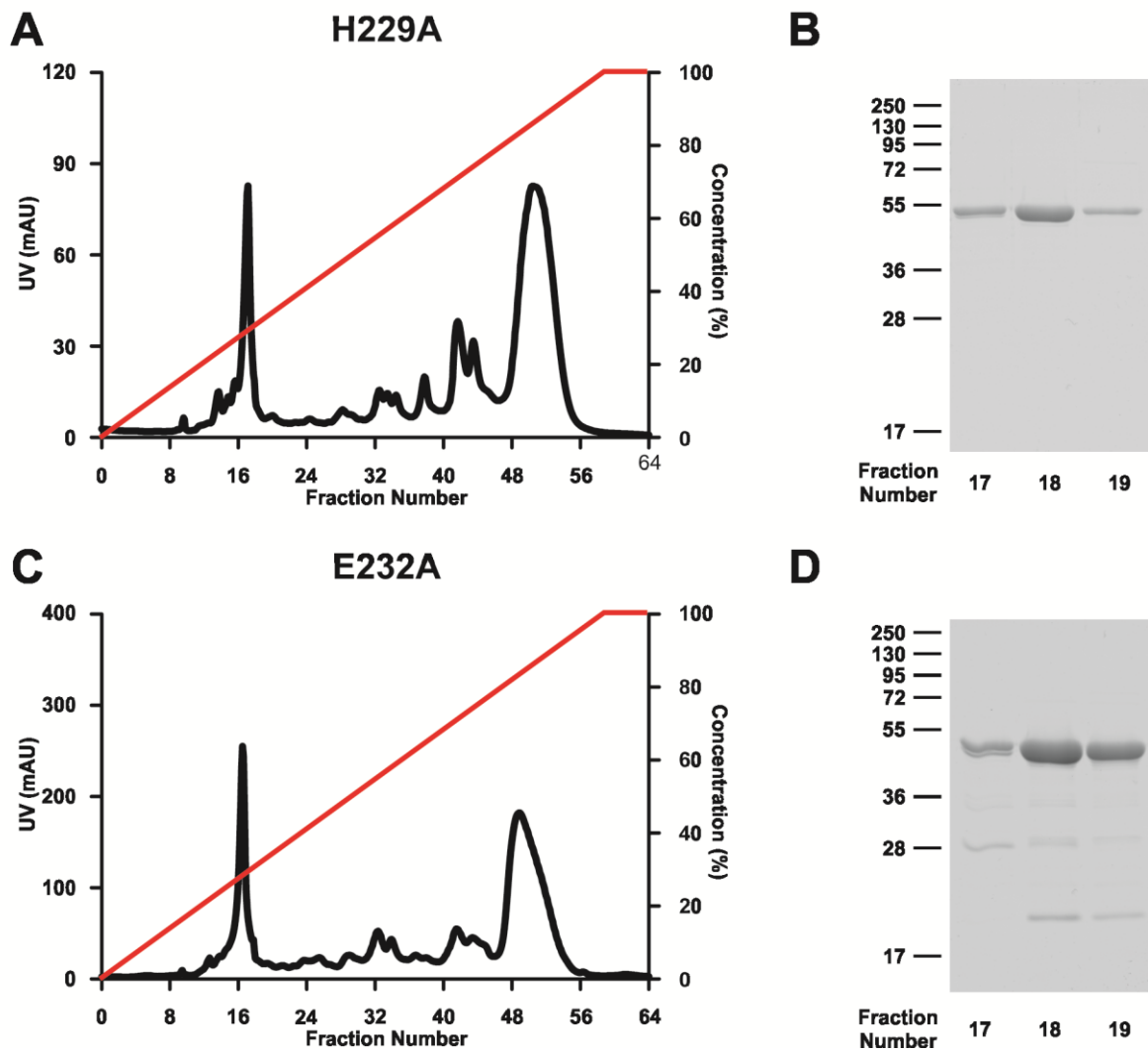


Figure 6.4. Analysis of recombinant β -sheet C α_2 -antiplasmin on Western and Native-PAGE. A) Purified H229A and E232 were transferred to a Western blot and analysed with an antibody against His-tag (1:2000). Relative molecular weight in kDa is as indicated on the left. **B)** Coomassie stained Native-PAGE analysis of H229A and E232A.

Figure 6.4.
Analysis of recombinant β -sheet C α_2 -antiplasmin
on Western and Native-PAGE



Table 6.3. Stoichiometry of inhibition (SI) and plasmin inhibition rate (k_a) of β -sheet C α_2 -antiplasmin versus WT α_2 -antiplasmin (n=3). Results of WT are from Chapter 4.

Recombinant α_2-antiplasmin	$SI \pm SE$ (n=3)	$k_a \pm SE$ ($M^{-1}s^{-1}$) (n=3)
WT	1.0 ± 0.02	$3.7 \pm 0.3 \times 10^7$
H229A	1.0 ± 0.02	$2.5 \pm 0.9 \times 10^7$
E232A	1.0 ± 0.003	$3.1 \pm 0.2 \times 10^7$

6.3.3 Stoichiometry of Inhibition (*S*) of β -sheet C mutant α_2 -antiplasmin

To ensure that mutations in the β -sheet C region of α_2 -antiplasmin had not affected the functional conformation and plasmin inhibition mechanism, the stoichiometry of inhibition (*S*) was determined. As previously described in Chapter 4, the *S* of each recombinant protein was determined by extrapolating to the serpin:protease ratio which resulted in a complete loss of protease activity (x-intercept). The plots used to determine the *S* of H229A and E232A are shown in Figures 6.5A and 6.5B respectively. Table 6.3 is a summary of *S* values obtained for β -sheet C α_2 -antiplasmin mutants. The *S* values determined for both β -sheet C mutants were ~1 which corresponds with WT α_2 -antiplasmin, indicating that the recombinant proteins remained in their native conformation despite the mutations that were introduced.

H229A and E232A mutants were assessed by CD spectrometry to further confirm that mutation introduced had not altered the conformation of α_2 -antiplasmin (Figure 6.6). Both mutants produced CD spectra similar to WT α_2 -antiplasmin (Figure 3.13), demonstrating that the mutant proteins retained their native fold.

Figure 6.5. Stoichiometry of inhibition (SI) of β -sheet C α_2 -antiplasmin with plasmin. A constant plasmin concentration was incubated with varying amount of recombinant α_2 -antiplasmin at the indicated serpin:protease ratio. Once the reaction was completed, residual protease activity was assayed. The SI was obtained by extrapolating to where protease activity equals zero. **A)** SI for H229A. **B)** SI for E232A.

Figure 6.5.
**Stoichiometry of inhibition (*S*) of β -sheet C α_2 -antiplasmin
with plasmin**

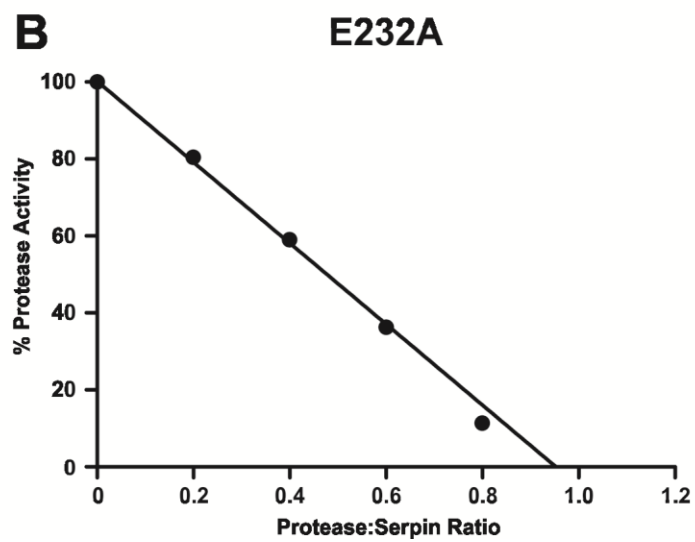
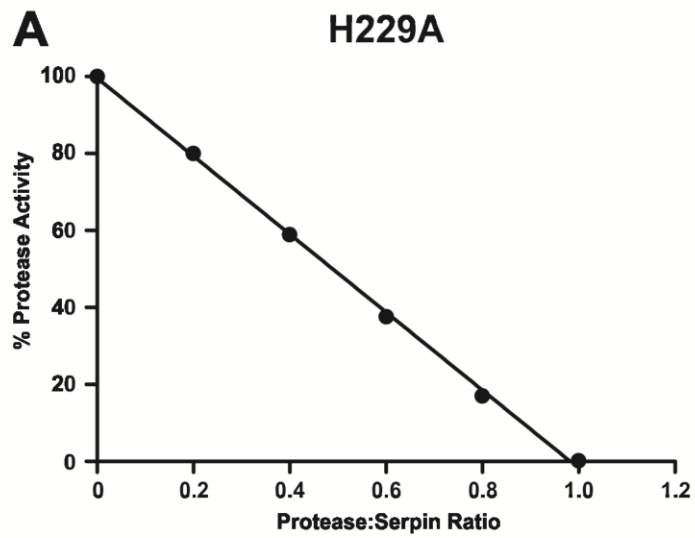
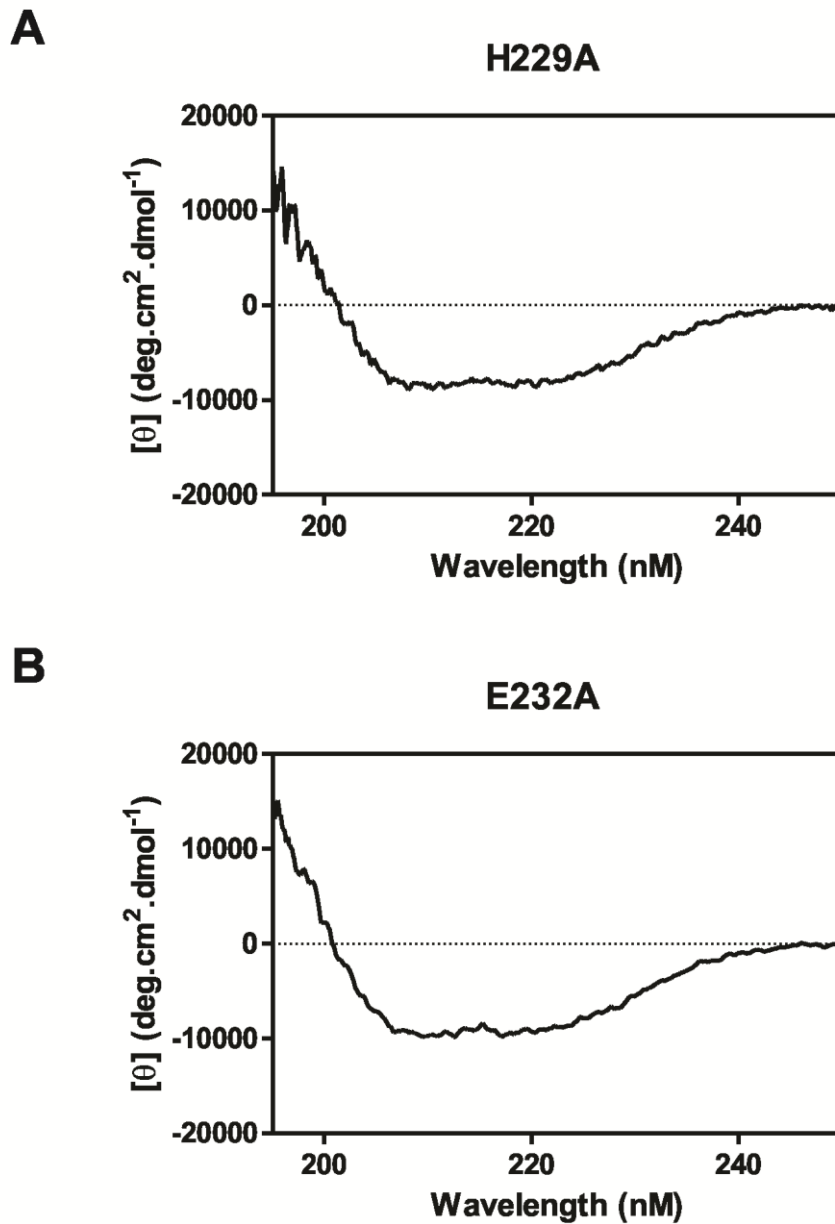


Figure 6.6. Circular dichroism analysis of β -sheet C α_2 -antiplasmin. The CD spectrum of 200 μ g/mL recombinant α_2 -antiplasmin was determined from 195-250nm using a 0.1cm path length cuvette. **A)** CD for H229A. **B)** CD for E232A.

Figure 6.6.
Circular dichroism analysis of β -sheet C α_2 -antiplasmin



This page has been intentionally left blank.

6.3.4 Plasmin Inhibition Rate of β -Sheet C α_2 -antiplasmin Mutants

The hypothesis being tested is whether the amino acids at position 229 and 232 within the β -sheet C of α_2 -antiplasmin accelerate the inhibition of plasmin. Kinetic studies using a protease inhibition assay were performed to measure the plasmin inhibition rate (k_a) of β sheet C α_2 -antiplasmin mutants.

The k_a of WT α_2 -antiplasmin was determined to be $3.7 \times 10^7 \text{ M}^{-1}\text{s}^{-1}$ (section 4.3.2). This value corresponds with published value (Christensen et al., 1996). This value was used as the base of comparison to β -sheet C α_2 -antiplasmin mutants analysed.

Figures 6.7A and B shows the analysis obtained from H229A with full-length plasmin. There was a decrease in plasmin inhibition rate with H229A ($k_a = 2.5 \times 10^7 \text{ M}^{-1}\text{s}^{-1}$) when compared with WT α_2 -antiplasmin (Table 6.3). Kinetic analysis of E232A with plasmin are shown in Figures 6.7C and D. The plasmin inhibition rate of E232A ($k_a = 3.1 \times 10^7 \text{ M}^{-1}\text{s}^{-1}$) showed a slight reduction when compared with WT. Both β -sheet C mutants showed no significance decrease in plasmin inhibition rate (Figure 6.8) suggesting that amino acids at position 229 and 232 result in minimal changes in the inhibition of plasmin by α_2 -antiplasmin.

Figure 6.7. Plasmin inhibition (k_a) by β -sheet C α_2 -antiplasmin. Progress curves of the interaction between plasmin (0.5nM) and α_2 -antiplasmin mutant (1-4nM) measured in fluorescence units. Black lines represent raw curves. Red line represents control protease only. Each curve was analysed and fitted (orange lines) using non-linear regression using Equation 4.1 to determine the k_{obs} at each serpin concentration. k_{obs} were plotted against α_2 -antiplasmin concentration and linear regression analysis was used to determine the k' . The plasmin inhibition rate (k_a) was determined by factoring in the Michaelis Menton (K_M), substrate concentration [S] and the S/I as described using Equation 4.2. **A&B)** Progress curves and k_a of H229A. **C&D)** Progress curves and k_a of E232A.

Figure 6.7.
Plasmin inhibition (k_a) by β -sheet C α_2 -antiplasmin

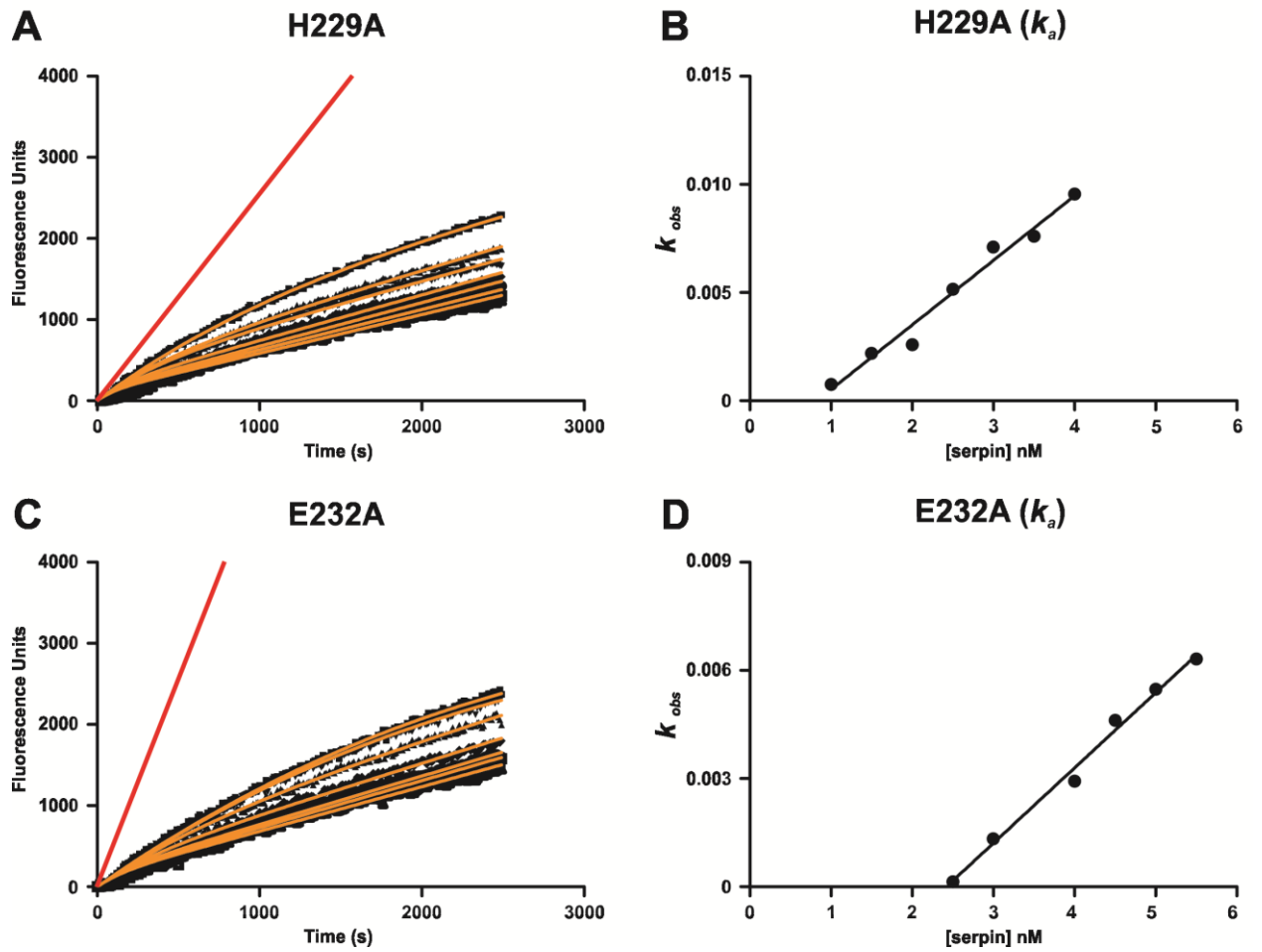


Figure 6.8. Comparison of plasmin inhibition rate (k_a) between wild-type and β -sheet C α_2 -antiplasmin. The k_a for plasmin and α_2 -antiplasmin variants were measured as described in Chapter 4. Statistics were assessed by one-way ANOVA with Newman-Keuls post-hoc correction. “ns” refers to non-statistically significant data ($p>0.05$). Data points represents the mean (n=3-4) with error bars representing \pm SE of each protein.

Figure 6.8.
Comparison of plasmin inhibition rate (k_a) between wild-type and β -sheet C α_2 -antiplasmin

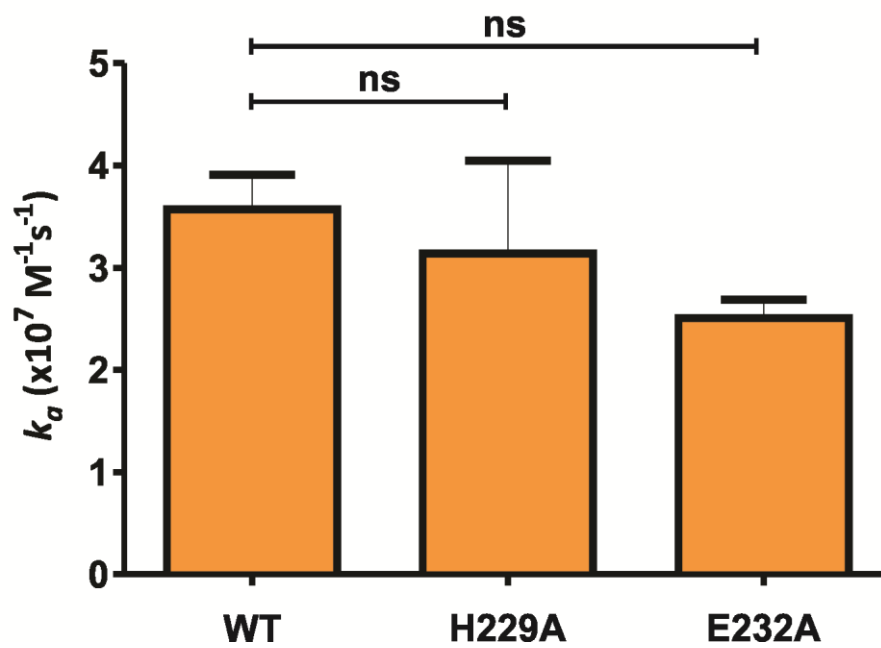


Table 6.4. Mean binding affinity, association and dissociation constants of WT and β -sheet C antiplasmin mutants for active site-blocked plasmin as measured by surface plasmon resonance (n=3-6). WT results are from Chapter 4.

Recombinant α_2-antiplasmin	$K_D \pm SE$ (nM)	k_{a1} ($M^{-1}s^{-1}$)	k_{d1} (1/s)	k_{a2} (1/s)	k_{d2} (1/s)
WT	1.6 \pm 0.1	2.1 $\times 10^7$	0.09	0.007	0.005
H229A	2.6 \pm 0.2	1.1 $\times 10^6$	0.01	0.01	0.005
E232A	2.7 \pm 0.4	1.0 $\times 10^6$	0.01	0.01	0.005

6.3.5 Binding Affinity of β -sheet C α_2 -antiplasmin Mutants with Active Site-blocked Plasmin

Surface plasmon resonance (SPR) was used to directly measure binding affinity of recombinant α_2 -antiplasmin to active site-blocked plasmin. WT and β -sheet C α_2 -antiplasmin mutants were reacted with active site-blocked plasmin (PlmCMK), and binding was observed in real time. The association and dissociation constants were calculated to obtain the binding affinity (K_D). Sensorgrams for the interaction between PlmCMK and β -sheet C α_2 -antiplasmin mutants are shown in Figure 6.9. A concentration range from 0-8nM of PlmCMK was used for all WT and β -sheet C mutants to achieve similar levels of response units (RU) seen on the sensorgrams.

The K_D of WT α_2 -antiplasmin for active PlmCMK was determined to be 1.6nM suggestive of a high affinity interaction (determined in Chapter 4). Single mutations of His-to-Ala at position 229 and Glu-to-Ala at position 232 showed a \sim 1.6-fold decrease in binding affinity (H229A, $K_D = 2.6$ nM; E232A, $K_D = 2.7$ nM) when compared to WT (Table 6.4). Both proteins showed significant difference in binding to active site-blocked plasmin (Figure 6.11). Therefore, this suggests that residues at position 229 and 232 in the β -sheet C region influence the binding of α_2 -antiplasmin to plasmin.

The rate of plasmin association (k_{a1}) of H229A and E232A showed a \sim 10-fold difference when compared to WT α_2 -antiplasmin. This suggests that residues at position 229 and 232 may play a role in accelerating the initial interaction with plasmin which decreases the overall affinity for plasmin, however the rate of plasmin inhibition (k_a) is not affected as described in section 6.3.4. The dissociation rate constant (k_{d1}) and the forward and reverse rate constants (k_{a2} and k_{d2}) obtained using SPR remained relatively unchanged for WT and β -sheet C α_2 -antiplasmin recombinant proteins with PlmCMK.

Figure 6.9. Sensorgrams of the binding of recombinant β -sheet C α_2 -antiplasmin to PImCMK as measured by SPR. β -sheet C mutant α_2 -antiplasmin (20nM) was immobilised on a NTA chip. The binding of various concentrations of active site-blocked plasmin to α_2 -antiplasmin was monitored in real time. Green lines are raw curves and fitted curves are in black. **A)** Binding of active site-blocked plasmin (2-8nM) to H229A ($\chi^2 = 0.60$). **B)** Binding of active site-blocked plasmin (2-8nM) to E232A ($\chi^2 = 0.69$).

Figure 6.9.
Sensorgrams of the binding of recombinant β -sheet C α_2 -antiplasmin to PlmCMK as measured by SPR

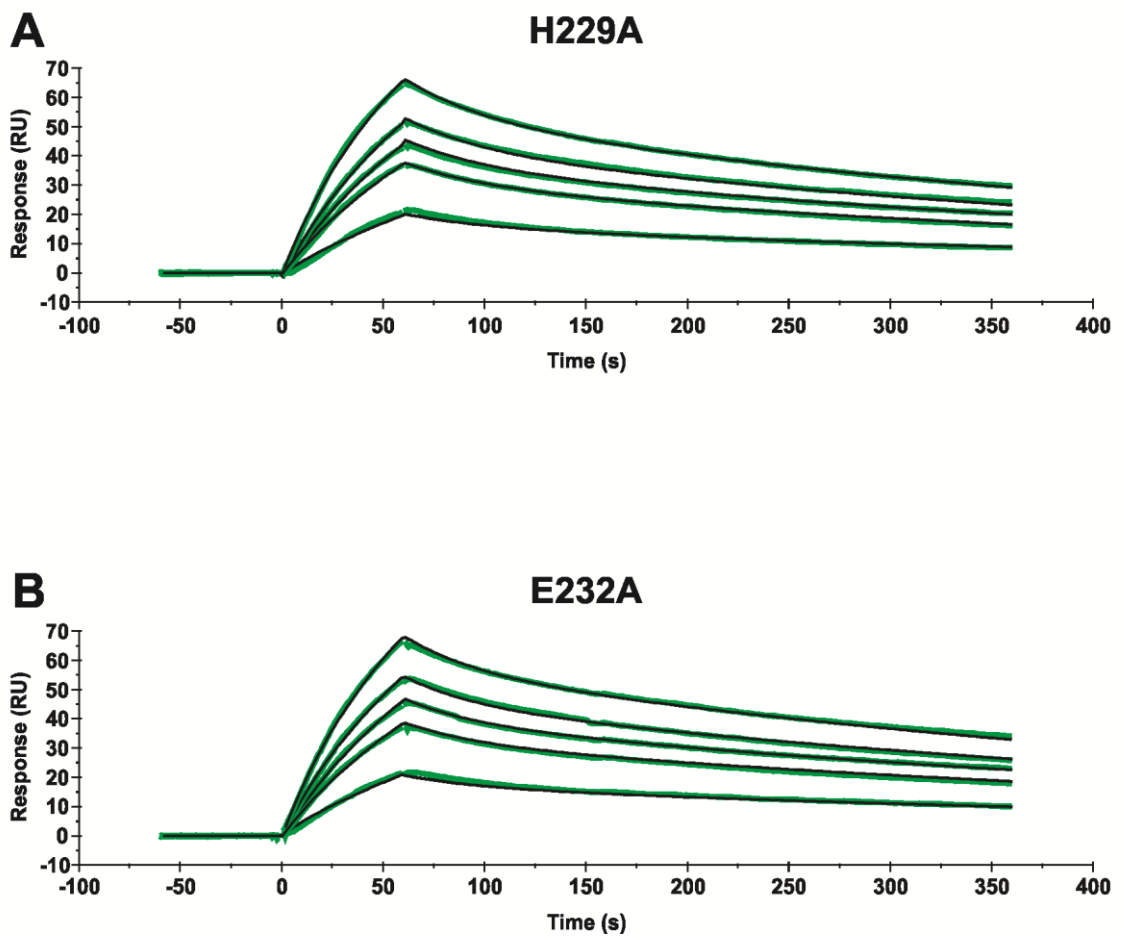


Table 6.5. Mean binding affinity, association and dissociation constants of WT and β -sheet C antiplasmin mutants for active site-blocked microplasmin as measure by surface plasmon resonance (n=3).

Recombinant α_2 -antiplasmin	$K_D \pm SE$ (nM)	k_{a1} ($M^{-1}s^{-1}$)	k_{d1} (1/s)	k_{a2} (1/s)	k_{d2} (1/s)
WT	105 \pm 12	2.9 $\times 10^4$	0.01	0.008	0.003
H229A	126 \pm 17	2.4 $\times 10^4$	0.01	0.008	0.003
E232A	79 \pm 15	3.7 $\times 10^4$	0.01	0.007	0.003

6.3.6 Binding Affinity of β -sheet C α_2 -antiplasmin with Active Site-blocked Microplasmin

To further examine the role of the β -sheet C of antiplasmin in the interaction with the protease domain of plasmin, β -sheet C α_2 -antiplasmin mutants were reacted with active site-blocked microplasmin (μ PlmCMK). By comparing binding of plasmin and microplasmin, a better understanding on whether β -sheet C region of α_2 -antiplasmin interacts with either the plasmin protease domain or kringles may be revealed. The sensorgrams of μ PlmCMK and β -sheet C α_2 -antiplasmin mutants are shown in Figure 6.10 (sensorgram for WT and μ PlmCMK is presented in Chapter 7). To achieve similar RU seen on the sensorgrams, 0-200nM of μ PlmCMK was used for all binding studies to WT and β -sheet C proteins.

The K_D of WT α_2 -antiplasmin for μ PlmCMK was determined to be 105nM. Single mutations to Ala at positions 229 and 232 showed a K_D of 126nM and 79nM respectively (Table 6.5). The binding affinities of these β -sheet C mutants were not significantly different when compared to WT α_2 -antiplasmin (Figure 6.11). This informed that the amino acid at position 229 and 232 does not play a role in the interaction with the protease domain, however may be involved with the kringle(s).

The rate of microplasmin association (k_{a1}), dissociation rate constant (k_{d1}) and the forward and reverse rate constants (k_{a2} and k_{d2}) obtained using SPR remained relatively unchanged for WT and β -sheet C α_2 -antiplasmin mutant recombinant proteins with μ PlmCMK.

Figure 6.10. Sensorgrams of the binding of recombinant β -sheet C α_2 -antiplasmin to μ PlmCMK as measured by SPR. β -sheet C mutant α_2 -antiplasmin (20nM) was immobilised on a NTA chip. The binding of various concentrations of μ PlmCMK to α_2 -antiplasmin was monitored in real time. **A)** Binding of μ PlmCMK (40-200nM) to H229A ($\chi^2 = 0.26$). **B)** Binding μ PlmCMK (40-200nM) to E232A ($\chi^2 = 0.37$).

Figure 6.10.
Sensorgrams of the binding of recombinant β -sheet C α_2 -antiplasmin to μ PlmCMK as measured by SPR

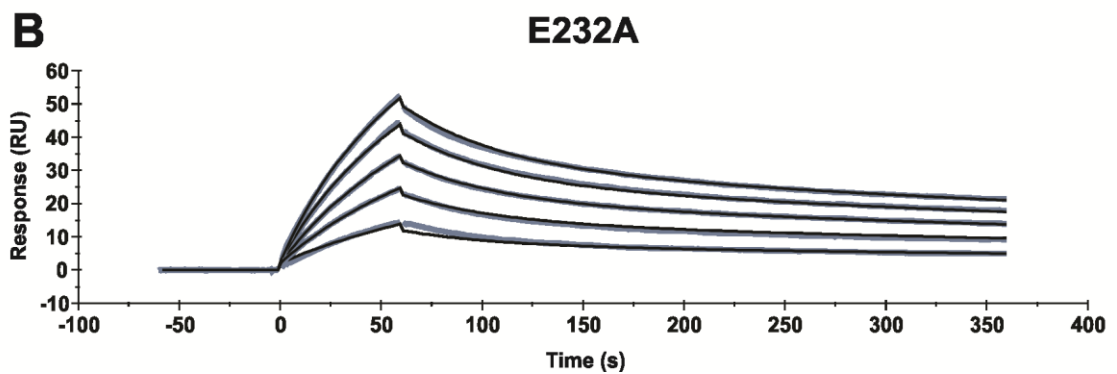
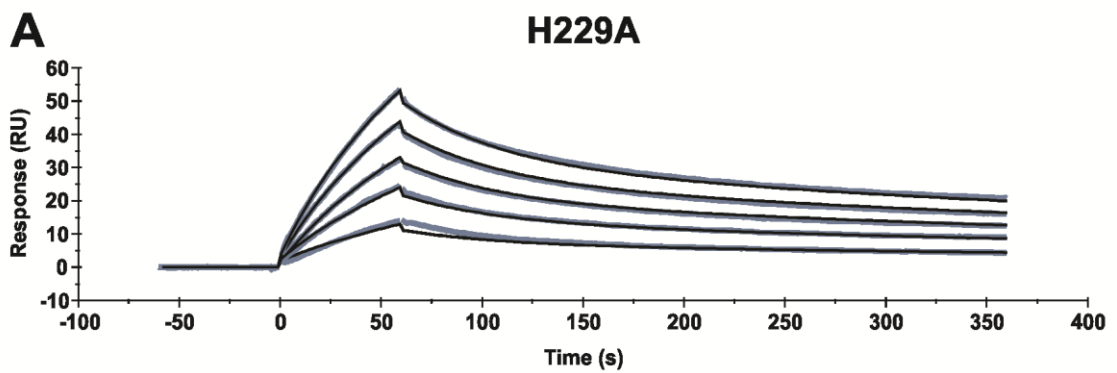
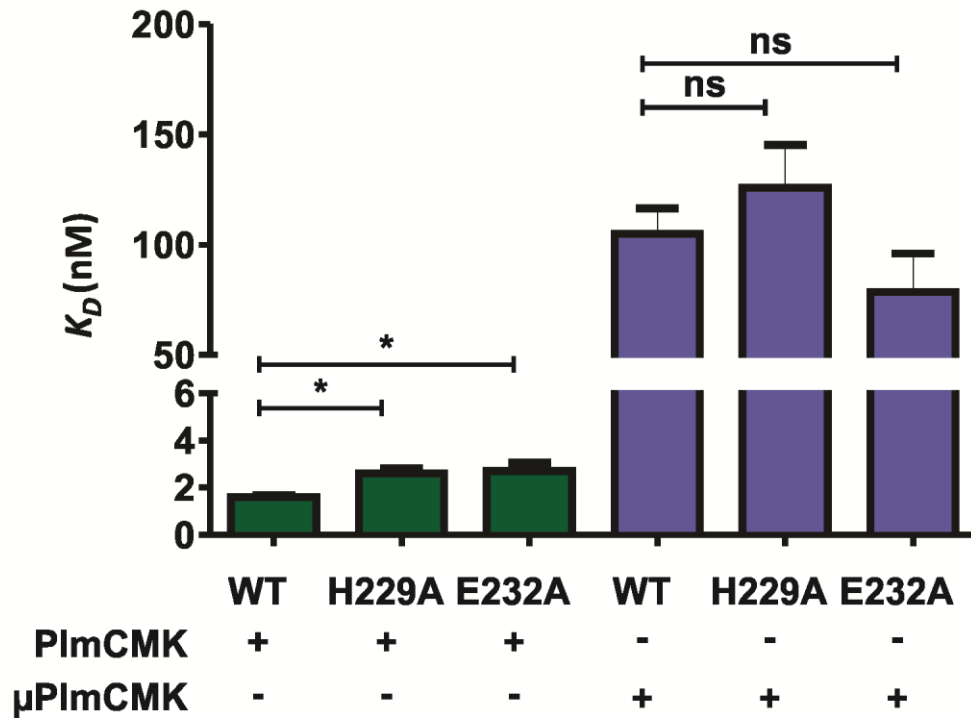


Figure 6.11. Comparison of the binding affinity (K_D) between β -sheet C α_2 -antiplasmin with PlmCMK or μ PlmCMK. The K_D of WT and β -sheet C mutants (H229A and E232A) were calculated based on Equation 4.4 as previously described. Statistics were assessed by one-way ANOVA with Newman-Keuls post-hoc correction. “*” refers to statistically significant data with a p-value of $p < 0.05$. “ns” refers to non-statistically significant data ($p > 0.05$). Each of the data points represents the mean ($n=3-6$) with error bars representing \pm SE. Green bar graphs are K_D of β -sheet C α_2 -antiplasmin mutants with PlmCMK. Blue bar graphs are K_D of β -sheet C α_2 -antiplasmin mutants with μ PlmCMK.

Figure 6.11.
Comparison of the binding affinity (K_D) between β -sheet C α_2 -antiplasmin with PlmCMK or μ PlmCMK



This page has been intentionally left blank.

6.4 Discussion

The SPR data in Chapter 4 suggested an additional exosite interaction that exists between α_2 -antiplasmin and plasmin. In Chapter 5, the identification of additional exosite interaction between the protease domain and serpin domain through the direct visualisation by crystallisation of the encounter complex was attempted. In this chapter, the possibility of the β -sheet C in this added recognition site was explored using modelling and mutagenesis. Therefore, based on superposition the uPA/PAI-I counter complex (Lin et al., 2011) with the murine α_2 -antiplasmin, three residues (His²²⁹, Glu²³² and Arg²³³) were identified as potential residues which may form contacts with plasmin(ogen) (Figure 6.12). Site-directed mutagenesis was used to explore this possibility. The plasmin inhibition rate and binding affinities of these mutants were measured to determine whether the residues influenced interaction with plasmin(ogen). Only residues His²²⁹ and Glu²³² were explored in this chapter as Arg²³³ is not conserved within species (Figure 1.11).

Recombinant β -sheet C α_2 -antiplasmin mutants were expressed and purified from *E.coli* as a soluble protein as previously described in Chapter 3. Purification on nickel affinity and anion exchange chromatography has successfully separated the protein of interest from bacterial contaminants. Protein purity was accessed by Western blot and Native-PAGE to ensure that the proteins are in monomeric form. Expression level was lower in H229A when compared to E232A, however sufficient protein was produced for kinetic and binding analysis. Production of H229A and E232A was achieved with a purity of ~98% and with a final protein yield of between 0.1-0.4 mg per litre of culture.

To assess the efficiency of recombinant β -sheet C mutants as a plasmin inhibitor, the stoichiometry of inhibition was determined. Recombinant β -sheet C mutants were observed to have an *SI* of approximately 1.0 which was similar to that obtained for wild-type (WT) α_2 -antiplasmin. This indicates that the efficiency of the mutants has not been affected by the substitution of His²²⁹ and Glu²³² to alanine in the β -sheet C of α_2 -antiplasmin. CD spectrum of H229A and E232A were obtained and further confirmed that recombinant proteins obtained remained in its native conformation.

It was determined that plasmin inhibition rates of both β -sheet C mutants were not altered when compared to WT α_2 -antiplasmin (WT, $k_a = 3.7 \times 10^7 \text{ M}^{-1}\text{s}^{-1}$; H229A, $k_a = 2.5 \times 10^7 \text{ M}^{-1}\text{s}^{-1}$; E232A, $k_a = 3.1 \times 10^7 \text{ M}^{-1}\text{s}^{-1}$). However, there was a slight decrease in binding affinity of β -sheet C mutants to active site-blocked plasmin in comparison to WT (WT, $K_D = 1.6\text{nM}$; H229A, $K_D = 2.6\text{nM}$; E232A, $K_D = 2.7\text{nM}$). Furthermore, the association rate constant (k_{a1}) of β -sheet C mutants showed a 10-fold decrease when compared to WT (Table 6.4). It is surprising that no significant reduction in plasmin inhibition rate (k_a) was observed with

β -sheet C α_2 -antiplasmin mutants. Therefore this implies that residues at position 229 and 232 play a minor role in increasing association rate (k_{a1}) and binding (K_D) to plasmin and that other residue(s) within α_2 -antiplasmin have a greater impact in the inhibition mechanism.

No significant difference in binding affinity was seen with β -sheet C mutants and active site-blocked microplasmin (WT, $K_D = 105\text{nM}$; H229A, $K_D = 105\text{nM}$; E232A, $K_D = 79\text{nM}$) which informs that the protease domain of plasmin does not interact with sheet C of α_2 -antiplasmin. Taken together, these results suggest that there is an interaction between β -sheet C of α_2 -antiplasmin and kringle domains of plasmin. The decrease in binding affinity observed in the single amino acid substitution is low implying that a region or multiple residues within the β -sheet C may be involved.

Individual substitution at residues His²²⁹ and Glu²³² of α_2 -antiplasmin have a modest reduction in plasmin binding (~2-fold) when compared to its wild-type counterpart. Future studies with combined mutation at positions 229 and 232 may demonstrate that these residues are important as a pair rather than singularly. Izaguirre and Olson (2006) showed that Tyr²⁵³ and Glu²⁵⁵ in β -sheet C strand 3 are key exosite residues in accelerating the inhibitory reaction with Factor Xa and IXa in the presence of heparin. When these residues were substituted individually, there was a reduction in the rate of inhibition between antithrombin with Factor Xa/IXa. However when both Tyr²⁵³ and Glu²⁵⁵ were mutated in combination, the inhibition rate was greatly decreased by ~100-folds in the presence of heparin (Izaguirre and Olson, 2006). Therefore, residues His²²⁹ and Glu²³² of α_2 -antiplasmin β -sheet C may demonstrate a multiplicative reduction in the binding to plasmin when mutated collectively.

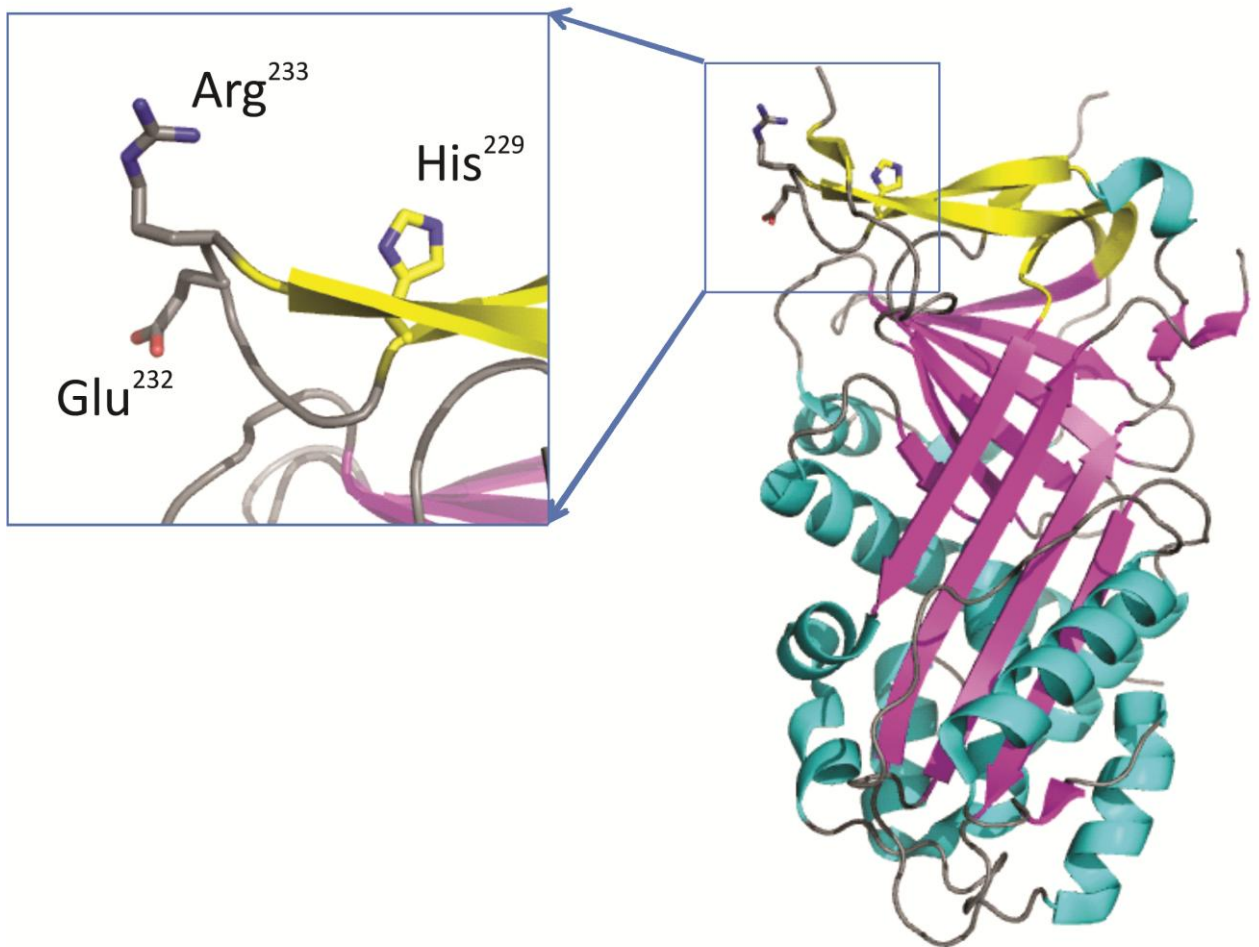
Another consideration is that the exosite interaction may exist distally from the catalytic site, as this is the case for tPA/PAI-I. It has been shown that the Glu residue at P4' and P5' of tPA enhance inhibition by PAI-I (Ibarra et al., 2004). In contrast, antitrypsin has a short α -helix structure at P7-P10 which forms an exosite interaction with trypsin (Dementiev et al., 2003). Based on the observations of the murine α_2 -antiplasmin structure, the RCL appears to be too short to form additional interactions outside of the P1-P1' (Law et al., 2008). However, these observations were made with mouse α_2 -antiplasmin and the RCL of human α_2 -antiplasmin may be different. Therefore, it is possible that additional contacts may be formed at the proximal or distal region of the RCL of α_2 -antiplasmin with surrounding regions of the catalytic site of plasmin.

In this chapter we have determined that His²²⁹ and Glu²³² have a minor role in the interaction with plasmin kringle domains. To further address the importance of His²²⁹ and Glu²³² in the interaction with plasmin, β -sheet C mutants in the absence of the C-terminal region should be studied to exclude the involvement of the C-terminus to the kringle domains. Additionally, binding studies with individual kringle (K1, K2, K3, K4 and K5) can be performed to

identify the specific kringle β-sheet C interacts with. Other conserved residues within β-sheet C may also be involved in this interaction and identifying additional amino acids or region is important in understanding its role in plasmin association. It is important to note that these residues were chosen based on the murine α₂-antiplasmin X-ray structure. This highlights the importance of obtaining the human α₂-antiplasmin X-ray structure as different residues may be exposed in the β-sheet C region compared to the mouse α₂-antiplasmin structure.

Figure 6.12. Structure of murine α_2 -antiplasmin highlighting His²²⁹, Glu²³² and Arg²³³ in the β -sheet C region. The three residues in the third and fourth strands of β -sheet C (yellow) is as indicated. β -sheets are in pink and α -helices are in cyan.

Figure 6.12.
**Structure of murine α_2 -antiplasmin highlighting His²²⁹, Glu²³²
and Arg²³³ in the β -sheet C region**



6.5 Conclusion

This chapter describes the expression and purification of recombinant mutant β -sheet C human α_2 -antiplasmin. Proteins produced were ~98% pure and functionally active. Plasmin binding affinity, but not plasmin inhibition rate and microplasmin binding, was affected by alanine substitution at position 229 and 232 of β -sheet C α_2 -antiplasmin mutants. It was determined that His²²⁹ and Glu²³² in the β -sheet C region of α_2 -antiplasmin is involved in plasmin interaction, presumably towards the kringle domains. Further studies with additional β -sheet C mutations are required to fully support this hypothesis.

Chapter 7:

Insights into the binding of different conformational forms of plasmin(ogen) to α_2 -antiplasmin

This page has been intentionally left blank.

7.1 Introduction

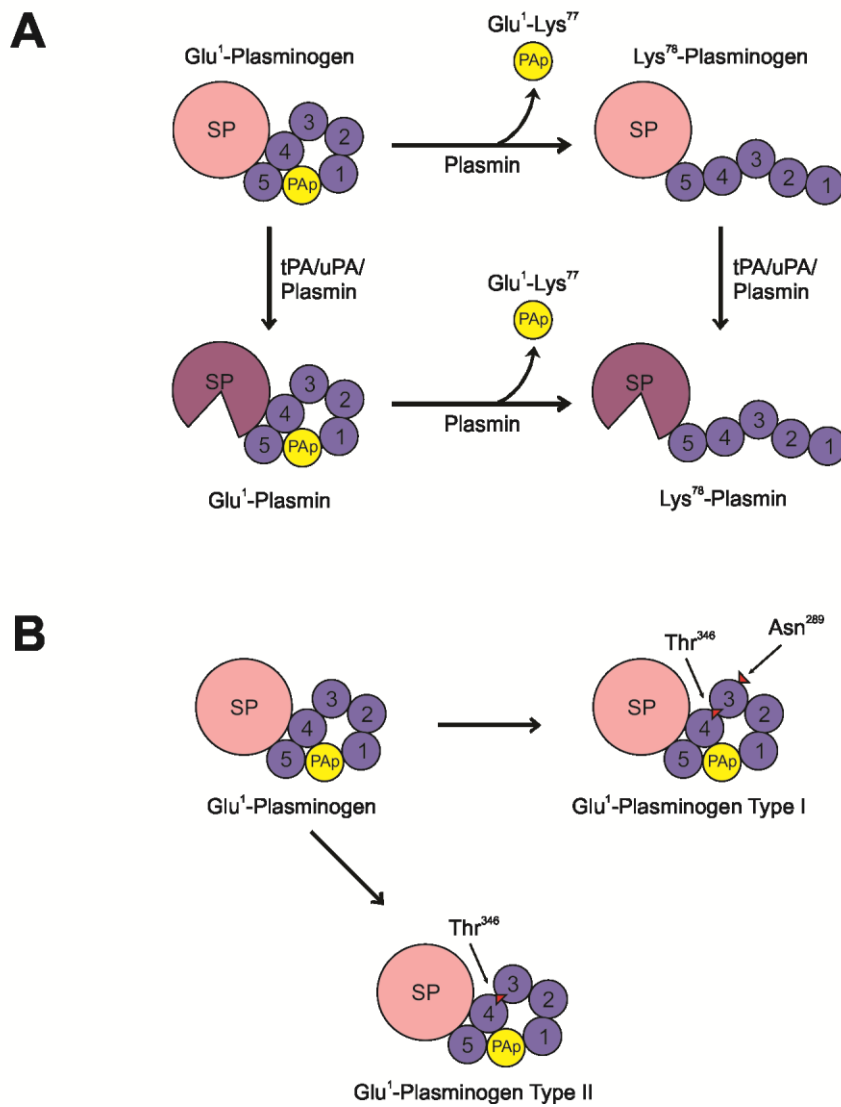
Native Glu-plasminogen exists as a 791 amino acid molecule containing a Pan-apple (PAP), five kringle domains (K1-5) and a serine protease domain (SP) (Law et al., 2012) (Figure 7.1A). In human circulation, Glu-plasminogen exists in two major glycoforms (Figure 7.1B) which can be separated based on their affinity for lysine sepharose. Glu-plasminogen Type I (30-40%) is glycosylated at Asn²⁸⁹ and Thr³⁴⁶, whereas Glu-plasminogen Type II (60-70%) is only glycosylated at Thr³⁴⁶ (Brockway and Castellino, 1972; Lijnen et al., 1981). Removal of the PAP domain (residues 1-77) at Lys⁷⁷-Lys⁷⁸ by the active enzyme plasmin, results in the conversion of Glu- to Lys-plasminogen (Markus, 1996; Peltz et al., 1982). Lys plasminogen is easily activated to plasmin by plasminogen activators because it has a more open conformation compared with its precursor, Glu-plasminogen. Ultimately, Lys-plasmin generation is required for efficient fibrin proteolysis during physiological conditions and thrombotic events (Xue et al., 2012).

The plasminogen molecule undergoes dramatic conformational change from Glu- to Lys-plasminogen and finally to plasmin (Marshall et al., 1994). The PAP domain has been shown to be important in maintaining the molecule in its closed conformation and removal of this region causes structural rearrangement of the molecule to a open conformation (Law et al., 2012; Marshall et al., 1994; Ponting et al., 1992). α_2 -antiplasmin, the main physiological inhibitor of plasmin has been shown to interact with the various forms of plasmin(ogen). A study by Lijnen and colleagues showed that α_2 -antiplasmin can recognise Lys-plasminogen Type I and Type II (Lijnen et al., 1981). A more recent study by Wang and colleagues used surface plasmon resonance to measure the affinities of wild-type α_2 -antiplasmin to plasminogen (mixture of both glycoforms) (Wang et al., 2006).

Continuing from Chapter 5, recombinant microplasmin (lacking the His-tag) was assessed with full-length (WT) and C-terminally truncated (CA) α_2 -antiplasmin to determine the rate of microplasmin inhibition. In this section, recombinant microplasmin(ogen) was abbreviated to μ PIg and uPIm. Prior to this work, there were no comprehensive studies investigating how different conformational forms of plasmin(ogen) influence the interaction with α_2 -antiplasmin. Therefore, this chapter presents a systematic study at measuring the binding affinities (K_D) of plasmin(ogen), namely Glu-plasminogen and its two glycoforms (GluPIg Type I and GluPIg Type II), Lys-plasminogen and microplasmin(ogen), with full-length (WT) and C-terminally truncated (CA) α_2 -antiplasmin using surface plasmon resonance (SPR). Furthermore, by exploring the interaction between plasmin(ogen) and α_2 -antiplasmin, a better understanding of which region(s) may be exposed and/or unavailable may be elucidated.

Figure 7.1. Schematic of the different conformations of plasmin(ogen). **A)** The preactivation peptide (PAP), kringle, serine protease (SP) and activated protease domain(s) are represented in yellow, purple, pink and maroon respectively. Plasmin cleaves Glu¹-plasminogen at Lys⁷⁷-Lys⁷⁸ to yield Lys⁷⁸-plasminogen. Tissue-type plasminogen activator (tPA) or urokinase (uPA) are required to activate plasminogen to active plasmin. **B)** Glu-plasminogen Type I is glycosylated at Asn²⁸⁹ and Thr³⁴⁶, whereas Glu-plasminogen Type II is only glycosylated at Thr³⁴⁶.

Figure 7.1.
Schematic of the different conformations of plasmin(ogen)



7.2 Methods

7.2.1 Kinetic Studies

7.2.1.1 Determining the Michaelis-Menten Constant

The Michaelis-Menten (K_M) for microplasmin (μPlm) with Ala-Phe-Lys-AMC (AMC) was determined by incubating 1nM μPlm with varying concentration of substrate (0-800 μM). To calculate the velocity for each reaction, linear regression analysis was performed on the plots of fluorescence units over time. The velocity of each reaction was plotted against substrate concentration and non-linear regression analysis was performed using the Michaelis-Menten equation on Graphpad Prism version 5.0 software. Data are mean of three experiments \pm SE (Figure 7.2). The final K_M value was determined to be 125 μM and this value was used in Equation 4.2 for the determination of the plasmin inhibition rates between μPlm and α_2 -antiplasmin.

7.2.1.2 Stoichiometry of Inhibition

Methods are as described in section 4.2.2. Briefly, 1nM of μPlm was incubated with recombinant WT and C Δ human α_2 -antiplasmin at various concentrations (0.2-1.5nM) for 1hr at 37°C. Residual plasmin activity was measured in the presence of 200 μM (final concentration) fluorogenic AMC substrate. Fluorescence signal was detected at 355/460 nm for 20 min, and the resulting plots were analysed using linear regression analysis. The value was plotted against serpin:protease ratio, and the points were analysed using linear regression and the line was extrapolated to the x-intercept. All experiments were performed in triplicates.

7.2.1.3 Rates of Inhibition – Continuous Assay

Methods were as described in section 4.2.3.1. Briefly, 0.5nM recombinant μPlm was reacted with various concentrations of recombinant WT and C Δ α_2 -antiplasmin (1-40nM), in the presence of 1mM (final concentration) of fluorogenic AMC substrate. The raw data was fitted to Equation 4.1 to determine the k_{obs} for each antiplasmin concentration. Linear regression analysis was performed to obtain the uncorrected rate of inhibition, k' , which was then corrected using Equation 4.2 to give the second order rate constant, k_a .

7.2.1.4 Rates of Inhibition – Discontinuous Assay

Methods were as described in section 4.2.3.2. Briefly, 5-10 nM of recombinant α_2 -antiplasmin (WT and C Δ) and 0.5 nM μ Plm were incubated at different time points (0-5 min). Residual protease activity was determined in the presence of 200 μ M fluorogenic AMC substrate. Fluorescence emission was monitored at 355/460 nm for 20 min.

7.2.2 Binding Studies

7.2.2.1 Preparation of Active Site-Blocked Microplasmin

Active site-blocked microplasmin (μ PlmCMK) was produced by incubating recombinant μ Plm with a 1000-fold molar excess of D-Val-Phe-Lys chloromethyl ketone (CMK) at 37°C for 1hr. Active site-blocked μ Plm was then dialysed overnight at 4°C in Running buffer (0.01M HEPES pH 7.4, 0.15M NaCl, 50 μ M EDTA and 0.05% surfactant P20). To confirm that the active site was completely blocked, the activity of μ PlmCMK was checked against active μ Plm in the presence of 200 μ M AMC substrate.

7.2.2.2 Surface Plasmon Resonance to Measure Binding Affinity

The interactions between plasmin(ogen) variants and recombinant α_2 -antiplasmin (WT and C Δ) were determined via surface plasmon resonance (SPR) using the BIAcore T100 system (which was upgraded to T200 in 2012). (GE Healthcare). The plasmin(ogen) variants used are as follows: Glu-plasminogen (GluPIg – Hematologic Technologies); Lys-plasminogen (LysPIg – Hematologic Technologies); Glu-plasminogen glycoform I (GluPIg Type I); Glu-plasminogen glycoform II (GluPIg Type II); microplasminogen (μ PIg WT); microplasmin (μ Plm WT); active site-blocked microplasmin (μ PlmCMK); plasmin (Plm – Hematologic Technologies). GluPIg Type I and II were purified and supplied by our collaborators (Dr Ruby Law and Mr Adam Quek).

The protocol to measure binding affinities was as described in section 4.2.4.2. Briefly, α_2 -antiplasmin (WT or C Δ) were immobilised on the NTA chop. Six different concentration of plasmin(ogen) variants (0-1200 nM) were injected for 1 min of association time, followed by 10 min of dissociation time. The NTA surface was regenerated at each concentration cycle. To obtain the binding affinity (K_D), the association and dissociation rate constants were fitted to Equation 4.4.

Figure 7.2. Determination of the K_M for μ Plm and AMC. 1nM of recombinant human μ Plm was incubated with varying concentration of fluorogenic substrate AMC (0-800 μ M). The reaction was allowed to proceed for 1 hr. The velocity of each reaction was calculated by linear regression analysis on the plots of fluorescence over time. The velocity was then plotted against substrate concentration and non-linear regression analysis using the Michaelis-Menten equation was performed. Plots are the average of three experiments \pm SEM. The value for K_M was calculated as $125 \pm 6 \mu$ M.

Figure 7.2.
Determination of the K_M for μ PII_m and AMC

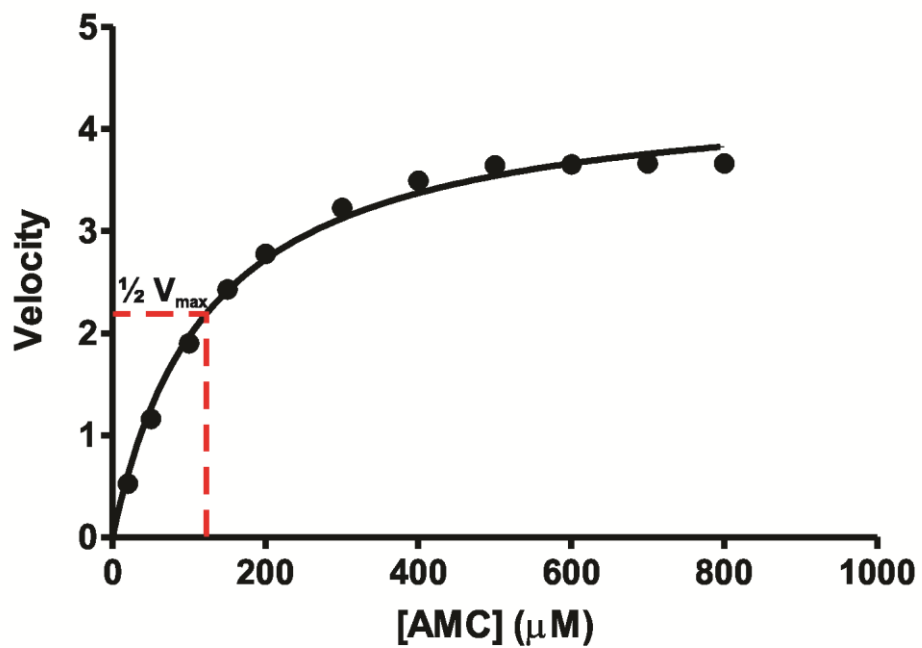


Table 7.1. Stoichiometry of inhibition (*SI*) and microplasmin inhibition rate (*k_a*) measured by continuous and discontinuous assays with WT and CΔ α₂-antiplasmin. Results of CΔ + Plm are from Chapter 4.

Recombinant Proteins	<i>SI</i> ±SE (n=3)	Continuous: <i>k_a</i> ± SE (M⁻¹s⁻¹)	Discontinuous: <i>k_a</i> ± SE (M⁻¹s⁻¹)
CΔ + Plm	1.5 ± 0.02	9.22 ± 0.24 × 10 ⁵	3.80 ± 0.08 × 10 ⁵
WT + μPlm WT	1.0 ± 0.02	1.08 ± 0.13 × 10 ⁶	4.03 ± 0.29 × 10 ⁵
CΔ + μPlm WT	1.2 ± 0.01	9.70 ± 0.79 × 10 ⁵	4.33 ± 0.29 × 10 ⁵

7.3 Results

7.3.1 Kinetic Analysis of Recombinant Microplasmin

To ensure that the removal of all five kringle domains of plasmin had not affected the functional domain and inhibition mechanism, the stoichiometry of inhibition (SI) and rate of inhibition (k_a) between recombinant microplasmin (μPlm) and α_2 -antiplasmin were determined. Table 7.1 is a summary of SI and k_a values obtained for α_2 -antiplasmin and μPlm .

SI between recombinant α_2 -antiplasmin and microplasmin

Figure 7.3A shows the reaction between WT α_2 -antiplasmin and μPlm which resulted in an SI value of 1.0. When $C\Delta$ was measured with μPlm , the SI was 1.2 (Figure 7.3B). This informs that the protease domain of μPlm was correctly folded and still reacted in a 1:1 ratio with its main inhibitor, α_2 -antiplasmin.

k_a between recombinant α_2 -antiplasmin and microplasmin – continuous method

Further kinetic characterisation of recombinant μPlm was performed by measuring inhibition rates (k_a) using the continuous method. The rate of microplasmin inhibition by WT α_2 -antiplasmin was determined to be $1.1 \times 10^6 \text{ M}^{-1}\text{s}^{-1}$ (Figures 7.4A & B). When $C\Delta$ α_2 -antiplasmin was reacted with μPlm , the inhibition rate was $9.7 \times 10^5 \text{ M}^{-1}\text{s}^{-1}$. Both values obtained are similar to the results obtained for $C\Delta$ and intact plasmin ($k_a = 9.2 \times 10^5 \text{ M}^{-1}\text{s}^{-1}$) (Figure 7.6) which is expected because in the absence of the kringle domain, the C-terminus of α_2 -antiplasmin is unable to accelerate the interaction.

k_a between recombinant α_2 -antiplasmin and microplasmin – discontinuous method

Analysis of the inhibition rate of recombinant μPlm WT with WT α_2 -antiplasmin (Figure 7.5A & B) and $C\Delta$ (Figure 7.5C & D) using the discontinuous assay revealed that the k_a was $4.03 \times 10^5 \text{ M}^{-1}\text{s}^{-1}$ and $4.33 \times 10^5 \text{ M}^{-1}\text{s}^{-1}$ respectively (Table 7.1). The values obtained are similar to C-terminally truncated α_2 -antiplasmin with intact plasmin measured with the same method ($k_a = 3.8 \times 10^5 \text{ M}^{-1}\text{s}^{-1}$) (Figure 7.6).

Figure 7.3. Stoichiometry of inhibition of human α_2 -antiplasmin with microplasmin. A constant μ Plm concentration was incubated with varying amount of recombinant α_2 -antiplasmin at the indicated serpin:protease ratio. Once the reaction was completed, residual protease activity was assayed. The *SI* was obtained by extrapolating to where protease activity equals zero. **A)** *SI* of WT α_2 -antiplasmin with μ Plm. **B)** *SI* of C Δ α_2 -antiplasmin with μ Plm.

Figure 7.3.
**Stoichiometry of inhibition of human α_2 -antiplasmin
with microplasmin**

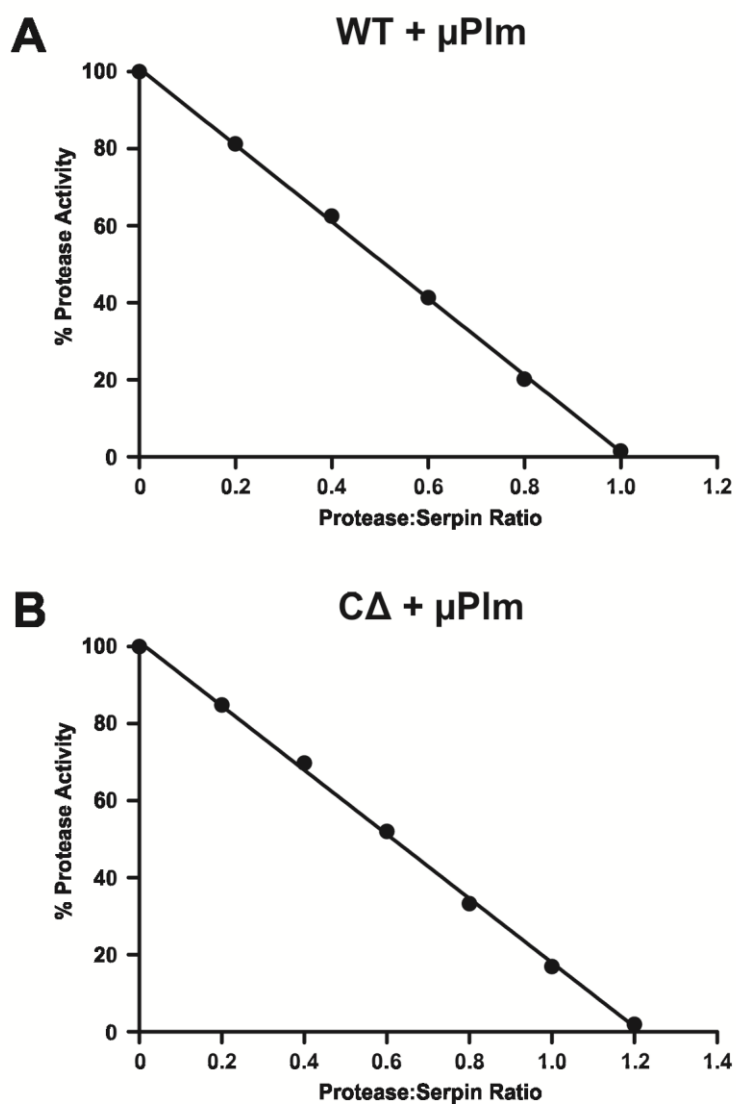


Figure 7.4. Microplasmin inhibition rate by wild-type and C-terminally truncated human α_2 -antiplasmin. Progress curves of the interaction between recombinant human μ Plm and α_2 -antiplasmin measured in fluorescence units. Black lines represent raw curves. Red line represents control protease only. Each curve was analysed and fitted (orange lines) using non-linear regression using Equation 4.1 to determine the k_{obs} at each serpin concentration. k_{obs} were plotted against α_2 -antiplasmin concentration and linear regression analysis was used to determine the k' . The plasmin inhibition rate (k_a) was determined by factoring in the Michaelis Menton (K_M), substrate concentration [S] and the S/I as described using Equation 4.2. **A&B)** Progress curves and k_a of WT α_2 -antiplasmin with μ Plm. **C&D)** Progress curves and k_a of C Δ α_2 -antiplasmin with μ Plm.

Figure 7.4.
Microplasmin inhibition rate by wild-type and C-terminally truncated human α_2 -antiplasmin

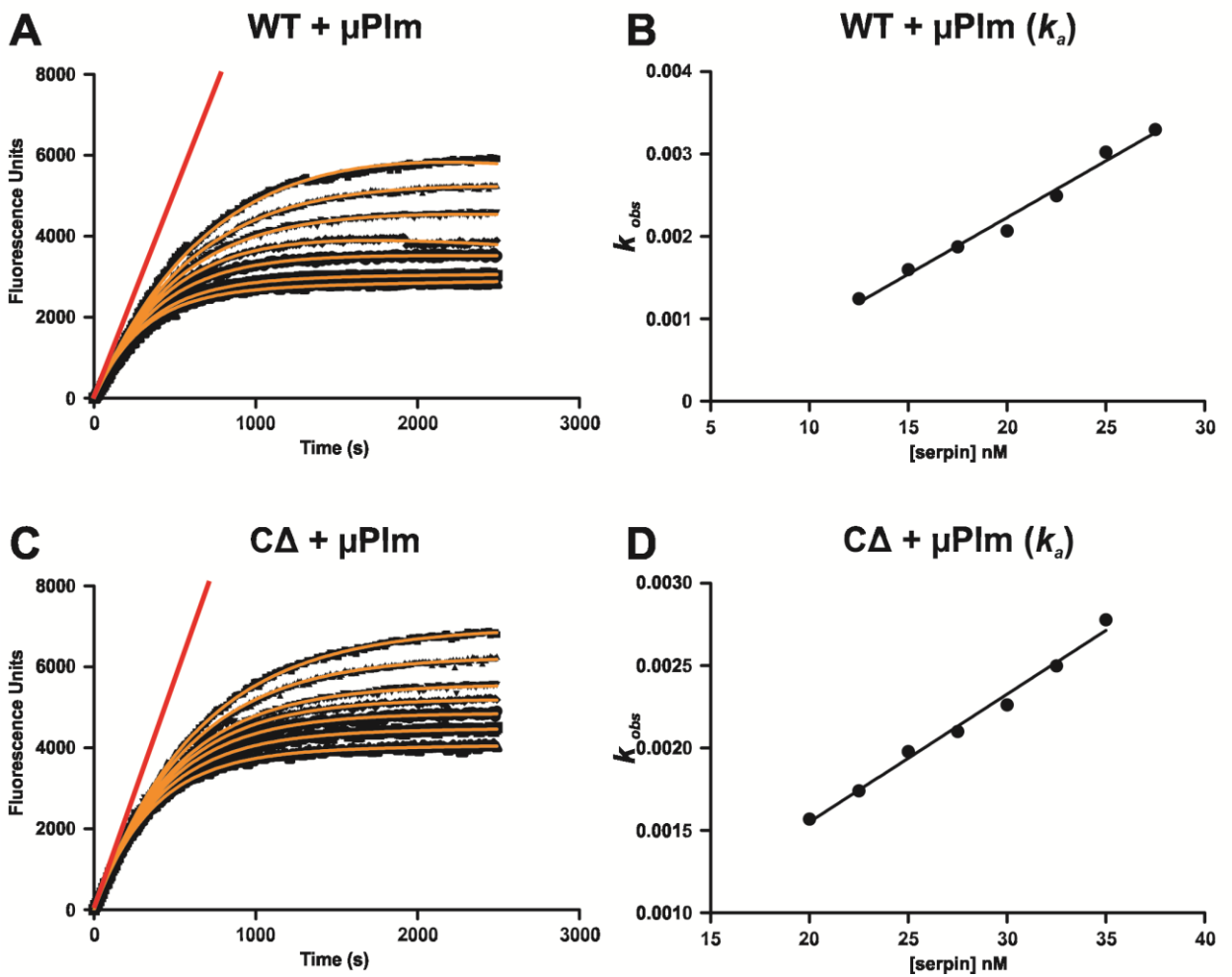


Figure 7.5. Microplasmin inhibition rate of recombinant human α_2 -antiplasmin determined by discontinuous method. Semilog plots in panels A, and C are of residual μ Plm activity versus time for reactions at varying concentration of recombinant α_2 -antiplasmin. Section 4.2.3.2 describes how the k_a for μ Plm and α_2 -antiplasmin variants were measured. **A&B)** Semilog plots and k_a of WT α_2 -antiplasmin with μ Plm. **C&D)** Semilog plots and k_a of C Δ α_2 -antiplasmin with μ Plm.

Figure 7.5.
Microplasmin inhibition rate of recombinant human α_2 -antiplasmin determined by discontinuous method

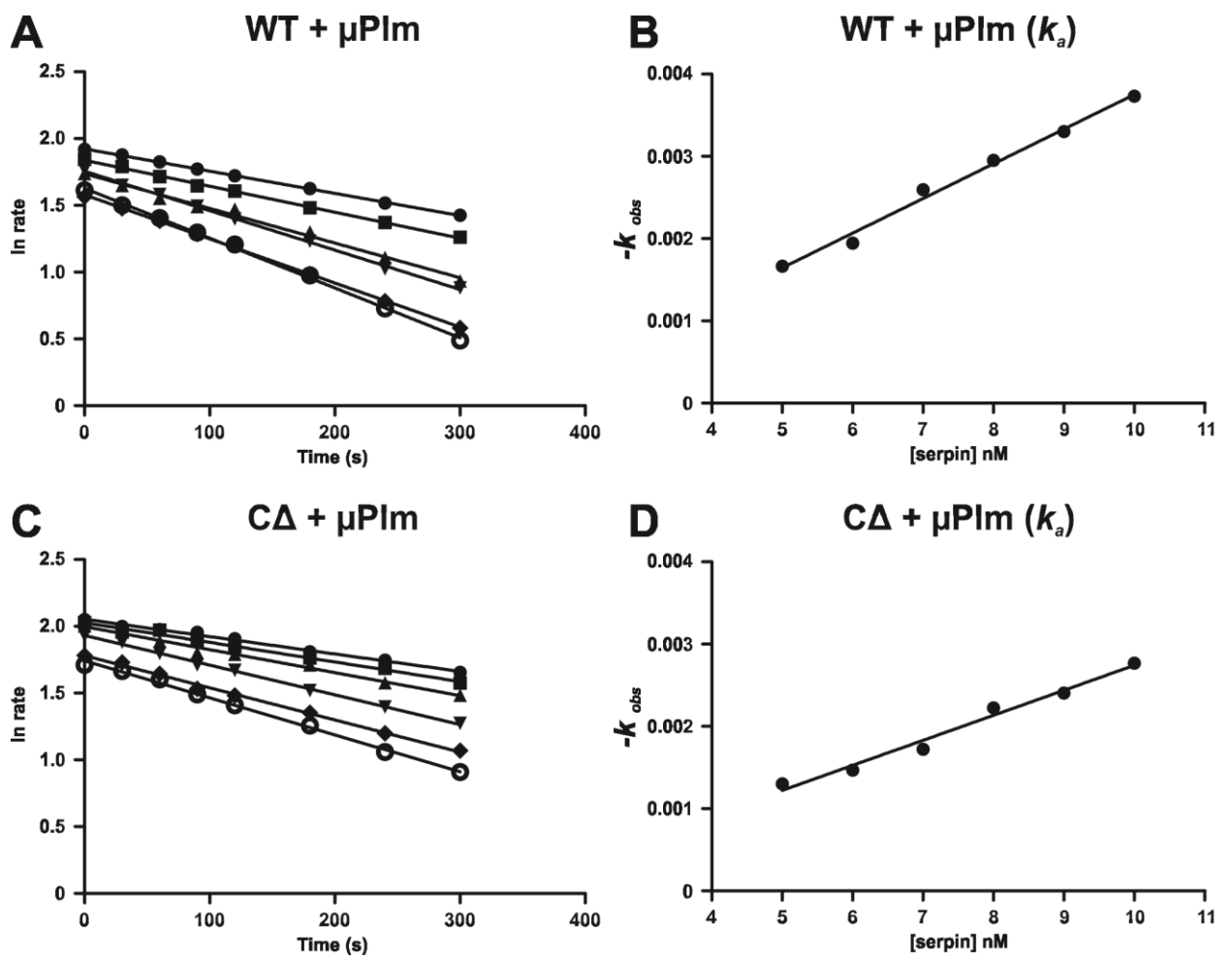
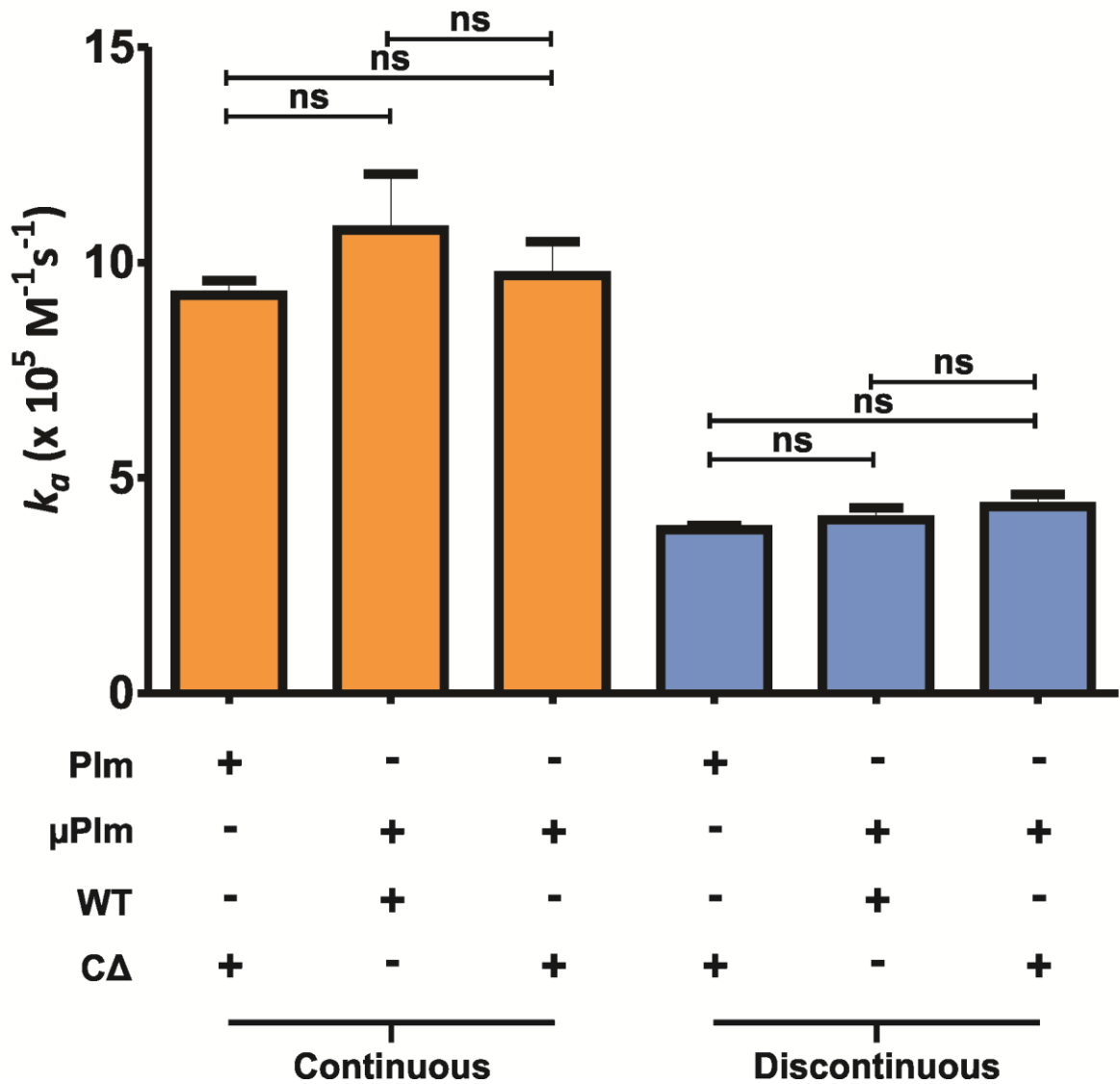


Figure 7.6. Comparison of the microplasmin inhibition rate between wild-type and C-terminally truncated α_2 -antiplasmin. Continuous and discontinuous methods are represented by orange and blue bars respectively. The k_a for μ PII and α_2 -antiplasmin variants were measured as described in Section 4.2.3.1 and 4.2.3.2. Statistics were assessed by one-way ANOVA with Newman-Keuls post-hoc correction. “ns” refers to non-statistically significant data ($p>0.05$). Each of data point represents the mean ($n=3$) with error bars representing \pm SE.

Figure 7.6.
Comparison of the microplasmin inhibition rate
between wild-type and C-terminally truncated
 α_2 -antiplasmin



7.3.2 Plasminogen Binding to α_2 -antiplasmin

In this section, the binding affinity for Glu-plasminogen (GluPIg), Lys-plasminogen (LysPIg), GluPIg Type I and GluPIg Type II were determined with WT or C Δ α_2 -antiplasmin using SPR as described in Chapter 4. GluPIg and LysPIg used were commercially prepared from Hematologic Technologies. Whereas GluPIg Type I and Type II were purified by our collaborators at the Department of Biochemistry, Monash University. Table 7.2 is the summary all binding data obtained with plasminogen variants. Residual plasmin activity of GluPIg, GluPIg Type I, GluPIg Type II and LysPIg were analysed with AMC fluoregenic substrate and compared with active plasmin. Fluorescence emission was not detected with all plasminogen preparations which indicated that there was no residual plasmin present in those purified samples (results not shown).

GluPIg binding to α_2 -antiplasmin

Figure 7.7A shows the sensorgram for the interaction between GluPIg and WT α_2 -antiplasmin. The K_D of WT α_2 -antiplasmin for GluPIg was determined to be 31nM. When GluPIg was measured with α_2 -antiplasmin lacking the C-terminus (C Δ) (Figure 7.7B), there was a slight reduction in binding affinity ($K_D = 48$ nM). However this decrease is not significant when both data were compared with the other (Figure 7.11). Association and dissociation constants (k_{a1} , k_{a2} , k_{d1} , k_{d2}) obtained from SPR remained unchanged when GluPIg was measured with WT or C Δ α_2 -antiplasmin (Table 7.2). It was surprising that the affinity of α_2 -antiplasmin for GluPIg was high at approximately ~30nM with the assumption that the active site cleft and kringle domains were unavailable. Therefore this suggests that interaction seen with α_2 -antiplasmin and GluPIg may be occurring via an exosite region which is exposed in the precursor plasminogen form. As mentioned in Chapter 4, each experiment was conducted with a blank flow cell and the test flow cell was subtracted with the control flow cell to produce the sensorgrams presented in this thesis. The baseline on the blank flow cell remained constant during the injection of GluPIg indicating that non-specific binding of the analyte to the chip surface was not observed (results not shown). This showed that the binding event observed was mediated through the interaction of GluPIg to α_2 -antiplasmin.

GluPIg Type I and Type II binding to α_2 -antiplasmin

As previously described, GluPIg exist in two glycoforms which are Type I and Type II. These two glycoforms were also analysed to determine if there was a difference in binding affinity for α_2 -antiplasmin. Figures 7.8A and B are sensorgrams for the analysis of GluPIg Type I with WT and C Δ α_2 -antiplasmin. The binding affinity for GluPIg Type I with WT and C Δ was determined to be 15nM and 14nM respectively. Association and dissociation constants (k_{a1} , k_{a2} ,

k_{d1} , k_{d2}) obtained from SPR remained unchanged when GluPlg Type I was measured with WT or C Δ α_2 -antiplasmin (Table 7.2).

Figures 7.9A and B are sensorgrams for the analysis of GluPlg Type II with WT and C Δ α_2 -antiplasmin. The binding affinity for GluPlg Type II was 52nM with WT α_2 -antiplasmin and decreased slightly to 68nM with C Δ . This change was not significant when both data sets were compared with each other (Figure 7.11). There was a ~2-fold decrease in association rate constant (k_{a1}) when the binding of GluPlg Type II and WT α_2 -antiplasmin was compared with GluPlg Type II and C Δ .

Affinities for Type I and Type II in the absence or presence of the C-terminal region of α_2 -antiplasmin were significantly different (Figure 7.11). This data informs that GluPlg Type I binds stronger to α_2 -antiplasmin by approximately 4-fold in comparison with GluPlg Type II. This also corresponds with the data obtained with GluPlg where the affinity is intermediate to Type I and Type II, which is as expected because GluPlg contains a mixture of both Type I and Type II.

LysPlg binding to α_2 -antiplasmin

LysPlg, the plasminogen molecule lacking the PAP domain, was analysed to determine if there was a difference in binding affinity for α_2 -antiplasmin when compared to GluPlg, the precursor form. The sensorgrams for LysPlg analysed with WT and C Δ α_2 -antiplasmin is seen in Figure 7.10A and B. Binding affinity of WT and C Δ for LysPlg was determined to be 7.8nM and 152nM respectively. In the absence of the C-terminus, the binding affinity to LysPlg is significantly decreased by ~20-fold when compared to WT α_2 -antiplasmin. The association constant (k_{a1}) was also reduced by ~22-fold when LysPlg and WT was compared to LysPlg and C Δ .

WT α_2 -antiplasmin had a ~4-fold increase in affinity for LysPlg when compared to GluPlg. In addition, the association rate constant (k_{a1}) increased by ~33-fold when the binding of WT α_2 -antiplasmin to LysPlg was compared with GluPlg. However in the absence of the C-terminus of α_2 -antiplasmin (C Δ), there was a ~3-fold decrease in affinity for LysPlg in comparison to GluPlg. This informs that the C-terminus plays a greater role in accelerating plasminogen/ α_2 -antiplasmin interaction in LysPlg than for GluPlg. This suggests that the kringles in LysPlg are more accessible and buried in GluPlg which further supports the concept that LysPlg is in a more open conformation.

Figure 7.7. Sensorgrams of the binding of recombinant α_2 -antiplasmin to GluPIg as measured by SPR. Recombinant α_2 -antiplasmin (20nM) was immobilised on a NTA chip. The binding of various concentrations of GluPIg to α_2 -antiplasmin was monitored in real time. Blue lines are raw curves and fitted curves are in black. **A)** Binding of GluPIg (20-200nM) to WT ($\chi^2 = 0.32$). **B)** Binding of GluPIg (50-500nM) to C Δ α_2 -antiplasmin ($\chi^2 = 0.32$).

Figure 7.7.
Sensorgrams of the binding of recombinant α_2 -antiplasmin to GluPIg as measured by SPR

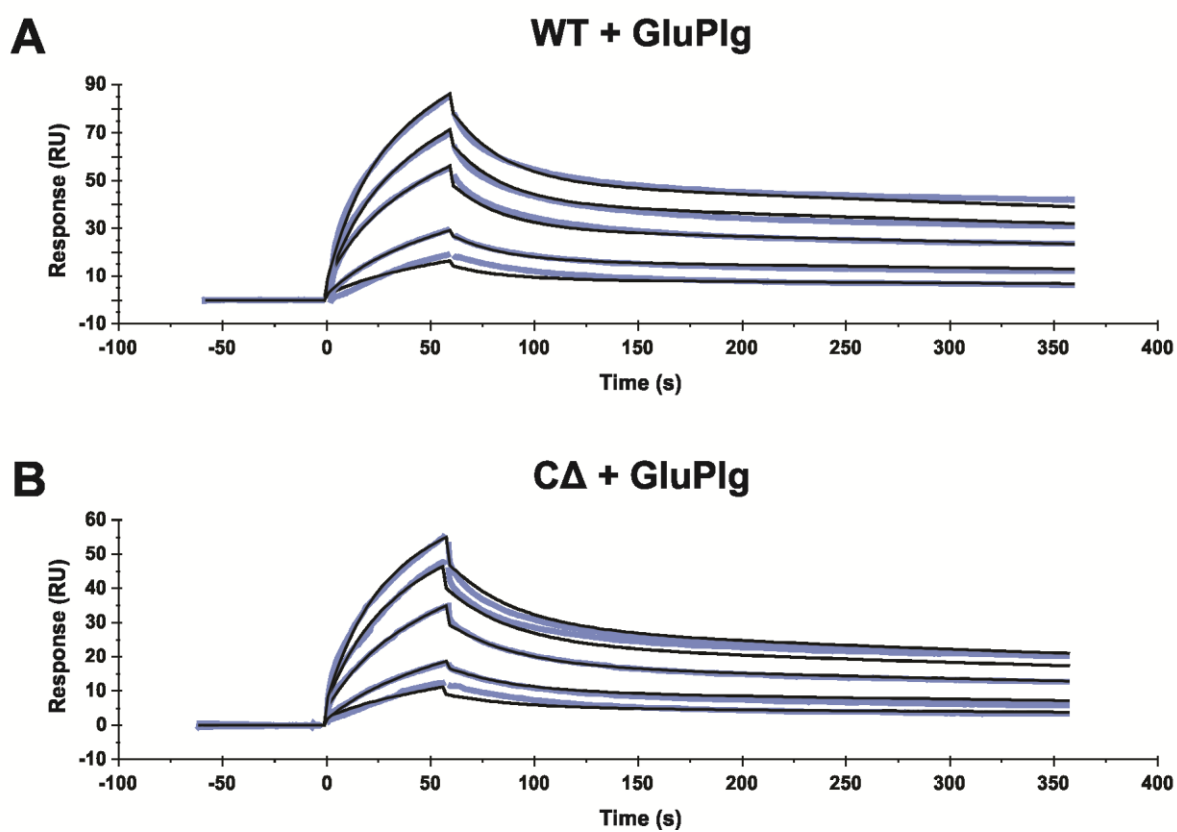


Figure 7.8. Sensorgrams of the binding of recombinant α_2 -antiplasmin to GluPIg Type I as measured by SPR. Recombinant α_2 -antiplasmin (20nM) was immobilised on a NTA chip. The binding of various concentrations of GluPIg Type I to α_2 -antiplasmin was monitored in real time. Blue lines are raw curves and fitted curves are in black. **A)** Binding of GluPIg Type I (50-400nM) to WT ($\chi^2 = 2.99$). **B)** Binding of GluPIg Type I (60-300nM) to C Δ ($\chi^2 = 0.56$).

Figure 7.8.
Sensorgrams of the binding of recombinant α_2 -antiplasmin to GluPIg Type I as measured by SPR

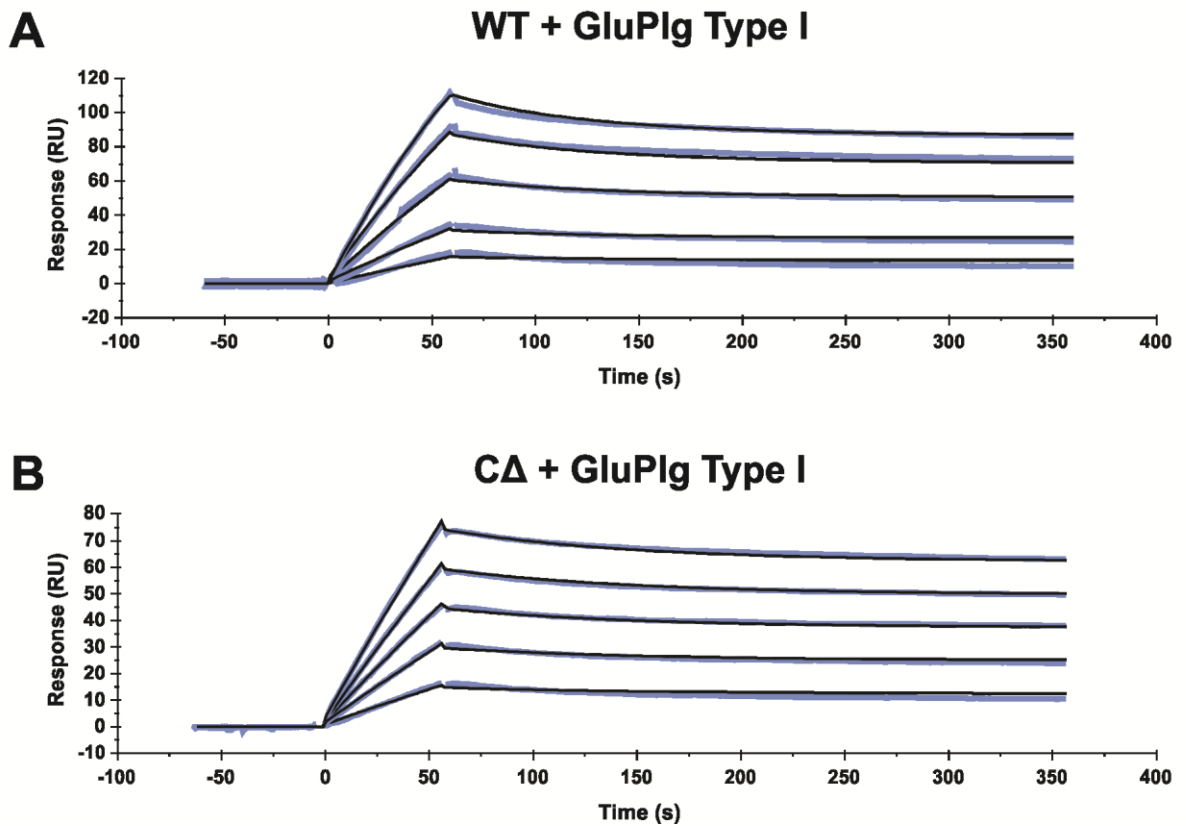


Figure 7.9. Sensorgrams of the binding of recombinant α_2 -antiplasmin to GluPIg Type II as measured by SPR. Recombinant α_2 -antiplasmin (20nM) was immobilised on a NTA chip. The binding of various concentrations of GluPIg Type II to α_2 -antiplasmin was monitored in real time. Blue lines are raw curves and fitted curves are in black. **A)** Binding of GluPIg Type II (100-500nM) to WT ($\chi^2 = 0.53$). **B)** Binding of GluPIg Type II (200-1200nM) to C Δ ($\chi^2 = 0.59$).

Figure 7.9.
Sensorgrams of the binding of recombinant α_2 -antiplasmin to GluPIg Type II as measured by SPR

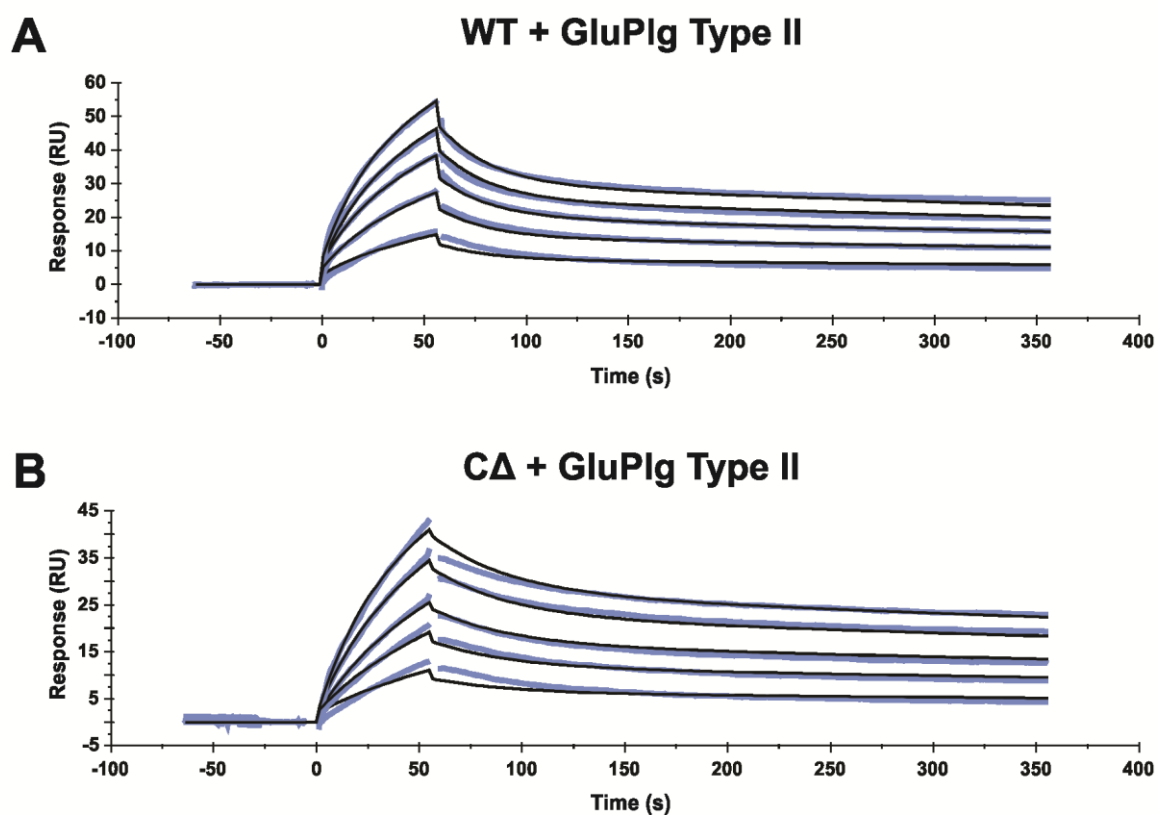


Figure 7.10. Sensorgrams of the binding of recombinant α_2 -antiplasmin to LysPIg as measured by SPR. Recombinant α_2 -antiplasmin (20nM) was immobilised on a NTA chip. The binding of various concentrations of LysPIg to α_2 -antiplasmin was monitored in real time. Blue lines are raw curves and fitted curves are in black. **A)** Binding of LysPIg (10-50nM) to WT ($\chi^2 = 0.87$). **B)** Binding of LysPIg (50-250nM) to C Δ ($\chi^2 = 1.09$).

Figure 7.10.
Sensorgrams of the binding of recombinant α_2 -antiplasmin to LysPIg as measured by SPR

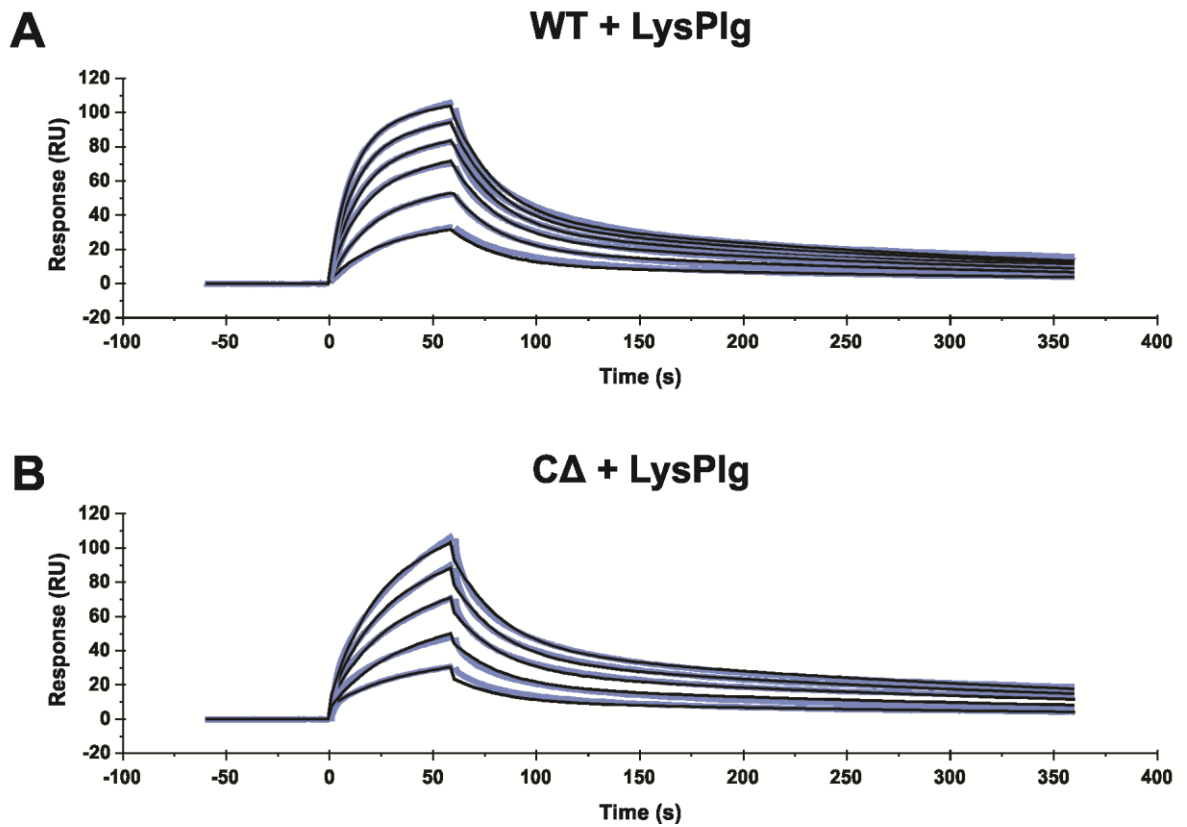


Figure 7.11. Comparison of the K_D between WT and CΔ α_2 -antiplasmin for plasminogen variants. The K_D for plasminogen and α_2 -antiplasmin variants were measured as described in Section 4.2.4. Statistics were assessed by one-way ANOVA with Newman-Keuls post-hoc correction. “*” refers to statistically significant data with a p-value of $p < 0.05$. “ns” refers to non-statistically significant data ($p > 0.05$). Each of the data point represents the mean ($n=3$) with error bars representing \pm SE.

Figure 7.11.
Comparison of the K_D between WT and C Δ
 α_2 -antiplasmin for plasminogen variants

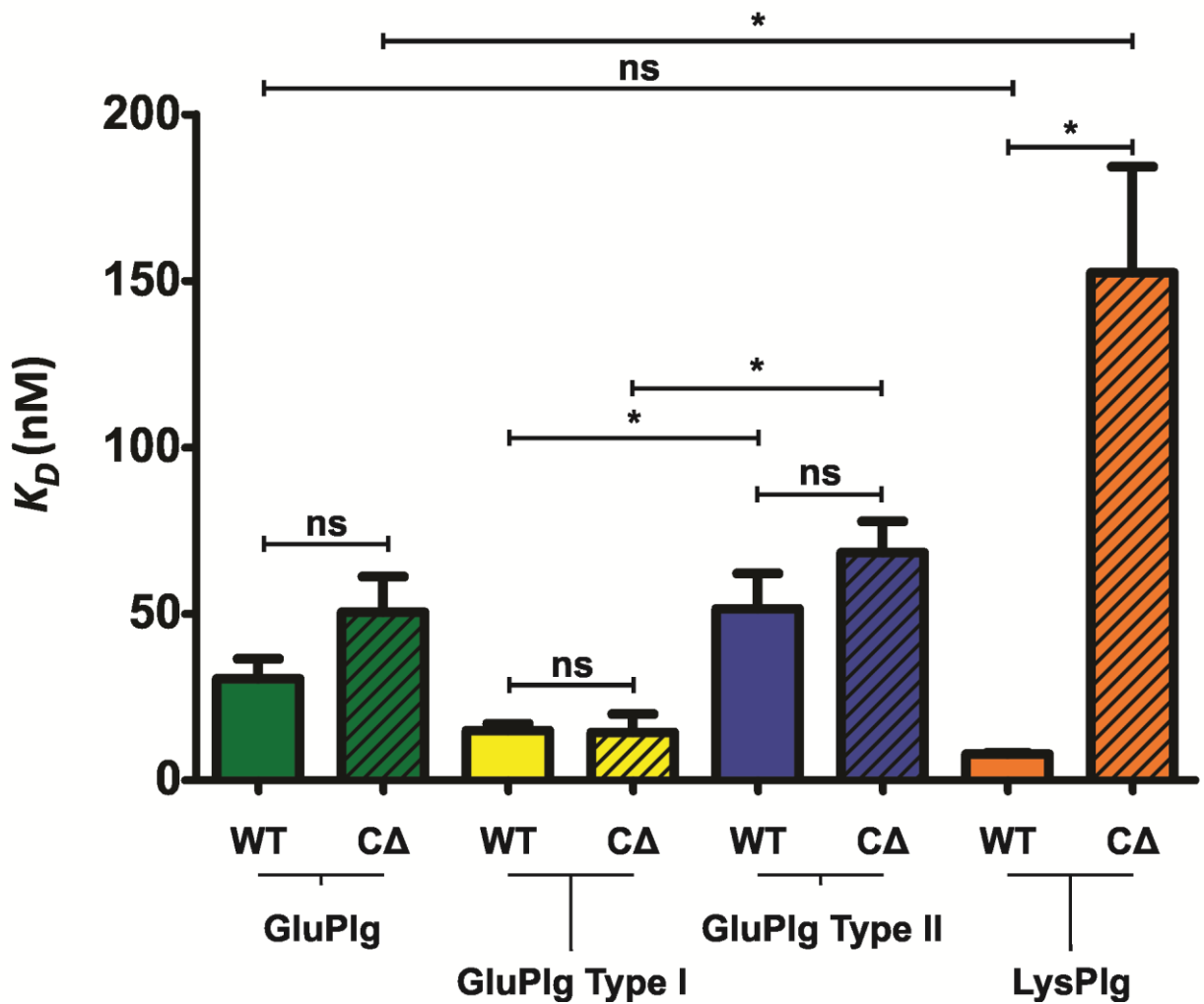


Table 7.2. Mean binding affinity, association and dissociation constants of plasmin(ogen) variants with WT or CΔ α_2 -antiplasmin as measured by SPR (n=3-6). Results of PlmCMK have been presented in Chapter 4. μ PlmCMK + WT was presented in Chapter 6.

Plasmin(ogen)	α_2 -antiplasmin	$K_D \pm SE$ (nM)	k_{a1} ($M^{-1}s^{-1}$)	k_{d1} (1/s)	k_{a2} (1/s)	k_{d2} (1/s)
GluPlg	WT	31 \pm 6.1	5.4 $\times 10^4$	0.03	0.01	0.001
	CΔ	48 \pm 7.9	7.0 $\times 10^4$	0.03	0.01	0.001
GluPlg Type I	WT	15 \pm 2.1	3.5 $\times 10^4$	0.03	0.01	0.0001
	CΔ	14 \pm 5.6	3.9 $\times 10^4$	0.06	0.01	0.0001
GluPlg Type II	WT	52 \pm 11	3.4 $\times 10^4$	0.02	0.01	0.001
	CΔ	68 \pm 9.5	1.8 $\times 10^4$	0.02	0.01	0.001
LysPlg	WT	7.8 \pm 0.4	1.8 $\times 10^6$	0.04	0.01	0.004
	CΔ	152 \pm 32	7.9 $\times 10^4$	0.04	0.01	0.004
Plm	WT	5.6 \pm 4.1 $\times 10^{-6}$	3.5 $\times 10^7$	4.5 $\times 10^{-6}$	0.02	0.001
	CΔ	0.4 \pm 0.03	2.6 $\times 10^6$	0.02	0.01	0.001
PlmCMK	WT	1.6 \pm 0.1	2.1 $\times 10^7$	0.09	0.01	0.005
	CΔ	49 \pm 1.7	1.1 $\times 10^7$	0.02	0.01	0.003
μ Plg	WT	1381 \pm 118	1.4 $\times 10^3$	0.02	0.001	0.002
	CΔ	1443 \pm 165	1.5 $\times 10^3$	0.02	0.001	0.002
μ PlmCMK	WT	105 \pm 12	2.9 $\times 10^4$	0.01	0.01	0.003
	CΔ	160 \pm 63	2.8 $\times 10^4$	0.01	0.01	0.003
μ Plm	WT	7.0 \pm 5.0 $\times 10^{-4}$	2.1 $\times 10^6$	0.004	0.02	1.0 $\times 10^{-5}$
	CΔ	1.0 \pm 0.6 $\times 10^{-3}$	1.6 $\times 10^6$	0.02	0.02	2.0 $\times 10^{-6}$

7.3.3 Plasmin Binding to α_2 -antiplasmin

In Chapter 4, active site-blocked plasmin (PlmCMK) was used to prevent the formation of the covalent α_2 -antiplasmin/plasmin complex. The binding of WT to PlmCMK was determined to be 1.6nM, whereas the binding of C Δ to PlmCMK was 50nM. In this section, the binding affinity of α_2 -antiplasmin to active plasmin (Plm) was described. As seen in the sensorgram of WT α_2 -antiplasmin with Plm (Figure 7.12A), no dissociation phase was seen as the stable α_2 -antiplasmin/plasmin covalent complex has formed. In contrast, slight dissociation is seen in C Δ with Plm until the complex stabilises ~1 min after the association phase (Figure 7.12B). From analysis of the sensorgrams, it was determined that WT and C Δ binding to Plm has a K_D value of 5.6×10^{-6} nM and 0.4nM respectively. In circulation, α_2 -antiplasmin forms an irreversible complex with plasmin. Therefore it is expected that tight binding was obtained when native Plm was analysed with WT α_2 -antiplasmin. Binding of α_2 -antiplasmin to plasmin was significantly improved when the active site of plasmin was accessible (Figure 7.13). All binding affinity values, association rate constants and dissociation rates are shown in Table 7.2.

As expected, the binding affinity of plasmin to α_2 -antiplasmin was the highest when compared to Glu- and Lys-plasminogen (Table 7.2). This was expected because plasminogen, the zymogen form, is catalytically inactive. Activation with plasminogen activators exposes the active site of plasmin which in turn increases interaction points for α_2 -antiplasmin.

Figure 7.12. Sensorgrams of the binding of WT and CΔ α_2 -antiplasmin to Plm as measured by SPR. Recombinant α_2 -antiplasmin (20nM) was immobilised on a NTA chip. The binding of various concentrations of active Plm to α_2 -antiplasmin was monitored in real time. Blue lines are raw curves and fitted curves are in black. **A)** Binding of Plm (1-4nM) to WT ($\chi^2 = 1.39$). **B)** Binding of Plm (4-20nM) to CΔ ($\chi^2 = 0.90$).

Figure 7.12.
Sensorgrams of the binding of WT and C Δ
 α_2 -antiplasmin to Plm as measured by SPR

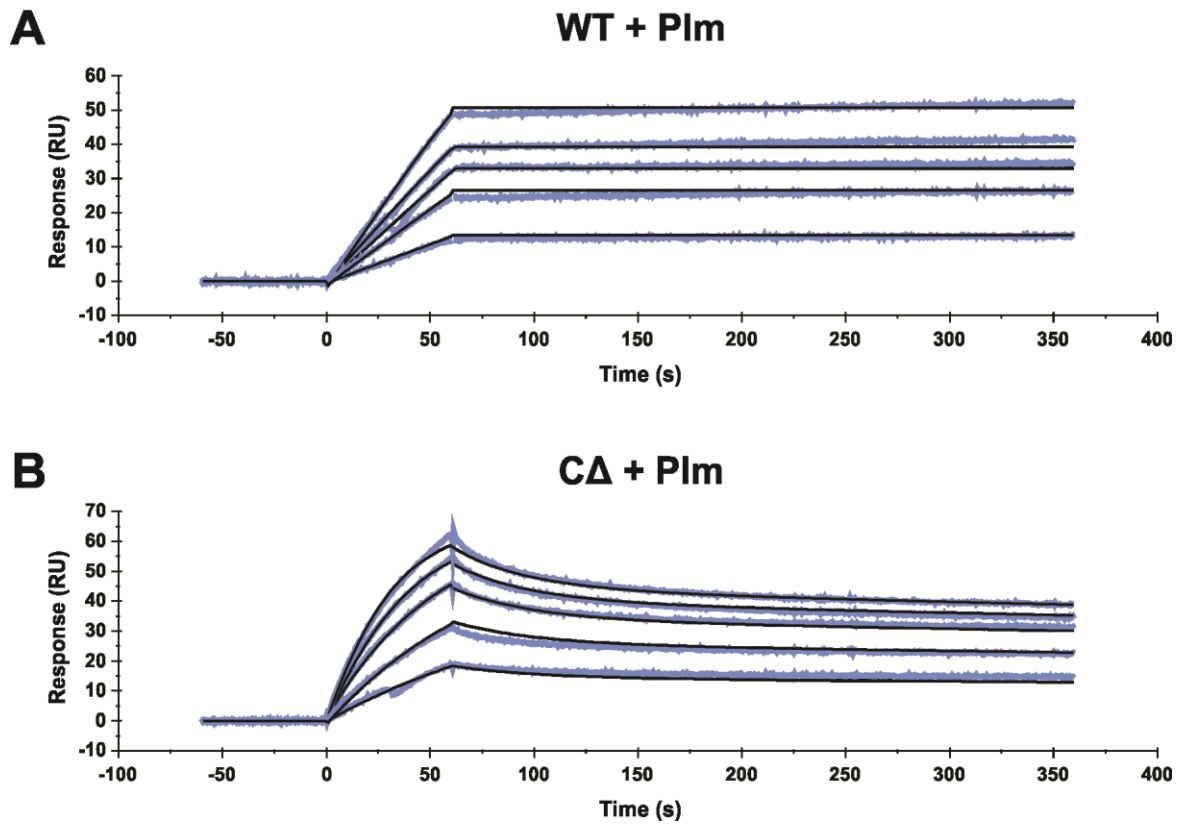
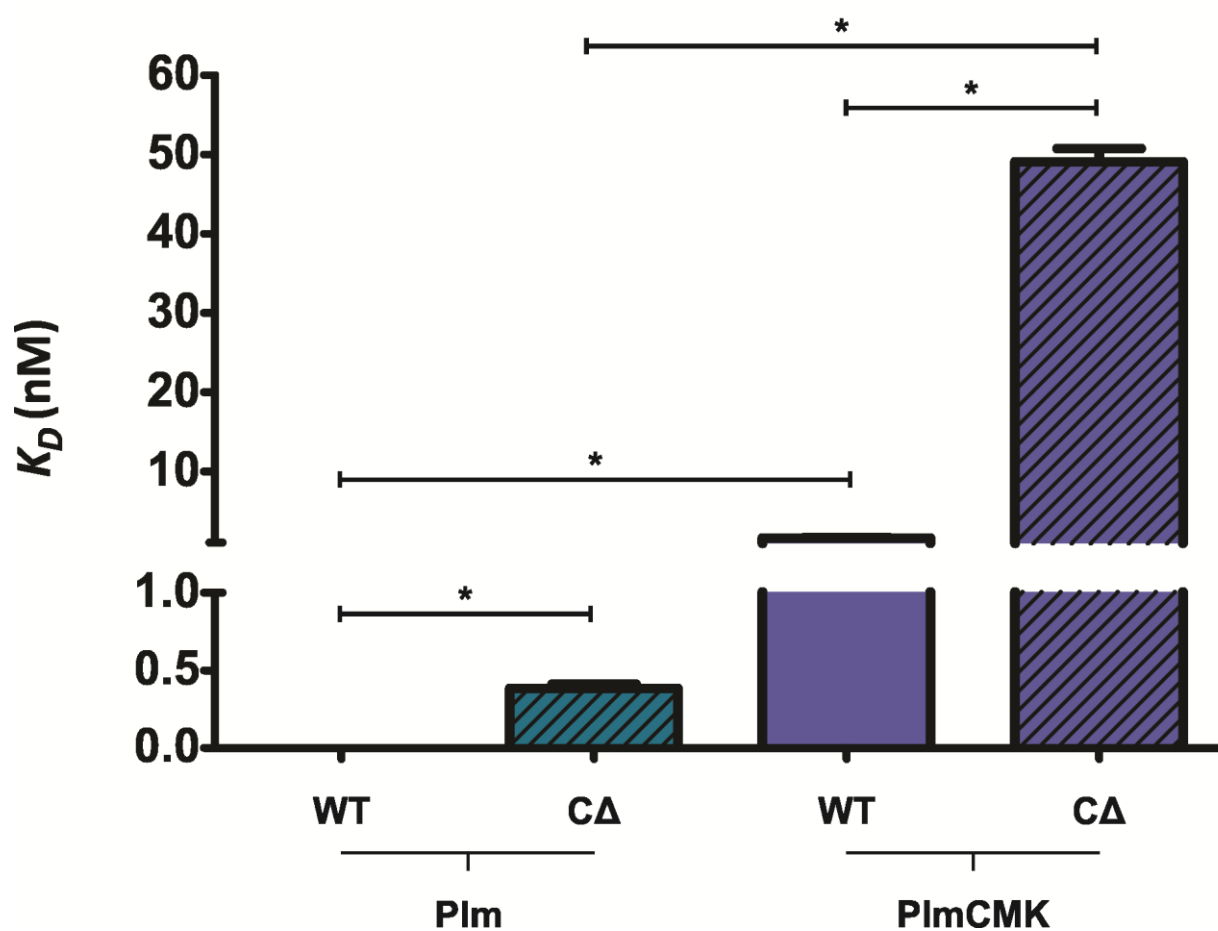


Figure 7.13. Comparison of the K_D between WT and CΔ α_2 -antiplasmin for plasmin variants. The K_D for plasmin and α_2 -antiplasmin variants were measured as described in Section 4.2.4. Statistics were assessed by one-way ANOVA with Newman-Keuls post-hoc correction. “*” refers to statistically significant data with a p-value of $p < 0.05$. “ns” refers to non-statistically significant data ($p > 0.05$). Each of the data point represents the mean ($n=3-6$) with error bars representing \pm SE.

Figure 7.13.
Comparison of the K_D between WT and C Δ
 α_2 -antiplasmin for plasmin variants



7.3.4 Microplasmin(ogen) Binding to α_2 -antiplasmin

This section describes the binding of α_2 -antiplasmin to variants of microplasmin(ogen). The generation of microplasminogen (μ PIg) was described in Chapter 5. μ PIg consists of only the serine protease domain where the activation site lies. Therefore, conversion to microplasmin (μ PIm) by plasminogen activators can occur. Prior to this work, the affinity of μ PIg/ μ PIm has never been determined with α_2 -antiplasmin. The contribution of the serine protease domain, in zymogen and enzyme form, can be evaluated with regards to the binding to α_2 -antiplasmin which may broaden our understanding of the interaction occurring between α_2 -antiplasmin/plasmin.

μ PIg binding to α_2 -antiplasmin

Figure 7.14A and B are sensorgrams of the interaction between μ PIg with WT and C Δ α_2 -antiplasmin. Binding affinity of WT and C Δ α_2 -antiplasmin to μ PIg was determined to be 1381nM and 1443nM respectively (Table 7.2). There was no significant difference between the binding of μ PIg to WT and C Δ (Figure 7.17). This result further confirms that the C-terminus of α_2 -antiplasmin interacts with the kringle domains of plasmin(ogen).

When binding of α_2 -antiplasmin to μ PIg was compared to full-length plasminogen (Glu-and Lys-plasminogen), it was evident that the binding affinity, in the absence of kringle domains, was reduced by ~35-folds (Table 7.2). This suggests that the interaction between full-length plasminogen and α_2 -antiplasmin is highly dependent on the kringle domain and serpin C-terminus. The results also informed that the non-activated serine protease domain of plasminogen plays a minor role in the binding to α_2 -antiplasmin.

μ PImCMK binding to α_2 -antiplasmin

Active site-blocked μ PIm (μ PImCMK) was generated by blocking with a plasmin inhibitor (CMK) as described in Section 7.2.2.1. Residual microplasmin activity was checked with the fluorogenic substrate (AMC) to ensure that the active site was completely blocked. Figure 7.15A and B are sensorgrams of the interaction between μ PImCMK with WT and C Δ α_2 -antiplasmin. μ PImCMK with WT gave a K_D value of 105nM, whereas C Δ and μ PImCMK interacted with an affinity of 160nM. There was no significant difference between the binding of μ PImCMK to WT and C Δ (Figure 7.17).

Conversion of μ PIg to μ PIm improved the binding affinity by approximately 9-fold, keeping in mind that the active site is inaccessible. This suggests that additional points of interaction may exist near the vicinity of the active site with the serpin domain of α_2 -antiplasmin.

μ PIIm binding to α_2 -antiplasmin

Active site-blocked μ PIImCMK was used to prevent the formation of the covalent complex with α_2 -antiplasmin. In this section, the binding of active μ PIIm was assessed. Figures 7.16A and B are sensorgrams of the binding between μ PIIm with WT and C Δ α_2 -antiplasmin. Analysis of the sensorgrams determined that the binding affinity of μ PIIm to WT and C Δ was 0.7pM and 1.0pM respectively. As seen with active plasmin (Figure 7.12), the sensorgram for active μ PIIm was similar in respects to the dissociation phase (Figure 7.16). There is an initial binding phase from 0-60s followed by no dissociation phase after a slight stabilisation from 60-360s. Covalent complex formation between μ PIIm and α_2 -antiplasmin resulted in a stable response where little dissociation is seen. There was no significant difference between the binding of μ PIIm to WT and C Δ (Figure 7.17). With the active site accessible for antiplasmin interaction, the binding affinity was significantly improved when compared to μ PIImCMK (Table 7.2).

The results with μ PIIm suggest that conversion to the active form by plasminogen activators causes major structural changes in the serine protease domain. The improvement in binding affinity from ~1.4 μ M to ~1pM observed with μ PIg and μ PIIm informed that the final inhibitory mechanism is completely driven by the serine protease domain and RCL of α_2 -antiplasmin. The interaction of plasmin kringle domains to the C-terminus of α_2 -antiplasmin are accessories in aiding the complex formation of the two molecules.

Figure 7.14. Sensorgrams of the binding of WT and CΔ α_2 -antiplasmin to μ PIg as measured by SPR. Recombinant α_2 -antiplasmin (20nM) was immobilised on a NTA chip. The binding of various concentrations of μ PIg to α_2 -antiplasmin was monitored in real time. Blue lines are raw curves and fitted curves are in black. **A)** Binding of μ PIg (200-1200nM) to WT ($\chi^2 = 0.77$). **B)** Binding of μ PIg (300-1200nM) to CΔ ($\chi^2 = 0.87$).

Figure 7.14.
Sensorgrams of the binding of WT and C Δ
 α_2 -antiplasmin to μ PIg as measured by SPR

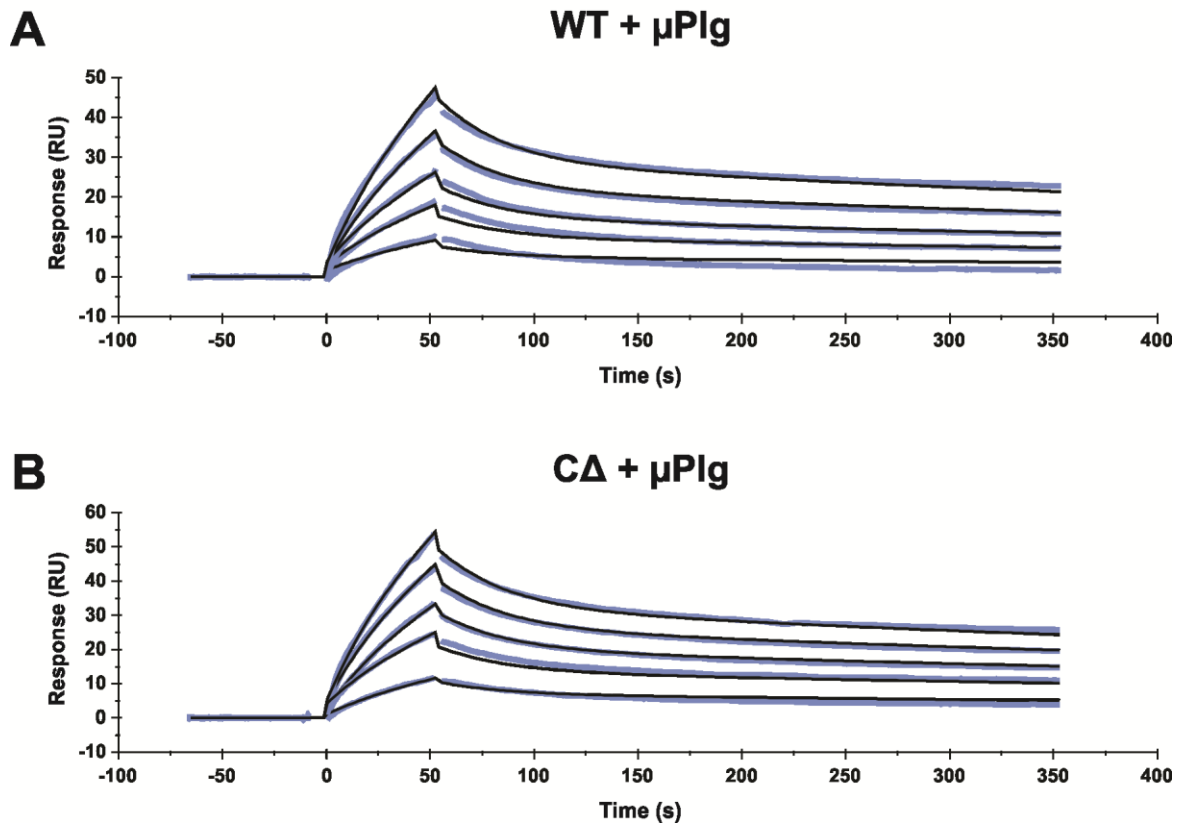


Figure 7.15. Sensorgrams of the binding of WT and CΔ α_2 -antiplasmin to μ PlmCMK as measured by SPR. Recombinant α_2 -antiplasmin (20nM) was immobilised on a NTA chip. The binding of various concentrations of μ PlmCMK to α_2 -antiplasmin was monitored in real time. Blue lines are raw curves and fitted curves are in black. **A)** Binding of μ PlmCMK (40-200nM) to WT ($\chi^2 = 0.13$). **B)** Binding of μ PlmCMK (40-200nM) to CΔ ($\chi^2 = 0.10$).

Figure 7.15.
Sensorgrams of the binding of WT and C Δ
 α_2 -antiplasmin to μ PIImCMK as measured by SPR

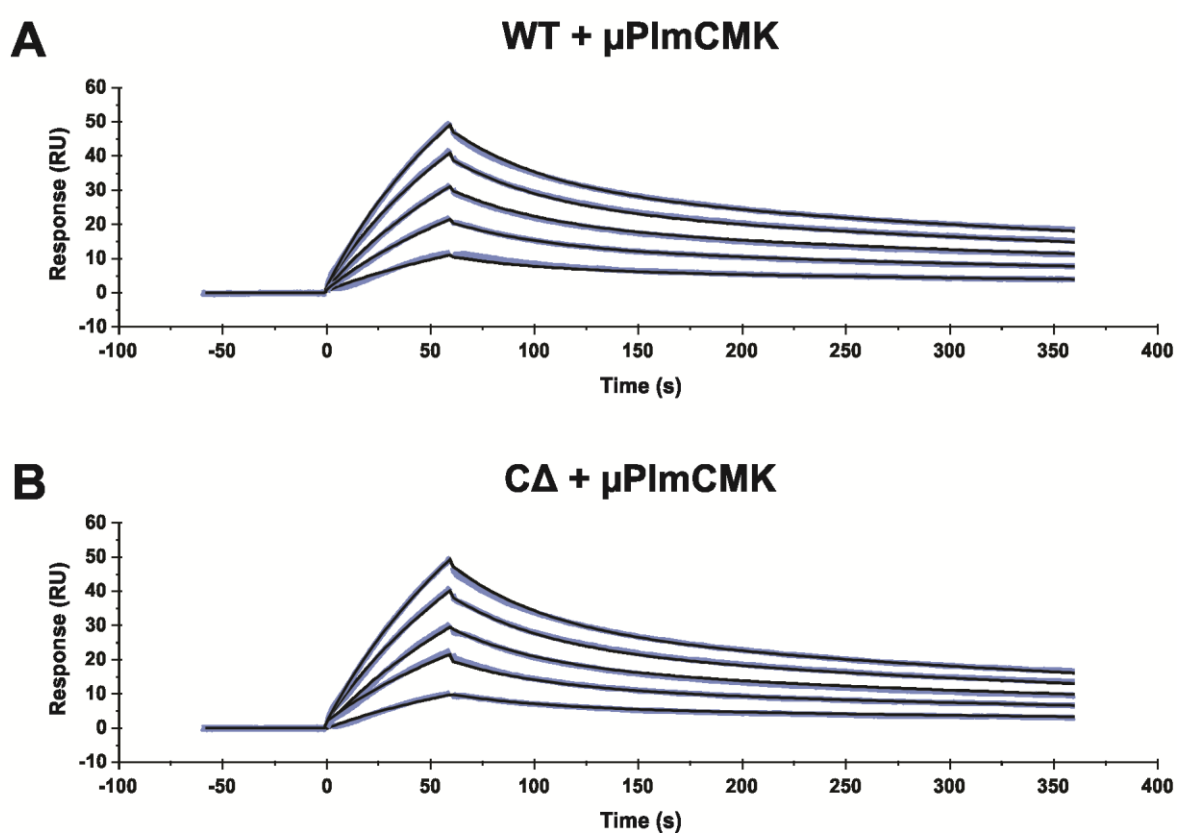


Figure 7.16. Sensorgrams of the binding of WT and CΔ α_2 -antiplasmin to μ Plm as measured by SPR. Recombinant α_2 -antiplasmin (20nM) was immobilised on a NTA chip. The binding of various concentrations of μ Plm to α_2 -antiplasmin was monitored in real time. Blue lines are raw curves and fitted curves are in black. **A)** Binding of μ Plm (7.5-60nM) to WT ($\chi^2 = 1.47$). **B)** Binding of μ Plm (7.5-60nM) to CΔ ($\chi^2 = 0.79$).

Figure 7.16.
Sensorgrams of the binding of WT and C Δ
 α_2 -antiplasmin to μ PIIm as measured by SPR

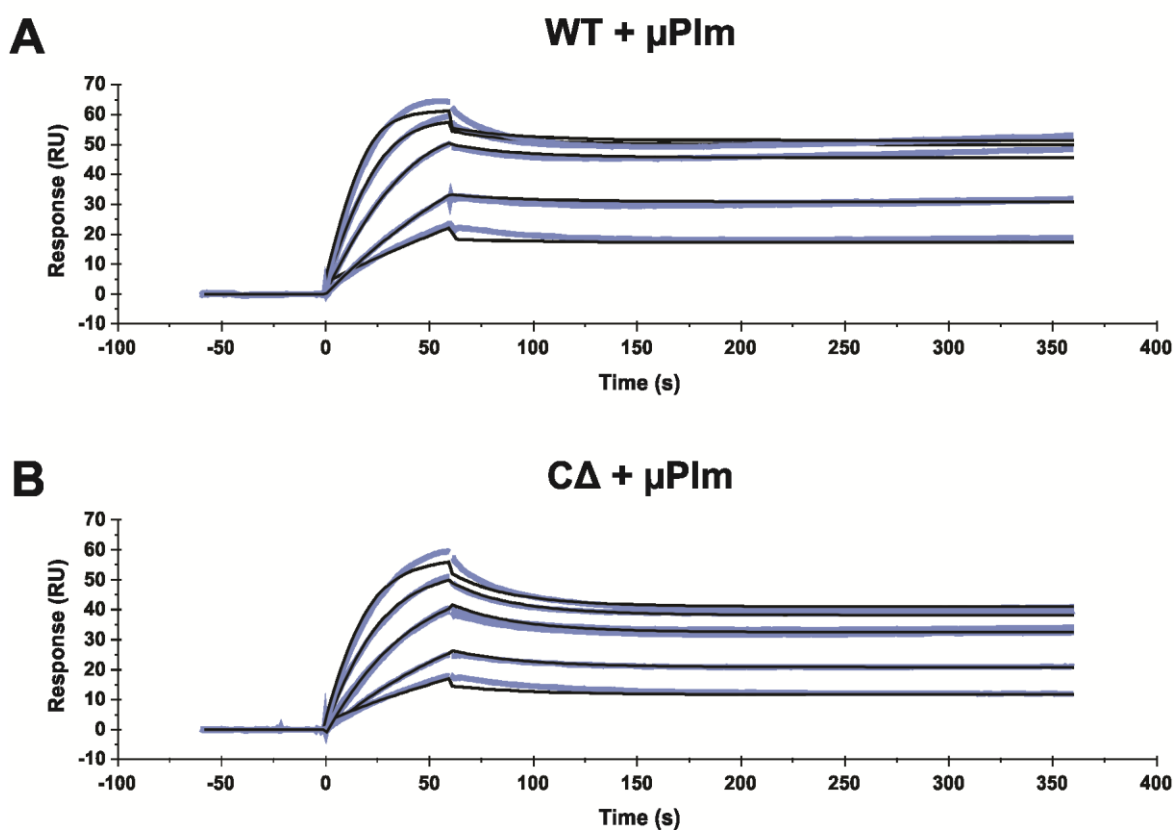
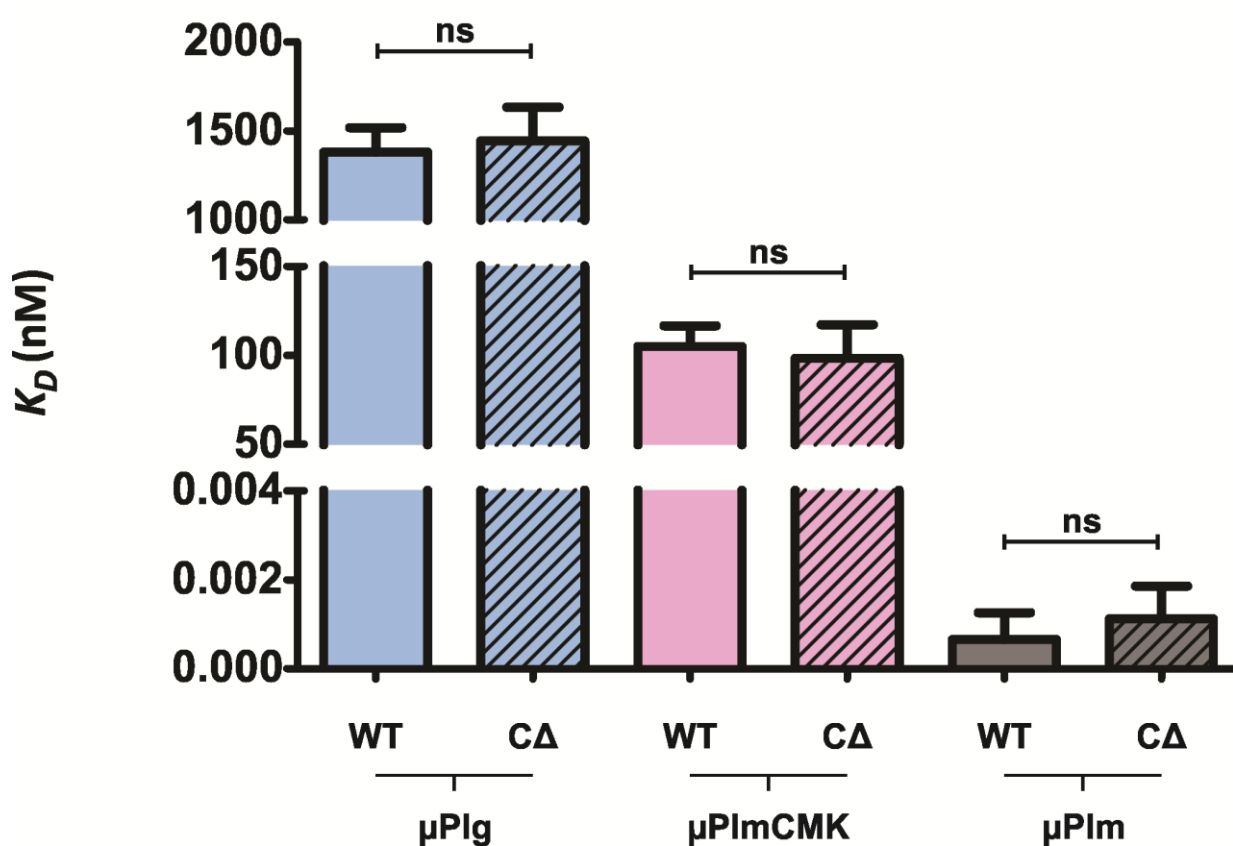


Figure 7.17. Comparison of the K_D between WT and CΔ α_2 -antiplasmin for microplasmin(ogen) variants. The K_D for microplasminogen and α_2 -antiplasmin variants were measured as described in Section 4.2.4. Statistics were assessed by one-way ANOVA with Newman-Keuls post-hoc correction. “*” refers to statistically significant data with a p-value of $p < 0.05$. “ns” refers to non-statistically significant data ($p > 0.05$). Each of the data point represents the mean ($n=3$) with error bars representing \pm SE.

Figure 7.17.
Comparison of the K_D between WT and C Δ
 α_2 -antiplasmin for microplasmin(ogen) variants



7.4 Discussion

Plasminogen is the key zymogen involved in the fibrinolysis system. The zymogen form consists of a leader sequence (PAp), serine protease domain, and five kringles which can be converted to its active counterpart, plasmin, which is responsible for fibrin clot degradation. Recently, the crystal structure of the precursor form of plasminogen (Glu-plasminogen) has been determined (Law et al., 2012; Xue et al., 2012). The structure provided new insights regarding domains which may have a role in conversion to plasmin and recruitment on the fibrin surface. However, the mechanism of how α_2 -antiplasmin, the natural inhibitor of plasmin, interacts with this multiple-domain-molecule remains unclear. To elucidate these complex interactions, this chapter presents the systematic study on the binding of plasmin(ogen) variants with full-length and C-terminally truncated α_2 -antiplasmin by surface plasmon resonance (SPR). By exploring the interaction of different forms of plasmin(ogen), a broader understanding on which region(s) may be exposed and/or unavailable for the interaction to α_2 -antiplasmin may be uncovered.

The precursor molecule, GluPIg, exists in two forms known as Type I and Type II and have different affinity for lysines (Hayes and Castellino, 1979). Both glycoforms are glycosylated at Thr³⁴⁶, while Type I contains an additional oligosaccharide chain at Asn²⁸⁹ (Figure 7.1B). It was previously determined that Type II binds 10 times more efficiently to cells when compared to Type I (Gonzalez-Gronow et al., 1989). Further characterisation of these two forms revealed that Type I preferentially binds to tissue factor receptors on cells whereas Type II has high affinity for the glycoprotein dipeptidyl peptidase IV (CD26) receptor on cells (Gonzalez-Gronow et al., 2002; Gonzalez-Gronow et al., 2001). Therefore, the favoured binding of Type I and Type II is dependent on receptor type present on cell surfaces. From data presented in this chapter, binding of Type I to α_2 -antiplasmin is ~4-fold higher in comparison with Type II. Binding of α_2 -antiplasmin to Type I and Type II cannot be compared with observations on cell binding as mechanism of interaction may be completely different. Furthermore, the crystal structure of full-length plasminogen revealed that Type I is more readily able to adopt the open conformation due to its labile structure (Law et al., 2012). As a consequence, plasminogen domains may be more accessible to α_2 -antiplasmin, which could possibly explain its increased affinity for Type I.

In a separate study by Lijnen and colleagues, binding of Glu- and Lys-plasminogen Type I and Type II to α_2 -antiplasmin and fibrin were determined (Lijnen et al., 1981). Glu-plasminogen Type II appeared to have a slightly increased affinity for α_2 -antiplasmin in comparison to Type I in Lijnen and colleague's work. It was observed that Lys-plasminogen Type II had an approximately 9-fold increase in binding to α_2 -antiplasmin when compared to Lys-plasminogen Type I (Lijnen et al., 1981). The discrepancies of their data with our current work could be due to the use of plasma purified α_2 -antiplasmin in their system. It was predicted that human

α_2 -antiplasmin contains four potential sites for glycosylation (Asn⁹⁹, Asn²⁶⁸, Asn²⁸⁰ and Asn²⁸⁹) (Lee et al., 1999; Lijnen et al., 1987) and the N-terminus of α_2 -antiplasmin undergoes proteolytic modification (Lee et al., 2004). Hence, purification of α_2 -antiplasmin from plasma may result in a heterogeneous protein sample and may influence the binding to plasminogen variants. Moreover, dissociation constants were determined by the concentration of plasminogen required to decrease α_2 -antiplasmin activity by 50% (Hayes and Castellino, 1979). Whereas in this study a new and sensitive assay using SPR technology was used to measure the direct binding affinity in real time. For a direct comparison of this work with Lijnen and colleague's results, Lys-plasminogen Type I and Type II binding to α_2 -antiplasmin should be considered in future work. Furthermore, recombinant α_2 -antiplasmin proteins produced in this thesis does not contain any glycosylation. Future experiments should include plasma purified α_2 -antiplasmin to explore the potential role of glycosylation sites in the binding of plasminogen. Perhaps the discrepancy seen with affinity between the study by Lijnen et al (1981) and this thesis could be resolved.

In circulation, Type I and Type II exists at approximately 40% and 60% respectively (Brockway and Castellino, 1972). For that reason, it was expected that our binding data of Glu-plasminogen (purchased from Hematologic Technologies) would be an intermediate value when compared to the binding affinity of Glu-plasminogen Type I and Type II. Our data obtained from analysing Glu-plasminogen and its two isoform revealed that the interaction was not influenced by the presence or absence of the C-terminal region of α_2 -antiplasmin (Figure 7.10). This suggests that the lysine binding sites of plasminogen are not exposed in this precursor form and may be purely mediated by an exosite interaction. From the crystal structure, it was determined that only kringle 1 (K1) is accessible in the closed conformation and the activation site on the serine protease domain is trapped between the linker of K2-K3 (Law et al., 2012).

Wang and colleagues determined that the binding affinity of plasminogen with Asn- α_2 -antiplasmin was 380nM (Wang et al., 2006) via SPR which is approximately 12-fold higher than the value obtained in this current study of 31nM. One limitation of their study was that the proportion of Glu-plasminogen and Lys-plasminogen used in their study was not reported. Therefore, their study may be compromised by a mixture of plasminogen isoforms in their binding assay. Furthermore, Wang and colleagues immobilised plasminogen on a CM5 chip. As described in Chapter 4, orientation of the plasminogen molecule on this surface will be random and important domains may be blocked. It is believed that binding of Glu-plasminogen to the cell surface can induce conformational change in the molecule (Han et al., 2011). Therefore, it is possible that the coupling of Glu-plasminogen onto the CM5 surface may render the molecule to the more open conformation.

Previous studies with Lys-plasminogen revealed that this form has a higher binding affinity to α_2 -antiplasmin in comparison to Glu-plasminogen (Lin et al., 2011; Wiman et al., 1979). Our results correspond with a published study where binding was increased ~4-fold when WT α_2 -antiplasmin interacted with Lys-plasminogen instead of Glu-plasminogen. Recent crystal structure of full-length plasminogen demonstrated that the PAp domain forms extensive interactions with K4 and K5 which maintain the molecule in its closed conformation (Law et al., 2012). Proteolytic cleavage of the PAp domain results in reshuffling of the molecule, exposing kringle domains and serine protease domain hence allowing access for α_2 -antiplasmin. When the C-terminal region of α_2 -antiplasmin was removed, the affinity was decreased ~20-fold. This data suggests that the Lys-plasminogen interaction is largely mediated by lysine binding sites in the kringle domains. An important observation was that the binding of C-terminally truncated α_2 -antiplasmin to Glu-plasminogen ($K_D = 48\text{nM}$) was greater than Lys-plasminogen ($K_D = 152\text{nM}$). This further supports the assertion that the interaction of α_2 -antiplasmin with Glu-plasminogen is mediated by an exosite region. It is possible that the exosite region is buried and made inaccessible upon conversion to Lys-plasminogen. In humans, plasminogen and α_2 -antiplasmin circulates at a concentration of $\sim 2.4\mu\text{M}$ and $\sim 1\mu\text{M}$ respectively. Based on this knowledge, results obtained from this chapter would suggest that α_2 -antiplasmin circulates in complex with plasminogen in plasma. In order to confirm this observation, co-purification of α_2 -antiplasmin and plasminogen from plasma should be attempted.

When α_2 -antiplasmin was analysed with active plasmin, it was clear from the sensorgram (Figure 7.12A) that a stable complex formed and that dissociation of plasmin could not be achieved. The binding value obtained was lower than the picomolar range which further supports the formation of a covalent α_2 -antiplasmin/plasmin complex. When compared with the active site-blocked plasmin counterpart, it was demonstrated that the inhibitory mechanism of α_2 -antiplasmin was driven by active site/RCL interaction. In turn, the C-terminal region and kringle domain are responsible for accelerating and orientating the α_2 -antiplasmin/plasmin molecule for efficient complex formation.

In Chapter 4, the *SI* of recombinant WT and C Δ α_2 -antiplasmin with plasmin was determined to be 1.0 and 1.5 respectively. Therefore, this confirmed that the recombinant α_2 -antiplasmin proteins were structurally sound. To ensure that the recombinant microplasmin produced in Chapter 5 is active, the *SI* was measured and determined to be 1.0 and 1.2 with recombinant WT and C Δ α_2 -antiplasmin respectively. This confirmed that μPIIm , which lacks all five kringle domains, was in its native conformation and able to recognise its natural inhibitor. Further kinetic analysis was performed to check inhibition rates of μPIIm by α_2 -antiplasmin. As expected, WT and C Δ inhibited μPIIm at a rate of $\sim 1.0\text{-}0.4 \times 10^6 \text{ M}^{-1}\text{s}^{-1}$ which corresponds with data from Chapter 4 when C Δ was reacted with full-length plasmin ($k_a = 9.2 \times 10^5 \text{ M}^{-1}\text{s}^{-1}$). There

was no difference in μ Plm inhibition rate in the absence or presence of the C-terminal region of α_2 -antiplasmin which was expected as μ Plm lacks any kringle domains.

Binding of microplasmin(ogen) was then studied by SPR. Microplasminogen bound to α_2 -antiplasmin with an affinity of ~ 1400 nM. There was no significant difference in the binding either in the presence or absence of the α_2 -antiplasmin C-terminus. This informed that the C-terminus does not interact with the serine protease domain of plasmin(ogen). Furthermore the data also suggested that the non-activated serine protease domain has low affinity towards the α_2 -antiplasmin serpin body. This further supports the observations seen with α_2 -antiplasmin and Glu-/Lys-plasminogen that these interactions are mainly mediated by lysine binding site to the C-terminal region and an additional exosite interaction that has not been identified.

There was a dramatic increase in binding affinity upon conversion of microplasminogen to microplasmin. A ~ 10 -fold increase was seen with active site-blocked microplasmin and an additional $\sim 10^5$ -fold increase was seen when the active site was accessible. The affinity seen with active microplasmin was similar to that seen in active plasmin which further supports the observation that the active site is crucial in the final inhibitory mechanism, whereas the kringle domains and exosite accelerates the initial interaction and assists in target recognition. This data also suggest that activation by plasminogen activator causes the protease domain to undergo remarkable conformational changes which supplements its recognition to α_2 -antiplasmin. Result seen with active site-blocked microplasmin with α_2 -antiplasmin provides added evidence that an interaction can occur. This data provided evidence that a non-covalent complex could be formed for crystallisation purposes in Chapter 5.

In Chapter 4, the striking observation made was that the binding affinity of active site-blocked plasmin with C-terminally truncated α_2 -antiplasmin was relatively high ($K_D = 49$ nM) when compared to WT α_2 -antiplasmin ($K_D = 1.6$ nM). It was then hypothesised that the exosite interaction may exist between the α_2 -antiplasmin serpin core and the plasmin protease domain. However, in this current chapter, it was revealed that the binding of active site-blocked microplasmin with α_2 -antiplasmin was ~ 100 nM. Therefore, a 2-fold difference is unaccounted for. With this new data, a new theory was formed that the exosite region lies between one of the kringle domains and the serpin core. Perhaps K5, which is the kringle adjacent to the protease domain, could form this additional interaction. Another possibility is K3, which unlike the other kringle domains, does not contain a lysine binding site and the role of this region is unclear (Christen et al., 2010).

7.5 Conclusion

In summary, detailed binding analysis of plasmin(ogen) variants with α_2 -antiplasmin was performed in this chapter. The interaction seen between Glu-plasminogen and α_2 -antiplasmin is likely mediated by exosite interaction as the molecule is in a closed conformation and the lysine binding sites are inaccessible. We demonstrated that Glu-plasminogen Type I has an increased affinity for α_2 -antiplasmin in comparison to Glu-plasminogen Type II. Conversion to Lys-plasminogen is predicted to undergo conformational change which exposes the lysine binding sites. Therefore, α_2 -antiplasmin C-terminus is able to bind to Lys-plasminogen resulting in a higher affinity when compared to Glu-plasminogen. Microplasminogen binds weakly to α_2 -antiplasmin, but affinity is dramatically increased once activated to microplasmin. Results revealed that the exosite interaction may lie between one or more kringle domains and the α_2 -antiplasmin serpin core.

Chapter 8:

General discussion

This page has been intentionally left blank.

The serine protease, plasmin, is the key molecule involved in the breakdown of fibrin clots triggering fibrinolysis in circulation. Balance between the components involved in the fibrinolytic system is important in maintaining a homeostatic environment. Excessive plasmin activity may lead to increased degradation of plasma proteins leading to hemorrhagic events. On the other hand, decreased plasmin activity may result in insufficient clot clearance during thrombotic conditions. Intravenous recombinant tPA (Alteplase), the current gold standard in the treatment of cardiovascular events, is used to enhance plasmin generation in the circulation. However, the administration of tPA is limited to a narrow time window and is associated with an increased bleeding tendency. Therefore, the development of new thrombolytics with decreased risk is required.

α_2 -antiplasmin, a serine protease inhibitor (serpin), is responsible for inactivating plasmin thus preventing further degradation of fibrin clots. Disrupting the interaction of the C-terminus region of α_2 -antiplasmin to plasmin has been shown to decrease plasmin inhibition resulting in increased fibrinolysis. Therefore, targeting the natural inhibitor may be a potential area of intervention in thrombotic diseases. By reducing or blocking the inhibitory mechanism of α_2 -antiplasmin, plasmin activity during thrombotic events may be prolonged. However, limited information is available regarding the molecular interactions which occurs between plasmin and α_2 -antiplasmin. It is also poorly understood how the lysine residues within the C-terminus of α_2 -antiplasmin accelerates the binding to plasmin. In order to develop new therapeutics, a better understanding of α_2 -antiplasmin/plasmin interaction is required. In this thesis, the basic biochemical and binding properties of α_2 -antiplasmin/plasmin were explored to further our knowledge of the complex interaction occurring between these multi-domain molecules.

A variety of recombinant human α_2 -antiplasmin proteins containing single or multiple lysine to alanine substitution within the C-terminus were generated and purified. Furthermore, the recombinant proteins lacking the N-terminus and/or C-terminus were also produced. Plasmin inhibition rate of each of the recombinant α_2 -antiplasmin proteins were determined using a sensitive kinetic assay. Prior to this work, there were limited studies investigating the binding affinity of full-length α_2 -antiplasmin to plasmin. Therefore, a sensitive assay to measure binding affinity was developed using SPR. A broad array of binding affinity data were obtained with α_2 -antiplasmin containing single/multiple lysine to alanine substitution within the C-terminus and active site-blocked plasmin (PlmCMK). Results obtained suggested that an additional exosite interaction may exist beyond the reactive centre loop (RCL) of the serpin and active site cleft of the protease, and the C-terminus of α_2 -antiplasmin and plasmin kringle domains. To further investigate this additional exosite, WT and active site mutated microplasmin were generated using recombinant protein technology. Subsequently, non-covalent complex formation studies with active site mutated microplasmin and N-terminally truncated α_2 -antiplasmin were performed. Additionally, β -sheet C of α_2 -antiplasmin was explored as the

potential exosite region in interacting with plasmin. Furthermore, there are no comprehensive studies investigating how different conformational forms of plasmin(ogen) influence the interaction with α_2 -antiplasmin. Therefore, by utilising the SPR technique developed, the binding affinity of different conformational forms of plasmin(ogen) were determined with WT and C-terminally truncated α_2 -antiplasmin. The main findings of this study will be discussed in this chapter.

N- and C-terminus of α_2 -antiplasmin: Potential role in stability

In Chapter 3, a range of recombinant human α_2 -antiplasmin proteins were generated in a bacterial expression system in this thesis which includes the α_2 -antiplasmin protein lacking both the N- and C-terminal extensions (N Δ C Δ). The expression and purification of soluble recombinant N Δ C Δ α_2 -antiplasmin was achieved, however it had the lowest yield when compared to all other proteins. Additionally, stoichiometry of inhibition (*SI*) measurement revealed that N Δ C Δ (*SI* = 1.8) had an increased value when compared to WT α_2 -antiplasmin. These observations suggest that the removal of N- and C-terminal regions may have affected structural stability and folding of α_2 -antiplasmin. At position 43 of the N-terminus, a cysteine residue is present and has been shown to form a disulphide bridge with Cys¹¹⁶ (Christensen et al., 1997). In this thesis, Cys⁴³ was removed when the N-terminus was truncated in both N Δ and N Δ C Δ α_2 -antiplasmin which may have affected disulphide bond formation to Cys¹¹⁶. When the N-terminus was truncated alone (N Δ), the *SI* was not altered which suggests that the two tails may interact and maintain stability of α_2 -antiplasmin. Therefore, future studies should aim to explore the potential role of N- and C-terminus in folding and stability of α_2 -antiplasmin. Examination of recombinant N Δ C Δ α_2 -antiplasmin which includes the Cys⁴³ may help to determine whether the Cys₄₃-Cys¹¹³ disulphide bond is required for protein stability. Progressive truncations of both N- and C-terminus may also reveal region(s) or amino acid(s) within the two tails which contributes to structural stability.

Lysine residues in the C-terminus of α_2 -antiplasmin mediate binding to kringle domains of plasmin

Prior to this work, it was found that the lysine residues within the C-terminus of α_2 -antiplasmin were responsible for interacting with the lysine binding sites contained within the kringle domains of plasmin. However, there was conflict in the literature in regards to which lysine residue was the most important in this interaction. Wang and colleagues identified Lys⁴⁴⁸ as the main binder, whereas Frank and colleagues determined that it was in fact Lys⁴⁶⁴ (Frank

et al., 2003; Wang et al., 2003). In my honours year, the plasmin inhibition rate was determined with full-length α_2 -antiplasmin containing single lysine to alanine substitution within the C-terminus. This differs from the work published by Wang and colleagues and Frank and colleagues because their studies used partial α_2 -antiplasmin or isolated kringle molecules. By using the sensitive kinetic assay established in our laboratory, it was established that Lys⁴⁶⁴ was the most important lysine residue in the C-terminus which agrees with observations by Frank and colleagues (Lu, 2008). However, the plasmin inhibition rate of a single lysine to alanine substitution at Lys⁴⁶⁴ does not equal the rate when the whole C-terminus was removed. Therefore, additional questions arose: 1) Can lysine be replaced with another amino acid containing the same charge? 2) What is the effect of multiple lysine to alanine mutations? and 3) Are residues other than the lysines within the C-terminus that are involved in the interaction? Answering these questions formed the basis of the first aim of this thesis.

To further demonstrate the importance of Lys⁴⁶⁴ in α_2 -antiplasmin, a single substitution from lysine to arginine (K464R) was generated. It was shown that binding to plasmin kringles was lysine specific and not based simply on the charge of the amino acid as plasmin inhibition and binding was reduced in the K464R mutant in comparison with WT α_2 -antiplasmin.

The plasmin inhibition rate of human WT α_2 -antiplasmin was determined to be $3.7 \times 10^7 \text{ M}^{-1}\text{s}^{-1}$ which corresponds with published data. Furthermore, binding affinity of WT α_2 -antiplasmin with active site-blocked plasmin was 1.6nM. When the N-terminus was absent, the plasmin inhibition rate and binding affinity remained unchanged which confirms that the N-terminus does not have a role in accelerating plasmin interaction. As expected, removal of the C-terminus (C Δ) resulted in a significant decrease in the rate of plasmin inhibition ($k_a = 4.2 \times 10^5 \text{ M}^{-1}\text{s}^{-1}$) indicating that the C-terminus mediates binding to plasmin. However it was surprising that the binding affinity of C Δ with active site-blocked plasmin ($K_D = 49\text{nM}$) still remained high in the absence of the C-terminus. In Chapter 4, it was shown that as the number of lysine to alanine substitutions were increased, there was a progressive loss in the rate of plasmin inhibition and binding. Additionally, when four of the conserved lysine residues were mutated (K434A/K444A/K448A/K464A), the rate of plasmin inhibition and binding affinity was similar to the C-terminally truncated α_2 -antiplasmin (C Δ). This demonstrates that the lysine residues are mediators in the binding to the kringle domains of plasmin. Recombinant α_2 -antiplasmin protein containing four internal lysine to alanine substitutions with the most C-terminal lysine retained (K427A/K434A/K441A/K448A/K464WT) further confirmed the importance of Lys⁴⁶⁴ and showed that the other lysine residues are required for efficient plasmin binding and inhibition. From these results, it was proposed that Lys⁴⁶⁴ acts as an anchor which orientates the remaining lysine residues to its corresponding kringle domains. Frank and colleagues proposed that the C-terminus potentially binds firstly to K1 followed by K4, K5 and K2 (Frank et al., 2003). The specifics regarding which lysine residue interacts with which kringle

domain remains unknown to date. Future studies should aim to identify the orientation in which the C-terminus of α_2 -antiplasmin interacts with the kringle domains of plasmin. This could be achieved by crystallising the kringle domains of plasmin with isolated C-terminus of α_2 -antiplasmin which may directly visualise the contacts made between these two regions.

One important observation from Chapter 4 was that the binding affinity of C-terminally truncated α_2 -antiplasmin to active site-blocked plasmin remained high ($K_D = 49\text{nM}$). This result suggests that there is an additional exosite interaction between the serpin core and plasmin molecule. This study has shown that the N-terminus does not play a role in accelerating plasmin binding and inhibition, therefore the contribution of N-terminus as the exosite region can be excluded. Using these findings, it was proposed that perhaps the exosite interaction could lie between the serpin core and the protease domain or serpin core or kringle domains of plasmin. As a result of these observations, the aims of Chapters 5 to 7 were to identify the additional interaction between α_2 -antiplasmin and plasmin.

Additional exosite interaction of α_2 -antiplasmin and plasmin

Structural studies: Non-covalent complex of microplasmin and α_2 -antiplasmin

To identify the exosite interaction between α_2 -antiplasmin and plasmin, different strategies were explored. Based on the binding affinity data of C Δ with active site-blocked plasmin, one of the assumptions was that the additional interaction may exist between the α_2 -antiplasmin core and protease domain. It has been shown that there are extensive additional contacts made between serpin/protease outside the active site and reactive centre loop (RCL) based on other studies (Lin et al., 2011, Izaguirre and Olson, 2006). Therefore, the first approach was to crystallise the encounter complex of active site mutated microplasmin (His- μ PIg S741A) and N-terminally truncated α_2 -antiplasmin (N Δ). In Chapter 5, expression and purification of μ PIg/ μ PIm were successfully established in the laboratory. Non-covalent complex formation between His- μ PIg S741A and N Δ α_2 -antiplasmin was demonstrated on a Native-PAGE however co-purification of the complex by size exclusion chromatography could not be shown. Furthermore, binding data in Chapter 7 showed that when active site-blocked microplasmin (μ PImCMK) analysed with WT α_2 -antiplasmin, the affinity was approximately 100nM. Together these results suggest that although His- μ PIg S741A and N Δ are interacting, the non-covalent complex formed is unstable and may be easily separated by the purification process. Crystallisation of His- μ PIg S741A in complex with N Δ α_2 -antiplasmin is still ongoing in our laboratory. If successful, this will provide the first structure of plasmin protease domain interacting with α_2 -antiplasmin, its natural binding partner and will also reveal contacts made between the serpin core and protease domain.

β -sheet C of α_2 -antiplasmin interacts with plasmin kringle domains

It is common for serpins to have additional points of interaction to increase its specificity towards its target protease. The X-ray crystal structure of murine α_2 -antiplasmin was superposed on the PAI-I/uPA encounter complex and two conserved residues (His²²⁹ and Glu²³²) within the β -sheet C of α_2 -antiplasmin were identified as potential point of interactions with plasmin (Lin et al., 2011). Single residue substitutions to alanine demonstrated that H229A and E232A had a 2-fold decrease in binding affinity with active site-blocked plasmin (PlmCMK) when compared to WT α_2 -antiplasmin. However, there was no significant decrease in the binding of H229A and E232A with μ PlmCMK. Therefore these results suggest that His²²⁹ and Glu²³² make contacts with the kringle(s) and not with the protease domain of plasmin. The exact kringle(s) in which β -sheet C interacts with remains unknown. Future studies should aim to investigate other residues within the β -sheet C of α_2 -antiplasmin which may contribute to binding to plasmin. Further experiments, such as producing proteins with combined mutations of His²²⁹ and Glu²³², should be performed to support the current hypothesis that these residues are involved in plasmin interaction. Other residues within the β -sheet C of α_2 -antiplasmin should also be explored to determine their role in interacting with plasmin.

Insight into the different conformational form of plasmin(ogen): Binding studies with α_2 -antiplasmin

Plasminogen, the key zymogen in the fibrinolytic system, is a multi-domain-molecule consisting on the pan-apple domain (PAP), five kringles and a serine protease domain. In human circulation, the native form, Glu-plasminogen exists in two major glycoforms (Type I and Type II). Removal of the PAP converts Glu-plasminogen to Lys-plasminogen which is proposed to be in a more open conformation. Ultimately, conversion to active plasmin is achieved by plasminogen activators. Due to the complex structural diversity of plasminogen/plasmin, there are limited studies available regarding the interaction with α_2 -antiplasmin. Therefore to elucidate these interactions, the work presented in Chapter 7 was aimed at studying the binding affinity of various plasmin(ogen) with WT and C Δ α_2 -antiplasmin. By exploring the interaction of different plasmin(ogen) variants, a broader understanding on which region(s) may be exposed and/or unavailable for the interaction to α_2 -antiplasmin may be uncovered.

The order in which WT α_2 -antiplasmin binds to the various plasmin(ogen) conformations, from lowest to highest affinity, is as follows: μ Plg< μ PlmCMK<Glu-plasminogen Type II<Glu-plasminogen (combination of Type I and II)<Glu-plasminogen Type I<Lys-plasminogen<PlmCMK< μ Plm<Plm. From these results, it was observed that Glu-plasminogen binds to α_2 -antiplasmin in a non-lysine dependent manner. Glu-plasminogen

Type I has a higher affinity for α_2 -antiplasmin in comparison with Type II. This supports observations seen in the recent X-ray crystal structure of human plasminogen that Type I is more conformationally labile and therefore readily able to adopt an open conformation (Law et al., 2012). The crystal structure also revealed that only kringle 1 (K1) is accessible in Glu-plasminogen (Law et al., 2012). This may explain results seen with C Δ α_2 -antiplasmin and Glu-plasminogen. There was a slight reduction in binding affinity with Glu-plasminogen when the C-terminus was absent which supports the suggestion that K1 is exposed.

As expected, Lys-plasminogen has a higher affinity for α_2 -antiplasmin when compared with Glu-plasminogen which corresponds with previously published data (Wiman et al., 1979). The PAP is absent in Lys-plasminogen, therefore the molecule is predicted to be in a more open conformation with multiple kringle domains exposed. With accessible kringles, it is unsurprising that the binding seen with α_2 -antiplasmin and Lys-plasminogen is lysine dependent. This was demonstrated with C Δ α_2 -antiplasmin which resulted in a significant decrease in affinity with Lys-plasminogen in the absence of the C-terminus.

When α_2 -antiplasmin binding to μ PIg was compared with μ PImCMK, there was a ~10-fold increase in affinity when the zymogen was converted to enzyme. Keeping in mind that the active site of μ PImCMK is chemically blocked, the increase in binding affinity from μ PIg is significant. This increase suggests that upon activation, the serine protease domain undergoes structural rearrangement exposing the active site cleft of plasmin and potentially additional interaction sites for α_2 -antiplasmin. As expected, when the active site of μ PIm is available, the binding affinity to α_2 -antiplasmin was similar to full-length plasmin. This confirmed that the active site is crucial for the final inhibitory mechanism of α_2 -antiplasmin.

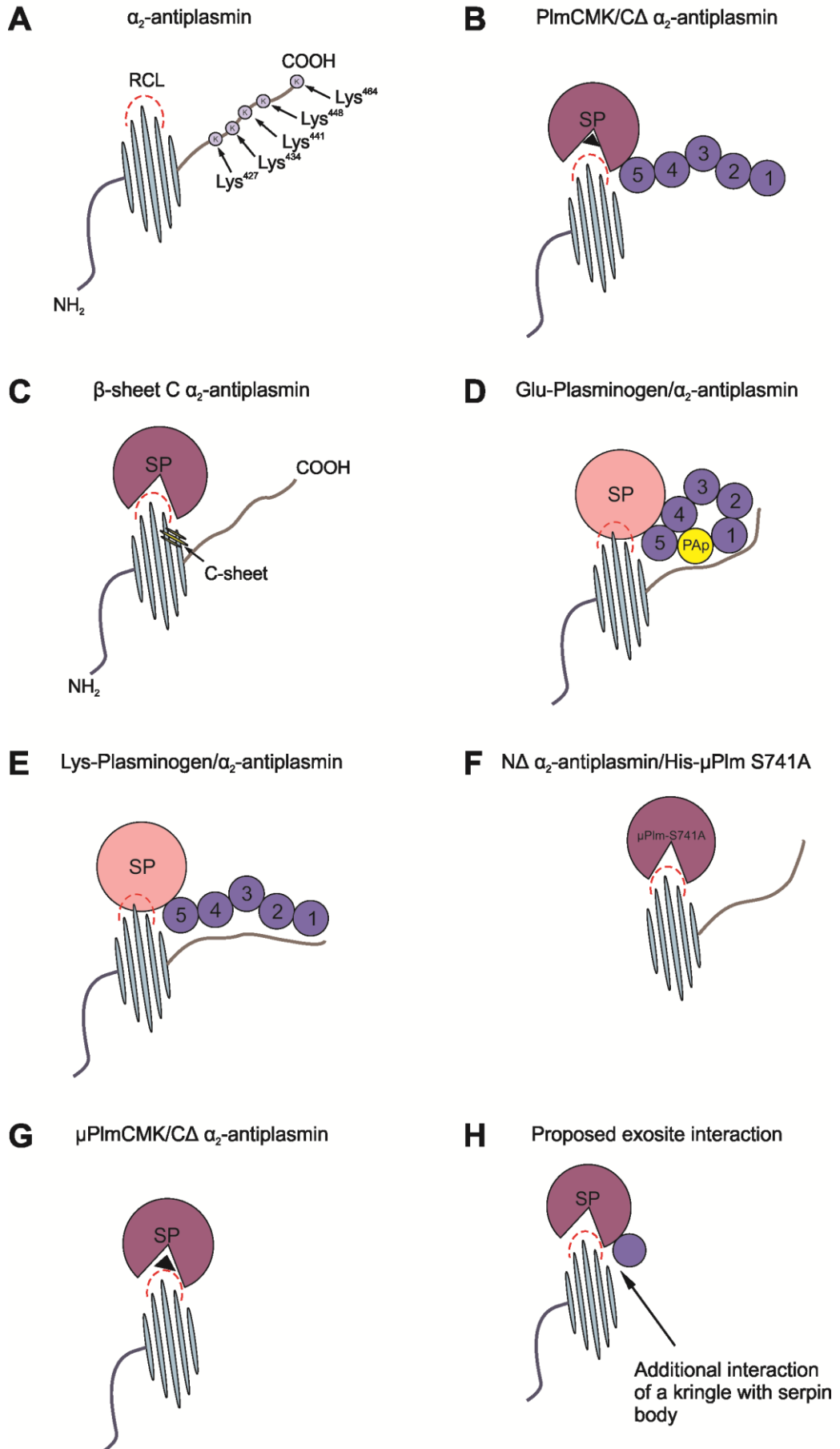
In Chapter 4, it was determined that the binding affinity of C Δ α_2 -antiplasmin with active site-blocked plasmin was high ($K_D = 49\text{nM}$). It was then proposed that an exosite interaction exist between the serpin core and protease domain. If this theory was true, the binding affinity of C Δ α_2 -antiplasmin and active site-blocked microplasmin should be ~50nM. However, it was revealed in Chapter 7 that the binding of C Δ α_2 -antiplasmin with active site-blocked microplasmin was 100nM. Therefore, a 2-fold difference in binding affinity was unaccounted for. Results have revealed that the exosite interaction may exist between the serpin core and one or more kringle domains. This proposal is supported by data obtained in Chapter 6 that β -sheet C of α_2 -antiplasmin form contacts with kringle(s) of plasmin. Future studies should aim to identify the kringle(s) which interacts with the α_2 -antiplasmin core. Miniplasmin, another form of plasmin which contains the serine protease domain and K5, could be generated and its binding affinity with C Δ α_2 -antiplasmin determined. Perhaps there are other regions in α_2 -antiplasmin other than β -sheet C that are able to form interactions with kringle(s) of plasmin.

Concluding remarks

In summary, a comprehensive and detailed analysis on inhibition and binding of plasmin(ogen) by α_2 -antiplasmin have been presented in this thesis. Figure 8.1 summarises the main findings of this work. This study highlighted the importance of individual lysine residues within the C-terminus of α_2 -antiplasmin and their role in combination in the binding to the plasmin molecule. It was shown that the C-terminus of α_2 -antiplasmin is crucial in accelerating the binding and inhibition of plasmin. Furthermore, it was identified that a novel exosite interaction exists between α_2 -antiplasmin and plasmin. From the results presented in this thesis, the additional exosite region has been revealed to exist between β -sheet C of α_2 -antiplasmin and kringle domain(s) of plasmin. Further experiments are required to identify the kringle(s) which are involved. The work presented in this thesis have provided new insights and improved understanding of the interaction that occurs between α_2 -antiplasmin and plasmin(ogen). This knowledge will enable us discover new therapeutics such as antibodies or small peptides which blocks the interaction sites of α_2 -antiplasmin to plasmin, thus up-regulating the activity of plasmin, the natural clot-busting molecule, in pathological thrombotic events.

Figure 8.1. Summary of main findings. **A)** Binding of kringle domains of plasmin is mediated by lysine residues in the C-terminus of α_2 -antiplasmin. **B)** Affinity of C Δ α_2 -antiplasmin with active site-blocked plasmin (PlmCMK) remains high at 50nM, suggesting an additional exosite interaction between the serpin and protease. **C)** Non-covalent complex of active site mutated microplasmin (His- μ Plm S741A) and N Δ α_2 -antiplasmin is unstable and crystallisation work is ongoing. **D)** His²²⁹ and Glu²³² of β -sheet C in α_2 -antiplasmin may form an exosite interaction with plasmin kringle(s). Further studies required to confirm this. **E)** Binding of Glu-plasminogen to α_2 -antiplasmin is not lysine mediated. **F)** Binding of Lys-plasminogen to α_2 -antiplasmin is mediated by lysine binding sites. **G)** Affinity of C Δ α_2 -antiplasmin with active site-blocked microplasmin (μ PlmCMK) does not equal C Δ α_2 -antiplasmin with PlmCMK. K_D was \sim 100nM which suggest that additional interaction does not involve serpin core and protease domain. **H)** Combined observations suggest that exosite interaction exist between kringle(s) and serpin core. Identity of kringle(s) is unknown. Region involved in α_2 -antiplasmin may be β -sheet C or another region that have not been identified.

Figure 8.1.
Summary of main findings



This page has been intentionally left blank.

Chapter 9:

Bibliography

This page has been intentionally left blank.

- Acharya, S.S., and Dimichele, D.M. (2008). Rare inherited disorders of fibrinogen. *Haemophilia* 14, 1151-1158.
- Aihara, K., Azuma, H., Akaike, M., Ikeda, Y., Sata, M., Takamori, N., Yagi, S., Iwase, T., Sumitomo, Y., Kawano, H., *et al.* (2007). Strain-dependent embryonic lethality and exaggerated vascular remodeling in heparin cofactor II-deficient mice. *The Journal of clinical investigation* 117, 1514-1526.
- Alessi, M.C., Declerck, P.J., De Mol, M., Nelles, L., and Collen, D. (1988). Purification and characterization of natural and recombinant human plasminogen activator inhibitor-1 (PAI-1). *European journal of biochemistry / FEBS* 175, 531-540.
- Aoki, N., Saito, H., Kamiya, T., Koie, K., Sakata, Y., and Kobakura, M. (1979). Congenital deficiency of alpha 2-plasmin inhibitor associated with severe hemorrhagic tendency. *The Journal of clinical investigation* 63, 877-884.
- Appella, E., Robinson, E.A., Ullrich, S.J., Stoppelli, M.P., Corti, A., Cassani, G., and Blasi, F. (1987). The receptor-binding sequence of urokinase. A biological function for the growth-factor module of proteases. *The Journal of biological chemistry* 262, 4437-4440.
- Armstrong, P.B., and Quigley, J.P. (1999). α 2-macroglobulin: an evolutionarily conserved arm of the innate immune system. *Developmental & Comparative Immunology* 23, 375-390.
- Askew, D.J., Cataltepe, S., Kumar, V., Edwards, C., Pace, S.M., Howarth, R.N., Pak, S.C., Askew, Y.S., Bromme, D., Luke, C.J., *et al.* (2007). SERPINB11 is a new noninhibitory intracellular serpin. Common single nucleotide polymorphisms in the scaffold impair conformational change. *The Journal of biological chemistry* 282, 24948-24960.
- Askew, Y.S., Pak, S.C., Luke, C.J., Askew, D.J., Cataltepe, S., Mills, D.R., Kato, H., Lehoczky, J., Dewar, K., Birren, B., *et al.* (2001). SERPINB12 is a novel member of the human ov-serpin family that is widely expressed and inhibits trypsin-like serine proteinases. *The Journal of biological chemistry* 276, 49320-49330.
- Aulak, K.S., Donaldson, V.H., Coutinho, M., and Davis, A.E., 3rd (1993). C1-inhibitor: structure/function and biologic role. *Behring Institute Mitteilungen*, 204-213.
- Baglin, T.P., Carrell, R.W., Church, F.C., Esmo, C.T., and Huntington, J.A. (2002). Crystal structures of native and thrombin-complexed heparin cofactor II reveal a multistep allosteric mechanism. *Proceedings of the National Academy of Sciences of the United States of America* 99, 11079-11084.
- Bajzar, L., Morser, J., and Nesheim, M. (1996). TAFI, or plasma procarboxypeptidase B, couples the coagulation and fibrinolytic cascades through the thrombin-thrombomodulin complex. *The Journal of biological chemistry* 271, 16603-16608.
- Bangert, K., Johnsen, A.H., Christensen, U., and Thorsen, S. (1993). Different N-terminal forms of alpha 2-plasmin inhibitor in human plasma. *The Biochemical journal* 291 (Pt 2), 623-625.
- Banyai, L., and Patthy, L. (1984). Importance of intramolecular interactions in the control of the fibrin affinity and activation of human plasminogen. *The Journal of biological chemistry* 259, 6466-6471.
- Bartalena, L., Farsetti, A., Flink, I.L., and Robbins, J. (1992). Effects of interleukin-6 on the expression of thyroid hormone-binding protein genes in cultured human hepatoblastoma-derived (Hep G2) cells. *Molecular endocrinology (Baltimore, Md)* 6, 935-942.
- Baumann, U., Huber, R., Bode, W., Grosse, D., Lesjak, M., and Laurell, C.B. (1991). Crystal structure of cleaved human alpha 1-antichymotrypsin at 2.7 Å resolution and its comparison with other serpins. *J Mol Biol* 218, 595-606.
- Beinrohr, L., Harmat, V., Dobó, J., Lőrincz, Z., Gál, P., and Závodszky, P. (2007). C1 Inhibitor Serpin Domain Structure Reveals the Likely Mechanism of Heparin Potentiation and Conformational Disease. *J Biol Chem* 282, 21100-21109.

Belorgey, D., Crowther, D.C., Mahadeva, R., and Lomas, D.A. (2002). Mutant Neuroserpin (S49P) that causes familial encephalopathy with neuroserpin inclusion bodies is a poor proteinase inhibitor and readily forms polymers in vitro. *The Journal of biological chemistry* 277, 17367-17373.

Belorgey, D., Sharp, L.K., Crowther, D.C., Onda, M., Johansson, J., and Lomas, D.A. (2004). Neuroserpin Portland (Ser52Arg) is trapped as an inactive intermediate that rapidly forms polymers: implications for the epilepsy seen in the dementia FENIB. *European journal of biochemistry / FEBS* 271, 3360-3367.

Belzar, K.J., Zhou, A., Carrell, R.W., Gettins, P.G., and Huntington, J.A. (2002). Helix D elongation and allosteric activation of antithrombin. *The Journal of biological chemistry* 277, 8551-8558.

Benarafa, C., Priebe, G.P., and Remold-O'Donnell, E. (2007). The neutrophil serine protease inhibitor serpinb1 preserves lung defense functions in *Pseudomonas aeruginosa* infection. *The Journal of experimental medicine* 204, 1901-1909.

Bennion, B.J., and Daggett, V. (2003). The molecular basis for the chemical denaturation of proteins by urea. *Proceedings of the National Academy of Sciences of the United States of America* 100, 5142-5147.

Bernik, M.B., and Kwaan, H.C. (1969). Plasminogen activator activity in cultures from human tissues. An immunological and histochemical study. *The Journal of clinical investigation* 48, 1740-1753.

Bjork, I., and Olson, S.T. (1997). Antithrombin. A bloody important serpin. *Advances in experimental medicine and biology* 425, 17-33.

Blomback, B., Hessel, B., and Hogg, D. (1976). Disulfide bridges in nh2 -terminal part of human fibrinogen. *Thrombosis research* 8, 639-658.

Blomback, B., Hessel, B., Hogg, D., and Therkildsen, L. (1978). A two-step fibrinogen--fibrin transition in blood coagulation. *Nature* 275, 501-505.

Blow, D.M., Birktoft, J.J., and Hartley, B.S. (1969). Role of a buried acid group in the mechanism of action of chymotrypsin. *Nature* 221, 337-340.

Boffa, M.B., Wang, W., Bajzar, L., and Nesheim, M.E. (1998). Plasma and recombinant thrombin-activable fibrinolysis inhibitor (TAFI) and activated TAFI compared with respect to glycosylation, thrombin/thrombomodulin-dependent activation, thermal stability, and enzymatic properties. *The Journal of biological chemistry* 273, 2127-2135.

Borders, C.L., Broadwater, J.A., Bekeny, P.A., Salmon, J.E., Lee, A.S., Eldridge, A.M., and Pett, V.B. (1994). A structural role for arginine in proteins: Multiple hydrogen bonds to backbone carbonyl oxygens. *Protein Sci* 3, 541-548.

Bornikova, L., Peyvandi, F., Allen, G., Bernstein, J., and Manco-Johnson, M.J. (2011). Fibrinogen replacement therapy for congenital fibrinogen deficiency. *Journal of Thrombosis and Haemostasis* 9, 1687-1704.

Borth, W. (1992). Alpha 2-macroglobulin, a multifunctional binding protein with targeting characteristics. *The FASEB Journal* 6, 3345-3353.

Bosma, P.J., Rijken, D.C., and Nieuwenhuizen, W. (1988). Binding of tissue-type plasminogen activator to fibrinogen fragments. *European journal of biochemistry / FEBS* 172, 399-404.

Bouma, B.N., Marx, P.F., Mosnier, L.O., and Meijers, J.C.M. (2001). Thrombin-Activatable Fibrinolysis Inhibitor (TAFI, Plasma Procarboxypeptidase B, Procarboxypeptidase R, Procarboxypeptidase U). *Thrombosis research* 101, 329-354.

Boyles, P.W., Meyer, W.H., Graff, J., Ashley, C.C., and Ripic, R.G. (1960). Comparative effectiveness of intravenous and intra-arterial fibrinolysin therapy. *The American journal of cardiology* 6, 439-446.

Brandt, J.T. (2002). Plasminogen and tissue-type plasminogen activator deficiency as risk factors for thromboembolic disease. *Archives of pathology & laboratory medicine* 126, 1376-1381.

- Brockway, W.J., and Castellino, F.J. (1972). Measurement of the binding of antifibrinolytic amino acids to various plasminogens. *Arch Biochem Biophys* 151, 194-199.
- Burgin, J., and Schaller, J. (1999). Expression, isolation and characterization of a mutated human plasminogen kringle 3 with a functional lysine binding site. *Cellular and molecular life sciences : CMLS* 55, 135-141.
- Caffrey, D.R., Dana, P.H., Mathur, V., Ocano, M., Hong, E.J., Wang, Y.E., Somaroo, S., Caffrey, B.E., Potluri, S., and Huang, E.S. (2007). PFAAT version 2.0: a tool for editing, annotating, and analyzing multiple sequence alignments. *BMC bioinformatics* 8, 381.
- Carmeliet, P., Schoonjans, L., Kieckens, L., Ream, B., Degen, J., Bronson, R., De Vos, R., van den Oord, J.J., Collen, D., and Mulligan, R.C. (1994). Physiological consequences of loss of plasminogen activator gene function in mice. *Nature* 368, 419-424.
- Carrell, R.W., Stein, P.E., Fermi, G., and Wardell, M.R. (1994). Biological implications of a 3 A structure of dimeric antithrombin. *Structure (London, England : 1993)* 2, 257-270.
- Castellino, F.J., and Ploplis, V.A. (2005). Structure and function of the plasminogen/plasmin system. *Thrombosis and haemostasis* 93, 647-654.
- Castellino, F.J., and Powell, J.R. (1981). [29] Human plasminogen. In *Methods Enzymol*, L. Laszlo, ed. (Academic Press), pp. 365-378.
- Casu, B., Oreste, P., Torri, G., Zoppetti, G., Choay, J., Lormeau, J.C., Petitou, M., and Sinay, P. (1981). The structure of heparin oligosaccharide fragments with high anti-(factor Xa) activity containing the minimal antithrombin III-binding sequence. *Chemical and 13C nuclear-magnetic-resonance studies. The Biochemical journal* 197, 599-609.
- Cesarman-Maus, G., and Hajjar, K.A. (2005). Molecular mechanisms of fibrinolysis. *British journal of haematology* 129, 307-321.
- Chakravarthi, S., Jessop, C.E., and Bulleid, N.J. (2006). The role of glutathione in disulphide bond formation and endoplasmic-reticulum-generated oxidative stress. *EMBO reports* 7, 271-275.
- Chang, W.S., and Lomas, D.A. (1998). Latent alpha1-antichymotrypsin. A molecular explanation for the inactivation of alpha1-antichymotrypsin in chronic bronchitis and emphysema. *The Journal of biological chemistry* 273, 3695-3701.
- Chang, W.S., Whisstock, J., Hopkins, P.C., Lesk, A.M., Carrell, R.W., and Wardell, M.R. (1997). Importance of the release of strand 1C to the polymerization mechanism of inhibitory serpins. *Protein science : a publication of the Protein Society* 6, 89-98.
- Chao, J., Schmaier, A., Chen, L.M., Yang, Z., and Chao, L. (1996). Kallistatin, a novel human tissue kallikrein inhibitor: levels in body fluids, blood cells, and tissues in health and disease. *The Journal of laboratory and clinical medicine* 127, 612-620.
- Chen, R. (2012). Bacterial expression systems for recombinant protein production: E. coli and beyond. *Biotechnol Adv* 30, 1102-1107.
- Cheret, J., Lebonvallet, N., Misery, L., and Le Gall-Ianotto, C. (2012). Expression of neuroserpin, a selective inhibitor of tissue-type plasminogen activator in the human skin. *Experimental dermatology* 21, 710-711.
- Christen, M.T., Frank, P., Schaller, J., and Llinas, M. (2010). Human plasminogen kringle 3: solution structure, functional insights, phylogenetic landscape. *Biochemistry* 49, 7131-7150.
- Christensen, S., Valnickova, Z., Thogersen, I.B., Olsen, E.H., and Enghild, J.J. (1997). Assignment of a single disulphide bridge in human alpha2-antiplasmin: implications for the structural and functional properties. *The Biochemical journal* 323 (Pt 3), 847-852.

Christensen, U., Bangert, K., and Thorsen, S. (1996). Reaction of human α 2-antiplasmin and plasmin Stopped-flow fluorescence kinetics. *FEBS Lett* 387, 58-62.

Christiansen, H.E., Schwarze, U., Pyott, S.M., AlSwaid, A., Al Balwi, M., Alrasheed, S., Pepin, M.G., Weis, M.A., Eyre, D.R., and Byers, P.H. (2010). Homozygosity for a missense mutation in SERPINH1, which encodes the collagen chaperone protein HSP47, results in severe recessive osteogenesis imperfecta. *American journal of human genetics* 86, 389-398.

Clark, E.D. (2001). Protein refolding for industrial processes. *Curr Opin Biotechnol* 12, 202-207.

Clemmensen, I., Thorsen, S., Mullertz, S., and Petersen, L.C. (1981). Properties of three different molecular forms of the alpha 2 plasmin inhibitor. *European journal of biochemistry / FEBS* 120, 105-112.

Colucci, M., and Semeraro, N. (2012). Thrombin activatable fibrinolysis inhibitor: At the nexus of fibrinolysis and inflammation. *Thrombosis research* 129, 314-319.

Connolly, B.M., Choi, E.Y., Gardsvoll, H., Bey, A.L., Currie, B.M., Chavakis, T., Liu, S., Molinolo, A., Ploug, M., Leppla, S.H., *et al.* (2010). Selective abrogation of the uPA-uPAR interaction in vivo reveals a novel role in suppression of fibrin-associated inflammation. *Blood* 116, 1593-1603.

Corral, J., Gonzalez-Conejero, R., Soria, J.M., Gonzalez-Porrás, J.R., Perez-Ceballos, E., Lecumberri, R., Roldan, V., Souto, J.C., Minano, A., Hernandez-Espinosa, D., *et al.* (2006). A nonsense polymorphism in the protein Z-dependent protease inhibitor increases the risk for venous thrombosis. *Blood* 108, 177-183.

Coughlin, P.B. (2005). Antiplasmin. *FEBS Journal* 272, 4852-4857.

Coutelier, M., Andries, S., Ghariani, S., Dan, B., Duyckaerts, C., van Rijckevorsel, K., Raftopoulos, C., Deconinck, N., Sonderegger, P., Scaravilli, F., *et al.* (2008). Neuroserpin mutation causes electrical status epilepticus of slow-wave sleep. *Neurology* 71, 64-66.

Coutinho, M., Aulak, K.S., and Davis, A.E. (1994). Functional analysis of the serpin domain of C1 inhibitor. *The Journal of Immunology* 153, 3648-3654.

Creemers, E., Cleutjens, J., Smits, J., Heymans, S., Moons, L., Collen, D., Daemen, M., and Carmeliet, P. (2000). Disruption of the plasminogen gene in mice abolishes wound healing after myocardial infarction. *The American journal of pathology* 156, 1865-1873.

Crumrine, R., Marder, V., Taylor, G., LaManna, J., Tsipis, C., Novokhatny, V., Scuderi, P., Petteway, S., and Arora, V. (2012). Safety evaluation of a recombinant plasmin derivative lacking kringle 2-5 and rt-PA in a rat model of transient ischemic stroke. *Experimental & Translational Stroke Medicine* 4, 10.

Dafforn, T.R., Mahadeva, R., Elliott, P.R., Sivasothy, P., and Lomas, D.A. (1999). A kinetic mechanism for the polymerization of alpha1-antitrypsin. *The Journal of biological chemistry* 274, 9548-9555.

Dahlen, J.R., Jean, F., Thomas, G., Foster, D.C., and Kisiel, W. (1998). Inhibition of soluble recombinant furin by human proteinase inhibitor 8. *The Journal of biological chemistry* 273, 1851-1854.

Davis, R.L., Shrimpton, A.E., Carrell, R.W., Lomas, D.A., Gerhard, L., Baumann, B., Lawrence, D.A., Yepes, M., Kim, T.S., Ghetti, B., *et al.* (2002). Association between conformational mutations in neuroserpin and onset and severity of dementia. *Lancet* 359, 2242-2247.

de Giorgio-Miller, A., Bottoms, S., Laurent, G., Carmeliet, P., and Herrick, S. (2005). Fibrin-induced skin fibrosis in mice deficient in tissue plasminogen activator. *The American journal of pathology* 167, 721-732.

de Koning, P.J., Bovenschen, N., Leusink, F.K., Broekhuizen, R., Quadir, R., van Gemert, J.T., Hordijk, G.J., Chang, W.S., van der Tweel, I., Tilanus, M.G., *et al.* (2009). Downregulation of SERPINB13 expression in head and neck squamous cell carcinomas associates with poor clinical outcome. *International journal of cancer Journal international du cancer* 125, 1542-1550.

Declerck, P.J. (2011). Thrombin activatable fibrinolysis inhibitor. *Hamostaseologie* 31, 165-166, 168-173.

- Dementiev, A., Simonovic, M., Volz, K., and Gettins, P.G. (2003). Canonical inhibitor-like interactions explain reactivity of alpha1-proteinase inhibitor Pittsburgh and antithrombin with proteinases. *The Journal of biological chemistry* 278, 37881-37887.
- Di Cera, E. (2009). Serine proteases. *IUBMB life* 61, 510-515.
- Doll, J.A., Stellmach, V.M., Bouck, N.P., Bergh, A.R., Lee, C., Abramson, L.P., Cornwell, M.L., Pins, M.R., Borensztajn, J., and Crawford, S.E. (2003). Pigment epithelium-derived factor regulates the vasculature and mass of the prostate and pancreas. *Nature medicine* 9, 774-780.
- Dommke, C., Turschner, O., Stassen, J.M., Van de Werf, F., Lijnen, H.R., and Verhamme, P. (2010). Thrombolytic efficacy of recombinant human microplasmin in a canine model of copper coil-induced coronary artery thrombosis. *Journal of thrombosis and thrombolysis* 30, 46-54.
- Donnan, G.A., Davis, S.M., Parsons, M.W., Ma, H., Dewey, H.M., and Howells, D.W. (2011). How to make better use of thrombolytic therapy in acute ischemic stroke. *Nat Rev Neurol* 7, 400-409.
- Doolittle, R.F. (1984). Fibrinogen and Fibrin. *Annu Rev Biochem* 53, 195-229.
- Doolittle, R.F. (2003). Structural basis of the fibrinogen–fibrin transformation: contributions from X-ray crystallography. *Blood Reviews* 17, 33-41.
- Doolittle, R.F., and Kollman, J.M. (2006). Natively unfolded regions of the vertebrate fibrinogen molecule. *Proteins: Structure, Function, and Bioinformatics* 63, 391-397.
- Dougherty, K.M., Pearson, J.M., Yang, A.Y., Westrick, R.J., Baker, M.S., and Ginsburg, D. (1999). The plasminogen activator inhibitor-2 gene is not required for normal murine development or survival. *Proceedings of the National Academy of Sciences of the United States of America* 96, 686-691.
- Ekici, O.D., Paetzel, M., and Dalbey, R.E. (2008). Unconventional serine proteases: variations on the catalytic Ser/His/Asp triad configuration. *Protein science : a publication of the Protein Society* 17, 2023-2037.
- Elliott, P.R., Lomas, D.A., Carrell, R.W., and Abrahams, J.P. (1996). Inhibitory conformation of the reactive loop of alpha 1-antitrypsin. *Nature structural biology* 3, 676-681.
- Ennis, S., Jomary, C., Mullins, R., Cree, A., Chen, X., Macleod, A., Jones, S., Collins, A., Stone, E., and Lotery, A. (2008). Association between the SERPING1 gene and age-related macular degeneration: a two-stage case-control study. *Lancet* 372, 1828-1834.
- Eriksson, S., Carlson, J., and Velez, R. (1986). Risk of cirrhosis and primary liver cancer in alpha 1-antitrypsin deficiency. *The New England journal of medicine* 314, 736-739.
- Favier, R., Aoki, N., and De Moerloose, P. (2001). Congenital α 2-plasmin inhibitor deficiencies: a review. *British journal of haematology* 114, 4-10.
- Fay, W.P., Parker, A.C., Condrey, L.R., and Shapiro, A.D. (1997). Human Plasminogen Activator Inhibitor-1 (PAI-1) Deficiency: Characterization of a Large Kindred With a Null Mutation in the PAI-1 Gene. *Blood* 90, 204-208.
- Fay, W.P., Shapiro, A.D., Shih, J.L., Schleef, R.R., and Ginsburg, D. (1992). Brief report: complete deficiency of plasminogen-activator inhibitor type 1 due to a frame-shift mutation. *The New England journal of medicine* 327, 1729-1733.
- Forsgren, M., Raden, B., Israelsson, M., Larsson, K., and Heden, L.O. (1987). Molecular cloning and characterization of a full-length cDNA clone for human plasminogen. *FEBS Lett* 213, 254-260.
- Fowler, W.E., Hantgan, R.R., Hermans, J., and Erickson, H.P. (1981). Structure of the fibrin protofibril. *Proceedings of the National Academy of Sciences of the United States of America* 78, 4872-4876.
- Frank, P.S., Douglas, J.T., Locher, M., Llinás, M., and Schaller, J. (2003). Structural/Functional Characterization of the α 2-Plasmin Inhibitor C-Terminal Peptide†. *Biochemistry* 42, 1078-1085.

Fredenburgh, J.C., and Nesheim, M.E. (1992). Lys-plasminogen is a significant intermediate in the activation of Glu-plasminogen during fibrinolysis in vitro. *The Journal of biological chemistry* 267, 26150-26156.

Freer, S.T., Kraut, J., Robertus, J.D., Wright, H.T., and Nguyen Huu, X. (1970). Chymotrypsinogen: 2,5-Å crystal structure, comparison with α -chymotrypsin, and implications for zymogen activation. *Biochemistry* 9, 1997-2009.

Fulton, K.F., Buckle, A.M., Cabrita, L.D., Irving, J.A., Butcher, R.E., Smith, I., Reeve, S., Lesk, A.M., Bottomley, S.P., Rossjohn, J., *et al.* (2005). The High Resolution Crystal Structure of a Native Thermostable Serpin Reveals the Complex Mechanism Underpinning the Stressed to Relaxed Transition. *J Biol Chem* 280, 8435-8442.

Gaffney, P.J. (2001). Fibrin Degradation Products. *Ann NY Acad Sci* 936, 594-610.

Geiger, M. (2007). Protein C inhibitor, a serpin with functions in- and outside vascular biology. *Thrombosis and haemostasis* 97, 343-347.

Genton, C., Kruithof, E.K., and Schleuning, W.D. (1987). Phorbol ester induces the biosynthesis of glycosylated and nonglycosylated plasminogen activator inhibitor 2 in high excess over urokinase-type plasminogen activator in human U-937 lymphoma cells. *The Journal of cell biology* 104, 705-712.

Gerber, S., Lejon, S., Locher, M., and Schaller, J. (2010). The human α 2-plasmin inhibitor: functional characterization of the unique plasmin(ogen)-binding region. *Cell Mol Life Sci* 67, 1505-1518.

Gettins, P.G. (2002). Serpin structure, mechanism, and function. *Chem Rev* 102, 4751-4804.

Gettins, P.G.W., and Olson, S.T. (2009). Exosite Determinants of Serpin Specificity. *J Biol Chem* 284, 20441-20445.

Gils, A., and Declerck, P.J. (2004). Plasminogen activator inhibitor-1. *Current medicinal chemistry* 11, 2323-2334.

Gonzalez-Gronow, M., Edelberg, J.M., and Pizzo, S.V. (1989). Further characterization of the cellular plasminogen binding site: evidence that plasminogen 2 and lipoprotein a compete for the same site. *Biochemistry* 28, 2374-2377.

Gonzalez-Gronow, M., Gawdi, G., and Pizzo, S.V. (2002). Tissue factor is the receptor for plasminogen type 1 on 1-LN human prostate cancer cells. *Blood* 99, 4562-4567.

Gonzalez-Gronow, M., Grenett, H.E., Weber, M.R., Gawdi, G., and Pizzo, S.V. (2001). Interaction of plasminogen with dipeptidyl peptidase IV initiates a signal transduction mechanism which regulates expression of matrix metalloproteinase-9 by prostate cancer cells. *The Biochemical journal* 355, 397-407.

Gooptu, B., Hazes, B., Chang, W.S., Dafforn, T.R., Carrell, R.W., Read, R.J., and Lomas, D.A. (2000). Inactive conformation of the serpin α (1)-antichymotrypsin indicates two-stage insertion of the reactive loop: implications for inhibitory function and conformational disease. *Proceedings of the National Academy of Sciences of the United States of America* 97, 67-72.

Gooptu, B., and Lomas, D.A. (2009). Conformational pathology of the serpins: themes, variations, and therapeutic strategies. *Annu Rev Biochem* 78, 147-176.

Gorkun, O.V., Veklich, Y.I., Medved, L.V., Henschen, A.H., and Weisel, J.W. (1994). Role of the alpha C domains of fibrin in clot formation. *Biochemistry* 33, 6986-6997.

Goulet, B., Chan, G., Chambers, A.F., and Lewis, J.D. (2012). An emerging role for the nuclear localization of maspin in the suppression of tumor progression and metastasis. *Biochemistry and cell biology = Biochimie et biologie cellulaire* 90, 22-38.

Goulet, B., Kennette, W., Ablack, A., Postenka, C.O., Hague, M.N., Mymryk, J.S., Tuck, A.B., Giguere, V., Chambers, A.F., and Lewis, J.D. (2011). Nuclear localization of maspin is essential for its inhibition of

- tumor growth and metastasis. *Laboratory investigation; a journal of technical methods and pathology* 91, 1181-1187.
- Grailhe, P., Nieuwenhuizen, W., and Angles-Cano, E. (1994). Study of tissue-type plasminogen activator binding sites on fibrin using distinct fragments of fibrinogen. *European journal of biochemistry / FEBS* 219, 961-967.
- Griffith, M.J., Carraway, T., White, G.C., and Dombrose, F.A. (1983). Heparin cofactor activities in a family with hereditary antithrombin III deficiency: evidence for a second heparin cofactor in human plasma. *Blood* 61, 111-118.
- Griffith, M.J., Noyes, C.M., Tyndall, J.A., and Church, F.C. (1985). Structural evidence for leucine at the reactive site of heparin cofactor II. *Biochemistry* 24, 6777-6782.
- Gunzler, W.A., Steffens, G.J., Otting, F., Kim, S.M., Frankus, E., and Flohe, L. (1982). The primary structure of high molecular mass urokinase from human urine. The complete amino acid sequence of the A chain. *Hoppe Seylers Z Physiol Chem* 363, 1155-1165.
- Hacke, W., Albers, G., Al-Rawi, Y., Bogousslavsky, J., Davalos, A., Eliasziw, M., Fischer, M., Furlan, A., Kaste, M., Lees, K.R., *et al.* (2005). The Desmoteplase in Acute Ischemic Stroke Trial (DIAS): a phase II MRI-based 9-hour window acute stroke thrombolysis trial with intravenous desmoteplase. *Stroke; a journal of cerebral circulation* 36, 66-73.
- Han, J., Baik, N., Kim, K.-H., Yang, J.-M., Han, G.W., Gong, Y., Jardí, M., Castellino, F.J., Felez, J., Parmer, R.J., *et al.* (2011). Monoclonal antibodies detect receptor-induced binding sites in Glu-plasminogen. *Blood* 118, 1653-1662.
- Han, M.H., Hwang, S.I., Roy, D.B., Lundgren, D.H., Price, J.V., Ousman, S.S., Fernald, G.H., Gerlitz, B., Robinson, W.H., Baranzini, S.E., *et al.* (2008). Proteomic analysis of active multiple sclerosis lesions reveals therapeutic targets. *Nature* 451, 1076-1081.
- Han, X., Fiehler, R., and Broze, G.J., Jr. (2000). Characterization of the protein Z-dependent protease inhibitor. *Blood* 96, 3049-3055.
- Hansen, A.P., Petros, A.M., Meadows, R.P., Nettesheim, D.G., Mazar, A.P., Olejniczak, E.T., Xu, R.X., Pederson, T.M., Henkin, J., and Fesik, S.W. (1994). Solution structure of the amino-terminal fragment of urokinase-type plasminogen activator. *Biochemistry* 33, 4847-4864.
- Harrop, S.J., Jankova, L., Coles, M., Jardine, D., Whittaker, J.S., Gould, A.R., Meister, A., King, G.C., Mabbutt, B.C., and Curmi, P.M.G. (1999). The crystal structure of plasminogen activator inhibitor 2 at 2.0 Å resolution: implications for serpin function. *Structure (London, England : 1993)* 7, 43-54.
- Hastings, G.A., Coleman, T.A., Haudenschild, C.C., Stefansson, S., Smith, E.P., Barthlow, R., Cherry, S., Sandkvist, M., and Lawrence, D.A. (1997). Neuroserpin, a Brain-associated Inhibitor of Tissue Plasminogen Activator Is Localized Primarily in Neurons: Implications for the regulation of motor learning and neuronal survival. *J Biol Chem* 272, 33062-33067.
- Hayes, M.L., and Castellino, F.J. (1979a). Carbohydrate of the human plasminogen variants. II. Structure of the asparagine-linked oligosaccharide unit. *The Journal of biological chemistry* 254, 8772-8776.
- Hayes, M.L., and Castellino, F.J. (1979b). Carbohydrate of the human plasminogen variants. III. Structure of the O-glycosidically linked oligosaccharide unit. *The Journal of biological chemistry* 254, 8777-8780.
- Hayes, M.L., and Castellino, J.F. (1979c). Carbohydrate of the human plasminogen variants. I. Carbohydrate composition, glycopeptide isolation, and characterization. *The Journal of biological chemistry* 254, 8768-8771.
- Hazell, A.S. (2007). Excitotoxic mechanisms in stroke: An update of concepts and treatment strategies. *Neurochemistry International* 50, 941-953.
- Hedstrom, L. (2002a). An overview of serine proteases. *Current protocols in protein science / editorial board, John E Coligan [et al] Chapter 21, Unit 21 10.*

Hedstrom, L. (2002b). Serine protease mechanism and specificity. *Chem Rev* 102, 4501-4524.

Hida, K., Wada, J., Eguchi, J., Zhang, H., Baba, M., Seida, A., Hashimoto, I., Okada, T., Yasuhara, A., Nakatsuka, A., *et al.* (2005). Visceral adipose tissue-derived serine protease inhibitor: a unique insulin-sensitizing adipocytokine in obesity. *Proceedings of the National Academy of Sciences of the United States of America* 102, 10610-10615.

Hirayoshi, K., Kudo, H., Takechi, H., Nakai, A., Iwamatsu, A., Yamada, K.M., and Nagata, K. (1991). HSP47: a tissue-specific, transformation-sensitive, collagen-binding heat shock protein of chicken embryo fibroblasts. *Molecular and cellular biology* 11, 4036-4044.

Hirosawa, S., Nakamura, Y., Miura, O., Sumi, Y., and Aoki, N. (1988). Organization of the human alpha 2-plasmin inhibitor gene. *Proceedings of the National Academy of Sciences of the United States of America* 85, 6836-6840.

Hoeprich, P.D., Jr., and Doolittle, R.F. (1983). Dimeric half-molecules of human fibrinogen are joined through disulfide bonds in an antiparallel orientation. *Biochemistry* 22, 2049-2055.

Holmes, W.E., Lijnen, H.R., Nelles, L., Kluft, C., Nieuwenhuis, H.K., Rijken, D.C., and Collen, D. (1987a). Alpha 2-antiplasmin Enschede: alanine insertion and abolition of plasmin inhibitory activity. *Science* 238, 209-211.

Holmes, W.E., Nelles, L., Lijnen, H.R., and Collen, D. (1987b). Primary structure of human alpha 2-antiplasmin, a serine protease inhibitor (serpin). *The Journal of biological chemistry* 262, 1659-1664.

Homan, E.P., Rauch, F., Grafe, I., Lietman, C., Doll, J.A., Dawson, B., Bertin, T., Napierala, D., Morello, R., Gibbs, R., *et al.* (2011). Mutations in SERPINF1 cause osteogenesis imperfecta type VI. *Journal of bone and mineral research : the official journal of the American Society for Bone and Mineral Research* 26, 2798-2803.

Hortin, G.L., Gibson, B.L., and Fok, K.F. (1988). α 2-antiplasmin's carboxy-terminal lysine residue is a major site of interaction with plasmin. *Biochem Biophys Res Commun* 155, 591-596.

Horvath, A.J., Lu, B.G.C., Pike, R.N., and Bottomley, S.P. (2011). Chapter Eleven - Methods to Measure the Kinetics of Protease Inhibition by Serpins. In *Methods Enzymol*, C.W. James, and I.B. Phillip, eds. (Academic Press), pp. 223-235.

Hoylaerts, M., Rijken, D.C., Lijnen, H.R., and Collen, D. (1982). Kinetics of the activation of plasminogen by human tissue plasminogen activator. Role of fibrin. *The Journal of biological chemistry* 257, 2912-2919.

Hunt, L.T., and Dayhoff, M.O. (1980). A surprising new protein superfamily containing ovalbumin, antithrombin-III, and alpha 1-proteinase inhibitor. *Biochem Biophys Res Commun* 95, 864-871.

Huntington, J.A. (2003). Mechanisms of glycosaminoglycan activation of the serpins in hemostasis. *Journal of Thrombosis and Haemostasis* 1, 1535-1549.

Huntington, J.A., Read, R.J., and Carrell, R.W. (2000). Structure of a serpin-protease complex shows inhibition by deformation. *Nature* 407, 923-926.

Hysi, P.G., Simpson, C.L., Fok, Y.K., Gerrelli, D., Webster, A.R., Bhattacharya, S.S., Hammond, C.J., Sham, P.C., and Rahi, J.S. (2012). Common polymorphisms in the SERPINI2 gene are associated with refractive error in the 1958 British Birth Cohort. *Investigative ophthalmology & visual science* 53, 440-447.

Ibarra, C.A., Blouse, G.E., Christian, T.D., and Shore, J.D. (2004). The contribution of the exosite residues of plasminogen activator inhibitor-1 to proteinase inhibition. *The Journal of biological chemistry* 279, 3643-3650.

Ichinose, A., Takio, K., and Fujikawa, K. (1986). Localization of the binding site of tissue-type plasminogen activator to fibrin. *The Journal of clinical investigation* 78, 163-169.

Ikematsu, S., Fukutake, K., and Aoki, N. (1996). Heterozygote for plasmin inhibitor deficiency developing hemorrhagic tendency with advancing age. *Thrombosis research* 82, 129-116.

- Im, H., Seo, E.J., and Yu, M.H. (1999). Metastability in the inhibitory mechanism of human alpha1-antitrypsin. *The Journal of biological chemistry* 274, 11072-11077.
- Irving, J.A., Cabrita, L.D., Rossjohn, J., Pike, R.N., Bottomley, S.P., and Whisstock, J.C. (2003). The 1.5 Å crystal structure of a prokaryote serpin: controlling conformational change in a heated environment. *Structure* (London, England : 1993) 11, 387-397.
- Irving, J.A., Pike, R.N., Lesk, A.M., and Whisstock, J.C. (2000). Phylogeny of the serpin superfamily: implications of patterns of amino acid conservation for structure and function. *Genome research* 10, 1845-1864.
- Izaguirre, G., and Olson, S.T. (2006). Residues Tyr253 and Glu255 in Strand 3 of β -Sheet C of Antithrombin Are Key Determinants of an Exosite Made Accessible by Heparin Activation to Promote Rapid Inhibition of Factors Xa and IXa. *J Biol Chem* 281, 13424-13432.
- Izaguirre, G., Zhang, W., Swanson, R., Bedsted, T., and Olson, S.T. (2003). Localization of an antithrombin exosite that promotes rapid inhibition of factors Xa and IXa dependent on heparin activation of the serpin. *The Journal of biological chemistry* 278, 51433-51440.
- Jankova, L., Harrop, S.J., Saunders, D.N., Andrews, J.L., Bertram, K.C., Gould, A.R., Baker, M.S., and Curmi, P.M. (2001). Crystal structure of the complex of plasminogen activator inhibitor 2 with a peptide mimicking the reactive center loop. *The Journal of biological chemistry* 276, 43374-43382.
- Jayakumar, A., Kang, Y., Frederick, M.J., Pak, S.C., Henderson, Y., Holton, P.R., Mitsudo, K., Silverman, G.A., AK, E.L.-N., Bromme, D., *et al.* (2003). Inhibition of the cysteine proteinases cathepsins K and L by the serpin headpin (SERPINB13): a kinetic analysis. *Arch Biochem Biophys* 409, 367-374.
- Jensen, P.E., and Sottrup-Jensen, L. (1986). Primary structure of human alpha 2-macroglobulin. Complete disulfide bridge assignment and localization of two interchain bridges in the dimeric proteinase binding unit. *The Journal of biological chemistry* 261, 15863-15869.
- Jespersen, J., Gram, J., and Astrup, T. (1986). The autodigestion of human plasmin follows a bimolecular mode of reaction subject to product inhibition. *Thrombosis research* 41, 395-404.
- Jeunemaitre, X., Gimenez-Roqueplo, A.P., Celerier, J., and Corvol, P. (1999). Angiotensinogen variants and human hypertension. *Current hypertension reports* 1, 31-41.
- Johnson, D.J.D., Li, W., Adams, T.E., and Huntington, J.A. (2006). Antithrombin-S195A factor Xa-heparin structure reveals the allosteric mechanism of antithrombin activation. *EMBO J* 25, 2029-2037.
- Kaiserman, D., Whisstock, J.C., and Bird, P.I. (2006). Mechanisms of serpin dysfunction in disease. *Expert reviews in molecular medicine* 8, 1-19.
- Karlsson, R., and Fält, A. (1997). Experimental design for kinetic analysis of protein-protein interactions with surface plasmon resonance biosensors. *Journal of Immunological Methods* 200, 121-133.
- Kasai, S., Arimura, H., Nishida, M., and Suyama, T. (1985). Primary structure of single-chain pro-urokinase. *The Journal of biological chemistry* 260, 12382-12389.
- Kimura, S., and Aoki, N. (1986). Cross-linking site in fibrinogen for alpha 2-plasmin inhibitor. *The Journal of biological chemistry* 261, 15591-15595.
- Kimura, S., Tamaki, T., and Aoki, N. (1985). Acceleration of fibrinolysis by the N-terminal peptide of alpha 2- plasmin inhibitor. *Blood* 66, 157-160.
- Klieber, M.A., Underhill, C., Hammond, G.L., and Muller, Y.A. (2007). Corticosteroid-binding globulin, a structural basis for steroid transport and proteinase-triggered release. *The Journal of biological chemistry* 282, 29594-29603.

Kluft, C., Nieuwenhuis, H.K., Rijken, D.C., Groeneveld, E., Wijngaards, G., van Berkel, W., Dooijewaard, G., and Sixma, J.J. (1987). α 2-Antiplasmin Enschede: dysfunctional α 2-antiplasmin molecule associated with an autosomal recessive hemorrhagic disorder. *The Journal of clinical investigation* 80, 1391-1400.

Koie, K., Kamiya, T., Ogata, K., and Takamatsu, J. (1978). Alpha2-plasmin-inhibitor deficiency (Miyasato disease). *Lancet* 2, 1334-1336.

Kollman, J.M., Pandi, L., Sawaya, M.R., Riley, M., and Doolittle, R.F. (2009). Crystal Structure of Human Fibrinogen. *Biochemistry* 48, 3877-3886.

Lähteenmäki, K., Edelman, S., and Korhonen, T.K. (2005). Bacterial metastasis: the host plasminogen system in bacterial invasion. *Trends in Microbiology* 13, 79-85.

Lapchak, P.A., Araujo, D.M., Pakola, S., Song, D., Wei, J., and Zivin, J.A. (2002). Microplasmin: A Novel Thrombolytic That Improves Behavioral Outcome After Embolic Strokes in Rabbits. *Stroke; a journal of cerebral circulation* 33, 2279-2284.

Laurens, N., Koolwijk, P., and De Maat, M.P.M. (2006). Fibrin structure and wound healing. *Journal of Thrombosis and Haemostasis* 4, 932-939.

Law, R.H., Caradoc-Davies, T., Cowieson, N., Horvath, A.J., Quek, A.J., Encarnacao, J.A., Steer, D., Cowan, A., Zhang, Q., Lu, B.G., *et al.* (2012). The X-ray crystal structure of full-length human plasminogen. *Cell reports* 1, 185-190.

Law, R.H., Sofian, T., Kan, W.T., Horvath, A.J., Hitchen, C.R., Langendorf, C.G., Buckle, A.M., Whisstock, J.C., and Coughlin, P.B. (2008). X-ray crystal structure of the fibrinolysis inhibitor α 2-antiplasmin. *Blood* 111, 2049-2052.

Law, R.H., Zhang, Q., McGowan, S., Buckle, A.M., Silverman, G.A., Wong, W., Rosado, C.J., Langendorf, C.G., Pike, R.N., Bird, P.I., *et al.* (2006). An overview of the serpin superfamily. *Genome biology* 7, 216.

Lawrence, D.A., Berkenpas, M.B., Palaniappan, S., and Ginsburg, D. (1994). Localization of vitronectin binding domain in plasminogen activator inhibitor-1. *The Journal of biological chemistry* 269, 15223-15228.

Lawrence, D.A., Palaniappan, S., Stefansson, S., Olson, S.T., Francis-Chmura, A.M., Shore, J.D., and Ginsburg, D. (1997). Characterization of the binding of different conformational forms of plasminogen activator inhibitor-1 to vitronectin. Implications for the regulation of pericellular proteolysis. *The Journal of biological chemistry* 272, 7676-7680.

Lecander, I., and Astedt, B. (1986). Isolation of a new specific plasminogen activator inhibitor from pregnancy plasma. *British journal of haematology* 62, 221-228.

Lee, K.N., Jackson, K.W., Christiansen, V.J., Chung, K.H., and McKee, P.A. (2004). A novel plasma proteinase potentiates α 2-antiplasmin inhibition of fibrin digestion. *Blood* 103, 3783-3788.

Lee, K.N., Jackson, K.W., Christiansen, V.J., Lee, C.S., Chun, J.G., and McKee, P.A. (2006). Antiplasmin-cleaving enzyme is a soluble form of fibroblast activation protein. *Blood* 107, 1397-1404.

Lee, K.N., Lee, C.S., Tae, W.-C., Jackson, K.W., Christiansen, V.J., and McKee, P.A. (2000). Cross-linking of Wild-type and Mutant α 2-Antiplasmins to Fibrin by Activated Factor XIII and by a Tissue Transglutaminase. *J Biol Chem* 275, 37382-37389.

Lee, K.N., Lee, C.S., Tae, W.-C., Jackson, K.W., Christiansen, V.J., and McKee, P.A. (2001). Crosslinking of α 2-Antiplasmin to Fibrin. *Ann NY Acad Sci* 936, 335-339.

Lee, K.N., Park, S.D., and Yu, M.H. (1996). Probing the native strain in α 1-antitrypsin. *Nature structural biology* 3, 497-500.

Lee, K.N., Tae, W.-C., Jackson, K.W., Kwon, S.H., and McKee, P.A. (1999). Characterization of Wild-Type and Mutant α 2-Antiplasmins: Fibrinolysis Enhancement by Reactive Site Mutant. *Blood* 94, 164-171.

- Lee, T.W., Montgomery, J.M., and Birch, N.P. (2012). The serine protease inhibitor neuroserpin regulates the growth and maturation of hippocampal neurons through a non-inhibitory mechanism. *J Neurochem* 121, 561-574.
- Lees, K.R., Bluhmki, E., von Kummer, R., Brott, T.G., Toni, D., Grotta, J.C., Albers, G.W., Kaste, M., Marler, J.R., Hamilton, S.A., *et al.* (2010). Time to treatment with intravenous alteplase and outcome in stroke: an updated pooled analysis of ECASS, ATLANTIS, NINDS, and EPITHET trials. *The Lancet* 375, 1695-1703.
- Li, X., Bokman, A.M., Llinas, M., Smith, R.A., and Dobson, C.M. (1994). Solution structure of the kringle domain from urokinase-type plasminogen activator. *J Mol Biol* 235, 1548-1559.
- Libourel, E.J., Bank, I., Meinardi, J.R., Balje -Volkers, C.P., Hamulyak, K., Middeldorp, S., Koopman, M.M., van Pampus, E.C., Prins, M.H., Buller, H.R., *et al.* (2002). Co-segregation of thrombophilic disorders in factor V Leiden carriers; the contributions of factor VIII, factor XI, thrombin activatable fibrinolysis inhibitor and lipoprotein(a) to the absolute risk of venous thromboembolism. *Haematologica* 87, 1068-1073.
- Lijnen, H.R. (2001). Elements of the fibrinolytic system. *Ann N Y Acad Sci* 936, 226-236.
- Lijnen, H.R., Holmes, W.E., van Hoef, B., Wiman, B., Rodriguez, H., and Collen, D. (1987). Amino-acid sequence of human alpha 2-antiplasmin. *European journal of biochemistry / FEBS* 166, 565-574.
- Lijnen, H.R., Okada, K., Matsuo, O., Collen, D., and Dewerchin, M. (1999). Alpha2-antiplasmin gene deficiency in mice is associated with enhanced fibrinolytic potential without overt bleeding. *Blood* 93, 2274-2281.
- Lijnen, H.R., Van Hoef, B., and Collen, D. (1981). On the role of the carbohydrate side chains of human plasminogen in its interaction with alpha 2-antiplasmin and fibrin. *European journal of biochemistry / FEBS* 120, 149-154.
- Lin, Z., Jiang, L., Yuan, C., Jensen, J.K., Zhang, X., Luo, Z., Furie, B.C., Furie, B., Andreasen, P.A., and Huang, M. (2011). Structural Basis for Recognition of Urokinase-type Plasminogen Activator by Plasminogen Activator Inhibitor-1. *J Biol Chem* 286, 7027-7032.
- Lind, B., and Thorsen, S. (1999). A novel missense mutation in the human plasmin inhibitor (alpha2-antiplasmin) gene associated with a bleeding tendency. *British journal of haematology* 107, 317-322.
- Lindahl, T.L., Sigurdardottir, O., and Wiman, B. (1989). Stability of plasminogen activator inhibitor 1 (PAI-1). *Thrombosis and haemostasis* 62, 748-751.
- Lindahl, U., Thunberg, L., Backstrom, G., and Riesenfeld, J. (1981). The antithrombin-binding sequence of heparin. *Biochem Soc Trans* 9, 499-451.
- Liu, Y., Bledsoe, G., Hagiwara, M., Shen, B., Chao, L., and Chao, J. (2012). Depletion of endogenous kallistatin exacerbates renal and cardiovascular oxidative stress, inflammation, and organ remodeling. *American journal of physiology Renal physiology* 303, F1230-1238.
- Lomas, D.A., Evans, D.L., Finch, J.T., and Carrell, R.W. (1992). The mechanism of Z alpha 1-antitrypsin accumulation in the liver. *Nature* 357, 605-607.
- Lomas, D.A., Evans, D.L., Stone, S.R., Chang, W.S., and Carrell, R.W. (1993). Effect of the Z mutation on the physical and inhibitory properties of alpha 1-antitrypsin. *Biochemistry* 32, 500-508.
- Longstaff, C., and Gaffney, P.J. (1991). Serpin-serine protease binding kinetics: .alpha.2-antiplasmin as a model inhibitor. *Biochemistry* 30, 979-986.
- Longstaff, C., Thelwell, C., Williams, S.C., Silva, M.M.C.G., Szabó, L., and Kolev, K. (2011). The interplay between tissue plasminogen activator domains and fibrin structures in the regulation of fibrinolysis: kinetic and microscopic studies. *Blood* 117, 661-668.

- Loscalzo, J. (1988). Structural and kinetic comparison of recombinant human single- and two-chain tissue plasminogen activator. *The Journal of clinical investigation* *82*, 1391-1397.
- Loskutoff, D.J., Linders, M., Keijer, J., Veerman, H., van Heerikhuizen, H., and Pannekoek, H. (1987). Structure of the human plasminogen activator inhibitor 1 gene: nonrandom distribution of introns. *Biochemistry* *26*, 3763-3768.
- Lu, B. (2008). Investigation of the Plasmin and Antiplasmin Interaction by Mutagenesis of the Antiplasmin C-terminus. Honours Thesis.
- Lu, B.G., Sofian, T., Law, R.H., Coughlin, P.B., and Horvath, A.J. (2011). Contribution of conserved lysine residues in the alpha2-antiplasmin C terminus to plasmin binding and inhibition. *The Journal of biological chemistry* *286*, 24544-24552.
- Lund-Katz, S., Nguyen, D., Dhanasekaran, P., Kono, M., Nickel, M., Saito, H., and Phillips, M.C. (2010). Surface plasmon resonance analysis of the mechanism of binding of apoA-I to high density lipoprotein particles. *J Lipid Res* *51*, 606-617.
- Ma, Z., Lu, W., Wu, S., Chen, J., Sun, Z., and Liu, J.-N. (2007). Expression and characterization of recombinant human micro-plasminogen. *Biotechnol Lett* *29*, 517-523.
- Madrazo, J., Brown, J.H., Litvinovich, S., Dominguez, R., Yakovlev, S., Medved, L., and Cohen, C. (2001). Crystal structure of the central region of bovine fibrinogen (E5 fragment) at 1.4-Å resolution. *Proceedings of the National Academy of Sciences of the United States of America* *98*, 11967-11972.
- Mannucci, P.M., Duga, S., and Peyvandi, F. (2004). Recessively inherited coagulation disorders. *Blood* *104*, 1243-1252.
- Mao, S.S., Cooper, C.M., Wood, T., Shafer, J.A., and Gardell, S.J. (1999). Characterization of plasmin-mediated activation of plasma procarboxypeptidase B. Modulation by glycosaminoglycans. *The Journal of biological chemistry* *274*, 35046-35052.
- Marder, V.J. (2008). Pre-clinical studies of plasmin: superior benefit-to-risk ratio of plasmin compared to tissue plasminogen activator. *Thrombosis research* *122 Suppl 3*, S9-S15.
- Marder, V.J. (2009). Thrombolytic therapy for deep vein thrombosis: potential application of plasmin. *Thrombosis research* *123, Supplement 4*, S56-S61.
- Marder, V.J., Jahan, R., Gruber, T., Goyal, A., and Arora, V. (2010a). Thrombolysis With Plasmin. *Stroke; a journal of cerebral circulation* *41*, S45-S49.
- Marder, V.J., Landskroner, K., Novokhatny, V., Zimmerman, T.P., Kong, M., Kanouse, J.J., and Jesmok, G. (2001). Plasmin induces local thrombolysis without causing hemorrhage: a comparison with tissue plasminogen activator in the rabbit. *Thrombosis and haemostasis* *86*, 739-745.
- Marder, V.J., Manyak, S., Gruber, T., Goyal, A., Moreno, G., Hunt, J., Bromirski, J., Scuderi, P., Petteway, S.R., Jr., and Novokhatny, V. (2010b). Haemostatic safety of a unique recombinant plasmin molecule lacking kringles 2-5. *Thrombosis and haemostasis* *104*, 780-787.
- Markus, G. (1996). Conformational changes in plasminogen, their effect on activation, and the agents that modulate activation rates — a review. *Fibrinolysis* *10*, 75-85.
- Markus, G., Evers, J.L., and Hobika, G.H. (1978). Comparison of some properties of native (Glu) and modified (Lys) human plasminogen. *The Journal of biological chemistry* *253*, 733-739.
- Marshall, J.M., Brown, A.J., and Ponting, C.P. (1994). Conformational studies of human plasminogen and plasminogen fragments: evidence for a novel third conformation of plasminogen. *Biochemistry* *33*, 3599-3606.
- Marti, D., Schaller, J., Ochensberger, B., and Rickli, E.E. (1994). Expression, purification and characterization of the recombinant kringle 2 and kringle 3 domains of human plasminogen and analysis of their binding affinity for ω -aminocarboxylic acids. *Eur J Biochem* *219*, 455-462.

- Marx, P.F., Brondijk, T.H., Plug, T., Romijn, R.A., Hemrika, W., Meijers, J.C., and Huizinga, E.G. (2008). Crystal structures of TAFI elucidate the inactivation mechanism of activated TAFI: a novel mechanism for enzyme autoregulation. *Blood* 112, 2803-2809.
- Matsuno, H. (2006). Alpha2-antiplasmin on cardiovascular diseases. *Current pharmaceutical design* 12, 841-847.
- Matsuno, H., Kozawa, O., Okada, K., Ueshima, S., Matsuo, O., and Uematsu, T. (2002). Plasmin generation plays different roles in the formation and removal of arterial and venous thrombus in mice. *Thrombosis and haemostasis* 87, 98-104.
- Matthews, B.W., Sigler, P.B., Henderson, R., and Blow, D.M. (1967). Three-dimensional structure of tosyl-alpha-chymotrypsin. *Nature* 214, 652-656.
- Matthijs, G., Devriendt, K., Cassiman, J.J., Van den Berghe, H., and Marynen, P. (1992). Structure of the human alpha-2 macroglobulin gene and its promotor. *Biochem Biophys Res Commun* 184, 596-603.
- Meagher, J.L., Olson, S.T., and Gettins, P.G. (2000). Critical role of the linker region between helix D and strand 2A in heparin activation of antithrombin. *The Journal of biological chemistry* 275, 2698-2704.
- Medved, L., and Nieuwenhuizen, W. (2003). Molecular mechanisms of initiation of fibrinolysis by fibrin. *Thrombosis and haemostasis* 89, 409-419.
- Medved, L., Weisel, J.W., On Behalf Of, F., Factor Xiii Subcommittee Of The Scientific Standardization Committee Of The International Society On, T., and Haemostasis (2009). Recommendations for nomenclature on fibrinogen and fibrin. *Journal of Thrombosis and Haemostasis* 7, 355-359.
- Medynski, D., Tuan, M., Liu, W., Wu, S., and Lin, X. (2007). Refolding, purification, and activation of miniplasminogen and microplasminogen isolated from E. coli inclusion bodies. *Protein Expression and Purification* 52, 395-402.
- Mehta, R., and Shapiro, A.D. (2008a). Plasminogen activator inhibitor type 1 deficiency. *Haemophilia* 14, 1255-1260.
- Mehta, R., and Shapiro, A.D. (2008b). Plasminogen deficiency. *Haemophilia* 14, 1261-1268.
- Melandri, G., Vagnarelli, F., Calabrese, D., Semprini, F., Nanni, S., and Branzi, A. (2009). Review of tenecteplase (TNKase) in the treatment of acute myocardial infarction. *Vascular health and risk management* 5, 249-256.
- Melchor, J.P., Pawlak, R., and Strickland, S. (2003). The tissue plasminogen activator-plasminogen proteolytic cascade accelerates amyloid-beta (Abeta) degradation and inhibits Abeta-induced neurodegeneration. *The Journal of neuroscience : the official journal of the Society for Neuroscience* 23, 8867-8871.
- Melchor, J.P., and Strickland, S. (2005). Tissue plasminogen activator in central nervous system physiology and pathology. *Thrombosis and haemostasis* 93, 655-660.
- Mikus, P., and Ny, T. (1996). Intracellular polymerization of the serpin plasminogen activator inhibitor type 2. *The Journal of biological chemistry* 271, 10048-10053.
- Mikus, P., Urano, T., Liljestrom, P., and Ny, T. (1993). Plasminogen-activator inhibitor type 2 (PAI-2) is a spontaneously polymerising SERPIN. Biochemical characterisation of the recombinant intracellular and extracellular forms. *European journal of biochemistry / FEBS* 218, 1071-1082.
- Miles, L.A., Plow, E.F., Donnelly, K.J., Hougie, C., and Griffin, J.H. (1982). A bleeding disorder due to deficiency of alpha 2-antiplasmin. *Blood* 59, 1246-1251.
- Mingers, A.M., Heimburger, N., Zeitler, P., Kreth, H.W., and Schuster, V. (1997). Homozygous type I plasminogen deficiency. *Seminars in thrombosis and hemostasis* 23, 259-269.

Miura, O., and Aoki, N. (1990). Impaired secretion of mutant alpha 2-plasmin inhibitor (alpha 2 PI-Nara) from COS-7 and HepG2 cells: molecular and cellular basis for hereditary deficiency of alpha 2-plasmin inhibitor. *Blood* 75, 1092-1096.

Miura, O., Sugahara, Y., and Aoki, N. (1989). Hereditary alpha 2-plasmin inhibitor deficiency caused by a transport-deficient mutation (alpha 2-PI-Okinawa). Deletion of Glu137 by a trinucleotide deletion blocks intracellular transport. *The Journal of biological chemistry* 264, 18213-18219.

Miyata, T., Inagi, R., Nangaku, M., Imasawa, T., Sato, M., Izuhara, Y., Suzuki, D., Yoshino, A., Onogi, H., Kimura, M., *et al.* (2002). Overexpression of the serpin megsin induces progressive mesangial cell proliferation and expansion. *The Journal of clinical investigation* 109, 585-593.

Miyata, T., Li, M., Yu, X., and Hirayama, N. (2007). Megsin gene: its genomic analysis, pathobiological functions, and therapeutic perspectives. *Current genomics* 8, 203-208.

Moroi, M., and Aoki, N. (1976). Isolation and characterization of alpha2-plasmin inhibitor from human plasma. A novel proteinase inhibitor which inhibits activator-induced clot lysis. *J Biol Chem* 251, 5956-5965.

Mosesson, M.W. (2005). Fibrinogen and fibrin structure and functions. *Journal of Thrombosis and Haemostasis* 3, 1894-1904.

Mosesson, M.W., DiOrio, J.P., Siebenlist, K.R., Wall, J.S., and Hainfeld, J.F. (1993). Evidence for a second type of fibril branch point in fibrin polymer networks, the trimolecular junction. *Blood* 82, 1517-1521.

Mosesson, M.W., Siebenlist, K.R., and Meh, D.A. (2001). The Structure and Biological Features of Fibrinogen and Fibrin. *Ann NY Acad Sci* 936, 11-30.

Mottonen, J., Strand, A., Symersky, J., Sweet, R.M., Danley, D.E., Geoghegan, K.F., Gerard, R.D., and Goldsmith, E.J. (1992). Structural basis of latency in plasminogen activator inhibitor-1. *Nature* 355, 270-273.

Murer, V., Spetz, J.F., Hengst, U., Altrogge, L.M., de Agostini, A., and Monard, D. (2001). Male fertility defects in mice lacking the serine protease inhibitor protease nexin-1. *Proceedings of the National Academy of Sciences of the United States of America* 98, 3029-3033.

Nesheim, M., Fredenburgh, J.C., and Larsen, G.R. (1990). The dissociation constants and stoichiometries of the interactions of Lys-plasminogen and chloromethyl ketone derivatives of tissue plasminogen activator and the variant delta FEIX with intact fibrin. *The Journal of biological chemistry* 265, 21541-21548.

Neurath, H., and Dixon, G.H. (1957). Structure and activation of trypsinogen and chymotrypsinogen. *Federation proceedings* 16, 791-801.

Ney, K.A., and Pizzo, S.V. (1982). Fibrinolysis and fibrinogenolysis by Val442-plasmin. *Biochim Biophys Acta* 708, 218-224.

Nobar, S.M., Guy-Crotte, O., Rabaud, M., and Bieth, J.G. (2004). Inhibition of human pancreatic proteinases by human plasma alpha2-antiplasmin and antithrombin. *Biol Chem* 385, 423-427.

Novokhatny, V. (2008). Structure and activity of plasmin and other direct thrombolytic agents. *Thrombosis research* 122, *Supplement 3*, S3-S8.

Ny, T., Elgh, F., and Lund, B. (1984). The structure of the human tissue-type plasminogen activator gene: correlation of intron and exon structures to functional and structural domains. *Proceedings of the National Academy of Sciences of the United States of America* 81, 5355-5359.

Olson, S.T., Bjork, I., Sheffer, R., Craig, P.A., Shore, J.D., and Choay, J. (1992). Role of the antithrombin-binding pentasaccharide in heparin acceleration of antithrombin-proteinase reactions. Resolution of the antithrombin conformational change contribution to heparin rate enhancement. *The Journal of biological chemistry* 267, 12528-12538.

- Olson, S.T., Bjork, I., and Shore, J.D. (1993). Kinetic characterization of heparin-catalyzed and uncatalyzed inhibition of blood coagulation proteinases by antithrombin. *Methods Enzymol* 222, 525-559.
- Olson, S.T., and Gettins, P.G.W. (2011). Chapter 5 - Regulation of Proteases by Protein Inhibitors of the Serpin Superfamily. In *Progress in Molecular Biology and Translational Science*, C. Enrico Di, ed. (Academic Press), pp. 185-240.
- Onda, M., Belorgey, D., Sharp, L.K., and Lomas, D.A. (2005). Latent S49P neuroserpin forms polymers in the dementia familial encephalopathy with neuroserpin inclusion bodies. *The Journal of biological chemistry* 280, 13735-13741.
- Osterwalder, T., Cinelli, P., Baici, A., Pennella, A., Krueger, S.R., Schrimpf, S.P., Meins, M., and Sonderegger, P. (1998). The axonally secreted serine proteinase inhibitor, neuroserpin, inhibits plasminogen activators and plasmin but not thrombin. *The Journal of biological chemistry* 273, 2312-2321.
- Ozaki, K., Nagata, M., Suzuki, M., Fujiwara, T., Miyoshi, Y., Ishikawa, O., Ohigashi, H., Imaoka, S., Takahashi, E., and Nakamura, Y. (1998). Isolation and characterization of a novel human pancreas-specific gene, pancpin, that is down-regulated in pancreatic cancer cells. *Genes, chromosomes & cancer* 22, 179-185.
- Pannekoek, H., Veerman, H., Lambers, H., Diergaarde, P., Verweij, C.L., van Zonneveld, A.J., and van Mourik, J.A. (1986). Endothelial plasminogen activator inhibitor (PAI): a new member of the Serpin gene family. *EMBO J* 5, 2539-2544.
- Parry, M.A.A. (2001). Over-Expression and Purification of Active Serine Proteases and Their Variants from *Escherichia coli* Inclusion Bodies. In *Current Protocols in Protein Science* (John Wiley & Sons, Inc.).
- Parry, M.A.A., Fernandez-Catalan, C., Bergner, A., Huber, R., Hopfner, K.-P., Schlott, B., Guhrs, K.-H., and Bode, W. (1998). The ternary microplasmin-staphylokinase-microplasmin complex is a proteinase-cofactor-substrate complex in action. *Nat Struct Mol Biol* 5, 917-923.
- Parsons, M., Spratt, N., Bivard, A., Campbell, B., Chung, K., Miteff, F., O'Brien, B., Bladin, C., McElduff, P., Allen, C., *et al.* (2012). A Randomized Trial of Tenecteplase versus Alteplase for Acute Ischemic Stroke. *New England Journal of Medicine* 366, 1099-1107.
- Paterson, M.A., Hosking, P.S., and Coughlin, P.B. (2008). Expression of the serpin centerin defines a germinal center phenotype in B-cell lymphomas. *American journal of clinical pathology* 130, 117-126.
- Pathy, L. (1993). [1] Modular design of proteases of coagulation, fibrinolysis, and complement activation: Implications for protein engineering and structure-function studies. In *Methods Enzymol*, K.G.M. Laszlo Lorand, ed. (Academic Press), pp. 10-21.
- Peisach, E., Wang, J., de los Santos, T., Reich, E., and Ringe, D. (1999). Crystal Structure of the Proenzyme Domain of Plasminogen[†],[‡]. *Biochemistry* 38, 11180-11188.
- Peltz, S.W., Hardt, T.A., and Mangel, W.F. (1982). Positive regulation of activation of plasminogen by urokinase: differences in Km for (glutamic acid)-plasminogen and lysine-plasminogen and effect of certain alpha, omega-amino acids. *Biochemistry* 21, 2798-2804.
- Pennica, D., Holmes, W.E., Kohr, W.J., Harkins, R.N., Vehar, G.A., Ward, C.A., Bennett, W.F., Yelverton, E., Seeburg, P.H., Heyneker, H.L., *et al.* (1983). Cloning and expression of human tissue-type plasminogen activator cDNA in *E. coli*. *Nature* 301, 214-221.
- Perry, D.J., and Carrell, R.W. (1996). Molecular genetics of human antithrombin deficiency. *Human mutation* 7, 7-22.
- Petersen, T.E., Martzen, M.R., Ichinose, A., and Davie, E.W. (1990). Characterization of the gene for human plasminogen, a key proenzyme in the fibrinolytic system. *The Journal of biological chemistry* 265, 6104-6111.
- Pirie-Shepherd, S.R., Jett, E.A., Andon, N.L., and Pizzo, S.V. (1995). Sialic Acid Content of Plasminogen 2 Glycoforms as a Regulator of Fibrinolytic Activity. *J Biol Chem* 270, 5877-5881.

- Ponting, C.P., Marshall, J.M., and Cederholm-Williams, S.A. (1992). Plasminogen: a structural review. *Blood coagulation & fibrinolysis : an international journal in haemostasis and thrombosis* 3, 605-614.
- Potempa, J., Shieh, B.H., and Travis, J. (1988). Alpha-2-antiplasmin: a serpin with two separate but overlapping reactive sites. *Science* 241, 699-700.
- Ranson, M., Andronicos, N.M., O'Mullane, M.J., and Baker, M.S. (1998). Increased plasminogen binding is associated with metastatic breast cancer cells: differential expression of plasminogen binding proteins. *British journal of cancer* 77, 1586-1597.
- Rathore, Y.S., Rehan, M., Pandey, K., Sahni, G., and Ashish (2012). First structural model of full-length human tissue-plasminogen activator: a SAXS data-based modeling study. *The journal of physical chemistry B* 116, 496-502.
- Rau, J.C., Beaulieu, L.M., Huntington, J.A., and Church, F.C. (2007). Serpins in thrombosis, hemostasis and fibrinolysis. *Journal of thrombosis and haemostasis : JTH* 5 Suppl 1, 102-115.
- Raum, D., Marcus, D., Alper, C.A., Levey, R., Taylor, P.D., and Starzl, T.E. (1980). Synthesis of human plasminogen by the liver. *Science* 208, 1036-1037.
- Rawlings, N.D., Barrett, A.J., and Bateman, A. (2012). MEROPS: the database of proteolytic enzymes, their substrates and inhibitors. *Nucleic Acids Res* 40, D343-350.
- Rehman, A.A., Ahsan, H., and Khan, F.H. (2012). Alpha-2-macroglobulin: A physiological guardian. *J Cell Physiol*, n/a-n/a.
- Remold-O'Donnell, E., Chin, J., and Alberts, M. (1992). Sequence and molecular characterization of human monocyte/neutrophil elastase inhibitor. *Proceedings of the National Academy of Sciences of the United States of America* 89, 5635-5639.
- Renatus, M., Engh, R.A., Stubbs, M.T., Huber, R., Fischer, S., Kohnert, U., and Bode, W. (1997). Lysine 156 promotes the anomalous proenzyme activity of tPA: X-ray crystal structure of single-chain human tPA. *EMBO J* 16, 4797-4805.
- Rezaie, A.R. (1998). Calcium enhances heparin catalysis of the antithrombin-factor Xa reaction by a template mechanism. Evidence that calcium alleviates Gla domain antagonism of heparin binding to factor Xa. *The Journal of biological chemistry* 273, 16824-16827.
- Rezaie, A.R., and Olson, S.T. (2000). Calcium enhances heparin catalysis of the antithrombin-factor Xa reaction by promoting the assembly of an intermediate heparin-antithrombin-factor Xa bridging complex. Demonstration by rapid kinetics studies. *Biochemistry* 39, 12083-12090.
- Ricagno, S., Caccia, S., Sorrentino, G., Antonini, G., and Bolognesi, M. (2009). Human neuroserpin: structure and time-dependent inhibition. *J Mol Biol* 388, 109-121.
- Riccio, A., Grimaldi, G., Verde, P., Sebastio, G., Boast, S., and Blasi, F. (1985). The human urokinase-plasminogen activator gene and its promoter. *Nucleic Acids Res* 13, 2759-2771.
- Riewald, M., Chuang, T., Neubauer, A., Riess, H., and Schleef, R.R. (1998). Expression of bomapin, a novel human serpin, in normal/malignant hematopoiesis and in the monocytic cell lines THP-1 and AML-193. *Blood* 91, 1256-1262.
- Rijken, D.C., and Lijnen, H.R. (2009). New insights into the molecular mechanisms of the fibrinolytic system. *Journal of thrombosis and haemostasis : JTH* 7, 4-13.
- Rijken, D.C., Wijngaards, G., and Welbergen, J. (1981). Immunological characterization of plasminogen activator activities in human tissues and body fluids. *The Journal of laboratory and clinical medicine* 97, 477-486.
- Rizzitelli, A., Meuter, S., Vega Ramos, J., Bird, C.H., Mintern, J.D., Mangan, M.S., Villadangos, J., and Bird, P.I. (2012). Serpinb9 (Spi6)-deficient mice are impaired in dendritic cell-mediated antigen cross-presentation. *Immunology and cell biology* 90, 916.

- Robbins, K.C., Summari, L., Hsieh, B., and Shah, R.J. (1967). The peptide chains of human plasmin. Mechanism of activation of human plasminogen to plasmin. *The Journal of biological chemistry* 242, 2333-2342.
- Rossi, V., Bally, I., Ancelet, S., Xu, Y., Frémeaux-Bacchi, V., Vivès, R.R., Sadir, R., Thielens, N., and Arlaud, G.J. (2010). Functional Characterization of the Recombinant Human C1 Inhibitor Serpin Domain: Insights into Heparin Binding. *The Journal of Immunology* 184, 4982-4989.
- Ryu, S.E., Choi, H.J., Kwon, K.S., Lee, K.N., and Yu, M.H. (1996). The native strains in the hydrophobic core and flexible reactive loop of a serine protease inhibitor: crystal structure of an uncleaved alpha1-antitrypsin at 2.7 Å. *Structure (London, England : 1993)* 4, 1181-1192.
- Saito, H., Goodnough, L.T., Knowles, B.B., and Aden, D.P. (1982). Synthesis and secretion of alpha 2-plasmin inhibitor by established human liver cell lines. *Proceedings of the National Academy of Sciences of the United States of America* 79, 5684-5687.
- Samson, A.L., Borg, R.J., Niego, B., Wong, C.H., Crack, P.J., Yongqing, T., and Medcalf, R.L. (2009). A nonfibrin macromolecular cofactor for tPA-mediated plasmin generation following cellular injury. *Blood* 114, 1937-1946.
- Samson, A.L., Knaupp, A.S., Sashindranath, M., Borg, R.J., Au, A.E., Cops, E.J., Saunders, H.M., Cody, S.H., McLean, C.A., Nowell, C.J., *et al.* (2012). Nucleocytoplasmic coagulation: an injury-induced aggregation event that disulfide crosslinks proteins and facilitates their removal by plasmin. *Cell reports* 2, 889-901.
- Sanglas, L., Arolas, J.L., Valnickova, Z., Aviles, F.X., Enghild, J.J., and Gomis-Ruth, F.X. (2010). Insights into the molecular inactivation mechanism of human activated thrombin-activatable fibrinolysis inhibitor. *Journal of thrombosis and haemostasis : JTH* 8, 1056-1065.
- Sazonova, I.Y., Thomas, B.M., Gladysheva, I.P., Houg, A.K., and Reed, G.L. (2007). Fibrinolysis is amplified by converting alpha-antiplasmin from a plasmin inhibitor to a substrate. *Journal of thrombosis and haemostasis : JTH* 5, 2087-2094.
- Schaller, J., and Gerber, S.S. (2011). The plasmin-antiplasmin system: structural and functional aspects. *Cellular and molecular life sciences : CMLS* 68, 785-801.
- Schechter, I., and Berger, A. (1967). On the size of the active site in proteases. I. Papain. *Biochem Biophys Res Commun* 27, 157-162.
- Schechter, I., and Berger, A. (1968). On the active site of proteases. III. Mapping the active site of papain; specific peptide inhibitors of papain. *Biochem Biophys Res Commun* 32, 898-902.
- Schechter, N.M., and Plotnick, M.I. (2004). Measurement of the kinetic parameters mediating protease-serpin inhibition. *Methods* 32, 159-168.
- Schick, C., Bromme, D., Bartuski, A.J., Uemura, Y., Schechter, N.M., and Silverman, G.A. (1998). The reactive site loop of the serpin SCCA1 is essential for cysteine proteinase inhibition. *Proceedings of the National Academy of Sciences of the United States of America* 95, 13465-13470.
- Schick, C., Kamachi, Y., Bartuski, A.J., Cataltepe, S., Schechter, N.M., Pemberton, P.A., and Silverman, G.A. (1997). Squamous cell carcinoma antigen 2 is a novel serpin that inhibits the chymotrypsin-like proteinases cathepsin G and mast cell chymase. *The Journal of biological chemistry* 272, 1849-1855.
- Schielen, J.G., Adams, H.P., Voskuilen, M., Tesser, G.J., and Nieuwenhuizen, W. (1991). Structural requirements of position A alpha-157 in fibrinogen for the fibrin-induced rate enhancement of the activation of plasminogen by tissue-type plasminogen activator. *The Biochemical journal* 276 (Pt 3), 655-659.
- Schrimpf, S.P., Bleiker, A.J., Brecevic, L., Kozlov, S.V., Berger, P., Osterwalder, T., Krueger, S.R., Schinzel, A., and Sonderegger, P. (1997). Human neuroserpin (PI12): cDNA cloning and chromosomal localization to 3q26. *Genomics* 40, 55-62.

Schuster, V., and Seregard, S. (2003). Ligneous conjunctivitis. *Survey of ophthalmology* 48, 369-388.

Seixas, S., Suriano, G., Carvalho, F., Seruca, R., Rocha, J., and Di Rienzo, A. (2007). Sequence diversity at the proximal 14q32.1 SERPIN subcluster: evidence for natural selection favoring the pseudogenization of SERPINA2. *Molecular biology and evolution* 24, 587-598.

Sharp, A.M., Stein, P.E., Pannu, N.S., Carrell, R.W., Berkenpas, M.B., Ginsburg, D., Lawrence, D.A., and Read, R.J. (1999). The active conformation of plasminogen activator inhibitor 1, a target for drugs to control fibrinolysis and cell adhesion. *Structure (London, England : 1993)* 7, 111-118.

Sheffield, W.P., Eltringham-Smith, L.J., Gataiance, S., and Bhakta, V. (2009). Addition of a sequence from alpha2-antiplasmin transforms human serum albumin into a blood clot component that speeds clot lysis. *BMC biotechnology* 9, 15.

Shi, G.Y., and Wu, H.L. (1988). Isolation and characterization of microplasminogen. A low molecular weight form of plasminogen. *The Journal of biological chemistry* 263, 17071-17075.

Shieh, B.H., and Travis, J. (1987). The reactive site of human alpha 2-antiplasmin. *J Biol Chem* 262, 6055-6059.

Silverman, G.A., Bird, P.I., Carrell, R.W., Church, F.C., Coughlin, P.B., Gettins, P.G.W., Irving, J.A., Lomas, D.A., Luke, C.J., Moyer, R.W., *et al.* (2001). The Serpins Are an Expanding Superfamily of Structurally Similar but Functionally Diverse Proteins: Evolution, mechanism of inhibition, novel functions, and a revised nomenclature. *J Biol Chem* 276, 33293-33296.

Silverman, G.A., Whisstock, J.C., Bottomley, S.P., Huntington, J.A., Kaiserman, D., Luke, C.J., Pak, S.C., Reichhart, J.-M., and Bird, P.I. (2010). Serpins Flex Their Muscle: I. Putting the clamps on proteolysis in diverse biological system. *J Biol Chem* 285, 24299-24305.

Simonovic, M., Gettins, P.G.W., and Volz, K. (2001). Crystal structure of human PEDF, a potent anti-angiogenic and neurite growth-promoting factor. *Proceedings of the National Academy of Sciences* 98, 11131-11135.

Sirmaci, A., Erbek, S., Price, J., Huang, M., Duman, D., Cengiz, F.B., Bademci, G., Tokgoz-Yilmaz, S., Hismi, B., Ozdag, H., *et al.* (2010). A truncating mutation in SERPINB6 is associated with autosomal-recessive nonsyndromic sensorineural hearing loss. *American journal of human genetics* 86, 797-804.

Sivaprasad, U., Askew, D.J., Ericksen, M.B., Gibson, A.M., Stier, M.T., Brandt, E.B., Bass, S.A., Daines, M.O., Chakir, J., Stringer, K.F., *et al.* (2011). A nonredundant role for mouse Serpinb3a in the induction of mucus production in asthma. *The Journal of allergy and clinical immunology* 127, 254-261, 261 e251-256.

Sofian, T. (2009). Structural and Functional Characterisation of the Serpin α_2 -Antiplasmin. PhD Thesis.

Sokalingam, S., Raghunathan, G., Soundrarajan, N., and Lee, S.-G. (2012). A Study on the Effect of Surface Lysine to Arginine Mutagenesis on Protein Stability and Structure Using Green Fluorescent Protein. *PLoS ONE* 7, e40410.

Sota, H., Hasegawa, Y., and Iwakura, M. (1998). Detection of Conformational Changes in an Immobilized Protein Using Surface Plasmon Resonance. *Anal Chem* 70, 2019-2024.

Spraggon, G., Everse, S.J., and Doolittle, R.F. (1997). Crystal structures of fragment D from human fibrinogen and its crosslinked counterpart from fibrin. *Nature* 389, 455-462.

Steffens, G.J., Gunzler, W.A., Otting, F., Frankus, E., and Flohe, L. (1982). The complete amino acid sequence of low molecular mass urokinase from human urine. *Hoppe Seylers Z Physiol Chem* 363, 1043-1058.

Stein, P.E., Leslie, A.G., Finch, J.T., Turnell, W.G., McLaughlin, P.J., and Carrell, R.W. (1990). Crystal structure of ovalbumin as a model for the reactive centre of serpins. *Nature* 347, 99-102.

Steiner, J.P., Migliorini, M., and Strickland, D.K. (1987). Characterization of the reaction of plasmin with .alpha.2-macroglobulin: effect of antifibrinolytic agents. *Biochemistry* 26, 8487-8495.

- Stout, T.J., Graham, H., Buckley, D.I., and Matthews, D.J. (2000). Structures of Active and Latent PAI-1: A Possible Stabilizing Role for Chloride Ions. *Biochemistry* 39, 8460-8469.
- Suenson, E., and Thorsen, S. (1981). Secondary-site binding of Glu-plasmin, Lys-plasmin and miniplasmin to fibrin. *The Biochemical journal* 197, 619-628.
- Sumi, Y., Ichikawa, Y., Nakamura, Y., Miura, O., and Aoki, N. (1989). Expression and characterization of pro alpha 2-plasmin inhibitor. *J Biochem* 106, 703-707.
- Summaria, L., Spitz, F., Arzadon, L., Boreisha, I.G., and Robbins, K.C. (1976). Isolation and characterization of the affinity chromatography forms of human Glu- and Lys-plasminogens and plasmins. *The Journal of biological chemistry* 251, 3693-3699.
- Sun, L.D., Cheng, H., Wang, Z.X., Zhang, A.P., Wang, P.G., Xu, J.H., Zhu, Q.X., Zhou, H.S., Ellinghaus, E., Zhang, F.R., *et al.* (2010). Association analyses identify six new psoriasis susceptibility loci in the Chinese population. *Nature genetics* 42, 1005-1009.
- Sveger, T. (1976). Liver disease in alpha1-antitrypsin deficiency detected by screening of 200,000 infants. *The New England journal of medicine* 294, 1316-1321.
- Tate, K.M., Higgins, D.L., Holmes, W.E., Winkler, M.E., Heyneker, H.L., and Vehar, G.A. (1987). Functional role of proteolytic cleavage at arginine-275 of human tissue plasminogen activator as assessed by site-directed mutagenesis. *Biochemistry* 26, 338-343.
- Taussky, P., Tawk, R.G., Daugherty, W.P., and Hanel, R.A. (2011). Medical Therapy for Ischemic Stroke: Review of Intravenous and Intra-Arterial Treatment Options. *World Neurosurgery* 76, S9-S15.
- Teshigawara, S., Wada, J., Hida, K., Nakatsuka, A., Eguchi, J., Murakami, K., Kanzaki, M., Inoue, K., Terami, T., Katayama, A., *et al.* (2012). Serum vaspin concentrations are closely related to insulin resistance, and rs77060950 at SERPINA12 genetically defines distinct group with higher serum levels in Japanese population. *The Journal of clinical endocrinology and metabolism* 97, E1202-1207.
- Thijs, V.N., Peeters, A., Vosko, M., Aichner, F., Schellinger, P.D., Schneider, D., Neumann-Haefelin, T., Rother, J., Davalos, A., Wahlgren, N., *et al.* (2009). Randomized, placebo-controlled, dose-ranging clinical trial of intravenous microplasmin in patients with acute ischemic stroke. *Stroke; a journal of cerebral circulation* 40, 3789-3795.
- Tollefsen, D.M., Pestka, C.A., and Monafu, W.J. (1983). Activation of heparin cofactor II by dermatan sulfate. *The Journal of biological chemistry* 258, 6713-6716.
- Tombran-Tink, J., Aparicio, S., Xu, X., Tink, A.R., Lara, N., Sawant, S., Barnstable, C.J., and Zhang, S.S.-M. (2005). PEDF and the serpins: Phylogeny, sequence conservation, and functional domains. *Journal of Structural Biology* 151, 130-150.
- Tordai, H., Banyai, L., and Patthy, L. (1999). The PAN module: the N-terminal domains of plasminogen and hepatocyte growth factor are homologous with the apple domains of the prekallikrein family and with a novel domain found in numerous nematode proteins. *FEBS Lett* 461, 63-67.
- Torpy, D.J., Bachmann, A.W., Gartside, M., Grice, J.E., Harris, J.M., Clifton, P., Easteal, S., Jackson, R.V., and Whitworth, J.A. (2004). Association between chronic fatigue syndrome and the corticosteroid-binding globulin gene ALA SER224 polymorphism. *Endocrine research* 30, 417-429.
- Tsai, S.P., and Drayna, D. (1992). The gene encoding human plasma carboxypeptidase B (CPB2) resides on chromosome 13. *Genomics* 14, 549-550.
- Tsurupa, G., Mahid, A., Veklich, Y., Weisel, J.W., and Medved, L. (2011). Structure, stability, and interaction of fibrin alphaC-domain polymers. *Biochemistry* 50, 8028-8037.
- Tsurupa, G., and Medved, L. (2001). Identification and characterization of novel tPA- and plasminogen-binding sites within fibrin(alpha) C-domains. *Biochemistry* 40, 801-808.

- Tsurupa, G., Tsonev, L., and Medved, L. (2002). Structural organization of the fibrin(ogen) alpha C-domain. *Biochemistry* *41*, 6449-6459.
- Tsurupa, G., Yakovlev, S., McKee, P., and Medved, L. (2010). Noncovalent Interaction of α 2-Antiplasmin with Fibrin(ogen): Localization of α 2-Antiplasmin-Binding Sites. *Biochemistry* *49*, 7643-7651.
- Turk, B., Brieditis, I., Bock, S.C., Olson, S.T., and Bjork, I. (1997). The oligosaccharide side chain on Asn-135 of alpha-antithrombin, absent in beta-antithrombin, decreases the heparin affinity of the inhibitor by affecting the heparin-induced conformational change. *Biochemistry* *36*, 6682-6691.
- Undas, A., and Ariëns, R.A.S. (2011). Fibrin Clot Structure and Function. *Arteriosclerosis, Thrombosis, and Vascular Biology* *31*, e88-e99.
- Van Deerlin, V.M., and Tollefsen, D.M. (1991a). The N-terminal acidic domain of heparin cofactor II mediates the inhibition of alpha-thrombin in the presence of glycosaminoglycans. *J Biol Chem* *266*, 20223-20231.
- Van Deerlin, V.M., and Tollefsen, D.M. (1991b). The N-terminal acidic domain of heparin cofactor II mediates the inhibition of alpha-thrombin in the presence of glycosaminoglycans. *The Journal of biological chemistry* *266*, 20223-20231.
- van Tilburg, N.H., Rosendaal, F.R., and Bertina, R.M. (2000). Thrombin activatable fibrinolysis inhibitor and the risk for deep vein thrombosis. *Blood* *95*, 2855-2859.
- van Zonneveld, A.J., Veerman, H., and Pannekoek, H. (1986a). Autonomous functions of structural domains on human tissue-type plasminogen activator. *Proceedings of the National Academy of Sciences of the United States of America* *83*, 4670-4674.
- van Zonneveld, A.J., Veerman, H., and Pannekoek, H. (1986b). On the interaction of the finger and the kringle-2 domain of tissue-type plasminogen activator with fibrin. Inhibition of kringle-2 binding to fibrin by epsilon-amino caproic acid. *The Journal of biological chemistry* *261*, 14214-14218.
- Verhamme, P., Heye, S., Peerlinck, K., Cahillane, G., Tangelder, M., Fourneau, I., Daenens, K., Belmans, A., Pakola, S., Verhaeghe, R., *et al.* (2012). Catheter-directed thrombolysis with microplasmin for acute peripheral arterial occlusion (PAO): an exploratory study. *International angiology : a journal of the International Union of Angiology* *31*, 289-296.
- von Kummer, R., Albers, G.W., Mori, E., and Committees, D.S. (2012). The Desmoteplase in Acute Ischemic Stroke (DIAS) clinical trial program. *International Journal of Stroke* *7*, 589-596.
- Walker, J.B., and Nesheim, M.E. (1999). The molecular weights, mass distribution, chain composition, and structure of soluble fibrin degradation products released from a fibrin clot perfused with plasmin. *The Journal of biological chemistry* *274*, 5201-5212.
- Wang, H., Karlsson, A., Sjöström, I., and Wiman, B. (2006). The interaction between plasminogen and antiplasmin variants as studied by surface plasmon resonance. *Biochimica et Biophysica Acta (BBA) - Proteins and Proteomics* *1764*, 1730-1734.
- Wang, H., Yu, A., Wiman, B., and Pap, S. (2003). Identification of amino acids in antiplasmin involved in its noncovalent 'lysine-binding-site'-dependent interaction with plasmin. *Eur J Biochem* *270*, 2023-2029.
- Wang, J., Brdar, B., and Reich, E. (1995). Structure and function of microplasminogen: I. Methionine shuffling, chemical proteolysis, and proenzyme activation. *Protein science : a publication of the Protein Society* *4*, 1758-1767.
- Wang, X., Lin, X., Loy, J.A., Tang, J., and Zhang, X.C. (1998). Crystal Structure of the Catalytic Domain of Human Plasmin Complexed with Streptokinase. *Science* *281*, 1662-1665.
- Wei, A., Rubin, H., Cooperman, B.S., and Christianson, D.W. (1994). Crystal structure of an uncleaved serpin reveals the conformation of an inhibitory reactive loop. *Nature structural biology* *1*, 251-258.

- Weisel, J.W., Nagaswami, C., Korsholm, B., Petersen, L.C., and Suenson, E. (1994). Interactions of plasminogen with polymerizing fibrin and its derivatives, monitored with a photoaffinity cross-linker and electron microscopy. *J Mol Biol* 235, 1117-1135.
- Whisstock, J., Skinner, R., and Lesk, A.M. (1998). An atlas of serpin conformations. *Trends Biochem Sci* 23, 63-67.
- Whisstock, J.C., and Bottomley, S.P. (2006). Molecular gymnastics: serpin structure, folding and misfolding. *Current opinion in structural biology* 16, 761-768.
- Whisstock, J.C., Silverman, G.A., Bird, P.I., Bottomley, S.P., Kaiserman, D., Luke, C.J., Pak, S.C., Reichhart, J.-M., and Huntington, J.A. (2010). Serpins Flex Their Muscle. *J Biol Chem* 285, 24307-24312.
- Wiman, B., Boman, L., and Collen, D. (1978). On the Kinetics of the Reaction between Human Antiplasmin and a Low-Molecular-Weight Form of Plasmin. *Eur J Biochem* 87, 143-146.
- Wiman, B., and Collen, D. (1977). Purification and characterization of human antiplasmin, the fast-acting plasmin inhibitor in plasma. *European journal of biochemistry / FEBS* 78, 19-26.
- Wiman, B., Lijnen, H.R., and Collen, D. (1979). On the specific interaction between the lysine-binding sites in plasmin and complementary sites in $\alpha 2$ -antiplasmin and in fibrinogen. *Biochimica et Biophysica Acta (BBA) - Protein Structure* 579, 142-154.
- Wong, A.P., Cortez, S.L., and Baricos, W.H. (1992). Role of plasmin and gelatinase in extracellular matrix degradation by cultured rat mesangial cells. *American Journal of Physiology - Renal Physiology* 263, F1112-F1118.
- Wu, H.L., Shi, G.Y., and Bender, M.L. (1987). Preparation and purification of microplasmin. *Proceedings of the National Academy of Sciences of the United States of America* 84, 8292-8295.
- Wun, T.C., Ossowski, L., and Reich, E. (1982). A proenzyme form of human urokinase. *The Journal of biological chemistry* 257, 7262-7268.
- Xue, Y., Bodin, C., and Olsson, K. (2012). Crystal structure of the native plasminogen reveals an activation-resistant compact conformation. *Journal of Thrombosis and Haemostasis* 10, 1385-1396.
- Yakovlev, S., Makogonenko, E., Kurochkina, N., Nieuwenhuizen, W., Ingham, K., and Medved, L. (2000). Conversion of fibrinogen to fibrin: mechanism of exposure of tPA- and plasminogen-binding sites. *Biochemistry* 39, 15730-15741.
- Ye, R.D., Ahern, S.M., Le Beau, M.M., Lebo, R.V., and Sadler, J.E. (1989). Structure of the gene for human plasminogen activator inhibitor-2. The nearest mammalian homologue of chicken ovalbumin. *The Journal of biological chemistry* 264, 5495-5502.
- Yee, V.C., Pratt, K.P., Cote, H.C., Trong, I.L., Chung, D.W., Davie, E.W., Stenkamp, R.E., and Teller, D.C. (1997). Crystal structure of a 30 kDa C-terminal fragment from the gamma chain of human fibrinogen. *Structure (London, England : 1993)* 5, 125-138.
- Yonekawa, O., Voskuilen, M., and Nieuwenhuizen, W. (1992). Localization in the fibrinogen gamma-chain of a new site that is involved in the acceleration of the tissue-type plasminogen activator-catalysed activation of plasminogen. *The Biochemical journal* 283 (Pt 1), 187-191.
- Yoshinaga, H., Nakahara, M., Koyama, T., Shibamiya, A., Nakazawa, F., Miles, L.A., Hirose, S., and Aoki, N. (2002). A single thymine nucleotide deletion responsible for congenital deficiency of plasmin inhibitor. *Thrombosis and haemostasis* 88, 144-148.
- Zhang, Q., Law, R.H., Bottomley, S.P., Whisstock, J.C., and Buckle, A.M. (2008). A structural basis for loop C-sheet polymerization in serpins. *J Mol Biol* 376, 1348-1359.
- Zhou, A., Huntington, J.A., and Carrell, R.W. (1999). Formation of the antithrombin heterodimer in vivo and the onset of thrombosis. *Blood* 94, 3388-3396.

Zhou, A., Wei, Z., Read, R.J., and Carrell, R.W. (2006). Structural mechanism for the carriage and release of thyroxine in the blood. *Proceedings of the National Academy of Sciences of the United States of America* 103, 13321-13326.

Chapter 10:

Appendices

Appendix 10.1 General Buffers

Table 10.1. General laboratory solutions

Buffer/Solution	Constituents/Composition
TAE	40mM Tris acetate 1mM EDTA
PBS	137mM NaCl 10mM Na ₂ HPO ₄ 1.76mM NaH ₂ PO ₄ 2.68mM KCl pH 7.4
PBS-T	137mM NaCl 10mM Na ₂ HPO ₄ 1.76mM NaH ₂ PO ₄ 2.68mM KCl 0.1% (v/v) Tween 20
SDS-PAGE running buffer	25mM Tris 190mM Glycine
Western transfer buffer	25mM Tris 190mM Glycine 10% (v/v) Methanol
Coomassie stain	0.05% (w/v) Coomassie brilliant blue G-250 50% (v/v) Methanol 10% (v/v) Acetic acid
Coomassie destain	40% (v/v) Methanol 10% (v/v) Acetic acid
LB (Luria Broth) media	1.0% (w/v) Tryptone 0.5% (w/v) Yeast extract 1.0% (w/v) NaCl
2x Tryptone-yeast (TY) media	1.6% (w/v) Tryptone 1.0% (w/v) Yeast 0.5% (w/v) NaCl
5x SDS-PAGE loading dye	123mM Tris-HCl pH6.8 25% (v/v) Glycerol 10% (w/v) SDS 0.5% (w/v) Bromophenol blue 5% (v/v) β-mercaptoethanol
5x Native-PAGE loading dye	235mM Tris-HCl pH6.8 10% (v/v) Glycerol 0.04% (w/v) Bromophenol blue

Table 10.2. Buffers used for the purification of recombinant human α_2 -antiplasmin.

Buffer/Solution	Constituents/Composition
HisTrap Buffer A	20mM NaPO ₄ 150mM NaCl 20mM Imidazole pH8.0
HisTrap Buffer B	20mM NaPO ₄ 150mM NaCl 500mM Imidazole pH8.0
MonoQ Buffer A	20mM Tris-HCl pH 8.0 0.1mM EDTA
MonoQ Buffer B	20mM Tris-HCl pH 8.0 0.1mM EDTA 500mM NaCl
Lysis Buffer	HisTrap Buffer A 1mg/mL Lysozyme 0.2mg/mL DNase 1:1000 Protease inhibitor cocktail 0.01% (v/v) PMSF

Table 10.3. Buffers used for kinetic and binding assays.

Buffer/Solution	Constituents/Composition
Kinetic Buffer	20mM Tris-HCl pH 8.0 150mM NaCl 0.01% Tween 20
Running Buffer (for SPR)	10mM HEPES pH7.4 150mM NaCl 50 μ M EDTA 0.05% Surfactant P20
Regeneration Buffer (for SPR)	10mM HEPES pH7.4 150mM NaCl 350mM EDTA 0.05% Surfactant P20
Nickel solution (for SPR)	500 μ M NiCl ₂

Table 10.4. Buffers used for the purification of recombinant microplasmin.

Buffer/Solution	Constituents/Composition
Lysis Buffer (for μPlm)	50mM Tris-HCl pH 8.0 100mM NaCl 1% (v/v) Triton X-100 5mM MgCl ₂ 1mg/mL Lysozyme 0.01% (v/v) PMSF 1:1000 Protease inhibitor cocktail
Wash Buffer 1	50mM Tris-HCl pH 8.0 0.5% (v/v) Triton X-100 100mM NaCl 1mM EDTA
Wash Buffer 2	50mM Tris-HCl pH 8.0 1mM EDTA
Denaturing Buffer	8M Urea 50mM Tris-HCl pH 8.0 1mM EDTA 10mM BME
Refolding Buffer	50mM Tris-HCl pH 8.0 50mM NaCl 1.25mM Reduced glutathione 0.125mM Oxidised glutathione
μPlg HisTrap Buffer A	50mM Tris-HCl pH 8.0 100mM NaCl 20mM Imidazole
μPlg HisTrap Buffer B	50mM Tris-HCl pH 8.0 100mM NaCl 500mM Imidazole
MonoS Buffer A	20mM MES pH 6.5 10% (w/v) Sucrose
MonoS Buffer B	20mM MES pH 6.5 10% (w/v) Sucrose 1M NaCl
Benzamidine Binding Buffer	50mM Tris-HCl pH 7.4 500mM NaCl
Benzamidine Wash Buffer	50mM Tris-HCl pH 7.4 1M NaCl 20mM <i>p</i> -aminobenzamidine
Benzamidine Elution Buffer	50mM Glycine pH 3.0
Gel Filtration Buffer (for μPlm and α_2-antiplasmin)	25mM Tris-HCl pH 8.0 150mM NaCl 5% (v/v) Glycerol 0.05% (w/v) NaAz

Appendix 10.2 Lu et al., 2011, published paper related to this thesis as described in Chapter 4

THE JOURNAL OF BIOLOGICAL CHEMISTRY VOL. 286, NO. 28, PP. 24544–24552, JULY 15, 2011
© 2011 BY THE AMERICAN SOCIETY FOR BIOCHEMISTRY AND MOLECULAR BIOLOGY, INC. PRINTED IN THE U.S.A.

Contribution of Conserved Lysine Residues in the α_2 -Antiplasmin C Terminus to Plasmin Binding and Inhibition*

Received for publication, February 7, 2011, and in revised form, April 19, 2011. Published, JBC Papers in Press, May 4, 2011, DOI 10.1074/jbc.M111.229013

Bernadine G. C. Lu[‡], Trifina Sofian[‡], Ruby H. P. Law[§], Paul B. Coughlin^{¶1,2}, and Anita J. Horvath^{‡1,2}

From the [‡]Australian Centre for Blood Diseases, Monash University, Melbourne, Victoria 3004, the [§]Department of Biochemistry and Molecular Biology, Monash University, Clayton, Victoria 3800, and the [¶]Department of Medicine and Haematology, Box Hill Hospital, Monash University, Box Hill, Victoria 3128, Australia

α_2 -Antiplasmin is the physiological inhibitor of plasmin and is unique in the serpin family due to N- and C-terminal extensions beyond its core domain. The C-terminal extension comprises 55 amino acids from Asn-410 to Lys-464, and the lysine residues (Lys-418, Lys-427, Lys-434, Lys-441, Lys-448, and Lys-464) within this region are important in mediating the initial interaction with kringle domains of plasmin. To understand the role of lysine residues within the C terminus of α_2 -antiplasmin, we systematically and sequentially mutated the C-terminal lysines, studied the effects on the rate of plasmin inhibition, and measured the binding affinity for plasmin via surface plasmon resonance. We determined that the C-terminal lysine (Lys-464) is individually most important in initiating binding to plasmin. Using two independent methods, we also showed that the conserved internal lysine residues play a major role mediating binding of the C terminus of α_2 -antiplasmin to kringle domains of plasmin and in accelerating the rate of interaction between α_2 -antiplasmin and plasmin. When the C terminus of α_2 -antiplasmin was removed, the binding affinity for active site-blocked plasmin remained high, suggesting additional exosite interactions between the serpin core and plasmin.

α_2 -Antiplasmin is unique among the serpin family due to the presence of N- and C-terminal extensions beyond its inhibitory core. The 42-amino acid N terminus is cross-linked to fibrin by factor XIIIa, localizing its activity to the clot (4, 5). The α_2 -antiplasmin C terminus extends 55 amino acids from Asn-410 to Lys-464 and is believed to be important in the initial interaction with kringle domains of plasmin (6). A form of α_2 -antiplasmin that lacks the C terminus interacts with plasmin much more slowly compared with the intact molecule (7). The crystal structure of murine α_2 -antiplasmin lacking the first 43 amino acids has been determined; however, the C terminus could not be modeled, which suggests that the C-terminal region of α_2 -antiplasmin is highly flexible (8).

The C terminus of α_2 -antiplasmin contains six lysines, five of which are conserved between species (Lys-427, Lys-434, Lys-441, Lys-448, and Lys-464), and it is known that lysines are key in mediating binding to kringle domains. Using a synthetic peptide corresponding to the final 26 amino acids of the C terminus, a previous study showed that the α_2 -antiplasmin/plasmin association was reduced, indicating that this region has high affinity for plasmin kringle domains (9). However, the relative importance assigned to the C-terminal lysine compared with other internal lysines differs in published studies. Frank *et al.* (6) and Gerber *et al.* (10) studied the binding of kringle domains to C-terminal peptide containing Lys-to-Ala mutations. They showed that the C-terminal lysine (Lys-464) was the most important contributor to binding affinity for plasmin kringle domains (6, 10). However, kinetic inhibitory studies by Wang *et al.* (11) indicated that Lys-448 in full-length α_2 -antiplasmin was most important in the interaction with plasmin.

At present, there are no comprehensive studies investigating the role of lysine residues using inhibitory rates as an end point. To fully understand the role of the C-terminal lysine residues in the interaction with kringle domains of plasmin, we present a systematic and sequential study on the mutagenesis of α_2 -antiplasmin C-terminal lysines (Lys-427, Lys-434, Lys-441, Lys-448, and Lys-464) and truncation of the C terminus. This is the first report describing the plasmin inhibition rate (k_a) for full-length human α_2 -antiplasmin and intact plasmin. Furthermore, we investigated the binding affinity (K_D) of wild-type α_2 -antiplasmin and various mutants for active site-blocked plasmin using plasmon surface resonance. These studies suggest additional exosite interactions between the serpin core domain and plasmin.

When tissue injury occurs, fibrinolysis and coagulation are activated in concert. Tissue plasminogen activator secreted by the injured endothelium activates plasminogen to plasmin, which in turn degrades the fibrin clot. Fibrinolysis remains localized because tissue plasminogen activator and plasminogen co-localize on fibrin strands, dramatically improving catalytic efficiency (1). In addition, free plasmin in plasma is rapidly inactivated by its principal regulator, α_2 -antiplasmin. Dysregulation of either fibrinolysis or coagulation has the potential to cause thrombosis, whereas on the other hand, therapeutic manipulation of these pathways can be used to treat thrombotic diseases (2). Currently, most therapeutic agents used to promote fibrinolysis directly activate plasminogen, but their use is limited by the risk of excessive bleeding. However, there is increasing evidence that α_2 -antiplasmin is a useful alternative target in the development of new therapeutics for thrombotic diseases (3).

* This work was supported by the National Health and Medical Research Council (NHMRC) of Australia.

¹ Both authors contributed equally to this work.

² To whom correspondence should be addressed: Australian Centre for Blood Diseases, Level 6 Burnet Bldg., 89 Commercial Rd., Melbourne, Victoria 3004, Australia. E-mail: [REDACTED]

α_2 -Antiplasmin Binding to Plasmin

EXPERIMENTAL PROCEDURES

Construction of α_2 -Antiplasmin Variants—Human WT α_2 -antiplasmin cDNA was isolated from a liver cDNA library using PCR with primers 5'-GGA TCC ACC CCA GGA GCA GGT GTC CC-3' and 5'-GGA TCC TCA CTT GGG GCT GCC AAA C-3'. The product was cloned into the pET-His(3a) expression vector and sequenced for authenticity (12). The QuikChange site-directed mutagenesis kit (Stratagene) was used on human WT α_2 -antiplasmin template in which alanine or stop codons were introduced at various lysine residues along the C terminus. Several mutations within the C terminus of human α_2 -antiplasmin were made as follows: K427A, K434A, K441A, K448A, K464A, P414stop (Cterm Δ), K448A/K464A, K434A/K448A/K464A, K434A/K441A/K448A/K464A, K427A/K434A/K441A/K448A/K464WT, L449stop, and K448A/L449stop (see Fig. 1).³ All constructs were nucleotide-sequenced to confirm the mutations introduced.

Expression and Purification of α_2 -Antiplasmin Variants—Recombinant human α_2 -antiplasmin (WT and mutants) was expressed in *Escherichia coli* BL21(DE3)pLysS cells. Cells were grown overnight at 37 °C with shaking at 220 rpm in 2 \times tryptone-yeast culture medium supplemented with 50 μ g/ml ampicillin. The cell cultures were then diluted 1:10 in fresh 2 \times tryptone-yeast medium supplemented with 50 μ g/ml ampicillin and grown for a further 2 h at 37 °C and 220 rpm. Human α_2 -antiplasmin was then induced with a final concentration of 0.02 mM isopropyl β -D-thiogalactopyranoside and incubated for 4 h at 30 °C and 220 rpm. Cells were harvested by centrifugation at 3500 rpm (Beckman JS-4.2 rotor) for 20 min and stored at -80 °C until used.

To obtain soluble recombinant α_2 -antiplasmin, the cell pellet was lysed in lysis buffer (50 mM NaPO₄ (pH 8.0), 500 mM NaCl, 20 mM imidazole, and 5 mM β -mercaptoethanol) containing 1 mg/ml lysozyme, 0.2 mg/ml DNase, 1:1000 protease inhibitor mixture (Sigma), and 0.01% phenylmethanesulfonyl fluoride per liter of cell culture. The cells were frozen in liquid nitrogen and then completely thawed three times in a 37 °C water bath. The lysate was centrifuged (Sorvall SS34 rotor) at 18,000 rpm for 20 min. To purify recombinant α_2 -antiplasmin, the supernatants were loaded onto a HisTrap column (GE Healthcare) and eluted with a linear imidazole gradient (0.02–0.5 M) in lysis buffer. The proteins were further purified on a Mono Q column (GE Healthcare) with a linear NaCl gradient (0–0.5 M) in 20 mM Tris (pH 8.0) and 0.1 mM EDTA. All recombinant human α_2 -antiplasmin was electrophoresed on 12.5% SDS-polyacrylamide gel to confirm the purity of peak fractions. Aliquots of recombinant protein were stored at -80 °C until used.

Determination of Stoichiometry of Inhibition—The stoichiometry of inhibition (SI)⁴ was determined by incubating 1 nM human plasmin (Hematologic Technologies, Essex Junction, VT) with WT α_2 -antiplasmin and mutants at various concentrations (0.2–1.5 nM) for 1 h at 37 °C. Residual plasmin activity was assayed at 25 °C using a FLUOstar Optima plate reader

(BMG Labtech, Victoria, Australia) set at 355/460 nm with 200 μ M fluorogenic substrate *H*-Ala-Phe-Lys-AMC (Bachem, Bubendorf, Switzerland). All reactions were done in triplicates in 20 mM Tris (pH 8.0), 150 mM NaCl, and 0.01% Tween 80 in a 1% bovine serum albumin-coated PerkinElmer OptiPlate.

Measuring the Rate of Plasmin Inhibition via Kinetic Assay—The rate of plasmin inhibition by recombinant α_2 -antiplasmin was determined using a continuous method described previously (13). Plasmin (0.5 nM) was reacted with various concentrations of recombinant α_2 -antiplasmin, WT (1.0–2.5 nM) or mutant (1.5–40 nM), in the presence of 1 mM *H*-Ala-Phe-Lys-AMC at 25 °C. Fluorescence emission was continuously measured using a FLUOstar Optima plate reader at 355/460 nm over time. Triplicate experiments were performed with each recombinant α_2 -antiplasmin in 20 mM Tris (pH 8.0), 150 mM NaCl, and 0.01% Tween 20 in a 1% bovine serum albumin-coated PerkinElmer OptiPlate.

The raw data were fitted using nonlinear regression in GraphPad Prism (Equation 1),

$$P = \frac{V_0}{k_{\text{obs}}} \times (1 - e^{(-k_{\text{obs}}t)}) \quad (\text{Eq. 1})$$

where P is the concentration of product at time t , V_0 is the initial velocity, and k_{obs} is the apparent first-order rate constant (14). The k_{obs} value for each serpin concentration was calculated by Equation 1. Each k_{obs} value was plotted against the respective α_2 -antiplasmin concentration. Linear regression analysis was performed to obtain the uncorrected rate of inhibition (k'). Equation 2 was used to account for fluorogenic substrate competition,

$$k_a = k' \times \left(1 + \frac{[S]}{K_m}\right) \times \text{SI} \quad (\text{Eq. 2})$$

where the rate of inhibition was adjusted with the SI, substrate concentration ($[S]$), and Michaelis constant (K_m) of the substrate to give the second-order rate constant (k_a) (14).

Binding of α_2 -Antiplasmin to Active Site-blocked Plasmin by Surface Plasmon Resonance—The interactions between active site-blocked plasmin and various recombinant α_2 -antiplasmin proteins were determined via surface plasmon resonance using the Biacore T100 system (GE Healthcare). Active site-blocked plasmin was produced by incubating human plasmin with a 1000-fold molar excess of D-Val-Phe-Lys chloromethyl ketone (Calbiochem) at 37 °C for 1 h. Active site-blocked plasmin was then dialyzed overnight at 4 °C in running buffer (0.01 M HEPES (pH 7.4), 0.15 M NaCl, 50 μ M EDTA, and 0.05% surfactant P20 (GE Healthcare)). To confirm that the active site was completely blocked, the activity of active site-blocked plasmin was checked against active plasmin in the presence of 200 μ M *H*-Ala-Phe-Lys-AMC fluorogenic substrate.

To measure the binding affinity and rate of plasmin association of α_2 -antiplasmin with active site-blocked plasmin, we immobilized hexahistidine-tagged WT or mutant α_2 -antiplasmin on the nitrilotriacetic acid (NTA) surface of a NTA chip (GE Healthcare) following the manufacturer's instructions. All experiments were carried out in running buffer at a flow rate of 10 μ l/min and performed in triplicates. Briefly, the NTA sur-

³ The numbering of recombinant α_2 -antiplasmin variants was based on the secreted 464-residue form (5).

⁴ The abbreviations used are: SI, stoichiometry of inhibition; AMC, 7-amino-4-methylcoumarin; NTA, nitrilotriacetic acid.

α_2 -Antiplasmin Binding to Plasmin

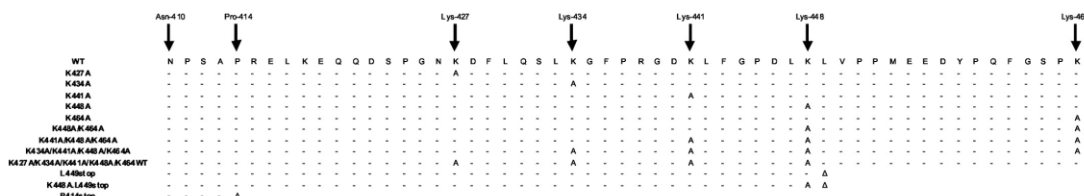


FIGURE 1. Schematic representation of the C terminus of α_2 -antiplasmin and positions at which mutations were introduced. Full-length WT α_2 -antiplasmin and various mutants (Lys-to-Ala mutations or truncation) of the C terminus were generated, expressed, and purified. Dashes represent the wild-type sequence, and the introduction of a stop codon is indicated (Δ).

face was activated by injecting 500 μM NiCl_2 for 1 min. 20 nM WT or mutant recombinant α_2 -antiplasmin was immobilized onto the surface on one flow cell for 1 min. A reference flow cell containing no α_2 -antiplasmin was used to account for nonspecific binding to the NTA surface. Six different concentrations of active site-blocked plasmin (analyte) were injected for 1 min of association time, followed by 10 min of dissociation time. The range of active site-blocked plasmin concentrations (2–120 nM) was adjusted for each α_2 -antiplasmin variant. At the end of each concentration cycle, the NTA surface was completely stripped with regeneration buffer (0.01 M HEPES (pH 7.4), 0.15 M NaCl, 0.35 M EDTA, and 0.05% surfactant P20) at a flow rate of 30 $\mu\text{L}/\text{min}$ for 2 min. NTA surface activation and α_2 -antiplasmin immobilization were performed at each active site-blocked plasmin concentration. The injection needle was cleaned with an extra wash of running buffer after each subsequent step.

Real-time binding curves were monitored on a sensorgram as resonance units over time. For kinetic and binding affinity analysis of recombinant α_2 -antiplasmin with active site-blocked plasmin, we used the two-state reaction model provided in the Biacore T100 evaluation software (Version 1.1.1) (Equation 3).

$$E + I \rightleftharpoons EI \rightleftharpoons EI^* \quad (\text{Eq. 3})$$

This model describes a 1:1 binding of analyte to immobilized ligand, followed by a secondary interaction that stabilizes the two molecules. χ^2 analysis supported this model. The overall equilibrium dissociation constant (K_D) was calculated using Equation 4 (15).

$$K_D = \frac{k_{d1}}{k_{a1}} \times \frac{k_{d2}}{k_{d2} + k_{a2}} \quad (\text{Eq. 4})$$

RESULTS

Stoichiometry of Inhibition between Recombinant Human α_2 -Antiplasmin and Plasmin—To examine the role of lysine residues in the α_2 -antiplasmin C terminus, we employed site-directed mutagenesis and produced a series of mutant recombinant proteins (Fig. 1). Mutations within the C-terminal region of α_2 -antiplasmin would not be expected to affect the inhibitory mechanism because this property resides in the serpin core domain. However, to verify that the recombinant proteins were correctly folded, the SI for human plasmin was determined for WT and mutant α_2 -antiplasmin.

The serpin/protease ratio that resulted in complete loss of protease activity was determined as the SI of the serpin (Fig. 2). The SI of WT α_2 -antiplasmin was found to be 1.0 (Fig. 2, A and

E) and corresponds with published values (16). Fig. 2E shows the SI values obtained for each recombinant protein produced. All mutants were shown to have an SI of between 0.9 and 1.5 (Fig. 2, B–E), indicating that the efficiency of mutant protein had not been structurally perturbed by the introduction of various amino acid substitutions in the C terminus. To confirm these observations, WT recombinant α_2 -antiplasmin and mutants were also assessed by CD spectrometry. Mutant α_2 -antiplasmin proteins produced CD spectra similar to WT α_2 -antiplasmin, demonstrating that the mutant proteins retained their native fold (data not shown).

Rate of Plasmin Inhibition of Recombinant Human α_2 -Antiplasmin Variants—The primary hypothesis being tested in this work is that lysine residues at the extreme C terminus of α_2 -antiplasmin as well as internally within the C-terminal extension accelerate inhibition of plasmin. Therefore, kinetic studies using a protease inhibition (progress curve) assay were performed to measure the rate of plasmin inhibition by WT and mutant α_2 -antiplasmin. Fig. 3 shows examples of progress and fitted curves obtained from the analysis of WT and P414stop (Cterm Δ) α_2 -antiplasmin.

As expected, recombinant human WT α_2 -antiplasmin was a fast inhibitor of human plasmin, with a plasmin inhibition rate (k_a) of $(3.7 \pm 0.3) \times 10^7 \text{ M}^{-1} \text{ s}^{-1}$, which corresponds to published results (17). Individual Lys-to-Ala mutations at positions 427, 434, 441, 448, and 464 caused decreases in the rate of plasmin inhibition of 1.5-, 1.6-, 1.7-, 2.8-, and 3.6-fold respectively (Fig. 4) compared with WT α_2 -antiplasmin. The K464A mutation produced the greatest reduction in the rate of plasmin inhibition; however, this was modest compared with the effect of removing the entire α_2 -antiplasmin C terminus (P414stop), which resulted in a 40-fold reduction ($k_a = (9.2 \pm 0.2) \times 10^5 \text{ M}^{-1} \text{ s}^{-1}$).

Because the reductions in the inhibition rate observed with individual Lys-to-Ala mutants were small compared with the effect of removal of the complete C terminus, we examined the effect of progressive mutations of the Lys residues in this domain. Compared with α_2 -antiplasmin K464A, each additional mutation (K448A/K464A, K441A/K448A/K464A, and K434A/K441A/K448A/K464A) resulted in an ~ 2 -fold reduction in the plasmin inhibition rate (Fig. 5). Therefore, the overall reduction in the rate of plasmin inhibition observed with the four-residue substitution (K434A/K441A/K448A/K464A) was 45-fold, which is comparable with the effect of removing the entire α_2 -antiplasmin C terminus (P414stop).

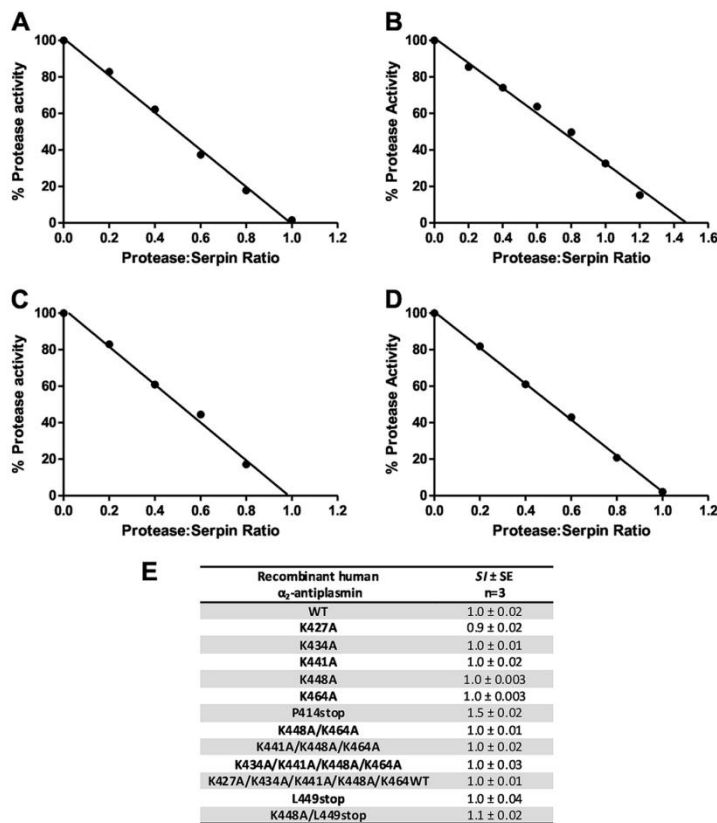
α_2 -Antiplasmin Binding to Plasmin

FIGURE 2. SI of plasmin by recombinant human α_2 -antiplasmin. Plasmin (1 nM) was incubated with WT or mutant α_2 -antiplasmin (0.2–1.5 nM) for 1 h at 37 °C. Residual protease activity was measured in the presence of H-Ala-Phe-Lys-AMC (0.2 mM). A, WT recombinant α_2 -antiplasmin; B, P414stop (Cterm Δ) mutant α_2 -antiplasmin; C, K464A mutant α_2 -antiplasmin; D, K434A/K441A/K448A/K464A mutant α_2 -antiplasmin; E, mean SI of plasmin by WT and mutant recombinant α_2 -antiplasmin.

It is conceivable that substitution of four lysine residues within the C terminus of α_2 -antiplasmin could produce a structural perturbation of the domain. We therefore measured the kinetic effect of adding the lysine analog ϵ -aminocaproic acid to the inhibitory reaction. When 1 mM ϵ -aminocaproic acid was added to the inhibitory reaction, a k_a of $(2.3 \pm 0.2) \times 10^6 \text{ M}^{-1} \text{ s}^{-1}$ was observed, which was comparable with the mutant with a deletion of the C terminus (P414stop) ($k_a = (9.2 \pm 0.2) \times 10^5 \text{ M}^{-1} \text{ s}^{-1}$) (Fig. 4). This suggests that most of the reduction in the plasmin inhibition rate caused by the removal of the C terminus can be accounted for by lysine-specific interactions.

The relative importance of the C-terminal Lys-464 compared with the internal lysine residues was further addressed by measuring the rate of inhibition of a mutant in which Lys-464 was preserved while the internal lysines were mutated to alanine (K427A/K434A/K441A/K448A/K464WT) (Fig. 5). This mutant demonstrated a 5.2-fold rate reduction ($k_a = (7.1 \pm 0.1) \times 10^6 \text{ M}^{-1} \text{ s}^{-1}$) compared with WT α_2 -antiplasmin.

The importance of the C-terminal lysine was further evaluated by producing a mutant in which a stop codon was intro-

duced after Lys-448 (L449stop). Despite this mutant possessing a C-terminal lysine, it still showed a rate reduction in plasmin inhibition ($k_a = (1.1 \pm 0.1) \times 10^5 \text{ M}^{-1} \text{ s}^{-1}$) of 3.4-fold compared with WT α_2 -antiplasmin. Additionally, when the L449stop mutant was modified by substituting Lys-448 with Ala (K448A/L449stop), there was a further decrease in the plasmin inhibition rate ($k_a = (2.8 \pm 0.1) \times 10^6 \text{ M}^{-1} \text{ s}^{-1}$).

Binding Affinity of Recombinant Human α_2 -Antiplasmin Variants for Active Site-blocked Plasmin—The association rate constants described above were derived from measurements of inhibition of plasmin amidolytic activity. To corroborate these results and to partition the α_2 -antiplasmin/plasmin interaction between the serpin core versus the C-terminal extension, we used surface plasmon resonance to directly measure the binding affinity of recombinant human α_2 -antiplasmin for human plasmin. WT α_2 -antiplasmin and various mutants were reacted with active site-blocked plasmin, and binding was observed in real time. The association and dissociation constants were calculated to obtain the binding affinity (K_D). Examples of sensorgrams for the interaction between active site-blocked plasmin

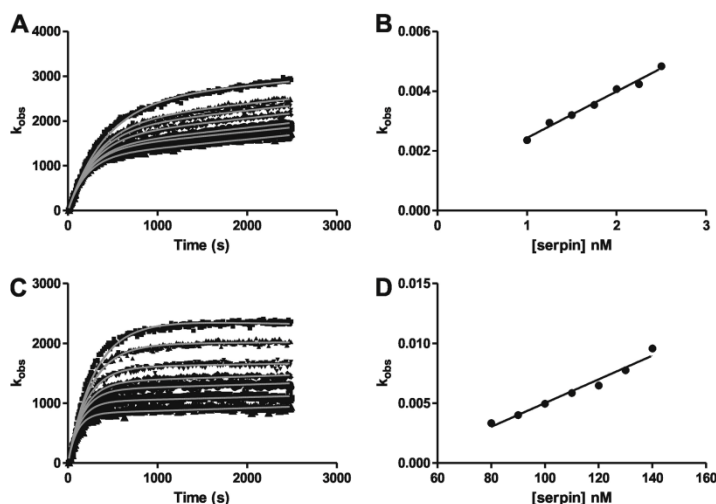
α_2 -Antiplasmin Binding to Plasmin

FIGURE 3. Plasmin inhibition by recombinant human α_2 -antiplasmin. A, progress curves of plasmin inhibition using plasmin (0.5 nM) and WT α_2 -antiplasmin (1–2.5 nM) in the presence of H-Ala-Phe-Lys-AMC (1 mM). Nonlinear regression analysis using Equation 1 was used to determine the first-order rate constant (k_{obs}). B, the k_{obs} is plotted against the WT α_2 -antiplasmin concentration, and linear regression analysis was performed to determine the uncorrected second-order rate constant (k'). To account for substrate inhibition, Equation 2 was applied to determine the corrected second-order rate constant (k_o). C, progress curves of plasmin inhibition using plasmin (0.5 nM) and P414stop (Cterm Δ) α_2 -antiplasmin (80–140 nM) in the presence of H-Ala-Phe-Lys-AMC (1 mM). The k_{obs} was obtained as described above. D, the k_{obs} is plotted against the Cterm Δ α_2 -antiplasmin concentration to determine the k' . The k_o of Cterm Δ α_2 -antiplasmin was calculated using Equation 2.

and recombinant α_2 -antiplasmin are shown in Fig. 6. To achieve similar response units for WT α_2 -antiplasmin (Fig. 6A), a higher concentration of active site-blocked plasmin was used with α_2 -antiplasmin mutants, which accounts for the difference in the shape of the binding curves observed in the sensorgrams (Fig. 6).

The K_D of WT α_2 -antiplasmin for active site-blocked plasmin was determined to be 1.6 nM, indicating a high affinity interaction. Single Lys-to-Ala mutants at positions 448 and 464 showed decreases in K_D of 1.3- and 3.3-fold, respectively (Fig. 7), compared with WT α_2 -antiplasmin. Removing the C terminus (P414stop) resulted in a 31-fold reduction in K_D (50 nM). Overall measurements of binding affinity were consistent with association rates observed using the progress curve plasmin inhibition assay.

Sequential mutation of the Lys residues within the C terminus resulted in a progressive decrease in the K_D , which corresponds to the observations made previously. K448A/K464A showed a 2.0-fold reduction in the K_D (10 nM) compared with K464A. K441A/K448A/K464A produced a 2.8-fold decrease compared with K448A/K464A. An additional 1.5-fold reduction in K_D was observed with K434A/K441A/K448A/K464A (K_D = 42 nM). The K_D for K434A/K441A/K448A/K464A was similar to that obtained by removing the C terminus of α_2 -antiplasmin (P414stop). The K_D for K427A/K434A/K441A/K448A/K464WT was 13 nM, corresponding to a 8.4-fold decrease compared with WT α_2 -antiplasmin.

The L449stop mutant demonstrated a K_D of 6.4 nM, which is similar to that obtained for K464A (K_D = 5.2 nM). This further confirms what was seen previously with the rate of plasmin inhibition. Subsequent mutation of L449stop to K448A/

L449stop resulted in a 17-fold reduction in K_D (27 nM) compared with WT α_2 -antiplasmin.

The rate of plasmin association (k_{a1}) obtained using surface plasmon resonance was very similar to the rate of plasmin inhibition (k_a) obtained using the kinetic assay described previously. The dissociation rate constant (k_{d1}) and the forward and reverse rate constants (k_{a2} and k_{d2}) remained relatively unchanged for WT α_2 -antiplasmin and mutants with active site-blocked plasmin.

DISCUSSION

In this work, we have reported the first comprehensive description of the kinetics of α_2 -antiplasmin/plasmin interactions employing two different methods. By incorporating a fluorogenic substrate with high affinity for plasmin, we have been able to use the “progress curve” method to accurately measure the association rates for WT α_2 -antiplasmin and mutants. In addition, we have independently observed the α_2 -antiplasmin/plasmin interaction via surface plasmon resonance. In both methods, we employed full-length α_2 -antiplasmin (WT and mutants) and intact plasmin containing the protease and all kringle domains. It is important to recognize that the two methods measure different kinetic rate constants. Using Fig. 8 as a reference schematic, surface plasmon resonance measures the initial rate of interaction (k_1) between α_2 -antiplasmin and plasmin. The protease inhibition assay (progress curve) measures the overall rate at which the irreversible covalent α_2 -antiplasmin-plasmin complex is formed, resulting in complete inhibition; therefore, this takes into account k_1 , k_2 , and k_4 (Fig. 8). We were able to obtain comparable rates of plasmin inhibition (k_a) and asso-

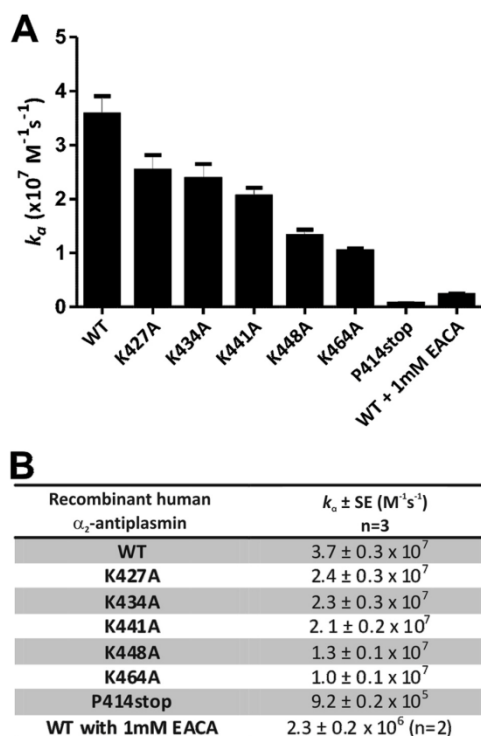


FIGURE 4. Effect of single Lys-to-Ala mutations in the human α_2 -antiplasmin C terminus on plasmin inhibition. A, mean rate of plasmin inhibition (k_a) by WT and mutant recombinant α_2 -antiplasmin ($n = 3$). B, mean k_a of plasmin for WT and mutant recombinant α_2 -antiplasmin.

ciation (k_{a1}) despite the fact that both methods measure different values. This indicates that the rapid interaction is predominantly due to the formation of the initial reversible encounter α_2 -antiplasmin-plasmin complex, thus suggesting that the rate-limiting step occurs when the covalent α_2 -antiplasmin-plasmin complex is formed.

Using protease inhibition and binding affinity data, we were able to demonstrate a progressive decrease in the rate of plasmin association, inhibition, and binding affinity with consecutive Lys-to-Ala mutations within the C terminus of α_2 -antiplasmin. We showed that all conserved Lys residues (Lys-427, Lys-434, Lys-441, Lys-448, and Lys-464) play a role in the interaction with kringle domains of plasmin, with Lys-464 being the main initiator, followed by Lys-448, which corresponds with previously published data (6, 10). Individually, the internal Lys residues appear to have a minor function in the interaction with plasmin. However, as demonstrated by several of our α_2 -antiplasmin mutants, primarily K434A/K441A/K448A/K464A and P414stop, we were able to show that when five of the lysines were mutated, the rates of plasmin inhibition and binding were reduced to those of the C-terminally truncated α_2 -antiplasmin protein. This indicates that the Lys residues within the C terminus of α_2 -antiplasmin are the primary mediators in the binding to the kringle domains and that removal of these

α_2 -Antiplasmin Binding to Plasmin

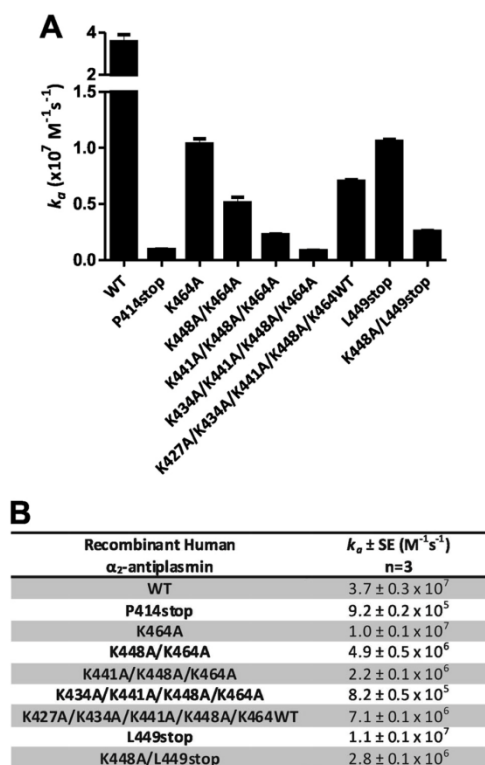


FIGURE 5. Effect of sequential Lys-to-Ala mutations and truncations in the human α_2 -antiplasmin C terminus on plasmin inhibition. A, mean rate of plasmin inhibition (k_a) by WT and mutant recombinant α_2 -antiplasmin ($n = 3$). B, mean k_a of plasmin for WT and mutant recombinant α_2 -antiplasmin.

residues will result in the loss of C-terminal binding. Furthermore, K427A/K434A/K441A/K448A/K464A demonstrated that even with the presence of the most C-terminal lysine with all the internal lysines mutated, the plasmin inhibition rate obtained was not comparable with WT α_2 -antiplasmin. Therefore, each conserved Lys in the α_2 -antiplasmin C terminus participates in the binding and inhibition of plasmin.

Previous studies by Frank *et al.* (6) using individual recombinant plasmin kringle domains (K1, K3, K3mut, K4, and K5) showed that the isolated α_2 -antiplasmin C terminus had the highest affinity for K1, followed by K4, K5, and K2. In further experiments, Gerber *et al.* (10) examined the affinity of the recombinant plasmin kringle domains (K1, K1-3, K4, and K4-5). They demonstrated that progressive mutations of lysine residues within the α_2 -antiplasmin C terminus decreased the affinity for K1-3, although the greatest contribution to binding was attributable to Lys-464 and Lys-448. The apparent lack of effect on the affinity of mutations of Lys-418, Lys-427, Lys-434, and Lys-441 may be explained by the fact that only two lysine-binding kringle domains were present in the K1-3 protein. The seeming discrepancy between our results and those of Gerber *et al.* can therefore be

α_2 -Antiplasmin Binding to Plasmin

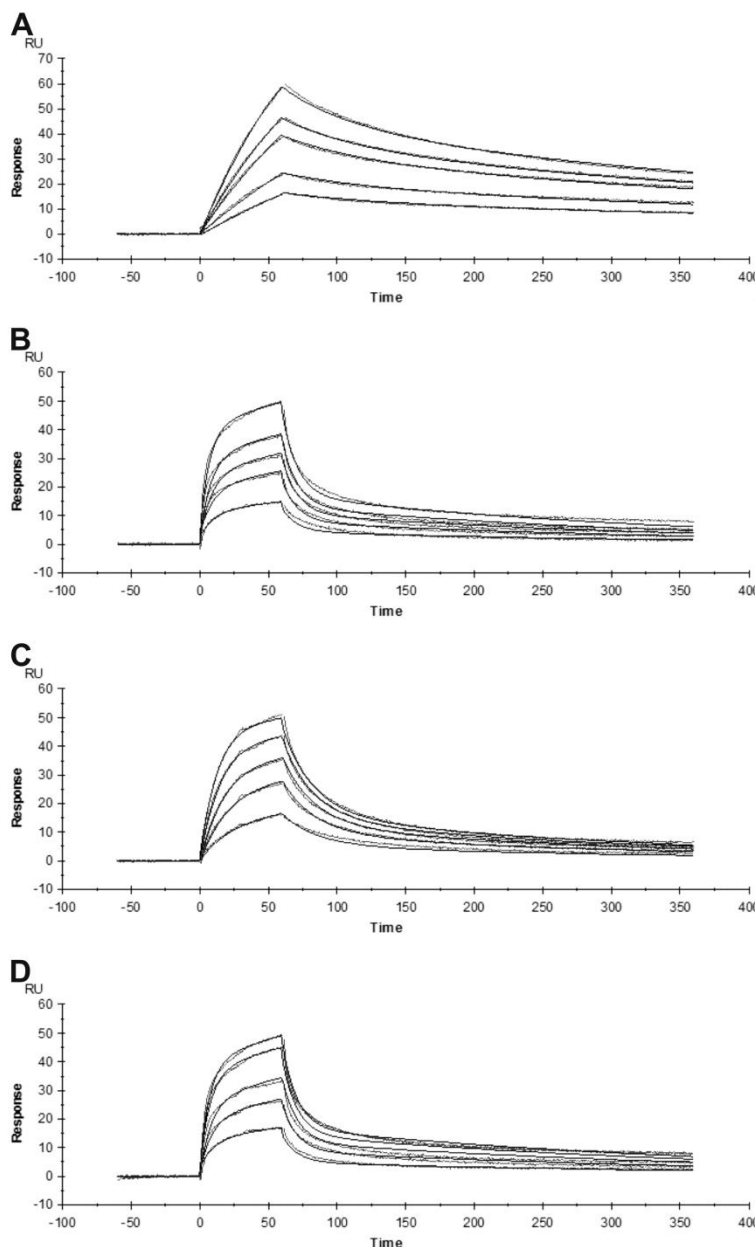


FIGURE 6. Sensorgrams of the binding of recombinant human α_2 -antiplasmin to active site-blocked plasmin measured by surface plasmon resonance. WT or mutant recombinant α_2 -antiplasmin (20 nM) was immobilized on a NTA chip. The binding of various concentrations of active site-blocked plasmin to α_2 -antiplasmin was monitored in real time. A, binding of active site-blocked plasmin (2–8 nM) to WT α_2 -antiplasmin ($\chi^2 = 0.21$). B, binding of active site-blocked plasmin (20–120 nM) to P414stop (Cterm Δ) recombinant α_2 -antiplasmin ($\chi^2 = 0.60$). C, binding of active site-blocked plasmin (4–20 nM) to K464A mutant α_2 -antiplasmin ($\chi^2 = 0.31$). D, binding of active site-blocked plasmin (20–100 nM) to K434A/K441A/K448A/K464A mutant α_2 -antiplasmin ($\chi^2 = 0.54$).

accounted for by differences in experimental approaches. They measured the association constants of isolated kringle domains (K1, K4, K1-3, and K4-5) with the C-terminal por-

tion of α_2 -antiplasmin. By contrast, this study describes the rate of plasmin inhibition and binding affinity of full-length α_2 -antiplasmin with intact plasmin.

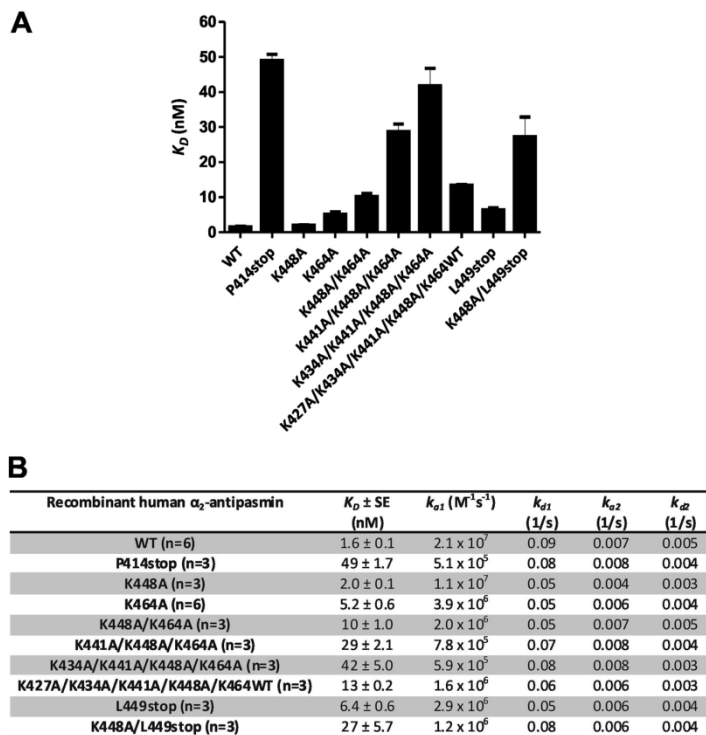
α_2 -Antiplasmin Binding to Plasmin

FIGURE 7. Effect of mutations in the α_2 -antiplasmin C terminus on binding to active site-blocked plasmin as studied via surface plasmon resonance. A, mean binding affinity (K_D) of WT and mutant recombinant α_2 -antiplasmin for active site-blocked plasmin ($n = 3$). B, mean K_D and association and dissociation constants of WT and mutant recombinant α_2 -antiplasmin for active site-blocked plasmin.

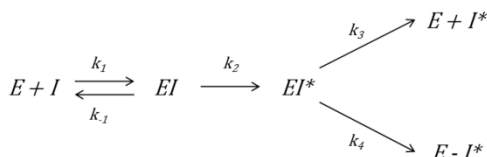


FIGURE 8. Mechanism of serpin inhibition. I represents serpin, and E represents the protease. The forward rate constant of serpin with protease is represented as k_1 . The association rate constant (k_{a1}) measured in surface plasmon resonance studies is equal to k_1 . k_{-1} is the reverse rate constant. The rate at which conformational change (EI^*) occurs is denoted as k_2 . k_3 occurs during the substrate reaction, which results in cleaved serpin and release of active protease ($E + I^*$). Formation of the covalent protease-serpin complex ($E-I^*$) results in complete inhibition, and the rate constant is represented as k_4 .

One striking observation made in this study is that the association rate and binding affinity of plasmin with C-terminally truncated α_2 -antiplasmin (P414stop) were relatively high ($k_{a1} = 5.1 \times 10^5 M^{-1} s^{-1}$; $K_D = 49$ nM). It is important to note that surface plasmon resonance studies were performed with active site-blocked plasmin, suggesting that the rapid association and high affinity observed in the absence of the C-terminal extension were mediated by exosite interactions between α_2 -antiplasmin and the plasmin protease domain. These important interactions between the α_2 -antiplasmin core domain, outside the immediate vicinity of P1-P1', and the

active site cleft of plasmin are also likely to contribute specificity to the serpin/protease interaction. Having additional exosite interactions is not uncommon in the serpin inhibition mechanism, as it may aid in the recognition of its target protein (18, 19). Together with the specific binding of the α_2 -antiplasmin C terminus to plasmin kringle domains, this leads to an exquisite specificity of the interaction minimizing off-target inhibition of non-cognate proteases.

In summary, we have performed detailed kinetic and binding studies of the interaction between α_2 -antiplasmin and plasmin. Within the α_2 -antiplasmin C terminus, we have measured the contribution of the conserved lysines to the interaction with the plasmin kringle domains. This study demonstrates that the C-terminal lysine (Lys-464) is the single most important amino acid in this domain. The remaining conserved lysine residues within the C terminus of α_2 -antiplasmin individually contribute less, but together significantly enhance the rate of association of serpin with plasmin. These data support the zipper model of interaction whereby Lys-464 binds initially to plasmin (most likely at K1), followed by progressive binding of the other conserved lysines (Lys-448, Lys-441, and Lys-434) to the remaining lysine-binding kringle domains (K4, K5, and K2) (6). Our data also highlight the importance of exosite interactions between the α_2 -antiplasmin core serpin and the plasmin

α_2 -Antiplasmin Binding to Plasmin

protease domain, which provide an additional mechanism of specificity in the serpin/protease interaction.

Acknowledgments—We thank Drs. Elizabeth Gardiner and Ping Fu for advice and guidance in setting up surface plasmon resonance experiments.

REFERENCES

- Lijnen, H. R. (2001) *Ann. N.Y. Acad. Sci.* **936**, 226–236
- Matsuno, H. (2006) *Curr. Pharm. Des.* **12**, 841–847
- Gross, P. L., and Weitz, J. I. (2009) *Clin. Pharmacol. Ther.* **86**, 139–146
- Lee, K. N., Lee, C. S., Tae, W. C., Jackson, K. W., Christiansen, V. J., and McKee, P. A. (2000) *J. Biol. Chem.* **275**, 37382–37389
- Coughlin, P. B. (2005) *FEBS J.* **272**, 4852–4857
- Frank, P. S., Douglas, J. T., Locher, M., Llinás, M., and Schaller, J. (2003) *Biochemistry* **42**, 1078–1085
- Clemmensen, I., Thorsen, S., Müllertz, S., and Petersen, L. C. (1981) *Eur. J. Biochem.* **120**, 105–112
- Law, R. H., Sofian, T., Kan, W. T., Horvath, A. J., Hitchen, C. R., Langendorf, C. G., Buckle, A. M., Whisstock, J. C., and Coughlin, P. B. (2008) *Blood* **111**, 2049–2052
- Hortin, G. L., Gibson, B. L., and Fok, K. F. (1988) *Biochem. Biophys. Res. Commun.* **155**, 591–596
- Gerber, S. S., Lejon, S., Locher, M., and Schaller, J. (2010) *Cell. Mol. Life Sci.* **67**, 1505–1518
- Wang, H., Yu, A., Wiman, B., and Pap, S. (2003) *Eur. J. Biochem.* **270**, 2023–2029
- Morris, E. C., Dafforn, T. R., Forsyth, S. L., Missen, M. A., Horvath, A. J., Hampson, L., Hampson, I. N., Currie, G., Carrell, R. W., and Coughlin, P. B. (2003) *Biochem. J.* **371**, 165–173
- Horvath, A. J., Irving, J. A., Rossjohn, J., Law, R. H., Bottomley, S. P., Quinsey, N. S., Pike, R. N., Coughlin, P. B., and Whisstock, J. C. (2005) *J. Biol. Chem.* **280**, 43168–43178
- Schechter, N. M., and Plotnick, M. I. (2004) *Methods* **32**, 159–168
- Morton, T. A., Myszka, D. G., and Chaiken, I. M. (1995) *Anal. Biochem.* **227**, 176–185
- Shieh, B. H., and Travis, J. (1987) *J. Biol. Chem.* **262**, 6055–6059
- Christensen, U., Bangert, K., and Thorsen, S. (1996) *FEBS Lett.* **387**, 58–62
- Whisstock, J. C., Silverman, G. A., Bird, P. I., Bottomley, S. P., Kaiserman, D., Luke, C. J., Pak, S. C., Reichhart, J. M., and Huntington, J. A. (2010) *J. Biol. Chem.* **285**, 24307–24312
- Lin, Z., Jiang, L., Yuan, C., Jensen, J. K., Zhang, X., Luo, Z., Furie, B. C., Furie, B., Andreassen, P. A., and Huang, M. (2011) *J. Biol. Chem.* **286**, 7027–7032

Appendix 10.3 Horvath et al., 2011, published paper related to the methods used in measuring the rate of plasmin inhibition by α_2 -antiplasmin as described in Chapters 4 and 6

CHAPTER ELEVEN

METHODS TO MEASURE THE KINETICS OF PROTEASE INHIBITION BY SERPINS

Anita J. Horvath,^{*} Bernadine G. C. Lu,^{*} Robert N. Pike,[†] and Stephen P. Bottomley[†]

Contents

1. Introduction	223
2. Determining the Rate of Protease Inhibition (k_a)	226
2.1. Initial assessment of the rate of inhibition	226
2.2. Discontinuous assay	227
2.3. Continuous assay	228
3. Efficiency of the Serpin Inhibitory Reaction	230
Acknowledgments	233
References	233

Abstract

The serpin molecule has evolved an unusual mechanism of inhibition, involving an exposed reactive center loop (RCL) and conformational change to covalently trap a target protease. Successful inhibition of the protease is dependent on the rate of serpin–protease association and the efficiency with which the RCL inserts into β -sheet A, translocating the covalently bound protease and thereby completing the inhibition process. This chapter describes the kinetic methods used for determining the rate of protease inhibition (k_a) and the stoichiometry of inhibition. These kinetic variables provide a means to examine different serpin–protease pairings, assess the effects of mutations within a serpin on protease inhibition, and determine the physiologically cognate protease of a serpin.

1. INTRODUCTION

Serpins inhibit serine proteases by a unique process known as the “suicide substrate inhibition mechanism” (Potempa *et al.*, 1994). Irreversible protease inhibition is achieved through the formation of a covalent

^{*} Australian Centre for Blood Diseases, Monash University, Melbourne, Victoria, Australia

[†] Department of Biochemistry and Molecular Biology, Monash University, Melbourne, Victoria, Australia

complex in which both serpin and protease are rendered inactive. This mechanism is distinct from other classes of protease inhibitors, such as Kunitz- and Kazal-type molecules, which inhibit the enzyme by using a reversible, tight, and noncovalent “lock and key” mechanism (Bode and Huber, 2000).

The exposed reactive center loop (RCL) acts as bait and is recognized as a substrate by target proteases. Cleavage of the RCL results in a dramatic conformational change in the serpin molecule and is characterized by insertion of the N-terminal portion of the cleaved RCL into β -sheet A (Carrell and Travis, 1985). The conformational change results in irreversible inhibition of the target protease as loop insertion translocates the protease and distorts its active site, thereby trapping it as an acyl-enzyme intermediate.

The initial interaction between a serpin (I) and protease (E) is a reversible Michaelis–Menten reaction, which proceeds to the formation of an acyl intermediate (Fig. 11.1). Cleavage of the peptide bond at P_1 – P_1' occurs by nucleophilic attack by the catalytic serine of the protease on the carbonyl carbon of the P_1 residue. The attack proceeds through the standard covalent tetrahedral intermediate of a substrate cleavage reaction, with the subsequent formation of an ester bond between the hydroxyl group of the Ser residue and the carbonyl carbon of the P_1 residue. This forms the covalent acyl-enzyme intermediate (EI') (Lawrence *et al.*, 1995; Wilczynska *et al.*, 1995). With the peptide bond between the serpin P_1 – P_1' residues broken, the N-terminal strand of the RCL is released and the loop can insert into the β -sheet A.

The mechanism becomes branched at this point with the rate of loop insertion determining whether the serpin behaves as a substrate or an

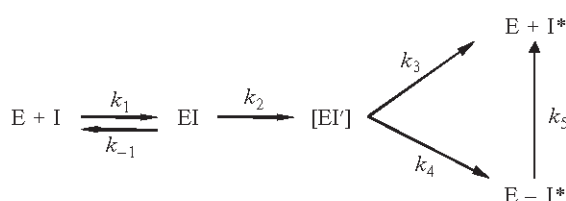


Figure 11.1 Schematic representation showing the mechanism of inhibition of a protease by a serpin. The Michaelis-like complex (EI) is formed after the initial interaction of the protease (E) and serpin (I), with the forward rate constant k_1 and the back constant of k_{-1} . This proceeds to formation of the covalent acylintermediate (EI'), with the rate constant of k_2 . From this point, the reaction can proceed down two different pathways which primarily depends on how rapidly the cleaved serpin loop is able to insert into the A β -sheet. The formation of cleaved serpin (I*) and active protease, with the rate constant k_3 , results from complete proteolysis. However, if the serpin kinetically traps the protease, the inhibitory complex (E – I*) is formed with the rate constant k_4 .

inhibitor (Lawrence *et al.*, 2000). If the loop insertion process is rapid ($k_3 > k_4$), the inhibitory pathway proceeds toward full protease inhibition ($E - I^*$) by trapping the acyl intermediate before the protease can complete the deacylation reaction. The rapid loop insertion, accompanied by conformational change in the serpin and translocation of the protease, distorts the protease active site and results in complete inhibition (Huntington *et al.*, 2000; Lawrence *et al.*, 2000). However, if loop insertion proceeds too slowly ($k_4 > k_3$), then the deacylation reaction continues, the serpin is cleaved without protease inhibition ($E + I$), and active protease is released. The inhibited serpin-protease complex is stable for days-weeks, depending on the serpin-protease pair (Calugaru *et al.*, 2001; Plotnick *et al.*, 2002; Zhou *et al.*, 2001). A typical inhibitory serpin forms a covalent complex with its cognate protease which is resistant to SDS and thermal denaturation, has a stoichiometry of inhibition (SI) close to 1 and an association constant (k_a) of $\geq 10^5 M^{-1} s^{-1}$ (Gettins, 2002).

Serpins are promiscuous inhibitors, able to inhibit multiple proteases. A number of serpins have been reported to possess inhibitory activity toward proteases outside the archetypal targets, that is, members of the chymotrypsin serine protease family. These include proteases of the subtilisin or cysteine protease family. α_1 -Antitrypsin is a rapid inhibitor of elastase but also inhibits both subtilisin *Carlsberg* and proteinase K (Beatty *et al.*, 1980; Komiyama *et al.*, 1996). The intracellular serpin PI-9 is an inhibitor of both the serine protease granzyme B and subtilisin A (Dahlen *et al.*, 1997, 1998; Sun *et al.*, 1996).

Both the caspase and cathepsin families of cysteine proteases are targeted for inhibition by serpins. The viral serpin crmA inhibits caspase1, caspase3, and caspase8, while PI-9 is a weak inhibitor of caspase1 (Annand *et al.*, 1999; Young *et al.*, 2000). Cathepsin L has been reported to be targeted by human SCCA1, SCCA-2, hurpin/headpin, protein C inhibitor, and chicken MENT (Fortenberry *et al.*, 2010; Higgins *et al.*, 2010; Irving *et al.*, 2002a; Schick *et al.*, 1998; Welss *et al.*, 2003). In the presence of DNA, cathepsin V is inhibited 10- to 50-fold more rapidly by both SCCA-1 and MENT (Ong *et al.*, 2007). A similar mechanism of inhibition by serpins is proposed for the interaction with cysteine proteases (Irving *et al.*, 2002b).

The accurate determination of inhibition constants provides a means to compare the rate and efficiency at which a serpin inhibits different proteases and is used to determine its most physiologically relevant cognate protease. This review will describe methods to calculate the rate of protease inhibition (k_a) by conventional protease-substrate assays, termed as discontinuous and continuous assays and a method for determining the SI (Horvath *et al.*, 2005; Le Bonniec *et al.*, 1995; Olson *et al.*, 1993). Intrinsic fluorescence-based assays, such as stopped flow kinetics, have been reviewed extensively elsewhere and are as such not included in this report.

2. DETERMINING THE RATE OF PROTEASE INHIBITION (K_A)

The type of assay used to determine the rate of inhibition is dependent on indications of how rapid the reaction is likely to be in preliminary experiments. The rate of protease inhibition by serpins is measured by utilizing either the discontinuous or the continuous/progress curve method. The discontinuous method is generally used for reactions when the rate of inhibition is $\leq 10^5 M^{-1} \text{sec}^{-1}$. Faster reaction rates, at $\geq 10^6 M^{-1} \text{sec}^{-1}$, are usually determined using progress curves (Horvath *et al.*, 2005; Olson *et al.*, 1993). If reactions proceed faster than can be measured by substrate-based assays, then stopped flow kinetics is commonly employed (Boudier *et al.*, 1999; Christensen *et al.*, 1996; Olson, 1988).

2.1. Initial assessment of the rate of inhibition

An initial assessment of the rate of inhibition can be made by incubating the protease with a more than five fold molar excess of serpin in the presence of substrate for the protease. The reaction is setup in a 96-well microtiter plate, thereby allowing continuous monitoring of the rate of substrate hydrolysis in a plate reader. The observed loss of proteolytic activity in the presence of the serpin, compared to protease alone, is then used to assess the rate of inhibition.

2.1.1. Example reaction 1: Assessing the rate of serpin inhibition

Assay

Into a well of a 96-well microtiter plate, add in the following order:

50 μl of 2–10 nM protease

50 μl of 5- and 10-fold molar excess of serpin

100 μl substrate solution

Place the plate into reader and follow the rate of substrate hydrolysis by taking readings every 10–30 s.

Figure 11.2 shows the expected profiles for slow and fast inhibitors of plasmin. The serpin α_2 -antiplasmin is a fast inhibitor of plasmin with an association rate (k_a) of $1 \times 10^7 M^{-1} \text{s}^{-1}$. As seen in Fig. 11.2, in the presence of α_2 -antiplasmin, there is an initial rapid increase in substrate hydrolysis followed by a steady-state phase reflective of complete loss of plasmin activity due to complete inhibition by the serpin. Reaching this steady-state phase is required in order to accurately calculate the association rate (k_a) using the continuous method.

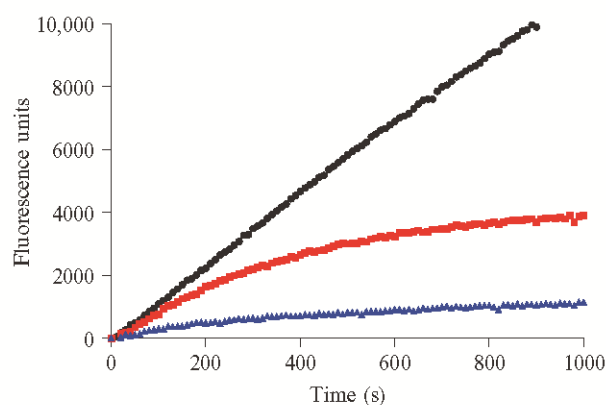


Figure 11.2 Example progress curves of the interaction of a fast and slow inhibitor of plasmin. Reactions were performed in the presence of plasmin (0.5 nM), wild-type α_2 -antiplasmin (2.5 nM), and α_2 -antiplasmin Δ C-term (40 nM) and the substrate H-Ala-Phe-Lys-AMC (1 mM). Change in fluorescence was measured by excitation/emission at 355 nm/460 nm. Reactions are plasmin + buffer (closed circle), plasmin + wild-type α_2 -antiplasmin (closed triangle), and plasmin + α_2 -antiplasmin Δ C-term (closed square).

In the presence of a slow inhibitor, a C-terminally truncated form of α_2 -antiplasmin, Lu *et al.* (2011) complete inhibition is not achieved and continued hydrolysis of the substrate is observed without reaching the steady-state phase. Therefore, the discontinuous assay is more suitable for measurement of the inhibition rate in this instance.

2.2. Discontinuous assay

The discontinuous assay is used when the rate of inhibition is low and cannot be determined through the use of progress curves, unless excessive amounts of protease and serpin are used; such high concentrations may not be feasible. In the discontinuous method, a constant concentration of protease is incubated with increasing amounts of serpin. The protease amount used should be low enough to achieve pseudo-first-order conditions with a more than five fold molar excess of serpin to protease. For each serpin–protease ratio, serpin and protease are preincubated together for various time lengths and a separate reaction mixture is prepared for each time point. If some initial estimate of the k_a for the reaction is available, the times and concentrations of serpin used for the assay may be estimated by calculating the predicted half-life ($t_{1/2}$) for the reaction using the following equation: $t_{1/2} = \ln 2/k_a \times [\text{Inhibitor}]$. The time for the full reaction may then be estimated by multiplying $t_{1/2}$ by 10. On completion of the

incubation, substrate is added to the reaction and the rate of substrate hydrolysis is monitored. The rate of protease activity at each time point is then calculated by linear regression analysis. The pseudo-first-order constant, k_{obs} , is determined by the slope of a semilogarithmic plot of the residual protease activity against time of incubation (Fig. 11.3). Linear regression analysis of the points provide the k_{obs} value. k_{obs} values are then plotted against serpin concentration and the slope of the linear regression of the line of best fit produces the second-order rate constant k_a .

2.2.1. Example reaction 2: Measurement of the rate of inhibition of plasmin–antiplasmin (C-trunc) variant

Reagents

A set concentration of protease	5 nM plasmin
Six different concentrations of serpin ^a	25–50 nM antiplasmin
Substrate	150 μM H-Ala-Phe-Lys-AMC

^aA separate reaction for eight time points for each serpin concentration ($t = 0$ –5 min).

Assay: Reactions are set up in a 96-well plate. For each concentration of serpin, eight time points are required and a separate reaction mixture is prepared. Aliquot 50 μl of 5 nM protease into eight wells of 96-well microtiter plate. Assign each well as a time point for the reaction. Add 50 μl of serpin at desired concentration to the first well of the microtiter plate (this becomes $t = 300$ s, or the longest incubation time point). Add another 50 μl of serpin to the next well containing protease when the next time point is reached. This process is repeated until time = 0 s is reached, and after the final addition of serpin, 100 μl of substrate is immediately added to each reaction and followed directly by measurement of substrate hydrolysis.

Analysis: Figure 11.3 shows the semilog plots of the residual rate of plasmin activity over time. The pseudo-first-order constant, k_{obs} , is determined by the slope of the semilogarithmic plot of the residual protease activity against time. The k_{obs} values are then plotted against serpin concentration and linear regression analysis is used to fit the points to a line (Lu *et al.*, 2011). The slope of this line provides the second-order rate constant, k_a .

2.3. Continuous assay

The continuous assay is the process by which the inhibition of the protease is measured by progress curves which are generated from monitoring the rate of product formation over time (Horvath *et al.*, 2005). A constant amount of protease is mixed with increasing amounts of serpin and a fixed concentration of substrate.

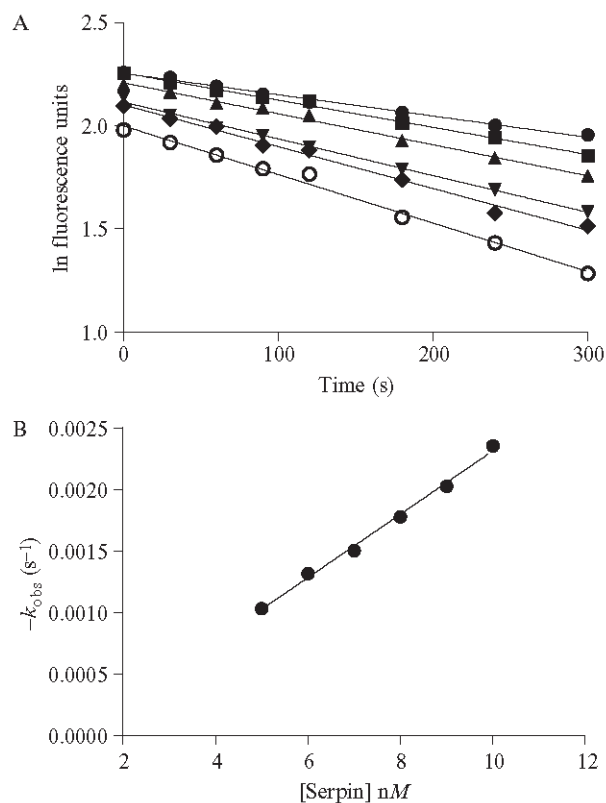


Figure 11.3 Discontinuous assay of the inhibition of plasmin by α_2 -antiplasmin ΔC -term. (A) Semilogarithmic plots of residual plasmin activity versus time for reactions at various concentrations of antiplasmin ((5–10 nM), 5 nM closed circle, 6 nM closed square, 7 nM closed triangle, 8 nM closed inverted triangle, 9 nM closed diamond and 10 nM open circle). (B) Plot of k_{obs} as a function of antiplasmin concentration. Linear regression of the slope gave the second-order rate constant k_i for the inhibition of plasmin by antiplasmin ΔC -term.

2.3.1. Example reaction 3: Measurement of the rate of inhibition of plasmin by α_2 -antiplasmin

<i>Reagents</i>	
A set concentration of protease	0.5 nM plasmin
Six different concentrations of serpin	1–10 nM antiplasmin
Substrate	1 mM H-Ala-Phe-Lys-AMC

Assay: A total of eight 200 μ l reactions, one with protease and substrate alone and seven with increasing serpin concentration, along with constant protease and substrate concentrations, are set up in a BSA-coated 96-well microtiter plate. Into the microtiter plate, aliquot 100 μ l of substrate into

each well, followed by 50 μl of serpin at the desired concentration. Place microtiter plate into plate reader. Add 50 μl of protease to each well and immediately commence measurement of substrate hydrolysis by taking readings at 15–30 s time intervals.

Analysis: Rate constants are measured under pseudo-first-order conditions using progress curves for the interaction of plasmin (0.5 nM) and antiplasmin (1–10 nM) in the presence of 1 mM fluorogenic substrate, H-Ala-Phe-Lys-AMC (Bachem, Bubendorf, Switzerland) (Lu *et al.*, 2011). The rate of product formation is measured using an excitation and emission wavelengths of 355 and 460 nm, respectively (Fig. 11.4A).

Product formation is described by Eq. (11.1), where P is the concentration of product at time t , k_{obs} is the apparent first-order rate constant, and v_0 is the initial velocity.

$$P = \frac{v_0}{k_{obs}} \left[1 - e^{-(1-k_{obs}t)} \right] \quad (11.1)$$

For each combination of protease and serpin, a k_{obs} value is calculated by nonlinear regression analysis of the data using Eq. (11.1) (Olson *et al.*, 1993; Rovelli *et al.*, 1992). The k_{obs} values are then plotted against the respective serpin concentration [serpin] and linear regression is used to provide a line to the points (Fig. 11.4B). The slope of this line provides the second-order rate constant, k' .

As the rate of inhibition is dependent on the SI and the inhibitor is in competition with the substrate [S], the second-order rate constant k' is corrected for substrate concentration, the K_M of the protease for substrate, and the SI (Eq. (11.2)) to calculate k_a , the rate of association.

$$k_a = k' \left(1 + \frac{[S]}{K_M} \right) \text{SI} \quad (11.2)$$

3. EFFICIENCY OF THE SERPIN INHIBITORY REACTION

To ascertain the efficiency of the serpin inhibitory reaction, the SI is calculated. This is a measure of the balance between the inhibitory reaction and the substrate reaction and describes the number of moles of serpin required to inhibit 1 mol of protease. If the inhibitory pathway proceeds faster than the substrate pathway, then the SI approaches 1. However, if serpin proteolysis and the substrate pathway prevail over the inhibitory pathway, then the SI is greater than 1. Physiological serpin–protease pairs, such as thrombin–anthrombin, plasmin–antiplasmin have 1:1 serpin–protease molar relationships (Moroi and Aoki, 1976; Olson, 1985). The SI can influence the measured association rate, and therefore, it is an important parameter to calculate when examining any protease–serpin interaction.

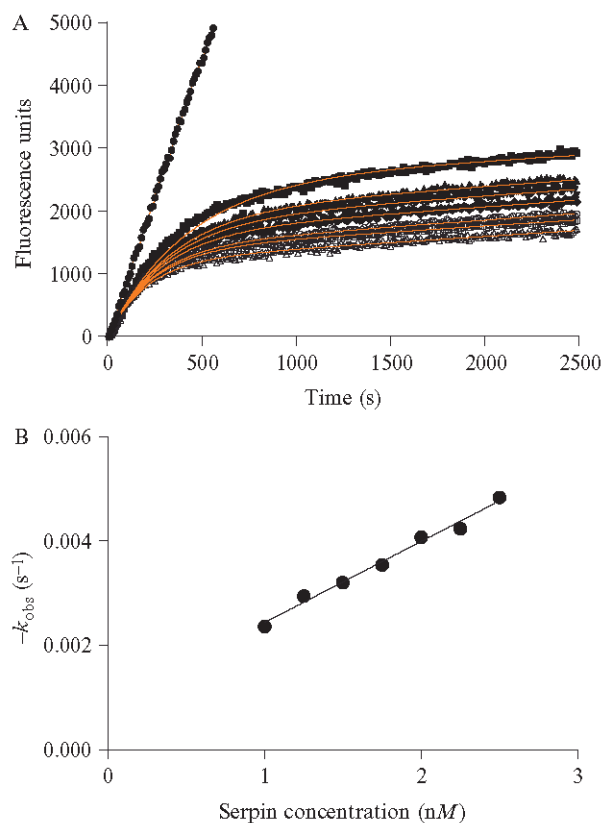


Figure 11.4 Continuous assay of the inhibition of plasmin by α_2 -antiplasmin. (A) Progress curves of the interaction between plasmin (0.5 nM) and wild-type α_2 -antiplasmin (1–2.5 nM) monitored by continuous measurement of the change in fluorescence excitation/emission at 355 nm/460 nm. k_{obs} at each serpin concentration was determined by nonlinear regression analysis of each curve using Eq. (11.1). (B) k_{obs} were plotted against α_2 -antiplasmin concentration and linear regression analysis was used to determine the second-order rate constant (k). k_a was determined by accounting for K_M of the protease for substrate (Eq. (11.2)).

To calculate the SI, a series of reactions are set up with a constant molar amount of protease and increasing molar amounts of serpin.

3.1. Example reaction 1: SI calculation using plasmin–antiplasmin

Reaction

30 μ l of 16 nM plasmin
 30 μ l of serpin (0–24 nM)
 Incubate at 37 °C for 1 h.

Assay: Aliquot duplicate 25 μl lots of each reaction into a 96-well microtiter plate. To assay for residual protease activity, add 75 μl of reaction buffer (20 mM Tris-HCl, pH 8.0, 150 mM NaCl, 0.01% Tween 20) and 100 μl of 150 μM H-Ala-Phe-Lys-AMC substrate and measure the rate of substrate hydrolysis.

Analysis: Figure 11.5 shows that as serpin concentration increases the rate of substrate hydrolysis decreases. The rate of substrate hydrolysis which is used as a measure of residual protease activity is measured by linear regression (Fig. 11.5A). The resultant rate is then converted to a percentage of maximal protease activity (from reactions with protease and buffer alone) and is then plotted against the serpin:protease ratio (Fig. 11.5B). The SI is

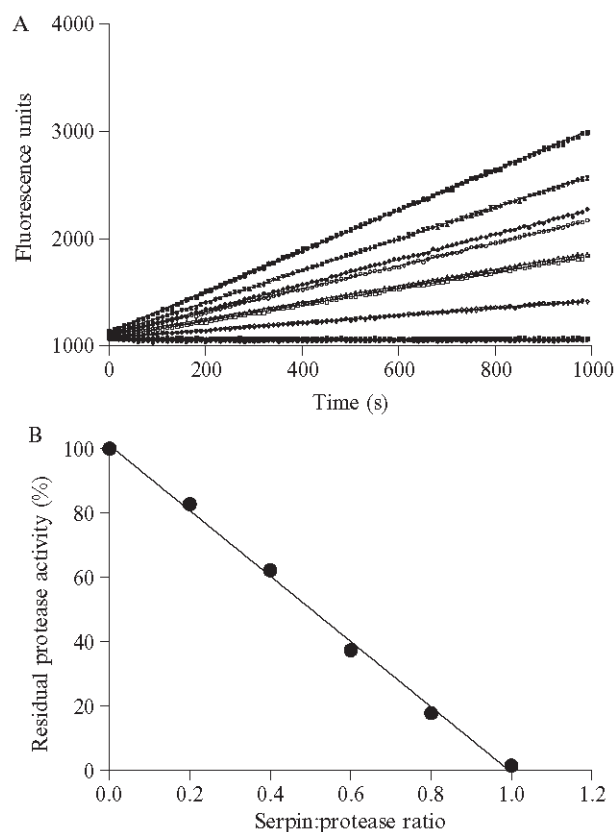


Figure 11.5 Stoichiometry of inhibition of plasmin by α_2 -antiplasmin. (A) Plasmin (1 nM) was incubated with wild-type α_2 -antiplasmin (0.2–1.5 nM) for 1 h at 37 °C. Residual protease activity was assayed in the presence of the substrate H-Ala-Phe-Lys-AMC (0.2 mM). Reactions were set up in duplicate. (B) The stoichiometry of inhibition was determined by plotting the percentage residual protease activity against serpin:protease ratio and extrapolation to the ratio which resulted in total loss of protease activity.

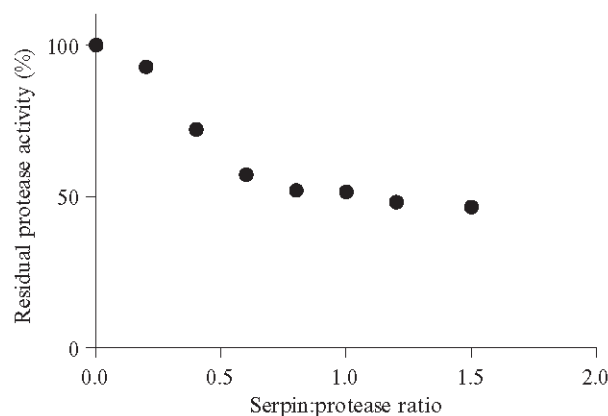


Figure 11.6 The effect of incubation time on the stoichiometry of inhibition. Plasmin (1 nM) was incubated with wild-type α_2 -antiplasmin (0.2–1.5 nM) for 5 min at 37 °C. Residual protease activity was assayed in the presence of the substrate H-Ala-Phe-Lys-AMC (0.2 mM). The percentage residual protease activity was plotted against serpin:protease ratio.

determined by extrapolating to the serpin:protease ratio where protease activity is zero.

A linear relationship should be observed between serpin:protease ratio and residual protease activity. Alternatives to this relationship may be observed if the protease and serpin are not incubated for sufficient time to ensure the inhibitory reaction has occurred to completion. In this instance, as seen in Fig. 11.6, residual protease activity has plateaued at 50%. This requires either a longer incubation time or an increase in both serpin and protease concentration in the reaction. It is for this reason that it is important to incubate the serpin–protease reactions for at least $5 \times t_{1/2}$.

The SI obtained through the use of the protease/substrate assay as described can also be confirmed by following the formation of the covalent serpin–protease complex on SDS-PAGE (Horvath *et al.*, 2005).

ACKNOWLEDGMENTS

The work presented in this report is supported with grants from the National Health and Medical Research Council (NHMRC) of Australia.

REFERENCES

- Annand, R. R., Dahlen, J. R., Sprecher, C. A., De Dreu, P., Foster, D. C., Mankovich, J. A., Talanian, R. V., Kiesel, W., and Giegel, D. A. (1999). Caspase-1 (interleukin-1 β -converting enzyme) is inhibited by the human serpin analogue proteinase inhibitor 9. *Biochem. J.* **342**(Pt. 3), 655–665.

- Beatty, K., Bieth, J., and Travis, J. (1980). Kinetics of association of serine proteinases with native and oxidized alpha-1-proteinase inhibitor and alpha-1-antichymotrypsin. *J. Biol. Chem.* **255**(9), 3931–3934.
- Bode, W., and Huber, R. (2000). Structural basis of the endoproteinase-protein inhibitor interaction. *Biochim. Biophys. Acta* **1477**(1–2), 241–252.
- Boudier, C., Cadène, M., and Bieth, J. G. (1999). Inhibition of neutrophil cathepsin G by oxidized mucus proteinase inhibitor. Effect of heparin. *Biochemistry* **38**(26), 8451.
- Calugaru, S. V., Swanson, R., and Olson, S. T. (2001). The pH dependence of serpin-proteinase complex dissociation reveals a mechanism of complex stabilization involving inactive and active conformational states of the proteinase which are perturbable by calcium. *J. Biol. Chem.* **276**(35), 32446–32455.
- Carrell, R. W., and Travis, J. (1985). α 1-Antitrypsin and the serpins: Variation and counter variation. *Trends Biochem. Sci.* **10**, 20–24.
- Christensen, U., Bangert, K., and Thorsen, S. (1996). Reaction of human alpha2-antiplasmin and plasmin stopped-flow fluorescence kinetics. *FEBS Lett.* **387**(1), 58.
- Dahlen, J. R., Foster, D. C., and Kisiel, W. (1997). Human proteinase inhibitor 9 (PI9) is a potent inhibitor of subtilisin A. *Biochem. Biophys. Res. Commun.* **238**, 329–333.
- Dahlen, J. R., Jean, F., Thomas, G., Foster, D. C., and Kisiel, W. (1998). Inhibition of soluble recombinant furin by human proteinase inhibitor 8. *J. Biol. Chem.* **273**, 1851–1854.
- Fortenberry, Y. M., Brandal, S., Bialas, R. C., and Church, F. C. (2010). Protein C inhibitor regulates both cathepsin L activity and cell-mediated tumor cell migration. *Biochim. Biophys. Acta* **1800**(6), 580–590.
- Gettins, P. G. (2002). Serpin structure, mechanism, and function. *Chem. Rev.* **102**(12), 4751–4804.
- Higgins, W. J., Fox, D. M., Kowalski, P. S., Nielsen, J. E., and Worrall, D. M. (2010). Heparin enhances serpin inhibition of the cysteine protease cathepsin L. *J. Biol. Chem.* **285**(6), 3722–3729.
- Horvath, A. J., Irving, J. A., Rossjohn, J., Law, R. H., Bottomley, S. P., Quinsey, N. S., Pike, R. N., Coughlin, P. B., and Whisstock, J. C. (2005). The murine orthologue of human antichymotrypsin: A structural paradigm for clade A3 serpins. *J. Biol. Chem.* **280**(52), 43168–43178.
- Huntington, J. A., Read, R. J., and Carrell, R. W. (2000). Structure of a serpin-protease complex shows inhibition by deformation. *Nature* **407**(6806), 923–926.
- Irving, J. A., Shushanov, S. S., Pike, R. N., Popova, E. Y., Bromme, D., Coetzer, T. H., Bottomley, S. P., Boulyenko, I. A., Grigoryev, S. A., and Whisstock, J. C. (2002a). Inhibitory activity of a heterochromatin-associated serpin (MENT) against papain-like cysteine proteinases affects chromatin structure and blocks cell proliferation. *J. Biol. Chem.* **277**(15), 13192–13201.
- Irving, J. A., Pike, R. N., Dai, W., Bromme, D., Worrall, D. M., Silverman, G. A., Coetzer, T. H., Dennison, C., Bottomley, S. P., and Whisstock, J. C. (2002b). Evidence that serpin architecture intrinsically supports papain-like cysteine protease inhibition: Engineering alpha(1)-antitrypsin to inhibit cathepsin proteases. *Biochemistry* **41**(15), 4998–5004.
- Komiyama, T., Gron, H., Pemberton, P. A., and Salvesen, G. S. (1996). Interaction of subtilisins with serpins. *Protein Sci.* **5**(5), 874–882.
- Lawrence, D. A., Ginsburg, D., Day, D. E., Berkenpas, M. B., Verhamme, I. M., Kvassman, J. O., and Shore, J. D. (1995). Serpin-protease complexes are trapped as stable acyl-enzyme intermediates. *J. Biol. Chem.* **270**(43), 25309–25312.
- Lawrence, D. A., Olson, S. T., Muhammad, S., Day, D. E., Kvassman, J. O., Ginsburg, D., and Shore, J. D. (2000). Partitioning of serpin-proteinase reactions between stable

- inhibition and substrate cleavage is regulated by the rate of serpin reactive center loop insertion into beta-sheet A. *J. Biol. Chem.* **275**(8), 5839–5844.
- Le Bonniec, B. F., Guinto, E. R., and Stone, S. R. (1995). Identification of thrombin residues that modulate its interactions with antithrombin III and alpha 1-antitrypsin. *Biochemistry* **34**(38), 12241–12248.
- Lu, B. C. G., Sofian, T., Law, R. H. P., Coughlin, P. B., and Horvath, A. J. (2011). Contribution of conserved lysine residues in the alpha 2 antiplasmin C terminus to plasmin binding and inhibition. *J. Biol. Chem.* **286**(28), 24544–24552.
- Moroi, M., and Aoki, N. (1976). Isolation and characterization of alpha2-plasmin inhibitor from human plasma. A novel proteinase inhibitor which inhibits activator-induced clot lysis. *J. Biol. Chem.* **251**(19), 5956–5965.
- Olson, S. T. (1985). Heparin and ionic strength-dependent conversion of antithrombin III from an inhibitor to a substrate of alpha-thrombin. *J. Biol. Chem.* **260**(18), 10153–10160.
- Olson, S. T. (1988). Transient kinetics of heparin-catalyzed protease inactivation by antithrombin III. Linkage of protease-inhibitor-heparin interactions in the reaction with thrombin. *J. Biol. Chem.* **263**(4), 1698–1708.
- Olson, S. T., Bjork, I., and Shore, J. D. (1993). Kinetic characterization of heparin-catalyzed and uncatalyzed inhibition of blood coagulation proteinases by antithrombin. *Methods Enzymol.* **222**, 525–559.
- Ong, P. C., McGowan, S., Pearce, M. C., Irving, J. A., Kan, W. T., Grigoryev, S. A., Turk, B., Silverman, G. A., Brix, K., Bottomley, S. P., Whisstock, J. C., and Pike, R. N. (2007). DNA accelerates the inhibition of human cathepsin V by serpins. *J. Biol. Chem.* **282**(51), 36980–36986.
- Plotnick, M. I., Rubin, H., and Schechter, N. M. (2002). The effects of reactive site location on the inhibitory properties of the serpin alpha(1)-antichymotrypsin. *J. Biol. Chem.* **277**(33), 29927–29935.
- Potempa, J., Korzus, E., and Travis, J. (1994). The serpin superfamily of proteinase inhibitors: Structure, function, and regulation. *J. Biol. Chem.* **269**(23), 15957–15960.
- Rovelli, G., Stone, S. R., Guidolin, A., Sommer, J., and Monard, D. (1992). Characterization of the heparin-binding site of glia-derived nexin/protease nexin-1. *Biochemistry* **31**(13), 3542–3549.
- Schick, C., Pemberton, P. A., Shi, G. P., Kamachi, Y., Cataltepe, S., Bartuski, A. J., Gornstein, E. R., Bromme, D., Chapman, H. A., and Silverman, G. A. (1998). Cross-class inhibition of the cysteine proteinases cathepsins K, L, and S by the serpin squamous cell carcinoma antigen 1: A kinetic analysis. *Biochemistry* **37**, 5258–5266.
- Sun, J. R., Bird, C. H., Sutton, V., McDonald, L., Coughlin, P. B., Dejong, T. A., Trapani, J. A., and Bird, P. I. (1996). A cytosolic granzyme B inhibitor related to the viral apoptotic regulator cytokine response modifier A is present in cytotoxic lymphocytes. *J. Biol. Chem.* **271**, 27802–27809.
- Wells, T., Sun, J., Irving, J. A., Blum, R., Smith, A. I., Whisstock, J. C., Pike, R. N., von Mikecz, A., Ruzicka, T., Bird, P. I., and Abts, H. F. (2003). Hurspin is a selective inhibitor of lysosomal cathepsin L and protects keratinocytes from ultraviolet-induced apoptosis. *Biochemistry* **42**(24), 7381–7389.
- Wilczynska, M., Fa, M., Ohlsson, P. I., and Ny, T. (1995). The inhibition mechanism of serpins. Evidence that the mobile reactive center loop is cleaved in the native protease-inhibitor complex. *J. Biol. Chem.* **270**(50), 29652–29655.
- Young, J. L., Sukhova, G. K., Foster, D., Kisiel, W., Libby, P., and Schonbeck, U. (2000). The serpin proteinase inhibitor 9 is an endogenous inhibitor of interleukin 1beta-converting enzyme (caspase-1) activity in human vascular smooth muscle cells. *J. Exp. Med.* **191**(9), 1535–1544.
- Zhou, A., Carrell, R. W., and Huntington, J. A. (2001). The serpin inhibitory mechanism is critically dependent on the length of the reactive center loop. *J. Biol. Chem.* **276**(29), 27541–27547.